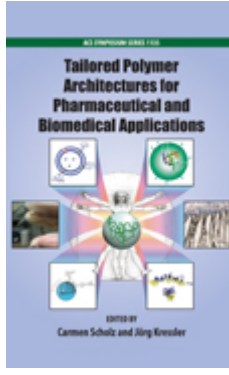
ACS SYMPOSIUM SERIES 1135
Tailored Polymer Architectures for Pharmaceutical and Biomedical Applications
EDITED BY
Carmen Scholz and Jörg Kressler

# Tailored Polymer Architectures for Pharmaceutical and Biomedical Applications

Downloaded by 217.118.78.91 on July 17, 2013 | http://pubs.acs.org
Publication Date (Web): July 8, 2013 | doi: 10.1021/bk-2013-1135.fw001

In Tailored Polymer Architectures for Pharmaceutical and Biomedical Applications; Scholz, C., et al.;
ACS Symposium Series; American Chemical Society: Washington, DC, 2013.

Downloaded by 217.118.78.91 on July 17, 2013 | http://pubs.acs.org
Publication Date (Web): July 8, 2013 | doi: 10.1021/bk-2013-1135.fw001

In Tailored Polymer Architectures for Pharmaceutical and Biomedical Applications; Scholz, C., et al.;
ACS Symposium Series; American Chemical Society: Washington, DC, 2013.

ACS SYMPOSIUM SERIES **1135**

# Tailored Polymer Architectures for Pharmaceutical and Biomedical Applications

**Carmen Scholz**, Editor
*University of Alabama in Huntsville*
*Huntsville, Alabama*

**Jörg Kressler**, Editor
*Martin Luther University Halle-Wittenberg*
*Halle, Germany*

Downloaded by 217.118.78.91 on July 17, 2013 | http://pubs.acs.org
Publication Date (Web): July 8, 2013 | doi: 10.1021/bk-2013-1135.fw001

**Sponsored by the**
**ACS Division of Polymer Chemistry, Inc.**

American Chemical Society, Washington, DC

Distributed in print by Oxford University Press

In Tailored Polymer Architectures for Pharmaceutical and Biomedical Applications; Scholz, C., et al.;
ACS Symposium Series; American Chemical Society: Washington, DC, 2013.

**Library of Congress Cataloging-in-Publication Data**

Tailored polymer architectures for pharmaceutical and biomedical applications / Carmen Scholz, editor, University of Alabama in Huntsville, Huntsville, Alabama, Jörg Kressler, editor, Martin Luther University Halle-Wittenberg, Halle, Germany ; sponsored by the ACS Division of Polymer Chemistry, Inc.
pages cm. -- (ACS symposium series ; 1135)
Includes bibliographical references and index.
ISBN 978-0-8412-2798-9 (alk. paper)
1. Polymers in medicine. 2. Polymers--Therapeutic use, 3. Biomedical materials 4. Drugs--Design. I. Scholz, Carmen, 1963- II. Kressler, Jörg, 1957- III. American Chemical Society. Division of Polymer Chemistry, Inc.
R857.P6T35 2013
610.28--dc23

2013020434

The paper used in this publication meets the minimum requirements of American National Standard for Information Sciences—Permanence of Paper for Printed Library Materials, ANSI Z39.48n1984.

Copyright © 2013 American Chemical Society

Distributed in print by Oxford University Press

All Rights Reserved. Reprographic copying beyond that permitted by Sections 107 or 108 of the U.S. Copyright Act is allowed for internal use only, provided that a per-chapter fee of $40.25 plus $0.75 per page is paid to the Copyright Clearance Center, Inc., 222 Rosewood Drive, Danvers, MA 01923, USA. Republication or reproduction for sale of pages in this book is permitted only under license from ACS. Direct these and other permission requests to ACS Copyright Office, Publications Division, 1155 16th Street, N.W., Washington, DC 20036.

The citation of trade names and/or names of manufacturers in this publication is not to be construed as an endorsement or as approval by ACS of the commercial products or services referenced herein; nor should the mere reference herein to any drawing, specification, chemical process, or other data be regarded as a license or as a conveyance of any right or permission to the holder, reader, or any other person or corporation, to manufacture, reproduce, use, or sell any patented invention or copyrighted work that may in any way be related thereto. Registered names, trademarks, etc., used in this publication, even without specific indication thereof, are not to be considered unprotected by law.

PRINTED IN THE UNITED STATES OF AMERICA

Downloaded by 217.118.78.91 on July 17, 2013 | http://pubs.acs.org
Publication Date (Web): July 8, 2013 | doi: 10.1021/bk-2013-1135.fw001

# Foreword

The ACS Symposium Series was first published in 1974 to provide a mechanism for publishing symposia quickly in book form. The purpose of the series is to publish timely, comprehensive books developed from the ACS sponsored symposia based on current scientific research. Occasionally, books are developed from symposia sponsored by other organizations when the topic is of keen interest to the chemistry audience.

Before agreeing to publish a book, the proposed table of contents is reviewed for appropriate and comprehensive coverage and for interest to the audience. Some papers may be excluded to better focus the book; others may be added to provide comprehensiveness. When appropriate, overview or introductory chapters are added. Drafts of chapters are peer-reviewed prior to final acceptance or rejection, and manuscripts are prepared in camera-ready format.

As a rule, only original research papers and original review papers are included in the volumes. Verbatim reproductions of previous published papers are not accepted.

**ACS Books Department**

Downloaded by 217.118.78.91 on July 17, 2013 | http://pubs.acs.org
Publication Date (Web): July 8, 2013 | doi: 10.1021/bk-2013-1135.fw001

In Tailored Polymer Architectures for Pharmaceutical and Biomedical Applications; Scholz, C., et al.;
ACS Symposium Series; American Chemical Society: Washington, DC, 2013.

Downloaded by 217.118.78.91 on July 17, 2013 | http://pubs.acs.org
Publication Date (Web): July 8, 2013 | doi: 10.1021/bk-2013-1135.pr001

# Preface

I am honored to present the Preface to this ACS book, "Tailored Polymer Architectures for Pharmaceutical and Biomedical Applications," dedicated to Professor Raphael (Ray) M. Ottenbrite. This ambitious title with its foundation in polymers implies broad coverage of medical applications including drugs, medical devices and combination products. This book is a perfectly appropriate way to honor Ray, since, as long as I have known him, he has exemplified and promoted the commendable "agnostic" premise that all scientific tools should be applied to the solution of unmet medical and other societal needs through his own research, the publications, conferences and symposia that he has sponsored and the professional service he has rendered.

How does Ray "walk the agnostic walk," in his personal research endeavors? A few examples follow. Included among his over 250 publications over 30 patents are descriptions of bulk polymers he has created that serve as immune-stimulators for treating HIV and cancer. He has developed synthetic, non-natural amino acids for combination with therapeutic biomolecules for oral delivery instead of injection. His small molecule therapy accomplishments include highly potent antibacterial agents with promising properties that combat bacterial resistance, novel anti-inflammatories deliverable transdermally or orally, and a new antiviral agent effective against the recent SARS virus. As a pioneer in surface coatings, Ray has generated functionally-coated nanoparticles for drug conjugation and delivery by injection.

Besides Ray's innovations in the medical arena, he has made numerous seminal contributions to surface science, nanoparticle technology and polymer structure modification. A notable example is the development of heat resistant adhesives for space shuttle re-entry shields.

In promoting and recognizing the work of diverse fellow medical innovators, Ray is in the top echelon of such colleagues. He has edited 21 polymer-related books. He has organized or co-organized over 20 ACS symposia and has chaired or served on the organizing committee of all Frontiers in Biomedical Polymers meetings, a biennial conference series of which he is a founding member. He has served continuously in leadership roles in the Polymer Division of the American Chemical Society since 1980, serving as chair in 1991. Ray has chaired two polymer-based Gordon conferences.

In recognition of his contributions, Ray has received numerous honors from ACS, NASA and from international universities (as Visiting Professor). He is a Fellow of the American Institute for Medical and Biological Engineering.

On a personal note, to know Ray is to appreciate a gentleman, always, who is driven to serve Society in the various creative ways that he can. This means


In Tailored Polymer Architectures for Pharmaceutical and Biomedical Applications; Scholz, C., et al.;
ACS Symposium Series; American Chemical Society: Washington, DC, 2013.

scouting unmet medical needs, highlighting them publicly and soliciting and publicizing approaches to their solution. He is respectful of and excited for the achievements of his colleagues and one of his greatest attributes is his ability to motivate people to provide service to the profession, to integrate them by sharing responsibilities and tasks such as editorships and symposia chairmanships, etc. To Ray, "Emeritus Professor" in no way implies relegation to the "rocking chair." It means continuing the unique service detailed above, perhaps without some of the "perks" previously enjoyed as a renowned educator. For this, our biomedical polymer community is not only profoundly grateful, but expectant of much more of the same service from Ray long after this book is published.

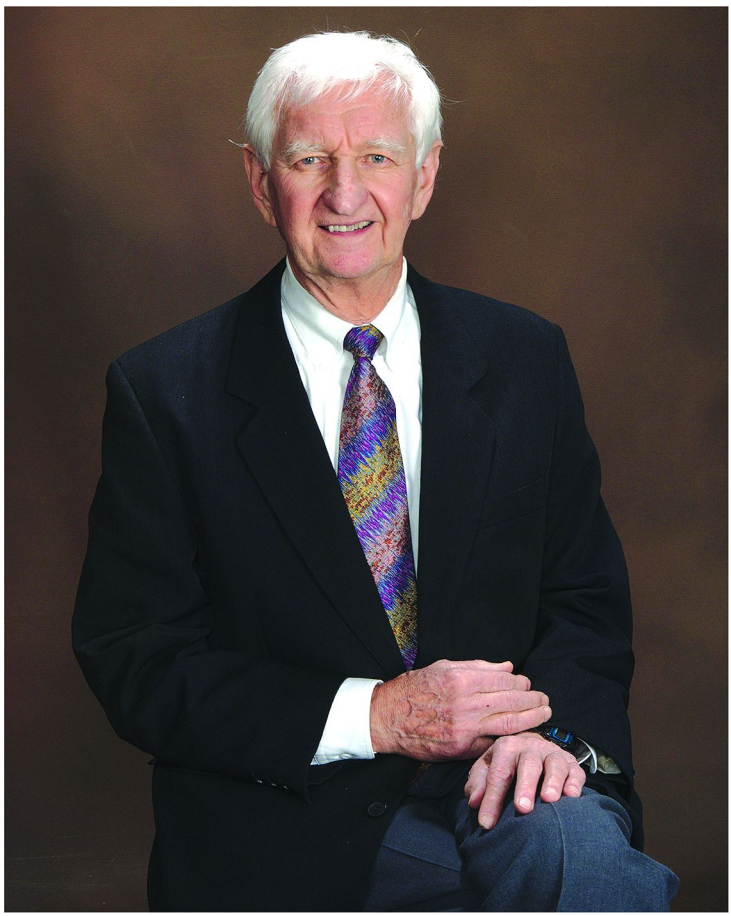

Professor Raphael (Ray) M. Ottenbrite

**Art Coury**
Coury Consultation Services
154 Warren Avenue
Boston, MA, U.S.A. 02116


In Tailored Polymer Architectures for Pharmaceutical and Biomedical Applications; Scholz, C., et al.;
ACS Symposium Series; American Chemical Society: Washington, DC, 2013.

Downloaded by 217.118.78.91 on July 17, 2013 | http://pubs.acs.org
Publication Date (Web): July 8, 2013 | doi: 10.1021/bk-2013-1135.pr001

Downloaded by 217.118.78.91 on July 17, 2013 | http://pubs.acs.org
Publication Date (Web): July 8, 2013 | doi: 10.1021/bk-2013-1135.ch001

## Chapter 1

# Introduction to Polymers in Today's Biomedical Realm

**Carmen Scholz*,[1] and Jörg Kressler[2]**

**[1]Department of Chemistry, University of Alabama in Huntsville, 301 Sparkman Drive, Huntsville, Alabama 35899, United States**
**[2]Department of Chemistry, Martin Luther University Halle-Wittenberg, D-06099 Halle (Saale), Germany**
***E-mail: cscholz@chemistry.uah.edu.**

New synthetic polymers and polymer architectures contribute widely to the progress in pharmacy and biomedicine. This book consists of five sections that describe and discuss recent developments in biorelated polymers; specifically, the focus is on the following subject areas: i) Synthesis of new polymers for pharmacy and biomedicine, ii) Using polymers for modern therapeutic approaches, iii) Delivery of biomacromolecules, i.e., drugs as well as nucleic acids, iv) Polymers for tissue engineering, and v) Polymers for surfaces and sensors. All chapters were written by the world's leading scientists in their respective fields. Research presented in these chapters demonstrates that these new polymers, new polymer architectures, and new polymer conjugates are well suited for demanding applications in biomedical diagnostics and therapies. Modern approaches to drug delivery systems, new scaffolds for tissue engineering, and surfaces for sensors or antimicrobial activity are discussed in detail. Novel strategies in polymer synthesis are presented, as e.g. the functionalization of dendrimers or hyperbranched polymers, exploiting the possibilities of 'click' chemistry for the synthesis of well-defined block and graft copolymers or bioconjugation, and introducing environmentally responsive polymer moieties. The characterization of these polymeric systems is a challenging

© 2013 American Chemical Society
In Tailored Polymer Architectures for Pharmaceutical and Biomedical Applications; Scholz, C., et al.; ACS Symposium Series; American Chemical Society: Washington, DC, 2013.

task in itself but becomes even more challenging when applying the *in vitro* and *in vivo* conditions that are relevant for pharmaceutical and biomedical applications.

## Introduction

Research into Biorelated Polymers is one of the most active fields in chemistry, physics, and materials science as it is intimately related to the progress in medical and pharmaceutical research. In the past few years new concepts were developed and several books and review articles appeared (*1–5*). With an advanced genetic understanding of diseases and the development of genetic therapeutic approaches biopolymers became essential and an integral part of modern biomedical research (*6*, *7*). Polymers can adopt manifold conformations, self-assemble into pre-determined structures, undergo stimuli-induced phase transitions or depolymerization steps and can act as probes. These characteristics together with their biocompatibility make them premier candidates for drug and gene delivery systems, for tissue engineering scaffolds, and for matrices for biomedical probes and many other biomedical applications (*8–10*).

Research into Biorelated Polymers resides at the interface of chemistry, pharmacy, medicine and biology and it continues to attract attention from scientists in academia, industry, and government research laboratories. Polymers made their entry into the realm of biomedical materials quite spectacularly when it was discovered that World War II fighter pilots did not suffer adverse affects from plastic fragments from their aircraft canopies that were launched into their bodies after being hit. Later on, poly(methyl methacrylate) (Plexiglas) found ample application as replacement for damaged or diseased skull bones (*11*). Another example are artificial blood vessels which were made initially from poly(ethylene terephthalate) (Dacron) knitted into flexible tubes; the same material that is used in the textile industry. While one would suspect that the hydrophobic material would cause heavy blood clotting, the success (survival) rate was surprisingly high. A third example that illustrates the crucial need of polymers in the biomedical field was the lack of a suitable (polymeric) delivery system for the administration of penicillin. Since this antibiotic degraded very fast after *in vivo* injection, it had to be administrated every three hours. The first drug delivery formulation for penicillin consisted of beeswax and peanut oil, the so-called Romansky-formulation. With that, penicillin had to be injected only once a day.

In recent years polymers have been tailored for specific biomedical and pharmaceutical applications starting with new and designed monomers and expanding to specific and controlled polymerizations that allow for tightly controlling molar masses and molar mass distributions. In addition, new polymerization techniques led to the production of new and well defined polymer architectures. This book provides five sections which focus on modern trends in biomedical and pharmaceutical polymers.

Downloaded by 217.118.78.91 on July 17, 2013 | http://pubs.acs.org
Publication Date (Web): July 8, 2013 | doi: 10.1021/bk-2013-1135.ch001


In Tailored Polymer Architectures for Pharmaceutical and Biomedical Applications; Scholz, C., et al.;
ACS Symposium Series; American Chemical Society: Washington, DC, 2013.

- Polymers with New Designs
- Modern Therapies
- Delivery of Biomacromolecules
- Tissue Engineering
- Surfaces and Sensors

This book was inspired by the 11th Biorelated Polymer Symposium that was held at the 243rd ACS meeting in March of 2012. The 20 chapters of this book provide detailed information on cutting edge research in the field of polymer science for biomedical and pharmaceutical applications. They are intended not only for polymer scientists but also for engineers and scientists working with polymers in life sciences.

Downloaded by 217.118.78.91 on July 17, 2013 | http://pubs.acs.org
Publication Date (Web): July 8, 2013 | doi: 10.1021/bk-2013-1135.ch001

## Polymers with New Designs

The development of new and designed monomers in the field of commercial mass plastics can be considered to be complete, but the synthesis of tailor-made monomers for biomedical application is only at its beginning. The unique advantage of polymers is their broad spectrum of chemical and physical properties, which can be exploited to complement and satisfy the broad spectrum of biomedical requirements. Challenging tasks for the future include stimuli-responsive polymer systems (responding to temperature, pH-value or pressure changes), chiral polymers for chiral recognition, tailored molar mass distributions that are not necessarily monodisperse, polyphilic polymers that carry additional functionalities and expand on the typical amphiphilic character, bioconjugate monomers and polymers, just to mention a few. This section describes important new synthetic routes that lead to tailor-made polymers for pharmaceutical and biomedical applications. New hyperbranched polyether-based lipids are presented, which might overcome some of the typical drawbacks of poly(ethylene glycol) (PEG), such as the lack of functional groups and non-biodegradability. An epoxide based monomer library is described including the monomers' subsequent modification with biocompatibilizing moieties, such as cholesterol. New bioactive polymers with reduced toxicity based on poly(anhydride-esters) are discussed. These polymers can be employed as controlled drug delivery systems and can also be formulated into hydrogels, microspheres, and electrospun fibers. Hydrophilic and biodegradable linear polyesters based on glycerol and derivates of dicarboxylic acids can be synthesized by enzymatic polymerization. The grafting of fatty acids to these polymers yields materials that are similar to glycerides and find widespread pharmaceutical applications. Another example are poly(oxazoline)s which are an important class of biomedical polymers due to their structural similarities to peptides and the ease of tailoring their hydrophilicity. Similarly, synthetic poly(amino acid)s consisting of naturally occurring *L*-amino acids are inherently biocompatible. The polymer properties can be tailored by judiciously selecting the ratio of hydrophilic to hydrophobic *L*-amino acids and/or incorporating amino acids with functional groups. Typically, polymer aggregates or polymeric micelles loaded with


In Tailored Polymer Architectures for Pharmaceutical and Biomedical Applications; Scholz, C., et al.;
ACS Symposium Series; American Chemical Society: Washington, DC, 2013.

drugs are delivered to solid tumors via the enhanced permeation and retention effect. The stabilization of micelles under i*n vivo* conditions can be achieved by electrostatic interactions as opposed to the classical covalent cross-linking of the core or the corona of micelles. Thus, the advantages of reversibility and maintained biodegradability are provided.

## Modern Therapies

This section addresses completely new therapeutic approaches that have emerged over the last two decades to combat the most serious of illnesses. Most recently, stem cell therapies entered into medical practice and while stem cells could cure a multitude of medical problems, delivering them and maintaining their viability still presents a tremendous challenge. Closely related to stem cell therapy is the cancer stem cell hypothesis, which provides completely new dimensions for the development of anti-cancer therapeutics. Progress in this field is linked to nanomedicines based on functional polymers. Another long lasting battle is the fight against HIV: The synthesis of peptide – synthetic polymer conjugates, which impede the host cell entry and the fusion of the HIV-1 virus, is addressed with a series of PEGylated fusion inhibitors. Here, the power of controlled radical polymerization techniques combined with chemo-selective coupling reactions is demonstrated. Significant progress was achieved in the field of drug delivery to solid tumors, but active targeting remains the main problem for the clinical translation of these polymeric systems. The new technique of plasmonic photothermal therapy combined with heat shock targeting is introduced and discussed in detail.

## Delivery of Biomacromecules

When considering the delivery of biologically active molecules the focus is moving from small drug molecules to macromolecules that actively interfere with cell biology, such as therapeutic proteins, DNA and RNA. The enhanced delivery of siRNA using polycationic structures in combination with the reduced toxicity of the carrier is a research focus discussed here. Poly(aspartamide)s with aminoethylene units in the side chains are designed to improve siRNA transfection based on: i) accelerated endosomal escape, and ii) stable siRNA complexation. Dendrimers are discussed for RNAi (RNA interference) delivery, a technique closely related to the process of gene silencing. Dendrimers of higher generations are of particular interest due to the high density of functional groups on their surface. Furthermore, alternatives for the PEGylation of proteins are discussed. PEG has some major drawbacks that are caused by its non-degradability even under *in vivo* conditions. Thus, technologies other than PEGylation are introduced, such as HESylation (conjugation with hydroxyethyl starch), Polysialylation, PASylation (coupling with polysialic acid) and Xten (fusion of a protein with an unstructured polypeptide) technologies. Polymer physics is utilized for biomedical applications when typical phase separation phenomena of polymers in solution are employed to control the affinity between

Downloaded by 217.118.78.91 on July 17, 2013 | http://pubs.acs.org
Publication Date (Web): July 8, 2013 | doi: 10.1021/bk-2013-1135.ch001


In Tailored Polymer Architectures for Pharmaceutical and Biomedical Applications; Scholz, C., et al.;
ACS Symposium Series; American Chemical Society: Washington, DC, 2013.

receptors and adhesion peptides. These phase transitions (UCST and LCST) can be controlled by the polymer architecture, specifically via the functional groups attached to thermo-responsive polymers.

## Tissue Engineering

Tissue engineering is an extraordinarily active and fast growing area in medical research. Researchers strive to re-grow and replace tissue and potentially entire organs that were lost to disease or trauma. Major progress has been made in the area of cell biology, but cells need a support system if they are expected to develop into functional tissue or even an organ. These scaffolds can be produced from synthetic as well as naturally occurring polymers and they provide the mechanical properties, including shape persistence and the adhesion sites for growing cells. This section presents different examples for polymeric scaffold materials. Porous hydogel spheres are described for the treatment of peripheral arterial disease; different polymer constructs are studied for their ability to promote angiogenesis. New cellulose derivates with mitogenic/angiogenic and osteogenic activity are introduced as potential scaffold materials for bone regeneration; here, the cellulose was sulfated to different degrees and the bioactivity varied strongly with the degree of sulfation as studied by interactions with various growth factors. Another natural polymer, silk, is discussed as scaffold material for applications in cartilage and also bone tissue regeneration. Silk fibroin has potentially bioactive properties such as promotion of cell adhesion and cell proliferation, and it supports metabolic activity. Technologies for the production of special scaffolds such as non-woven nets, sponges, and hydrogels are explained. A new aspect is the ability of these materials to support the osteogenic differentiation of stem cells for regenerative medicine therapy.

## Surfaces and Sensors

The interface between any synthetic or natural polymer and a living system is the most crucial area; this is the only surface that the living system "sees" and to the physical and chemical properties of which it will respond. The success of a biomedically relevant polymer, that can be a drug delivery system, implant, temporary deposit etc., depends primarily on its interaction with the living system it targets. Hence, polymer surfaces garner a lot of attention and can be designed to elicit very different responses, which range from "biological invisibility" to direct interaction, such as recognition or biocidal activity. Numerous reports focus on the functionalization of polymer surfaces in order to render them biocompatible. Yet, polymer surfaces are also the breeding ground for harmful microorganisms. Therefore, it is not only important to develop techniques that make surface biocompatible, it is equally important to develop the chemistries that render surfaces biocidal. Polymers that carry alkylammonium groups belong to a class of materials that effectively contact-kill pathogenic bacteria. Especially polyurethanes can be tailored for these purposes since the broad variety of soft and hard segments together with the tuning of hydrophilic/hydrophobic properties

Downloaded by 217.118.78.91 on July 17, 2013 | http://pubs.acs.org
Publication Date (Web): July 8, 2013 | doi: 10.1021/bk-2013-1135.ch001


In Tailored Polymer Architectures for Pharmaceutical and Biomedical Applications; Scholz, C., et al.;
ACS Symposium Series; American Chemical Society: Washington, DC, 2013.

can be utilized. Also, cationic amphiphilic copolymers containing different methacrylates are employed to fight drug-resistant bacterial infections. On the other hand, the tailoring of polymer surfaces is a very important facet in the design and generation of biosensors. The ability of sugar-decorated chips to discriminate between different viral strains and to detect viruses with an extremely high sensitivity is described here.

## Conclusion

This book demonstrates that research in the field of new polymers for pharmaceutical and biomedical applications is a very active research endeavor and it is also intimately related to the progress achieved by the medical sciences over the last years. Progress in polymer synthetic techniques such as controlled polymerizations, 'click' chemistry or enzymatic polymerizations was immediately adopted by the pharmaceutical and medical sciences. Equally, new polymer architectures such as dendrimers and hyperbranched polymers have been introduced for biomedical applications and the bioconjugation of synthetic polymers with drugs and proteins led to break-through therapies. Thus, progress in medicine was in part enabled by advances made in polymer science.

Downloaded by 217.118.78.91 on July 17, 2013 | http://pubs.acs.org
Publication Date (Web): July 8, 2013 | doi: 10.1021/bk-2013-1135.ch001

## References

1. *Polymeric Biomaterials*, 3rd ed.; Dumitriu, S., Popa, V., Eds.; CRC Press: Boca Raton, 2012.
2. Dvir, T.; Timko, B. P.; Kohane, D. S.; Langer, R. Nanotechnological strategies for engineering complex tissues. *Nat. Nanotechnol.* **2011**, *6*, 13–22.
3. Ratner, B. D. A Paradigm Shift: biomaterials that heal. *Polym. Int.* **2007**, *56*, 1183–1185.
4. Hoffman, A. S. Applications of "Smart polymers" as biomaterials. In *Biomaterials Science*, 2nd ed.; Ratner, B. D., ed.; Academic Press, Inc.: New York, 2004; pp 107−115.
5. Kopecek, J. Hydrogel biomaterials: A smart future? *Biomaterials* **2007**, *28*, 5185–5192.
6. Miyata, K.; Nishiyama, N.; Kataoka, K. Rational design of smart supramolecular assemblies for gene delivery: chemical challenges in the creation of artificial viruses. *Chem. Soc. Rev.* **2012**, *41*, 2562–2574.
7. Edinger, D.; Wagner, E. Bioresponsive polymers for the delivery of therapeutic nucleic acids. *Nanomed. Nanobiotechnol.* **2011**, *3*, 33–46.
8. Nair, L.; Laurencin, C. Biodegradable polymers as biomaterials. *Progr. Polym. Sci.* **2007**, *32*, 762–798.
9. Mikos, A.; et al. Engineering complex tissues. *Tissue Eng.* **2006**, *12*, 3307–3339.
10. Goddard, J. M.; Hotchkiss, J. H. Polymer surface modification for the attachment of bioactive compounds. *Progr. Polym. Sci.* **2007**, *32*, 698–725.
11. *Biomaterials, Principles and Applications*; Park, J. B., Bronzino, J. D., Eds.; CRC Press: Boca Raton, 2003.


In Tailored Polymer Architectures for Pharmaceutical and Biomedical Applications; Scholz, C., et al.; ACS Symposium Series; American Chemical Society: Washington, DC, 2013.

Downloaded by UNIV OF MINNESOTA on July 16, 2013 | http://pubs.acs.org
Publication Date (Web): July 8, 2013 | doi: 10.1021/bk-2013-1135.ch002

## Chapter 2

# Polyether-Based Lipids Synthesized with an Epoxide Construction Kit: Multivalent Architectures for Functional Liposomes

**Sophie S. Müller,[1,2] Carsten Dingels,[1] Anna Maria Hofmann,[1] and Holger Frey*[,1]**

**[1]Institute of Organic Chemistry, Johannes Gutenberg University Mainz, Duesbergweg 10-14, 55128 Mainz, Germany**
**[2]Graduate School MAINZ, Staudingerweg 9, 55128 Mainz, Germany**
***E-mail: hfrey@uni-mainz.de.**

Liposomes, vesicles consisting of phospholipids, are well known drug carriers, especially in anti-cancer treatment. Due to their improved pharmacokinetics, "stealth" liposomes, which are polymer coated vesicles, are being used in clinical applications with good results. One of the drawbacks of poly(ethylene glycol) (PEG) that is preferentially incorporated, is its lack of functional groups and its non-biodegradability. In this article new polyether-based lipids are presented that can be synthesized from an epoxide monomer library, resulting in tailored multivalent architectures. The cholesterol-based lipid-like structures offer further possibilities for functionalization, which is important for active targeting. Furthermore, a rather simple synthetic route has been developed, which leads to acid-cleavable cholesteryl PEG, thus leading to possible controlled destabilization of the liposome formulation. This process is crucial for drug release *in vivo*.

## Introduction

The formation of liposomes by self-assembly of phospholipids in water was discovered almost 40 years ago. Liposomes are colloidal vesicles consisting of a lipid bilayer with an aqueous medium interior (*1*). Fundamental research on the preparation, stability, release profile, encapsulation efficiency and targeting

© 2013 American Chemical Society
In Tailored Polymer Architectures for Pharmaceutical and Biomedical Applications; Scholz, C., et al.; ACS Symposium Series; American Chemical Society: Washington, DC, 2013.

of liposomes has led to clinical application. Especially for cancer therapies, the use of extremely toxic and aggressive drugs shows serious side effects. Effective delivery-systems, like liposomes, enabled an important step towards minimizing these undesired properties on healthy tissue. Advantages of these systems include a high local concentration of the anticancer drug, while protecting the body from a cytostatic drug before its release at the target site. A well known example is doxorubicin, an anthracycline, which has severe cardiotoxic effects in humans when applied directly. However, when encapsulated in lipid formulations it shows considerably increased circulation time compared to the free drug, and more importantly, lower concentration of the free drug and consequently lower cardiotoxicity. The respective product, known as Doxil™, was one of the first liposome formulations approved in the US.

Conventional liposomes (see Figure 1) as lipoidal carriers have been extensively studied as drug-delivery systems, motivated by the combination of reduced side effects on healthy tissue and passive targeting (*1*, *2*). However, the main disadvantages of such systems are the rapid removal from the blood by macrophages (mononuclear phagocyte system, MPS) after opsonin binding and uptake into the liver and spleen (*3*). Additionally, their physical and chemical instability results in uncontrollable properties *in vivo* (*4*, *5*). To overcome these drawbacks, so-called "stealth liposomes" with surfaces modified by mainly poly(ethylene glycol) (PEG), but also polysaccharides, were developed. The presence of PEG for example effects prolonged blood circulation time (*6*, *7*), reduced MPS uptake (*8*), reduced aggregation of PEGylated carriers and better (storage) stability of liposomal carriers (*9*).

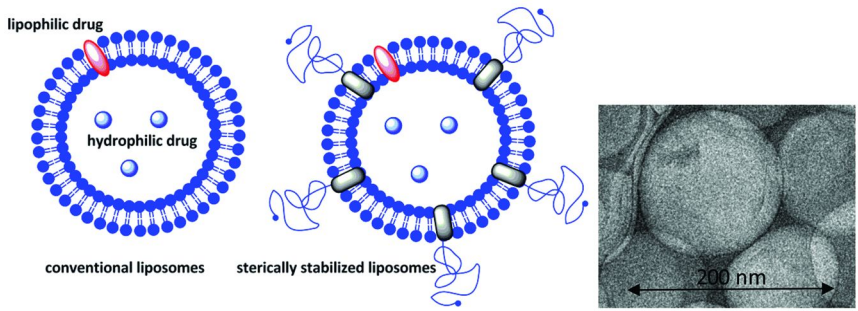


*Figure 1. left: Schematic picture of conventional liposomes and sterically stabilized liposomes, right: TEM image of liposomes containing a lipid and cholesterol-PEG.*

The present chapter will give a short overview of the recent development in multifunctional "stealth" liposome preparations. This interdisciplinary area between synthetic polymer chemistry, advances in their characterization combined with new liposome preparation techniques leads to interesting new aspects in the area of "stealth" liposomes. Next to a short overview of polymeric amphiphiles currently used in "stealth" liposome preparations, the main focus will be on


In Tailored Polymer Architectures for Pharmaceutical and Biomedical Applications; Scholz, C., et al.; ACS Symposium Series; American Chemical Society: Washington, DC, 2013.

Downloaded by UNIV OF MINNESOTA on July 16, 2013 | http://pubs.acs.org
Publication Date (Web): July 8, 2013 | doi: 10.1021/bk-2013-1135.ch002

polyethers such as poly(ethylene glycol) (PEG) and alternative branched and hyperbranched structures recently developed in our group. Additionally, we will give a short summary of acid-cleavable polymers in the application of degradable liposomes.

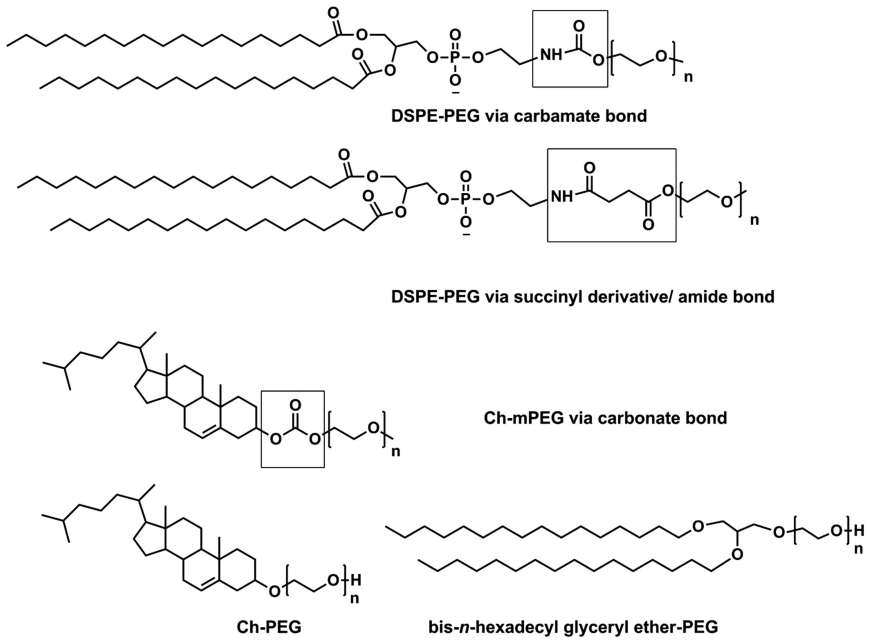


*Figure 2. A selection of lipid-polymer conjugates for the incorporation into vesicle membranes to generate long-circulating "stealth" liposomes (DSPE= 1,2-Distearoyl-sn-glycero-3-phosphoethanolamine; Ch=cholesterol; PEG= poly(ethylene glycol); mPEG=methoxy poly(ethylene glycol)).*

## Liposome Stabilization: A Polymer Shell Is Necessary

*In vivo* studies of conventional liposomes have shown that they are rapidly opsonized by serum proteins, and therefore taken up by cells of the mononuclear phagocyte system (MPS), such as Kupffer-cells or macrophages from the liver. This process is a key to control drug delivery, since the particles are not capable of performing their desired therapeutic task (*10*). Although the exact mechanism is not clearly understood yet, it is known that the type and number of proteins that attach to the vesicle's surface can vary dramatically. Factors that influence the opsonization process include liposome size, composition and charges. Harashima et al. demonstrated a correlation between decreasing liposome size and decreasing opsonization. Furthermore, phagocytic cells remove liposomes in proportion to the amount of opsonization (*11*). Negatively charged liposomes increase intracellular uptake into phagocytic cells and therefore accelerate their own clearance after administration (*12*, *13*). Since the binding of proteins


In Tailored Polymer Architectures for Pharmaceutical and Biomedical Applications; Scholz, C., et al.; ACS Symposium Series; American Chemical Society: Washington, DC, 2013.

Downloaded by UNIV OF MINNESOTA on July 16, 2013 | http://pubs.acs.org
Publication Date (Web): July 8, 2013 | doi: 10.1021/bk-2013-1135.ch002

depends on a variety of physicochemical characteristics, the initial approaches to increase circulation time relied on changing these parameters. The simplest way to achieve this goal is to reduce the liposome size by sonication, extrusion or microfluidization (*1*). A rather recent method for the preparation of small liposomes was presented by Massing et al. They used a so-called dual asymmetric centrifuge (DAC) to produce a viscous vesicular phophoplipid gel (VPG), which can be diluted to a conventional liposome dispersion. The procedure is based on shear forces for efficient homogenization due to two rotating movements in this special centrifuge (*14*). The authors also showed high entrapping efficiencies of siRNA under sterile conditions (*15*).

Another route to improve circulation time is to graft a polymer shell onto the surface of the particles (see Figure 1). The attachment of e.g., poly(ethylene glycol) (PEG), can lead to a protective, hydrophilic polymer layer, which prevents opsonin adsorption via steric repulsion. Hence, opsonization is reduced, and the probability for the uptake by the MPS system is decreased. Research groups who studied the half-life times *in vivo* could show extended retention periods from 5 h up to 5 days (*16–19*). Furthermore, it was proven that PEGylated liposomes showed improved biodistribution, which resulted in low amounts of "stealth" liposomes (10-15%) being taken up by the liver (*20*).

Covalent attachment to lipids is clearly more stable than mere physical adsorption. Hence, "stealth" liposomes are prepared by polymer-modified lipids, which can be phospholipids or cholesterol, both natural membrane components. These polymer conjugates function as an anchor in the vesicle membrane. Selected biocompatible amphiphilic compounds used for this purpose are shown in Figure 2.

Several lipid-polymer conjugates consist of phospholipids, i.e. phosphatidyl ethanolamine (PE), which is coupled to methoxy poly(ethylene glycol) (mPEG) via carbamate or amide bond formation. Furthermore, cholesterol can be used as the hydrophobic anchor. Monomethoxy poly(ethylene glycol) can be coupled to cholesteryl chloroformate by a carbonate bond (*21*). Our group also demonstrated an alternative method, which relies on aliphatic initiators, such as cholesterol or bis-*n*-hexadecyl glyceryl ether, for the ring-opening polymerization of ethylene oxide (EO). These syntheses are advantageous, since they do not require multiple reaction steps, coupling chemistry or laborious purifications steps. Furthermore, the synthesized lipids contain a hydroxyl end group, which can be used for further functionalization (*22*, *23*).

## Clinical Applications

Extensive studies on the biodistribution of liposomal formulations and improved pharmacokinetic behavior of "stealth" liposomes have been done in numerous clinical tests. The best known and commercially available liposomal anti-cancer treatment, doxorubicin, is sold under the name Doxil™. The following table (Table 1) shows a selection of conventional and PEGylated liposomes for clinical usage.


In Tailored Polymer Architectures for Pharmaceutical and Biomedical Applications; Scholz, C., et al.;
ACS Symposium Series; American Chemical Society: Washington, DC, 2013.

Downloaded by UNIV OF MINNESOTA on July 16, 2013 | http://pubs.acs.org
Publication Date (Web): July 8, 2013 | doi: 10.1021/bk-2013-1135.ch002

Downloaded by UNIV OF MINNESOTA on July 16, 2013 | http://pubs.acs.org
Publication Date (Web): July 8, 2013 | doi: 10.1021/bk-2013-1135.ch002



**Table 1. Conventional and PEGylated liposomes in clinical usage (*9*, *21*, *24*)**

| | *Drug* | *Company* | *Product name* | *Indication* |
|---|---|---|---|---|
| **Conventional Liposomes** | Doxorubicin | Elan | Myocet/ Evacet | Breast cancer |
| | Amphoterecin B | Astellas Pharma | Ambisome | Fungal infection |
| | Daunomycin | Gilead | DaunoXome | Kaposi's sarcoma |
| | Vincristine | Hana Biosciences | Marqibo | Non-Hodgkin's lymphoma |
| **PEGylated Liposomes** | Doxorubicin | Schering Plough | Doxil/ Caelyx | Kaposi's sarcoma, ovarian cancer |
| | Cisplatin | Regulon | Lipoplatin | Various cancer types |
| | Mitoxantone | Wyeth Lederle | Novantrone | Multiple sclerosis, prostate cancer, acute myeloid leukemia |

In Tailored Polymer Architectures for Pharmaceutical and Biomedical Applications; Scholz, C., et al.;
ACS Symposium Series; American Chemical Society: Washington, DC, 2013.

## Liposome Stabilization: Alternatives to PEG

PEG attached to lipids in pharmaceutical formulations has been investigated intensely, and these system have shown the best performance in clinical studies to date. Nevertheless, alternatives are being studied, since there is the hope for improved performance in targeting, physicochemical properties, and biocompatibility. In a recent review by Schubert et al. the disadvantages of PEG, such as its non-biodegradability, the possible degradation under stress and potential toxic side-product, were highlighted. Furthermore, the authors mention the hypersensitivity found in some cases, indicated by an activation of the complement system by PEGylated liposomes. More studies on the mechanism and the influence of other factors are necessary. Additionally, it has to be elucidated, whether other factors or the combinations of several components lead to side effects (*25*).

General requirements for an alternative to PEG are high water-solubility, i.e., hydrophilicity of the polymer, high biocompatibility, and flexibility of the respective chain (*9*). Among non-biodegradable polymers poly(vinyl pyrrolidone) (PVP, commercially available) and poly(acryl amide) (PAA) have shown prolonged blood circulation times *in vivo* of coated liposomes (*26*). Poly(2-oxazoline)s are studied intensely at present, since for this type of polymer similar behavior compared to PEG has been proven (*27*). Figure 3 shows a selection of molecular structures of polymers currently considered for "stealth" liposome preparation.

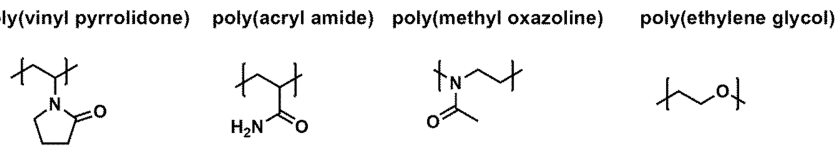


*Figure 3. Molecular structures of polymers for "stealth" liposome preparation including poly(vinyl pyrrolidone), poly(acryl amide), poly(methyl oxazoline), and poly(ethylene glycol).*

In general polyethers are interesting polymers in biomedical application. Not only linear poly(ethylene glycol), but also hyperbranched structures are promising with regard to their shielding behavior in drug delivery or liposome formulations. In fact, such systems have been used as hydrophilic shells, micelles or hydrogels (*28*). Interestingly, surfaces covered with hyperbranched polyglycerol (*hb*PG) having a molecular weight around 1500-5000 g/mol showed slightly better protein repulsion than linear PEG. Presumably, the branched structure makes the polymer even more bulky, and more hydrophilic due to the high amount of hydroxyl groups, leading to a brush-like structure (*29*, *30*).


In Tailored Polymer Architectures for Pharmaceutical and Biomedical Applications; Scholz, C., et al.; ACS Symposium Series; American Chemical Society: Washington, DC, 2013.

Downloaded by UNIV OF MINNESOTA on July 16, 2013 | http://pubs.acs.org
Publication Date (Web): July 8, 2013 | doi: 10.1021/bk-2013-1135.ch002

To date, there have been very few publications on "stealth" liposomes functionalized with polyglycerols. Maruyama et al. published the synthesis and investigation of dipalmitoylphosphatidyl polyglycerols (DPP-PG), which consisted of oligomeric linear polyglycerol (*l*PG) attached to the phospholipid via phospholipase D (*31*). Effective shielding for diglycerol or tetraglycerol was observed upon using 8 mol% incorporation of the polymer-conjugate, while octaglycerol only required 4 mol% for good performance with respect to circulation times. The best result was found for DPP-hexaglycerol, which prolonged the blood circulation time, when 6 mol% were incorporated. Interestingly, such PG oligomers displayed improved performance in relation to linear PEG. Usually, PEG chains with molecular weights between 1000-5000 g/mol are used for liposomal formulations, and around 5-8 mol% is necessary to generate a considerable "stealth" effect.

Downloaded by UNIV OF MINNESOTA on July 16, 2013 | http://pubs.acs.org
Publication Date (Web): July 8, 2013 | doi: 10.1021/bk-2013-1135.ch002

## Polyether-Based Lipids: Multivalent Architectures

Poly(ethylene glycol) (PEG) is the most widely studied polymer for the preparation of "stealth" liposomes, which is due to its outstanding properties as a shielding layer around the vesicular carriers. Its good biocompatibility, very low toxicity as well as immunogenicity, low cost and facile coupling chemistry to hydrophobic molecules render it attractive for biomedical applications. Furthermore, its flexibility and water solubility are crucial for *in vivo* applications (*32*). However, as mentioned above, similar polyethers with different architectures exhibit the same or even better performance compared to PEG. In the following section we will highlight the recent work on polyether-based amphiphiles synthesized and characterized in our group.

Phospholipids are sensitive molecules that are not stable under the very basic conditions required for the polymerization of epoxides. In general, this polymerization is an anionic ring-opening polymerization (ROP) of ethylene oxide (EO). Since the labile phospholipids are excluded under these conditions, we looked for other biocompatible options, which led us to bisalkyl glyceryl ethers and cholesterol as suitable initiators for the polymerization. These two aliphatic molecules withstand the basic ring-opening conditions as well as acidic conditions used for the deprotection of other epoxide derivatives (see Figure 4). Using a combination of ethylene oxide (EO), ethoxyethyl glycidyl ether (EEGE), isopropylidene glycidyl glyceryl ether (IGG), and glycidol as an epoxide-based construction kit, a vast variety of linear and branched architectures becomes available. Among them are complex structures, such as linear-hyperbranched amphiphiles, which combine the advantageous properties of PEG and the polyfunctionality of polyglycerol (*22*, *33*). This aspect is one of the most important improvements compared to conventional "stealth" liposomes: the additional hydroxyl groups increase water-solubility and provide the possibility for further functionalization, such as the attachment of markers (labeling), antibodies or targeting groups. Maximum biocompatibility is achieved by using cholesterol as the initiator and *hb*PG as a polymer with excellent biocompatibility (*28*, *34–36*).


In Tailored Polymer Architectures for Pharmaceutical and Biomedical Applications; Scholz, C., et al.;
ACS Symposium Series; American Chemical Society: Washington, DC, 2013.

## Synthesis of Multivalent Architectures

The synthesis of multivalent lipids is described with cholesterol as an initiator, since the resulting polymer is expected to show very good biocompatibility. Cholesterol is a natural membrane component and also commercially available. In the lipid structures prepared, cholesterol can function as the membrane anchor.

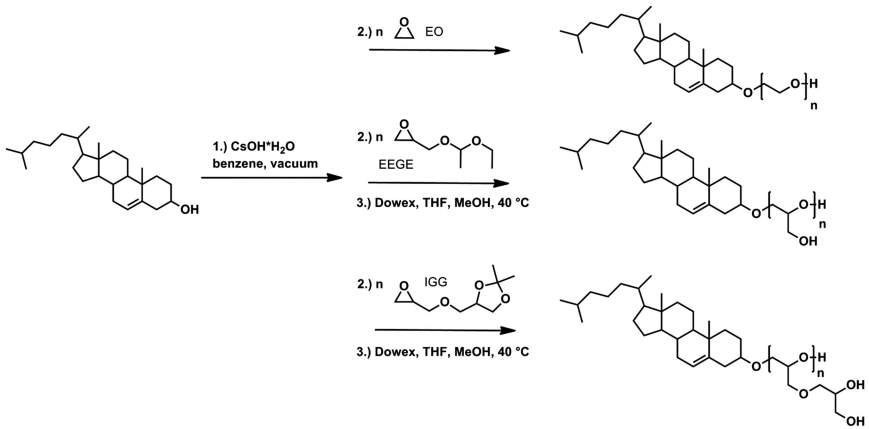


*Figure 4. Reaction sequence for the synthesis of cholesterol initiated polyethers: Ch-PEG, Ch-lPG, Ch-lPGG.*

The first step is the formation of the cholesterol alkoxides, which represent the initiator for the subsequent polymerization. The degree of deprotonation employed is 90% in the case of CsOH as the deprotonating agents. Due to the rapid proton exchange between cholesterol and the growing chain, almost 100% of the initiator molecules are incorporated into the resulting polyether amphiphile. To form the linear polymer, ethylene oxide can be polymerized using the standard oxyanionic ring-opening polymerization technique (*37*). In order to obtain linear polyglycerol protected epoxide derivatives such as ethoxyethyl glycidyl ether (EEGE) or isopropylidene glycidyl glyceryl ether (IGG) can be used. Deprotection of the acetal groups leads to one (EEGE) or two (IGG) hydroxyl groups per monomer unit. Using this protocol, multifunctional, linear polyglycerol can be synthesized in a one-pot approach (Figure 4).

Using a two-step procedure, it is possible to tailor hyperbranched structures based on linear macroinitiators. Glycidol is polymerized by the ring-opening multibranching technique in a slow monomer addition step (Figure 5). The multihydroxy-precursor polymer is crucial for the "hypergrafting" of glycidol since excellent conditions and low polydispersities are required. Usually the degree of deprotonation is around 25%, which allows good control over the anion concentration and prevents homopolymerization of glycidol. For the slow monomer addition step a syringe pump is used, which adds the monomer in low concentration over a certain amount of time (around 18-24 h, depending on the batch size).


In Tailored Polymer Architectures for Pharmaceutical and Biomedical Applications; Scholz, C., et al.;
ACS Symposium Series; American Chemical Society: Washington, DC, 2013.

Downloaded by UNIV OF MINNESOTA on July 16, 2013 | http://pubs.acs.org
Publication Date (Web): July 8, 2013 | doi: 10.1021/bk-2013-1135.ch002

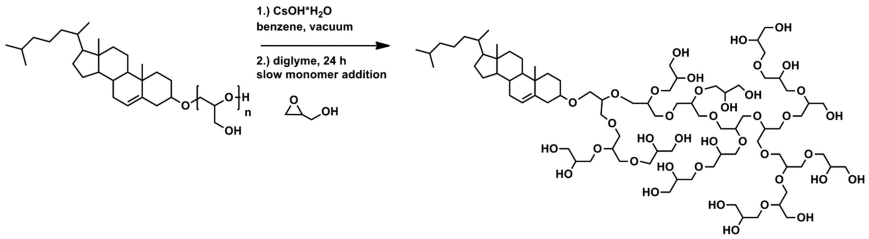


*Figure 5. Reaction sequence for the synthesis of cholesterol initiated hyperbranched structures (Ch-hbPG).*

Downloaded by UNIV OF MINNESOTA on July 16, 2013 | http://pubs.acs.org
Publication Date (Web): July 8, 2013 | doi: 10.1021/bk-2013-1135.ch002

Following the above mentioned reaction sequence, one can combine any epoxide derivative in the way of a molecular construction kit, permitting rapid access to polyfunctional lipids via ROP (see Figure 6). Random copolymerization allows for the synthesis of Ch-PEG-co-PGG or Ch-PEG-co-*l*PG using EO and IGG or EEGE, respectively. Additionally, linear hyperbranched structures are available via the ROP of ethylene oxide followed by EEGE or IGG, the deprotection step and subsequent slow monomer addition of glycidol onto the macroinitiator polymer. The resulting architectures show low to moderate polydispersities (PDI= 1.1-1.6) and can be characterized by size exclusion chromatography (SEC), NMR spectroscopy or matrix assisted laser desorption time-of-flight mass spectrometry (MALDI ToF MS). Furthermore the critical micelle concentration was determined to be in the range of 1.4-40.7 mg/L, depending on the molecular structure (*33*).

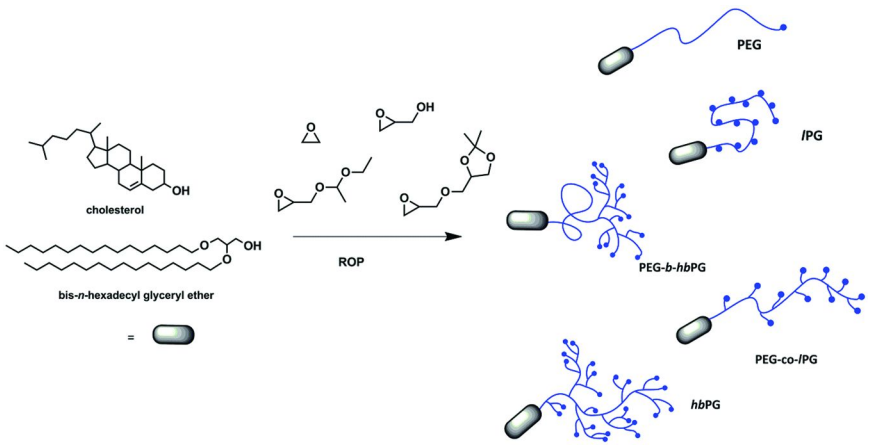


*Figure 6. Possible lipid architectures available by using EO, EEGE, IGG, and glycidol for the ring-opening polymerization initiated by either cholesterol or bis-n-hexadecyl glyceryl ether.*


In Tailored Polymer Architectures for Pharmaceutical and Biomedical Applications; Scholz, C., et al.;
ACS Symposium Series; American Chemical Society: Washington, DC, 2013.

In a recent work by Kressler et al. the linear poly(ethylene glycol)$_{30}$-*b*-*hb*PG$_{24}$ copolymer was investigated in mixed layers with 1,2-dipalmitoyl-*sn*-glycero-3-phosphocholine (DPPC). In adsorption measurements it was demonstrated that an intense affinity of the amphiphilic block copolymer to DPPC is given after the injection of the polymer into the water subphase. The surface pressure was determined to be 48.2 mN/m, showing the fast penetration of the hydrophobic cholesterol into the lipid monolayer, as well as good interaction with DPPC. Figure 7 shows the DPPC monolayer at the air-water interface with the amphiphilic polymer, which is attached to the lipid layer via its cholesterol moiety (*38*).

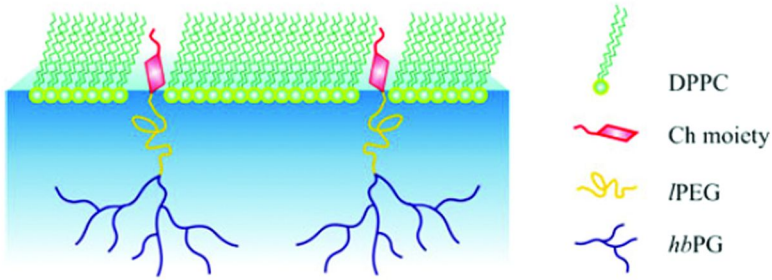


*Figure 7. DPPC monolayer and adsorbed cholesterol moiety of Ch-PEG-hbPG to the air-water interface. (Reproduced with permission from reference (38). Copyright 2012 Springer Verlag.)*

Downloaded by UNIV OF MINNESOTA on July 16, 2013 | http://pubs.acs.org
Publication Date (Web): July 8, 2013 | doi: 10.1021/bk-2013-1135.ch002

Several multifunctional polymers have been synthesized, showing generally good adsorption behavior at DPPC monolayers. In future work, the properties in liposomal formulations *in vivo* will be studied. These novel coatings combine the advantages of PEG as well as PG and might increase liposome stability. Furthermore, it is important to target the vesicles, which can be easily accomplished by the functionalization of peripheral hydroxyl groups. Model reactions, such as the attachment of the dye rhodamine B by click chemistry demonstrated the utility of the branched structure (*33*). The performance in blood serum is currently under investigation, and further experiments *in vivo* will be carried out in the near future.

## Liposome Destabilization: pH-Sensitive Lipids with an Acid-Labile Moiety

Acid-sensitive PEG amphiphiles, such as lipids, have attracted considerable attention in biomedical applications, since controlled destabilization of liposomes is necessary for the release of the drug incorporated in the vesicular transporter.

Those "stealth" systems are usually stable at neutral pH, which translates to stability during the circulation in the body, whereas destabilization is needed for the fusion with membranes or the escape from endosomal vesicles (*39*). The fusion and the release of the drug in slightly acidic tissue, such as tumor tissue or inflammatory tissues, can be realized with pH-sensitive PEG coated liposomes, where the protecting shell can be shed at a pH around 6.5 for tumor tissues. One major advantage is that no external stimulus is required for triggering the drug release.

In this section we would like to focus on acid-sensitive PEG lipid analogs that have been used for liposome preparation. Furthermore, we present very recent work that has been carried out in our group, which is based on an acid-labile cholesterol derivative as the initiator for the ring-opening polymerization of ethylene glycol.

Downloaded by UNIV OF MINNESOTA on July 16, 2013 | http://pubs.acs.org
Publication Date (Web): July 8, 2013 | doi: 10.1021/bk-2013-1135.ch002

Different approaches have been developed to tune the pH-sensitivity of the polymer shell around nanoparticles or liposomes. Recently, Clawson et al. have published the synthesis and characterization of lipid-polymer hybrid nanoparticles with a PEG shell that sheds under acidic conditions. They used a lipid-(succinate)-mPEG as the amphiphilic polymer, which was synthesized via the coupling of 1,2-dipalmitoyl-*sn*-glycer-3-phospho(ethylene glycol) and methoxy poly(ethylene glycol), endfunctionalized with succinate prior to the coupling step (*40*).

In 2003 an acid-labile poly(ethylene glycol) PEG-conjugated lipid, (*R*)-1,2-di-*O*-(1'*Z*,9'*Z*-octadecadienyl)-glyceryl-3-(ω-methoxy-poly(ethylene glycolate, MW5000) (BVEP), was synthesized and mixed with 1,2-dioleoyl-*sn*-glycero-3-phosphoethanolamine (DOPE) in liposomes to investigate destabilization and membrane-membrane fusion after acid-catalyzed hydrolysis of the vinyl ether linkages. The research group showed that PEG removal occurred after hydrolysis, but that it resulted in undesired payload leakage and liposome collapse as well (*41*).

Using cholesterol as the lipophilic part, Boomer et al. presented a six-step synthesis for the preparation of cholesterol-vinyl ether-PEG conjugates (CVEP), which degraded under mildly lowered pH values. Cleavage resulted in PEG removal, leading to content release and thus an increased bioavailability of a potent drug (*42*).

In our group a cholesterol derivative was used directly as the initiator for the ring-opening polymerization of ethylene oxide (EO) (*43*). The addition of the steroid (**1**) to 2-acetoxyethyl vinyl ether (AcVE, **2**) was carried out in dichloromethane, catalyzed by *p*-toluene sulfonic acid, leading to acetoxyethyl 1-(cholesteryloxy)ethyl ether (**3**). The advantages of AcVE are the following: The acetate group can be used as a protection group and is removed under basic conditions with little effort, leading to glycol 1-(cholesteryloxy)ethyl ether (**4**). Hence, the hydroxyl group, which is important for the oxyanionic polymerization, is liberated easily. This group is used as an alkoxide after deprotonation and is structurally related to the growing chain end, which results in good initiation kinetics. Hence, it was possible to synthesize a scissile initiator for the polymerization of EO in three steps (Figure 8). The polymer (**5**) was characterized by NMR spectroscopy, SEC, and MALDI-ToF MS.

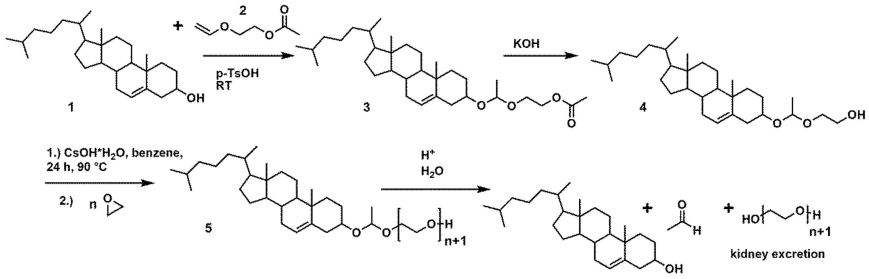


*Figure 8. Synthesis of the pH-sensitive cholesterol derivative for the initiation of ethylene oxide.*

Downloaded by UNIV OF MINNESOTA on July 16, 2013 | http://pubs.acs.org
Publication Date (Web): July 8, 2013 | doi: 10.1021/bk-2013-1135.ch002

The insertion of such a scissile hydrophobic unit leads to responsive materials that are cleaved under acidic condition leading to a loss of their amphiphilicity. This is a desired feature, when it comes to destabilizing the "stealth" liposomes.

Acid-sensitivity was demonstrated as a proof of principle in a UV-Vis spectrometer. An aqueous solution of the scissile lipid analog was acidified by adding hydrochloric acid. After a while the solutions turned turbid, as the released cholesterol precipitated and the transmission began to decrease. Almost all light was scattered in the end, due to cholesterol precipitation. As expected, cholesterol was released faster at higher reaction temperature (T=25 °C vs. T=37 °C), as indicated by the shorter initial phase and more negative slope of the trace. To confirm complete removal of the steroid, a similar experiment was performed with the scissile cholesteryl PEG, in which the precipitated cholesterol and the aqueous solution were separated and $^1$H spectra were recorded. A clean cholesterol spectrum was obtained, whereas the aqueous phase exhibited pure PEG diol. Hence, the cholesteryl initiator was released completely under these reaction conditions.

This system represents a novel approach towards cleavable amphiphiles, which are promising for "stealth" liposome preparation. One acid-sensitive moiety can be cleaved resulting in biocompatible cholesterol and PEG, respectively. The molecular weight of the PEG polymer chain is typically around 2000-5000 g/mol, so the polymer is small enough to be excreted by the kidney and be eliminated from the body.

We believe this approach to be promising in shedding the protecting layer, and thus destabilizing liposomes at the site of action, where lower pH-values are present. Further studies are planned to synthesize acid-cleavable, hyperbranched lipids for multifunctional liposomes.

## Conclusion

Many approaches have been made in the development of effective drug delivery systems, especially in the field of liposomes. The vesicles used as a transporter for hydrophilic or hydrophobic drugs suffered from several disadvantages such as low stability and low circulation times *in vivo*. One of the biggest steps towards long-circulating liposomes was the incorporation of


In Tailored Polymer Architectures for Pharmaceutical and Biomedical Applications; Scholz, C., et al.;
ACS Symposium Series; American Chemical Society: Washington, DC, 2013.

a biocompatible, water-soluble polymer, such as poly(ethylene glycol) (PEG). The improved performance of the liposomal formulation resulted from the stabilizing polymer shell around the vesicle, which protects the drug carrier and additionally prevents opsonin adsorption. These unique properties lead to reduced blood clearance and hence prolonged blood circulation times. Additionally, the enhanced accumulation and retention effect (EPR) helps to increase drug concentration at the site of action. It is no surprise that liposomal formulations, with or without a polymer shell, are used in clinical applications, especially in cancer treatment, due to their outstanding pharmacokinetics.

PEG coated liposomes, so-called "stealth liposomes" are applied in various treatments such as Kaposi's sarcoma, breast cancer or fungal infections. Nevertheless, new synthetic polymers offer various advantages that may further enhance the applicability of "stealth" liposomes. Among these are biodegradability and multifunctionality, which is important for the attachment of markers and targeting moieties. In this context we presented new polymeric amphiphiles based on poly(ethylene glycol) and polyglycerol (linear and hyperbranched) that represent a new class of multifunctional lipid analogs with various architectures. The multiple hydroxyl groups increase aqueous solubility of the polymer and offer the possibility for effective targeting through further functionalization. In addition, the degradability of acid-sensitive Ch-PEG polymers was discussed, in contrast to chemically inert PEG, resulting in possible destabilization of the "stealth" liposome in the acidic tumor tissue or acidic endosomes. The desired destabilization is still one of the key tasks that remain problematic in liposome research. Regarding the advantages of the hyperbranched lipids, we believe that this class of lipids is promising with respect to drug delivery and "stealth" components. Investigations on the stealth effect *in vivo,* as well as monolayer studies, are currently in progress.

Downloaded by UNIV OF MINNESOTA on July 16, 2013 | http://pubs.acs.org
Publication Date (Web): July 8, 2013 | doi: 10.1021/bk-2013-1135.ch002

## References

1. Sharma, A.; Sharma, U. S. *Int. J. Pharm.* **1997**, *154* (2), 123–140.
2. Lian, T.; Ho, R. J. Y. *J. Pharm. Sci.* **2001**, *90* (6), 667–680.
3. Lasic, D.; Papahadjopoulos, D. *Science* **1995**, *267* (5202), 1275–1276.
4. Allen, T. M.; Chonn, A. *FEBS Lett.* **1987**, *223* (1), 42–46.
5. Woodle, M. C.; Lasic, D. D. *Biochim. Biophys. Acta* **1992**, *1113* (2), 171–199.
6. Woodle, M. C.; Matthay, K. K.; Newman, M. S.; Hidayat, J. E.; Collins, L. R.; Redemann, C.; Martin, F. J.; Papahadjopoulos, D. *Biochim. Biophys. Acta* **1992**, *1105* (2), 193–200.
7. Torchilin, V. P.; Omelyanenko, V. G.; Papisov, M. I.; Bogdanov, A. A.; Trubetskoy, V. S.; Herron, J. N.; Gentry, C. A. *Biochim. Biophys. Acta, Biomembr.* **1994**, *1195* (1), 11–20.
8. Blume, G.; Cevc, G. *Biochim. Biophys. Acta, Biomembr.* **1990**, *1029* (1), 91–97.
9. Immordino, M. L.; Dosio, F.; Cattel, L. *Int. J. Nanomed.* **2006**, *1* (3), 297–315.


In Tailored Polymer Architectures for Pharmaceutical and Biomedical Applications; Scholz, C., et al.;
ACS Symposium Series; American Chemical Society: Washington, DC, 2013.

10. Owens, D. E.; Peppas, N. A. *Int. J. Pharm.* **2006**, *307* (1), 93–102.
11. Harashima, H.; Sakata, K.; Funato, K.; Kiwada, H. *Pharm. Res.* **1994**, *11* (3), 402–406.
12. Lee, K. D.; Hong, K.; Papahadjopoulos, D. *Biochim. Biophys. Acta* **1992**, *1103* (2), 185–197.
13. Gabizon, A.; Papahadjopoulos, D. *Biochim. Biophys. Acta* **1992**, *1103* (1), 94–100.
14. Massing, U.; Cicko, S.; Ziroli, V. *J. Controlled Release* **2008**, *125* (1), 16–24.
15. Hirsch, M.; Ziroli, V.; Helm, M.; Massing, U. *J. Controlled Release* **2009**, *135* (1), 80–88.
16. Klibanov, A. L.; Maruyama, K.; Torchilin, V. P.; Huang, L. *FEBS Lett.* **1990**, *268* (1), 235–237.
17. Senior, J.; Delgado, C.; Fisher, D.; Tilcock, C.; Gregoriadis, G. *Biochim. Biophys. Acta, Biomembr.* **1991**, *1062* (1), 77–82.
18. Papahadjopoulos, D.; Allen, T. M.; Gabizon, A.; Mayhew, E.; Matthay, K.; Huang, S. K.; Lee, K. D.; Woodle, M. C.; Lasic, D. D.; Redemann, C.; Martin, F. J. *Proc. Natl. Acad. Sci. U.S.A.* **1991**, *88* (24), 11460–11464.
19. Stathopoulos, G. P.; Boulikas, T.; Vougiouka, M.; Deliconstantinos, G.; Rigatos, S.; Darli, E.; Viliotou, V.; Stathopoulos, J. G. *Oncol. Rep.* **2005**, *13* (4), 589–595.
20. Allen, T. M.; Hansen, C.; Martin, F.; Redemann, C.; Yau-Young, A. *Biochim. Biophys. Acta, Biomembr.* **1991**, *1066* (1), 29–36.
21. Zhao, X. B.; Muthusamy, N.; Byrd, J. C.; Lee, R. J. *J. Pharm. Sci.* **2007**, *96* (9), 2424–2435.
22. Hofmann, A. M.; Wurm, F.; Hühn, E.; Nawroth, T.; Langguth, P.; Frey, H. *Biomacromolecules* **2010**, *11* (3), 568–574.
23. Reuter, S.; Hofmann, A. M.; Busse, K.; Frey, H.; Kressler, J. *Langmuir* **2010**, *27* (5), 1978–1989.
24. Torchilin, V. P. *Nat. Rev. Drug Discovery* **2005**, *4* (2), 145–160.
25. Knop, K.; Hoogenboom, R.; Fischer, D.; Schubert, U. S. *Angew. Chem., Int. Ed.* **2010**, *49* (36), 6288–6308.
26. Torchilin, V. P.; Shtilman, M. I.; Trubetskoy, V. S.; Whiteman, K.; Milstein, A. M. *Biochim. Biophys. Acta, Biomembr.* **1994**, *1195* (1), 181–184.
27. Zalipsky, S.; Hansen, C. B.; Oaks, J. M.; Allen, T. M. *J. Pharm. Sci.* **1996**, *85* (2), 133–137.
28. Calderon, M.; Quadir, M. A.; Sharma, S. K.; Haag, R. *Adv. Mater.* **2010**, *22* (2), 190–218.
29. Siegers, C.; Biesalski, M.; Haag, R. *Chem.—Eur. J.* **2004**, *10* (11), 2831–2838.
30. Kainthan, R. K.; Zou, Y.; Chiao, M.; Kizhakkedathu, J. N. *Langmuir* **2008**, *24* (9), 4907–4916.
31. Maruyama, K.; Okuizumi, S.; Ishida, O.; Yamauchi, H.; Kikuchi, H.; Iwatsuru, M. *Int. J. Pharm.* **1994**, *111* (1), 103–107.
32. Roberts, M. J.; Bentley, M. D.; Harris, J. M. *Adv. Drug Delivery Rev.* **2002**, *54* (4), 459–476.

Downloaded by UNIV OF MINNESOTA on July 16, 2013 | http://pubs.acs.org
Publication Date (Web): July 8, 2013 | doi: 10.1021/bk-2013-1135.ch002

33. Hofmann, A. M.; Wurm, F.; Frey, H. *Macromolecules* **2011**, *44* (12), 4648–4657.
34. Wilms, D.; Wurm, F.; Nieberle, J.; Boehm, P.; Kemmer-Jonas, U.; Frey, H. *Macromolecules* **2009**, *42* (9), 3230–3236.
35. Wilms, D.; Stiriba, S.-E.; Frey, H. *Acc. Chem. Res.* **2010**, *43* (1), 129–141.
36. Kainthan, R. K.; Gnanamani, M.; Ganguli, M.; Ghosh, T.; Brooks, D. E.; Maiti, S.; Kizhakkedathu, J. N. *Biomaterials* **2006**, *27* (31), 5377–5390.
37. Mangold, C.; Wurm, F.; Frey, H. *Polym. Chem.* **2012**, *3* (7), 1714–1721.
38. Peng, X.; Hofmann, A.; Reuter, S.; Frey, H.; Kressler, J. *Colloid. Polym. Sci.* **2012**, *290* (7), 579–588.
39. Hong, R. L.; Huang, C. J.; Tseng, Y. L.; Pang, V. F.; Chen, S. T.; Liu, J. J.; Chang, F. H. *Clin. Cancer Res.* **1999**, *5* (11), 3645–3652.
40. Clawson, C.; Ton, L.; Aryal, S.; Fu, V.; Esener, S.; Zhang, L. *Langmuir* **2011**, *27* (17), 10556–10561.
41. Boomer, J. A.; Inerowicz, H. D.; Zhang, Z. Y.; Bergstrand, N.; Edwards, K.; Kim, J. M.; Thompson, D. H. *Langmuir* **2003**, *19* (16), 6408–6415.
42. Boomer, J. A.; Qualls, M. M.; Inerowicz, H. D.; Haynes, R. H.; Patri, V. S.; Kim, J.-M.; Thompson, D. H. *Bioconjugate Chem.* **2009**, *20* (1), 47–59.
43. Dingels, C.; Müller, S. S.; Steinbach, T.; Tonhauser, C.; Frey, H. *Biomacromolecules* **2013** DOI:10.1021/bm3016797.

Downloaded by UNIV OF MINNESOTA on July 16, 2013 | http://pubs.acs.org
Publication Date (Web): July 8, 2013 | doi: 10.1021/bk-2013-1135.ch002

Downloaded by UNIV OF PITTSBURGH on July 20, 2013 | http://pubs.acs.org
Publication Date (Web): July 8, 2013 | doi: 10.1021/bk-2013-1135.ch003

## Chapter 3

# Bioactive-Based Poly(anhydride-esters) and Blends for Controlled Drug Delivery

**R. Fogaça,[1,2] M. A. Ouimet,[1] L. H. Catalani,[2] and K. E. Uhrich*,[1]**

**[1]Department of Chemistry and Chemical Biology, Rutgers University, Piscataway, New Jersey 08854, United States**
**[2]Instituto de Química, Universidade de São Paulo, São Paulo, SP 05513-970, Brasil**
***E-mail: keuhrich@rutgers.edu.**

Biodegradable polymers exhibit several potential therapeutic advantages for controlled release due to their biologically relevant (i.e., bioactive) molecules. Bioactive-based poly(anhydride-esters) are one such example. Compared to conventional drug formulations, these polymers offer improved efficacy and reduced toxicity. Utilizing specific synthetic methods, various bioactive agents can be chemically incorporated within the polymer backbone and then released in a sustained manner, thus overcoming current issues of drug delivery, such as poor patient compliance due to repeated administration. Moreover, the polymers can be formulated into hydrogels, microspheres, or electrospun fibers to increase their potential use and applications.

## Introduction

Biodegradable polymers have been extensively studied in recent years for biomaterials, gene delivery, drug delivery, and tissue engineering (*1*). Polyanhydrides are of particular interest as advantageous biomedical delivery systems because of their surface erosion behavior. This property enables a near zero-order drug release profile for bioactives physically entrapped within the polymer matrix (*2–5*). Poly(anhydride-esters) (PAEs), in particular, have been investigated over the past decade as drug delivery systems for a wide variety of bioactive molecules. Typically bioactive molecules are physically incorporated

© 2013 American Chemical Society
In Tailored Polymer Architectures for Pharmaceutical and Biomedical Applications; Scholz, C., et al.; ACS Symposium Series; American Chemical Society: Washington, DC, 2013.

within PAE matrices and released through a combination of matrix degradation and diffusion. Unfortunately, this method of drug incorporation can suffer from low drug loading, poor mechanical properties, and limited control over drug release rates. To overcome issues associated with physical incorporation, chemical incorporation of bioactives into PAEs has been investigated. By chemically incorporating the bioactives within a polymer backbone, drug loading can be increased without compromising the material's mechanical properties and the bioactives can be released in a controlled, sustained fashion during subsequent polymer degradation. Furthermore, the degradation rate and drug release rate can be manipulated based on the polymer's chemical structure (*2*, *6*).

Many prevalent bioactive molecules have been chemically incorporated within PAE backbones for controlled release. PAEs based on morphine, a potent narcotic analgesic, have shown sustained release of the opioid leading to extended analgesia in the treatment of chronic pain – extending analgesia from 3 hours for free morphine to 3 days (*7*). Hydroxycinnamic acid (HC) derivatives such as ferulic, sinapic, and coumaric acids – which exhibit antioxidant, antibacterial, and anti-inflammatory activities (*8*) – have also been incorporated within PAE backbones. In addition to providing sustained release, incorporation of ferulic acid into a polymer backbone overcomes its chemical instability, which results in decomposition and thus limited bioactivity. Salicylic acid (SA), a nonsteroidal anti-inflammatory drugs (NSAIDs) well known for its anti-inflammatory and analgesic properties (*9*, *10*), has the most extensive research to date as a bioactive incorporated within PAEs.

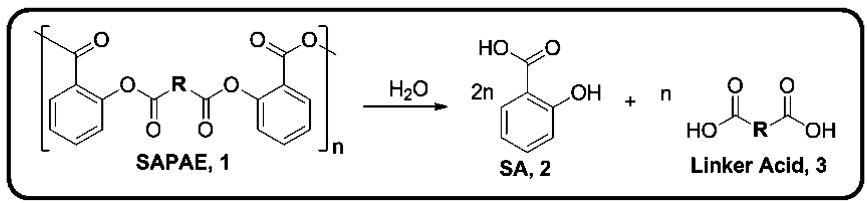


*Figure 1. Hydrolytic degradation of polymer **1** to therapeutic SA and compatible linker acid.*

The incorporation of SA into PAEs and subsequent formulation has been a major focus of the Uhrich laboratory. The SA-containing PAEs (SAPAEs) are polymeric prodrugs in which SA has been incorporated into a PAE backbone using linker molecules, and upon hydrolytic cleavage of the labile anhydride and ester bonds, the drug (e.g., SA (2)) and the biocompatible "linker" molecule (3) are released (Figure 1). The degradation rate of the polymer (1) can be altered by changing the chemical structure of the linker (*6*) to vary polymer hydrophilicity or by copolymerizing the bioactive-based monomer with a non-bioactive monomer with appropriate hydrophilic characteristics.

As noted above, these polymers are unique in their composition. In addition, the SAPAEs are biocompatible (*11–14*), stable under storage conditions (*15*), and can be exposed to ionizing radiation for sterilization without changing their


In Tailored Polymer Architectures for Pharmaceutical and Biomedical Applications; Scholz, C., et al.;
ACS Symposium Series; American Chemical Society: Washington, DC, 2013.

Downloaded by UNIV OF PITTSBURGH on July 20, 2013 | http://pubs.acs.org
Publication Date (Web): July 8, 2013 | doi: 10.1021/bk-2013-1135.ch003

physicochemical properties (*16*). Further, SAPAEs are effective for controlling inflammation (*11*, *14*), promoting bone growth (*11*, *17*), and preventing biofilm formation (*14*, *18*) and can be fabricated into different geometries including disks (*6*), fibers (*19*), microspheres (*20*, *21*), coatings (*18*), and stents (*22*).

## Poly(anhydride-ester) Polymerization Methods

Several polymerization methods have been used to synthesize polyanhydrides including melt-condensation, solution, inter-facial, and ring-opening approaches. For SAPAEs, specifically, melt-condensation and solution methods have been successfully employed (*6*, *12*, *23*, *24*). In melt-polymerization, a diacid (i.e., polymer precursor) is first activated with an excess of acetic anhydride to yield the monomer. The monomer is then melted under high temperature (e.g., 160 – 180 °C) and vacuum (e.g., > 2 mm Hg) to initiate polymerization (Figure 2). Although this method is highly reproducible and allows for easy scale-up, it may not be suitable for thermally sensitive bioactives, especially if the difference between a monomer's melting temperature and decomposition temperature is narrow.

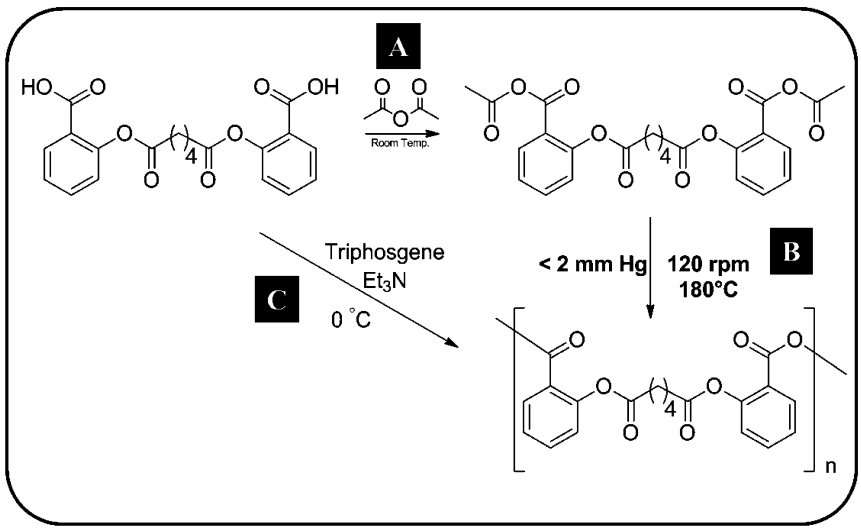


*Figure 2. Synthesis of SAPAEs via melt-condensation polymerization by acetylating the diacid (A) and polymerizing monomer under vacuum at high temperatures (B). Solution polymerization (C) is an alternative method.*

For these thermally sensitive monomers, solution polymerization at low or ambient temperatures is necessary. In solution polymerization, where strict control of stoichiometry is required, the diacid is reacted with triphosgene in the presence of a base, forming phosgene *in situ* as a coupling agent. As compared to melt-polymerization, polymers with lower molecular weights are obtained and scale-up can be difficult.


In Tailored Polymer Architectures for Pharmaceutical and Biomedical Applications; Scholz, C., et al.;
ACS Symposium Series; American Chemical Society: Washington, DC, 2013.

Downloaded by UNIV OF PITTSBURGH on July 20, 2013 | http://pubs.acs.org
Publication Date (Web): July 8, 2013 | doi: 10.1021/bk-2013-1135.ch003

## Poly(anhydride-esters) as Delivery Systems

As mentioned previously, the SAPAE physicochemical properties can be altered by changing the chemical structure of the linker (*6*, *12*, *23*, *24*). Uhrich et al. demonstrated that the glass transition temperature, hydrophobicity, and release rates were altered as the previously described linker molecules were changed. Several linkers were evaluated including linear and branched aliphatic, heteroatomic, and aromatic structures (*6*, *23*). Glass transition temperatures decreased with increasing alkyl chain length and polymers containing aromatic linkers exhibited the highest values. Hydrolytic degradation of the polymer to release SA was also found to be a function of linker structure. The general trends demonstrated that more hydrophilic linkers (leading to a more hydrophilic polymer overall) exhibited faster *in vitro* degradation than did more hydrophobic structures (*23*, *25*).

In addition to their linker-guided tunability, drug delivery devices based on the SAPAEs can be formulated into microspheres, hydrogels, and electrospun fibers, for example, depending upon their intended application. These devices could be introduced *in vivo* via numerous delivery routes including topical (e.g., subcutaneous and epicutaneous), enteral (e.g., oral and rectal), and parenteral (e.g., intravenous and intramuscular) administration. The formulation of SAPAE microspheres, hydrogels, and fibers for controlled release applications are detailed below.

Downloaded by UNIV OF PITTSBURGH on July 20, 2013 | http://pubs.acs.org
Publication Date (Web): July 8, 2013 | doi: 10.1021/bk-2013-1135.ch003

### Poly(anhydride-ester) Microspheres

Microsphere-based drug delivery systems have garnered significant attention in recent years as they can be easily administered via non-surgical methods (e.g., by injection) (*26*). As a result, compounds with pharmaceutical activity are routinely encapsulated within polymer microspheres (*27–30*). Microspheres exhibit increased release rates compared to other systems such as polymer discs due to the larger surface area-to-volume ratio offered by the microspheres (*3*, *29*). For example, three different SAPAE compositions with a heteroatomic (**4**), linear aliphatic (**5**), and branched aliphatic linkers (**6**) were evaluated as microsphere formulations (Figure 3A) (*21*).

SAPAE microspheres were produced using an oil-in-water single emulsion, solvent evaporation technique. As shown in representative scanning electron microscopy (SEM) images (Figure 3B-D), the resulting microspheres exhibited smooth morphologies and did not aggregate, which is important as aggregated microspheres could potentially hinder efficient injection (*31*). In addition, the microspheres showed a relatively narrow size distribution with diameters ranging from 2 to 34 μm (*21*), allowing for uniform microsphere degradation and thus more predictable drug release profiles (*31*).


In Tailored Polymer Architectures for Pharmaceutical and Biomedical Applications; Scholz, C., et al.;
ACS Symposium Series; American Chemical Society: Washington, DC, 2013.

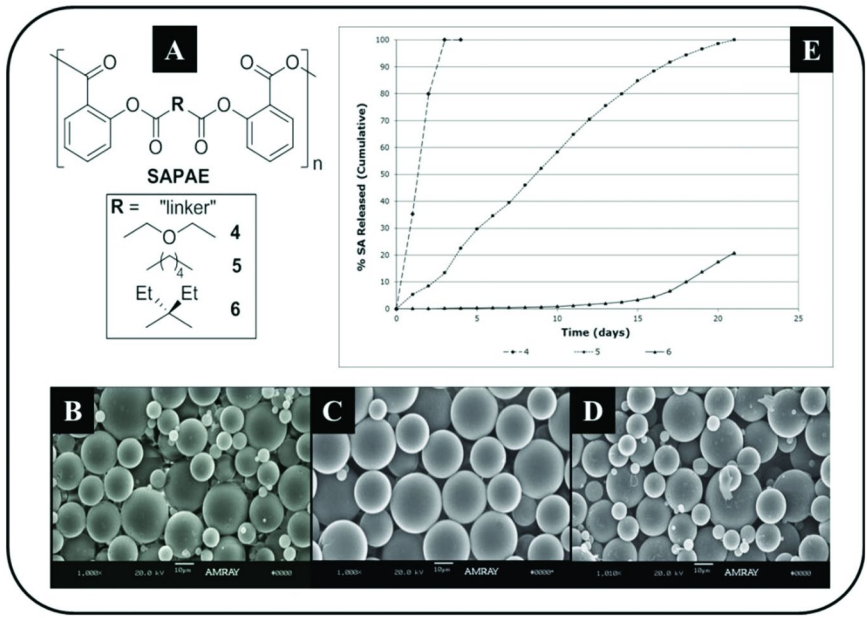


*Figure 3. SAPAE chemical structures with varying linkers 4-6 used to formulate microspheres (A), SEM images of the SAPAE microspheres according to linker structure **4-6** (B-D), and SA release profile from the SAPAE microspheres (E). Adapted with permission from reference (1). Copyright 2012 Springer Science.*

Downloaded by UNIV OF PITTSBURGH on July 20, 2013 | http://pubs.acs.org
Publication Date (Web): July 8, 2013 | doi: 10.1021/bk-2013-1135.ch003

According to the release profiles presented in Figure 3E, the three different linker molecules demonstrate short- and long-term SA release. This can be explained by the varying hydrophobicity of each polymer used for microsphere formulation. SA release was a direct function of the linker structure; polymer microspheres comprised of the heteroatomic linker released 100% SA faster *in vitro* (3 days) than did the linear aliphatic linker (21 days). The polymer microspheres with the branched aliphatic linker have a projected 100% SA release over 3.5 months (*21*). Thus, SA can be delivered over days or months providing potential use for a variety of applications.

## Poly(anhydride-ester) Hydrogels

Hydrogels are comprised of hydrophilic polymeric networks that can absorb substantial amounts of water without dissolving (*32*). If covalent bonds are formed between adjacent polymer chains to cause crosslinking, the resulting hydrogels are considered "chemically produced". The covalent bonds can be produced though different pathways (e.g., chemical reactions) (*33–35*). In the case of chemical crosslinking, residual toxic crosslinking agents may remain within the hydrogel structure, making these systems less desirable for *in vivo* applications. To circumvent this limitation, hydrogels can be produced with

physical crosslinks formed through hydrogen bonds, crystallized domains, or hydrophobic interactions between adjacent polymer chains (*36*). These physical hydrogels are reversible and offer safer alternatives for drug delivery.

Due to their high water content, hydrogels are soft materials that are suitable for a wide variety of applications such as contact lenses, controlled delivery systems, scaffolds, regenerative medicine, skin grafts, and wound dressings (*32*, *37*). In wound healing, hydrogels can provide an ideal moisturizing environment (with unobstructed visibility of the wound bed) which can minimize pain and enhance healing. Moreover, an ideal dressing would be capable of delivering bioactive molecules to improve the healing process. Poly(*N*-vinyl-2-pyrrolidone) (PVP) (Figure 4A, left) is a common hydrogel material due to its mechanical and water-absorption properties when chemically crosslinked (*35*, *38*). One major drawback, however, is that PVP alone does not have inherent bioactivity. In contrast, SAPAEs have inherent bioactivity but can be brittle and lack the swelling properties necessary for hydrogels.

Consequently, Uhrich et al. (*39*) have combined these two polymer systems to produce physically crosslinked hydrogels with appropriate physical characteristics and drug delivery behavior as potential wound dressing materials. These PVP:SAPAE-based hydrogels would be ideal wound dressings as water absorption by the hydrogel would initiate the PAE degradation and trigger bioactive release. As the bioactives are not physically admixed within the hydrogel matrix, immediate and uncontrolled release of the bioactives can be avoided.

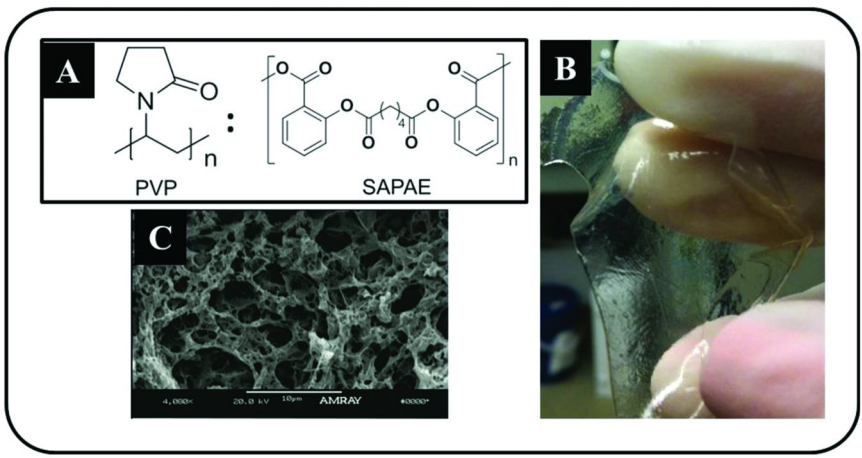


*Figure 4. Chemical structures of PVP (A, left) and SAPAE (A, right), representative image of the PVP:SAPAE hydrogel (B), and SEM image of the PVP:SAPAE (70:30) hydrogel porous structure at 4080X magnification (C).*

PVP:SAPAE hydrogels (Figure 4A-B) were prepared at various ratios. Water uptake, as indicated by swelling ratio (*Q*) (see Table 1), changed in relation to the PVP:SAPAE ratio, with higher PVP content correlating to larger swelling values.


In Tailored Polymer Architectures for Pharmaceutical and Biomedical Applications; Scholz, C., et al.; ACS Symposium Series; American Chemical Society: Washington, DC, 2013.

Downloaded by UNIV OF PITTSBURGH on July 20, 2013 | http://pubs.acs.org
Publication Date (Web): July 8, 2013 | doi: 10.1021/bk-2013-1135.ch003

Furthermore, water uptake and swelling resulted in pore formation throughout the hydrogel structure (Figure 4C) and promoted SA release. The SA release profiles are currently being investigated to ascertain the time frame over which all SA is released; this outcome will be the subject of a future publication.

**Table 1. Swelling ratio (*Q*) variation according to PVP content (*39*)**

| *PVP:SAPAE ratio* | *Swelling ratio (Q)* |
|---|---|
| 70:30 | 14.2 ± 1.4 |
| 60:40 | 7.2 ± 0.8 |
| 50:50 | 4.9 ± 0.1 |

Downloaded by UNIV OF PITTSBURGH on July 20, 2013 | http://pubs.acs.org
Publication Date (Web): July 8, 2013 | doi: 10.1021/bk-2013-1135.ch003

PAEs containing bioactives other than SA have been successfully blended with PVP to form hydrogels as well. Uhrich et. al. (*40*) have prepared PAEs based on HC derivatives (ferulic, sinapic, and coumaric acids) that could be beneficial for wound dressing applications due to the therapeutic properties of the HC (released via PAE hydrolysis). The chemical structures of the HC-based PAEs (HCPAEs) are presented in Figure 5.

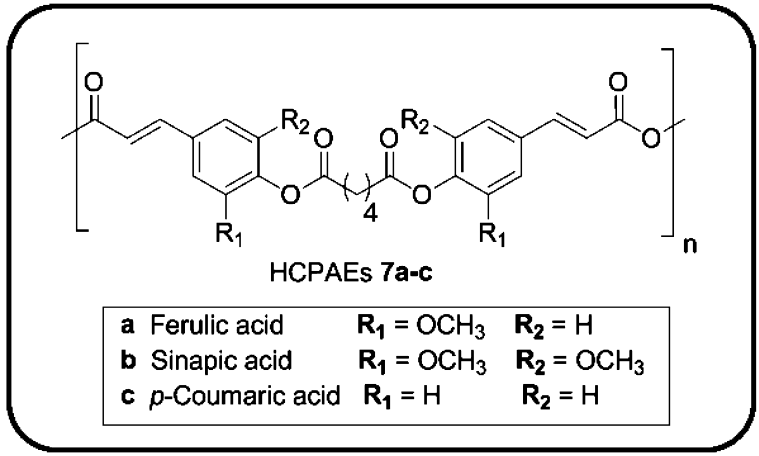


*Figure 5. HCPAE polymers (**7a-c**) used to prepare physically crosslinked hydrogels.*

PVP:HCPAE hydrogels exhibited similar swelling behaviors as compared to PVP:SAPAE hydrogels. As with the SAPAEs, higher PVP content yielded higher swelling ratios. A wide range of PVP-to-HCPAE ratios were investigated with many showing appreciable swelling values relevant for wound dressing applications. A notable exception, however, was the 90:10 PVP:HCPAE system which did not swell, but completely dissolved when exposed to water.

Downloaded by UNIV OF PITTSBURGH on July 20, 2013 | http://pubs.acs.org
Publication Date (Web): July 8, 2013 | doi: 10.1021/bk-2013-1135.ch003

**Poly(anhydride-ester) Electrospun Fibers**

Electrospinning is a well-established technique for producing polymeric fibers with diameters ranging from nanometers to micrometers. Polymer fibers possess large surface areas and can be useful in a wide variety of applications including controlled drug release systems, scaffolds for tissue engineering, and in regenerative medicine (*41*). Due to their low molecular weight and poor mechanical properties, the SAPAEs previously discussed are not suitable for electrospinning when used alone. However, highly uniform SAPAE micro- and nanofibers have been successfully prepared when blended with poly(lactic-co-glycolic acid) (PLGA) or PVP (*42*, *43*). Notably, highly aligned PLGA:SAPAE (70:30) electrospun nanofibers were prepared to promote cell alignment for nerve regeneration applications. The environment provided by the nanofibers mimics that found *in vivo* for cell alignment, promoting nerve cell differentiation and directing the attachment and morphology of nerve cells. Specifically, Schwann cells showed directed cell elongation and proliferation in directions parallel to the oriented nanofibers along with aligned neurite outgrowth. In addition, the fibers degraded over 42 days to locally release SA and reduce inflammation during the neurite outgrowth and regeneration processes.

As another example, PVP:HCPAE blended electrospun microfibers (PVP:HCPAE 70:30) were produced for bioactive wound dressing applications. Figure 6A-B shows the microstructure of PVP:HCPAE electrospun fibers exhibiting diameters of ca. 10 μm. The fibers present a ribbon-like structure, which can be related to both solvent evaporation during the electrospinning process (*44*); electrospinning parameters must be adjusted to optimize the fiber morphology. These electrospun systems are suitable materials to produce hydrogels given their physicochemical properties. Electrospun PVP-based hydrogels have been described as appropriate materials for wound healing; in additional to the benefits of using hydrogels as a wound dressing, an electrospun material can control the rate of debriding protein release to ultimately enhance the healing process (*45*). Therefore, these electrospun fibers have the capabilities of a hydrogel, the ability to remove non-viable tissue, and exhibit controlled drug release from the bioactive-based PAEs.

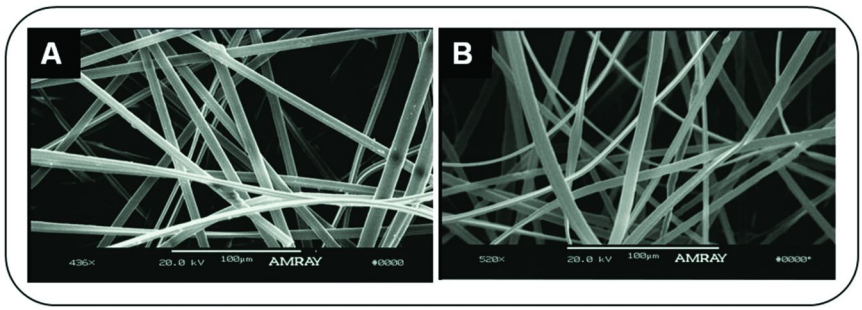


*Figure 6. SEM images of PVP:HCPAE (ferulic acid 70:30) (A) and PVP:HCPAE (sinapic acid 70:30) electrospun fibers (B).*


In Tailored Polymer Architectures for Pharmaceutical and Biomedical Applications; Scholz, C., et al.;
ACS Symposium Series; American Chemical Society: Washington, DC, 2013.

## Summary

Biodegradable polymers play an integral role in drug delivery, particularly in the realm of biomaterials. Bioactive-based PAEs are a unique class of polymers that allows for controlled drug delivery, high drug loading, and can be fabricated into various devices depending on the end use. The bioactive-based PAEs described here have been fabricated into microspheres, hydrogels, and fibers, yielding novel biomaterials capable of sustained bioactive release upon polymer hydrolytic degradation. SAPAE formulation into microspheres provides a non-invasive method for drug delivery and provides the potential to be used as a carrier device. Innovative physical hydrogels and electrospun fibers utilizing SAPAEs and HCPAEs blended with PVP and/or PLGA have significant potential as enhanced wound dressings. The polymer design allows for more control current delivery systems which can improve upon current treatments. The drug release tunability, ease of fabrication, and ability to change the bioactive molecule allows for these polymers to be employed in a broad range of applications within the biomaterial field.

Downloaded by UNIV OF PITTSBURGH on July 20, 2013 | http://pubs.acs.org
Publication Date (Web): July 8, 2013 | doi: 10.1021/bk-2013-1135.ch003

## Acknowledgments

The authors acknowledge the many contributions of Ray Ottenbrite, who has been a leader and inspiration to the polymer field, specifically for biomedical applications. Dr. Bryan Langowski and Uhrich group members are thanked for intellectual contributions to this work.

## References

1. Brannon-Peppas, L. *Med. Plast. Biomater* **1997**.
2. Uhrich, K. E.; Cannizzaro, S. M.; Langer, R. S.; Shakesheff, K. M. *Chem. Rev.* **1999**, *99* (11), 3181–98.
3. Whitaker-Brothers, K.; Uhrich, K. *J. Biomed. Mater. Res., Part A* **2006**, *76A* (3), 470–479.
4. Göpferich, A.; Tessmar, J. *Adv. Drug Delivery Rev.* **2002**, *54* (7), 911–31.
5. Tamada, J. A.; Langer, R. *Proc. Natl. Acad. Sci. U.S.A.* **1993**, *90* (2), 552–6.
6. Prudencio, A.; Schmeltzer, R. C.; Uhrich, K. E. *Macromolecules* **2005**, *38* (16), 6895–901.
7. Rosario-Meléndez, R.; Harris, C. L.; Delgado-Rivera, R.; Yu, L.; Uhrich, K. E. *J. Controlled Release* **2012**, *162*, 538–44.
8. Carbone, A. L. *Natural bioactive-based polyanhydrides for controlled release applications*; Rutgers, The State Univeristy of New Jersey: New Brunswick, 2009.
9. Schmeltzer, R. C.; Schmalenberg, K. E.; Uhrich, K. E. *Biomacromolecules* **2005**, *6* (1), 359–67.
10. Schmeltzer, R. C.; Uhrich, K. E. *J. Bioact. Compat. Polm.* **2006**, *21* (2), 123–33.
11. Erdmann, L.; Macedo, B.; Uhrich, K. E. *Biomaterials* **2000**, *21* (24), 2507–12.

12. Schmeltzer, R. C.; Johnson, M.; Griffin, J.; Uhrich, K. *J. Biomater. Sci., Polym. Ed.* **2008**, *19* (10), 1295–306.
13. Reynolds, M. A.; Prudencio, A.; Aichelmann-Reidy, M. E.; Woodward, K.; Uhrich, K. E. *Curr. Drug Delivery* **2007**, *4* (3), 233–9.
14. Bryers, J. D.; Jarvis, R. A.; Lebo, J.; Prudencio, A.; Kyriakides, T. R.; Uhrich, K. *Biomaterials* **2006**, *27* (29), 5039–48.
15. Deronde, B. M.; Carbone, A. L.; Uhrich, K. E. *Polym. Degrad. Stab.* **2010**, *95* (9), 1778–82.
16. Rosario-Meléndez, R.; Lavelle, L.; Bodnar, S.; Halperin, F.; Harper, I.; Griffin, J.; Uhrich, K. E. *Polym. Degrad. Stab.* **2011**, *96* (9), 1625–30.
17. Harten, R. D.; Svach, D. J.; Schmeltzer, R.; Uhrich, K. E. *J. Biomed. Mater., Res. A* **2005**, *72* (4), 354–62.
18. Rosenberg, L. E.; Carbone, A. L.; Romling, U.; Uhrich, K. E.; Chikindas, M. L. *Lett. Appl. Microbiol.* **2008**, *46* (5), 593–9.
19. Whitaker-Brothers, K.; Uhrich, K. *J. Biomed. Mater. Res., Part A* **2004**, *70A* (2), 309–18.
20. Yeagy, B. A.; Prudencio, A.; Schmeltzer, R. C.; Uhrich, K. E.; Cook, T. J. *J. Microencapsulation* **2006**, *23* (6), 643–53.
21. Rosario-Meléndez, R.; Ouimet, M. A.; Uhrich, K. E. *Polym. Bull.* **2013**, *70* (1), 343–51.
22. Jabara, R.; Chronos, N.; Robinson, K. *Catheter Cardiovasc. Interventions* **2008**, *72* (2), 186–94.
23. Carbone, A. L.; Uhrich, K. E. *Macromol. Rapid Commun.* **2009**, *30* (12), 1021–6.
24. Schmeltzer, R. C.; Anastasiou, T. J.; Uhrich, K. E. *Polym. Bull.* **2003**, *49* (6), 441–8.
25. Prudencio, A.; Schmeltzer, R. C.; Uhrich, K. E. *Macromolecules* **2005**, *38* (16), 6895–901.
26. Kipper, M. J.; Shen, E.; Determan, A.; Narasimhan, B. *Biomaterials* **2002**, *23* (22), 4405–4412.
27. Vasir, J. K.; Tambwekar, K.; Garg, S. *Int. J. Pharm.* **2003**, *255* (1-2), 13–32.
28. Freitas, S.; Merkle, H. P.; Gander, B. *J. Controlled Release* **2005**, *102* (2), 313–32.
29. Freiberg, S.; Zhu, X. X. *Int. J. Pharm.* **2004**, *282* (1-2), 1–18.
30. Edlund, U.; Albertsson, A. *Degradable Polymer Microspheres for Controlled Drug Delivery*; Springer: Berlin, 2002; Vol. 157, pp 67−112.
31. Kawaguchi, H. *Prog. Polym. Sci.* **2000**, *25* (8), 1171–210.
32. Hennink, W. E.; van Nostrum, C. F. *Adv. Drug Delivery Rev.* **2002**, *54* (1), 13–36.
33. Peppas, N. A.; Huang, Y.; Torres-Lugo, M.; Ward, J. H.; Zhang, J. *Annu. Rev. Biomed. Eng.* **2000**, *2*, 9–29.
34. Hamidi, M.; Azadi, A.; Rafiei, P. *Adv. Drug Delivery Rev.* **2008**, *60* (15), 1638–49.
35. Lopérgolo, L. C.; Lugão, A. B.; Catalani, L. H. *Polymer* **2003**, *44* (20), 6217–22.
36. Peppas, N. A.; Bures, P.; Leobandung, W.; Ichikawa, H. *Eur. J. Pharm. Biopharm.* **2000**, *50* (1), 27–46.

Downloaded by UNIV OF PITTSBURGH on July 20, 2013 | http://pubs.acs.org
Publication Date (Web): July 8, 2013 | doi: 10.1021/bk-2013-1135.ch003


In Tailored Polymer Architectures for Pharmaceutical and Biomedical Applications; Scholz, C., et al.;
ACS Symposium Series; American Chemical Society: Washington, DC, 2013.

37. Mohan, Y. M.; Thomas, V.; Namdeo, M.; Bajpai, S. K.; Bajpai, M. *J. Macromol. Sci., Part A: Pure Appl. Chem.* **2008**, *45* (1), 107–19.
38. Barros, J. A. G.; Fechine, G. J. M.; Alcantara, M. R.; Catalani, L. H. *Polymer* **2006**, *47* (26), 8414–19.
39. Ouimet, M. A.; Nguyen, V.; Smith, K.; Uhrich, K. E. *Polym. Prepr. (Am. Chem. Soc., Div. Polym. Chem.)* **2012**, *53* (1), 548–549.
40. Fogaça, R.; Ouimet, M. A.; Catalani, L. H.; Uhrich, K. E. Synthesis and Characterization of Novel Bioactive PVP-based Hydrogels. *Proc. ACS Div. Polym. Mater: Sci. Eng.*; Amercian Chemical Society: Washington, DC, 2010; Vol. 2.
41. Schiffman, J. D.; Schauer, C. L. *Polym. Rev.* **2008**, *48* (2), 317–52.
42. Griffin, J.; Delgado-Rivera, R.; Meiners, S.; Uhrich, K. E. *J. Biomed. Mater. Res., Part A* **2011**, *97A* (3), 230–42.
43. Griffin, J.; Carbone, A.; Delgado-Rivera, R.; Meiners, S.; Uhrich, K. E. *Acta Biomater.* **2010**, *6* (6), 1917–24.
44. Ramakrishna, S. F., K.; Teo, W. E.; Lim, T. C.; Ma, Z. *An Introduction to Electrospinning and Nanofibers*; World Scientific: River Edge, NJ, 2005.
45. Fogaça, R.; Catalani, L. H. *Soft Matter* **2013**, *11* (1), 61–8.

Downloaded by UNIV OF PITTSBURGH on July 20, 2013 | http://pubs.acs.org
Publication Date (Web): July 8, 2013 | doi: 10.1021/bk-2013-1135.ch003

Downloaded by UNIV OF MICHIGAN ANN ARBOR on July 17, 2013 | http://pubs.acs.org
Publication Date (Web): July 8, 2013 | doi: 10.1021/bk-2013-1135.ch004

## Chapter 4

# Fatty Acid Modified Poly(glycerol adipate) - Polymeric Analogues of Glycerides

**T. Naolou,[1] V. M. Weiss,[2] D. Conrad,[1] K. Busse,[1] K. Mäder,[2] and J. Kressler***

**[1]Institute of Chemistry, Martin Luther University Halle-Wittenberg, D-06099 Halle (Saale), Germany**
**[2]Institute of Pharmacy, Martin Luther University Halle-Wittenberg, D-06099 Halle (Saale), Germany**
***E-mail: joerg.kressler@chemie.uni-halle.de.**

Poly(glycerol adipate) PGA is synthesized by enzymatic polymerization using glycerol and either divinyl adipate or dimethyl adipate. The PGA is linear when the enzymatic reaction is carried out at 40°C while branching occurs at higher temperatures. The linear PGA backbone is modified by esterification with fatty acids of different lengths yielding comb-like polymers. The melting temperature and specific enthalpy of fusion increase with increasing degree of substitution and/or by increasing length of the saturated fatty acids used to modify the PGA backbone. Furthermore, the comb-like polymers have a higher thermal stability compared to the original PGA backbone. The shape of nanoparticles prepared by an optimized interfacial deposition method depends on the type of fatty acid used and on the degree of substitution. The nanoparticles are phase separated as a result of the incompatibility between the polymer backbone and the teeth of the comb-like polymers. When saturated fatty acids are used, additionally crystallization of the side chains takes place. Also the esterification with non-crystallizing oleic acid allows for preparation of phase separated nanoparticles.

© 2013 American Chemical Society
In Tailored Polymer Architectures for Pharmaceutical and Biomedical Applications; Scholz, C., et al.;
ACS Symposium Series; American Chemical Society: Washington, DC, 2013.

The conversion of glycerol with different fatty acids may result in mono-, di- or triglycerides (*1*). Triglycerides are usually hydrophobic and the mono- or diglycerides can be considered as amphiphilic molecules due to remaining OH-groups (*2*). Thus, they are surface active and reduce the surface tension of water or they are effective emulsifiers (*3*). Additionally, they are able to form lyotropic liquid crystalline phases (*4*). Especially, the monoolein/water system is interesting since it can form nanoparticles exhibiting a bicontinuous cubic phase (cubosomes) when stabilized by poloxamers (*5*). These nanoparticles can dissolve both hydrophilic and lipophilic drugs and additionally they can be used as scaffold for therapeutic proteins (*6*).

It is reasonable to assume that polyesters based on glycerol can possess similar properties as low-molar mass glycerides discussed above; but they would have the advantage of higher mechanical stability and longer *in vivo* circulation times. Synthetic, aliphatic polyesters are some of the most widely used polymers in modern life. Their biodegradability and low costs of production are considered to be the main factors for their widespread use. Nevertheless, many physical, biological and mechanical properties of polyesters are not always meeting the crucial requirements for some applications. Therefore, synthesizing new polyesters with functional groups able for post-polymerization functionalization is a challenging task (*7*). Actually, many routes have been developed to synthesize polyesters with functional groups such as ring opening polymerization of substituted lactones (*8–11*), and polycondensation of multifunctional monomers (*12–16*). Utilization of enzymes as a catalyst to synthesize functional polyester has been attracting many interests for two decades due to advantages that enzymes provide over conventional chemical catalysts (*17*). Actually, enzymatic polymerization can be performed under mild reaction conditions and does not require protection-deprotection steps due to the regio- and enantioselectivity of enzymes (*18*). This will omit deprotection steps that might degrade the polyester backbone. Poly(glycerol adipate) (PGA) was enzymatically synthesized first by Kline et al. (*19*) using glycerol and divinyl adipate as monomers and lipase enzyme from *Candida Antarctica* type B (CAL-B) as catalyst to yield linear polyesters with free pendent hydroxyl groups. The enzyme is immobilized on an acrylic macroporous resin which facilitates the processes of separating it from the final polymer. The overall synthesis process could be described as simple, clean, easy to conduct, easy to purify the final product, and easy to scale up to 500 g (*20*). Using glycerol as a monomer has a big advantage since it is a cheap, widely used, and biocompatible compound. On the other hand, the utilization of divinyl adipate as monomer for synthesis is not appropriate for commercial purposes. Using dimethyl adipate (DMA) instead of divinyl adipate to synthesize PGA is more appropriate since it is a large-scale and cheap commodity chemical compound. On the other hand, esterification of the hydroxyl pendent groups at the PGA backbone with fatty acids has been found to yield promising materials for application in the field of nano-drug carriers (*21–24*). However, further characterization for these polymers and corresponding nanoparticles is necessary in order to tune their properties and to ensure their suitability to be applicable *in vivo*. Furthermore, additional applications in pharmacy and medicine can be envisioned due to their biocompatibility and biodegradability.

Downloaded by UNIV OF MICHIGAN ANN ARBOR on July 17, 2013 | http://pubs.acs.org
Publication Date (Web): July 8, 2013 | doi: 10.1021/bk-2013-1135.ch004



In Tailored Polymer Architectures for Pharmaceutical and Biomedical Applications; Scholz, C., et al.;
ACS Symposium Series; American Chemical Society: Washington, DC, 2013.

# Experimental Section

## Materials

All chemicals were purchased from Sigma-Aldrich and used without further purification unless otherwise stated. Lauroyl chloride 98%, stearoyl chloride 97%, behenoyl chloride ≥99.0%, oleoyl chloride, dimethyl adipate (DMA) (99.5%) are used as received. Tetrahydrofuran is dried over sodium under anaerobic conditions. Pyridine (99%) was dried over calcium hydride over night, distilled under atmospheric pressure and stored over molecular sieve (3Å). Solvents for column chromatography and precipitation were distilled prior to use. CAL B (lipase B from *Candida Antarctica* immobilized on an acrylic macroporous resin) is dried under vacuum at 4 °C over $P_2O_5$ for two days prior to use. Divinyl adipate (DVA) is obtained from TCI-Europe.

Downloaded by UNIV OF MICHIGAN ANN ARBOR on July 17, 2013 | http://pubs.acs.org
Publication Date (Web): July 8, 2013 | doi: 10.1021/bk-2013-1135.ch004

## Synthesis of Poly(glycerol adipate) PGA

Poly(glycerol adipate) was synthesized at 50°C from glycerol and DVA as described by Kallinteri et al (*21*). A typical procedure for the synthesis of PGA backbone using DMA and glycerol as monomers was as follows: (11.5 g, 0.12 mol) glycerol, (21.7g, 0.12mol) DMA, and 13 mL anhydrous THF were charged into an oven dried two-necked 250 mL round bottom flask. The flask was equipped with a soxhlet extractor (150 mL) attached to a condenser. The soxhlet extractor was charged with 105 g of molecular sieve 5Å and then filled with about 100 mL anhydrous THF. The mixture was stirred by magnetic stirrer to allow reactants to warm up to the bath's temperature (60°C) for about 30 min. The reaction was started by adding (0.73 g) of enzyme. The pressure was then reduced gradually to 300 mbar in order to allow for the evaporation process. The azeotropic mixture of THF and methanol was collected gradually into the soxhlet extractor and came into contact with the molecular sieve. As a result the methanol was entrapped gradually by the molecular sieve. The conditions (temperature and pressure) were adjusted to allow one cycle of soxhlet filling to be 20 min. The enzyme was removed at the end of polymerization by filtration followed by washing with 35 mL THF. The solvent was removed by rotary evaporation at 60°C under vacuum. Finally, the temperature was raised up to 95°C for 10 min in order to deactivate any remaining free enzyme. The polymer was used for the next step without further purification.

## Acylation of PGA Backbone with Fatty Acid Chains

Acylation reaction was carried out between hydroxyl groups on PGA backbone and an acyl halide of lauroyl, stearoyl, behenoyl, and oleoyl chains. The acylation reaction was performed using the procedure described by Kallinteri et al (*21*). However, further purification step was necessary in order to remove unreacted fatty acid. The purification was carried out by precipitation into cold n-hexane in the case of acylation with lauroyl chloride or for low substitution degrees in the case of the other fatty acids. Whereas, dialysis against THF for 5 days, using regenerated cellulose membrane of a MWCO of 1000 g/mol, was performed in the case of higher substitution degrees.


In Tailored Polymer Architectures for Pharmaceutical and Biomedical Applications; Scholz, C., et al.;
ACS Symposium Series; American Chemical Society: Washington, DC, 2013.

PGA with molar mass 3700 g/mol was used for the acylation reaction. The acylation degrees (given in mol% of converted OH-groups of PGA) were as follows:

lauroyl chains: 30%, 50%, 75% called L30, L50 L75.

stearoyl chains: 8%, 20%, 45%, 65%, 85% called S8, S20, S45, S65, S85.

behenoyl chains: 45%, 65% called B45, B65 respectively.

oleoyl chains: 15%, 23%, 30%, 67%, 92% called O15, O20, O30, O67, O92.

The acylation degrees were calculated form $^1$H NMR spectra

## Polymer Nanoparticle Preparation

Nanoparticles were prepared according to the optimized interfacial deposition method (*25*). Shortly, 10 mg of polymer were dissolved in 1 mL of acetone which was then injected slowly into 15 mL of 60°C water using a glass syringe under rapid magnetic stirring. The hot nanoparticle dispersion was subsequently poured into an empty iced beaker under magnetic stirring. The remaining solvent and some water were then removed by a rotary evaporator to obtain finally an 1% dispersion (10 mg polymer/g solution).

## Differential Scanning Calorimetry

Differential scanning calorimetry (DSC) experiments were carried under continuous nitrogen flow using a Mettler Toledo DSC 823e module. Aluminum pans were filled with about 10 mg of sample. Every sample was heated up to 100°C and kept at this temperature for 20 min. The sample was then cooled to -50°C with a cooling rate of -1 K/min. The sample was kept at -50°C for further 20 min; afterwards the sample was heated up again to 100°C with a heating rate 1 K/min. DSC traces were baseline-corrected. The maximum of the endothermal peak during the second heating was taken as the melting temperature $T_m$, whereas the minimum of the exothermal peak was taken as a crystallization temperature $T_c$. Specific enthalpy of melting $\Delta\widetilde{H}_m$ was obtained from integration of the endothermal peak divided by the weight of alkyl side chains of the sample. The degree of crystallization $X_{DSC}= \Delta\widetilde{H}_{m/} \Delta\widetilde{H}^0_m$ where $\Delta\widetilde{H}^0_m$ is the enthalpy of melting of the respective fatty acid.

## Transmission Electron Microscopy (TEM)

Samples were negatively stained using aqueous solution of uranyl acetate The samples for freeze-fracture were cryofixed using a propane jet-freeze device JFD 030 (BAL-TEC, Balzers, Liechtenstein). Thereafter, the samples were freeze-fractured at −150 °C without etching with a freeze-fracture/freeze-etching system BAF 060 (BAL-TEC). Cryo-TEM grids were prepared in the same way as TEM. Measurements were carried out immediately after preparation of the grids with a Zeiss 902 A microscope operating at 80 kV.



In Tailored Polymer Architectures for Pharmaceutical and Biomedical Applications; Scholz, C., et al.; ACS Symposium Series; American Chemical Society: Washington, DC, 2013.

Downloaded by UNIV OF MICHIGAN ANN ARBOR on July 17, 2013 | http://pubs.acs.org
Publication Date (Web): July 8, 2013 | doi: 10.1021/bk-2013-1135.ch004

Downloaded by UNIV OF MICHIGAN ANN ARBOR on July 17, 2013 | http://pubs.acs.org
Publication Date (Web): July 8, 2013 | doi: 10.1021/bk-2013-1135.ch004

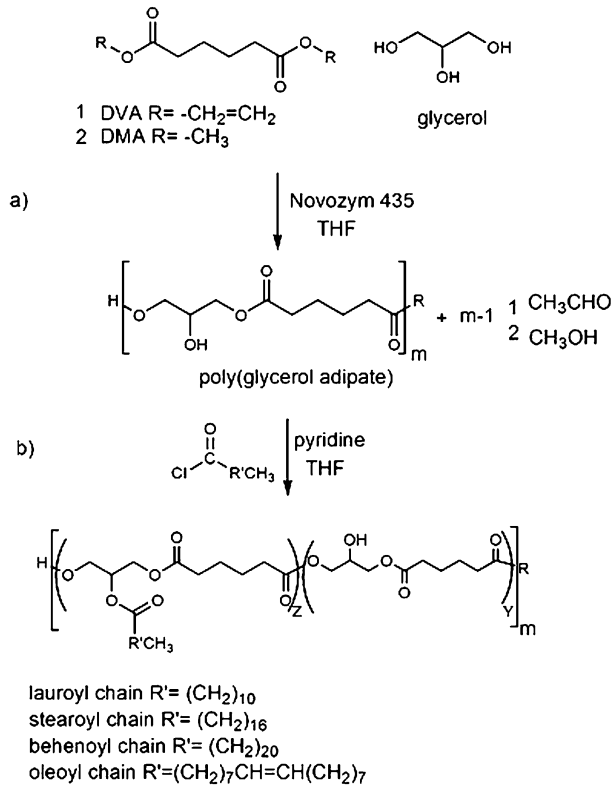


*Figure 1. Synthesis of a) poly(glycerol adipate) backbone by using glycerol and either DVA or DMA as monomers and CAL-B as a catalyst. b) Esterification reaction between acyl chloride of fatty acids and PGA using pyridine.*

## Results and Discussion

### Synthesis of Poly(glycerol adipate) (PGA) Backbone

PGA is an amphiphilic, water insoluble, yellowish, and highly viscous liquid. The overall synthesis route for the PGA backbone is shown in Figure 1. The polymer is enzymatically synthesized using two strategies. In the first one glycerol is enzymatically polymerized with divinyl adipate (DVA) in the presence of *CAL-B* as catalyst. The regioselectivity of lipase towards primary alcohols of the glycerol yields linear polyesters with free pendent hydroxyl groups at the backbone. The absence of enzyme, on the other hand, results in cross-linked products (*26*). The vinyl alcohol produced as by-product, beside PGA during the enzymatic reaction, is directly converted into acetaldehyde by tautomerization and will finally evaporate at the reaction temperature. This shifts the equilibrium of the polycondensation reaction towards the products. The second strategy to


In Tailored Polymer Architectures for Pharmaceutical and Biomedical Applications; Scholz, C., et al.;
ACS Symposium Series; American Chemical Society: Washington, DC, 2013.

synthesize PGA is using dimethyl adipate (DMA) instead of divinyl adipate (DVA). Utilization of DMA causes some problems of shifting the direction of the equilibrium towards the polymer since methanol will be the by-product of this reaction which has to be removed. Actually, methanol and tetrahydrofurane (THF) form an azeotropic mixture which makes their separation impossible by distillation during the enzymatic reaction. Thus the polymerization reaction would cease at low conversions. Therefore, the polymerization reaction is carried out in the presence of molecular sieves placed into a soxhlet apparatus attached on the top of the reaction vessel as depicted in Figure 2. Both methanol and THF evaporate together during the enzymatic polymerization and condense again by the condenser to be collected finally into soxhlet extractor where the mixture comes into contact with the molecular sieve.

Downloaded by UNIV OF MICHIGAN ANN ARBOR on July 17, 2013 | http://pubs.acs.org
Publication Date (Web): July 8, 2013 | doi: 10.1021/bk-2013-1135.ch004

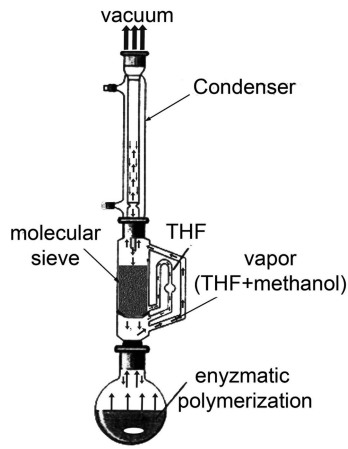


*Figure 2. Experimental setup to prepare poly(glycerol adipate) using DMA and glycerol in the presence of CAL-B as a catalyst and THF as solvent.*

The molecular sieve has a pore size of 5Å. This size allows for only methanol to be captured by the molecular sieve and thus only pure THF will reflux to the reaction vessel. The capacity of the molecular sieve to entrap methanol is around 14 wt% of its own weight. An excess of about 80 wt% of molecular sieve is added in order to prevent the system to reach a state of saturation of the molecular sieve with methanol. The procedure described above to remove the resulting by-product has many advantages, e.g. easy to scale-up by increasing the amount of molecular sieve and the molecular sieve is not in contact with the polymer formed. Many strategies have been suggested to remove the resulting by-product in order to shift the reaction equilibrium towards the products in polycondensation processes (*27*). However, not all of these strategies are convenient for both laboratories and industrial applications (*28–30*). Using the solvent route instead of bulk route for


In Tailored Polymer Architectures for Pharmaceutical and Biomedical Applications; Scholz, C., et al.;
ACS Symposium Series; American Chemical Society: Washington, DC, 2013.

the polycondensation provides a better distribution for both enzyme beads and temperature within the reaction vessel. Furthermore, Juais et al. (*31*) proved that carrying out enzymatic polymerization in solvents gives a higher $M_w$ than in bulk. The procedure can be extended to be suitable for large scale process. Table I shows the results of enzymatic polymerization of divinyl adipate or dimethyl adipate with glycerol at different reaction times. Increasing $M_n$ of the polymer causes also an increase of its polydispersity *D*. The number-average molecular weights $M_n$ obtained from the reaction of DVA are higher than that of DMA within a shorter time of reaction. The low reactivity of alkyl esters towards alcohols in lipase-catalyzed transesterification could be the reason for these results (*18*).

Downloaded by UNIV OF MICHIGAN ANN ARBOR on July 17, 2013 | http://pubs.acs.org
Publication Date (Web): July 8, 2013 | doi: 10.1021/bk-2013-1135.ch004

**Table I. SEC Measurements of PGA Synthesized Using Either DVA or DMA and Glycerol**

| *Type of adipate* | *Time [h]* | $M_w$[a] *[g/mol]* | $M_n$[a] *[g/mol]* | *PD*[a] |
|---|---|---|---|---|
| Divinyl adipate | 4 | 5070 | 2700 | 1.9 |
| Divinyl adipate | 8 | 7650 | 3500 | 2.1 |
| Dimethyl adipate | 18 | 1660 | 890 | 1.8 |
| Dimethyl adipate | 48 | 4800 | 1950 | 2.4 |

[a] $M_w$, $M_n$, and *PD* were determined by SEC using THF as eluent and poly(styrene) a standard.

PGA ($M_n$ is 1950 g/mol) is characterized first by $^1$H-$^{13}$C COSY NMR carried out in $CDCl_3$ and shown in Figure 3.Actually, the peaks at 51.1, 66.1, 68.6, 69.2, and 71.9 ppm in the $^{13}$CNMR spectrum appear as negative value in APT CNMR spectrum which indicates that they are related to methine (CH) and methyl ($CH_3$) groups. The peak at 51.1 ppm is well known to be related to the methyl group of dimethyl adipate. This means essentially that the other peaks are related to the methine group of glyceride units within the PGA backbone. The peaks in the H-C COSY NMR spectrum are assigned to the polymer structure as shown in Figure 3. The presence of many peaks for methine groups indicates some imperfections of the enzyme regioselectivity during polymerization towards primary alcohols. This imperfection causes the formation of 1,2-disubstituted and 1,2,3-trisubstituted glyceride units within the backbone whereas only 1,3-disubstituted and 1-substituted species should appear in the case of ideal regioselectivity of the enzyme during polymerization. The presence of some imperfections of the regioselectivity has been noticed before (*19*, *32*). Actually, the presence of 1,2,3-trisubstituted glyceride has the worst effect on the properties of the backbone since it decreases the number of hydroxyl groups on PGA backbone and will effect also the linearity of the total polymer backbone. The ratio of trisubstitution is calculated using the integral ratio between the peaks R or S and the peak C and it is equal to about 8 mol%.


In Tailored Polymer Architectures for Pharmaceutical and Biomedical Applications; Scholz, C., et al.;
ACS Symposium Series; American Chemical Society: Washington, DC, 2013.

Downloaded by UNIV OF MICHIGAN ANN ARBOR on July 17, 2013 | http://pubs.acs.org
Publication Date (Web): July 8, 2013 | doi: 10.1021/bk-2013-1135.ch004

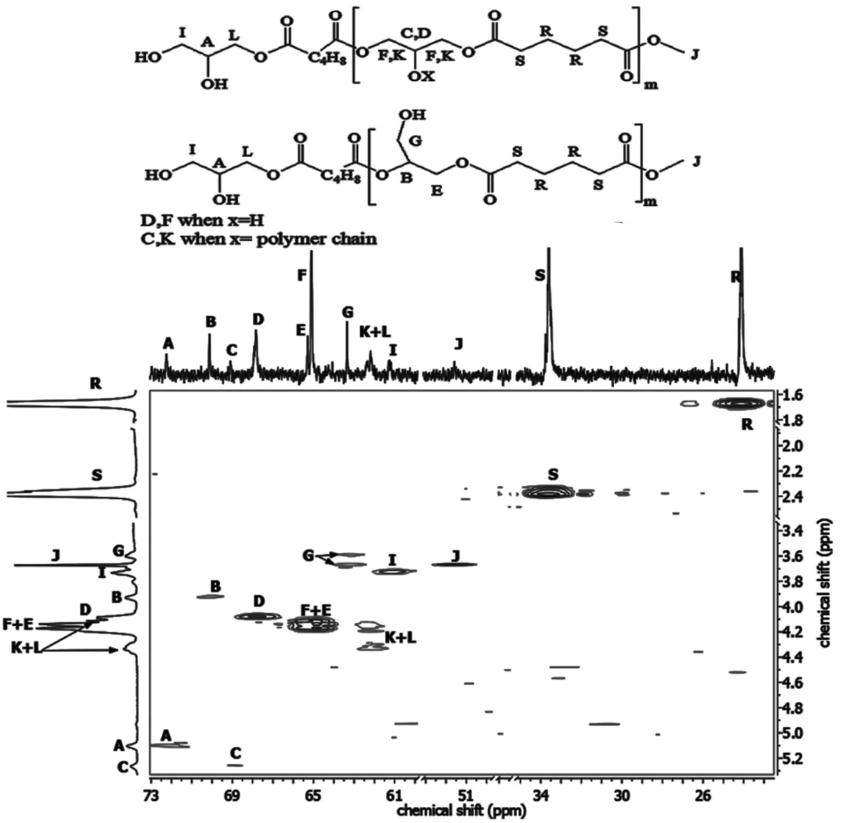


*Figure 3. $^{1}H$-$^{13}C$ COSY NMR spectrum of PGA measured in $CDCl_3$ at room temperature.*

## Temperature Dependence of Regioselectivity

Two enzymatic reactions are carried between divinyl adipate and glycerol but at different temperatures (60°C and 40°C) in order to investigate the influence of reaction temperature on the regioselectivity of the CAL-B. The corresponding $^{13}C$ NMR spectra of both reaction products are shown in Figure 4. The comparison between both spectra shows a complete disappearance of the peaks related to 1,2-disubstituted and 1,2,3-trisubstituted glycerides for the polymer synthesized at 40°C. This indicates a perfect regioselectivity of the enzyme at 40°C. These results match the results reported before for the enzymatic polymerization of divinyl sebacate with glycerol at different temperatures (*33*).


In Tailored Polymer Architectures for Pharmaceutical and Biomedical Applications; Scholz, C., et al.;
ACS Symposium Series; American Chemical Society: Washington, DC, 2013.

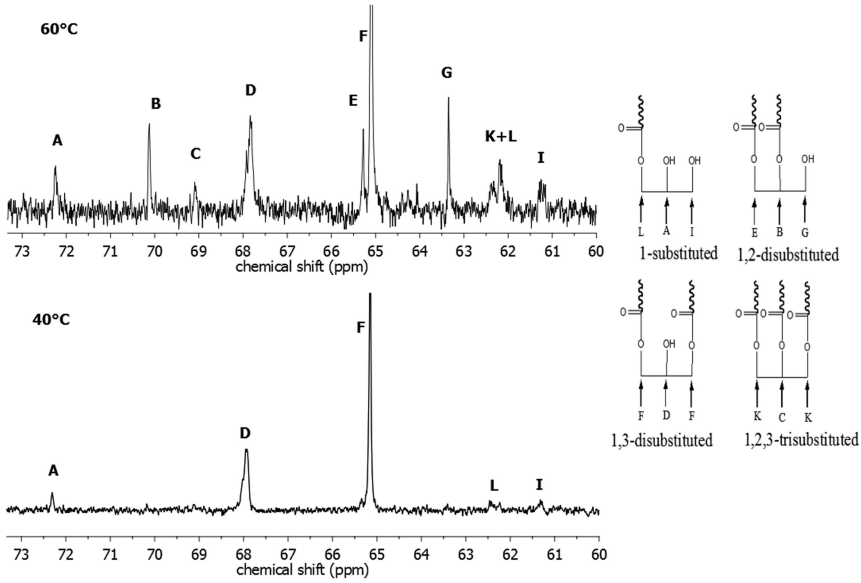


*Figure 4. Expanded $^{13}C$ NMR spectra of PGA obtained from glycerol and DVA in $CDCl_3$ at 40°C, and at 60°C.*

Downloaded by UNIV OF MICHIGAN ANN ARBOR on July 17, 2013 | http://pubs.acs.org
Publication Date (Web): July 8, 2013 | doi: 10.1021/bk-2013-1135.ch004

## DSC Measurements

Table II shows the results obtained by DSC. The PGA backbone is an amorphous polymer which means that the crystallization of the substituted polymer is related only to the alkyl side chains. The results reflect an increase of $T_m$ and $\Delta\widetilde{H}_m$ with increasing degree of substitution and with increasing length of alkyl side chains.

The increase of $T_m$ and $\Delta\widetilde{\boldsymbol{H}}_{\boldsymbol{m}}$ with increasing side chain length is mainly related to the thicker crystalline lamellae, which causes an increase of the energy required for melting the polymer (*34*). The decrease of $T_m$ with decreasing degree of substitution must be related to thinner or more imperfect crystals, whereas the decrease $\Delta\widetilde{\boldsymbol{H}}_{\boldsymbol{m}}$ indicates also a higher amount of amorphous alkyl chains. The results show also a decrease of the degree of crystallinity with decreasing degree of substitution. Nevertheless, the degree of crystallinity is always lower than the crystallinity of the free fatty with identical chain length alone.


In Tailored Polymer Architectures for Pharmaceutical and Biomedical Applications; Scholz, C., et al.;
ACS Symposium Series; American Chemical Society: Washington, DC, 2013.

## Thermogravimetry

The thermal decomposition temperatures of the stearic acid, PGA, S20, and S45 are investigated using thermo-gravimetric analyses in an air stream with a heating rate of 5°C/min. The results are shown in Figure 5. The comparison between the thermograms shows that the stability of S45 is higher than stearic acid or PGA. On the other hand, no big effect of substitution on the stability of the overall polymer is noticed in the case of S20 which has a low degree of substitution.

Downloaded by UNIV OF MICHIGAN ANN ARBOR on July 17, 2013 | http://pubs.acs.org
Publication Date (Web): July 8, 2013 | doi: 10.1021/bk-2013-1135.ch004

**Table II. Melting Temperature $T_m$, Crystallization Temperature $T_c$, Specific Enthalpy of Melting $\Delta\tilde{H}_m$, Degree of Crystallinity $X_{DSC}$**

| *Sample* | $T_m$ *[°C]* | $T_c$ *[°C]* | $\Delta\tilde{H}_m$ *[J/g]* | $X_{DSC}$ *[%]* |
|---|---|---|---|---|
| L30 | -37 | --[a] | 16.4 | 8.4 |
| L50 | -22 | -25 | 61.3 | 26.4 |
| L75 | -20.6 | -32 | 56.8 | 29.1 |
| Lauric acid | 45.3 | -41 | 195.2 | 100 |
| S8 | 29.1 | 21 | 34 | 14.6 |
| S20 | 33.9 | 29.7 | 29.9 | 12.8 |
| S45 | 36.9 | 35.4 | 100.7 | 43.2 |
| S65 | 39 | 36.9 | 159.7 | 68.5 |
| S85 | 38.7 | 34.8 | 162.9 | 69.9 |
| Stearic acid | 69.7 | 66.6 | 233 | 100 |
| B45 | 57.9 | 57.3 | 145.2 | 59.6 |
| B65 | 51.9 | 51.18 | 158.1 | 64.9 |
| Behenic acid | 80.1 | 76.1 | 243.7 | 100 |

[a] No DCS peak is present under the measurements conditions. The samples with oleic acid are amorphous.

## Transmission Electron Microscopy

It has been reported by Kallinteri et al. (*21*) that PGA substituted with stearoyl chains forms spherical nanoparticles. However, our investigation shows that the shape of these nanoparticles strongly depends on the degree of substitution. The cryo-TEM and negative stain-TEM images (Fig. 6a, 6b) show various non- spherical shapes of nanoparticles with linear boarders and defined geometries such as hexagons, pentagons, squares, and triangles.


In Tailored Polymer Architectures for Pharmaceutical and Biomedical Applications; Scholz, C., et al.;
ACS Symposium Series; American Chemical Society: Washington, DC, 2013.

Downloaded by UNIV OF MICHIGAN ANN ARBOR on July 17, 2013 | http://pubs.acs.org
Publication Date (Web): July 8, 2013 | doi: 10.1021/bk-2013-1135.ch004

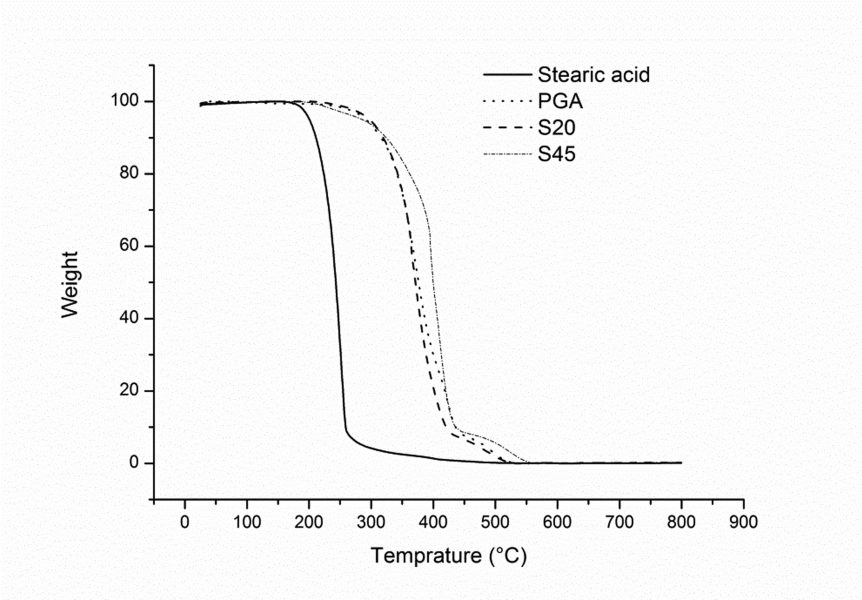


*Figure 5. Thermal gravimetric analysis (TGA) thermograms of stearic acid, PGA, S20, and S45 using a heating rate of 5 K/min in air.*

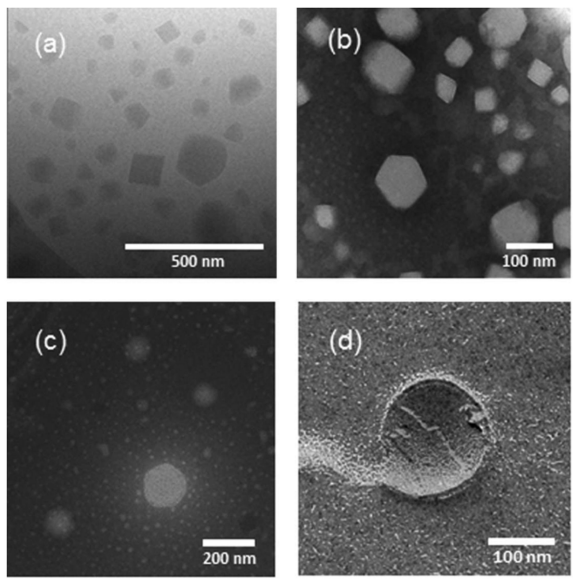


*Figure 6. (a) Cryo-TEM image of S20 nanoparticles prepared in aqueous suspension. (b) Negative-stain TEM of S20 nanoparticles. (c) Negative-stain TEM of O20 nanoparticles. (d) Internal structure of S85 nanoparticles after freeze fracture showing a layered morphology.*


In Tailored Polymer Architectures for Pharmaceutical and Biomedical Applications; Scholz, C., et al.;
ACS Symposium Series; American Chemical Society: Washington, DC, 2013.

Further investigations into these nanoparticles show the presence of well-ordered pseudo-hexagonal structures (*35*). A freeze fracture image of S85 (Fig. 6d) reveals the presence of internal lamellar structure inside the nanoparticles which is explained as onion-like morphology. Such onion structure is suggested to be as results of alternating crystalline and amorphous phases the nanoparticles (*35*). Finally, also the O20 sample shows phase separation between the polymer backbone and the side chains (Fig. 6c). This is surprising since the oleic acid side chains are not able to crystallize. Thus, it can be assumed that a liquid-liquid like phase separation takes place.

Downloaded by UNIV OF MICHIGAN ANN ARBOR on July 17, 2013 | http://pubs.acs.org
Publication Date (Web): July 8, 2013 | doi: 10.1021/bk-2013-1135.ch004

## Conclusion

This report describes the synthesis and characterization of poly(glycerol adipate) (PGA) and fatty acid modified poly(glycerol adipate). PGA is synthesized by enzymatic polymerization using glycerol and either divinyl adipate or dimethyl adipate. Methanol which is produced as a by-product during the enzymatic polymerization in the case of using DMA is removed by molecular sieves packed into a soxhlet extractor on the top of the reaction vessel. DMA shows a slower enzymatic polymerization rate compared with DVA. The regioselectivity of CAL-B is affected by reaction temperature. It has been found that branched PGAs are produced when the enzymatic polymerization is carried out at 60°C because of the regioselectivity imperfection of CAL-B at this temperature. On the other hand, linear PGA can be produced when the reaction is carried out at 40°C. Both $T_m$ and $\Delta\tilde{H}_m$ increase with increasing the ratio of substitution and/or with increasing the length of alkyl side chains. This is explained as a result of improvement of the compact packing of the complete comb-like polymers. Substitution is also found to increase the stability of the polymers against thermal decomposition. Transmission electron microscopy images of the nanoparticles depict shapes of the resulting nanoparticles depending on the degree of substitution. *S20* is found to form nanoparticles with straight boarders with polyhedral geometries whereas S85 forms onion-like spherical nanoparticles. These nanoparticles have potential applications in pharmacy caused by their biodegradability and biocompatibility (*36*).

## Acknowledgments

We gratefully acknowledge the Deutsche Forschungsgemeinschaft (DFG, SFB 418) for financial support.

## References

1. Shipley, G. G. In *Handbook of Lipid Research*; Small, D. M., Ed.; Plenum Press: New York, 1986; Vol. 4, Chapter 5, pp 123−129.
2. Lutton, E. S. *J. Am. Oil Chem. Soc.* **1972**, *49*, 1–9.
3. Zwierzykowski, W.; Orzecka, B.; Spich, K. *Tenside Deterg.* **1976**, *13*, 313–316.

Downloaded by UNIV OF MICHIGAN ANN ARBOR on July 17, 2013 | http://pubs.acs.org
Publication Date (Web): July 8, 2013 | doi: 10.1021/bk-2013-1135.ch004

4. Hong Qiu, H.; Caffrey, M. *Biomaterials* **2000**, *21*, 223–234.
5. Gustafsson, J.; Ljusberg-Wahren, H.; Almgren, M.; Larsson, K *Langmuir* **1997**, *13*, 6964–6971.
6. Rizwan, S. B.; Assmus, D.; Boehnke, A.; Hanley, T.; Boyd, B. J.; Rades, T.; Hook, S. *Eur. J. Pharm. Biopharm.* **2011**, *79*, 15–22.
7. Williams, C. K. *Chem. Soc. Rev.* **2007**, *36*, 1573–1580.
8. Rieger, J.; Van Butsele, K.; Lecomte, P.; Detrembleur, C.; Jérôme, R.; Jérôme, C. *Chem. Commun. (Cambridge, U. K.)* **2005**, 274–276.
9. Grignard, B.; Schmeits, S.; Riva, R.; Detrembleur, C.; Lecomte, P.; Jérôme, C. *Green Chem.* **2009**, *11*, 1525–1529.
10. Parrish, B.; Breitenkamp, R. B.; Emrick, T. *J. Am. Chem. Soc.* **2005**, *127*, 7404–7410.
11. Xu, N.; Wang, R.; Du, F.; Li, Z. *J. Polym. Sci., Part A: Polym. Chem.* **2009**, *47*, 3583–3594.
12. Naolou, T.; Busse, K.; Kressler, J. *Biomacromolecules* **2010**, *11*, 3660–3667.
13. Billiet, L.; Fournier, D.; Du Prez, F. *J. Polym. Sci., Part A: Polym. Chem.* **2008**, *46*, 6552–6564.
14. Hu, J.; Gao, W.; Kulshrestha, A.; Gross, R. A. *Macromolecules* **2006**, *39*, 6789–6792.
15. Gross, R. A.; Ganesh, M.; Lu, W. *Trends Biotechnol.* **2010**, *28*, 435–443.
16. Yang, Y.; Lu, W.; Cai, J.; Hou, Y.; Ouyang, S.; Xie, W.; Gross, R. A. *Macromolecules* **2011**, *44*, 1977–1985.
17. Kobayashi, S.; Makino, A. *Chem. Rev.* **2009**, *109*, 5288–5353.
18. Uyama, H.; Kobayashi, S. *Enzyme-Catalyzed Synthesis of Polymers*; Kobayashi, S., Ritter, H., Kaplan, D., Eds.; Springer-Verlag: Berlin/ Heidelberg, 2006; Vol. 194, p 133.
19. Kline, B. J.; Beckman, E. J.; Russell, A. J. *J. Am. Chem. Soc.* **1998**, *120*, 9475–9480.
20. Korupp, C.; Weberskirch, R.; Müller, J. J.; Liese, A.; Hilterhaus, L. *Org. Process Res. Dev.* **2010**, *14*, 1118–1124.
21. Kallinteri, P.; Higgins, S.; Hutcheon, G. A.; St Pourçain, C. B.; Garnett, M. C. *Biomacromolecules* **2005**, *6*, 1885–1894.
22. Meng, W.; Parker, T. L.; Kallinteri, P.; Walker, D. a; Higgins, S.; Hutcheon, G. a; Garnett, M. C. *J. Controlled Release* **2006**, *116*, 314–321.
23. Puri, S.; Kallinteri, P.; Higgins, S.; Hutcheon, G. A.; Garnett, M. C. *J. Controlled Release* **2008**, *125*, 59–67.
24. Meng, W.; Kallinteri, P.; Walker, D. a; Parker, T. L.; Garnett, M. C. *Exp. Biol. Med. (London, U. K.)* **2007**, *232*, 1100–1108.
25. Weiss, V. M.; Naolou, T.; Hause, G.; Kuntsche, J.; Kressler, J.; Mäder, K. *J. Controlled Release* **2012**, *158*, 156–164.
26. Brioude, M. D. M.; Guimarães, D. H.; Fiúza, R. D. P.; Prado, L. A. S. D. A.; Boaventura, J. S.; José, N. M. *Mater. Res.* **2007**, *10*, 335–339.
27. Ebata, H.; Toshima, K.; Matsumura, S. *Chem. Lett.* **2001**, 798–799.
28. Binns, F.; Roberts, S. M.; Taylor, A.; Williams, C. F. *J. Chem. Soc., Perkin Trans. 1* **1993**, 899.
29. Mezoul, G.; MARECHAL, E.; Brigodiot, M. *J. Polym. Sci., Part A: Polym. Chem.* **1995**, *33*, 2691–2698.

30. Trusek-Holownia, A.; Noworyta, A. *J. Biotechnol.* **2007**, *130*, 47–56.
31. Juais, D.; Naves, A. F.; Li, C.; Gross, R. a.; Catalani, L. H. *Macromolecules* **2010**, *43*, 10315–10319.
32. Uyama, H.; Inada, K.; Kobayashi, S. *Macromol. Rapid Commun.* **1999**, *20*, 171–174.
33. Uyama, H.; Inada, K.; Kobayashi, S. *Macromol. Biosci.* **2001**, *1*, 40–44.
34. Shi, H.; Zhao, Y.; Zhang, X.; Zhou, Y.; Xu, Y.; Zhou, S.; Wang, D.; Han, C. C.; Xu, D. *Polymer* **2004**, *45*, 6299–6307.
35. Weiss, V. M.; Naolou, T.; Amado, E.; Busse, K.; Mäder, K.; Kressler, J. *Macromol. Rapid Commun.* **2012**, *33*, 35–40.
36. Weiss, V. M.; Naolou, T.; Groth, T.; Kressler, J.; Mäder, K. *J. Appl. Biomater. Function. Mater.* **2012**, *10*, 163–169.

Downloaded by UNIV OF MICHIGAN ANN ARBOR on July 17, 2013 | http://pubs.acs.org
Publication Date (Web): July 8, 2013 | doi: 10.1021/bk-2013-1135.ch004

Downloaded by UNIV OF PITTSBURGH on July 20, 2013 | http://pubs.acs.org
Publication Date (Web): July 8, 2013 | doi: 10.1021/bk-2013-1135.ch005

## Chapter 5

# Poly(oxazoline) Block Copolymers for Biomedical Applications

**Michael J. Isaacman[1] and Luke Theogarajan[*,2]**

**[1]Department of Chemistry, University of California, Santa Barbara, Santa Barbara, California 93106**
**[2]Department of Electrical and Computer Engineering, University of California, Santa Barbara, Santa Barbara, California 93106**
**[*]E-mail: ltheogar@ece.ucsb.edu.**

Poly(oxazolines) have emerged as a viable alternative to poly(ethyleneglycol), as a polymer coating for therapeutic applications. In this chapter, we will outline some of the key features of poly(oxazoline), its synthesis and its use as a hydrophilic segment of an amphiphilic block copolymer. Both macrointiation based block copolymer synthesis and polymer-polymer conjugation by click chemistry will be discussed in the context of synthesizing these block copolymers. The self-assembling properties of these block copolymers are then discussed. We show that nanoscale vesicular topologies are readily formed by these polymers.

## Introduction and Motivation

Translation from the lab-bench to the bedside of effective therapies, especially against cancer, has proved enormously challenging (*1*). A key reason for this gap between the advances in our knowledge of cancer biology and effective outcome in the clinic can be mainly attributed to the ineffectiveness of the drug delivery techniques employed. For example, only 1-10 parts in a 100,000 of intravenously delivered monoclonal anti-bodies reach the intended target (*2*). The main challenges to effective targeted delivery are the biological and physiological barriers that need to be overcome (*3*). Accumulation of the drug in the desired tissue is achieved by most targeted therapies via antigen binding,

© 2013 American Chemical Society
In Tailored Polymer Architectures for Pharmaceutical and Biomedical Applications; Scholz, C., et al.; ACS Symposium Series; American Chemical Society: Washington, DC, 2013.

since molecular targets that are different between cancerous and normal tissue are hard to find. Liposomal delivery has been the main approach to overcoming some of the barriers. Liposomes that utilize antibody based targeting, termed immunoliposomes, have been moderately successful in pre-clinical (*4*).

The main challenge in using liposomes, apart from their poor scale-up, high-cost and short shelf-life, is that they are rapidly cleared by the reticulo-endothelial system (RES). High circulation times are essential for liposomes to effectively deliver their payload to targets such as tumors. Stealth properties that prevent rapid clearance by the RES can be imparted to liposomes by incorporating a small fraction (3-7 mol%) of lipids that have been conjugated to hydrophilic polymers. The increased circulation times are believed to be due to the increase in the hydrodynamic radius, thus avoiding renal clearance. For many decades, PEG has been the hydrophilic polymer of choice for biomedical conjugation (or PEGylation). One school of thought is that PEGylation of liposomes reduces surface opsonization by steric repulsion thus enabling macrophage resistance, though it is increasingly becoming clear that this is not the case (*5*). It seems a combination of effects such as limited concentration of opsonins in the blood; weak interaction, hydrophobic effects and favorable dysopsonin interaction with the polymer surface are responsible for the prolonged circulation times (*5*). Despite some commercial success PEGylation has its drawbacks. One major cause for concern is the so-called accelerated blood clearance (ABC) effect (*6*), where a second dose of PEGylated liposomes, administered within a few days, are rapidly cleared by the RES. It is believed that the complement activation by the serum proteins by the first dose is responsible for this effect (*7*), though an antibody activated pathway may also be at work (*8*, *9*). Irrespective of the exact mechanism, it is widely suspected that the type of surface presented to the cell by the liposome is largely responsible for the fate of the liposome *in-vivo* (*10*). Unfortunately, liposome surfaces are not easily amenable to manipulation since a delicate balance exists between the amounts of PEGylated (3-10 mol%) to non-PEGylated lipids (*11*).

Another polymer that has been investigated for drug delivery applications is Hydroxyethyl starch (HES), a polymer derived from the natural polymer amylopectin. HES found its main use as plasma volume substitute. Recently, it has been shown that conjugation of Hydroxyethyl starch (Hesylation) to proteins and drugs have been found to be more effective than the unconjugated versions of the drug (*31*). The main attribute that makes Hydroxyethyl starch useful is that it can degraded extracellularly by the plasmatic α–amylase (primary pathway) or intracellularly by α-glucosidase enzyme (*32*), enabling clearance through the renal pathway. The rate of clearance can be tailored via the amount of hyroxyethylation of the natural polymer. Hesylated drugs and proteins exhibit low immunogenicity, less interference with bindig sites *in-vitro* and exhibit low viscocity enabling high concentration formulations (*31*). Recently, it has been shown that by modification of HES, via esterification, with fatty acid chains such as lauric, stearic and palmitic acids, amphiphillic polymers that assemble into micelles and vesicles can be synthesized (*30*). Despite these advantages due to its highly branched nature, it is more difficult to synthesize polymers that exhibit a well-defined structure-function relationship.

Downloaded by UNIV OF PITTSBURGH on July 20, 2013 | http://pubs.acs.org
Publication Date (Web): July 8, 2013 | doi: 10.1021/bk-2013-1135.ch005


In Tailored Polymer Architectures for Pharmaceutical and Biomedical Applications; Scholz, C., et al.;
ACS Symposium Series; American Chemical Society: Washington, DC, 2013.

## ABA Self-Assembling Triblock Copolymers

Clearly, a targeted, tailored, cost-effective and versatile method for drug delivery is needed. Rather than use the problematic lipid-centric approach, a modular polymer-centric approach would be preferable. The membrane of the vesicle will then be composed of a triblock copolymer that mimics the lipid-bilayer, transforming the liposome into a polymersome. The triblock comprises of a hydrophobic siloxane block flanked by two hydrophilic polymethyloxazoline blocks, an approach originally pioneered by Meier and co-workers (*15*). Polyoxazolines display the same "stealth" behavior like PEG without its adverse biological side-effects (*12*, *13*). Since the packing density of the hydrophilic polymer is extremely high, the polymersome has an intrinsic advantage over PEGylated-lipid containing liposomes. The ease of tailoring the properties of the polymer makes it more attractive than HESylation. Additionally, we have extended the above concept to enable functionalization of the hydrophobic block (*22*). This allows for either tuning of the self-assembling properties or enabling a prodrug strategy. In the next few sections we will briefly review the polymerization of the individual blocks and then synthesis of the ABA triblock copolymer, followed by its self-assembly properties.

Downloaded by UNIV OF PITTSBURGH on July 20, 2013 | http://pubs.acs.org
Publication Date (Web): July 8, 2013 | doi: 10.1021/bk-2013-1135.ch005

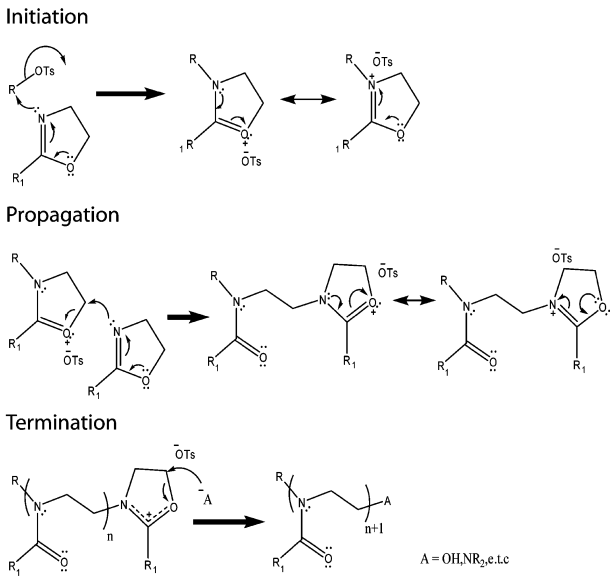


*Figure 1. Mechanism of cationic ring-opening polymerization of 2-oxazolines. R can either be a small molecule such as propargyl or a macromolecule. $R_1$ is an alkyl substituent, such as methyl, ethyl or phenyl, on the oxazoline monomer and OTs is the Tosylate leaving group.*


In Tailored Polymer Architectures for Pharmaceutical and Biomedical Applications; Scholz, C., et al.;
ACS Symposium Series; American Chemical Society: Washington, DC, 2013.

## Cationic Ring Opening Polymerization of Polyoxazolines

Oxazolines belong to the class of endocyclic imino ethers susceptible to ring-opening isomerization polymerization. The polymerization of oxazolines are initiated by electrophilic species like protic acids, alkyl sulfonates like triflates and tosylates and aklyl halides and hence it is also called electrophilic polymerization. The mechanism of polymerization is shown in Figure 1. Depending on the nature of the initiator the propagation can proceed through an ionic species or a covalent species or in some cases both. The stability of the propagating species makes the nature of the polymerization living under appropriate conditions, 2-oxazolines can be unsubstituted or substituted and the nature of the substituent determines much of the properties of the polymeric block. If the substituent is methyl or ethyl the block is hydrophillic and bulkier substituents make it hydrophobic. The living nature of the polymerization makes it possible to terminate the polymerization with functional groups yielding macroinitiators and telechelics. One very useful end group is the acrylate group, which can be conveniently introduced by terminating the reaction with acrylic acid in an appropriate base like triethylamine or 2,6-lutidine. The carboxylate being nucleophilic enough to terminate the polymerization yielding post-polymerizable acrylate end-groups. Recently, Hoogenboom *et. al*. (*14*) have shown that under microwave irradiation conditions oxazolines bearing pendant alkyl groups can be readily polymerized.

## Polysiloxanes as Hydrophobic Cores

Polysiloxanes are generally prepared from cyclic monomers by ring opening polymerization using an acid catalyst (cationic) or base (anionic) initiator. Though the Si-O bond is highly stable under neutral conditions it is readily cleaved in highly acidic or basic conditions. Siloxane bonds are constantly broken and reformed in both anionic and cationic polymerizations, leading to both linear and cyclic species being formed until the reaction reaches a thermodynamic equilibrium. Hence, this polymerization is often termed an equilibration or redistribution polymerization. However in anionic ring-opening, the beginning of the reaction is most probably a kinetically controlled process and only in the later stages does the equilibration process take over. To obtain high molecular weights with low polydispersity careful time-controlled quenching of the reaction mixture is necessary. The main advantage of anionic polymerization is that it can be used to polymerize cycles that contain bulky side groups like phenyls that cannot proceed via equilibrium polymerization. However, anionic polymerization requires strained cycosiloxane rings such as trisiloxanes. Cationic polymerization, is poorly understood and the current state of understanding is that the acid catalyzes the ring-opening in the initiation step and continues to catlyze the reaction via the silyl ester that is formed via the condensation of the silanol group and the counterion. The other mechanism that is thought to be active in the propagation step is the conversion of the sianol end-group to a leaving group (water) by the acid catalyst. Unlike the Si-O bond the Si-C bond is stable under these reaction conditions and if molecules containing Si-C bonds are present, they will terminate the growing chain and serve as the end-blocker (*17*).


In Tailored Polymer Architectures for Pharmaceutical and Biomedical Applications; Scholz, C., et al.;
ACS Symposium Series; American Chemical Society: Washington, DC, 2013.

Downloaded by UNIV OF PITTSBURGH on July 20, 2013 | http://pubs.acs.org
Publication Date (Web): July 8, 2013 | doi: 10.1021/bk-2013-1135.ch005

The remaining cyclic non-functional side products can be removed by vacuum distillation or precipitation. If the end-blocker is a siloxane dimer it will yield bifunctional siloxane telechelics and simultaneously provide a method for the control of the molecular weight.

## Polyoxazoline Containing Triblock Block Copolymers

### Triblock Synthesis by Macroinitation

Previously reported syntheses of non-functionalized poly(siloxane)-b-poly(oxazoline) triblock copolymers relied on one of two major strategies. One approach is to convert a commercially available α,ω-bishydroxy-poly(dimethylsiloxane) into a macroinitator by converting the hydroxyl group into a trifluoromethanesulfonic acid ester (triflate) (*15*), that initiate the ring-opening polymerization of 2-methyl-2-oxazoline. The second approach is to synthesize the poly(siloxane) with reactive end-groups, namely benzyl chloride, and use those as a macroinitiator for the ring-opening polymerization of 2-ethyl-2-oxazoline with Sodium iodide as catalyst (*16*). Another approach to the synthesis of a diblock copolymer that merits attention is based upon the hydrosilylation of a SiH-terminated poly(dimethylsiloxane) with allyl alcohol. The hydroxyl end group thus obtained is converted into a tosylate (*17*) and used as the macroinitiator as in the syntheses described above. The central theme of all the reported syntheses has been to generate a macrointiator capable of initiating the ring-opening polymerization of oxazolines. A wide variety of intiators have been reported of which the triflates are the most effective since they are highly electrophilic (*18*). However, triflates are generally less air and moisture stable, requiring very careful handling. The approach of using chlorides was also not very attractive since it needed fairly high temperatures (130°C) and the use of iodide as a catalyst can cause unwanted side reactions in the functional groups. Tosylates offer a good balance between the required leaving group ability, tolerance to other functional groups and stability.

Functionalization of the hydrophobic core requires a copolymer of dimethylsiloxane and methylhydrosiloxane, P(DMS-co-MHS. Therefore reported schemes like the one mentioned earlier (*17*) cannot be used since it involves a hydrosilylation step. Also, post derivatization of a hydroxyl end-group is not attractive since the termination may neither be quantitative or bi-functional, and may lead to very tedious work-up strategies to isolate the bifunctional tosylates. Additionally, hydroxybutyl and hydroxypropyl terminated polysiloxanes degrade upon heating, through the loss of the end-groups (*20*). Recently, we reported (*22*) a novel and facile route to synthesizing quantitatively terminated bifunctional P(DMS-co-MHS) tosylated telechelics, which is a modification of a reaction reported by Yilgor et al. (*16*, *19*).

Triblock copolymers were synthesized by cationic ring opening polymerization of 2-methyl-2-oxazoline using the bistosylate terminated siloxane telechelics as a macroinitiator. As in the telechelic synthesis, reaction conditions were first determined using the PDMS homopolymer. The reaction scheme (Generation I) is shown in Figure 2 along with the $^{1}$H NMR spectrum of the


In Tailored Polymer Architectures for Pharmaceutical and Biomedical Applications; Scholz, C., et al.;
ACS Symposium Series; American Chemical Society: Washington, DC, 2013.

Downloaded by UNIV OF PITTSBURGH on July 20, 2013 | http://pubs.acs.org
Publication Date (Web): July 8, 2013 | doi: 10.1021/bk-2013-1135.ch005

triblock copolymer. The spectrum exhibits the classical polyoxazoline segment peaks of the side chain methyl protons between 2. 0 and 2.3 ppm, and the protons connected to the nitrogen appear at 3.3-3.5 ppm. Similarly, triblock copolymers were formed when P(DMS-co-HMS) was used as macroinitiator, Figure 2, Generation II. The $^1$H NMR spectrum verifies the structure of the triblock copolymer, clearly indicating the presence of the poly(oxazoline), Si-CH3, and Si-H moieties. The presence of the fairly reactive Si-H groups does not seem to hinder the block polymerization under the reaction conditions used.

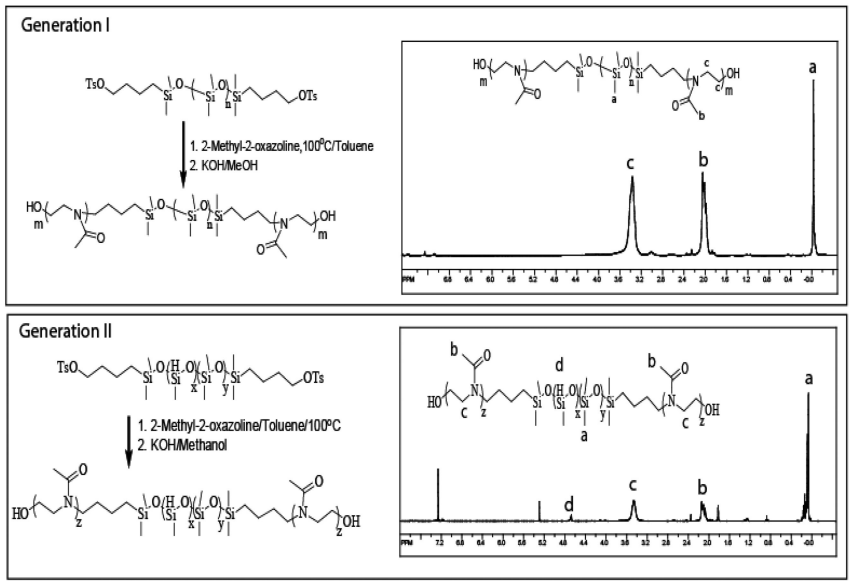


*Figure 2. Generation I was used as a proof of concept to verify the synthetic scheme of using a tosylate terminated polysiloxane as a macroinitiator for the ring opening polymerization of 2-methyl-2-oxazoline. The $^1$H NMR spectrum shows the classical polyoxazoline peaks and are indicated as peaks b and c. Generation II was designed so that the polymeric backbone could be derivatized with functional molecules via the hydrosilylation reaction. The Si-H peak d at 4.7 ppm clearly indicate that under the reactions conditions the Si-H protons do no hinder the polymerization. (Reprinted with permission from Ref. (22), Copyright 2008 John Wiley & Sons.)*

The triblock copolymers described above with the methylhydrosiloxane moieties containing B-block were further derivatized via a hydrosilylation reaction. The effect of the reaction order was investigated by either (i) first forming the triblock copolymers followed by the hydrosilylation reaction, and (ii) the hydrosilylation was conducted first, followed by the ring-opening polymerization


In Tailored Polymer Architectures for Pharmaceutical and Biomedical Applications; Scholz, C., et al.;
ACS Symposium Series; American Chemical Society: Washington, DC, 2013.

Downloaded by UNIV OF PITTSBURGH on July 20, 2013 | http://pubs.acs.org
Publication Date (Web): July 8, 2013 | doi: 10.1021/bk-2013-1135.ch005

of 2-methyl-2-oxazoline. It was discovered that the hydrosilylation reaction, that is the attachment of the tethered supramolecules to the P(DMS-co-HMS) block, needs to be conducted prior to the block copolymer formation with 2-methyl-2-oxazoline (i.e. option (ii)). Reactions in which the triblock copolymer was formed first, option (i), and the side-chain moieties were tethered later met with failure. We believe this is due to the interaction of the platinum metal catalyst with the poly(oxazoline) block. We have not investigated the use of platinum catalyst's other than Kardsedt's catalyst since it is the most widely used and gentle method of hydrosilylation. Hence, the reaction scheme was modified so that after the copolymerization of D4 and D4H, a hydrosilylation reaction was performed yielding a P(DMS-co-HMS) copolymer derivatized with an appropriate side-chain, see Figure 3, Generation III.

Downloaded by UNIV OF PITTSBURGH on July 20, 2013 | http://pubs.acs.org
Publication Date (Web): July 8, 2013 | doi: 10.1021/bk-2013-1135.ch005

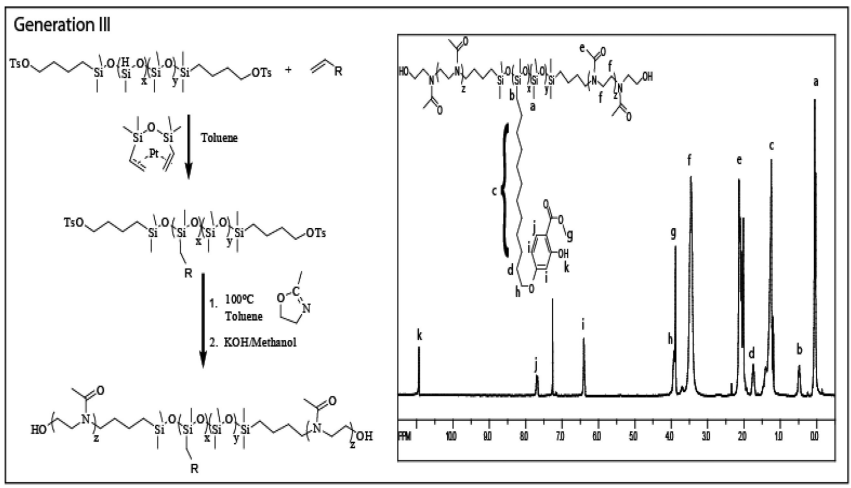


*Figure 3. Generation III shows a modification to the earlier scheme to yield a functionalized triblock copolymer. Here the backbone was first derivatized and then used as a macroinitiator for the ring opening polymerization of 2-methyl-2-oxazoline. As evidenced by the $^{1}H$ NMR spectrum this route is successful and is the preferred route for the synthesis of functionalized triblock co-polymers. (Reprinted with permission from Ref. (22), Copyright 2008 John Wiley & Sons.)*

## Triblock Formation via Click Chemistry

Recently, click chemistry has found considerable use in polymer-polymer conjugation via the copper-catalyzed azide-alkyne cycloaddtion (CuAAC) reaction (*33–35*). Click-based conjugation allows for the modular synthesis of block copolymer architectures with well-defined block lengths and end-groups.


In Tailored Polymer Architectures for Pharmaceutical and Biomedical Applications; Scholz, C., et al.;
ACS Symposium Series; American Chemical Society: Washington, DC, 2013.

The basic idea of the approach is shown in Figure 4. This allows for systematic investigation of the effect of a single parameter variation on the self-assembling properties of the macromolecular system. For example, by using individually well-characterized hydrophobic and hydrophilic blocks, the effect of the hydrophilic block length on the self-assembling properties could be studied. This exquisite level of control allows for sophisticated scientific exploration and will enable the understanding of the underlying structure-function relationships that influence the physics of self-assembly in these macromolecules.

Downloaded by UNIV OF PITTSBURGH on July 20, 2013 | http://pubs.acs.org
Publication Date (Web): July 8, 2013 | doi: 10.1021/bk-2013-1135.ch005

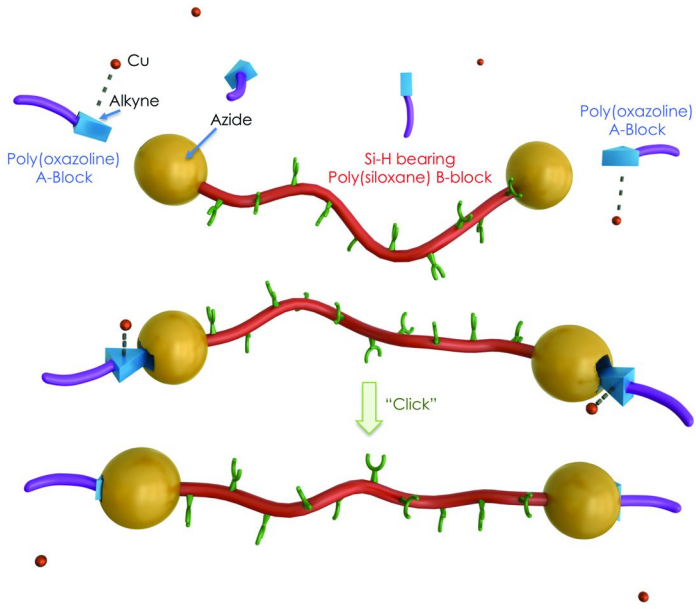


*Figure 4. Schematic view of our click-based triblock copolymer synthesis. (Reprinted with permission from Ref. (21), Copyright 2012 John Wiley & Sons.)*

Poly(siloxane)s were converted into clickable partners for the alkyne-functionalized poly(oxazoline) A-blocks by conversion of the iodide or tosylate end groups into azides, using sodium azide. We found that while tosylate end-groups can be converted into azides under mild heating, this was not suitable for Si-H bearing copolymers. To circumvent this we used an iodide end-blocker that could be converted to an azide at room-temperature and was tolerant to the Si-H groups in the copolymer. The hydrophilic PMOXA A-block was synthesized via CROP using a propargyl tosylate initiator, which ensured terminal alkyne functionality on one end of the polymer.

Downloaded by UNIV OF PITTSBURGH on July 20, 2013 | http://pubs.acs.org
Publication Date (Web): July 8, 2013 | doi: 10.1021/bk-2013-1135.ch005



**Table 1. Copper-Catalyzed Alkyne-Azide Cycloaddition Methodology**

| *No.* | *Poly(siloxane) B-block* | *Copper Source* | *Solvent* | *Time (hours)* | *Result* | *Product* |
|---|---|---|---|---|---|---|
| **1** | $N_3$-PDMS-$N_3$ | Cu/Asc | $H_2O$/THF | 12 | <60% Conversion | **10** |
| **2** | $N_3$-PDMS-$N_3$ | Cu/Asc | EtOH | 2 | Quantitative Conversion | **10** |
| **3** | $N_3$-PDMS-$N_3$ | $CuSO_4$ | EtOH | 15 | Quantitative Conversion | **10** |
| **4** | $N_3$-PDMS-$N_3$ | CuBr/PMDETA | PhMe/DMF | 1 | Quantitative Conversion | **10** |
| **5** | $N_3$-PDMS-$N_3$ | CuNPs | EtOH | 2 | Quantitative Conversion | **10** |
| **6** | $N_3$-P(DMS-*co*-PHS)-$N_3$ | Cu/Asc | $H_2O$/THF | 2 | Insoluble Gel Produced | **11** |
| **7** | $N_3$-P(DMS-*co*-PHS)-$N_3$ | CuNPs no EDTA | EtOH | 2 | Si-H Peak Perturbed | **11** |
| **8** | $N_3$-P(DMS-*co*-PHS)-$N_3$ | CuNPs with EDTA | EtOH | 2 | Quantitative Conversion | **11** |

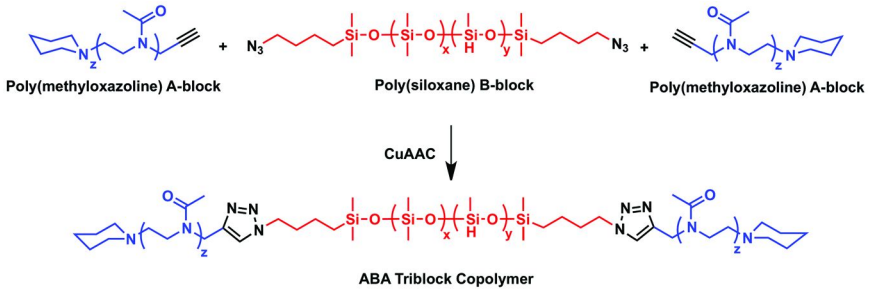


*Figure 5. Synthesis of ABA triblock copolymer from alkyne-functionalized poly(oxazoline) A-block and bis-azide poly(siloxane) B-block homopolymers via copper-catalyzed alkyne-azide cycloaddtion reaction. (Reprinted with permission from Ref. (21), Copyright 2012 John Wiley & Sons.)*

Downloaded by UNIV OF PITTSBURGH on July 20, 2013 | http://pubs.acs.org
Publication Date (Web): July 8, 2013 | doi: 10.1021/bk-2013-1135.ch005

Polymer-polymer conjugation of amphiphilic blocks is especially challenging due to the inherent incompatibility of the blocks. We explored several popular CuAAC methods including Copper(I) salt with an amine ligand, Copper(II) salt in conjunction with a reducing agent, and a heterogeneous coupling catalyst, namely copper nanoparticles, see Figure 5. The results of all methods studied are shown in Table 1.

Click reactions with polymer applications frequently employ CuBr/PMDETA as the catalyst (*23*) thus we attempted to conjugate homopolymers PMOXA and $N_3$-PDMS-$N_3$ using this catalytic method. Although tetrahydrofuran and dimethylformamide are frequently used solvents, we found the toulene:dimethylformamide v/v 1:1 solvent system was most effective since toluene is a θ solvent for siloxanes (*24*). Many CuAAC reactions are known to proceed at room temperature, however full conjugation did not occur at room temperature-even after 2 days. Thus heat was required to drive the reaction to completion. Quantitative conversion occurred after 1h using 1 equivalent of $N_3$-PDMS-$N_3$ and 2 equivalents of PMOXA, circumventing the need for an excess of either block. Although conversion was quantitative and rapid, the reaction yielded a dark-green product due to the presence of copper, which was rather difficult to purify. Removal of copper contaminate from PMOXA-PDMS-PMOXA was challenging for two reasons. Firstly, the polyamide functionality of PMOXA can chelate copper, making its disassociation from the polyamide difficult. Secondly, any attempt to remove copper in a solvent that does not solubilize both blocks can cause polymer aggregation, allowing the copper to be "hidden" in the polymer aggregate. Efficient copper removal from CuBr/PMDETA click reactions proved unsuccessful-even after purification steps such as EDTA (aq) wash, solvent precipitation, soxhlet extraction, silica chromatography, alumina chromatography, or the use of Dowex M4195 chelating resin (*25*). Sodium sulfide has been used for removal of copper from amine groups (*26*), owing to the insoluble copper sulfide salt that is formed. When 1 equivalent (to copper) of 1M $Na_2S$ (aq) was added to a solution of


In Tailored Polymer Architectures for Pharmaceutical and Biomedical Applications; Scholz, C., et al.;
ACS Symposium Series; American Chemical Society: Washington, DC, 2013.

copper-contaminated triblock in dichloromethane, a brown solution immediately formed along with the insoluble copper sulfide, which was removed by filtration. Although copper was successfully removed using this method, the product was pale orange, indicating the presence of trace amounts of sulfur.

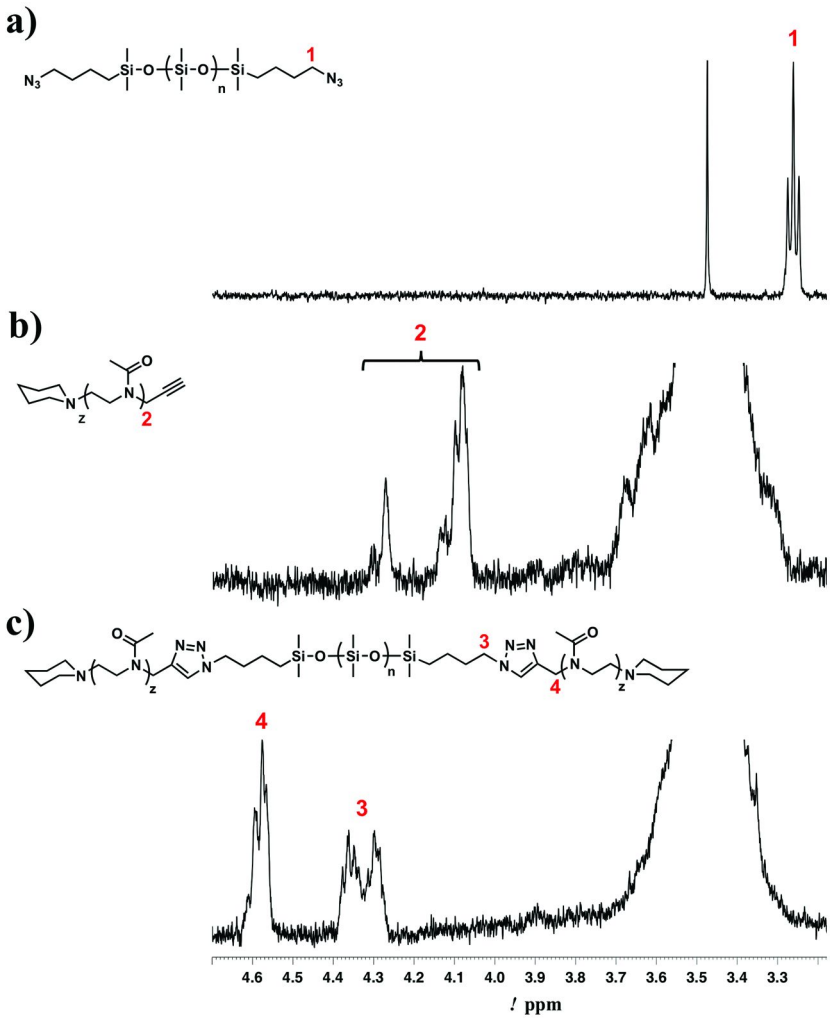


*Figure 6. $^1$H NMR spectra of $N_3$-PDMS-$N_3$, **6** (a), PMOXA, **9** (b), and CuAAC product PMOXA-PDMS-PMOXA, **10** (c). The disappearance of azide and alkyne peaks along with the appearance of triazole peaks indicated quantitative conversion to the triazole click product. (Reprinted with permission from Ref. (21), Copyright 2012 John Wiley & Sons.)*


In Tailored Polymer Architectures for Pharmaceutical and Biomedical Applications; Scholz, C., et al.; ACS Symposium Series; American Chemical Society: Washington, DC, 2013.

Downloaded by UNIV OF PITTSBURGH on July 20, 2013 | http://pubs.acs.org
Publication Date (Web): July 8, 2013 | doi: 10.1021/bk-2013-1135.ch005

Both PDMS (*27*) and PMOXA (*28*) have been used successfully in CuAAC reactions using the $CuSO_4$/sodium L-ascorbate (Cu/Asc) method, leading us to consider it for PMOXA-PDMS-PMOXA triblock synthesis. Most conditions involve a binary solvent system that includes water, which serves to solubilize Cu/Asc. All attempts to synthesize the triblock using an aqueous-based binary solvent system were met with moderate conversion <60%. We reasoned that the extreme hydrophobicity of poly(siloxane) causes self-aggregation in the presence of water, thus hiding the azide end-groups and preventing the reaction from proceeding to completion. We therefore attempted the CuAAC reaction in ethanol, which has the ability to solubilize both blocks, minimizing self-aggregation. Despite the heterogeneous nature of Cu/Asc in ethanol, the CuAAC reaction occurred quantitatively in 2h at 60°C. Furthermore, the product can be isolated by simple filtration, albeit the triblock polymer was yellow/green - indicating the presence of trace amounts of copper. When $CuSO_4$ was used as the catalyst, in the absence of sodium L-ascorbate reducing agent, the reaction proceeded to 50% completion after 2 hours, and quantitative completion in 15h at 60°C. This reaction was also successful when acetone, 2-propanol, or chloroform was used as the solvent system.

The heterogeneous nature of Cu/Asc in ethanol led us to attempt our conjugation reactions using copper nanoparticles (CuNPs), owing to their use in the synthesis of block copolymers (*29*). When the CuAAC reaction was conducted using CuNPs in ethanol with 1 equivalent of $N_3$-PDMS-$N_3$ and 2 equivalents of PMOXA at 60°C, $^1$H NMR spectroscopy revealed quantitative conjugation after 2h, as shown in Figure 6. Furthermore, after removal of the CuNPs via filtration, triblock copolymer was obtained as a beige solid, unlike the yellow, green or blue products of previous methods, indicating negligible copper contamination.

In all of our triblock preparations, the proof of triblock rather than a diblock formation was gleaned by carefully comparing the integration of the Si-$CH_3$ protons of the poly(siloxane)s block to the N-$CH_2$-$CH_2$ and O=C-$CH_3$ protons of the poly(oxazoline) block using $^1$H NMR spectroscopy. The integration of the Si-CH3 protons in the triblock were set to the value obtained for the poly(siloxane) homopolymer and the resulting value of the poly(oxazoline) protons in the triblock integrated to twice the value (within experimental error) of that obtained from the poly(oxazoline) homopolymer. This clearly indicates triblock formation and further lends credence to power of the modular approach. Such characterization is not trivial, since in a macrointiation method it could always be argued that the hydrophilic block is just longer than anticipated. Furthermore, the amphiphilic nature of these polymers does not allow for corroboration using classical characterization techniques such as GPC due to aggregation in the column. This coupled with the excellent PDI of the poly(oxazoline), obtained due to the modular synthesis, makes the click-based approach very attractive for synthesizing this family of triblock polymers.

Downloaded by UNIV OF PITTSBURGH on July 20, 2013 | http://pubs.acs.org
Publication Date (Web): July 8, 2013 | doi: 10.1021/bk-2013-1135.ch005


In Tailored Polymer Architectures for Pharmaceutical and Biomedical Applications; Scholz, C., et al.;
ACS Symposium Series; American Chemical Society: Washington, DC, 2013.

## Self-Assembly of Triblock Copolymer

### Large Unilamellar Vesicles

Though the self assembling properties of poly(oxazoline-co-polysiloxane) triblock copolymers have been established (*15*), the self-assembly properties of copolymers with Si-H repeat units or copolymers with long side chains have not yet been demonstrated.

In order to ensure that the synthesized copolymers retain their self-assembling properties, copolymers were assembled into vesicular structures before and after derivatizations. Electroformation was chosen, since this method yields large-sized vesicles that can be readily imaged using conventional light microscopy. The resulting vesicles are shown in Figure 7.

Downloaded by UNIV OF PITTSBURGH on July 20, 2013 | http://pubs.acs.org
Publication Date (Web): July 8, 2013 | doi: 10.1021/bk-2013-1135.ch005

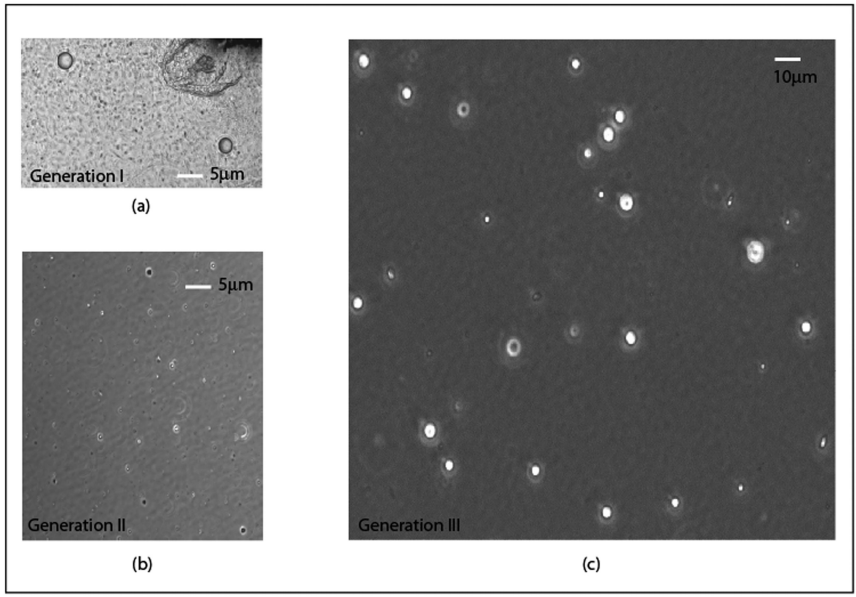


*Figure 7. Vesicles are in the range of 1-5µm. The size distribution correlates with the backbone lipophlicity. a) Vesicles of size between 2-3µm formed by co-polymers that have a polydimethylsiloxane hydrophobic core. b) Vesicles of size between 1-2µm by co-polymers that have a poly(dimethylsiloxane-co-methylhydrosiloxane hydrophobic core. c) Vesicles of size between 3-5µm formed by co-polymers that have a methyl (2-hydroxy, 4-undeceneloxy) benzoate derivatized siloxane hydrophobic block. (Reprinted with permission from Ref. (22), Copyright 2008 John Wiley & Sons.)*

Vesicle size is determined by the composition of the main chain as well as by the nature of the side chains. Conventional triblock copolymers (Generation I) form vesicles, 2-3µm in diameter. Converting the B-block into a random


In Tailored Polymer Architectures for Pharmaceutical and Biomedical Applications; Scholz, C., et al.;
ACS Symposium Series; American Chemical Society: Washington, DC, 2013.

copolymer of dimethylsiloxane and hydroxymethyl siloxane results in smaller sized vesicles with a diameter between 1-2 μm, which is believed due to the increased polar character of Si-H bond. This hypothesis is further validated by the fact that the vesicles formed by the copolymers containing the lipophilic 2-hydroxy, 4 undecenyloxy-methyl-benzoate forms larger sized vesicles, with diameters between 2-5 μm.

**Nanoscale Vesicles**

The ability of amphiphilic ABA triblock copolymers to self-assemble into higher architectures at the nanoscale is well known (*15*), thus vesicles of PMOXA-PDMS-PMOXA were prepared by an ethanol injection method.7 Briefly, an ethanolic solution of the triblock was dropped into water under vigorous stirring and then filtered through a 200nm filter. Vesicle size in solution was determined using dynamic light scattering (DLS), which revealed the hydrodynamic diameter of these vesicles to be 80 nm. Vesicles were also imaged using transmission electron microscopy (TEM) and shown to posses an average diameter of 150 nm (Figure 8). The flattening of the vesicles under drying accounts for the larger vesicle size observed with TEM.

Downloaded by UNIV OF PITTSBURGH on July 20, 2013 | http://pubs.acs.org
Publication Date (Web): July 8, 2013 | doi: 10.1021/bk-2013-1135.ch005

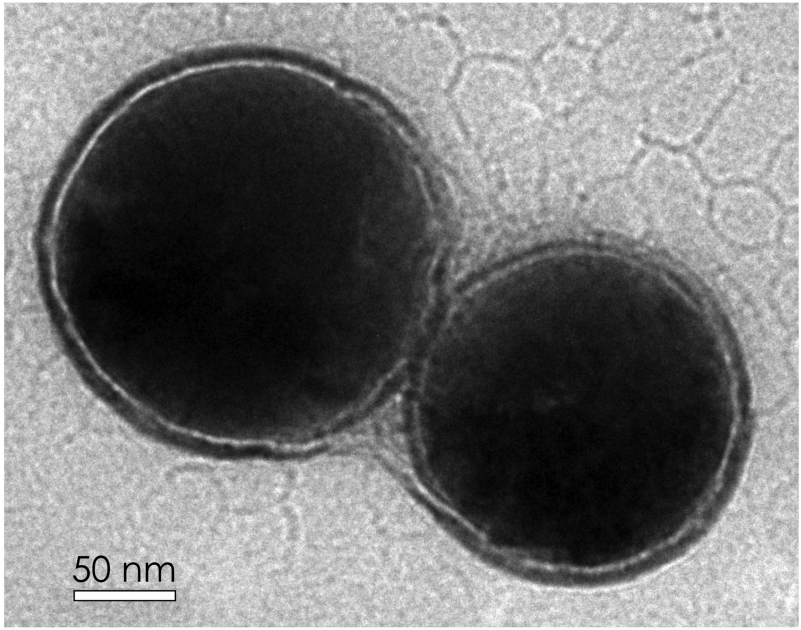


*Figure 8. Transmission electron micrograph of PMOXA-PDMS-PMOXA triblock copolymer vesicles showing the self-assembling nature of these amphiphilic copolymers. (Reprinted with permission from Ref. (21), Copyright 2012 John Wiley & Sons.)*


In Tailored Polymer Architectures for Pharmaceutical and Biomedical Applications; Scholz, C., et al.;
ACS Symposium Series; American Chemical Society: Washington, DC, 2013.

## Outlook and Conclusions

Polyoxazolines are emerging as viable alternative to PEG and are uniquely suited to the synthesis of block copolymers either via macroinitiation or click chemistry. We have present a novel and facile route to synthesizing, both functionalized and non-functionalized self-assembling triblock. Furthermore, a derivatized siloxane with pendant side groups still retains its macrointiating ability. We have also demonstrated a versatile yet facile method for synthesizing amphiphilic triblock copolymers using click chemistry. We have presented a matrix of conditions under which such polymers can be synthesized, the optimal method being that which uses copper nanoparticles. We believe that the modular synthesis of these polymers will allow for systematic investigation of the their structure-function relationships. The poly(oxazoline)-poly(siloxane)-poly(oxazoline) ABA blocks can self-assemble into vesicles under appropriate conditions. The synthesized triblocks have been electroformed into vesicles. Vesicle size seems to correlate with side chain lipophilicity. Side chain receptor density does not seem to affect the self-assembling properties of these polymeric membranes. These polymers are ideal systems for biomedical applications such as drug-delivery and synthetic lipid bilayers for ion-channel studies. Furthermore, we have shown that polymers with the Si-H functionality in the middle block that allows for further functionality via a hydrosilylation reaction. We are currently exploring the functionalization of these polymers and their use in bioengineering and medicine.

Downloaded by UNIV OF PITTSBURGH on July 20, 2013 | http://pubs.acs.org
Publication Date (Web): July 8, 2013 | doi: 10.1021/bk-2013-1135.ch005

## References

1. Ferrari, M. *Nat. Rev. Cancer* **2005**, *5* (3), 161–17103.
2. Li, K.; Pandit, S.; Samira Guccione, S.; Bednarski, M. *Biomed. Microdevices* **2004**, *6* (2), 113–116.
3. Jain, R. *Cancer Res.* **1990**, *50*, 814–819.
4. Torchilin, V. *Nat. Rev. Drug Discovery* **2005**, *4* (2), 145–160.
5. Xuedong Yan, X.; Gerrit L. Scherphof, G.; Jan A. A. M. Kamps, J. *J. Liposome Res.* **2005**, *15* (1-2), 109–139.
6. Ishida, T.; Harada, M.; Wang, X.; Ichihara, M.; Irimura, K.; Kiwada, H. *J. Controlled Release* **2005**, *105* (3), 305–317.
7. Dams, E.; Peter Laverman, P.; Oyen, W.; Storm, G.; Scherphof, G.; van der Meer, J.; Corstens, F.; Boerman, O. C. *J. Pharmacol. Exp. Ther.* **2000**, *292* (3), 1071–1079.
8. Ishida, T.; Kiwada, H. *Int. J. Pharm.* **2008**, *354* (1-2), 56–62.
9. Sroda, K.; Rydlewski, J.; Langner, M.; Kozubek, K.; Grybek, M.; Sikorsi, A. *Cell. Mol. Biol. Lett.* **2005**, *10*, 3747.
10. Moghimi, S. M.; Szebeni, J. *Prog. Lipid Res.* **2003**, *42* (6), 463–478.
11. Bedu-Addo, K.; Tang, P.; Xu, Y.; Huang, L. *Pharm. Res.* **1996**, *13*, 710–717.
12. Viegas, T.; Bentley, M.; Harris, J.; Fang, Z.; Yoon, K.; Dizman, B.; Weimer, R.; Mero, A.; Pasut, G.; Veronese, F. *Bioconjugate Chem.* **2011**, *22* (5), 976–986.


In Tailored Polymer Architectures for Pharmaceutical and Biomedical Applications; Scholz, C., et al.;
ACS Symposium Series; American Chemical Society: Washington, DC, 2013.

13. Zalipsky, S.; Hansen, C.; Oaks, J.; Allen, T. *J. Pharm. Sci.* **1996**, *85* (2), 133–137.
14. Hoogenboom, R.; Wiesbrock, F.; Huang, H.; Leenen, M. A. M.; Thijs, H. M. L.; Van Nispen, S. F. G. M.; Van der loop, M.; Fustin, C.-A.; Jonas, A. M.; Gohy, J.-F.; Schubert, U. S. *Macromolecules* **2006**, *39*, 4719–4725.
15. Nardin, C.; Hirt, T.; Leukel, J.; Meier, W. *Langmuir* **2000**, *16*, 1035–1041.
16. Yilgor, I; Steckle, W. P.; Yilgor, E; Freelin, G; Riffle, J. *J. Polym. Sci., Part A: Polym. Chem.* **1989**, *27*, 3673–3690.
17. Kazama, H; Tezuka, Y.; Imai, K. *Polymer* **1987**, *19* (9), 1091–1100.
18. Einzmann, M; Binder, W. H. *J. Polym. Sci., Part A: Polym. Chem.* **2001**, *39*, 2821–2831.
19. Yilgor, I.; Riffle, J..; McGrath, J. *Reactive Oligmers*; Harris, F. W., Spinelli, H. J., Eds.; ACS Symposium Series 282; American Chemical Society: Washington, DC, 1985; pp 162−174.
20. Yilgor, I.; Yilgor, E. *Polym. Bull.* **1998**, *40*, 525–532.
21. Isaacman, M.; Barraon, K.; Theogarajan, L. *J. Polym. Sci., Part A: Polym. Chem.* **2012**, *50* (12), 2319–2329.
22. Theogarajan, L.; Desai, S.; Baldo, M.; Scholz, C. *Polym. Int.* **2008**, *57*, 660–667.
23. Meldal, M.; Tornøe, C. W. *Chem. Rev.* **2008**, *108*, 2952–3015.
24. Guiselin, O.; Lee, L. T.; Farnoux, B.; Lapp, A. *J. Chem. Phys.* **1991**, *95*, 4632–4640.
25. Matyjaszewski, K.; Pintauer, T.; Gaynor, S. *Macromolecules* **2000**, *33*, 1476–1478.
26. Nowshuddin, S.; Reddy, A. R. *Tetrahedron Lett.* **2006**, *47*, 5159–5161.
27. Halila, S.; Manguian, M.; Fort, S.; Cottaz, S.; Hamaide, T.; Fleury, E.; Driguez, H. *Macromol. Chem. Phys.* **2008**, *209*, 1282–1290.
28. Fijten, M. W. M.; Haensch, C.; van Lankvelt, B. M.; Hoogenboom, R.; Schubert, U. S. *Macromol. Chem. Phys.* **2008**, *209*, 1887–1895.
29. Pressly, E. D.; Amir, R. J.; Hawker, C. J. *J. Polym. Sci., Part A: Polym. Chem.* **2011**, *49*, 814–819.
30. Besheer, A.; Hause, G.; J. Kressler, J.; Mäder, K. *Biomacromolecules* **2007**, *8*, 359–367.
31. Hey, T.; Knoller, H.; Vorstheim, P. *Half-Life Extension through HESylation®, in Therapeutic Proteins: Strategies to Modulate Their Plasma Half-Lives*; Kontermann, R., Ed.; Wiley-VCH Verlag GmbH & Co. KGaA: Weinheim, Germany, 2012; doi: 10.1002/9783527644827.ch7.
32. Kiehl, P.; Metze, D.; Kresse, H.; Reimann, S.; Kraft, D.; Kapp, A. *Br. J. Dermatol.* **1998**, *138*, 672–677.
33. Binder, W. H.; Sachsenhofer, R. *Macromol. Rapid Commun.* **2007**, *28*, 15–54.
34. Fournier, D.; Hoogenboom, R.; Schubert, U. S. *Chem. Soc. Rev.* **2007**, *36*, 1369.
35. Barner-Kowollik, C.; Du Prez, F. E.; Espeel, P.; Hawker, C. J.; Junker, T.; Schlaad, H.; Van Camp, W. *Angew. Chem., Int. Ed.* **2011**, *50*, 60.

Downloaded by UNIV OF PITTSBURGH on July 20, 2013 | http://pubs.acs.org
Publication Date (Web): July 8, 2013 | doi: 10.1021/bk-2013-1135.ch005


In Tailored Polymer Architectures for Pharmaceutical and Biomedical Applications; Scholz, C., et al.;
ACS Symposium Series; American Chemical Society: Washington, DC, 2013.

Downloaded by UNIV TENNESSEE KNOXVILLE CAMPUS on July 17, 2013 | http://pubs.acs.org
Publication Date (Web): July 8, 2013 | doi: 10.1021/bk-2013-1135.ch006

## Chapter 6

# Investigating the Secondary Structure of Oligomeric Poly(amino acid)s

**David Ulkoski, Tracy Armstrong, and Carmen Scholz***

**Department of Chemistry, University of Alabama in Huntsville, 301 Sparkman Drive, Huntsville, Alabama 35899**
***E-mail: cscholz@chemistry.uah.edu.**

Poly(amino acid)s have garnered significant interest as biomedical materials. They consist of naturally occurring *L*-amino acids, which are linked via peptide bonds, both factors contribute to the inherent biocompatibility of this material. Furthermore, due to their isotacticity these polymers readily undergo self-assembly, which is exploited for the formation of drug and gene delivery vehicles and tissue engineering scaffolds and gels. However, this strong propensity for self-assembly also interferes with the polymerization process (ring-opening polymerization of amino acid N-carboxyanhydrides), as nascent chains adopt preferably a β-sheet conformation whose rigidity impedes chain growth and leads to early chain termination. This work investigates the tendencies of γ-benzyl *L*-glutamate, $N^{\varepsilon}$-trifluoroacetyl-*L*-lysine and S- carboxybenzyl-*L*-cysteine to form β-sheets in the beginning of a polymerization. The results of detailed FTIR investigations of the amide I and II bands support qualitatively the quantitative results obtained by circular dichroism spectroscopy. Poly(bz-*L*-Glu) and p(TFA-*L*-Lys) form α-helices when the oligomer length reaches 10 repeat units thus, readily sustaining the living character of the polymerization. Poly(Cbz- *L*-Cys) oligomers have the strongest tendency to form β-sheets, however, the addition of hydrogen-bond breaking urea to the reaction mixture diminishes β-sheet formation and forces the growing chains into unstructured conformations.

© 2013 American Chemical Society
In Tailored Polymer Architectures for Pharmaceutical and Biomedical Applications; Scholz, C., et al.;
ACS Symposium Series; American Chemical Society: Washington, DC, 2013.

# Introduction

Mankind has utilized protein materials for a long time, starting with wool and silk to keep warm and protect against the elements to using recombinant DNA techniques to produce proteins with unique and useful properties (*1*). Poly(amino acid)s, PAA's, are similar to proteins and peptides in that they consist of amino acid building blocks linked via amide bonds. This backbone architecture contributes to the overall biocompatibility of these materials and *L*-amino acid as potential degradation products are inherently biocompatible as well. However, there is no specific amino acid sequence associated with these polymers. In fact, most PAA's consist of no more than two different amino acids that are linked to yield either random or block copolymers.

Due to their isotacticity PAA's form distinct secondary structures and these self-assembling properties have been utilized for the formation of drug delivery systems and biomedical gels (*2*, *3*). Deming et al. showed that amphiphilic PAA copolymers readily undergo gelation. Special emphasis was placed on investigating these gels for applications in the central nervous system, specifically, to fill defects and at the same time deliver drugs and/or growth factors locally. Results indicated that amphiphilic diblock copolymers consisting of *L*-Leu in combination with *L*-Lys, *L*-Arg or *L*-Glu were biocompatible and did not cause excessive glia formation, inflammation or any other detrimental effect, and a sustained delivery of nerve growth factors was achieved (*4–6*). One aspect that was very important to the research on PAA's for applications in the central nervous system was the self-assembly behavior of these diblock copolymers, which re-assemble *in vivo* into 3D deposits after being injected. This is a significant advantage when working in a confined and not readily accessible area such as the inside of the skull. Furthermore, the physical properties of PAA hydrogels, such as the modulus and viscosity can be tuned to achieve preset drug release kinetics and/or cell ingrowth behaviors (*7*). The observed remarkable stability and robustness of these hydrogels is comparable to that of H- bonded β-sheet fibrils, which led to establishing a new model for the assembly of helical PAA's into structures termed twisted fibrils.

Other target areas, such as for instance liver tissue, have been identified where PAA's lend themselves as drug and gene delivery systems. Here, the synthesis of PAA's has been designed in such a way that the initiator used in the ring-opening polymerization of N- carboxyanhydrides of amino acids (NCA-ROP) served as a liver-specific homing device. Specifically, liver-targeting moieties such as bile, glycyrrhetinic or glycyrrhizic acid were derivatized with amino groups, which initiated the polymerization of an amino acid NCA's, here specifically p(*L*-Glu) (*8*). In a different liver-targeting approach, a non- viral gene delivery system was built based upon p(*L*-Lys), which served to condense plasmid DNA, and was synthesized by NCA-ROP using α- galactose-ω-amino poly(ethylene glycol), PEG, as macroinitiator. This delivery system yielded good transfection results and was less cytotoxic than p(*L*-Lys) alone due to the biocompatibilizing effect of PEG. Here, the galactose moiety at the PEG chain end served as homing device towards hepatocytes (*9*).



In Tailored Polymer Architectures for Pharmaceutical and Biomedical Applications; Scholz, C., et al.;
ACS Symposium Series; American Chemical Society: Washington, DC, 2013.

Downloaded by UNIV TENNESSEE KNOXVILLE CAMPUS on July 17, 2013 | http://pubs.acs.org
Publication Date (Web): July 8, 2013 | doi: 10.1021/bk-2013-1135.ch006

Furthermore, PAA's have been investigated as adjuvants in inorganic-organic hybrid biomaterials, where they were grafted onto silica nanoparticles. The covalent attachment of p(*L*-Glu) yielded coated nanoparticles that displayed a pH sensitivity (*10*). Heise et al. found that PAA's can also play a vital role in bioinorganic processes. The interaction of PAA copolymers with Calcium ions was investigated in an attempt to mimic biomineraliztion processes. A direct correlation between the *L*-Glu-content in a PAA copolymer and the $CaCO_3$ nucleation as well as the amount of soluble Calcium ions was found (*11*).

Downloaded by UNIV TENNESSEE KNOXVILLE CAMPUS on July 17, 2013 | http://pubs.acs.org
Publication Date (Web): July 8, 2013 | doi: 10.1021/bk-2013-1135.ch006

## Poly(amino acid) Polymerization Mechanisms

Unlike proteins, which have a polydispersity index of 1.0, PAA's are made by synthetic methods and show a molecular weight distribution. Depending on the synthetic approach, the polydispersity index of PAA's can be low, but does not equal unity. The formation of PAA's has been thoroughly investigated and described in the past by Kricheldorf (*12*). Three different mechanisms have been identified for the NCA-ROP: amine, carbamate and activated monomer mechanism, Figure 1. Which of those mechanisms dominates a specific polymerization depends primarily on the temperature, solvent, and $CO_2$ pressure and proton concentration in the reaction mixture (*12–14*). The amine mechanism is the most likely NCA polymerization pathway when primary aliphatic amines are used as initiators. The nucleophilic attack of the amine on the C(O)-2 of the NCA causes the ring-opening of the NCA and concurrent release of $CO_2$ . If the decarboxylation reaction is however, too slow or otherwise hindered the carbamate mechanism takes over. This leads to the formation of carboxylate end groups, and the living character of the polymerization is lost at this point. It is possible for the carboxylate to perform a nucleophilic attack on an NCA monomer, leading to ring- opening and the continuance of the polymerization whereat the mechanism could revert to the amine mechanism. The likelihood for chain growth to proceed via the carbamate mechanism is however, very low, as the weakly basic amines do not stabilize the carbamic acid by deprotonation. The absence of decarboxylation results in the incorporation of an anhydride function into the polymer chain, which significantly impacts the polymer properties, and in particular the degradation behavior. Tertiary amines deprotonate the NH group of the NCA thereby generating an activated monomer, which initiates the NCA-ROP. The polymerization proceeds via the nucleophilic attack of another activated NCA monomer on the C(O)-2 carbonyl carbon in the NCA ring structure that forms the chain end of the growing chain with concurrent or subsequent decarboxylation (*15*).

Aside from the polymerization mechanism that can be influenced by the choice of initiator and reaction conditions, the aforementioned strong tendency to form secondary structures in the nascent chain is also chiefly responsible for maintaining (or losing) the living character of an NCA- ROP. While the hydrogen-bond formation is beneficial in several PAA applications, as discussed


In Tailored Polymer Architectures for Pharmaceutical and Biomedical Applications; Scholz, C., et al.;
ACS Symposium Series; American Chemical Society: Washington, DC, 2013.

above, it can be detrimental during the early stages of polymer formation. Secondary structures of the developing polymer chains influence the overall chain growth. As PAA oligomers start to form, they have a tendency to form β-sheets prior to having sufficient chain length to form α-helices. The magnitude of this tendency to form β-sheets depends on the chemical nature of the amino acid. *L*-Cysteine for instance has a strong tendency to form β-sheets, which can be diminished, but the polymer chain will not adopt a helical conformation at any chain length (*16*). *L*-Lysine on the other hand forms α-helices quite readily.

The strong H-bond interactions within β-sheets are hypothesized to be responsible for early chain termination as the rigidity of these structures suppresses the ability of the growing chain to undergo continued nucleophilic attacks on NCA monomers, and in most severe scenarios, these structures precipitate out of solution (*17*). This study focuses on the investigation of nascent PAA chains, their tendencies to form initially β-sheets that convert into α-helices as the polymerization progresses and the potential of urea, which readily breaks hydrogen- bonds, to diminish or suppress the formation of β-sheets, thus maintaining the living character of the polymerization.

This project was spurred by and is part of research to produce PEGylated PAA's for the surface modification of biomedical implants (*18–22*). The PEG, in PEGylated PAA block copolymers conveys a stealth character to an implant and renders its surface biocompatible. Since PEG by itself is chemically inert, it needs an anchoring moiety that facilitates the polymer's covalent attachment to the implant surface and ideally this anchoring moiety also enhances the biocompatibility of the polymer coating. Poly(amino acid)s with functional side groups could serve as anchors and they are inherently biocompatible, as *L*-amino acids are natural molecules and they are linked via peptide linkages. Cysteine e.g. readily reacts with gold surfaces or gold nanoparticles and can thus establish the desired covalent linkage between the substrate surface and polymeric coating. Typically, the reactive SH-group is dispersed within a second amino acid building block, thus guaranteeing flexibility and mobility for the reactive cysteine groups. PEGylated PAA's in biomedical applications need to have a low polydispersity and must not contain any metal traces. Hence, polymerizations need to follow a living mechanism and no metal catalysts should be used. It became evident that maintaining a living character for the PAA polymerization was crucially dependent upon the first couple of polymerization steps.

It is hypothesized that a low polydispersity can be achieved if the nascent PAA chains can grow past the oligomer stage and the formation of β-sheets is successfully kept in check. Poly(amino acid) oligomers with five to twenty repeat units were synthesized and their secondary structures were analyzed by circular dichroism and FTIR spectroscopy in an effort to test the hypothesis that secondary structures, in particular β- sheets are prevalent in the early polymerization stage and can be influenced by H-bond breaking reagents such as urea (*23*).

Downloaded by UNIV TENNESSEE KNOXVILLE CAMPUS on July 17, 2013 | http://pubs.acs.org
Publication Date (Web): July 8, 2013 | doi: 10.1021/bk-2013-1135.ch006


In Tailored Polymer Architectures for Pharmaceutical and Biomedical Applications; Scholz, C., et al.;
ACS Symposium Series; American Chemical Society: Washington, DC, 2013.

Downloaded by UNIV TENNESSEE KNOXVILLE CAMPUS on July 17, 2013 | http://pubs.acs.org
Publication Date (Web): July 8, 2013 | doi: 10.1021/bk-2013-1135.ch006



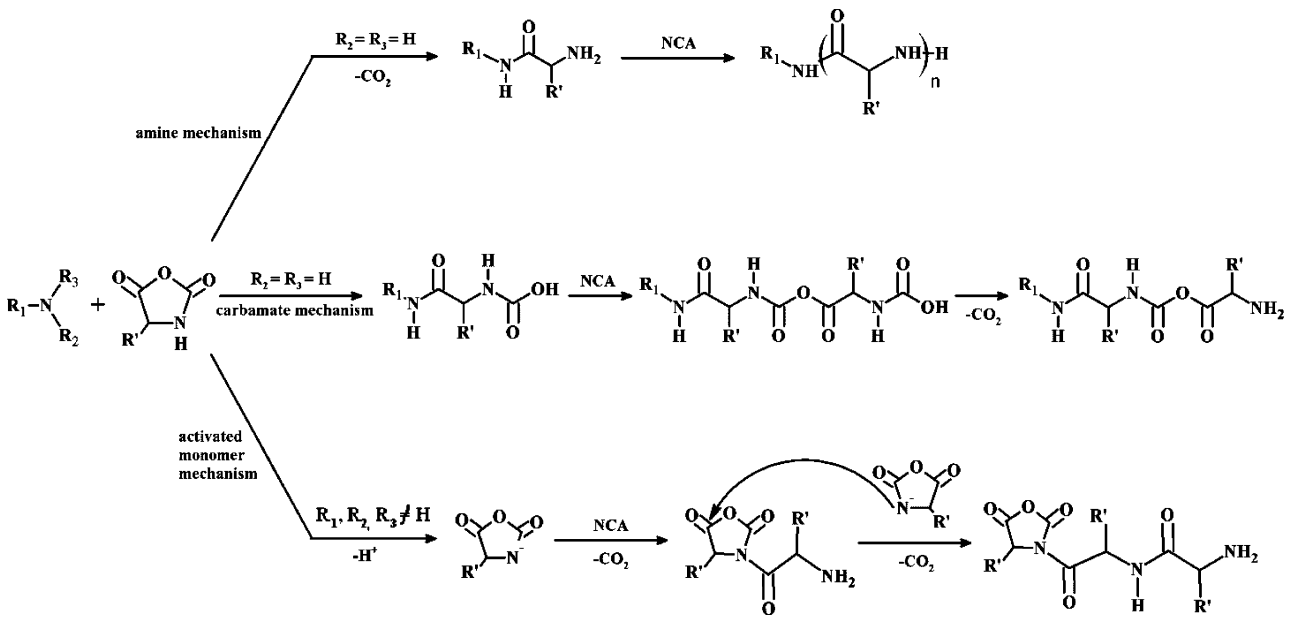


*Figure 1. Amine-initiated ring-opening polymerization of amino acid N-carboxyanhydrides (NCAs): amine, carbamate, and activated monomer mechanism, Scheme developed from Kricheldorf (12).*

# Secondary Structures of Nascent Poly(amino acid) Chains

## I. Synthesis of Amino Acid Oligomers

Poly(amino acid)s are synthesized by a ROP from their respective NCA's. If amino acids carry functional side groups, these functional groups need to be protected prior to the formation of the NCA and during the subsequent polymerization in order to prevent uncontrolled side reactions. Here, NCA-ROP's were performed on the NCA's of the following amino acids: γ-benzyl *L*-glutamate, (bz-*L*-Glu), $N^{\varepsilon}$- trifluoroacetyl-*L*-lysine (TFA-*L*-Lys) and S-carboxybenzyl-*L*-cysteine (Cbz-*L*-Cys) and yielded the respective protected oligomers. All studies of secondary structures were conducted on these protected moieties as the nascent chain in NCA-ROP's carries the protective groups during the polymerization and the properties of the developing polymer are in part determined by the properties of the protective groups. The formation of all oligomers was initiated with n-hexylamine and 5-, 10-, and 20-mers were produced. The characteristics of the resulting oligomers are listed in Table 1.

The targeted oligomer length, 5-, 10-, and 20-mer was achieved within experimental error for all oligomers. One somewhat distinct deviation from the targeted chain length was observed in n-Hex-p(Cbz- *L*-Cys), where the 20-mer polymerized without urea, resulted in a product with an average of only 16 repeat units. Shorter n-Hex-p(Cbz-*L*- Cys) oligomers achieved the targeted oligomer length within acceptable deviations. Typical yields ranged at about 90%, again with n-Hex- p(Cbz-*L*-Cys) oligomers showing somewhat lower yields. Missing the target length for the longest p(Cbz-*L*-Cys) oligomer, produced without urea, together with overall slightly lower yields indicate that Cbz-*L*-Cys NCA polymerizations are more strained than those of other amino acid NCA's.

## II. Investigation of the Secondary Structure of PAA Oligomers by Circular Dichroism, CD

Circular dichroism spectroscopy is a proven technique to identify the secondary structures of peptides and proteins. Schmidt et al. used it successfully to observe coil-to-helix transitions in polymers with p(*L*- Lys) side chains ("bottlebrush polymers") in aqueous salt solutions that either favor helix or coil conformations (*24*). Representative CD- spectra of n-Hex-p(bz-*L*-Glu), n-Hex-p(TFA-*L*-Lys) and n-Hex-p(Cbz-*L*- Cys), with and without urea, are shown in Figures 2 through 5. While the secondary structure could not be observed directly during the synthesis, the purified 5-, 10-, and 20-mers were re-dissolved in acetonitrile (0.2 mg/mL) for CD analyses (Olis CD spectrometer, Model RSM-100). Acetonitrile was chosen as solvent, because it is well suited for CD measurements, yields a high signal-to-noise ratio in the UV range of 195 – 260 nm, and it has similar properties as dimethylformamide, which was used as solvent in the polymerization process. It was thus anticipated that oligomer-solvent interactions would resemble the synthesis conditions. CDPRO prediction software was used to identify and quantify the secondary structures of the PAA oligomers, Table 2.



In Tailored Polymer Architectures for Pharmaceutical and Biomedical Applications; Scholz, C., et al.;
ACS Symposium Series; American Chemical Society: Washington, DC, 2013.

Downloaded by UNIV TENNESSEE KNOXVILLE CAMPUS on July 17, 2013 | http://pubs.acs.org
Publication Date (Web): July 8, 2013 | doi: 10.1021/bk-2013-1135.ch006

**Table 1. Amino acid oligomers for the investigation of the secondary structure of nascent PAA chains. * indicates that the oligomers were synthesized in the presence of 0.1M urea. All reactions were performed at room temperature.**

| *DP* | *Oligomers* | *Actual $\overline{DP}_n$ (Reaction time in days)* | *Theoret. $M_w$ (g/mol)* | *Actual $M_w$ (g/mol) (NMR)* | *Yield (%)* |
|---|---|---|---|---|---|
| 5 | n-Hex-p(bz-*L*-Glu) | 6 (2) | 1196 | 1415 | 92 |
| 5 | n-Hex-p(TFA-*L*-Lys) | 5 (2) | 1221 | 1221 | 89 |
| 5 | n-Hex-p(Cbz-*L*-Cys) | 4 (2) | 1286 | 1049 | 86 |
| 10 | n-Hex-p(bz-*L*-Glu) | 11 (3) | 2291 | 2510 | 91 |
| 10 | n-Hex-p(TFA-*L*-Lys) | 12 (3) | 2341 | 2789 | 89 |
| 10 | n-Hex-p(Cbz-*L*-Cys) | 10 (3.5) | 2471 | 2471 | 92 |
| 20 | n-Hex-p(bz-*L*-Glu) | 20 (4) | 4481 | 4481 | 88 |
| 20 | n-Hex-p(TFA-*L*-Lys) | 17 (4) | 4581 | 3909 | 86 |
| 20 | n-Hex-p(Cbz-*L*-Cys) | 16 (4.5) | 4841 | 3893 | 91 |
| 5 | n-Hex-p(Cbz-*L*-Cys)* | 4 (2) | 1286 | 1049 | 84 |
| 10 | n-Hex-p(Cbz-*L*-Cys)* | 9 (3) | 2471 | 2234 | 90 |
| 20 | n-Hex-p(Cbz-*L*-Cys)* | 18 (4) | 4841 | 4367 | 89 |

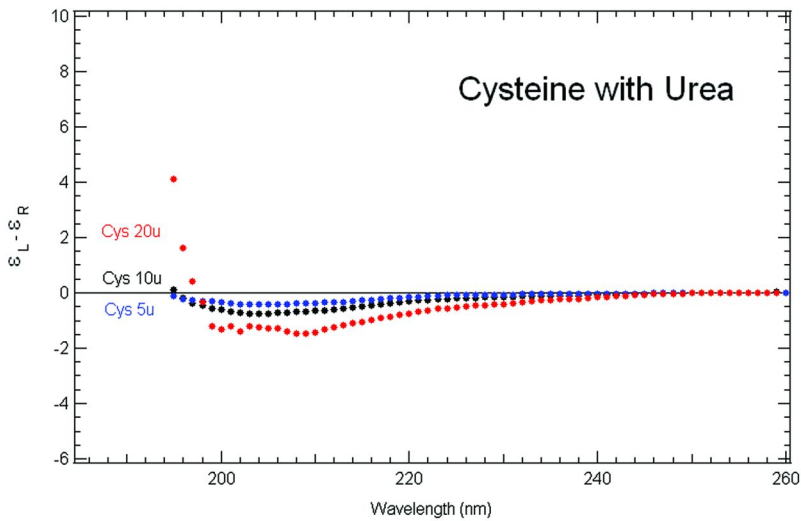


*Figure 2. CD spectra of poly(TFA-L-cysteine) in acetonitrile, synthesized with 0.1 M urea.*



In Tailored Polymer Architectures for Pharmaceutical and Biomedical Applications; Scholz, C., et al.; ACS Symposium Series; American Chemical Society: Washington, DC, 2013.

Downloaded by UNIV TENNESSEE KNOXVILLE CAMPUS on July 17, 2013 | http://pubs.acs.org
Publication Date (Web): July 8, 2013 | doi: 10.1021/bk-2013-1135.ch006

Downloaded by UNIV TENNESSEE KNOXVILLE CAMPUS on July 17, 2013 | http://pubs.acs.org
Publication Date (Web): July 8, 2013 | doi: 10.1021/bk-2013-1135.ch006

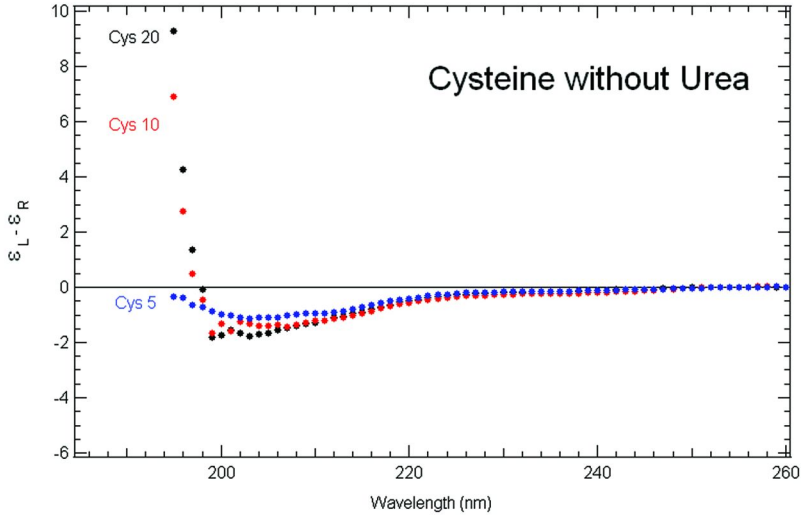


*Figure 3. CD spectra of poly(Cbz-L-cysteine) in acetonitrile.*

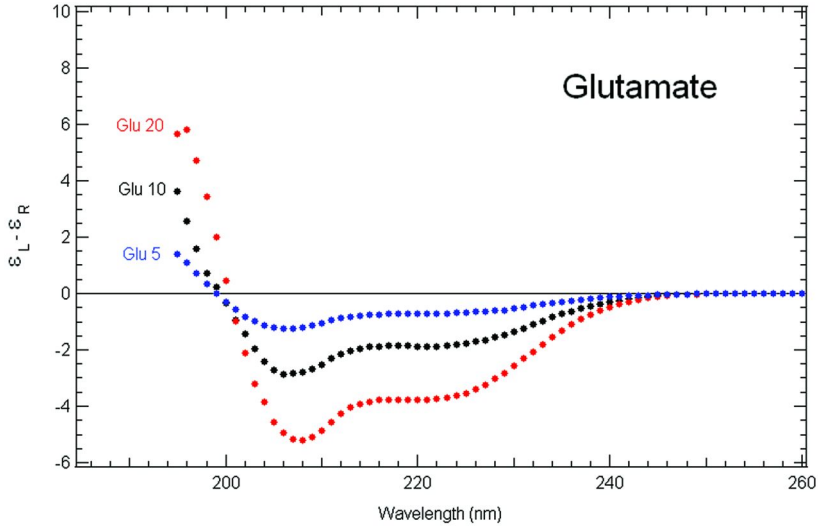


*Figure 4. CD spectra of N-hexylamino-poly(bz-L-glutamate) in acetonitrile.*


In Tailored Polymer Architectures for Pharmaceutical and Biomedical Applications; Scholz, C., et al.;
ACS Symposium Series; American Chemical Society: Washington, DC, 2013.

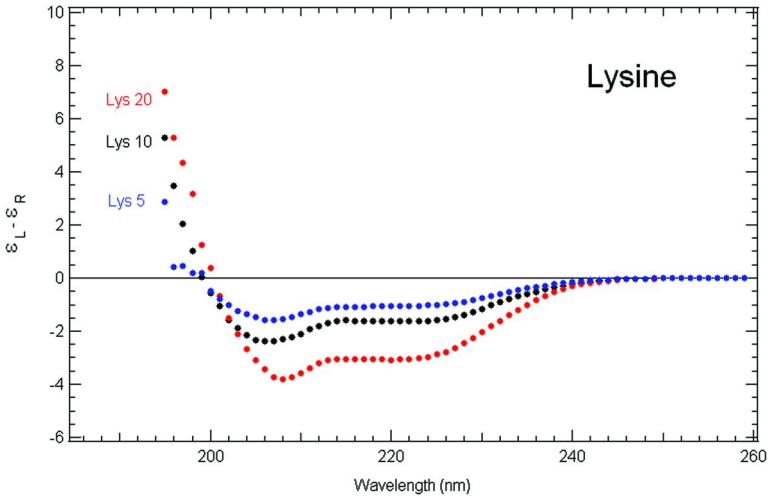


*Figure 5. CD spectra of poly(Cbz-L-lysine) in acetonitrile.*

Since p(Cbz-*L*-Cys) does not form α-helices at any chain length, this oligomer presents an excellent opportunity to study the impact of urea on the nascent chain. When *L*-Cys NCA is polymerized in the absence of urea about 75% of the growing chains adopt an overall β-sheet conformation. The remainder of the chains exists either in turns or is unstructured. It should be noticed that no turns were observed for the 20- mer. No distinct difference is observed between 5-, 10-, and 20-mers with respect to unstructured regions. Resolving the β-sheet structure in greater detail, that is, distinguishing between regular and distorted β- sheets, Table 3, indicates that with increasing chain length the regular β- sheets start to undergo distortion, as the percentage of chains in a regular β-sheet conformation decreases from 63% to 22%, and the percentage of chains in distorted β-sheets increases from 11% for the 5-mer to 53% for 20-mer.

The formation of secondary structures changes when urea is present during the polymerization, only between 15% (5-mer) and 40% (20-mer) of the chains are in a β-sheet conformation. The majority of the chains is forced into an unstructured conformation by the H-bond breaking action of the urea. The H-bond breaking activity becomes very obvious in the case of the p(Cbz-*L*-Cys) 5-mer, where the formation of the β-sheets, the natural state of the nascent chain, is clearly hindered which results in the formation of a significant amount of unstructured oligomer, 68%. This is highest amount of unstructured conformation observed throughout all experiments. The amount of turns formed by the chains is relatively unchanged compared to the urea-free polymerization, except for 20% of turns observed for p(Cbz-*L*-Cys) 20-mer, compared to 0% turns in the oligomer produced without urea. It can be assumed that the increased chain flexibility achieved by urea allows the chains to form turns. A closer analysis of the β-sheets reveals that in the beginning of the polymerization no chains can adopt a regular β-sheet, all are in the distorted β-sheet conformation; for comparison in the absence of urea 63% of the chains existed at that stage in a regular β-sheet. As the chains grow, the effect of


In Tailored Polymer Architectures for Pharmaceutical and Biomedical Applications; Scholz, C., et al.;
ACS Symposium Series; American Chemical Society: Washington, DC, 2013.

Downloaded by UNIV TENNESSEE KNOXVILLE CAMPUS on July 17, 2013 | http://pubs.acs.org
Publication Date (Web): July 8, 2013 | doi: 10.1021/bk-2013-1135.ch006

urea seems to be somewhat overcome as the chains start to form regular β-sheets at the expense of the distorted ones, up to 34% for the 20-mer. But even in the presence of urea the polymerization does not yield any α-helices.

**Table 2. Secondary structure prediction from CD data for PAA oligomers in acetonitrile. * indicates the synthesis was carried out with the addition of 0. 1 M urea. Experimental errors were based upon the deviance from the average percentage of secondary structure determined by each of CDPRO's inherent algorithms.**

| *Oligomer* | *[%] α-helix (r+d)* | *[%] β- sheet (r+d)* | *[%] Turn* | *[%] Unstructured* |
|---|---|---|---|---|
| n-Hex-p(Cbz-*L*-Cys) $_5$ | 0 ± 0 | 73.7 ± 2 | 12.2 ± 1 | 13.0 ± 3 |
| n-Hex-p(Cbz-*L*-Cys) $_{10}$ | 0 ± 0 | 77.4 ± 2 | 11.8 ± 2 | 11.2 ± 4 |
| n-Hex-p(Cbz-*L*-Cys) $_{20}$ | 0 ± 0 | 75.6 ± 3 | 0 ± 0 | 14.3 ± 4 |
| n-Hex-p(Cbz-*L*-Cys) $_5$ * | 0 ± 0 | 15.0 ± 1 | 16.4 ± 2 | 68.6 ± 3 |
| n-Hex-p(Cbz-*L*-Cys) $_{10}$ * | 0 ± 0 | 31.0± 1 | 11.0 ± 2 | 57.6 ± 2 |
| n-Hex-p(Cbz-*L*-Cys) $_{20}$ * | 0 ± 0 | 39.7 ± 2 | 19.9 ± 2 | 40.4± 2 |
| n-Hex-p(TFA-*L*-Lys) $_5$ | 13.6 ± 1 | 54.5 ± 2 | 4.3 ± 1 | 27.6 ± 2 |
| n-Hex-p(TFA-*L*-Lys) $_{10}$ | 60.5 ± 2 | 20.2 ± 2 | 5.0 ± 1 | 14.0 ± 2 |
| n-Hex-p(TFA-*L*-Lys) $_{20}$ | 80.5 ± 1 | 0.4 ± 0 | 5.4 ± 1 | 15.1 ± 2 |
| n-Hex-p(bz-*L*-Glu) $_5$ | 2 ± 1 | 61.3 ± 2 | 19.4 ± 1 | 17.1 ± 3 |
| n-Hex-p(bz-*L*-Glu) $_{10}$ | 58.5 ± 2 | 19.5 ± 1 | 5.4 ± 1 | 14.6 ± 1 |
| n-Hex-p(bz-*L*-Glu) $_{20}$ | 70.9 ± 2 | 11.0 ± 0.1 | 18.1 ± 1 | 0 ± 0 |

The H-bond breaking action of urea is schematically shown in Figure 6. In the polymerization of Cbz-*L*-Cys NCA, urea induced a change in the β-sheet conformation from a regular β-sheet structure to a distorted β-sheet structure, it could however not suppress the formation of β-sheets completely. The consequences of these more strained polymerizations were observed in the oligomer characteristics described above, Table 1, which showed more deviations from the target chain length and lower yields for the p(Cbz-*L*-Cys) oligomers.

Poly(*L*-Lys) and p(bz-*L*-Glu) are known to undergo α-helix formation rather readily. These oligomers were synthesized in the absence of urea to study the impact of chain length on the secondary structure of the growing chain. As shown in Table 2, a small percentage (2%) of 5-mers of p(*L*-Glu) exists already in α-helix conformation, while the majority of the chains forms β-sheets (61%) as hypothesized for very short oligomers. As the p(*L*-Glu) chain length increases to 10- and 20- mers the amount of α-helices increases significantly to 58% and 71%, respectively, at the expense of β-sheets, which diminish from 61% (5-mer) to 11% for the 20-mer. The p(*L*-Glu) 20-mer has no unstructured regions, the chains are predominantly in α-helix conformation with 18% turns and a remainder of 11% in β-sheet conformation. It can be concluded from these data that p(*L*-Glu) turns from a β-sheet into an α- helix when the oligomer length reached about 10 repeat units.


In Tailored Polymer Architectures for Pharmaceutical and Biomedical Applications; Scholz, C., et al.;
ACS Symposium Series; American Chemical Society: Washington, DC, 2013.

Downloaded by UNIV TENNESSEE KNOXVILLE CAMPUS on July 17, 2013 | http://pubs.acs.org
Publication Date (Web): July 8, 2013 | doi: 10.1021/bk-2013-1135.ch006

**Table 3. In depth analysis of the secondary structure of n-Hex-p(Cbz-*L*-Cys) oligomers, synthesized without and with (*) 0.1 M urea. A distinction was made between regular and distorted versions of β-sheets.**

| *Oligomer* | *[%] regular β-sheet* | *[%] distorted β-sheet* |
|---|---|---|
| n-Hex-p(Cbz-*L*-Cys) $_5$ | 63.5 ± 2 | 11.2 ± 1 |
| n-Hex-p(Cbz-*L*-Cys) $_{10}$ | 48.7 ± 2 | 28.7 ± 1 |
| n-Hex-p(Cbz-*L*-Cys) $_{20}$ | 22.2 ± 1 | 53.5 ±2 |
| n-Hex-p(Cbz-*L*-Cys) $_5$ * | 0.0 | 15.0 ± 1 |
| n-Hex-p(Cbz-*L*-Cys) $_{10}$ * | 24.3 ± 1 | 6.7 ± 0.5 |
| n-Hex-p(Cbz-*L*-Cys) $_{20}$ * | 34.4 ± 1 | 5.3 ± 0.5 |

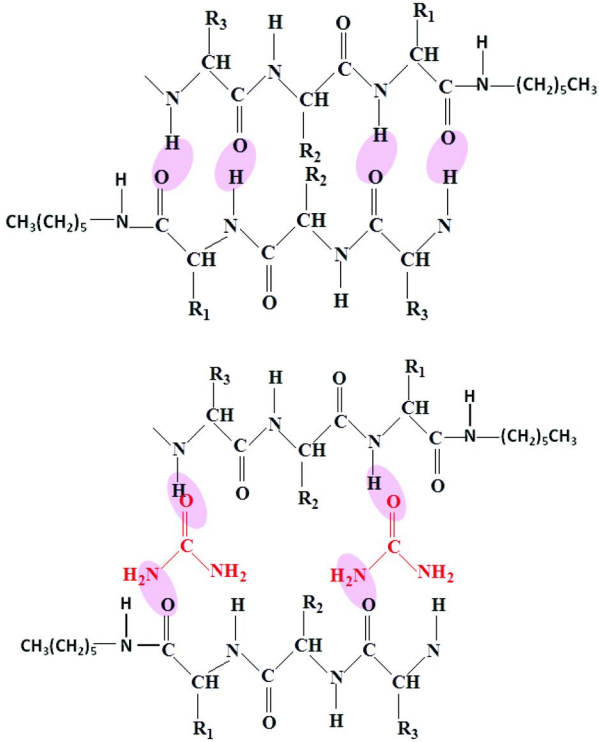

*Figure 6. Schematic representation of urea interfering with β-sheet formation.*

Poly(TFA-*L*-Lys) is even more prone to adopt an α-helix conformation. In the 5-mer, already 14% of chains are in α-helix conformation, this percentage increases to 80% for the 20-mer. Correspondingly, the β-sheet conformation diminishes from 54% for the 5-mer to 0.4% for the 20 mer. The data indicate that p(TFA-*L*-Lys) will not retain any β-sheets structures once higher molecular


In Tailored Polymer Architectures for Pharmaceutical and Biomedical Applications; Scholz, C., et al.; ACS Symposium Series; American Chemical Society: Washington, DC, 2013.

Downloaded by UNIV TENNESSEE KNOXVILLE CAMPUS on July 17, 2013 | http://pubs.acs.org
Publication Date (Web): July 8, 2013 | doi: 10.1021/bk-2013-1135.ch006

weight polymers are formed. Turns and unstructured regions remain rather constant at 5% and between 15% and 25%, respectively. The transition from a β-sheet into an α-helix occurs when the nascent chain consists of about 10 repeat units, as observed for p(bz-*L*-Glu). However, while p(bz-*L*-Glu) retained some degree of β-sheets and may retain those even in its polymeric form, p(TFA-*L*-Lys) does not retain any β-sheet structures. The impact of the protective group on the secondary structure development becomes obvious when comparing theses results with work by Blout and Kricheldorf who used $N^{\varepsilon}$-Cbz-protected L-Lys and found that at least 12 repeat units were necessary to form α-helices (*12*, *16*).

Conducting actual polymerizations, i.e. synthesizing high molecular weight PAA's, of bz-*L*-Glu and TFA-*L*-Lys NCA's in the presence of urea will further suppress the initial formation of β-sheets, which are responsible for chain death and loss of living polymerization character due to precipitation from the reaction mixture. Hence, the H-bond breaking activity of urea guarantees living polymerization mechanisms.

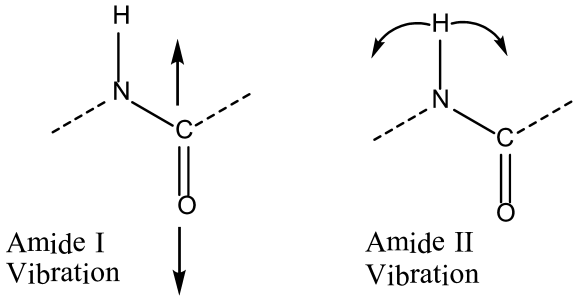


*Figure 7. Schematic depictions of vibrations causing the amide I (carbonyl stretching) and amide II (NH bending) bands in the infrared spectra of PAA's polypeptides, and proteins (25).*

## III. Investigation of the Secondary Structure of PAA Oligomers by Attenuated Total Reflectance-Fourier Transform Infrared, ATR- FTIR, Spectroscopy

Data obtained on the secondary structure of nascent PAA chains from CD spectroscopy measurements were further verified by ATR- FTIR spectroscopy (Perkin Elmer Spectrometer, Spectrum One, 126 scans with a scanning range of 4000 to 600 $cm^{-1}$). The amide I and amide II bands were used for the analysis of the secondary structure of the oligomers, their relative positioning yields information on the secondary structure of PAA's. The amide I band is the result of carbonyl stretching vibrations, while the amide II band is due to amine NH bending vibrations, Figure 7. While CD spectroscopy yields rather exact and quantifiable ratios of α-helices, β-sheets, unstructured regions and turns, FTIR spectroscopy only gives information on predominant structures. Representative ATR-FTIR spectra of the 20-mers (synthesized without urea) are provided in


In Tailored Polymer Architectures for Pharmaceutical and Biomedical Applications; Scholz, C., et al.;
ACS Symposium Series; American Chemical Society: Washington, DC, 2013.

Downloaded by UNIV TENNESSEE KNOXVILLE CAMPUS on July 17, 2013 | http://pubs.acs.org
Publication Date (Web): July 8, 2013 | doi: 10.1021/bk-2013-1135.ch006

Figure 8. Analyzing the secondary structures of PAA's by FTIR is a qualitative technique, which is however, excellently suited to evaluate the secondary structure of PAA copolymers as well as PEGylated PAA copolymers that cannot be investigated by CD-spectroscopy. The following information on the secondary structure of PAA's is obtained from amide I and amide II bands (*25–27*):

Amide I:

- o α-helices: band at approximately 1650 $cm^{-1}$.
- o β-sheet bands are located between 1620 and 1630 $cm^{-1}$.

Amide II

- o α-helices are located between 1540 and 1550 $cm^{-1}$.
- o β-sheet bands are located at approximately 1520 $cm^{-1}$
- o a broadening of the band at 1520 $cm^{-1}$ is indicative of a less structured β-sheet

**Table 4. Summary of amide I and amide II band positions as observed by ATR-FTIR spectroscopy. * indicates oligomers synthesized in the presence of 0.1 M urea.**

| *Oligomer* | *Amide I Position $cm^{-1}$* | *Amide II Position $cm^{-1}$* | *Secondary Structure* |
|---|---|---|---|
| n-Hex-p(Cbz-*L*-Cys) $_5$ | 1631 | 1522 | β-sheet |
| n-Hex-p(Cbz-*L*-Cys) $_{10}$ | 1630 | 1522 | β-sheet |
| n-Hex-p(Cbz-*L*-Cys) $_{20}$ | 1629 | 1517 | β-sheet |
| n-Hex-p(Cbz-*L*-Cys) $_5$ * | 1639 | 1516 | Unstructured |
| n-Hex-p(Cbz-*L*-Cys) $_{10}$ * | 1638 | 1518 | Unstructured |
| n-Hex-p(Cbz-*L*-Cys) $_{20}$ * | 1639 | 1517 | Unstructured |
| n-Hex-p(TFA-*L*-Lys) $_5$ | 1633/1654 | 1558 | α-helix + β-sheet |
| n-Hex-p(TFA-*L*-Lys) $_{10}$ | 1627/1648 | 1551 | α-helix + β-sheet |
| n-Hex-p(TFA-*L*-Lys) $_{20}$ | 1648 | 1557 | α-helix |
| n-Hex-p(bz-*L*-Glu) $_5$ | 1632/1651 | 1545 | α-helix + β-sheet |
| n-Hex-p(bz-*L*-Glu) $_{10}$ | 1626/1645 | 1546 | α-helix + β-sheet |
| n-Hex-p(bz-*L*-Glu) $_{20}$ | 1650 | 1546 | α-helix |

The FTIR data presented in Table 4 clearly show that the preferred conformation for p(Cbz-*L*-Cys) is a β-sheet, with the amide I bands positioned between 1630 and 1640 $cm^{-1}$ and the amide II band between 1515 and 1522 $cm^{-1}$, independent whether the oligomers were synthesized in the presence or absence of urea. However, n-Hex-p(Cbz- *L*-Cys) oligomers prepared in the presence of urea show a broadening of the amide II band at ~1520 $cm^{-1}$, Figure 9, which is an indication that the β-sheet is perturbed and starting to adopt a more distorted


In Tailored Polymer Architectures for Pharmaceutical and Biomedical Applications; Scholz, C., et al.;
ACS Symposium Series; American Chemical Society: Washington, DC, 2013.

Downloaded by UNIV TENNESSEE KNOXVILLE CAMPUS on July 17, 2013 | http://pubs.acs.org
Publication Date (Web): July 8, 2013 | doi: 10.1021/bk-2013-1135.ch006

and unstructured conformation. While the CD analyses clearly indicated that n-Hex-p(Cbz-*L*-Cys) synthesized in the presence of urea is mostly (40 – 68%) unstructured, the FTIR analysis confirms this observation in so far that a β-sheet structure is observed, and its indicative amide II band is broadened. The amide I band is indicative of a β-sheet for all n-Hex- p(Cbz-*L*-Cys) samples independent of whether they were produced with and without urea. A slight shift to somewhat lower wavelengths, 1638 $cm^{-1}$, is observed for samples produced with urea, however, more detailed studies would be necessary to determine whether this is also an indication for distortions in the β-sheets.

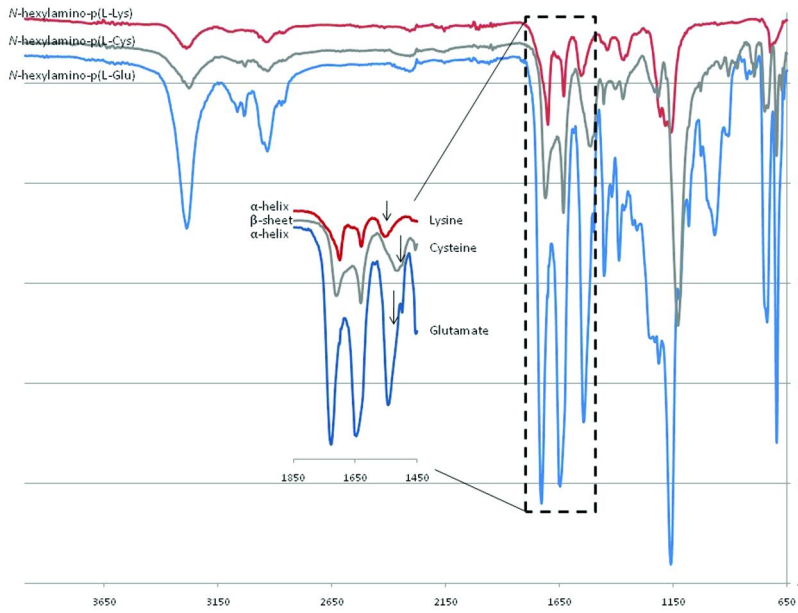


*Figure 8. ATR-FTIR spectrum of n-Hex-p(TFA-L-Lys)* $_{20}$ *(top spectrum), n-Hex-p(Cbz-L-Cys)* $_{20}$*, synthesized without urea middle spectrum), and n-Hex-p(bz-L-Glu)* $_{20}$ *(bottom spectrum). The arrows show the amide I stretching band.*

FTIR analyses of n-Hex-p(TFA-*L*-Lys) and n-Hex-p(bz-*L*-Glu) oligomers clearly indicate the impact of chain length on the secondary structures of nascent chains. Here, the amide II bands are less sensitive to the structures and all amide II signals indicate that the chains exist predominantly as α-helices, with band positions between 1545 and 1560 $cm^{-1}$. The amide I bands are more sensitive to actual structures and two amide I bands are observed for the 5- and 10-mers, respectively; one at around 1530 $cm^{-1}$ and a second one at around 1650 $cm^{-1}$. The band at 1530 $cm^{-1}$ is indicative of β-sheets and the band at 1650 $cm^{-1}$ indicates the presence of α-helices. These results suggest that a mixed secondary structure


In Tailored Polymer Architectures for Pharmaceutical and Biomedical Applications; Scholz, C., et al.; ACS Symposium Series; American Chemical Society: Washington, DC, 2013.

Downloaded by UNIV TENNESSEE KNOXVILLE CAMPUS on July 17, 2013 | http://pubs.acs.org
Publication Date (Web): July 8, 2013 | doi: 10.1021/bk-2013-1135.ch006

exists, as it was suggested by the CD spectra. A small deviation is observed for n-Hex-p(bz-*L*-Glu)$_5$ where the CD analysis predicted a negligible 2% of chains in α-helix conformation, whereas the FTIR analysis suggests a mixed structure of α-helices and β-sheets. It can be concluded that the amide I band is a good indicator for the presence of mixed secondary structures in PAA oligomers.

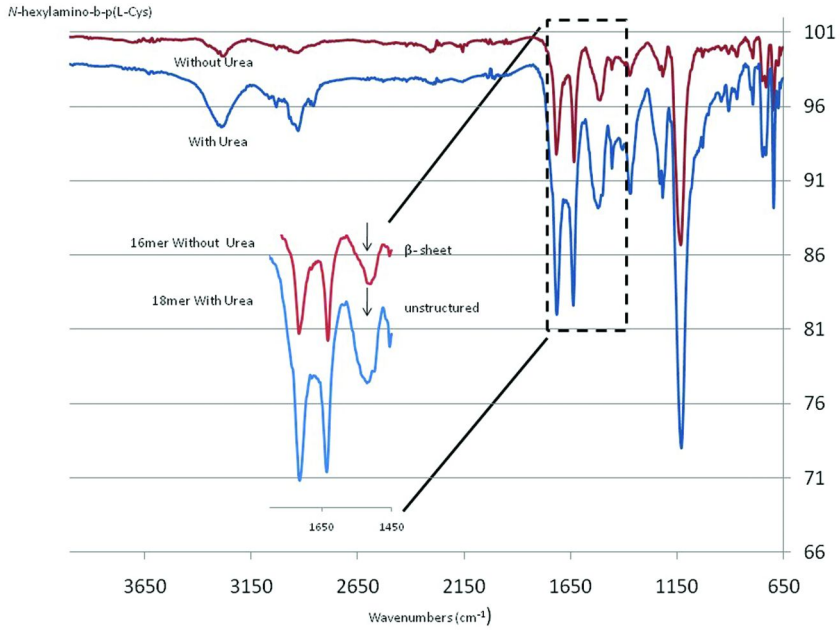


*Figure 9. ATR-FTIR spectrum of n-Hex-p(Cbz-L-Cys)* $_{20}$ *synthesized without urea (top spectrum), and with urea (bottom spectrum).*

## Conclusion

It has been shown that nascent PAA chains adopt preferentially a β- sheet conformation in the initial stages of the polymerization. The strength of this tendency depends on the chemical nature of the amino acid being polymerized; p(Cbz-*L*-Cys) has a very strong tendency to form β-sheets (about 75% of oligomers, independent of oligomer chain length are in β-sheet conformation), in p(TFA-*L*-Lys) on the other hand this tendency is less pronounced and 13% of 5-mer oligomers are already in α-helix conformation. As the oligomer length increases for p(TFA-*L*- Lys) and p(bz-*L*-Glu), β-sheets convert to α-helices. About 80% of all 20-mer p(TFA-*L*-Lys) oligomers and 70% of the p(bz-*L*-Glu) 20-mers are in a-helix conformation, but p(Cbz-*L*-Cys) does not adopt a helical conformation at all. The strong tendency of p(Cbz-*L*-Cys) to form β- sheets can be perturbed by adding a H-bond breaking reagent, like urea to the polymerization.


In Tailored Polymer Architectures for Pharmaceutical and Biomedical Applications; Scholz, C., et al.;
ACS Symposium Series; American Chemical Society: Washington, DC, 2013.

Downloaded by UNIV TENNESSEE KNOXVILLE CAMPUS on July 17, 2013 | http://pubs.acs.org
Publication Date (Web): July 8, 2013 | doi: 10.1021/bk-2013-1135.ch006

In that case regular β-sheets become distorted and oligomers are also forced into unstructured conformations. The development of these secondary structures can be quantitatively monitored by CD spectroscopy and qualitatively assessed by analyzing the positions of the amide I and II bands in FTIR spectra. The results of both techniques are in very good agreement.

## Acknowledgments

This is a collaborative research effort with the Boston Retinal Implant Project and financial support from NIH 1RO1EY016674-04 and NIH ARRA 2RO1 EY016674-04A1 is greatly acknowledged.

Downloaded by UNIV TENNESSEE KNOXVILLE CAMPUS on July 17, 2013 | http://pubs.acs.org
Publication Date (Web): July 8, 2013 | doi: 10.1021/bk-2013-1135.ch006

## References

1. Tirrell, J. G.; Tirrell, D. A.; Fournier, M. J.; Mason, T. L. Artificial Proteins: de novo design, synthesis and solid state properties. In *Protein-Based Materials*; Kaplan, D., McGrawth, K., Eds.; Springer: New York, 1997; pp 61−99.
2. Holowka, E. P.; Pochan, D. J.; Deming, T. J. Copolypeptide Vesicles with Controllable Diameter. *J. Am. Chem. Soc.* **2005**, *127* (35), 12423–12428.
3. Bellomo, E. G.; Wyrsta, M. D.; Pakstis, L.; Pochan, D. J.; Deming, T. J. Stimuli-responsive polypeptide vesicles by conformation-specific assembly. *Nat. Mater.* **2004**, *3* (4), 244–248.
4. Nowak, A. P.; Breedveld, V.; Pakstis, L.; Ozbas, B.; Pine, D. J.; Pochan, D.; Deming, T. J. Rapidly recovering hydrogel scaffolds from self-asembling diblock copolypetides amphiphiles. *Nature* **2002**, *417* (6887), 424–428.
5. Yang, C.; Song, B.; Ao, Y.; Nowak, A. P.; Abelowitz, R. B.; Korsak, R. A.; Hafton, L. A.; Deming, T. J.; Sofroniew, M. V. Biocompatibility of amphiphilic diblock copolypetides hydrogels in the central nervous system. *Biomaterials* **2009**, *30* (15), 2881–2898.
6. Song, B.; Song, J.; Zhang, S.; Anderson, M.; Ao, Y.; Yang, C.; Deming, T. J.; Sofroniev, M. V. Sustained local delivery of bioactive nerve growth factor in the central nervous system via tunable diblock copolypeptide hydrogel depots. *Biomaterials* **2012**, *33*, 9105–9116.
7. Deming, T. J. Polypeptide hydrogels via a unique assembly mechanism. *Soft Matter* **2005**, *1*, 28–35.
8. Cha, R.; Du, T.; Li, J.; Yuan, Z. Synthesis and Characterization of polypeptide containing liver-targeting group. *Polym. Int.* **2006**, *55*, 1057–1062.
9. Hu, H.; Zhang, X.; Zhong, N.; Pan, S. Study on galactose- poly(ethylene glycol)-poly(L-lysine) as novel gene vector targeting hepatocytes in vitro. *J. Biomater. Sci., Polym. Ed.* **2012**, *23* (5), 677–95.
10. Borase, T.; Iacono, M.; Ali, S. I.; Thornton, P. D.; Heise, A. Polypeptide core-shell silica nanoparticles with high grafting density by *N*-carboxyanhydride (NCA) ring opening polymerization as responsive materials and for bioconjugation. *Polym. Chem.* **2012**, *3*, 1267–1275.
11. Dmitrivic, V.; Habraken, G. J. M.; Hendrix, M. M. R. M.; Habraken, W. J. E. M.; Heise, A.; de Wirth, G.; Sommerdijk, N. A. J. M. Random Poly(amino

Acid)s Synthesized by Ring Opening Polymerization as Additives in the Biomimetic mineralization of $CaCO_3$. *Polymers* **2012**, *4*, 1195–1210.
12. Kricheldorf, H. R. Polypeptides and 100 Years of Chemistry of α- Amino Acid N-Carboxyanhydrides. *Angew. Chem., Int. Ed.* **2006**, *45*, 5752–5784.
13. Szwarc, M. The kinetics and mechanism of N-carboxy-α-amino acid anhydride (NCA) polymerization to poly-amino acids. *Fortschr. Hochpolym.-Forsch.* **1965**, *4* (1), 1–65.
14. Ballard, D. G. H.; Bamford, C. H. Heterogenous polymerization of a- N-carboxyamino-acid anhydrides. *J. Chem. Soc.* **1959**, 1039–1044.
15. Dubois, P.; Coulembier, O. In *Handbook of Ring-opening Polymerization*; Wiley-VCH: New York, 2009
16. Blout, E. R.; de Loze, C; Bloom, S. M.; Fasman, G. D. The ependance of the Conformation of Synthetic Polypeptides on Amino Acid Composition. *J. Am. Chem. Soc.* **1960**, *82*, 3787–3789.
17. Komoto, T.; Kim, K. Y.; Oya, M.; Kawai, T. Crystallization of polypeptides in the course of polymerization, 5. Effect of the steric hindrance on the crystal growth by the side chains. *Makromol. Chem.* **1974**, *175* (1), 283–299.
18. Scholz, C. Perspectives on: Material Aspects of Retinal Prostheses. *J. Bioact. Compat. Polymers* **2007**, *22* (5), 539–568.
19. Obeid, R.; Scholz, C. Synthesis and self-assembly of well-defined Poly(amino acid) end Capped Poly(ethylene glycol) and Poly(2- methyl-2-oxazoline). *Biomacromolecules* **2011**, *12* (10), 3797–3804.
20. Obeid, R.; Armstrong, T.; Ulkoski, D.; Peng, X.; Kressler, J.; Scholz, C. PEGylated poly(amino acid) block copolymers for surface modification and self-assembly: synthesis and characterization. *Polym. Prepr.* **2012**, *53* (2), 334–335.
21. Ulkoski, D.; Scholz, C. Novel synthesis of ABS terpolymers based on poly(ethylene glycol) and poly(amino acid) copolymers. *Polym. Prepr.* **2012**, *53* (1), 623–624.
22. Scholz, C. Vayaboury Controlled Molecular weight amino acid polymers having functionalizable backbones and end groups and process of preparing the same. Provisional Patent Application #20090131589.
23. Armstrong, T. L. Synthesis and Characterization of Biocompatible PEGylated Poly(amino acid) Random and Block Copolymers for Application to Solid Surfaces, Dissertation, University of Alabama in Huntsville, Huntsville, AL, 2012,
24. Sahl, M.; Muth, S.; Branscheid, R.; Fischer, K.; Schmidt, M. Helix- Coil Transition in Cylindrical Brush polymers with Poly-L-lysine Side Chains. *Macromolecules* **2012**, *45* (12), 5167–5175.
25. Yang, W. J.; Griffiths, P. R.; Byler, D. M.; Susi, H Protein Conformation by Infrared Spectrscopy: Resolution Enhancement by Fourier Self-Deconvolution. *Appl. Spectrosc.* **1985**, *39* (2), 282–287.
26. Byler, D. M.; Susi, H. Examination of the secondary structure of proteins by deconvolved FTIR spectra. *Biopolymers* **1986**, *25* (3), 469–487.
27. Susi, H.; Byler, D. M. Fourier Deconvolution of the Amide I Raman Band of Proteins as Related to Conformation. *Appl. Spectrosc.* **1988**, *42* (5), 819–826.

Downloaded by UNIV TENNESSEE KNOXVILLE CAMPUS on July 17, 2013 | http://pubs.acs.org
Publication Date (Web): July 8, 2013 | doi: 10.1021/bk-2013-1135.ch006


In Tailored Polymer Architectures for Pharmaceutical and Biomedical Applications; Scholz, C., et al.;
ACS Symposium Series; American Chemical Society: Washington, DC, 2013.

Downloaded by UNIV OF ROCHESTER on July 20, 2013 | http://pubs.acs.org
Publication Date (Web): July 8, 2013 | doi: 10.1021/bk-2013-1135.ch007

## Chapter 7

# Polymeric Micelles Stabilized by Electrostatic Interactions for Drug Delivery

**Yuichi Ohya***

**Department of Chemistry and Materials Engineering, Kansai University, 3-3-35 Yamate, Suita, Osaka 564-8680, Japan**
***E-mail: yohya@kansai-u.ac.jp.**

Polymeric micelle is one of the most fascinating nanoparticles formed by self-assemblies of block copolymers as vehicles for drug delivery system. The therapeutic effects of polymeric micelles carrying antitumor agents in cancer chemotherapy are derived from the results of their localization at tumor sites by EPR (enhanced permeability and retention) effect. To achieve efficient drug delivery to tumor site, stealth character and stability of the polymeric micelles in blood stream are very important. Cross-linking in core or shell of polymeric micelles with covalent bonds has been carried out to achieve stabilization of polymeric micelles. However, covalent cross-linking has some drawbacks, such as toxicity, loss of biodegradability etc. Although electrostatic interactions (including ionic bonds and coordination bonds with metal ion) are weaker than covalent bonds, there may be some advantages such as reversibility, degradability and low toxicity. In this review, recent studies on the stabilization of polymeric micelles by electrostatic interactions including coordination bonds are introduced.

## 1. Introduction: Polymeric Micelles As Drug Carriers

Recently, drug delivery systems using nanoparticles (liposomes, polymeric micelles, polymersomes, and nanogels) consisting of physically assembled molecules as vehicles have been extensively investigated. Among them,

© 2013 American Chemical Society
In Tailored Polymer Architectures for Pharmaceutical and Biomedical Applications; Scholz, C., et al.; ACS Symposium Series; American Chemical Society: Washington, DC, 2013.

polymeric micelles especially have attracted many researchers because of the convenience in preparation, relatively narrow diameter distributions, and high performance as drug delivery vehicles. Polymeric micelles are generally formed by self-assembly of amphiphilic diblock (sometimes triblock or multiblock) copolymers composed of hydrophobic segment and hydrophilic segment, and have core-shell type structures with hydrophobic inner cores surrounded by hydrophilic outer shell layers. Most of them have diameters within 100 nm and hydrophobic drugs can be entrapped in the core. Poly(ethylene glycol) (PEG) have been used frequently as hydrophilic segment forming outer shell layer, because PEG has high water-solubility, large exclusion volume, low affinity with serum components to achieve stealth characters (long half-life in blood stream) and biocompatibility. There have been many excellent reviews for drug or gene delivery system using polymeric micelles (*1–9*). Several kinds of polymeric micelles having PEG as outer shell carrying antitumor drugs are now under clinical trials for cancer chemotherapy.

Downloaded by UNIV OF ROCHESTER on July 20, 2013 | http://pubs.acs.org
Publication Date (Web): July 8, 2013 | doi: 10.1021/bk-2013-1135.ch007

## 2. Toward EPR Effect

As described above, polymeric micelles can be applied as drug delivery carriers especially for cancer chemotherapy, because EPR (enhanced permeability and retention) effect (*10–12*) (Figure 1) is expected for them. EPR effect can be understood as follows:

Usual low-molecular-weight drugs are excreted by renal clearance, however nanoparticles having larger sizes than serum proteins are not, because renal clearance was governed by the size of objects that can or cannot go through the membrane at Bowman's capsule in glomerulus. Simultaneously, nanoparticles with several tens nanometer diameter and hydrophilic outer shells have much possibility to escape from immobilization by reticuloendothelial system (RES) such as phagocytic cells in liver, lung, spleen etc. Therefore, macromolecules and nanoparticles like polymeric micelles have a tendency to show longer circulation period in blood stream (stealth character). On the other hand, normal blood vessels have well-organized thick layers of endothelial cells. Only small molecules can be diffused outside from normal blood vessels, and larger objects (macromolecules and particles) cannot. However, there are many defects on tumor neovascular capillary walls, and large objects (~300 nm) can leak outside of the newborn blood capillary. Since the chance to go outside of blood vessels for long circulating nanoparticles is limited at neovascular sites around tumor tissue, these nano-objects tend to intrude around tumor tissues. In addition, around tumor tissue there was no lymph node, which scavenges objects leaked from blood vessels. So the macromolecules and nanoparticles leaked from neovascular capillaries can stay longer period at that site.

Of course, to achieve high antitumor activity by this EPR effect, there are several hurdles to overcome (Figure 1) as follows:


In Tailored Polymer Architectures for Pharmaceutical and Biomedical Applications; Scholz, C., et al.;
ACS Symposium Series; American Chemical Society: Washington, DC, 2013.

(1) Escaping from renal clearance
(2) Escaping from RES and opsonization (absorption of serum proteins, which enhance entrapment by RES)
(3) Stability during circulation in blood stream: no dissociation, no aggregation, and no (or very small) release of drugs
(4) Leakage from neovascular capillary
(5) Internalization into tumor cells
(6) Release of drugs in cytosol or endosome / Escaping from endosome to active site of the cell

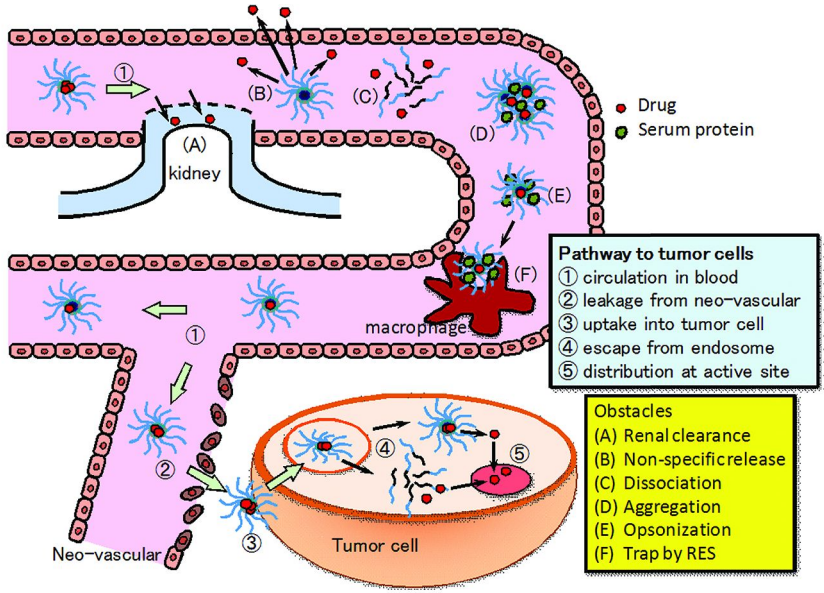


*Figure 1. Schematic illustration of enhanced permeability and retention (EPR) effect, the pathway to tumor cells and obstacles on the way. (see color insert)*

Escaping from renal clearance (1) and leakage from neovascular capillary (4) can be achieved by the size of nanoparticles as described above. Escaping from RES and opsonization (2) may be achieved by surrounding by PEG and the enough small particle sizes. Specific uptake into tumor cells (5) can be achieved by the introduction of specific ligands for the receptors on surface of tumor cells. Release of drugs (6) depends on degradability of the particles in cytosol or endosomal condition. Escaping from endosome to active site might not be matter if the antitumor agents are hydrophobic and permeable across cell membrane, and the micelle would be decomposed by lysosomal digestion. However, the improvement of stability of the polymeric micelle during the circulation (3) must be one of the most important obstacles still to be overcome.


In Tailored Polymer Architectures for Pharmaceutical and Biomedical Applications; Scholz, C., et al.; ACS Symposium Series; American Chemical Society: Washington, DC, 2013.

Downloaded by UNIV OF ROCHESTER on July 20, 2013 | http://pubs.acs.org
Publication Date (Web): July 8, 2013 | doi: 10.1021/bk-2013-1135.ch007

## 3. Importance of Stability of Polymeric Micelle Systems

Generally, polymeric micelles obtained by physical assemblies of the block copolymers have relatively higher stability (lower critical micelle concentration (CMC) and high colloidal stability) compared with conventional low-molecular-weight amphiphile micelles, especially when the inner core is kinetically "frozen" in a solid state. However, the micelle formation by non-covalent interaction is basically reversible process, and there are possibilities of dissociation when diluted below CMC. The amount of blood for an adult human is said to be about 7-8% of the body weight. So, a human whose body weight is 60 kg has about 4.5 L of blood. This means after intravenous injection of 10 mg of polymeric micelle, the concentration would go down to 0.002 g/L. Moreover, there are various serum components in blood such as ions, proteins, lipids and so on. The interaction of polymeric micelles with these serum components may lead aggregation or dissociation of the polymeric micelles. In addition, the release of drugs during circulation in blood stream should be suppressed to avoid non-specific drug distribution to whole body. Although site-specific drug delivery (targeting) has been investigated by introduction of specific pilot moieties on polymeric micelles, such pilot moieties can act only when the polymeric micelles contact with target tumor cell surfaces. Drug leakage before contacting with tumor cells by unexpected dissociation and diffusion must reduce the therapeutic effects of the polymeric micelle in drug delivery. So we should remind the targeting can be achieved only when the stability in blood stream is guaranteed.

From these stand points, various approaches have been proposed to stabilize polymeric micelles by chemical cross-linking of their cores or shells (*13–19*). There were excellent reviews for these approaches (*20–22*). However, covalent cross-linking might have some drawbacks. To stabilize polymeric micelles by covalent bonds, cross-linking reactions should be carried out in the cores, shells or interface of core and shell. In these cases, cross-linking reagents or initiator of polymerization should be used, and they may be potentially toxic. So, the reagents should be carefully chosen. When the cross-linking reaction is polymerization of vinyl monomers, the products would have a problem in biodegradability.

On the other hand, ionic complex formations by electrostatic interaction or coordination bonds formation with metal ions have also been used for stabilization of polymeric micelles. Ionic bonds, electrostatic interactions and reversible coordination bonds with metal ion are much weaker than covalent bonds. But there may be some advantages such as reversibility, degradability and low toxicity. In this review, some examples of recent studies on the stabilization of polymeric micelles by electrostatic interactions including coordination bonds are introduced.

As described above, since electrostatic interaction does not need cross-linking reagents, and the reaction (bond formation) can proceed under very mild condition (usually in aqueous solution at room temperature), it is very fascinating for the stabilization of polymeric micelles. However, polycation has some cytotoxicity against living cells, and electrostatic interaction would be influenced by pH and ionic strength of the solution. There have been many reports on polymeric micelles using electrostatic interaction as a driving force, polyion complex (PIC) micelles


In Tailored Polymer Architectures for Pharmaceutical and Biomedical Applications; Scholz, C., et al.;
ACS Symposium Series; American Chemical Society: Washington, DC, 2013.

Downloaded by UNIV OF ROCHESTER on July 20, 2013 | http://pubs.acs.org
Publication Date (Web): July 8, 2013 | doi: 10.1021/bk-2013-1135.ch007

(*23–27*). For example, polycation-*b*-PEG block copolymers can form PIC micelles with anionic polynucleotides, and such PIC micelles carrying polynucleotide have been investigated as gene delivery carriers (*28*, *29*).

## 4. Stabilization by Complex Formation with Metal Ion

It is well known that multivalent metal ion can form chelate-type complex, and can be a cross-linking reagents. For example, $Ca^{2+}$ can induce hydrogel formation on mixing with alginate. Platinum ion forms square-type tetra-coordination structure. It is well known some platinum complexes (II) (Figure 2) such as *cis*-dichlorodiamine platinum(II) (CDDP) (**1**) and *cis*-dichloro(cyclohexane-*trans*-*l*-1,2-diamine)platinum(II) (Dach-Pt) (**2**) have strong antitumor activity, and have been used for cancer chemotherapy. These *cis*-type platinum complexes can form chelate-type coordination bonds with polycarboxylates. We previously reported preparation of soluble polycarboxylate/platinum complexes conjugates as macromolecular prodrugs for cancer chemotherapy (*30–32*). Kataoka and coworkers reported polymeric micelles using the coordination bonds between PEG-*b*-polyglutamate diblock copolymer (Figure 2) (**3**) and platinum complexes as driving force of micelle formation (*33–36*). The obtained complex micelles with metal coordination showed improvement solubility of Dach-Pt, longer blood circulation, and good therapeutic results for tumor bearing mice. Recently, they reported the importance of the micellar size to deliver drugs into especially poorly permeable tumors based on direct evidences using this system (*36*).

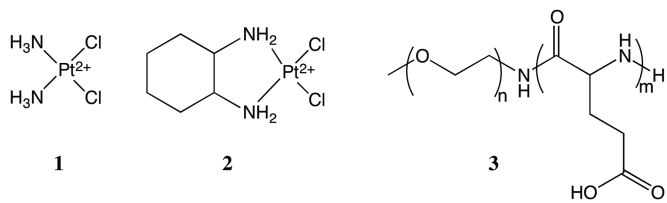


**1** **2** **3**

*Figure 2. Molecular structures of platinum complexes and the PEG-b-polyglutamate.*

Yan and coworkers reported formation of polymeric micelles using poly(2-vinyl-*N*-methylpyridinium iodide)-*b*-PEG (**4**) mixing with zinc nitrate and bisligand (**5**) (Figure 3) (*37*). The obtained mixture formed polymeric micelle having 25-27 nm of diameter with a narrow distribution. Their approaches utilized bisligand as an additive cross-linker. Wang and coworkers reported formation of polymeric micelle directly driven by metal-ligand coordination (*38*). They synthesized poly(4-vinyl-pyridinium)-*b*-PEG derivative (**6**) having pendant ligand moiety with similar structure as Yan's work (Figure 3). The polyvalent polymer formed stable polymeric micelles having 15 nm of diameter


In Tailored Polymer Architectures for Pharmaceutical and Biomedical Applications; Scholz, C., et al.; ACS Symposium Series; American Chemical Society: Washington, DC, 2013.

Downloaded by UNIV OF ROCHESTER on July 20, 2013 | http://pubs.acs.org
Publication Date (Web): July 8, 2013 | doi: 10.1021/bk-2013-1135.ch007

in the presence of $Zn^{2+}$. The addition of salt and ethylenediaminetetraacetic acid (EDTA) hardly affects of the micelles, and the CMC was in the range of 0.010-0.020 g/L.

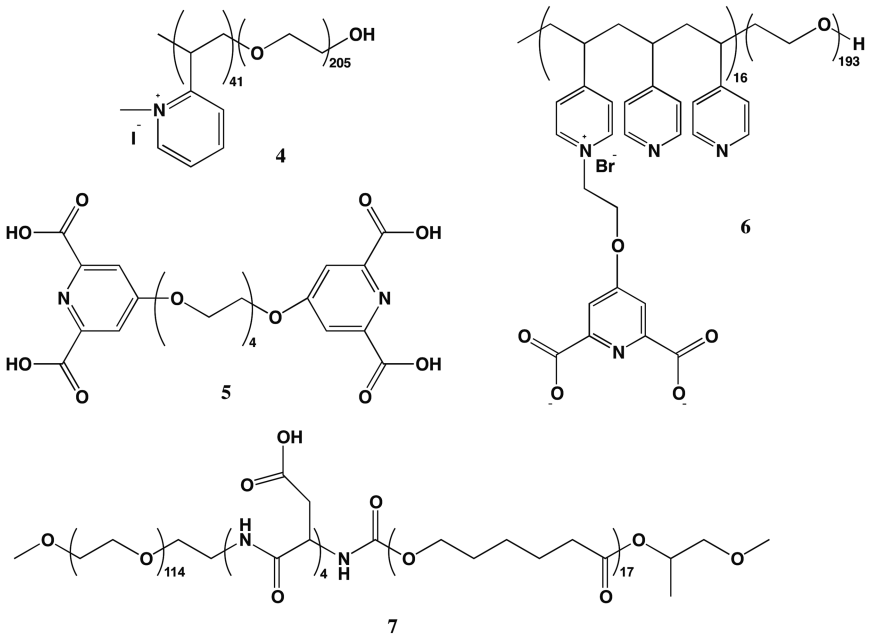


*Figure 3. Molecular structures of polymers and ligands used for preparation of polymeric micelles stabilized by metal coordination.*

These studies introduced above are core cross-linking approaches using metal coordination bonds as a main driving force for micelle formation. Ahn and coworkers reported shell cross-linking (exactly saying, cross-linking at the interface of core and shell) approach for stabilization of polymeric micelles (*39*). They synthesized ABC-type triblock copolymer, methoxy-poly(ethylene glycol)-*b*-oligo(aspartic acid)-*b*-poly(ε-caprolactone) (MeO-PEG-*b*-PAsp-*b*-PCL) (Figure 3) (**7**) having oligocarboxylate segment in the middle of the triblock copolymer for complex formation with metal ions. The triblock copolymer could form polymeric micelle having 73 nm of diameter without $Ca^{2+}$, and the CMC was 0.078 g/L. In the presence of $Ca^{2+}$, the copolymer formed polymeric micelle having 70 nm of diameter. Almost no effect on the diameter was observed for the addition of $Ca^{2+}$. They prepared paclitaxel-loaded polymeric micelle in the presence and absence of $Ca^{2+}$. After dilution of these micelle solutions below CMC of the copolymer (0.078 g/L) to 0.02 g/L, precipitation of paclitaxel was observed for non-stabilized paclitaxel-loaded polymeric micelle. But paclitaxel-loaded ionically stabilized micelle showed clear solution even


In Tailored Polymer Architectures for Pharmaceutical and Biomedical Applications; Scholz, C., et al.; ACS Symposium Series; American Chemical Society: Washington, DC, 2013.

Downloaded by UNIV OF ROCHESTER on July 20, 2013 | http://pubs.acs.org
Publication Date (Web): July 8, 2013 | doi: 10.1021/bk-2013-1135.ch007

after dilution below CMC to 0.02 g/L. Moreover, the suppression of release of paclitaxel was observed for paclitaxel-loaded ionically stabilized micelle compared with non-stabilized micelle.

## 5. Stabilization by Polyion Complex Formation

PIC formation between oppositely charged polyelectrolytes is a well-known technique to prepare, for example, layer-by-layer (LbL) self-assembled membranes (*40*). PIC offers several advantages over covalent bond and also coordination bond with metal ion: (1) Cross-linking reagents and metal ions, which may potentially be toxic, are not necessary; (2) There are no small-molecule by-products; (3) The reaction proceeds under mild conditions (in aqueous solution at room temperature); (4) Multiple electrostatic interaction leads to high thermodynamic stability; (5) But electrostatic interaction, in principle, reversible.

Downloaded by UNIV OF ROCHESTER on July 20, 2013 | http://pubs.acs.org
Publication Date (Web): July 8, 2013 | doi: 10.1021/bk-2013-1135.ch007

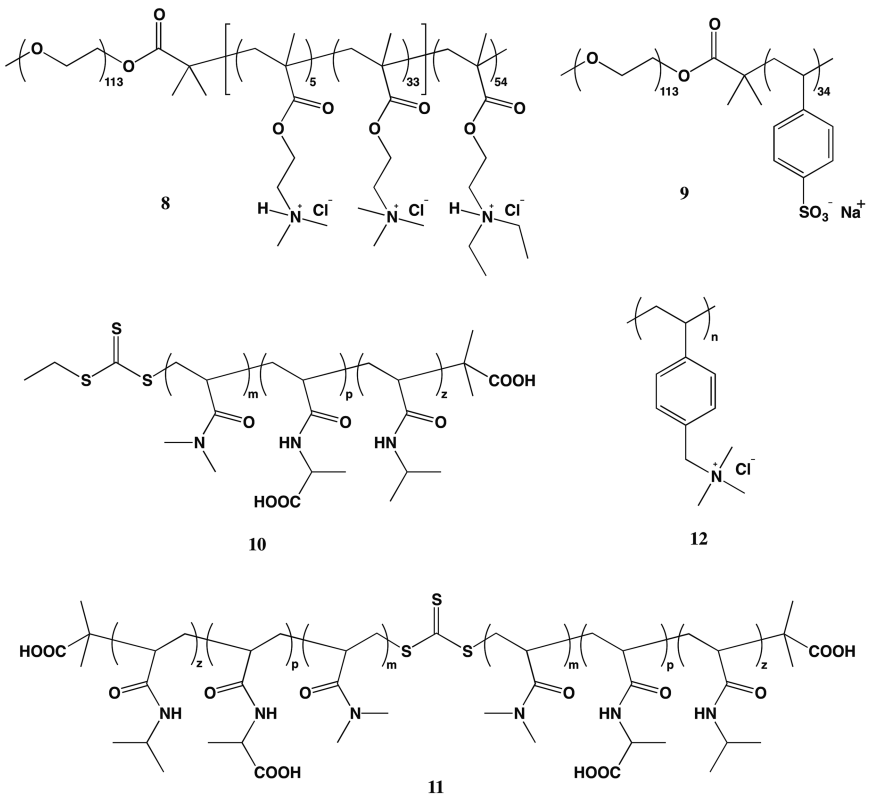


*Figure 4. Molecular structures of polymers used for preparation of polymeric micelles stabilized by polyion complex formation.*


In Tailored Polymer Architectures for Pharmaceutical and Biomedical Applications; Scholz, C., et al.;
ACS Symposium Series; American Chemical Society: Washington, DC, 2013.

Downloaded by UNIV OF ROCHESTER on July 20, 2013 | http://pubs.acs.org
Publication Date (Web): July 8, 2013 | doi: 10.1021/bk-2013-1135.ch007

Weaver, Armes and coworkers reported preparation of shell cross-linked micelle by PIC formation (*41*). They prepared triblock copolymer of PEG, poly[2-(dimethylamino)ethyl methacrylate] (DMAEM) and poly[2-(diethylamino)ethyl methacrylate] (DEAEM) by atom transfer radical polymerization (ATRP). After quaternization of DMAEM segment, the obtained block copolymer, PEG-*b*-[QDMAEM/DMAEM]-*b*-DEAEM (**8**) (Figure 4) could form polymeric micelle with 27 nm diameter under neutral pH. The obtained positively charged polymeric micelle was further mixed with anionic block copolymer, PEG-*b*-poly(sodium 4-styrenesulfate) (**9**), in various ratios to form ionically cross-linked micelles with 35-50 nm of diameters. The obtained micelles cross-linked by PIC showed good stability against pH change and salt. The CMC value of the stabilized micelle was 0.08 g/L.

Lokitz, McCormick and coworkers also reported PIC stabilized micelle having temperature-responsive segment by similar strategy (*42*). They synthesized triblock copolymer (**10**) and pentablock copolymer (**11**) consisting of *N,N*-dimethylacrylamide (DMA), *N*-acryloylalanine (AAL) and *N*-isopropylacrylamide (NIPAM) unit segments (Figure 4) by reversible addition fragmentation chain transfer (RAFT) polymerization. These copolymers were soluble as unimers in water at 25°C, but formed polymeric micelle having 35-86 nm upon heating by dehydration of PNIPAM segments. The micelles were reacted with polycation, poly[(ar-vinylbenzyl)ammonium chloride] (PVBTAC), to give micelle stabilized by PIC (Figure 5). The micelle stabilized by PIC did not show dissociation upon cooling, although non-stabilized block copolymer micelle dissociate upon cooling the solution to 25°C. The micelles remained intact at salt concentration as high as 0.3 M NaCl while dissociation into unimers was observed at 0.4 M NaCl, demonstrating the reversibility of the PIC cross-linking.

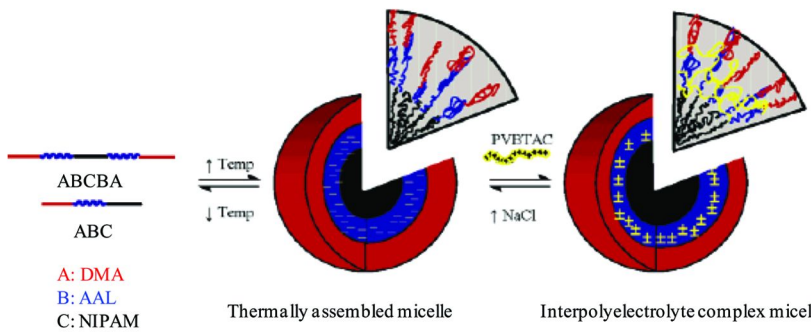


*Figure 5. Illustration for temperature-responsive micelle formation and reversible interpolyelectrolyte complexed micelle formation. (Reproduced with permission from reference (42). Copyright 2006 American Chemical Society.) (see color insert)*

These approaches introduced above utilized PIC formation as cross-linking at the interface of core and shell, where outer shells were composed of nonionic hydrophilic polymers. We recently reported PIC coating strategy to achieve


In Tailored Polymer Architectures for Pharmaceutical and Biomedical Applications; Scholz, C., et al.;
ACS Symposium Series; American Chemical Society: Washington, DC, 2013.

higher stability of polymeric micelle (*43*, *44*). There are also some reports on the stabilization of vesicles by PIC coating on the surfaces (*45–48*). Significant improvements in the stability of the vesicles were achieved. Caruso and coworkes reported the preparation of hollow capsules based on electrostatic interaction and their application for drug delivery systems (*49–51*).

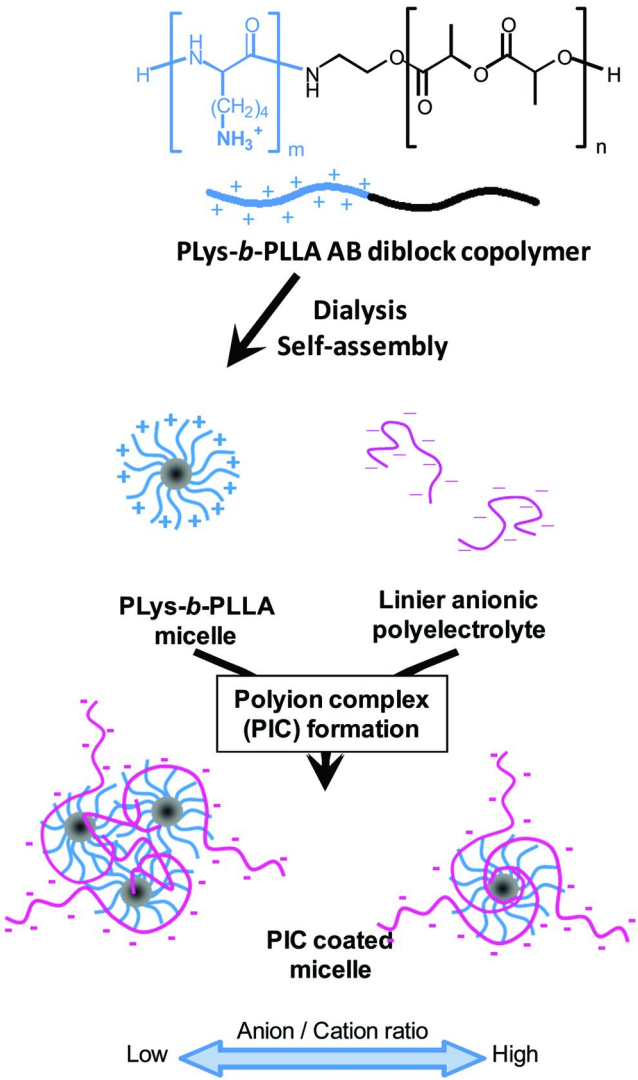


*Figure 6. Schematic illustration for the preparation of HA-coated micelles. (Reproduced with permission from reference (43). Copyright 2010 John Wiley & Sons.) (see color insert)*



In Tailored Polymer Architectures for Pharmaceutical and Biomedical Applications; Scholz, C., et al.; ACS Symposium Series; American Chemical Society: Washington, DC, 2013.

Downloaded by UNIV OF ROCHESTER on July 20, 2013 | http://pubs.acs.org
Publication Date (Web): July 8, 2013 | doi: 10.1021/bk-2013-1135.ch007

We previously prepared negatively charged polymeric micelles from biodegradable AB-type diblock copolymers composed of poly(L-aspartic acid) (PAsp) and poly(L-lactide) (PLLA), PAsp-*b*-PLLAs. The obtained polymeric micelles had negatively charged shell-layers and pH responsibility (*52–54*). We also synthesized positively charged AB-type diblock copolymers of poly(L-lysine) (PLys) and PLLA, PLys-*b*-PLLA by similar synthetic methods. This polymer could form polymeric micelles with positively charged surfaces. The positively charged micelles did not show excellent stability, and are not good as drug delivery vehicle, because polycation shows cytotoxicity and high opsonization possibility in blood stream. To improve the stability of the polymeric micelles and impart various functionalities including biocompatibility, the positively charged micelles were coated with polyanionic polysaccharide, hyaluronic acid (HA), using PIC formation (Figure 6) (*43*). HA, a linear mucopolysaccharide composed of repeating disaccharide subunits of *N*-acetyl-D-glucosamine and D-glucuronic acid, is one of the main components of the extracellular matrix (ECM) with good biocompatibility, and has been used as biomaterials.

Downloaded by UNIV OF ROCHESTER on July 20, 2013 | http://pubs.acs.org
Publication Date (Web): July 8, 2013 | doi: 10.1021/bk-2013-1135.ch007

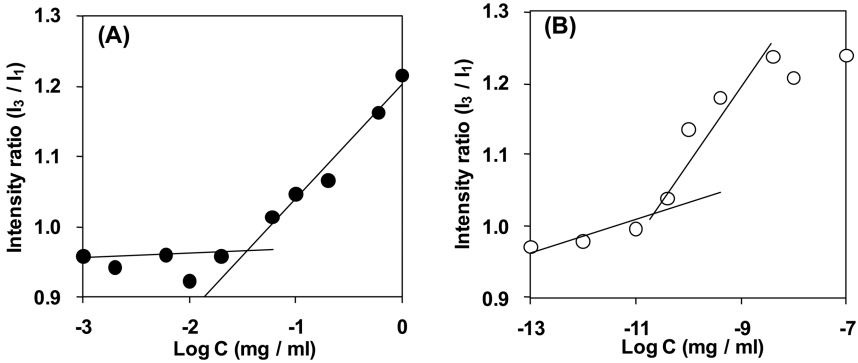


*Figure 7. Plots of fluorescence intensity ratio for $I_1$ (373 nm) to $I_3$ (393 nm) peaks of pyrene, as a function of micelle concentration in water (excitation wavelength: 339 nm). (A) PLys-b-PLLA micelles and (B) HA-coated micelles. (Reproduced with permission from reference (43). Copyright 2010 John Wiley & Sons.)*

The diameter of HA-coated micelle was typically 40 nm when the anion/cation (A/C) ratio was 1.4, larger than that of PLys-*b*-PLLA non-coated micelle (about 25 nm) under the same condition. The HA-coated micelles had larger diameters, 1.5–5 times that of the non-coated PLys-*b*-PLLA micelle. The diameter of the micelle became larger when the A/C ratio decreased. These results suggest that several PLys-*b*-PLLA micelles could be wrapped together into

one HA-coated micelle at a sufficiently low A/C ratio. The positive ζ-potential value for the PLys-*b*-PLLA micelle in PBS became negative by coating with HA. The stability of the micelle against dilution was evaluated as CMC values by fluorescence measurements using pyrene as a probe in PBS (Figure 7) (*43*). Although CMC for PLys-*b*-PLLA micelle was at 0.035 g/L, HA-coated micelle (A/C = 1.4) had a single inflection point at $2.1\times10^{-11}$ g/L. This value might not be a correct CMC for HA-coated micelle, because polymer/probe ratio is not sufficient high at such low polymer concentration. But we can say that the CMC value for the HA-coated micelle is below the limit of this method and the micelle has a significantly higher stability against dilution. We also confirmed the improvement of colloidal stability of the HA-coated micelle than non-coated micelle in the absence and presence of serum components (*43*). The diameter of the HA-coated micelle was almost constant for 24 h in the presence of serum componets. However, the diameter of the non-coated micelle increased with incubation time, and precipitation was observed after 12 h at the same condition. These results suggest that non-coated micelle become self-aggregated or interact with serum proteins to form insoluble aggregates within 12 h, but the HA-coated micelle does not exhibit self-aggregation or interaction with serum proteins for 24 h. Moreover, the HA-coated micelle did not show cytotoxicity although cationic non-coated micelle showed weak cytotoxicity. The release of model drug from the micelle could be suppressed by coating with HA (*44*).

It was reported that HA can be recognized by the receptors existing on the liver sinusoidal endothelial cells (LSECs) (*55–57*), and more than 90% of HA in the bloodstream is known to be taken up and metabolized by LSECs. To evaluate HA-coated micelles as cyto-specific drug carriers, uptake of the FITC-labeled HA-coated micelle into LSECs and Kupffer cells were investigated by flow cytometeric analysis (*44*). Other anionic polysaccharides, heparin (Hep) and carboxymethyl-dextran (CMDex), were used as controls for outer polyelectrolyte to coat the positively charged micelles. Figure 8 shows the results of flow cytometric analysis (*44*). A large amount of Hep-coated micelles were incorporated into Kupffer cells, while a smaller amount of the micelles was incorporated into LSECs. CMDex-coated micelle showed efficient uptake into both of LSECs and Kupffer cells, exhibiting no specificity. Interestingly, almost no HA-coated micelles were incorporated into Kupffer cells. Although the uptake amount was lower than Hep-coated micelles, HA-coated micelles showed a certain amount of uptake into LSECs. These results suggested HA-coated micelles were taken up into LSECs via specific interactions with HA-receptors expressed on LSEC and could escape from Kupffer cell, which is one of RES cells. Thus, we could control the liver cellular uptake behavior of polyanion-coated polymeric micelles by changing the outer polyanions. We can use other polyelectrolytes, such as polyanions having specific pilot moieties as outer PIC layers. Such polyelectrolyte-coated micelles having specific outer layers can be prepared only by changing the outer polyelectrolytes, like a “dress-up doll”. Therefore, the polyelectrolyte-coated micelle system having high stability in body fluids, exhibiting sustained release of drugs, low cytotoxicity and changeable specificity with target cells is an excellent candidate for drug delivery vehicles, realizing efficient drug targeting to a specific site.

Downloaded by UNIV OF ROCHESTER on July 20, 2013 | http://pubs.acs.org
Publication Date (Web): July 8, 2013 | doi: 10.1021/bk-2013-1135.ch007



In Tailored Polymer Architectures for Pharmaceutical and Biomedical Applications; Scholz, C., et al.;
ACS Symposium Series; American Chemical Society: Washington, DC, 2013.

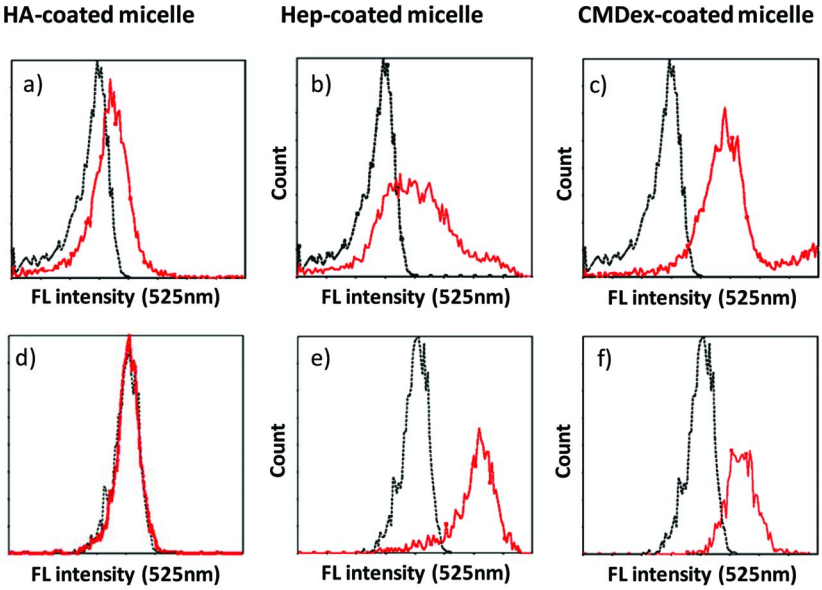


*Figure 8. The results of flow cytometric analysis for uptake of HA-coated micelles, Hep-coated micelles, and CMDex-coated micelles into LSECs and Kupffer cells. Black line: cells only; red line: cells + micelles. a, b, c: LSECs and d, e, f: Kupffer cells; a, d: HA-coated micelles; b, e: Hep-coated micelles; c, f: CMDex-coated micelles. (Reproduced with permission from reference (44). Copyright 2011 Elsevier.) (see color insert)*

Downloaded by UNIV OF ROCHESTER on July 20, 2013 | http://pubs.acs.org
Publication Date (Web): July 8, 2013 | doi: 10.1021/bk-2013-1135.ch007

## 6. Summary and Outlook

The preparation and stabilization of polymeric micelles by electrostatic interaction were reviewed. As described, electrostatic interaction has many advantages and possibility to prepare biomedical materials and systems. It is very important to achieve enough stability in blood stream and to suppress non-specific interactions for efficient drug delivery to specific sites (cells or organs) by EPR effect and pilot moiety immobilization. Electrostatic interaction can offer both of reversible (dissociable) characters and certain level of thermodynamic stability at the same time. This character is very convenient for design of biomedical materials, which are expected to be degraded, dissociated, excreted and metabolized after the temporal use.

## Acknowledgments

The author's works introduced in this review were financially supported by a Grant-in-Aid for Scientific Research (B) (No. 22300172) from the *Japan Society for the Promotion of Science (JSPS)* and "Strategic Project to Support the Formation of Research Bases at Private Universities": Matching Fund Subsidy from *MEXT (Ministry of Education, Culture, Sports, Science and Technology, Japan)*, 2010-2014.

## References

1. Ohya, Y.; Takahashi, A.; Nagahama, K. *Adv. Polym. Sci.* **2012**, *247*, 65–114.
2. Kataoka, K.; Harada, A.; Nagasaki, Y. *Adv. Drug Delivery Rev.* **2001**, *47*, 113–131.
3. Torchilin, V. P. *Adv. Drug Delivery Rev.* **2002**, *54*, 235–252.
4. Kwon, G. S. *Crit. Rev. Ther. Drug Carrier Syst.* **2003**, *20*, 357–403.
5. van Nostrum, C. F. *Adv. Drug Delivery Rev.* **2004**, *56*, 9–16.
6. Gaucher, G.; Dufresne, M. H.; Sant, V. P.; Kang, N.; Maysinger, D.; Leroux, J. C. *J. Controlled Release* **2005**, *109*, 169–188.
7. Nishiyama, N.; Kataoka, K. *Pharmacol. Ther.* **2006**, *112*, 630–648.
8. Matsumura, Y. *J. Drug Targeting* **2007**, *15*, 507–517.
9. Xiong, X. B.; Falamarzian, A.; Garg, S. M.; Lavasanifar, A. *J. Controlled Release* **2011**, *155*, 248–261.
10. Matsumura, Y.; Maeda, H. *Cancer Res.* **1986**, *46*, 6387–6392.
11. Maeda, H.; Matsumura, Y. *Crit. Rev. Ther. Drug Carrier Syst.* **1989**, *6*, 193–210.
12. Greish, K. *J. Drug Targeting* **2007**, *15*, 457–464.
13. Rijcken, C. J.; Snel, C. J.; Schiffelers, R. M.; van Nostrum, C. F.; Hennink, W. E. *Biomaterials* **2007**, *28*, 5581–5593.
14. Jiang, J.; Qi, B.; Lepage, M.; Zhao, Y. *Macromolecules* **2007**, *40*, 790–792.
15. Zhang, Q.; Remsen, E. E.; Wooley, K. L. *J. Am. Chem. Soc.* **2000**, *122*, 3642–3651.
16. Wooley, K. L. *J. Polym. Sci., Part A.: Polym. Chem.* **2000**, *38*, 1397–1407.
17. Butun, V.; Lowe, A. B.; Billingham, N. C.; Armes, S. P. *J. Am. Chem. Soc.* **1999**, *121*, 4288–4289.
18. Stewart, S.; Liu, G. *Chem. Mater.* **1999**, *11*, 1048–1054.
19. Thurmond, K. B., II; Kowalewski, T.; Wooley, K. L. *J. Am. Chem. Soc.* **1996**, *118*, 7239–7240.
20. van Nostrum, C. F. *Soft Matter* **2011**, *7*, 3246–3259.
21. O'Reilly, R. K.; Hawker, C. J.; Wooley, K. L. *Chem. Soc. Rev.* **2006**, *35*, 1068–1083.
22. Read, E. S.; Armes, S. P. *Chem. Commun.* **2007**, 3021–3035.
23. Harada, A.; Kataoka, K. *Macromolecules* **1995**, *28*, 5294–5299.
24. Harada, A.; Kataoka, K. *Science* **1999**, *283*, 65–67.
25. Harada, A.; Kataoka, K. *J. Am. Chem. Soc.* **1999**, *121*, 9241–9242.
26. Kabanov, A. V.; Bronich, T. K.; Kabanov, V. A.; Yu, K.; Eisenberg, A. *Macromolecules* **1996**, *29*, 6797–6802.



In Tailored Polymer Architectures for Pharmaceutical and Biomedical Applications; Scholz, C., et al.; ACS Symposium Series; American Chemical Society: Washington, DC, 2013.

Downloaded by UNIV OF ROCHESTER on July 20, 2013 | http://pubs.acs.org
Publication Date (Web): July 8, 2013 | doi: 10.1021/bk-2013-1135.ch007

27. Bronich, T. K.; Keifer, P. A.; Shlyakhtenko, L. S.; Kabanov, A. V. *J. Am. Chem. Soc.* **2005**, *127*, 8236–8237.
28. Osada, K.; Kataoka, K. *Adv. Polym. Sci.* **2006**, *202*, 113–153.
29. Kakizawa, K.; Kataoka, K. *Adv. Drug Delivery Rev.* **2002**, *54*, 203–222.
30. Ohya, Y.; Masunaga, T.; Baba, T.; Ouchi, T. *J. Biomater. Sci., Polym. Ed.* **1996**, *7*, 1085–1096.
31. Ohya, Y.; Oue, H.; Nagatomi, K.; Ouchi, T. *Biomacromolecules* **2001**, *2*, 927–933.
32. Ichinose, K.; Tomiyama, N.; Nakashima, M.; Ohya, Y.; Ichikawa, M.; Ouchi, T.; Kanematsu, T. *Anticancer Drugs* **2000**, *11*, 33–38.
33. Cabral, H.; Nishiyama, N.; Kataoka, K. *J. Controlled Release* **2007**, *121*, 146–155.
34. Cabral, H.; Nishiyama, N.; Okazaki, S.; Koyama, H.; Kataoka, K. *J. Controlled Release* **2005**, *101*, 223–232.
35. Nishiyama, N.; Okazaki, S.; Cabral, H.; Miyamoto, M.; Kato, Y.; Sugiyama, Y.; Nishio, K.; Matsumura, Y.; Kataoka, K. *Cancer Res.* **2003**, *63*, 8977–8983.
36. Cabral1, H.; Matsumoto, Y.; Mizuno, K.; Chen, Q.; Murakami, M.; Kimura, M.; Terada, Y.; Kano, M. R.; Miyazono, K.; Uesaka, M.; Nishiyama, N.; Kataoka, K. *Nat. Nanotechnol.* **2011**, *6*, 815–823.
37. Yan, Y.; Besseling, N. A. M.; de Keizer, A.; Marcelis, A. T. M.; Drechsler, M.; Stuart, M. A. C. *Angew. Chem., Int. Ed.* **2007**, *46*, 1807–1809.
38. Wang, J.; Stuart, M. A. C.; Marcelis, A. T. M.; Colomb-Delsuc, M.; Otto, S.; van der Gucht, J. *Macromolecules* **2012**, *45*, 7179–7185.
39. Cha, E.-J.; Kim, J. E.; Ahn, C.-H. *Eur. J. Pharm. Sci.* **2009**, *38*, 341–346.
40. Decher, G. *Science* **1997**, *277*, 1232–1237.
41. Weaver, J. V. M.; Tang, Y. Q.; Liu, S.; Iddon, P. D.; Grigg, R.; Billingham, N. C.; Armes, S. P.; Hunter, R.; Rannard, S. P. *Angew. Chem., Int. Ed.* **2004**, *43*, 1389–1392.
42. Lokitz, B. S.; Convertine, A. J.; Ezell, R. G.; Heidenreich, A.; Li, Y.; McCormick, C. L. *Macromolecules* **2006**, *39*, 8594–8602.
43. Ohya, Y.; Takeda, S.; Shibata, Y.; Ouchi, T.; Maruyama, A. *Macromol. Chem. Phys.* **2010**, *211*, 1750–1756.
44. Ohya, Y.; Takeda, S.; Shibata, Y.; Ouchi, T.; Kano, A.; Iwata, T.; Mochizuki, S.; Taniwaki, Y.; Maruyama, A. *J. Controlled Release* **2011**, *155*, 104–110.
45. Ciobanu, M.; Heurtault, B.; Shultz, P.; Ruhlmann, C.; Muller, C. D.; Frisch, B. *Int. J. Pharm.* **2007**, *344*, 154–157.
46. Lee, H.; Jeong, Y.; Park, T. G. *Biomacromolecules* **2007**, *8*, 3705–3711.
47. Germain, M.; Grube, S.; Carriere, V.; Richard-Foy, H.; Winterhalter, M.; Fournier, D. *Adv. Mater.* **2006**, *18*, 2868–2871.
48. Ito, Y.; Matsusaki, M.; Kida, T.; Akashi, M. *Biomacromolecules* **2006**, *7*, 2715–2718.
49. Johnston, A. P. R.; Such, G. K.; Ng, S. L.; Caruso, F. *Curr. Opin. Colloid Interface Sci.* **2011**, *16*, 171–181.
50. Ochs, C. J.; Such, G. K.; Caruso, F. *Langmuir* **2010**, *27*, 1275–1280.


In Tailored Polymer Architectures for Pharmaceutical and Biomedical Applications; Scholz, C., et al.;
ACS Symposium Series; American Chemical Society: Washington, DC, 2013.

Downloaded by UNIV OF ROCHESTER on July 20, 2013 | http://pubs.acs.org
Publication Date (Web): July 8, 2013 | doi: 10.1021/bk-2013-1135.ch007

51. Chandrawati, R.; Hosta-Rigau, L.; Vanderstraaten, D.; Lokuliyana, S.; Stadler, B.; Albericio, F.; Caruso, F. *ACS Nano* **2010**, *4*, 1351–1361.
52. Arimura, H.; Ohya, Y.; Ouchi, T. *Macromol. Rapid Commun.* **2004**, *25*, 743–747.
53. Arimura, H.; Ohya, Y.; Ouchi, T. *Biomacromolecules* **2005**, *6*, 720–725.
54. Ouchi, T.; Miyazaki, H.; Arimura, H.; Tasaka, F.; Hamada, A.; Ohya, Y. *J. Polym. Sci., Part A: Polym. Chem.* **2002**, *40*, 1426–1432.
55. Yannariello-Brown, J.; Frost, S. J.; Weigel, P. H. *J. Biol. Chem.* **1992**, *267*, 20451–20456.
56. Weigel, J. A.; Weigel, P. H. *J. Biol. Chem.* **2003**, *278*, 42802–42811.
57. Mochizuki, S.; Kano, A.; Shimada, N.; Maruyama, A. *J. Biomater. Sci., Polym. Ed.* **2009**, *20*, 83–97.

Downloaded by UNIV OF ROCHESTER on July 20, 2013 | http://pubs.acs.org
Publication Date (Web): July 8, 2013 | doi: 10.1021/bk-2013-1135.ch007

Downloaded by UNIV TENNESSEE KNOXVILLE CAMPUS on July 17, 2013 | http://pubs.acs.org
Publication Date (Web): July 8, 2013 | doi: 10.1021/bk-2013-1135.ch008

## Chapter 8

# Combating HIV-1 Entry and Fusion with Peptide–Synthetic Polymer Conjugates

**Maarten Danial[1,2] and Harm-Anton Klok[*,1]**

**[1]École Polytechnique Fédérale de Lausanne, Institut des Matériaux and Institut des Sciences et Ingénierie Chimiques, Laboratoire des Polymères, Bâtiment MXD, 1015 Lausanne, Switzerland**
**[2]Current affiliation: Key Centre for Polymers & Colloids, The University of Sydney, School of Chemistry, Building F11, Sydney NSW 2006, Australia**
**[*]E-mail: Harm-Anton.Klok@epfl.ch.**

This Chapter presents the preparation and properties of two families of peptide–synthetic polymer conjugates that are designed to combat HIV-1–host cell entry and fusion. In a first example, a post-polymerization modification strategy is used to prepare synthetic polymers that contain a large number of short peptides that can bind in a polyvalent fashion to the gp120 envelope proteins on HIV-1 and thereby prevent subsequent binding of the HIV-1 virion to the CD4 receptors on the host cell. In the second example, site-specific PEGylation is explored to modify peptide-based fusion inhibitors. Screening of a small library of PEGylated fusion inhibitors reveals that judicious selection of the site of PEGylation allows to increase the proteolytic stability of the peptides, while minimizing the loss of efficacy due to the attachment of the PEG chain. These two examples exemplify the power of the modern polymer chemistry toolbox, and more specifically of controlled radical polymerization in combination with site-specific chemo-selective coupling chemistry such as thiol-acrylate Michael addition and thiol-ene addition, to provide access to therapeutic peptide−synthetic polymer conjugates with improved efficacies and pharmacokinetics as compared to non-modified peptide and protein drugs.

© 2013 American Chemical Society
In Tailored Polymer Architectures for Pharmaceutical and Biomedical Applications; Scholz, C., et al.; ACS Symposium Series; American Chemical Society: Washington, DC, 2013.

Downloaded by UNIV TENNESSEE KNOXVILLE CAMPUS on July 17, 2013 | http://pubs.acs.org
Publication Date (Web): July 8, 2013 | doi: 10.1021/bk-2013-1135.ch008

# Introduction

The human immunodeficiency virus type 1 (HIV-1) has globally affected more than 33 million individuals with 1.8 million deaths and 2.6 million new infections estimated in 2009 (*1*). Although advances in the fundamental understanding of the HIV-1 life cycle have led to the availability of a range of effective antiretroviral inhibitors and broadly neutralizing antibodies, an effective vaccine against this virus that causes acquired immune deficiency syndrome (AIDS) remains to be developed (*2*).

The HIV-1 life cycle (Figure 1) consists of four main events that ultimately lead to the release of new HIV-1 virions: (i) viral recognition and fusion that lead to viral entry into the host cell, (ii) reverse transcription of viral RNA into double stranded DNA, which is subsequently (iii) integrated into the host cell genome via integrase activity. Through cellular mechanisms, the infected host cell DNA is transcribed into messenger RNA that is translated into polypeptides, and is converted into functional proteins through (iv) protease activity. Therapeutics that prevent HIV-1 infection can intervene at each of these four stages by inhibiting (i) cellular attachment (entry) and membrane fusion, (ii) reverse transcription (iii) viral double stranded DNA integration, and (iv) maturation/proteolysis (Figure 1) (*3*).

Fusion and entry inhibitors are particularly attractive therapeutics since they prohibit the virus from entering the host cell as opposed to the other classes of antivirals that only act after the virus has already penetrated the host cell membrane. As Figure 2 illustrates, HIV-1 entry and fusion is caused by the glycoprotein Env, which consists of a closely associated trimer of heterodimers ($gp120_3/gp41_3$) on the virion surface (*4*, *5*). An HIV-1 virion displays ~ 14 copies of the Env trimer on its surface, although a notable number of these glycoproteins adopt a non-functional form that is incapable of initiating viral entry (*6*, *7*). HIV-1 cell infection starts with the interaction of the gp120 subunits with the CD4 receptor and a CXCR4 or CCR5 coreceptor on the host cell membrane. Binding of gp120 with CD4 and a coreceptor then leads to a series of conformational changes causing the exposure of the gp41 trimer. In its prefusogenic state, a glycine-rich region at the N-terminus of gp41 trimer anchors into the host cell membrane. Subsequently, the heptad repeat 1 domain (HR1) folds onto the HR2 domain on gp41 forming a trimer-of-hairpins (also known as a six-helix bundle), which brings the viral and host cell membrane into close proximity and ultimately leads to the fusion of the membranes releasing the viral contents in to the host cell (post-fusogenic state, Figure 2) (*8*).

One approach in the development of HIV-1 entry inhibitors involves the use of small molecules that block the interaction of gp120 with the CD4 receptor and/or coreceptor. The FDA-approved drug maraviroc binds to the CCR5 coreceptor and thereby blocks its interaction with gp120 on HIV-1. A drawback of maraviroc is that it is only potent against CCR5-tropic HIV-1, which means that the drug is ineffective against HIV-1 that utilizes CXCR4 (*9*). In addition, broadly neutralizing antibodies that bind to gp120 envelope proteins are also attractive entry inhibitors since many of these interfere with gp120-CD4 receptor binding and thus prevent the virus from entering the host cell (*10*). One particular


In Tailored Polymer Architectures for Pharmaceutical and Biomedical Applications; Scholz, C., et al.;
ACS Symposium Series; American Chemical Society: Washington, DC, 2013.

example of a neutralizing antibody is IgG1 b12 that was developed from the bone marrow of an HIV positive patient (*11*). Elucidation of this IgG1 b12 antibody crystal structure revealed an unusual long CDR H3 loop located on both Fab regions of the antibody (*12*). The CDR H3 loop consists of 18 amino acids with a tryptophan residue located at its apex, which rises approximately 15 Å above the surface of the Fab domain. Computational docking studies between IgG b12 Fab (containing the CDR H3 loop) and gp120 suggested that the projected structure adopted by CDR H3 in Fab inserts into a polar pocket on gp120. Comparison of the model obtained between IgG1 b12 Fab and gp120 and the CD4-gp120 crystal structure revealed that a peptide loop in CD4 present binds to that same polar pocket on gp120. Binding to gp120 and entry inhibition was further confirmed with the ligation of the CDR H3 peptide to bovine serum albumin which was capable of HIV-1 neutralization (*12*).

Several strategies to generate polyvalent HIV-1 entry inhibitors have been explored. Examples of polymeric compounds that have been used to prevent HIV-1 entry include polyanions such as natural sulfated polysaccharides (*13*, *14*) or synthetic sulfated polymers (*15–17*) that bind to the positively charged residues on the gp120 envelope protein (*18*). In addition, attempts have also been made to develop target-specific polyvalent HIV-1 entry inhibitors. Li et al., for example developed bivalent CD4 miniproteins, which consist of polypeptides that mimic the CD4 receptor linked by a poly(ethylene glycol) (PEG) spacer. The bivalent CD4 miniproteins were found to be 21-fold more effective against HIV-1 entry than the CD4 mimicking polypeptide alone (*19*). In a subsequent paper, these authors reported the development of trivalent CD4 miniproteins that consisted of CD4 mimicking peptides that were attached to Kemp's acid or triazacyclododecane (*20*). The trivalent CD4 miniproteins, however, exhibited anti-HIV activities that were comparable to the bivalent CD4 miniproteins. More recently, effective multivalent anti-HIV inhibitors have been developed using methacrylamide-based polymers that have pendant benzoboroxole functionalities (*21*). The benzoboroxole moieties bind to the 4,6-diols on the mannopyranose residues present on gp120 and thus block the interaction between CD4 receptor and HIV-1. In a follow-up study, the efficacy of the benzoboroxole methacrylamide polymers against HIV-1 entry was further improved through the addition of 10 mole percent sulfonic acid pendant groups throughout polymer chain. These sulfonic acid pendant groups not only improved solubility but also improved electrostatic interactions between the polymer and the positively charged V3 loop on gp120 thereby mediating a higher efficacy (*18*, *22*).

Another approach to combat HIV-1 is to prevent virus–host cell fusion. One strategy to accomplish this, is by the use of peptides derived from the HR1 or HR2 regions of gp41, which act as competitive inhibitors by binding to the HR2 and HR1 domains on gp41, respectively (*23–26*). A prominent example of a HR2 derived fusion inhibitor is T-20 (Enfuvirtide or Fuzeon®), which was approved by the FDA in 2003. T-20 works by binding to the HR1 domain of gp41 on HIV-1, which prevents the formation of the trimer-of-hairpins between the HR1 and HR2 domains of gp41, thus abrogating virus and host cell membrane fusion (*27–29*). However, due to the high cost of production and requirement


In Tailored Polymer Architectures for Pharmaceutical and Biomedical Applications; Scholz, C., et al.;
ACS Symposium Series; American Chemical Society: Washington, DC, 2013.

Downloaded by UNIV TENNESSEE KNOXVILLE CAMPUS on July 17, 2013 | http://pubs.acs.org
Publication Date (Web): July 8, 2013 | doi: 10.1021/bk-2013-1135.ch008

for parenteral administration, it is primarily used as salvage therapy for HIV-1 patients, who show little response to standard antiretroviral therapy (*9*). Another drawback of T-20 is that its effectiveness is short lived due to its short plasma half-life (3.8 h) (*30*) and susceptibility to proteolytic degradation.

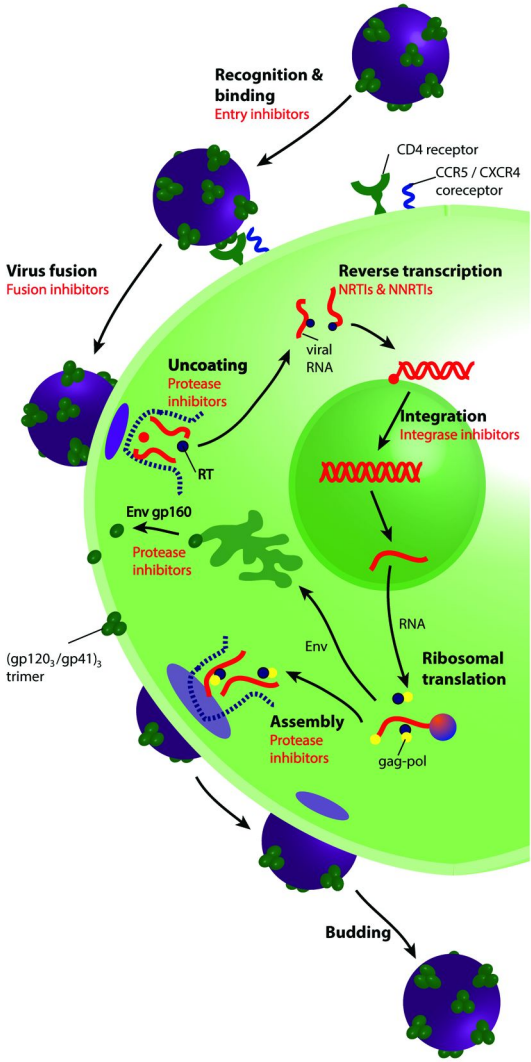


*Figure 1. An illustration depicting the HIV-1 life cycle highlighting the different possibilities for therapeutic intervention. Strategies to combat HIV-1 infection include (i) entry and fusion inhibition, (ii) reverse transcriptase inhibition via nucleotide, nucleoside and non-nucleoside inhibitors; (iii) integrase inhibition and (iv) protease inhibition.*



In Tailored Polymer Architectures for Pharmaceutical and Biomedical Applications; Scholz, C., et al.; ACS Symposium Series; American Chemical Society: Washington, DC, 2013.

Downloaded by UNIV TENNESSEE KNOXVILLE CAMPUS on July 17, 2013 | http://pubs.acs.org
Publication Date (Web): July 8, 2013 | doi: 10.1021/bk-2013-1135.ch008

Downloaded by UNIV TENNESSEE KNOXVILLE CAMPUS on July 17, 2013 | http://pubs.acs.org
Publication Date (Web): July 8, 2013 | doi: 10.1021/bk-2013-1135.ch008

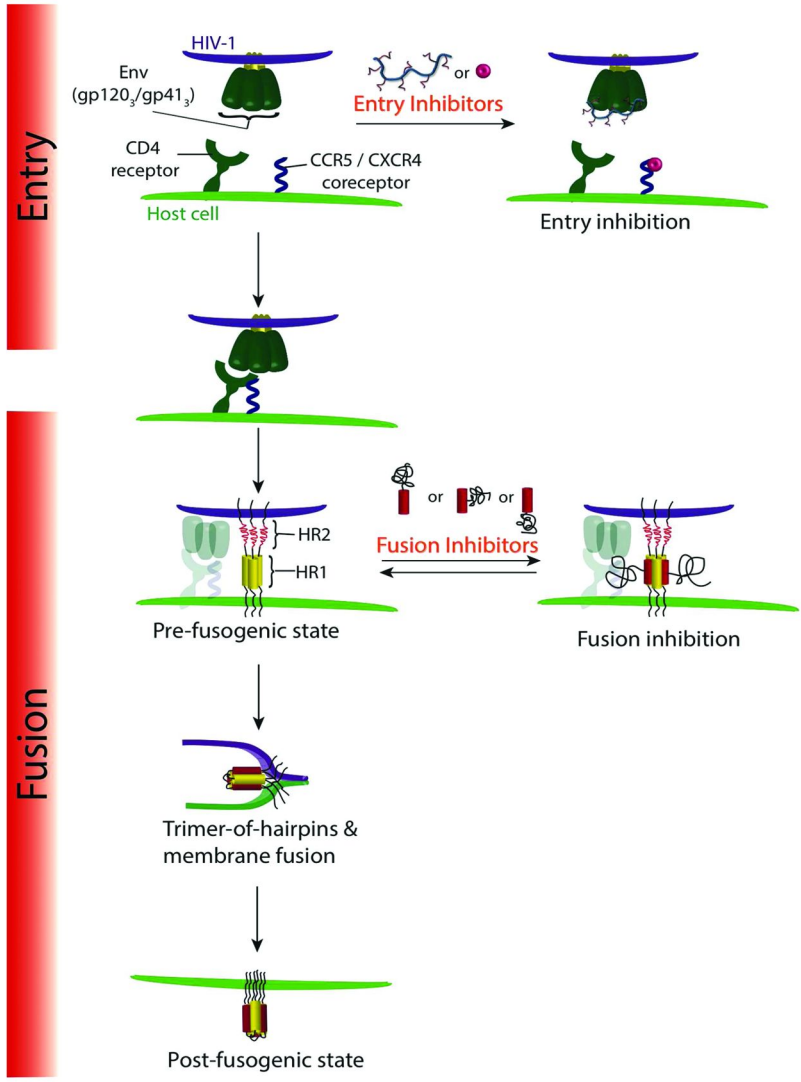


*Figure 2. An illustration showing entry and fusion inhibition. HIV-1 entry inhibition can be achieved by polyvalent polymer inhibitors or chemokine antagonists. Fusion inhibition can be achieved using peptide - synthetic polymer conjugates that form competitive inhibitors.*

Several strategies have been developed to improve the pharmacokinetics and *in vivo* half-life of peptide-based HIV-1 fusion inhibitors. One approach encompasses the design of 'third generation' fusion inhibitors that contain stabilizing intramolecular salt-bridges (*25*) or covalent bonds (*23*, *31*). Another


In Tailored Polymer Architectures for Pharmaceutical and Biomedical Applications; Scholz, C., et al.;
ACS Symposium Series; American Chemical Society: Washington, DC, 2013.

option is the use of small peptide inhibitors that contain D-amino acids (*32*) or β-amino acids (*33*) which are both resistant to proteases. Alternatively, conjugation of polymers such as poly(ethylene glycol) (PEG) has proven an attractive strategy to improve the pharmacokinetics and stablitiy of peptide/protein drugs. PEGylation is widely used to prevent proteolytic degradation and reduce renal elimination of peptide/protein drugs (*34–37*) including HR2-derived peptides intended as anti-HIV fusion inhibitors (*38*, *39*). Exemplified by the PEGylation of the HR2 derived peptides T-20 and T-1249, a common drawback of PEGylation is the reduction in biological activity of the peptide or protein drug (*38*, *39*). However, through a judicial choice of PEGylation via site-specific chemistry the detrimental effects upon biological activity can be minimized. An example is the mono-PEGylation of erythropoiesis protein, which leads to a 2-fold increase in the plasma residence time and elimination time while maintaining the cell proliferation activity (*40*).

From the short survey presented above, it is apparent that peptides and proteins are attractive therapeutics to fight HIV-1 entry and fusion. The efficacy of such peptide and protein based inhibitors, however, is often compromised due to their relatively short plasma half-life and susceptibility to proteolysis as well as due to the fact that virus-host cell recognition processes often involve multivalent interactions, which are challenging to antagonize with a monovalent ligand. Polymer chemistry provides a powerful toolbox to overcome these problems and improve the stability, half-life and activity of peptide and protein based therapeutics. This Chapter will present a summary of two recently published studies from our laboratory, which serve to illustrate this. The first example will present the design, synthesis and performance of multivalent HIV-1 entry inhibitors based on side-chain peptide–polymer conjugates (*41*). The second example will underline the importance of site-selective PEGylation to improve the stability of peptide-based HIV-1 fusion inhibitors while minimizing the loss of activity upon polymer modification (*42*).

## Polyvalent Side Chain Peptide–Synthetic Polymer Conjugates as HIV-1 Entry Inhibitors

In the mid 1990s, an antibody Fab b12 was identified from a combinatorial phage display library developed from the bone marrow of an HIV-1 infected individual (*11*). After the conversion of the Fab b12 to a whole immunoglobulin molecule, the resultant antibody IgG1 b12 proved to be effective against laboratory HIV-1 strains using a syncytial formation assay as well as against a set of 10 primary HIV-1 isolates using a p24 reporter assay (*11*). In 2001, Saphire et al. reported the crystal structure of IgG1 b12 and elucidated the molecular basis by which the antibody IgG1 b12 causes HIV-1 neutralization (*12*). In this study, an 18 amino acid sequence known as the CDR H3 region in the antibody IgG1 b12 was identified, which was proposed to dock onto the gp120 envelope protein on HIV-1 and prevent subsequent binding of the CD4 receptor on the host cell


In Tailored Polymer Architectures for Pharmaceutical and Biomedical Applications; Scholz, C., et al.;
ACS Symposium Series; American Chemical Society: Washington, DC, 2013.

Downloaded by UNIV TENNESSEE KNOXVILLE CAMPUS on July 17, 2013 | http://pubs.acs.org
Publication Date (Web): July 8, 2013 | doi: 10.1021/bk-2013-1135.ch008

thereby preventing virus-host cell membrane fusion (*12*). In addition, a bovine serum albumin conjugate that displays this peptide was shown to neutralize the virus. Based on the work by Saphire et al. (*12*), we hypothesized that the peptide derived from CDR H3 could be an attractive candidate for the development of polyvalent entry inhibitors.

To explore the feasibility of the CDR H3 peptide for the development of polyvalent HIV-1 entry inhibitors, a library of 10 side chain peptide–synthetic polymer conjugates was prepared via a sequential post-polymerization modification strategy. As has been reviewed recently by Günay, Theato and Klok, the versatility of post-polymerization modification has been demonstrated as a facile route for the synthesis of (multi)functional polymers from well-defined, easy-modifiable polymeric precursors (*43*). In addition, sequential (or double) post-polymerization modifications have enabled diversification of chemical functionality and permit introduction of chemical moieties that are otherwise not accessible from direct polymerization (*44*, *45*). Employing this strategy, the design of these polymer conjugates and in particular their degree of polymerization can be tailored towards the structure of the HIV-1 virion envelope proteins. The design of these polymer conjugates and in particular their degree of polymerization, takes into account the structure of the HIV-1 virion envelope proteins and the fact that polyvalent inhibition can occur at two length scales: (i) polymers with a low degree of polymerization with two of three pendant CDR H3 peptide ligands may span 15 nm (*7*) and bind simultaneously to a single envelope spike, while (ii) polymers with a high degree of polymerization could span at least two envelope spikes, which corresponds to a distance of 7–80 nm (*7*). The polymer conjugates were prepared following a 3-step ester-amide/thiol-ene post-polymerization modification strategy, which is illustrated in Scheme 1. In a first step, pentafluorophenyl methacrylate (PFMA) (*46*) was polymerized either via reversible addition-fragmentation chain transfer (RAFT) polymerization using a 4-cyanopentanoic acid dithiobenzoate as chain transfer agent (CTA) or by conventional free radical polymerization (FRP) to yield polymers with varying degrees of polymerization. Poly(pentafluorophenyl methacrylate) (PPFMA) precursor polymers with degrees of polymerization of 199, 269, 372 were obtained by RAFT, while a PPFMA polymer with a degree of polymerization of 539 was obtained by FRP (*41*). For the PPFMA precursor polymers synthesized by RAFT, the dithiobenzoate end-group was then replaced with an isobutyronitrile group using 30 mol % of the initiator azobisisobutyronitrile (AIBN) (*47*). Post-polymerization modification of the pendant active ester moieties on PPFMA can be easily achieved with primary amines in the presence of a base e.g. triethylamine (*48*). The PPFMA polymers presented here were reacted with 1 equivalent (relative to the PFMA moieties) of a 50/50 or 20/80 (mol/mol) mixture of allylamine and 2-hydroxypropylamine. In a final post-polymerization modification reaction, a thiol-ene coupling of the CDR H3 peptide via the thiol group on N-terminal cysteine residue to the pendant allyl side chains was performed (*48*). Table I presents the library of the CDR H3 pendant peptide–polymer conjugates that was prepared. In addition to polyvalent CDR H3 peptide–polymer conjugates, a peptide with a scrambled amino acid sequence was conjugated via thiol-ene addition to the poly(allyl

Downloaded by UNIV TENNESSEE KNOXVILLE CAMPUS on July 17, 2013 | http://pubs.acs.org
Publication Date (Web): July 8, 2013 | doi: 10.1021/bk-2013-1135.ch008


In Tailored Polymer Architectures for Pharmaceutical and Biomedical Applications; Scholz, C., et al.;
ACS Symposium Series; American Chemical Society: Washington, DC, 2013.

methacrylamide-*co*-2-hydroxypropyl methacrylamide) copolymer to create a negative control (**11**) for the HIV-1 entry inhibition assays (*vide infra*). All polyvalent peptide–polymer conjugates were analyzed by $^1$H-NMR to determine the number of peptides per polymer chain (Table I) (*41*).

The side-chain peptide–synthetic polymer conjugates were evaluated with regards to their ability to inhibit infection of HOS CCR5 cells by single cycle HIV-1 viruses. For these experiments, HOS CCR5 cells were used that expressed the CD4 receptor as well as the CCR5 coreceptor and the CXCR4 coreceptor (*49*). The presence of both coreceptors on the HOS CCR5 cells permitted the evaluation of the infectivity inhibition of both X4- and R5-tropic strains of HIV-1 (pseudotyped HXB2 and JRFL, respectively). Both HIV-1 strains carried a luciferase reporter construct, which allowed luminescent detection of productive infection. Infection of the HOS CCR5 cells would lead to luciferase activity while complete inhibition of the HIV-1 would lead to no lucerifase activity. The inhibitory potencies of all the polyvalent conjugates along with the CDR H3 peptide, as well as the polyvalent scrambled peptide–polymer conjugate and IgG1 b12 controls are presented in Figure 3. While the side chain peptide–polymer conjugates showed efficacies in the low micromolar range, neither the polyvalent scrambled peptide–polymer conjugate (**11**) nor the CDR H3 peptide alone showed anti-HIV-1 activity up to 100 μM (Figure 3A). Comparison of the $IC_{50}$ values derived from the titration experiments of the polyvalent peptide–polymer conjugates revealed a clear influence of the number-average degree of polymerization (DP) on antiviral activity. As shown in Figure 3B, the $IC_{50}$ values are around 10 μM for the peptide–polymer conjugates with DP's of 199 and 269, respectively, whereas the larger copolymer with a DP of 372 were the most effectitive with $IC_{50}$ values ~ 2 μM. The largest polyvalent peptide–polymer conjugate with a DP of 539 yielded an $IC_{50}$ value of ~ 10 μM. Performing the infection inhibition assays with the HIV-$1_{JRFL}$ viral strain lead to similar results, albeit with slightly higher $IC_{50}$ values (~10–30 μM) as compared to the HIV-$1_{HXB2}$ strain. The polyvalent peptide–synthetic polymer inhibitors have similar efficacies as compared to a variety of other polyvalent HIV-1 entry inhibitors. The bivalent CD4M9 entry inhbitors reported by Li et al. showed a maximum efficacy of 0.12 μM with an intermediate spacer length (*19*). Furthermore, trivalent entry inhibitors by the same group exhibited efficacies ranging from 0.4–3.0 μM (*20*).

The chain length dependency observed in Figure 3, can be attributed to the opposing contributions of the enthalpy and entropy of binding to the overall free energy (*50*). While the polyvalent peptide–polymer conjugates **1**–**4** may not be sufficiently long to span the distance between two neighboring Env spikes, conjugates **5**–**9** are sufficiently long to bridge the distance between Env spikes. While conjugate **10** is sufficiently long to span the distance between multiple spikes, the $IC_{50}$ value is higher as compared to **5**–**9**, which is attributed to the increased entropic penalty that goes with polyvalent binding of these long chain polymer conjugates as compared to the lower molecular weight analogues.

Downloaded by UNIV TENNESSEE KNOXVILLE CAMPUS on July 17, 2013 | http://pubs.acs.org
Publication Date (Web): July 8, 2013 | doi: 10.1021/bk-2013-1135.ch008


In Tailored Polymer Architectures for Pharmaceutical and Biomedical Applications; Scholz, C., et al.;
ACS Symposium Series; American Chemical Society: Washington, DC, 2013.

Downloaded by UNIV TENNESSEE KNOXVILLE CAMPUS on July 17, 2013 | http://pubs.acs.org
Publication Date (Web): July 8, 2013 | doi: 10.1021/bk-2013-1135.ch008



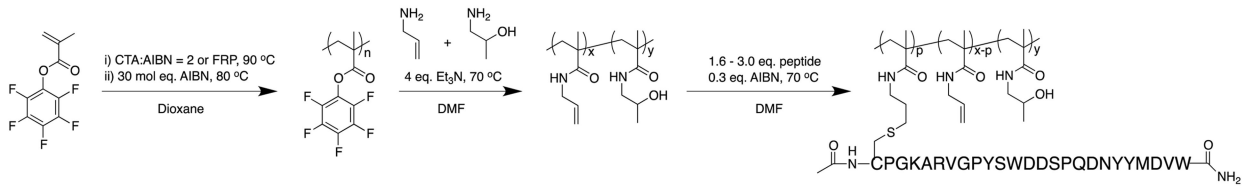


*Scheme 1. Synthesis of side chain peptide–synthetic polymer conjugates via polymerization of pentafluorophenyl methacrylate and successive post-polymerization modification with allylamine/2-hydroxypropylamine and thiol-ene reaction of the cysteine containing peptide. Adapted with permission from Danial et al. (41) Copyright 2012 American Chemical Society.*

**Table I. Properties of the peptide modified copolymers. Adapted with permission from Danial et al. (*41*) Copyright 2012 American Chemical Society.**

| *Peptide-copolymer* | *Copolymer DP*[a] *(-)* | *Peptide per copolymer (%)*[b] | *Number of peptides per copolymer*[c] *(-)* |
|---|---|---|---|
| **1** | 199 | 10.9 | 18 |
| **2** | 199 | 7.2 | 12 |
| **3** | 269 | 7.5 | 19 |
| **4** | 269 | 7.6 | 18 |
| **5** | 372 | 4.2 | 15 |
| **6** | 372 | 9.1 | 32 |
| **7** | 372 | 11.1 | 39 |
| **8** | 372 | 5.6 | 19 |
| **9** | 372 | 11.7 | 40 |
| **10** | 539[d] | 6.0 | 30 |
| **11**[e] | 372 | 13.9 | 49 |

[a] Number-average degree of polymerization of the PPFMA precursor as determined from $^1$H-NMR spectroscopy from comparison of the protons on the RAFT agent end group to the -C**H**$_2$ backbone peaks. [b] Calculated from $^1$H-NMR spectra as: number of peptides per polymer /(total number of original allyl units prior to thiol-ene addition + number of HPMA units). [c] The number of peptide chains per copolymer based on the total polymer DP derived from $^1$H-NMR presented in Table I. [d] The number average degree of polymerization of copolymer **10** is determined by DMF SEC. [e] Copolymer **11** functions as a negative control with the scrambled peptide grafted on to the copolymer via thiol-ene reaction.

Comparison of the $IC_{50}$ values of **5**–**9**, which are expressed in total peptide concentration, does not reveal a significant influence of the peptide content on the inhibitory activity of the conjugates. However, when the $IC_{50}$ values are considered from the perspective of copolymer concentration, a small increase in efficacy was observed. For example, polyvalent peptide–polymer conjugates **5**, **6**, and **7**, yielded $IC_{50}$ values of 170, 78 and 64 nM respectively when based on copolymer concentration.

Figure 3 indicates that all peptide–polymer conjugates are less active as the IgG1 b12 antibody, suggesting that the tertiary structure of the antibody plays a significant role when binding to gp120. While the CDR H3 domain on IgG1 b12 is presented in a defined conformation, the CDR H3 peptides pendant to the copolymer chain have more conformational freedom, which presents a higher entropic barrier toward binding. In addition, the domains located at the periphery of the CDR H3 domain on the antibody may also contribute towards effective binding to gp120 (*12*, *51*), and could further add to the the differences


In Tailored Polymer Architectures for Pharmaceutical and Biomedical Applications; Scholz, C., et al.; ACS Symposium Series; American Chemical Society: Washington, DC, 2013.

Downloaded by UNIV TENNESSEE KNOXVILLE CAMPUS on July 17, 2013 | http://pubs.acs.org
Publication Date (Web): July 8, 2013 | doi: 10.1021/bk-2013-1135.ch008

in efficacy between IgG1 b12 and the polyvalent peptide–polymer conjugates. Despite the lower efficacy compared to the IgG1 b12 antibody, the polyvalent peptide–polymer conjugates may present a cost-effective alternative to existing therapies, especially for microbicidal applications (*52*).

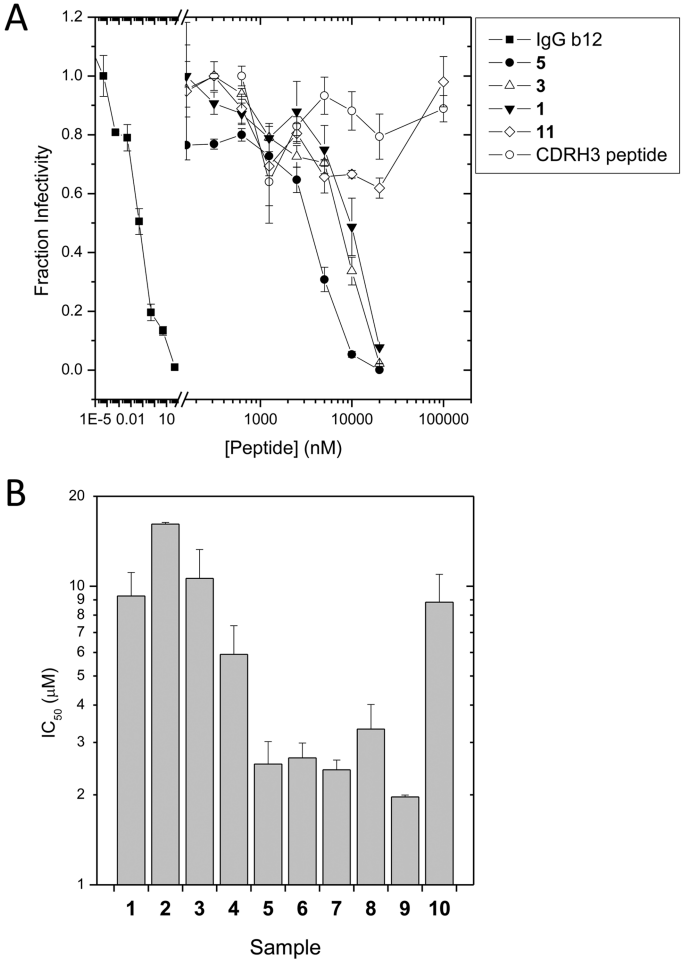


*Figure 3. (A) HIV-1$_{HXB2}$ viral infectivity inhibition by the IgG1 b12 antibody and side chain peptide-synthetic polymer conjugates **1**, **3** and **5**. As controls, a copolymer containing a scrambled peptide (**11**) and the CDR H3 peptide alone are included. The error bars are the standard error observed within one experiment. (B) Efficacy of the polyvalent peptide copolymers against HIV-1 HXB2 wild type on HOS CCR5 cells. The error bars depict the standard error over three or more independent experiments. Adapted with permission from Danial et al. (41) Copyright 2012 American Chemical Society.*

Downloaded by UNIV TENNESSEE KNOXVILLE CAMPUS on July 17, 2013 | http://pubs.acs.org
Publication Date (Web): July 8, 2013 | doi: 10.1021/bk-2013-1135.ch008


In Tailored Polymer Architectures for Pharmaceutical and Biomedical Applications; Scholz, C., et al.;
ACS Symposium Series; American Chemical Society: Washington, DC, 2013.

# PEGylation of HIV-1 Fusion Inhibiting Peptides

As depicted in Figure 2, HIV-1–host cell membrane fusion proceeds via the formation of a trimer of antiparallel coiled coil dimers between the HR1 and HR2 domains on the gp41 glycoprotein (*53*, *54*). Inhibition of the formation of this trimer-of-hairpins using peptides derived from either HR1 (*23*) or HR2 (*27*) domains is an attractive strategy to inhibit HIV-1 virus-host cell fusion. As with all peptide and protein drugs, however, a drawback of these peptide based fusion inhibitors is that they typically possess relatively short plasma half-lives. For the HR2 derived peptide T-20 (Fuzeon®), for example, a plasma half-life of 3.8 hours have been reported (*30*).

Despite being a well-established approach to increase the stability and plasma half-life of peptide and proteins, site-specific polymer conjugation (or poly(ethylene glycol (PEG) modification) of HR2-derived peptides to prolong the lifetime of HIV-1 fusion inhibitors has only been reported in a few instances. Bailon and Won have reported that N-terminal conjugation of a 10kDa PEG to T-20 lowers HIV-1 fusion efficacy by one order of magnitude relative to the unmodified T-20 peptide (*38*). Similarly, in a second patent, Bailon and Won describe synthesis and potency of an N-terminal PEGylated version of T1249 (a more potent HR2-derived variant of T-20) and showed that the T1249-PEG20k conjugates had 13.7–56.7 fold lower efficacy relative to the unmodified T1249 peptide (*39*). In addition to PEG, also various other, biological macromolecules have been conjugated to HR2-derived peptide fusion inhibitors to prolong their life-time (*55*, *56*). Stoddart et al., for example, have shown that conjugation of human serum albumin to the C-terminus of C34 (an HR2-derived peptide) resulted in an order of magnitude loss in fusion inhibition efficacy, while N-terminal conjugation yielded only a minor loss in HIV-1 fusion inhibition efficacy (*55*). In another example, Huet et al. described the synthesis and HIV-1 fusion inhibition efficacy of T-20 modified at the N-terminus with an anti-thrombin binding carrier pentasaccharide (*56*). Although the N-terminal pentasaccharide conjugates showed up to a six-fold reduction in HIV-1 fusion inhibition efficacy, a moderate increase in plasma half-life in rats from 2.8 hours for the unmodified T-20 to 10.4 hours for the conjugates was shown. None of the above studies, however, systematically examine the effect of the site of polymer conjugation and its effect upon HIV-1 fusion inhibition and proteolytic stability.

To study the effect of the site of PEGylation as well as PEG molecular weight on HIV inhibition properties, a series of PEGylated variants of an HR2 derived fusion inhibitor (C41) was prepared (Figure 4). The design of the HR2 derived peptide C41 was based on the peptide T-20 (*27*) but adding an N-terminal extension that includes Trp-2 and Ile-6 that bind to the deep-pocket on HR1 (*57*), while truncating the C-terminal residues of T-20 that are not part of the HR2 region (*58*). The HR2 derived peptide C41 was PEGylated at the *c* and *f* sites of the helical wheel located at the periphery of the six-helix bundle, so as to minimize interference of the PEG chain with the formation of the six-helix bundle (Figure 4C). To enable site-specific PEGylation of C41, cysteine mutants were synthesized to which a PEG-acrylate could easily be


In Tailored Polymer Architectures for Pharmaceutical and Biomedical Applications; Scholz, C., et al.;
ACS Symposium Series; American Chemical Society: Washington, DC, 2013.

Downloaded by UNIV TENNESSEE KNOXVILLE CAMPUS on July 17, 2013 | http://pubs.acs.org
Publication Date (Web): July 8, 2013 | doi: 10.1021/bk-2013-1135.ch008

conjugated via a Michael addition reaction (Scheme 2). Moreover, cysteine residues replaced the amino acids at positions 4, 11, 15, 18, 22 and 29 of the C41 peptide that are present on the c and f positions of the heptad repeat to allow for site-specific PEGylation (Figure 4B, C). In addition, N- and C-terminal cysteine extended variants were prepared as well as a negative control where cysteine was placed at position *a* of the heptad repeat in order to assess the impact of the PEGylation site with respect to PEGylation at the *c* and *f* positions of the heptad repeat. Table II presents the library of cysteine peptide mutants and the original HR2-derived peptide C41 that was PEGylated with PEG750 or PEG2000 (DP ~ 17 or ~ 45 respectively). All PEGylated cysteine mutant peptides were purified by reverse phase HPLC and characterized by matrix assisted laser desorption–ionization–time of flight (MALDI-ToF) mass spectrometry, circular dichroism and analytical ultracentrifugation (*42*).

Downloaded by UNIV TENNESSEE KNOXVILLE CAMPUS on July 17, 2013 | http://pubs.acs.org
Publication Date (Web): July 8, 2013 | doi: 10.1021/bk-2013-1135.ch008

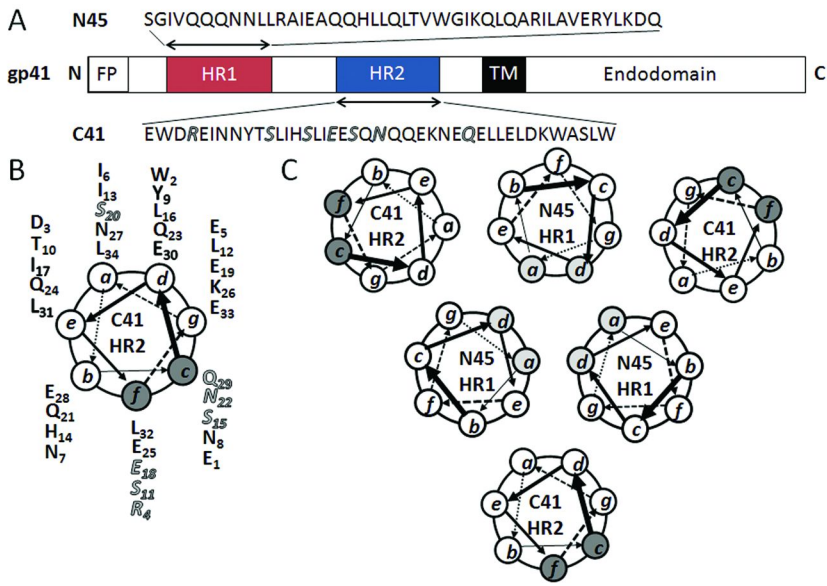


*Figure 4. (A) Heptad repeat domains HR1 and HR2 located within the glycoprotein41 (gp41) polypeptide. (B) Helical wheel representation of the HR2 derived C41 wild-type peptide and the residues present at each position. The residues in the c and f mutated to cysteine are highlighted. (C) The helical wheel representation of the six-helix bundle formed between 3 N45 peptides and 3 C41 peptides. The sequences of the peptides N45 and C41 are derived from HR1 and HR2 domains defined as published in Ref (58). Adapted with permission from Danial et al. (42) Copyright 2012 American Chemical Society.*


In Tailored Polymer Architectures for Pharmaceutical and Biomedical Applications; Scholz, C., et al.;
ACS Symposium Series; American Chemical Society: Washington, DC, 2013.

Downloaded by UNIV TENNESSEE KNOXVILLE CAMPUS on July 17, 2013 | http://pubs.acs.org
Publication Date (Web): July 8, 2013 | doi: 10.1021/bk-2013-1135.ch008



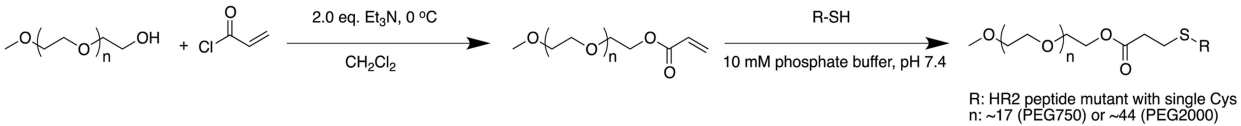


*Scheme 2. Michael addition of the cysteine containing mutant HR2 peptides to PEG-acrylate, where n is ~ 18 for PEG750 and ~ 44 for PEG2000. Adapted with permission from Danial et al. (42) Copyright 2012 American Chemical Society.*

**Table II. The HR2 peptide–PEG conjugates discussed in this contribution. Reprinted with permission from Danial et al. (*42*) Copyright 2012 American Chemical Society.**

| Sample | *f c f c f c f c f* |
|---|---|
| WT | EWDREINN YTSLIHSLIEESQNQQEKNEQELLELDKWASLW |
| N terminus | CEWDREINN YTSLIHSLIEESQNQQEKNEQELLELDKWASLW |
| R4C | EWDCEINN YTSLIHSLIEESQNQQEKNEQELLELDKWASLW |
| S11C | EWDREINN YTCLIHSLIEESQNQQEKNEQELLELDKWASLW |
| S15C | EWDREINN YTSLIHCLIEESQNQQEKNEQELLELDKWASLW |
| E18C | EWDREINN YTSLIHSLICESQNQQEKNEQELLELDKWASLW |
| N22C | EWDREINN YTSLIHSLIEESQCQQEKNEQELLELDKWASLW |
| Q29C | EWDREINN YTSLIHSLIEESQNQQEKNECELLELDKWASLW |
| C terminus | EWDREINN YTSLIHSLIEESQNQQEKNEQELLELDKWASLWC |
| S20C | EWDREINN YTSLIHSLIEECQNQQEKNEQELLELDKWASLW |

n = the degree of polymerization of PEG is either 17 or 45.

The influence of the site of PEGylation as well as the PEG chain length on the membrane fusion inhibition was assessed using a model cell-cell fusion assay, which involved adherent Chinese Hamster Ovarian cells expressing the HIV-1 gp120 and gp41 envelope glycoproteins (CHO-WT) (*59*) and CD4 positive SupT1 (*60*) cells. Addition of SupT1 cells to CHO-WT cells in the absence of a peptide fusion inhibitor leads to multiple fusion events resulting in large cell-like structures with multiple nuclei known as syncytia (*59*). To measure the anti-fusion efficacy of the PEGylated HR2 peptides, conjugates at


In Tailored Polymer Architectures for Pharmaceutical and Biomedical Applications; Scholz, C., et al.; ACS Symposium Series; American Chemical Society: Washington, DC, 2013.

Downloaded by UNIV TENNESSEE KNOXVILLE CAMPUS on July 17, 2013 | http://pubs.acs.org
Publication Date (Web): July 8, 2013 | doi: 10.1021/bk-2013-1135.ch008

concentrations between 0 and 500 nM were added to a mixture of CHO-WT and SupT1 cells and the syncytia were counted after 4 hours. From these titration experiments a dose-response curve, which represents the relative number of syncytia as a function of conjugate concentration, could be generated. From these dose-response curves the inhibitory concentration at which 50 % of the relative number of syncytia was inhibited ($IC_{50}$) was determined. Figure 5 represents the results of the syncytia assay for the investigated peptides and peptide conjugates.

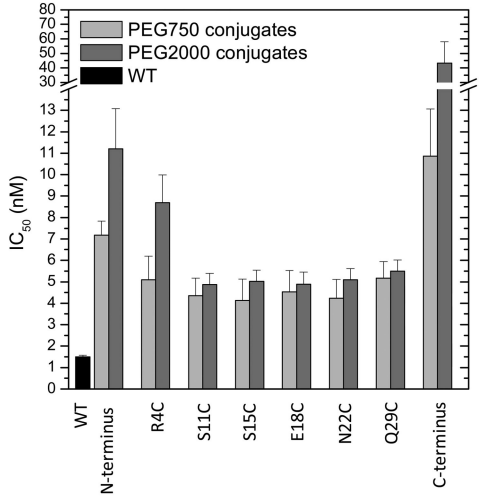


*Figure 5. Efficacy of the HR2 mutant peptide–PEG conjugates compared to the non-modified HR2 wild-type peptide (WT) against cell-cell membrane fusion. Reprinted with permission from Danial et al. (42) Copyright 2012 American Chemical Society.*

As illustrated by Figure 5, all PEGylated HR2 peptide conjugates inhibited the formation of syncytia with $IC_{50}$ values between 4 and 40 nM. For the S20C-PEG750 and S20C-PEG2000 conjugates (data not included in Figure 5), however, $IC_{50}$ values exceeded 400 nM, which is not surprising since this peptide mutant was PEGylated at position *a* of the heptad repeat, which was suggested to interfere with the interaction of HR1 domain on gp41. In comparison to the unmodified wild-type peptide C41, all the PEGylated HR2 peptide conjugates had lower membrane fusion inhibition potencies. However, the site of PEGylation has a significant effect on the in the inhibitory potency. PEGylation at or near the N- or C-terminus seemed to negatively influence the membrane fusion inhibition potency the most, while PEGylation along the middle of the chain at positions 11, 15, 18, 22, and 29 seemed to yield higher efficacies than their N- or C-terminated conjugate counterparts. The $IC_{50}$ values of both C-terminal-PEG750 and C-terminal-PEG2000 were significantly higher than all other conjugates synthesized. This observation can be attributed to the antiparallel nature of the six-helix bundle, which places the C-terminus in close proximity


In Tailored Polymer Architectures for Pharmaceutical and Biomedical Applications; Scholz, C., et al.; ACS Symposium Series; American Chemical Society: Washington, DC, 2013.

Downloaded by UNIV TENNESSEE KNOXVILLE CAMPUS on July 17, 2013 | http://pubs.acs.org
Publication Date (Web): July 8, 2013 | doi: 10.1021/bk-2013-1135.ch008

to the host-cell membrane and causes steric hindrance between the PEG chains and the cell membrane and ultimately leads to less efficient membrane fusion inhibition. PEG chain length when conjugated at positions 11, 15, 18, 22 and 29 of the HR2 derived peptide mutants did not influence the membrane fusion inhibitions significantly ($IC_{50}$ ~ 4.5 nM). Taken together, the results presented in Figure 5 illustrate the importance of judicious control of the site of PEGylation and demonstrate that by careful conjugate design, loss in the membrane fusion inhibitory potency of the peptides can be minimized.

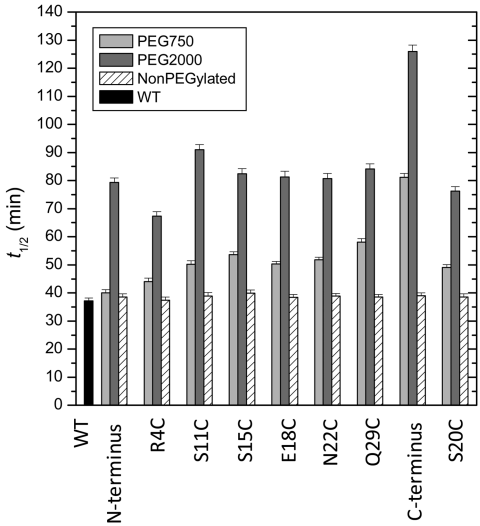


*Figure 6. Degradation half-lives of the HR2 peptide–PEG conjugates measured in a trypsin assay and compared to the non-modified HR2 wild-type peptide (WT). Reprinted with permission from Danial et al. (42) Copyright 2012 American Chemical Society.*

To assess the influence of PEGylation on the proteolytic stability of the HR2 peptides, a model assay that involves the use of trypsin, which is a cheap enzyme and selectively cleaves amide bonds at the C-terminus of basic amino acids such as lysine and arginine (*61*) was set up. This assay involved the incubation of 10 μM of the peptide or PEGylated HR2 mutant peptide with 1 μM of trypsin at 37 °C, over a time-frame of about 100 minutes. At regular intervals, 50 μL aliquots were taken and added to 50 μL of a freshly prepared solution containing 5 % acetic acid and 5 mM phenylmethanesulfonyl fluoride (PMSF), which serves as an inhibitor to trypsin. The degradation products were subsequently analyzed by analytical reverse phase HPLC (*42*). From the HPLC analyses, degradation half-lives ($t_{1/2}$) were determined, which are shown in Figure 6. While PEG750 conjugates only showed minor improvements in half-life, PEG2000 conjugation resulted in a 1.8 to 3.4-fold increase in the trypsin degradation half-life as compared to the unmodified peptide. Moreover, the degradation


In Tailored Polymer Architectures for Pharmaceutical and Biomedical Applications; Scholz, C., et al.;
ACS Symposium Series; American Chemical Society: Washington, DC, 2013.

Downloaded by UNIV TENNESSEE KNOXVILLE CAMPUS on July 17, 2013 | http://pubs.acs.org
Publication Date (Web): July 8, 2013 | doi: 10.1021/bk-2013-1135.ch008

half-life progressively increases the closer PEGylation occurs at the C-terminus, it is still unclear why C-terminal-PEG conjugates have higher trypsin degradation half-lives than the other conjugates.

## Concluding Remarks

In this Chapter, two classes of novel peptide–polymer conjugates that target the fusion and entry of HIV-1 have been presented. Potent polyvalent entry inhibitors ($IC_{50}$ 2–15 μM) have been prepared, which show a more than 100 fold increase in efficacy relative to CDR H3 peptide alone ($IC_{50}$ >100 μM). Although the potencies are not comparable to antibodies such as IgG1 b12, the polyvalent peptide–synthetic polymer conjugates could prove an interesting alternative in microbicidal applications. PEGylated peptides that are derived from the HR2 region of gp41 also form interesting, potentially longer lasting fusion inhibitors. One of the major drawbacks of PEGylation is the loss in biological activity. However, as demonstrated, judicial site-specific PEGylation allows access to PEGylated fusion inhibitors that show improved stability towards proteolyic degradation while minimizing loss of activity. Taken together, the two examples discussed in this Chapter nicely illustrate the power of controlled radical polymerization in combination with site-specific chemo-selective coupling chemistry such as thiol-acrylate Michael addition and thiol-ene addition to provide access to peptide–synthetic polymer therapeutics with improved efficacies and pharmacokinetics as compared to the non-modified peptides and protein drugs.

## Acknowledgments

This work was supported by the European Commission, FP6 project "NanoBioPharmaceutics" (NMP4-CT-2006-026723). Prof. Michael J. Root (Thomas Jefferson University, Philadelphia, USA) and Dr. Andy J. G. Pötgens (Syntab Therapeutics GmbH, Aachen, Germany) are thanked for fruitful discussions and assistance with virological and cell biological assays.

## References

1. *UNAIDS Report on the Global AIDS Epidemic*; 2010.
2. Virgin, H. W.; Walker, B. D. *Nature* **2010**, *464*, 224–231.
3. Mehellou, Y.; De Clercq, E. *J. Med. Chem.* **2010**, *53*, 521–538.
4. Eckert, D. M.; Kim, P. S. *Annu. Rev. Biochem.* **2001**, *70*, 777–810.
5. Root, M. J.; Steger, H. K. *Curr. Pharm. Des.* **2004**, *10*, 1805–1825.
6. Moore, P. L.; Crooks, E. T.; Porter, L.; Zhu, P.; Cayanan, C. S.; Grise, H.; Corcoran, P.; Zwick, M. B.; Franti, M.; Morris, L.; Roux, K. H.; Burton, D. R.; Binley, J. M. *J. Virol.* **2006**, *80*, 2515–2528.
7. Zhu, P.; Liu, J.; Bess, J., Jr.; Chertova, E.; Lifson, J. D.; Grisé, H.; Ofek, G. A.; Taylor, K. A.; Roux, K. H. *Nature* **2006**, *441*, 847–852.
8. Klasse, P. J. *Cellular Microbiol.* **2012**, *14*, 1183–1192.
9. Volberding, P. A.; Deeks, S. G. *Lancet* **2010**, *376*, 49–62.


In Tailored Polymer Architectures for Pharmaceutical and Biomedical Applications; Scholz, C., et al.; ACS Symposium Series; American Chemical Society: Washington, DC, 2013.

Downloaded by UNIV TENNESSEE KNOXVILLE CAMPUS on July 17, 2013 | http://pubs.acs.org
Publication Date (Web): July 8, 2013 | doi: 10.1021/bk-2013-1135.ch008

Downloaded by UNIV TENNESSEE KNOXVILLE CAMPUS on July 17, 2013 | http://pubs.acs.org
Publication Date (Web): July 8, 2013 | doi: 10.1021/bk-2013-1135.ch008

10. Pantophlet, R.; Burton, D. R. *Annu. Rev. Immunol.* **2006**, *24*, 739–769.
11. Burton, D. R.; Pyati, J.; Koduri, R.; Sharp, S. J.; Thornton, G. B.; Parren, P. W. H. I.; Sawyer, L. S. W.; Hendry, R. M.; Dunlop, N.; Nara, P. L.; Lamacchia, M.; Garratty, E.; Stiehm, E. R.; Bryson, Y. J.; Cao, Y.; Moore, J. P.; Ho, D. D.; Barbas Iii, C. F. *Science* **1994**, *266*, 1024–1027.
12. Saphire, E. O.; Parren, P. W. H. I.; Pantophlet, R.; Zwick, M. B.; Morris, G. M.; Rudd, P. M.; Dwek, R. A.; Stanfield, R. L.; Burton, D. R.; Wilson, I. A. *Science* **2001**, *293*, 1155–1159.
13. Ito, M.; Baba, M.; Sato, A. *Antiviral Res.* **1987**, *7*, 361–367.
14. Shaunak, S.; Gooderham, N. J.; Edwards, R. J.; Payvandi, N.; Javan, C. M.; Baggett, N.; MacDermot, J.; Weber, J. N.; Davies, D. S. *Br. J. Pharmacol.* **1994**, *113*, 151–158.
15. McCarthy, T. D.; Karellas, P.; Henderson, S. A.; Giannis, M.; O'Keefe, D. F.; Heery, G.; Paull, J. R. A.; Matthews, B. R.; Holan, G. *Mol. Pharmaceutics* **2005**, *2*, 312–318.
16. Rusconi, S.; Moonis, M.; Merrill, D. P.; Pallai, P. V.; Neidhardt, E. A.; Singh, S. K.; Willis, K. J.; Osburne, M. S.; Profy, A. T.; Jenson, J. C.; Hirsch, M. S. *Antimicrob. Agents Chemother.* **1996**, *40*, 234–236.
17. Kensinger, R. D.; Yowler, B. C.; Benesi, A. J.; Schengrund, C. L. *Bioconjugate Chem.* **2004**, *15*, 349–358.
18. Batinic, D.; Robey, F. A. *J. Biol. Chem.* **1992**, *267*, 6664–6671.
19. Li, H.; Song, H.; Heredia, A.; Le, N.; Redfield, R.; Lewis, G. K.; Wang, L. X. *Bioconjugate Chem.* **2004**, *15*, 783–789.
20. Li, H.; Guan, Y.; Szczepanska, A.; Moreno-Vargas, A. J.; Carmona, A. T.; Robina, I.; Lewis, G. K.; Wang, L. X. *Bioorg. Med. Chem.* **2007**, *15*, 4220–4228.
21. Jay, J. I.; Lai, B. E.; Myszka, D. G.; Mahalingam, A.; Langheinrich, K.; Katz, D. F.; Kiser, P. F. *Mol. Pharmaceutics* **2010**, *7*, 116–129.
22. Mahalingam, A.; Geonnotti, A. R.; Balzarini, J.; Kiser, P. F. *Mol. Pharmaceutics* **2011**, *8*, 2465–2475.
23. Bianchi, E.; Finotto, M.; Ingallinella, P.; Hrin, R.; Carella, A. V.; Hou, X. S.; Schleif, W. A.; Miller, M. D.; Geleziunas, R.; Pessi, A. *Proc. Natl. Acad. Sci. U.S.A.* **2005**, *102*, 12903–12908.
24. Melikyan, G. B. *Retrovirology* **2008**, *5*, 111.
25. Dwyer, J. J.; Wilson, K. L.; Davison, D. K.; Freel, S. A.; Seedorff, J. E.; Wring, S. A.; Tvermoes, N. A.; Matthews, T. J.; Greenberg, M. L.; Delmedico, M. K. *Proc. Natl. Acad. Sci. U.S.A.* **2007**, *104*, 12772–12777.
26. Tilton, J. C.; Doms, R. W. *Antiviral Res.* **2010**, *85*, 91–100.
27. Wild, C.; Greenwell, T.; Matthews, T. *AIDS Res. Hum. Retroviruses* **1993**, *9*, 1051–1053.
28. De Clercq, E. *Int. J. Antimicrob. Agents* **2009**, *33*, 307–320.
29. Eggink, D.; Berkhout, B.; Sanders, R. W. *Curr. Pharm. Des.* **2010**, *16*, 3716–3728.
30. *Fuzeon Product Information*; http://www.fuzeon.com.
31. Wang, D.; Lu, M.; Arora, P. S. *Angew. Chem., Int. Ed.* **2008**, *47*, 1879–1882.
32. Welch, B. D.; VanDemark, A. P.; Heroux, A.; Hill, C. P.; Kay, M. S. *Proc. Natl. Acad. Sci. U.S.A.* **2007**, *104*, 16828–16833.


In Tailored Polymer Architectures for Pharmaceutical and Biomedical Applications; Scholz, C., et al.;
ACS Symposium Series; American Chemical Society: Washington, DC, 2013.

Downloaded by UNIV TENNESSEE KNOXVILLE CAMPUS on July 17, 2013 | http://pubs.acs.org
Publication Date (Web): July 8, 2013 | doi: 10.1021/bk-2013-1135.ch008

33. Stephens, O. M.; Kim, S.; Welch, B. D.; Hodsdon, M. E.; Kay, M. S.; Schepartz, A. *J. Am. Chem. Soc.* **2005**, *127*, 13126–13127.
34. Caliceti, P.; Veronese, F. M. *Adv. Drug Delivery Rev.* **2003**, *55*, 1261–1277.
35. Pasut, G.; Veronese, F. M. *Prog. Polym. Sci.* **2007**, *32*, 933–961.
36. Veronese, F. M. *Biomaterials* **2001**, *22*, 405–417.
37. Klok, H.-A. *Macromolecules* **2009**, *42*, 7990–8000.
38. Bailon, P. S.; Won, C.-Y. *PEGylated T20 Polypeptide*; WO/2004/013164, 2004.
39. Bailon, P. S.; Won, C.-Y. *PEGylated T1249 Polypeptide*; WO/2004/013165, 2004.
40. Kochendoerfer, G. G.; Chen, S. Y.; Mao, F.; Cressman, S.; Traviglia, S.; Shao, H.; Hunter, C. L.; Low, D. W.; Cagle, E. N.; Carnevali, M.; Gueriguian, V.; Keogh, P. J.; Porter, H.; Stratton, S. M.; Con Wiedeke, M.; Wilken, J.; Tang, J.; Levy, J. J.; Miranda, L. P.; Crnogorac, M. M.; Kalbag, S.; Botti, P.; Schindler-Horvat, J.; Savatski, L.; Adamson, J. W.; Kung, A.; Kent, S. B. H.; Bradburne, J. A. *Science* **2003**, *299*, 884–887.
41. Danial, M.; Root, M. J.; Klok, H.-A. *Biomacromolecules* **2012**, *13*, 1438–1447.
42. Danial, M.; van Dulmen, T. H. H.; Aleksandrowicz, J.; Pötgens, A. J. G.; Klok, H.-A. *Bioconjugate Chem.* **2012**, *23*, 1648–1660.
43. Günay, K. A.; Theato, P.; Klok, H.-A. *J. Polym. Sci., Part A: Polym. Chem.* **2013**, *51*, 1–28.
44. Jochum, F. D.; Theato, P. *Macromolecules* **2009**, *42*, 5941–5945.
45. Singha, N. K.; Gibson, M. I.; Koiry, B. P.; Danial, M.; Klok, H.-A. *Biomacromolecules* **2011**, *12*, 2908–2913.
46. Eberhardt, M.; Mruk, R.; Zentel, R.; Théato, P. *Eur. Polym. J.* **2005**, *41*, 1569–1575.
47. Perrier, S.; Takolpuckdee, P.; Mars, C. A. *Macromolecules* **2005**, *38*, 2033–2036.
48. Gibson, M. I.; Fröhlich, E.; Klok, H.-A. *J. Polym. Sci., Part A: Polym. Chem.* **2009**, *47*, 4332–4345.
49. Kahle, K. M.; Steger, H. K.; Root, M. J. *PLoS Pathogens* **2009**, *5*, e1000674.
50. Mammen, M.; Shakhnovich, E. I.; Whitesides, G. M. *J. Org. Chem.* **1998**, *63*, 3168–3175.
51. Zhou, T.; Xu, L.; Dey, B.; Hessell, A. J.; Van Ryk, D.; Xiang, S. H.; Yang, X.; Zhang, M. Y.; Zwick, M. B.; Arthos, J.; Burton, D. R.; Dimitrov, D. S.; Sodroski, J.; Wyatt, R.; Nabel, G. J.; Kwong, P. D. *Nature* **2007**, *445*, 732–737.
52. Lederman, M. M.; Jump, R.; Pilch-Cooper, H. A.; Root, M.; Sieg, S. F. *Retrovirology* **2008**, *5*, 116.
53. Gallo, S. A.; Finnegan, C. M.; Viard, M.; Raviv, Y.; Dimitrov, A.; Rawat, S. S.; Puri, A.; Durell, S.; Blumenthal, R. *Biochim. Biophys. Acta, Biomembr.* **2003**, *1614*, 36–50.
54. Chan, D. C.; Kim, P. S. *Cell* **1998**, *93*, 681–684.
55. Stoddart, C. A.; Nault, G.; Galkina, S. A.; Thibaudeau, K.; Bakis, P.; Bousquet-Gagnon, N.; Robitaille, M.; Bellomo, M.; Paradis, V.; Liscourt, P.;

Lobach, A.; Rivard, M. È.; Ptak, R. G.; Mankowski, M. K.; Bridon, D.; Quraishi, O. *J. Biol. Chem.* **2008**, *283*, 34045–34052.
56. Huet, T.; Kerbarh, O.; Schols, D.; Clayette, P.; Gauchet, C.; Dubreucq, G.; Vincent, L.; Bompais, H.; Mazinghien, R.; Querolle, O.; Salvador, A.; Lemoine, J.; Lucidi, B.; Balzarini, J.; Petitou, M. *Antimicrob. Agents Chemother.* **2010**, *54*, 134–142.
57. Chan, D. C.; Chutkowski, C. T.; Kim, P. S. *Proc. Natl. Acad. Sci. U.S.A.* **1998**, *95*, 15613–15617.
58. Weissenhorn, W.; Dessen, A.; Harrison, S. C.; Skehel, J. J.; Wiley, D. C. *Nature* **1997**, *387*, 426–430.
59. Weiss, C. D.; White, J. M. *J. Virol.* **1993**, *67*, 7060–7066.
60. Smith, S. D.; Morgan, R.; Link, M. P. *Blood* **1986**, *67*, 650–656.
61. *Sigma-Aldrich Enzyme Explorer – Trypsin*; http://www.sigmaaldrich.com/life-science/metabolomics/enzyme-explorer/analytical-enzymes/trypsin.html.

Downloaded by UNIV TENNESSEE KNOXVILLE CAMPUS on July 17, 2013 | http://pubs.acs.org
Publication Date (Web): July 8, 2013 | doi: 10.1021/bk-2013-1135.ch008

Downloaded by UNIV OF ROCHESTER on July 20, 2013 | http://pubs.acs.org
Publication Date (Web): July 8, 2013 | doi: 10.1021/bk-2013-1135.ch009

## Chapter 9

# Cancer Stem Cells: Potential Target For Anti-Cancer Nanomedicines

**Yan Zhou,[1] Jiyuan Yang,[1] and Jindřich Kopeček[*,1,2]**

**[1]Department of Pharmaceutics and Pharmaceutical Chemistry, University of Utah, Salt Lake City, Utah 84112**
**[2]Department of Bioengineering, University of Utah, Salt Lake City, Utah 84112**
**[*]E-mail: jindrich.kopecek@utah.edu. Address: University of Utah, Center for Controlled Drug Delivery, 2030 E 20 S BPRB Room 205B, Salt Lake City, Utah 84112-9452. Tel.: + 801 581 7211. Fax: + 801 581 7848.**

The recently revived Cancer Stem Cell (CSC) hypothesis adds a new and important dimension to the development of anti-cancer therapeutics. Evidences suggest that the drug resistant CSCs contribute to cancer progression, recurrence and metastasis and are responsible for the failure of conventional anti-cancer treatments. In this chapter, the concept, the biological/functional properties and therapeutic implications of CSCs are covered. Furthermore, design and approaches of nanomedicines for targeting CSCs are discussed. In particular, the CSC inhibitory effect of a nanosized HPMA (*N*-(2-hydroxypropyl)methacrylamide) copolymer-based cyclopamine delivery system towards prostate CSCs is described.

The understanding of tumor initiation, progression and metastasis has been improved and anti-cancer treatments have been advanced in the past several decades, whereas cancer still remains one of the top causes of morbidity and mortality (*1*). A major obstacle to develop effective anti-cancer treatments is the heterogeneity of cancer cells (*2*, *3*). Nowadays, tumors are recognized

© 2013 American Chemical Society
In Tailored Polymer Architectures for Pharmaceutical and Biomedical Applications; Scholz, C., et al.; ACS Symposium Series; American Chemical Society: Washington, DC, 2013.

as complex as organs, rather than just a mass of homogeneous cancer cell population. Cancer cells are biologically and functionally heterogeneous, in terms of phenotype, proliferation, tumorigenesis and invasiveness, etc. Noticeably, accumulated evidences have recently revealed a new dimension of cancer cell heterogeneity, that is, cancer cells are present in various differentiation statuses, with relatively undifferentiated Cancer Stem Cells (CSCs) maintaining the hierarchical organization of the tumor mass, similar to the role of normal stem cells (NSCs) in healthy tissues (*4*, *5*). Moreover, the CSC theory suggests that the often observed treatment failures are largely due to the failure of conventional cytotoxic anti-cancer therapies to eliminate CSCs. Thus, the CSC theory may hold previously underappreciated but important implications for successful development of anti-cancer treatment strategies. Below we will discuss the development of CSC concept, CSC properties, therapeutic implications and our design of polymeric anti-cancer therapeutics based on CSC concept.

Downloaded by UNIV OF ROCHESTER on July 20, 2013 | http://pubs.acs.org
Publication Date (Web): July 8, 2013 | doi: 10.1021/bk-2013-1135.ch009

## Models of Cancer Heterogeneity: Clonal Evolution versus Cancer Stem Cells

Cancer heterogeneity has long been observed experimentally and considerable research investigated the reasons of the heterogeneity since many decades ago (*5*, *6*). The stem cell concept in tumors was brought up around the same time as the concept of cancer as a genetic disease (*7*). As early as 1937, it was observed that a new tumor could be generated from a single mouse tumor cell by tumor cell transplantation to a recipient mouse (*7*). This tumor seeding capacity was found to be only possessed by a small tumor cell population in later research (*8*). Similar to the development of normal tissues, the tumor-initiating cells identified in undifferentiated areas within tumors could give rise to more differentiated cancer cells as observed by radiolabeling approach (*9*). However, no breakthrough was made in this area since 1970s due in part to the technical limitations in isolating and characterizing stemlike cells within tumors. On the other hand, the clonal evolution concept thrived in past decades, along with the rapid advances in the studies of oncogenes and tumor suppressor genes (*10*).

Based on the clonal evolution model, tumor is generated from a monoclonal cancer cell population; however, triggered by both intrinsic and extrinsic environmental factors, cancer progression is driven by genetic changes acquired randomly within the original clone (Figure 1). Thus, cancer cells develop into genetically heterogeneous subclones through clonal selection (*5*, *6*). Adhering to this model, cancer cells stochastically acquire the tumorigenic potential. On the contrary, the CSC model postulates that not all cancer cells have an equal tumorigenic potential; instead, similar to the growth and maintenance of normal organs, the tumor growth and progression is driven by only limited number of stemlike cancer cells with the ability to self-renew and differentiate (*4*, *5*). Only these CSCs are able to generate phenotypically heterogeneous tumor cell populations that resemble the original organization of the parent tumor (Figure 1).


In Tailored Polymer Architectures for Pharmaceutical and Biomedical Applications; Scholz, C., et al.;
ACS Symposium Series; American Chemical Society: Washington, DC, 2013.

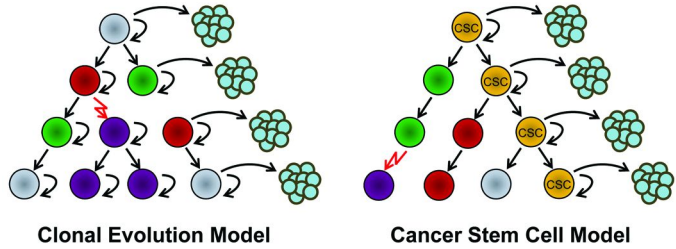


*Figure 1. The illustration of the two cancer heterogeneity models-clonal evolution (left) and cancer stem cell model (right). Adapted with permission from ref. (3). Copyright 2001 Nature.*

Downloaded by UNIV OF ROCHESTER on July 20, 2013 | http://pubs.acs.org
Publication Date (Web): July 8, 2013 | doi: 10.1021/bk-2013-1135.ch009

To prove the CSC hypothesis, isolation and thorough characterization of CSCs is a must. Recently, the CSC concept was revived with stronger supporting evidences. The identification of leukemia stem cells (in hematopoietic malignancy) and breast CSCs (in solid tumor) by transplantation assays using highly immunodeficient mice are milestones of this effort (*11*, *12*). Since then, in a series of studies, cancer stemlike cells were isolated in other solid tumors including brain (*13*), prostate (*14*, *15*) and colon cancers (*16*).

## Key Properties of Cancer Stem Cells

### Self-Renewal and Differentiation

Consistent with NSCs, the core property of CSCs is the ability to self-renew and differentiate into diverse progenies (*4*, *5*). Nowadays, Fluorescent Activated Cell Sorting (FACS) can be utilized for efficient isolation of a subset of cancer cell population with a particular phenotype distinctive from the rest of cancer cells (*11*). This method has been used widely to separate putative CSCs with a certain combination of stem cell-related surface marker expressions. For example, Bonnet and Dick isolated CD34+/CD38- leukemic cells from different subtypes of acute myeloid leukemia (AML) (*11*). They found that the ability to propagate and initiate human AML in non-obese diabetic/severe combined immunodeficiency mice (NOD/SCID mice) was exclusively restricted to CD34+/CD38- cancer cells, but not cells with other phenotypes, demonstrating the self-renew property of these leukemic stem cells (*11*). Limiting dilution transplantation into highly immunodeficient mice (most commonly NOD/SCID mice) has become a standard method to evaluate the tumorigenicity of human CSCs (*4*). In addition, differentiation capacity of CSCs can be tested in mice transplantation assay. The phenotype and histopathology of the new tumor grown from CSCs should resemble the original human tumor, with more differentiated descendant cancer


In Tailored Polymer Architectures for Pharmaceutical and Biomedical Applications; Scholz, C., et al.;
ACS Symposium Series; American Chemical Society: Washington, DC, 2013.

cells that comprise the bulk of tumor (*12*). Strikingly, except for differentiating into subsets of cancer epithelial cells, it has been reported recently that CSCs have the potential to transdifferentiate into endothelial cells which line the tumor vasculature, as demonstrated in brain tumor models (*17*, *18*).

### Resistance to Anti-Cancer Therapies

Another important property of CSCs is their intrinsic resistance to a variety of traditional anti-cancer chemo- or radiation therapies, which target rapidly dividing cancer cells (*19*, *20*). Drug resistance of CSCs has been observed in many hematopoietic and solid tumors experimentally and clinically. For example, leukemic stem cells were found to be resistant to Imatinib in chronic myeloid leukemia (CML) patients (*21*). In breast cancer patients, $CD44^{+}CD24^{low}$ CSC population surviving within the residual tumor expanded to a larger proportion following standard chemotherapy, although the tumor bulk was shrunk by the therapy (*22*). Several possible mechanisms contributing to CSC drug resistance have been demonstrated. One important mechanism is the enhanced expression of drug efflux proteins, such as P-glycoprotein and ABCG2, on the surface of CSCs than on non-CSCs (*23*). The ability of CSCs to pump out the substrate of the efflux protein is utilized to enrich the CSC population, which is also called the "side population" (*24*). Besides, overexpression of genes essential for the enhanced DNA damage repair or the antiapoptotic signaling pathway increases CSC resistance (*19*, *25*). For instance, due to the overexpression of checkpoint activation protein CHK1, CD133+ colon CSCs showed enhanced survival than bulk tumor cells following cisplatin treatment (*26*).

Overall, CSCs contribute to the treatment failure of anti-cancer therapies at least for two reasons: firstly, CSCs are more resistant than bulk tumor cells and they survive from cytotoxic therapies, even if the tumor mass can be shrunk efficiently; secondly, these surviving CSCs can proliferate and regenerate a tumor after the cease of treatment, resulting in recurrence and metastasis (*5*, *6*).

## Regulation of Cancer Stem Cell Growth and Maintenance

Studies have shown that CSCs share similar gene and transcriptional profiles with normal tissue stem cells. Consistent with this, a network of signaling pathways regulating the self-renewal, growth and maintenance of NSCs, including hedgehog (Hh) (*27*, *28*), notch (*29*) and wnt (*30*) pathways, plays an important role in CSCs.

Recent studies have implicated the critical roles of Hh signaling pathway in various cancers (*31*). The aberrant activation of Hh is responsible for the development of several cancers, especially those originating in organs whose development require Hh signaling, such as medulloblastoma, glioblastoma, prostate, basal cell carcinoma and pancreatic cancer (*32*). In particular, Hh pathway elements are usually found to be more active in CSC population than in bulk tumor population (*33*).


In Tailored Polymer Architectures for Pharmaceutical and Biomedical Applications; Scholz, C., et al.;
ACS Symposium Series; American Chemical Society: Washington, DC, 2013.

Downloaded by UNIV OF ROCHESTER on July 20, 2013 | http://pubs.acs.org
Publication Date (Web): July 8, 2013 | doi: 10.1021/bk-2013-1135.ch009

The notch pathway is another important signaling pathway associated with stem cell survival, proliferation and differentiation (*34*). So far, the role of notch signaling in CSCs is mostly supported in breast and brain tumors (*35*). The overexpression of notch elements increases the chemo- or radio-resistance of CSCs (*36*). Notch inhibition could decrease the mammosphere formation as tested in many breast cancer cell lines as well as patient samples (*37*). Notch pathway inhibitor GSI (γ-secretase inhibitor) could selectively get rid of medulloblastoma CSCs but not non-CSCs (*38*). Wnt pathway is also implicated in CSC maintenance and proliferation, with more supporting evidences in lung and colon cancers (*35*). These pathways form an interactive network to regulate the CSC fate. It would be critical to identify the determining element for CSC maintenance as the best target for anti-CSC treatment.

Another issue is to identify the similarities and differences of these regulation pathways on NSCs versus CSCs. It is important for developing therapies targeting these pathways with minimal NSC related toxicities, since normal adult stem cells and CSCs may share these signaling systems. Although there are more and more studies on this, it is still not clearly stated yet. The notch pathway inhibitors showed side effects on normal intestinal stem cells and could cause intestinal cell metaplasia (*39*, *40*). On the other hand, the inhibition of hedgehog pathway did not show adverse effect on hematopoietic stem cells (HSCs) maintenance and functions (*41*, *42*). Hedgehog pathway may be dispensable in adult HSCs, different from its critical function in stem cells during embryonic development. To be noted, leukemic stem cells and HSCs have shown the opposite response towards PI3K/mTOR pathway inhibition, indicating the possibility to target CSCs while sparing NSCs (*43*).

## Challenges for the CSC Model

As research in CSC field advances, more challenges have been brought up (*4–6*, *44*). Instead of considering CSCs as a strictly fixed cancer cell population within tumors, increasing number of studies indicate that CSCs may be more plastic than hypothesized in the CSC model (*45*, *46*). For example, the inter-conversion between CSCs and non-CSCs has been observed in breast cancer cell lines. The sorted relatively pure non-CSC population could generate cells with CSC phenotype and functions under the culture condition, reaching a dynamic equilibrium between CSC and non-CSC phenotypes (*47*). Moreover, it has been found that microenvironmental factors, such as secreted IL-6, could interact with cancer cells and induce the formation of CSCs (*48*). Thus, the two models, CSC and clonal evolution, are not mutually exclusive in terms of explaining the development of cancer heterogeneity (*4*, *5*). Cancer cells would accumulate genetic differences during tumor progression; meanwhile, genetically homogeneous cancer cells may hold distinct hierarchical differentiation status driven by epigenetic modification (*2*). For instance, evidence strongly supports that hematopoietic malignancies such as CML follow the CSC model, but except for the intrinsic resistance of CSCs, the acquired resistance to Imatinib is partially due to the generation of a new subclone with genetic mutation in the drug target

Downloaded by UNIV OF ROCHESTER on July 20, 2013 | http://pubs.acs.org
Publication Date (Web): July 8, 2013 | doi: 10.1021/bk-2013-1135.ch009


In Tailored Polymer Architectures for Pharmaceutical and Biomedical Applications; Scholz, C., et al.;
ACS Symposium Series; American Chemical Society: Washington, DC, 2013.

gene (*49*). On the other hand, epigenetic regulation itself could be responsible for drug resistance (*4*, *50*). For example, the epithelial growth factor receptor (EGFR) inhibitor tolerance could be due to the up-regulation of histone demethylase KDM5A (*50*).

Despite the complexicity of cancer development and cancer cell response to anti-cancer therapies, the CSC concept holds significant therapeutic implications. Targeting the CSC properties, which have not been successfully addressed by current traditional therapies, would be a promising anti-cancer approach. Furthermore, considering the plasticity of CSCs, it is beneficial to develop therapeutics that target bulk tumor cells and CSCs simultaneously, or prevent the non-CSC to CSC transition, in order to eliminate all cancer cells (*47*).

Downloaded by UNIV OF ROCHESTER on July 20, 2013 | http://pubs.acs.org
Publication Date (Web): July 8, 2013 | doi: 10.1021/bk-2013-1135.ch009

## Current Strategies Employed in Anti-CSC Therapies

Since CSCs are intrinsically resistant to cytotoxic anti-cancer agents, it is necessary to develop novel therapeutics to which CSCs are sensitive, or to develop strategies to overcome the resistance. Based on the properties and key regulation factors of CSCs that are uncovered, small molecule agents targeting the key stem cell regulation pathways that govern CSC self-renewal and differentiation have been selected as candidates for CSC inhibition. Several dozens of modulators for hedgehog, notch, wnt and PI3K pathways, as molecularly targeted anti-cancer small molecule agents, have already entered clinical trials for evaluations of the anti-cancer effects. Currently, these pathways have been further correlated with CSC properties, cancer progression, recurrence and metastasis. Thus, the anti-CSC effects are also being evaluated in several clinical studies (*51*, *52*). For example, the anti-cancer as well as anti-CSC effects of an Hh inhibitor GDC-0449, alone or in combination with gemcitabine, have been investigated in advanced pancreatic cancer in a pilot clinical study (*51*). In another phase I/II study of the MK-0752 and docetaxel combination therapy in advanced or metastatic breast cancer, one of the study endpoints is to evaluate whether the notch pathway (γ-secretase) inhibitor MK-0752 would kill breast CSCs (*52*).

Besides known pathway regulators, the search and screening of specific anti-CSC agents is underway. Some drugs with known indications in non-cancerous diseases have been found to have new potential applications in cancer treatment, due to their inhibitory effects on CSCs. As shown in one study, an antibiotic salinomycin was selected via high throughput small molecule screening as a potential anti-CSC agent, with specific toxicity on breast CSCs but not on the bulk tumor cells (*53*). However, the mechanism of salinomycin to selectively kill CSCs is yet to be identified. Metformin, a first-line drug for the treatment of type 2 diabetes, was recently found to selectively kill breast CSCs as tested in four genetically different subtypes of breast cancer (*54*). In combination with a standard chemotherapeutic drug, metformin significantly reduced the relapse and prolonged the tumor-free periods in mice model. Metformin is currently under investigation in clinical trials of colorectal cancer and advanced ovarian cancer for its effect to target CSCs and prevent recurrence.


In Tailored Polymer Architectures for Pharmaceutical and Biomedical Applications; Scholz, C., et al.;
ACS Symposium Series; American Chemical Society: Washington, DC, 2013.

Other possible ways to inhibit CSC growth and function include overcoming multidrug resistance of CSCs, sensitizing CSCs to conventional therapies, inducing CSC differentiation, or remodeling the CSC-supporting microenvironment.

## Anti-CSC Nanomedicines

Most of the above mentioned small molecule anti-CSC agents have similar drawbacks as traditional anti-cancer drugs: they are poorly water-soluble and may exert nonspecific toxicity to normal tissues. Thus, the development of anti-CSC nanomedicines would offer advantageous anti-CSC behaviors than small molecule agents. Additionally, macromolecular drug delivery system can provide a more versatile treatment modality and potentially improve the anti-CSC effect by multiple mechanisms. Nanocarriers can enhance the accumulation of the therapeutic agents in tumor area due to the enhanced permeation and retention (EPR) effect (*55*). Secondly, biodistribution of the nanocarriers to several most actively self-renewing organs, such as intestine and skin, is relatively low (*56*, *57*), potentially reducing the stem cell toxicity of some anti-CSC agents. Nanocarriers allow the conjugation of targeting ligands to the identified surface markers on CSCs (*58*), which may increase the targeting specificity to certain CSCs. The uptake of either non-targeted or targeted nanocarriers by pinocytosis or receptor-mediated endocytosis may help to circumvent the drug efflux transporters which are often overexpressed on CSCs (*59*). Last but not least, multiple treatment modalities such as radiation, hyperthermia and ultrasound may be combined with the macromolecular delivery system, to further enhance its tumor accumulation, penetration or therapeutic effects.

An example of the nanocarriers for anti-CSC therapy under development is the nanoparticle (NanoCurc™) loaded with hedgehog pathway inhibitor-curcumin. Evaluation of this formulation showed the induction of CD133+ CSC deaths and the inhibition of anchorage-independent growth in brain tumor cell lines (*60*). The inhibition of CSC properties was tested in the in vitro stem cell assay, but not yet validated in vivo.

There are also designs of nanocarriers incorporated with targeting moieties to CSC surface biomarkers. The commonly targeted biomarkers include CD44, CD133 and certain integrins, which are often employed to identify NSCs and CSCs. For example, the anti-cancer effects of hyaluronan-drug conjugates (*58*) and anti-CD133 antibody targeted nanoparticles (*61*) have been tested in cancer cell lines. However, in the above studies, the direct anti-CSC effects were not evaluated. The main advantage of the actively targeted therapeutics is to enhance the cellular uptake of nanomedicines into CD44+ or CD133+ cancer cells, thus improving the cell killing effects. However, it is important to note that CSC markers may be different for cancers from different tissues of origin as well as different subtypes of the same cancer (*4*, *6*). Furthermore, CSCs could still be resistant to the actively targeted therapeutics.

A promising design for the sensitization of the resistant CSCs to conventional radiation therapy has been reported recently (*62*). It was to sensitize breast


In Tailored Polymer Architectures for Pharmaceutical and Biomedical Applications; Scholz, C., et al.;
ACS Symposium Series; American Chemical Society: Washington, DC, 2013.

Downloaded by UNIV OF ROCHESTER on July 20, 2013 | http://pubs.acs.org
Publication Date (Web): July 8, 2013 | doi: 10.1021/bk-2013-1135.ch009

CSCs to radiation therapy by gold nanoshell-mediated hyperthermia. The study showed that the breast CSC population expanded after ionizing radiation treatment in both the triple-negative breast cancer syngeneic mouse model and xenograft model, demonstrating the intrinsic resistance of these CSCs. However, following combination of hyperthermia at 42°C and ionizing radiation, the frequency of breast CSCs, the mammosphere forming ability, and the in vivo tumorigenicity of the residual tumor cells were significantly decreased compared to the radiation only-treated tumors and mock-treated tumors. More studies were needed to identify the detailed mechanism of the CSC sensitization, for possible generalization in other CSC models.

It is encouraging to witness the emergence of nanomedicine designs based on CSC concept, however, only few of the current studies evaluate the direct inhibitory effects of nanomedicines on the CSC subpopulation (*35*). Efforts in both nanocarrier design and efficacy evaluation development are in great need for successful development of anti-CSC nanomedicines.

Downloaded by UNIV OF ROCHESTER on July 20, 2013 | http://pubs.acs.org
Publication Date (Web): July 8, 2013 | doi: 10.1021/bk-2013-1135.ch009

## Anti-Prostate CSC Nanomedicine Based on HPMA Copolymer-Cyclopamine Conjugate

Nanosized polymer-drug conjugates based on HPMA (*N*-(2-hydroxypropyl)methacrylamide) copolymers have been broadly used as linear water soluble macromolecular carriers for targeting and therapeutic applications (*63–65*). HPMA copolymer conjugates carrying anti-cancer drugs have shown excellent biocompatibility, enhanced targetability to tumor tissues and significant antiproliferative effects on cancer cells both in animal models and in clinical studies (*63–68*). The ability to improve drug solubility and pharmacokinetics, to reduce nonspecific toxicity, and to overcome multidrug resistance, as well as the physicochemical properties to allow the incorporation of sufficient amount of drugs and efficient drug release, makes HPMA copolymer a suitable nanocarrier to improve the efficacy of anti-CSC therapies.

We choose prostate cancer as a study model for the evaluation of anti-CSC macromolecular therapeutics. Thus far, improving the clinical outcome of advanced/progressive prostate cancer is an unmet medical need. Although the tumor bulk can be effectively shrunk by traditional chemo- or radio-therapies or by androgen deprivation therapy, almost all late stage prostate cancer patients suffer from tumor relapse or widespread metastasis (*69*). Prostate cancer remains the second lethal malignancy in men in the United States, largely due to the treatment failure in advanced prostate cancer patients.

Recently a subset of tumorigenic prostate cancer cells, in most cases identified as androgen-independent and with the similar phenotypic profile to normal prostatic stem cells, was found to possess CSC properties, including in vitro self-renewing sphere formation, differentiation and in vivo regeneration of tumor that recapitulate the cellular hierarchy of the original parental tumor (*70*, *71*). These putative prostate CSCs showed aberrantly upregulated stem cell related transcriptional profiles and are more resistant to anti-prostate cancer therapies than the rest of cancer cells (*70*, *71*). These evidences support the


In Tailored Polymer Architectures for Pharmaceutical and Biomedical Applications; Scholz, C., et al.;
ACS Symposium Series; American Chemical Society: Washington, DC, 2013.

hypothesis that the failure of traditional therapies for prostate cancer is largely attributed to the failure to kill prostate CSCs. Therefore, targeting prostate CSCs would improve patient survival and reduce cancer recurrence and metastasis.

Based on several lines of evidence, Hh signaling inhibition would be an effective and possibly safe strategy to deplete prostate CSCs. Firstly, the critical role of Hh pathway in both prostate cancer progression and prostate CSC maintenance has been proved in animal models and suggested in patient samples (*28*, *31*). Secondly, as discussed above, Hh inhibition does not show side effect on normal adult HSCs.

Hh signaling pathway has been found to be involved in prostate cancer development and progression for a long time. It was firstly discovered to be critical in regulating stem cell self-renewal during normal embryonic development in Drosophila, and later identified in vertebrate development (*31*). Sonic, Desert and Indian Hh are three known secreted Hh proteins (ligands) with different tissue specificities in mammals. Among these, Sonic hedgehog (SHh) is the most widely expressed including in the prostate (*72*). In the absence of SHh ligands, a 12-transmembrane protein receptor Patched (PTCH) functions to silence the pathway by repression of another seven-transmembrane protein Smoothened (SMO). While upon binding of Hh ligands to PTCH, the inhibitory effect of PTCH on SMO is relieved. The activated SMO triggers a series of intracellular transductions, eventually inducing the activation of GLI transcription factor and transcription of multiple Hh responsive genes, including cyclin D1, N-Myc, Bcl-2, Bmi-1, nanog and Snail (*73*).

SHh pathway elements SHh, PTCH, SMO and GLI is found to be up-regulated in prostate cancer cell lines, primary prostate tumor cultures, mouse prostate cancer xenografts and prostate cancer patients (*28*, *74*). The blockade of SHh signaling pathway in vitro and in vivo leads to decreased proliferation of prostate cancer cells and induction of apoptosis (*32*, *75*). In addition, activation of SHh pathway enhanced the migration and invasiveness of prostate cancer cells by up-regulating genes involved in epithelial-mesenchymal transition (*28*). The level of the SHh pathway activity in prostate cancer patient samples is associated with the degree of metastatic potential.

More importantly, the SHh pathway is important in prostate CSC maintenance, as revealed in several studies. Compared to bulk tumor cells, invasive prostate CSC population holds more elevated SHh signaling activity (*76*). SHh signaling was shown to be required in stem/progenitor cell self-renewal and it prompts the expression of stem cell renewal factors in cancer cells (*28*). Sustained over-activation of SHh signaling by stably transfected GLI was able to transform prostate progenitor cells into tumorigenic malignant cancer cells. On the other hand, inhibition of SHh pathway by cyclopamine could successfully improve the cancer-free survivals of mice bearing prostate cancer xenograft and achieve long-term prostate cancer regression (*28*). These evidences suggest that SHh signaling is required for prostate CSC maintenance.

Currently there are several small molecule Hh pathway inhibitors targeting to diverse elements along the stream of Hh signaling under clinical development. Cyclopamine is one of the earliest found classic Hh inhibitors and it shows definite inhibitory effect on Hh pathway. It prevented the invasion of metastatic prostate

Downloaded by UNIV OF ROCHESTER on July 20, 2013 | http://pubs.acs.org
Publication Date (Web): July 8, 2013 | doi: 10.1021/bk-2013-1135.ch009


In Tailored Polymer Architectures for Pharmaceutical and Biomedical Applications; Scholz, C., et al.;
ACS Symposium Series; American Chemical Society: Washington, DC, 2013.

cancer cells in vitro and in lethal metastatic rodent models of prostate cancer (*28*, *75*, *77*). The mechanism of action of cyclopamine is to directly bind to SMO heptahelical bundle and suppress SMO receptor. In addition, down-regulation of drug efflux transporters in androgen-independent prostate cancer was observed upon treatment of cyclopamine, indicating its effect to reverse the multidrug resistance of cancer cells (*78*).

## Design and Synthesis of HPMA Copolymer-Cyclopamine Conjugate

As a natural steroidal alkaloid, cyclopamine contains active functional groups potentially useful for versatile chemical modifications. In the HPMA copolymer-cyclopamine conjugate, cyclopamine was chemically conjugated to the side chains of the linear HPMA copolymer backbone, via the reaction of the secondary amine in cyclopamine with thiazolidine-2-thione (TT) functional groups at side chains termini (Figure 2) (*79*, *80*). GFLG (glycylphenylalanylleucylglycyl) biodegradable terapeptide linker was employed as a spacer between the HPMA copolymer carrier and cyclopamine, considering the binding of cyclopamine to its SMO receptor might take place both from outside and inside of the SMO-expressing cells (*81*).

Downloaded by UNIV OF ROCHESTER on July 20, 2013 | http://pubs.acs.org
Publication Date (Web): July 8, 2013 | doi: 10.1021/bk-2013-1135.ch009

**Table 1. Characterization of HPMA Copolymer Precursor Containing Thiazolidine-2-thione (TT) Functional Groups (*79*, *80*)**

| *Mth (kDa)* | *Mn (kDa)* | *Mw (kDa)* | *Mw/Mn* | *Conversion (%)* | *TT feed mol%* | *TT mol%* |
|---|---|---|---|---|---|---|
| 45 | 47.7 | 50.8 | 1.07 | 45 | 6.0 | 6.1 |
| 45 | 32.4 | 35.8 | 1.08 | 45 | 10.0 | 9.8 |

Mth: theoretical molecular weight.

The synthetic scheme of the HPMA copolymer-cyclopamine conjugate is shown in Figure 2. To obtain well controlled molecular weight and polydispersity of the polymeric carrier, RAFT (Reversible Addition-Fragmentation chain Transfer) copolymerization was employed for the synthesis of HPMA copolymer precursor containing TT functional groups. The reaction was conducted at 40°C in methanol using VA 044 as initiator and 4-cyanopentanoic acid dithiobenzoate as chain transfer agent (*82*). The characterization of P-GFLG-TT (HPMA copolymer containing TT groups in the side chains), in two scenarios with different TT feed ratios, is shown in Table 1 (*79*). The actual molecular weight of the resulting copolymer precursor is similar to the theoretical molecular weight and it possesses a very narrow molecular weight distribution. The TT content, determined by its typical UV absorbance at 305 nm in the end-modified copolymer removing the chain-end dithiobenzoate groups, is close to the TT feed ratio in both cases as shown in Table 1.


In Tailored Polymer Architectures for Pharmaceutical and Biomedical Applications; Scholz, C., et al.;
ACS Symposium Series; American Chemical Society: Washington, DC, 2013.

Downloaded by UNIV OF ROCHESTER on July 20, 2013 | http://pubs.acs.org
Publication Date (Web): July 8, 2013 | doi: 10.1021/bk-2013-1135.ch009



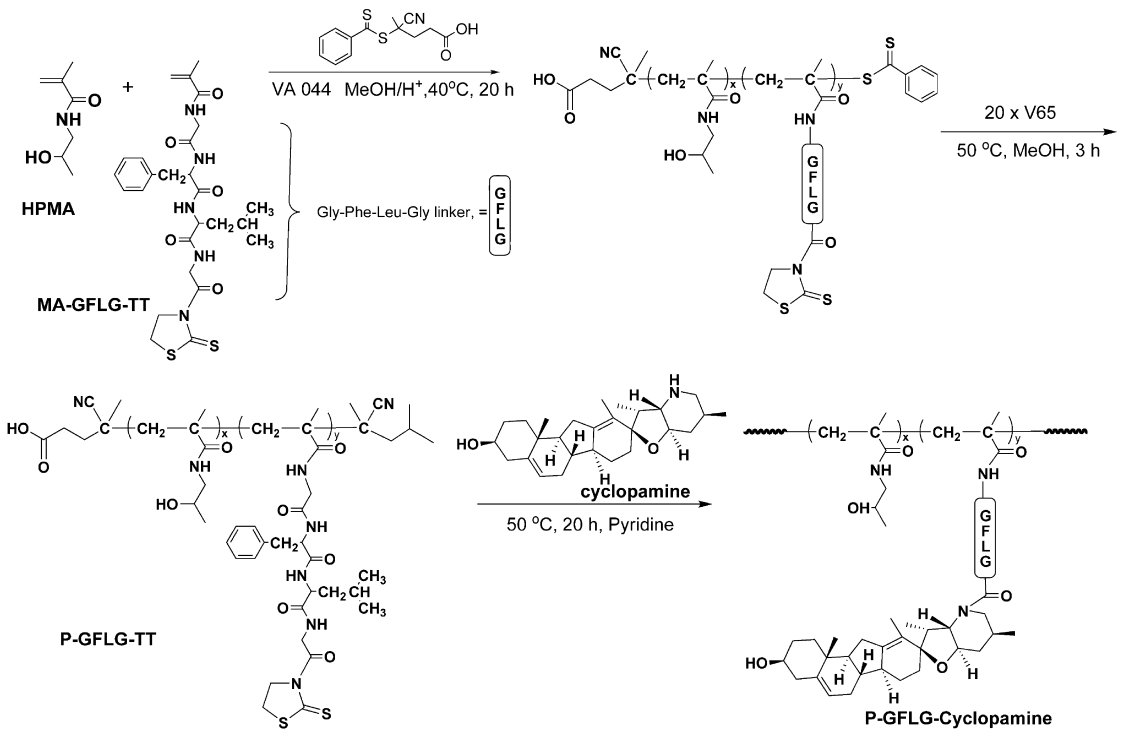


*Figure 2. Synthetic scheme of HPMA copolymer-cyclopamine conjugate. Adapted with permission from ref. (79). Copyright 2012 Elsevier.*

The final HPMA copolymer-cyclopamine conjugate was obtained by the reaction of end-modified P-GFLG-TT with cyclopamine under basic condition. The conversion of TT reactive groups to cyclopamine was around 50%, as estimated from the HPLC profile of the conjugate after model lysosomal enzyme cathepsin B cleavage. To be noted, cathepsin B cleavage resulted in the majority of free cyclopamine fraction ($[CYP+H]^+$, 412.1), while cleavage catalyzed by papain produced the major cleaved product glycine-cyclopamine ($[Gly\text{-}CYP+H]^+$, 469.4) as confirmed by HPLC and LC-MS (*79*). This is due to the preference of papain for phenylalanine in position $P_2$ (nomenclature of Schechter and Berger (*83*)) of the substrate, forming the papain-substrate complex with F in $P_2$ despite the steric hindrance of the HPMA copolymer backbone. Thus, GFLG side-chains interact with the active site of papain in two modes (F in $P_2$ and F in $P_3$), leading to two cleaved products. As indicated in previous research of cyclopamine and its derivatives (*84*), modified cyclopamine could retain its biological activity if the hydroxyl group is retained.

Downloaded by UNIV OF ROCHESTER on July 20, 2013 | http://pubs.acs.org
Publication Date (Web): July 8, 2013 | doi: 10.1021/bk-2013-1135.ch009

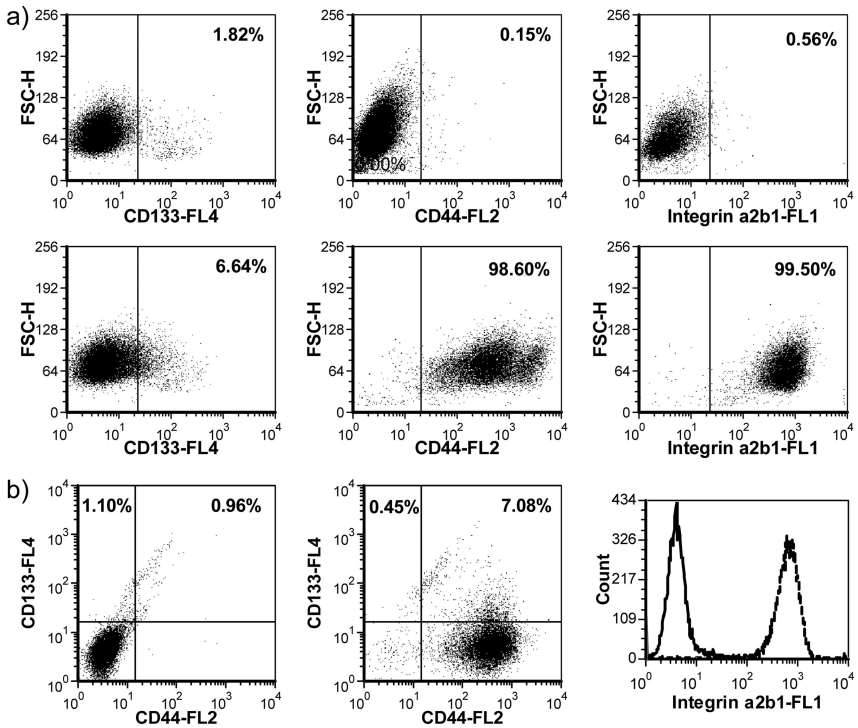


*Figure 3. Cell surface marker expressions of CD133, CD44 and integrin α2β1 on RC-92a/hTERT cells. a) single antigen staining (the upper panels are the negative controls; the lower panels are the stained samples); b) multiparameter staining (the left is the negative control; the middle profile is CD133 and CD44 double staining; the right profile is the integrin expression in CD133+/CD44+ cells). Adapted with permission from ref. (79). Copyright 2012 Elsevier.*


In Tailored Polymer Architectures for Pharmaceutical and Biomedical Applications; Scholz, C., et al.;
ACS Symposium Series; American Chemical Society: Washington, DC, 2013.

In addition, the conjugate was stable in growth medium under tissue culture condition, with no release of free cyclopamine for at least 72 hours, due to the stability of the amide bond formed between the side chain and cyclopamine.

## Characterization of Cancer Stemlike Cells in RC-92a/hTERT Prostate Cancer Model

Preceding the evaluation of the conjugate effect on prostate CSCs, the CSC properties in our prostate cancer model, an hTERT-immortalized human primary prostate cancer-derived cell line, was characterized. Previous results in Rhim's group (who established the RC-92a/hTERT cells) showed that the prostate CSC-enriched populations express surface markers CD133, CD44 and integrin α2β1, with enhanced sphere forming ability and differentiation capacity in vitro and increased tumorigenicity in vivo (*85*, *86*). We further validated the use of surface markers as the biomarkers for CSC enrichment and identification. We observed that CD133 is stably expressed in about 5% of the whole RC-92a/hTERT cell population throughout long-term passages (*79*, *80*). Although 5% of CSCs is a small proportion of cells, it is much higher than the prostate CSCs isolated from other commonly used prostate cancer cell lines and primary tumors. Possibly it is due to the hTERT transfection that imposes stem cell properties to this cell line. On the contrary, both CD44 and integrin α2β1 are expressed in the majority of cancer cells; they do express in all CD133+ cells, although they also appear in CD133- cells (Figure 3) (*79*). Therefore, CD133 is the most specific marker among the above three surface antigens for cancer stemlike cells in this prostate cancer cell line.

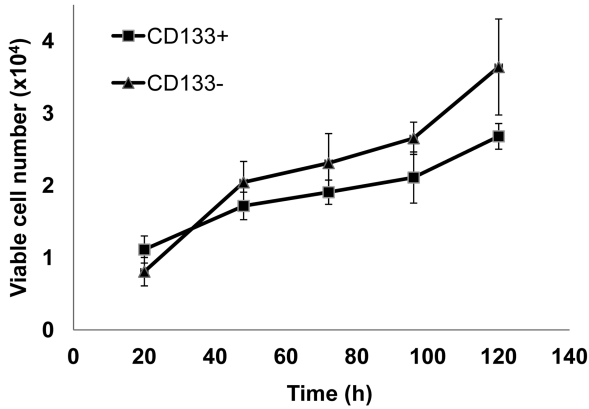


*Figure 4. Growths of FACS sorted CD133+ and CD133- cells in monolayer under normal cell culture condition immediately after cell sorting.*

In addition, we compared the growth behavior of the FACS isolated CD133+ and CD133- cells in monolayer under normal cell culture conditions. After seeding the pure (confirmed by post FACS flow cytometry analysis) CD133+ and CD133- cells, respectively, in tissue culture plate, cells in both groups proliferated


In Tailored Polymer Architectures for Pharmaceutical and Biomedical Applications; Scholz, C., et al.; ACS Symposium Series; American Chemical Society: Washington, DC, 2013.

Downloaded by UNIV OF ROCHESTER on July 20, 2013 | http://pubs.acs.org
Publication Date (Web): July 8, 2013 | doi: 10.1021/bk-2013-1135.ch009

and the growth rate of CD133+ cells was only slightly slower than that of CD133- cells (Figure 4). This result suggests that instead of being quiescent, these CD133+ putative CSCs grow and differentiate into phenotypically diverse cancer cell populations, which is consistent with observation in the in vitro culture of other types of CSCs (*47*). Indeed, the expression of CD133 in CD133+ cells decreased to 30% following two passages, and further decreased during long-term culture (*79*). On the other hand, CD133 expression in cells subcultured from CD133- cells remained similar to the background level of unstained CD133- cells within two passages (*79*).

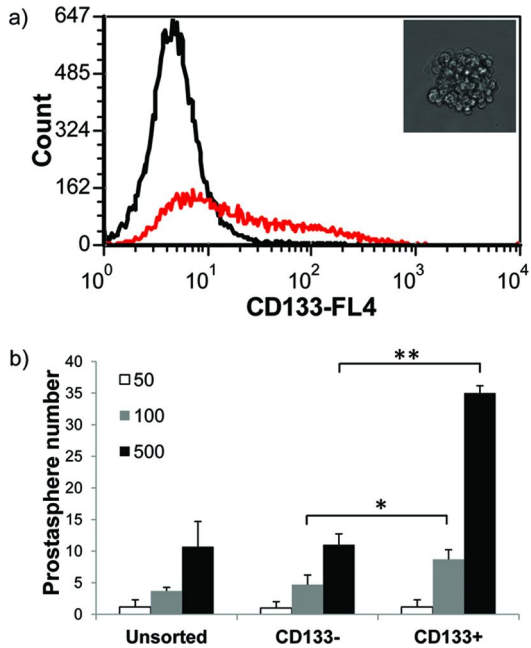


*Figure 5. a) CD133 expression in spheres formed from RC-92a/hTERT cells (black: negative control; red: anti CD133-APC stained cells) and b) Prostasphere formation from unsorted, sorted CD133+ and CD133- cells (*, $p<0.05$; **, $p<0.01$). Adapted with permission from refs. (79) (Copyright 2012 Elsevier) and (80) (Copyright 2012 American Chemical Society).*

To evaluate the self-renewal ability of CD133+ cells, sphere forming assay was performed on both RC-92a/hTERT cells and sorted cells. Under nonadherent culture conditions, only cells with self-renewal and differentiation capacities can survive and grow into prostaspheres - cell clusters clonally grown from a single prostate cancer cell, whereas differentiated cells can hardly grow (*84*). The whole RC-92a/hTERT cells generate prostaspheres following 10 days of anchorage-independent growth, with the CSC marker CD133 expressed in about


In Tailored Polymer Architectures for Pharmaceutical and Biomedical Applications; Scholz, C., et al.;
ACS Symposium Series; American Chemical Society: Washington, DC, 2013.

Downloaded by UNIV OF ROCHESTER on July 20, 2013 | http://pubs.acs.org
Publication Date (Web): July 8, 2013 | doi: 10.1021/bk-2013-1135.ch009

30% of cancer cells within the spheres (Figure 5a) (*79*, *80*). To directly prove the sphere-forming ability of CD133+ prostate CSCs, the nonadherent culture of sorted CD133+ and CD133- cells was compared following seeding the same number of viable cells with each phenotype respectively. CD133+ cells formed significantly more spheres than CD133- cells under all the three conditions with different initial cell seeding densities (Figure 5b) (*79*, *80*). In addition, the number of spheres generated from CD133+ cells was approximately proportional to its seeding densities. This suggests a low extent of sphere fusion/aggregation (*87*). Furthermore, to avoid the intrinsic limitation of the sphere-forming assay, which is the possible occurrence of sphere fusion/aggregation, we seeded RC-92a/hTERT cells in ultra low density, with 0-5 cells per well of the nonadherent 96-well tissue culture plate. The frequency of the sphere-forming cells calculated from the above assay was 1-2%, the same magnitude as the frequency of CD133+ cells. Concluding from the above series of characterizations, the CD133+ cancer cell population is enriched with CSC properties within the RC-92a/hTERT prostate cancer model.

Downloaded by UNIV OF ROCHESTER on July 20, 2013 | http://pubs.acs.org
Publication Date (Web): July 8, 2013 | doi: 10.1021/bk-2013-1135.ch009

## Evaluations of Cyclopamine and HPMA Copolymer-Cyclopamine Conjugate on RC-92a/hTERT Cells

First, the cytotoxic effect of cyclopamine was tested on RC-92a/hTERT cells. However, cyclopamine, especially at concentrations under 10 μM (the concentration range commonly used in published studies), did not decrease the whole cell viability significantly (Figure 6a). Consistent with this observation, cyclopamine could only induce very low levels of apoptotic cell deaths as detected in Annexin V apoptosis assay (Figure 6b). The results indicate that Hh pathway, although shown to be widely up-regulated in certain prostate cancer models (*32*, *74*), is not widely active in the majority of prostate cancer cells in the RC-92a/hTERT model. This is reasonable since in vitro prostate cancer models derived via different methods could show various phenotypic and functional properties. However, interestingly, cyclopamine treatment of FACS sorted CD133+ prostate CSCs showed significant induction of apoptosis (Figure 6b). Taken together, CD133+ prostate CSC-enriched subpopulation from the RC-92a/hTERT cells are more sensitive to Hh inhibition and cyclopamine treatment, which makes it an ideal model for HPMA copolymer-cyclopamine conjugate evaluation.

The first step for cyclopamine to exert specific Hh inhibitory effect is the binding of cyclopamine to SMO receptor. We evaluated whether HPMA copolymer conjugated cyclopamine can still have access to and interact with the cell surfaces of RC-92a/hTERT cells. Similar to the established BODIPY-cyclopamine binding assay reported in previous studies, we incubated FITC labeled HPMA copolymer-cyclopamine conjugate with RC-92a/hTERT cells seeded in glass bottom dishes at 37 °C for 2 hours, to minimize the intracellular uptake of the conjugate or control polymers. The positive FITC fluorescent signals on cell surfaces was only observed following HPMA copolymer-cyclopamine conjugate incubation, but not in the control FITC labeled


In Tailored Polymer Architectures for Pharmaceutical and Biomedical Applications; Scholz, C., et al.;
ACS Symposium Series; American Chemical Society: Washington, DC, 2013.

HPMA copolymer with no cyclopamine conjugation (*79*). The interaction of HPMA copolymer-cyclopamine conjugate with prostate cancer cells was also confirmed in flow cytometry study (data not shown). Since the Hh pathway may be heterogeneously activated in the whole cell line, we did not observe the binding of HPMA copolymer-cyclopamine conjugate on all the cultured cells.

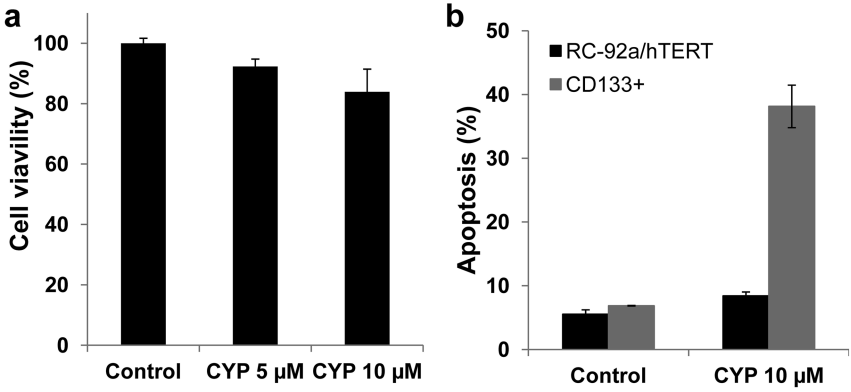


*Figure 6. a) Cytotoxicity of cyclopamine on RC-92a/hTERT cells as determined by CCK-8 cell counting kit; b) Apoptosis levels induced by cyclopamine on the whole RC-92a/hTERT cells (black) and sorted CD133+ prostate CSCs (grey).*

Next, we examined whether the HPMA copolymer-cyclopamine conjugate shows inhibitory effect on CD133+ prostate CSCs. As shown in our characterization, CD133+ cells maintain a stable proportion within the whole cell population without any therapeutic interventions (*79*, *80*). Thus, the change in the percentage of CD133+ cells within the whole viable prostate cancer cells before and after certain treatment would suggest its therapeutic effect on the CD133+ prostate CSC subpopulation. This strategy, instead of directly evaluating treatment effects on monolayer cultured CD133+/- cells, is much more convenient, and most importantly, avoid the problem that sorted CSCs grown in monolayer usually undergo quick phenotypic and/or functional property changes. As expected, the CD133+ cell percentages in the surviving residual cancer cells were decreased in the dose-dependent manner, following the treatments of different concentrations of HPMA copolymer-cyclopamine conjugate (*79*, *80*). The mechanism of action of free cyclopamine proved in our studies (Figure 6b) suggests that the decrease of CD133+ subpopulation is most probably due to cell death instead of differentiation, although further studies are needed to reveal the mechanism of the inhibitory effect of the conjugate on CD133+ cells.

We also evaluated whether the depletion of CD133+ cells is correlated to the inhibition of CSC functional properties, self-renewal and differentiation. To this end, HPMA copolymer-cyclopamine conjugate was added into the ultra low adherent plate containing suspended single RC-92a/hTERT cells during


In Tailored Polymer Architectures for Pharmaceutical and Biomedical Applications; Scholz, C., et al.;
ACS Symposium Series; American Chemical Society: Washington, DC, 2013.

Downloaded by UNIV OF ROCHESTER on July 20, 2013 | http://pubs.acs.org
Publication Date (Web): July 8, 2013 | doi: 10.1021/bk-2013-1135.ch009

the whole period of prostasphere culture. It turned out that the number of spheres formed in the conjugate treated group was decreased compared to the untreated group (Figure 7). In addition, the sizes of the spheres were smaller in treated group than in untreated one. This result further demonstrate that HPMA copolymer-cyclopamine conjugate can interrupt the stem cell related function of prostate cancer cells, potentially reducing their tumorigenic capacity, thus improving the prognosis of prostate cancer.

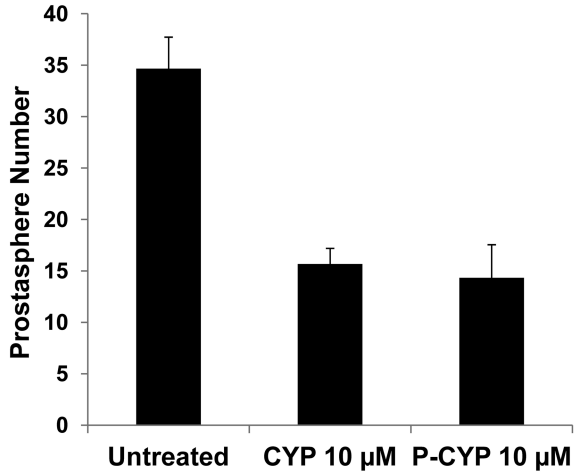


*Figure 7. Prostasphere formation following the treatment of RC-92a/hTERT cells with cyclopamine and HPMA copolymer-cyclopamine conjugate.*

Downloaded by UNIV OF ROCHESTER on July 20, 2013 | http://pubs.acs.org
Publication Date (Web): July 8, 2013 | doi: 10.1021/bk-2013-1135.ch009

To further compare the therapeutic effect of cyclopamine conjugate with docetaxel, the commonly used first line chemotherapeutics for prostate cancer, we analyzed the changes in CD133 expression as well as the whole cell cytotoxicity on the same batch of RC-92a/hTERT cells following different treatments. HPMA copolymer-cyclopamine conjugate (or cyclopamine) and docetaxel showed the opposite effect on the two subpopulations-CD133+ prostate CSCs and CD133- bulk tumor cells (Figure 8) (*79*, *80*). Cyclopamine conjugate and cyclopamine treatment could not decrease the whole cell viability, but they led to significantly decreased percentages of viable CD133+ cells. On the other hand, 10%, 20% and 45% decrease of whole cell viability was observed following 0.5 nM, 1 nM and 2 nM docetaxel treatment, respectively. However, docetaxel failed to inhibit the growth of CD133+ prostate CSCs at all three concentrations. The experimental data suggests that following conventional anti-prostate cancer therapy such as docetaxel treatment, cancer cells with CSC properties could still survive and may generate new malignant tumor cells. HPMA copolymer-cyclopamine conjugate holds the potential to kill these surviving prostate CSCs and improve the therapeutic effect of the traditional therapy with docetaxel (*88*).


In Tailored Polymer Architectures for Pharmaceutical and Biomedical Applications; Scholz, C., et al.;
ACS Symposium Series; American Chemical Society: Washington, DC, 2013.

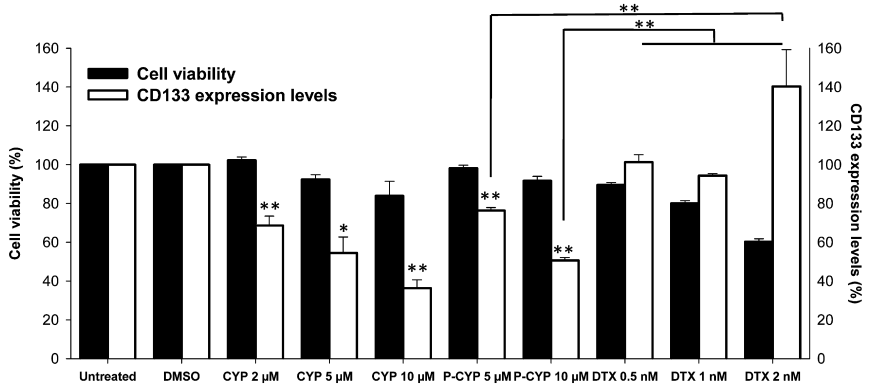


*Figure 8. Changes of cell viabilities (black columns) and CD133+ prostate CSC percentages (white columns) following HPMA copolymer-cyclopamine conjugate, free cyclopamine or docetaxel treatments on RC-92a/hTERT cells. *, $p < 0.05$; **, $p < 0.01$. Adapted with permission from refs. (79) (Copyright 2012 Elsevier) and (80) (Copyright 2012 American Chemical Society).*

Downloaded by UNIV OF ROCHESTER on July 20, 2013 | http://pubs.acs.org
Publication Date (Web): July 8, 2013 | doi: 10.1021/bk-2013-1135.ch009

If the CSC population is a fixed population, it might be adequate to selectively target only the CSCs for long-term cancer remission. However, accumulated evidence supports that CSCs are a dynamic cancer cell population which can be generated de novo. So targeting CSCs alone will probably not lead to complete cancer regression. To both effectively remove the tumor mass and reduce the tumorigenic potential of prostate cancer, combination therapeutics of HPMA copolymer-cyclopamine conjugate and docetaxel (or docetaxel conjugate) would be a promising strategy, due to the preferential therapeutic effects of HPMA copolymer-cyclopamine conjugate and docetaxel on two prostate cancer subpopulations with distinct properties. Our evaluations of the combinational therapeutic effect of HPMA copolymer-cyclopamine conjugate and docetaxel are still going on, with some promising initial results in vitro.

## Future Perspectives

Although more and more investigations on CSCs are taking place, there are still controversies around the CSC theory. For instance, it is not clear that whether CSC model fits all types of cancer; what are unique biomarkers for CSCs; and whether the frequency of CSCs in a certain tumor is dynamically changing. However, it is clear that CSCs identified based on current knowledge do escape traditional therapies and contribute to cancer relapse. Therefore, the CSC population represents an important therapeutic target. Nanomedicines have the potential to improve the small molecule anti-CSC therapeutics and may offer new multimodal strategies to kill CSCs. Given that the clonal evolution and CSCs both play critical roles in cancer progression, combination therapy that takes

into account both the genetic and epigenetic heterogeneity would be a promising solution to improve cancer treatment. It is foreseeable that the end point for the anti-cancer therapy evaluation may switch from short-term tumor regression to long-term prognosis in the future.

## Acknowledgments

The research was supported in part by NIH grant RO1 CA132831 from the National Cancer Institute. We thank Dr. J.S. Rhim for the gift of RC92a/hTERT cells.

Downloaded by UNIV OF ROCHESTER on July 20, 2013 | http://pubs.acs.org
Publication Date (Web): July 8, 2013 | doi: 10.1021/bk-2013-1135.ch009

## References

1. Jemal, A.; Siegel, R.; Xu, J.; Ward, E. *CA-Cancer J. Clin.* **2010**, *60* (5), 277–300.
2. Hanahan, D.; Weinberg, R. A. *Cell* **2011**, *144* (5), 646–674.
3. Reya, T.; Morrison, S. J.; Clarke, M. F.; Weissman, I. L. *Nature* **2001**, *414* (6859), 105–111.
4. Shackleton, M.; Quintana, E.; Fearon, E. R.; Morrison, S. J. *Cell* **2009**, *138* (5), 822–829.
5. Dick, J. E. *Nat. Biotechnol.* **2009**, *27* (1), 44–46.
6. Clevers, H. *Nat. Med.* **2011**, *17* (3), 313–319.
7. Furth, J.; Kahn, M. *Am. J. Cancer* **1937**, *31*, 276–282.
8. Bruce, W. R.; Van Der Gaag, H. *Nature* **1963**, *199*, 79–80.
9. Pierce, G. B.; Wallace, C. *Cancer Res.* **1971**, *31* (2), 127–134.
10. Nowell, P. C. *Science* **1976**, *194* (4260), 23–28.
11. Bonnet, D.; Dick, J. E. *Nat. Med.* **1997**, *3* (7), 730–737.
12. Al-Hajj, M.; Wicha, M. S.; Benito-Hernandez, A.; Morrison, S. J.; Clarke, M. F. *Proc. Natl. Acad. Sci. U.S.A.* **2003**, *100* (7), 3983–3988.
13. Singh, S. K.; Hawkins, C.; Clarke, I. D.; Squire, J. A.; Bayani, J.; Hide, T.; Henkelman, R. M.; Cusimano, M. D.; Dirks, P. B. *Nature* **2004**, *432* (7015), 396–401.
14. Collins, A. T.; Maitland, N. J. *Nat. Rev. Urol.* **2009**, *6* (4), 184–186.
15. Wang, Z. A.; Shen, M. M. *Oncogene* **2010**, *30* (11), 1261–1271.
16. Ricci-Vitiani, L.; Lombardi, D. G.; Pilozzi, E.; Biffoni, M.; Todaro, M.; Peschle, C.; De Maria, R. *Nature* **2007**, *445* (7123), 111–115.
17. Ricci-Vitiani, L.; Pallini, R.; Biffoni, M.; Todaro, M.; Invernici, G.; Cenci, T.; Maira, G.; Parati, E. A.; Stassi, G.; Larocca, L. M.; De Maria, R. *Nature* **2010**, *468* (7325), 824–828.
18. Wang, R.; Chadalavada, K.; Wilshire, J.; Kowalik, U.; Hovinga, K. E.; Geber, A.; Fligelman, B.; Leversha, M.; Brennan, C.; Tabar, V. *Nature* **2010**, *468* (7325), 829–833.
19. Dean, M.; Fojo, T.; Bates, S. *Nat. Rev. Cancer* **2005**, *5* (4), 275–284.
20. Tang, C.; Ang, B. T.; Pervaiz, S. *FASEB J.* **2007**, *21* (14), 3777–3785.


In Tailored Polymer Architectures for Pharmaceutical and Biomedical Applications; Scholz, C., et al.; ACS Symposium Series; American Chemical Society: Washington, DC, 2013.

21. Oravecz-Wilson, K. I.; Philips, S. T.; Yilmaz, O. H.; Ames, H. M.; Li, L.; Crawford, B. D.; Gauvin, A. M.; Lucas, P. C.; Sitwala, K.; Downing, J. R.; Morrison, S. J.; Ross, T. S. *Cancer Cell* **2009**, *16* (2), 137–148.
22. Yu, F.; Yao, H.; Zhu, P.; Zhang, X.; Pan, Q.; Gong, C.; Huang, Y.; Hu, X.; Su, F.; Lieberman, J.; Song, E. *Cell* **2007**, *131* (6), 1109–1123.
23. Chow, E. K. *J. Lab. Autom.* **2013**, *18* (1), 6–11.
24. Hirschmann-Jax, C.; Foster, A. E.; Wulf, G. G.; Nuchtern, J. G.; Jax, T. W.; Gobel, U.; Goodell, M. A.; Brenner, M. K. *Proc. Natl. Acad. Sci. U.S.A.* **2004**, *101* (39), 14228–14233.
25. Bao, S.; Wu, Q.; McLendon, R. E.; Hao, Y.; Shi, Q.; Hjelmeland, A. B.; Dewhirst, M. W.; Bigner, D. D.; Rich, J. N. *Nature* **2006**, *444* (7120), 756–760.
26. Gallmeier, E.; Hermann, P. C.; Mueller, M. T.; Machado, J. G.; Ziesch, A.; De Toni, E. N.; Palagyi, A.; Eisen, C.; Ellwart, J. W.; Rivera, J.; Rubio-Viqueira, B.; Hidalgo, M.; Bunz, F.; Göke, B.; Heeschen, C. *Stem Cells* **2011**, *29*, 418–429.
27. Thayer, S. P.; di Magliano, M. P.; Heiser, P. W.; Nielsen, C. M.; Roberts, D. J.; Lauwers, G. Y.; Qi, Y. P.; Gysin, S.; Fernández-del Castillo, C.; Yajnik, V.; Antoniu, B.; McMahon, M.; Warshaw, A. L.; Hebrok, M. *Nature* **2003**, *425* (6960), 851–856.
28. Karhadkar, S. S.; Steven Bova, G.; Abdallah, N.; Dhara, S.; Gardner, D.; Maitra, A.; Isaacs, J. T.; Berman, D. M.; Beachy, P. A. *Nature* **2004**, *431* (7009), 707–712.
29. Wang, Z.; Li, Y.; Kong, D.; Banerjee, S.; Ahmad, A.; Azmi, A. S.; Ali, S.; Abbruzzese, J. L.; Gallick, G. E.; Sarkar, F. H. *Cancer Res.* **2009**, *69* (6), 2400–2407.
30. Teng, Y.; Wang, X.; Wang, Y.; Ma, D. *Biochem. Biophys. Res. Commun.* **2010**, *392* (3), 373–379.
31. Magliano, M. P.; Hebrok, M. *Nat. Rev. Cancer* **2003**, *3*, 903–911.
32. Shaw, A.; Bushman, W. *J. Urol.* **2007**, *177*, 832–838.
33. Kobune, M.; Takimoto, R.; Murase, K.; Lyama, S.; Sato, T.; Kikuchi, S.; Kawano, Y.; Miyanishi, K.; Sato, Y.; Niitsu, Y.; Kato, J. *Cancer Sci.* **2009**, *100* (5), 948–955.
34. Pannuti, A.; Foreman, K.; Rizzo, P.; Osipo, C.; Golde, T.; Osborne, B.; Miele, L. *Clin. Cancer Res.* **2010**, *16*, 3141–3152.
35. Vinogradov, S.; Wei, X. *Nanomedicine* **2012**, *7* (4), 597–615.
36. Wang, J.; Wakeman, T. P.; Lathia, J. D.; Hjelmeland, A. B.; Wang, X. F.; White, R. R.; Rich, J. N.; Sullenger, B. A. *Stem Cells* **2010**, *28*, 17–28.
37. Farnie, G.; Clarke, R. B. *Stem Cell Rev.* **2007**, *3*, 169–175.
38. Fan, X.; Matsui, W.; Khaki, L.; Stearns, D.; Chun, J.; Li, Y. M.; Eberhart, C. G. *Cancer Res.* **2006**, *66*, 7445–7452.
39. Milano, J.; McKay, J.; Dagenais, C.; Foster-Brown, L.; Pognan, F.; Gadient, R.; Jacobs, R. T.; Zacco, A.; Greenberg, B.; Ciaccio, P. J. *Toxicol Sci.* **2004**, *82* (1), 341–358.
40. Watters, J. W.; Cheng, C.; Majumder, P. K.; Wang, R.; Yalavarthi, S.; Meeske, C.; Kong, L.; Sun, W.; Lin, J.; Heyer, J.; Ware, C.; Winter, C.;

Downloaded by UNIV OF ROCHESTER on July 20, 2013 | http://pubs.acs.org
Publication Date (Web): July 8, 2013 | doi: 10.1021/bk-2013-1135.ch009

Reilly, J. F.; Demuth, T.; Clark, S.; Chiu, M. I.; Robinson, M. O.; Kohl, N.; Kannan, K. *Cancer Res.* **2009**, *69*, 8949–8957.
41. Hofmann, I.; Stover, E. H.; Cullen, D. E.; Mao, J.; Morgan, K. J.; Lee, B. H.; Kharas, M. G.; Miller, P. G.; Cornejo, M. G.; Okabe, R.; Armstrong, S. A.; Ghilardi, N.; Gould, S.; de Sauvage, F. J.; McMahon, A. P.; Gilliland, D. G. *Cell Stem Cell* **2009**, *4*, 559–567.
42. Gao, J.; Graves, S.; Koch, U.; Liu, S.; Jankovic, V.; Buonamici, S.; Andaloussi, A. E.; Nimer, S. D.; Kee, B. L.; Taichman, R.; Radtke, F.; Aifantis, I. *Cell Stem Cell* **2009**, *4* (6), 548–558.
43. Yilmaz, O. H.; Valdez, R.; Theisen, B. K.; Guo, W.; Ferguson, D. O.; Wu, H.; Morrison, S. J. *Nature* **2006**, *441* (7092), 475–482.
44. Rosen, J. M.; Jordan, C. T. *Science* **2009**, *234* (26), 1670–1677.
45. Quintana, E.; Shackleton, M.; Sabel, M. S.; Fullen, D. R.; Johnson, T. M.; Morrison, S. J. *Nature* **2008**, *456* (7222), 593–598.
46. Roesch, A.; Fukunaga-Kalabis, M.; Schmidt, E. C.; Zabierowski, S. E.; Brafford, P. A.; Vultur, A.; Basu, D.; Gimotty, P.; Vogt, T.; Herlyn, M. *Cell* **2010**, *141* (4), 583–594.
47. Gupta, P. B.; Fillmore, C. M.; Jiang, G.; Shapira, S. D.; Tao, K.; Kuperwasser, C.; Lander, E. S. *Cell* **2011**, *146* (4), 633–644.
48. Iliopoulos, D.; Hirsch, H. A.; Wang, G.; Struhl, K. *Proc. Natl. Acad. Sci. U.S.A.* **2011**, *108* (4), 1397–1402.
49. Shah, N. P.; Skaggs, B. J.; Branford, S.; Hughes, T. P.; Nicoll, J. M.; Paquette, R. L.; Sawyers, C. L. *J. Clin. Invest.* **2007**, *117* (9), 2562–2569.
50. Sharma, S. V.; Lee, D. Y.; Li, B.; Quinlan, M. P.; Takahashi, F.; Maheswaran, S.; McDermott, U.; Azizian, N.; Zou, L.; Fischbach, M. A.; Wong, K. K.; Brandstetter, K.; Wittner, B.; Ramaswamy, S.; Classon, M.; Settleman, J. *Cell* **2010**, *141* (1), 69–80.
51. Dlugosz, A.; Agrawal, S.; Kirkpatrick, P. *Nat. Rev. Drug Discovery* **2012**, *11* (6), 437–438.
52. http://www.clinicaltrials.gov/ct2/show/NCT00645333?term=cancer+stem+cell&rank=20.
53. Gupta, P. B.; Onder, T. T.; Jiang, G.; Tao, K.; Kuperwasser, C.; Weinberg, R. A.; Lander, E. S. *Cell* **2009**, *138* (4), 645–659.
54. Hirsch, H. A.; Iliopoulos, D.; Tsichlis, P. N.; Struhl, K. *Cancer Res.* **2009**, *69* (19), 7507–7511.
55. Fang, J.; Nakamura, H.; Maeda, H. *Adv. Drug Delivery Rev.* **2011**, *63* (3), 136–151.
56. Alexis, F.; Pridgen, E.; Molnar, L. K.; Farokhzad, O. C. *Mol. Pharm.* **2008**, *5* (4), 505–515.
57. Lammers, T.; Kühnlein, R.; Kissel, M.; Subr, V.; Etrych, T.; Pola, R.; Pechar, M.; Ulbrich, K.; Storm, G.; Huber, P.; Peschke, P. *J. Controlled Release* **2005**, *110*, 103–118.
58. Banzato, A.; Bobisse, S.; Rondina, M.; Renier, D.; Bettella, F.; Esposito, G.; Quintieri, L.; Meléndez-Alafort, L.; Mazzi, U.; Zanovello, P.; Rosato, A. *Clin. Cancer Res.* **2008**, *14* (11), 3598–3606.
59. Minko, T.; Kopečková, P.; Kopeček, J. *Int. J. Cancer* **2000**, *86*, 108–117.

Downloaded by UNIV OF ROCHESTER on July 20, 2013 | http://pubs.acs.org
Publication Date (Web): July 8, 2013 | doi: 10.1021/bk-2013-1135.ch009


In Tailored Polymer Architectures for Pharmaceutical and Biomedical Applications; Scholz, C., et al.;
ACS Symposium Series; American Chemical Society: Washington, DC, 2013.

60. Lim, K. J.; Bisht, S.; Bar, E. E.; Maitra, A.; Eberhart, C. G. *Cancer Biol. Ther.* **2011**, *11* (5), 464–473.
61. Bourseau-Guilmain, E.; Béjaud, J.; Griveau, A.; Lautram, N.; Hindré, F.; Weyland, M.; Benoit, J. P.; Garcion, E. *Int. J. Pharm.* **2011**, *423* (1), 93–101.
62. Atkinson, R. L.; Zhang, M.; Diagaradjane, P.; Peddibhotla, S.; Contreras, A.; Hilsenbeck, S. G.; Woodward, W. A.; Krishnan, S.; Chang, J. C.; Rosen, J. M. *Sci. Transl. Med.* **2010**, *2* (55), 55–79.
63. Kopeček, J.; Kopečková, P. *Adv. Drug Delivery Rev.* **2010**, *62*, 122–149.
64. Zhou, Y.; Kopeček, J. *J. Drug Targeting* **2013**, *21* (1), 1–26.
65. Kopeček, J. *Adv. Drug Delivery Rev.* **2013**, *65* (1), 49–59.
66. Seymour, L. W.; Ferry, D. R.; Kerr, D. J.; Rea, D.; Whitlock, M.; Ponyer, R.; Boivin, C.; Hesslewood, S.; Twelves, C.; Blackie, R.; Schätzlein, A.; Jodrell, D.; Bissett, D.; Calvert, H.; Lind, M.; Robbins, A.; Burtless, S.; Duncan, R.; Cassidy, J. *Int. J. Oncol.* **2009**, *34*, 1629–1636.
67. Shoemaker, N. E.; van Kesteren, C.; Rosing, H.; Jansen, S.; Swart, M.; Lieverst, J.; Fraier, D.; Breda, M.; Pellizzoni, C.; Spinelli, R.; Grazia Porro, M.; Beijnen, J. H.; Schellens, J. H. M.; ten Bokkel Huinink, W. W. *Br. J. Cancer* **2002**, *87*, 608–614.
68. Rademaker-Lakhai, J. M.; Terret, C.; Howell, S. B.; Baud, C. M.; De Boer, R. F.; Pluim, D.; Beijnen, J. H.; Schellens, J. H.; Droz, J. P. *Clin. Cancer Res.* **2004**, *10*, 3386–3395.
69. Shah, R. B.; Mehra, R.; Chinnaiyan, A. M.; Shen, R.; Ghosh, D.; Zhou, M.; Macvicar, G. R.; Varambally, S.; Harwood, J.; Bismar, T. A.; Kim, R.; Rubin, M. A.; Pienta, K. J. *Cancer Res.* **2004**, *64* (24), 9209–9216.
70. Collins, A. T.; Berry, P. A.; Hyde, C. *Cancer Res.* **2005**, *65* (23), 10946–10951.
71. Patrawala, L.; Calhoun, T.; Schneider-Broussard, R.; Li, H.; Bhatia, B.; Tang, S.; Reilly, J. G.; Chandra, D.; Zhou, J.; Claypool, K.; Coghlan, L.; Tang, D. G. *Oncogene* **2006**, *25* (12), 1696–1708.
72. Pathi, S.; Pagan-Westphal, S.; Baker, D. P.; Garber, E. A.; Rayhorn, P.; Bumcrot, D.; Tabin, C. J.; Blake, R. P.; Williams, K. P. *Mech. Dev.* **2001**, *106*, 107–117.
73. Ruiz, A.; Altaba, I.; Sánchez, P.; Dahmane, N. *Nat. Rev. Cancer* **2002**, *2* (5), 361–372.
74. Shaw, G.; Price, A. M.; Ktori, E.; Bisson, I.; Purkis, P. E.; McFaul, S.; Oliver, R. T. D.; Prowse, D. M. *Eur. Urol.* **2008**, *54*, 1333–1343.
75. Sanchez, P.; Hernandez, A. M.; Stecca, B. *Proc. Natl. Acad. Sci. U.S.A.* **2004**, *101*, 12561–12566.
76. Klarmann, G. J.; Hurt, E. M.; Matthews, L. A.; Zhang, X.; Duhagon, M. A.; Mistree, T.; Thomas, S. B.; Farrar, W. L. *Clin. Exp. Metastasis* **2009**, *26*, 433–446.
77. Kumar, S. K.; Roy, I.; Anchoori, R. K.; Fazli, S.; Maitra, A.; Beachy, P. A.; Khan, S. R. *Bioorg. Med. Chem.* **2008**, *16*, 2764–2768.
78. Sims-Mourtada, J.; Izzo, J. G.; Ajani, J.; Chao, K. S. *Oncogene* **2007**, *26* (38), 5674–5679.
79. Zhou, Y.; Yang, J.; Kopeček, J. *Biomaterials* **2012**, *33* (6), 1863–1872.

Downloaded by UNIV OF ROCHESTER on July 20, 2013 | http://pubs.acs.org
Publication Date (Web): July 8, 2013 | doi: 10.1021/bk-2013-1135.ch009


In Tailored Polymer Architectures for Pharmaceutical and Biomedical Applications; Scholz, C., et al.;
ACS Symposium Series; American Chemical Society: Washington, DC, 2013.

80. Zhou, Y.; Yang, J.; Kopeček, J. *Polymer Preprints*; Division of Polymer Chemistry, 11th International Symposium on Biorelated Polymers, 243th American Chemical Society Meeting, San Diego, CA, March 22−25, 2012.
81. Chen, J. K.; Taipale, J.; Cooper, M. K.; Beachy, P. A. *Genes Dev.* **2002**, *16* (21), 2743–2748.
82. Yang, J.; Luo, K.; Pan, H.; Kopečková, P.; Kopeček, J. *React. Funct. Polym.* **2011**, *71* (3), 294–302.
83. Schechter, I.; Berger, A. *Biochem. Biophys. Res. Commun.* **1967**, *27* (2), 157–162.
84. Sinha, S.; Chen, J. K. *Nat. Chem. Biol.* **2006**, *2* (1), 29–30.
85. Miki, J.; Furusato, B.; Li, H.; Gu, Y.; Takahashi, H.; Egawa, S.; Sesterhenn, I. A.; McLeod, D. G.; Srivastava, S.; Rhim, J. S. *Cancer Res.* **2007**, *67* (7), 3153–3161.
86. Gu, Y.; Li, H.; Miki, J.; Kim, K. H.; Furusato, B.; Sesterhenn, I. A.; Chu, W. S.; McLeod, D. G.; Srivastava, S.; Ewing, C. M.; Isaacs, W. B.; Rhim, J. S. *Exp. Cell Res.* **2006**, *312* (6), 831–843.
87. Singec, I.; Knoth, R.; Meyer, R. P.; Maciaczyk, J.; Volk, B.; Nikkhah, G.; Frotscher, M.; Snyder, E. Y. *Nat. Methods* **2006**, *10* (3), 801–806.
88. Liu, J.; Kopečková, P.; Pan, H.; Sima, M.; Bühler, P.; Wolf, P.; Elsässer-Beile, U.; Kopeček, J. *Macromol. Biosci.* **2012**, *12*, 412–422.

Downloaded by UNIV OF ROCHESTER on July 20, 2013 | http://pubs.acs.org
Publication Date (Web): July 8, 2013 | doi: 10.1021/bk-2013-1135.ch009

Downloaded by MICHIGAN STATE UNIV on July 17, 2013 | http://pubs.acs.org
Publication Date (Web): July 8, 2013 | doi: 10.1021/bk-2013-1135.ch010

## Chapter 10

# Enhanced Delivery of Polymer Therapeutics to Solid Tumors

**Adam J. Gormley,[1,2,4] Nate Larson,[2,3] and Hamidreza Ghandehari[*,1,2,3]**

**[1]Department of Bioengineering, University of Utah, Salt Lake City, Utah 84112**
**[2]Center for Nanomedicine, Nano Institute of Utah, and University of Utah, Salt Lake City, Utah 84112**
**[3]Department of Pharmaceutics and Pharmaceutical Chemistry, University of Utah, Salt Lake City, Utah, 84112**
**[4]Present address: Department of Materials, Imperial College London, London, SW7 2BP, United Kingdom**
**[*]E-mail: hamid.ghandehari@pharm.utah.edu. Ph: 801-587-1566. Fax: 801-581-6321. Address: 36 S. Wasatch Dr., Salt Lake City, Utah, 84112-5001.**

The conjugation of anticancer drugs to water-soluble polymers can improve their plasma solubility, biodistribution and tumor accumulation. Despite these advantages, poor overall delivery to the tumor microenvironment remains the greatest challenge towards achieving clinical translation. In this review, various strategies to improve their delivery to tumors are discussed. This includes passive and active targeting as well as pharmacologic and physical ways of augmenting delivery. A new technique using plasmonic photothermal therapy (PPTT) with heat shock targeting is introduced. By taking advantage of laser-initiated hyperthermia, heat shock targeted copolymers can be guided to achieve greater tumor accumulation, penetration, retention and anticancer activity. In the future, it will be interesting to see what additional techniques emerge to facilitate greater delivery of these conjugates.

© 2013 American Chemical Society
In Tailored Polymer Architectures for Pharmaceutical and Biomedical Applications; Scholz, C., et al.; ACS Symposium Series; American Chemical Society: Washington, DC, 2013.

# 1. Introduction

The concept of developing therapies which are targeted to specific cells while leaving the healthy ones intact is credited to Paul Ehrlich who postulated "we have to learn how to aim chemically" (*1*). Indeed, when the goal is to impose a pharmacologic or physical effect on diseased tissue, any collateral damage to healthy tissue can have devastating consequences. Ehrlich's concept of the magic bullet ultimately led to the development of today's chemotherapeutic strategies which have some pharmacologic bias towards cancerous cells, though uptake in non-intended cells still remains the greatest challenge.

With advances in polymer chemistry and antibody-based therapies in the 1970's, macromolecular based targeted therapies were born. In systems like those conceptualized by Helmut Ringsdorf (*2*), large carriers can be used to target sites of disease and deliver therapeutic payloads. Such targeted therapies evolved into a field now coined "polymer therapeutics", and represent a significant improvement in cancer therapies the goal of which is to limit adverse effects while maximizing efficacy (*3*). These targeted therapies are increasingly attracting widespread attention in oncology and are likely to provide substantial benefits in future cancer therapies.

Despite these indications for improved treatment performance, the number of available polymer therapeutics in the market remains limited. The reasons for this have to do with problems with the therapeutics' overall design as well as the biological barriers that prevent them from reaching the target. Of these limitations, possibly the most influential barrier to success is limited tumor delivery and penetration. A common method for displaying tumor accumulation data is by calculating the percent injected dose per gram of tissue (%ID/g). Using these units, a nanomedicine is considered to have high tumor localization when above 10 %ID/g. If one considers, however, that most tumors used in preclinical studies are on average 100 mg by weight, then the total dose delivered to the tumor is only 1.0 %ID. Translating this idealized scenario in mice bearing subcutaneous tumors to humans, where the average cost of treatment using an approved polymer therapeutic is about $30,000, not including hospital costs (*4*, *5*), then only about $300 worth of therapeutic is actually imposing any therapeutic effect. The remaining $29,700 is either urinated or accumulates in organs of the RES where toxicity occurs. This major imbalance coupled with severe adverse effects that patients have to endure highlight the need for improved methods of drug delivery.

Such limited tumor delivery is mostly a consequence of the many biological barriers that restrict cancer cell access. For a particular drug or protein within a polymer therapeutic to reach from the injection site to the subcellular target, it must successfully navigate these barriers (*6*). Upon injection, the therapeutic must become soluble in the blood plasma and be resistant to protein opsonization (*7*). If significant opsonization occurs and forms a protein corona, phagocytic detection and reticuloendothelial system (RES) clearance is probable. As most drug delivery systems require prolonged blood circulation to be efficacious, the therapeutic must then avoid both RES and renal clearance for an extended period of time (several

Downloaded by MICHIGAN STATE UNIV on July 17, 2013 | http://pubs.acs.org
Publication Date (Web): July 8, 2013 | doi: 10.1021/bk-2013-1135.ch010


In Tailored Polymer Architectures for Pharmaceutical and Biomedical Applications; Scholz, C., et al.;
ACS Symposium Series; American Chemical Society: Washington, DC, 2013.

hours to days). As the polymer therapeutic enters the tumor's vasculature, it must then permeate through the vascular endothelium and enter the tumor interstitial space. In order to have maximal effect, it must then be transported through the dense interstitial space and reach cells which are distant from the tumor's viable vasculature (*8*, *9*). As macromolecules are unable to diffuse across the cell's plasma membrane, they must then bind to the cell's surface and initiate endo- or phagocytic uptake. If bound via degradable linker, the drugs must then be cleaved from the polymeric carrier and be released. Finally, binding to the target protein, or transport through the nuclear envelope and subsequent binding to nucleic acids represents the last step before therapy can initiate. Given this daunting journey, it is perhaps not surprising that much less than 1% of the injected dose exerts its effect.

Given this grand challenge, many strategies are employed by drug delivery scientists to improve outcome. In the following sections, some of these strategies are reviewed in the context of improving the delivery of polymer therapeutics to solid tumors. Also, recent work (*10*–*13*) using plasmonic photothermal therapy (PPTT) as well as heat shock targeting to improve delivery will be reviewed. It is likely that as the field matures, new and interesting tools will continue to be developed to navigate around these delivery limitations.

Downloaded by MICHIGAN STATE UNIV on July 17, 2013 | http://pubs.acs.org
Publication Date (Web): July 8, 2013 | doi: 10.1021/bk-2013-1135.ch010

## 2. Tools for Improved Delivery to Solid Tumors

To increase the delivery of polymer therapeutics to solid tumors, one can either make modifications to the conjugate itself or to the tumor microenvironment. In the context of therapeutic design, there are several physicochemical parameters that can be modified to improve delivery. Primarily, these parameters focus on characteristics such as size, shape, charge and plasma solubility to reduce RES detection and prolong blood circulation. Indeed, prolonged blood circulation is positively correlated with favorable tumor accumulation and is thus of high importance when designing a new therapeutic (*14*). The present review, however, focuses on strategies to enhance delivery when considering the tumor microenvironment itself. Concepts such as passive and active targeting will be discussed, as well as methods to chemically or physically modify this environment to facilitate delivery. Such information is important as the poor tissue structure of tumors provides both barriers and opportunities to enhance the delivery of nanocarriers.

### 2.1. Passive Targeting and the EPR Effect

It has been known for a long time that the blood vessels which supply solid tumors are disorganized and have higher than average permeability to macromolecules (*15*, *16*). In the 1970's, this increased permeability was leveraged to screen for tumors by scintigraphy using gallium-67 which has known affinity for transferrin (*17*, *18*). In 1986, when Maeda and colleagues were studying the tumor delivery of SMANCS (SMA-neocarzinostatin), they observed that


In Tailored Polymer Architectures for Pharmaceutical and Biomedical Applications; Scholz, C., et al.;
ACS Symposium Series; American Chemical Society: Washington, DC, 2013.

this hyperpermeability in combination with poor lymphatic drainage caused the micelles to accumulate and be retained in tumors (*19*). Recognizing the contributions of hyperpermeability and poor drainage, they described their observation by coining the phrase 'Enhanced Permeability and Retention' (EPR) effect (*20*). Since this landmark paper (*19*), the EPR effect has been applied ubiquitously to describe the passive delivery of macromolecules and nanomedicines to solid tumors.

The translatability of EPR to a broad spectrum of polymer therapeutics remains a challenge, particularly considering that most studies are performed in rodents bearing fast growing, subcutaneous tumors. However, studies with these tumor models provide some insight. When one initially compares the vasculature of tumors versus healthy tissue, it is apparent that tumor vessels form with an abnormal and disorganized architecture (*21–23*). The spatial distribution of blood vessels lacks order and continuity which ultimately generates a heterogeneous distribution of poorly perfused tissue (*24*). The structure of individual blood vessels is also poorly formed and lacks smooth muscle. The endothelial cells have overlapping and branched morphologies with large intercellular and transcellular openings up to 4.7 μm in size (*25*). These large fenestrae then explain tumor blood vessel leakiness which allows macromolecules such as albumin to permeate.

The disorganized and tortuous nature of tumor vasculature coupled with macromolecular hyperpermeability and limited lymphatic drainage has a consequential impact on the tumor microenvironment (*26*). Poor plasma drainage and increased red blood cell accumulation causes a significant increase in the viscosity of the blood in tumors (*27*). This increased viscosity provides resistance and may be responsible for overall decreased blood flow in tumors (*28*). The higher concentration of albumin and other proteins in this tissue also causes hypertension which increases the tumor's interstitial pressure (*29*, *30*). This too limits the degree of convective transport of small and large molecules into the tumor interstitial space. Finally, high cell and extracellular matrix (ECM) density provides more resistance to convective and diffusive transport of macromolecules (*31*). Taken together, these transport barriers reduce the availability of oxygen and other essential nutrients in tumors thereby creating large regions which are hypoxic and necrotic (*32*).

In the context of delivering nanomedicines to solid tumors, these transport barriers become exaggerated due to their large size. The population of intercellular openings in the tumor's vasculature is highly heterogeneous in size, location and density. While some may exist as large as several microns in size, the majority are 1-2 μm (*25*). This size cutoff thereby excludes particles which are greater than roughly 1.5 μm from taking advantage of the EPR effect (*33*). Also, as much of the transport of molecules out of the tumor's vasculature and through the interstitial space depends on diffusion, the size of the particle will dictate how far it can travel. As described by the Stokes-Einstein equation, larger particles will have less diffusive transport than smaller particles and therefore may not access cancerous cells which are distant from the vasculature. Also, given that the density of the ECM in tumors is prohibitively high for effective diffusive transport over long distances (*34*), larger particles such as liposomes and inorganic colloids may lack overall effectiveness even though they are within the size range of EPR (*35*, *36*).


In Tailored Polymer Architectures for Pharmaceutical and Biomedical Applications; Scholz, C., et al.;
ACS Symposium Series; American Chemical Society: Washington, DC, 2013.

Downloaded by MICHIGAN STATE UNIV on July 17, 2013 | http://pubs.acs.org
Publication Date (Web): July 8, 2013 | doi: 10.1021/bk-2013-1135.ch010

Despite these barriers, the passive delivery of polymer therapeutics by EPR remains a viable approach. Many drug delivery systems from polymer therapeutics, to monoclonal antibodies, to AuNPs rely on EPR to selectively accumulate in cancerous tissue (*37*). And while issues such as human translatability and pervasive distribution throughout the whole tumor mass raise significant concerns over the effectiveness of this approach, it is partially responsible for the biologicals and nanomedicines available in the clinic.

### 2.2. Receptor-Mediated Active Targeting

Monoclonal antibody therapies have received significant attention in the last two decades and many are currently used in the clinic. When properly humanized and protected from the immune system, they are able to circulate for extended periods of time and bind with high specificity and affinity to their target receptors on cancer cells (*38*). In this way, antibodies can directly initiate cancer cell apoptosis upon binding, tag cancer cells for immune detection and elimination, or be used as carriers for drugs and radionuclides (*39*). Such systems therefore represent a series of emerging nanomedicine based technologies which utilize receptor-mediated active targeting to deliver therapeutics with high cellular specificity.

Inspired by Paul Ehrlich's concept of targeted therapies, many drug delivery scientists aim to improve the delivery of their 'magic bullets' by conjugating a wide variety of biomolecules which have known specificity to cancer cell receptors. Examples of targeting approaches include antibodies against epidermal growth factor receptor (EGFR) such as anti-HER2 (*40–42*), folate receptor targeting with folic acid (*43–45*), transferrin receptor targeting (*46–49*), and angiogenesis targeting with RGD (*50–54*). Each of these examples has proven selectivity towards cancerous tissues due to overexpression of the targeted receptors.

Many liposomal based systems have been functionalized with antibody or antibody fragments for this purpose (*41*, *55–57*). In some cases, this approach has resulted in increased delivery of the targeted liposomes relative to control liposomes (*58*). In most examples, however, equal or less tumor accumulation is achieved (*41*, *59*). Such results do not necessarily preclude these systems from being more valuable than the untargeted systems. Unless the targeting ligand is used to target the tumor's vasculature, passive delivery by EPR is the necessary first and often delivery-limiting step (*60*). As the nanocarriers diffuse through the tumor interstitium, receptor-mediated targeting may facilitate cellular binding and uptake and therefore drug delivery (*61*).

Due to the known advantages of this approach, clinical translation of an actively targeted HPMA copolymer-doxorubicin conjugate was attempted (*62*). Galactosamine, a derivative of galactose, has known affinity for asialoglycoprotein receptors which are overly expressed in liver and hepatocellular tissue (*63*). When linked to an HPMA copolymer containing doxorubicin, liver targeting was achieved in both rats and mice (*64–66*). These results led to pursuing this conjugate in a Phase I clinical trial (*62*, *67*). Results from these studies showed that targeting to the liver was high (15-20 %ID), but that targeting to hepatic


In Tailored Polymer Architectures for Pharmaceutical and Biomedical Applications; Scholz, C., et al.;
ACS Symposium Series; American Chemical Society: Washington, DC, 2013.

Downloaded by MICHIGAN STATE UNIV on July 17, 2013 | http://pubs.acs.org
Publication Date (Web): July 8, 2013 | doi: 10.1021/bk-2013-1135.ch010

tumors was substantially lower (3.3 %ID). Additionally, relative to its untargeted PK1, targeting to the liver significantly lowered the MTD of this conjugate. Such accumulation in the healthy liver tissue is thus limiting and highlights the need for active targeting improvements.

Based on the number of reports which provide conflicting support for active targeting, there are clearly a large number of challenges that may reduce the viability of this approach. From a formulation or colloidal dispersion standpoint, functionalization with antibodies, antibody fragments, peptides, etc. may reduce the overall stability of the nanocarriers in water or plasma. Once in the blood, these ligands which are designed to be biorecognizable may then facilitate RES clearance and dramatically reduce blood circulation time. As was the case for the HPMA copolymer-galactosamine conjugates, targeting to healthy cells which also express the targeted receptor may expose these cells to the drug and result in unwanted toxicity. Other examples of variables which may impact active targeting viability include ligand-receptor binding affinity, receptor expression heterogeneity within the same tumor or across patient populations and receptor saturation. Each of these barriers prevents the majority of active targeted nanomedicines from having real clinical benefit, and a better understanding of these events is ultimately required.

Downloaded by MICHIGAN STATE UNIV on July 17, 2013 | http://pubs.acs.org
Publication Date (Web): July 8, 2013 | doi: 10.1021/bk-2013-1135.ch010

### 2.3. Pharmacologic Enhancement of Delivery

There are several tumor microenvironment characteristics that resist diffusive and convective transport of drugs and polymer therapeutics. These characteristics are: 1) vascular heterogeneity, 2) high blood viscosity, 3) sluggish blood flow, 4) elevated interstitial pressure, 5) poor lymphatic drainage, and 6) dense interstitial matrix due to abnormally high cellular and ECM densities (*68*). Though most often discussed in the context of improving delivery, neither EPR, a natural phenomenon, nor receptor-mediated targeting act to alleviate any of these major delivery barriers. This may be due to the fact that these barriers are a direct consequence of tumor physiology which cannot be easily resolved by changing the design of the therapeutic. Therefore, efforts which aim to improve delivery by decreasing the contribution of each of these barriers have focused on pharmacologic based interventions.

One method which Maeda, Jain and others have used to increase tumor blood flow and transmural pressure (ratio of arterial pressure to tumor interstitial pressure) between the vasculature and tumor interstitial space is to elevate overall blood pressure (*69–73*). It was previously observed that raising the mean arterial blood pressure to 150 mmHg using angiotensin II results in a marked increase in tumor blood flow (*74*). This effect was found to be selective to cancerous tissue. The mechanism behind this phenomenon is most likely related to the inability of tumor microvessels to respond to elevated blood pressure by autoregulatory contraction as well as increased transmural pressure which drives convective transport (*69*). To show then that this technique can be used to improve the delivery of macromolecules, Maeda and colleagues artificially raised the blood pressure in mice using angiotensin II followed by administration of SMANCS (*70*). Treatment in this way resulted in a 1.2-1.8-fold increase in overall tumor


In Tailored Polymer Architectures for Pharmaceutical and Biomedical Applications; Scholz, C., et al.;
ACS Symposium Series; American Chemical Society: Washington, DC, 2013.

delivery while less accumulation occurred in the bone marrow and small intestine. Translating this concept into a clinical setting, patients with a variety of carcinomas were co-administered angiotensin II and SMANCS and evaluated for tumor delivery and overall outcome (*71*). Similar to their previous findings, hypertension was able to improve the delivery of SMANCS as well as overall response to the drug. This pharmacologic based technique is thus an interesting and clinically relevant approach for improving the delivery of nanomedicines.

Similar approaches using other vasoactive drugs to modulate tumor blood flow and permeability have been tried (*75*). Maeda and others have leveraged nitric oxide (NO) as a tool to vasodialate surrounding blood vessels to improve blood flow and therefore drug delivery (*69*, *76*). Indeed, topical application of nitroglycerin on the tumor resulted in 2 to 3-fold enhancement of polymer-drug conjugate delivery (*76*). Alternatively, when inhibitors of NO were tested, significant decreases in tumor blood flow occurred (*77*). Interestingly, when vasoconstrictor drugs other than angiotensin II such as phenylephrine were tested for similar purposes, no changes or slight decreases in tumor blood flow were observed (*78*).

Vascular disrupting agents (VDAs), drugs or proteins which act on the already established tumor vasculature, have also been tested. For example, tumor necrosis factor-α (TNF-α), a major proinflammatory cytokine, acts strongly on vascular endothelial cells and increases vascular permeability by formation of large intercellular gaps (*79*). Administration of TNF-α is capable of enhancing EPR and the delivery of macromolecules (*80*). Because systemic administration of TNF-α produces significant toxicity, delivery by adsorption to AuNPs is being evaluated in a Phase II clinical trial (*81*). Using this delivery scheme, AuNP-TNF-α conjugates also improved macromolecular permeability (*82*).

Because of its known effect on macrophages to stimulate TNF-α production, 5,6-dimethylxanthenone-4-acetic acid (DMXAA) has also been tested for its capacity to increase tumor vascular permeability. Administration of DMXAA in mice with or without TNF receptor or gene knockdown was found to enhance EPR (*83*). Because enhanced permeability occurred in mice with or without TNF receptor or gene knockdown, these authors suggest that DMXAA can improve vascular permeability in a TNF-α independent manner. Though VDAs have shown to increase vascular permeability, they are also well known to reduce tumor blood flow (*84*), and an appropriate balance of dose may therefore be required to leverage the full potential of these drugs to improve macromolecular delivery.

Unlike VDAs whose target is already established vasculature, antiangiogenic drugs aim to prevent the formation of new tumor blood vessels. In the 1970's, Judah Folkman postulated that tumor growth is dependent on continual angiogenesis and that inhibition of this process might stunt its growth (*85*). Since this landmark paper, a large number of groups have investigated the utility of this line of therapy, and many antiangiogenic therapies are used clinically. Rakesh Jain has described an alternative use of antiangiogenic therapy (*22*). The inhibition of angiogenic stimulators such as vascular angiogenic growth factor (VEGF) initiates vascular remodeling (*86*). This remodeling process effectively prunes those vessels which are characteristically leaky and immature, and thus limit blood flow. The result is a "normalization" of the tumor's vasculature to

Downloaded by MICHIGAN STATE UNIV on July 17, 2013 | http://pubs.acs.org
Publication Date (Web): July 8, 2013 | doi: 10.1021/bk-2013-1135.ch010


In Tailored Polymer Architectures for Pharmaceutical and Biomedical Applications; Scholz, C., et al.;
ACS Symposium Series; American Chemical Society: Washington, DC, 2013.

a state which has improved blood flow and therefore tissue perfusion (*21*). The impact of this vessel normalization was observed when antiangiogenic therapy was combined with radiation therapy. Increased vascular function and therefore tumor oxygenation due to antiangiogenic normalization has been shown to synergistically improve radiation therapy (*87*). When anti-VEGF antibodies were used to decrease colon adenocarcinoma microvessel density, increased tumor perfusion and chemotherapeutic delivery was achieved (*88*). While increased blood flow and decreased intratumoral pressure occur after this process, it is likely that decreased vessel leakiness and therefore EPR will also result. To study this, Jain et. al. evaluated the passive delivery of differently sized nanoparticles after vascular normalization. Indeed, antiangiogenic treatment did reduce vascular pore size suggesting that smaller nanocarriers are required for efficient delivery after vascular normalization (*89*).

Each of the previously described methods for enhancing delivery pharmacologically has used drugs which act on the tumor's vasculature to improve blood flow and/or vascular permeability. This is because drug delivery is primarily limited by degree of vascularization. However, improving local blood flow and permeability may not necessarily improve overall outcome because the dense tumor interstitium limits the diffusivity of small and large molecules (*9*). High cellular and ECM density coupled with high interstitial fluid pressure (IFP) resists transport in a size dependent manner. One method to improve overall delivery is to reduce interstitial density and IFP. For example, treatment of tumors with chemotherapy initiates cell death and therefore reduces cellular density (*90*). This decompression allows for greater transport of drug after repeated administration. Direct injection of ECM enzymes such as collagenase produces a similar result. Digestion of ECM components increases the diffusion of macromolecules in a size dependent manner (*91*). For this reason, many now are developing multistage nanoparticle systems which are initially large for prolonged blood circulation, but then break apart into smaller particles or release free drug once in the tumor space (*92–94*).

Downloaded by MICHIGAN STATE UNIV on July 17, 2013 | http://pubs.acs.org
Publication Date (Web): July 8, 2013 | doi: 10.1021/bk-2013-1135.ch010

### 2.4. Physical Enhancement of Delivery

Tumor blood vessels are also subject to externally applied forces to increase blood flow and permeability. If the location of the diseased tissue is known, the physician may be able to treat the region with either ultrasound or heat for this purpose. Each of these may be useful tools for enabling the clinician to play a more active role in choosing the location of enhanced drug delivery.

Ultrasound has been used primarily for medical imaging due in part to its low cost and safety. The absorption of ultrasound by various tissues can also be used with therapeutic intentions (*95*). High-intensity focused ultrasound (HIFU) can ablate tissue through heating and is used in some cases in the treatment of prostate cancer (*96*). Another interesting application of ultrasound in the context of the current review topic is in its ability to improve the delivery of macromolecules across biological barriers (*97*). Depending on the frequency and intensity of the ultrasound, acoustic cavitations can occur in tissue during ultrasound treatment. These cavitations produce mechanical deformations and


In Tailored Polymer Architectures for Pharmaceutical and Biomedical Applications; Scholz, C., et al.;
ACS Symposium Series; American Chemical Society: Washington, DC, 2013.

cell-cell junction disruption which causes normally semi-permeable barriers to become hyperpermeable (*98*). For example, Mitragotri and Langer have used ultrasound to permeabilize skin and enable transdermal adsorption of proteins (*99*). The transport of drugs, macromolecules and nucleic acids through the plasma membrane can also be improved using ultrasound through sonoporation (*100*, *101*). In regards to transvascular transport, the effect is similar. Ultrasound treatment of the blood-brain barrier, an endothelial lining with characteristically tight cell-cell junctions, temporarily disrupts this tissue and allows for drug delivery to the brain (*102*, *103*). In tumors, such treatment can also improve transvascular delivery (*104*). Increased vascular permeability from ultrasound treatment improves tumor accumulation of drug carrying macromolecules (*105*). This effect is, however, significantly less advantageous in tumor tissue relative to that observed with the BBB as tumor tissue is already permeable to macromolecules (*106*).

There are many advantages of combining hyperthermia with chemotherapy. At the cellular level, hyperthermia improves the intracellular delivery of small molecular weight drugs which can provide synergistic treatment (*107*). When these drugs are incorporated in polymer therapeutics, the same may also be true but by a different mechanism. Recent findings, for example, have shown that hyperthermia can increase the rate of both endo- and phagocytosis which may then potentiate macromolecular uptake and intracellular delivery (*108*, *109*). Another level of synergism is obtained when the temperature does not significantly exceed 43°C where severe vascular damage occurs. At such elevated temperatures (41-43°C), tumor blood flow can increase roughly two-fold (*110*). This change in blood flow then increases the overall availability of macromolecules to extravasate. Unfortunately, the extent of this increased blood flow is not to the same degree as healthy tissue due to the lack of a smooth muscle layer and the overall tortuous nature of intravascular circulation (*111*, *112*). In fact, this observed increase may be due to changes in surrounding blood vessels which supply the tumor and therefore force more blood inflow.

A consequence of this forced blood perfusion is increased vascular pressure. Similar to the tumor microvascular changes which occur with elevated blood pressure, the weak endothelial layer is not able to resist this pressure and heat adequately, and increased vascular permeability results (*113*, *114*). Such increased permeability is believed to be a result of cytoskeletal disaggregation in endothelial cells leading to further expansion of the intercellular junctions that already surround them (*115–118*). This increase in vascular permeability and therefore EPR has been leveraged to improve nanomedicine delivery. Initial studies in this area focused on the extravasation of liposomes when combined with hyperthermia (*119–122*). The application of heat facilitated the extravasation of PEGylated liposomes in a time and temperature dependent manner. In most cases, a low thermal dose (temperature < 42°C, time < 30 min) does not result in a substantial increase in liposomal delivery (*120*). As the thermal dose is increased, so does the delivery of liposomes where a 47-fold increase has been observed using intravital microscopy (*122*). Of particular interest in these studies was the use of temperature sensitive liposomes which could release their drug contents with increased temperature. A similar study using hyperthermia to enhance the


In Tailored Polymer Architectures for Pharmaceutical and Biomedical Applications; Scholz, C., et al.;
ACS Symposium Series; American Chemical Society: Washington, DC, 2013.

Downloaded by MICHIGAN STATE UNIV on July 17, 2013 | http://pubs.acs.org
Publication Date (Web): July 8, 2013 | doi: 10.1021/bk-2013-1135.ch010

delivery of HPMA copolymers was also completed, however in this case, no thermal enhancement of delivery was observed (*123*).

Dewhirst and colleagues have evaluated the increased vascular permeability and its impact on nanoparticle delivery due to local hyperthermia (*124–127*). In one study, the thermal dose was varied and the extravasation of liposomes was imaged using intravital microscopy (*126*). They observed that at temperatures below 40°C, no increased extravasation occurred. As the tumors were treated with temperatures above 40°C, liposomes began to extravasate in a temperature and time dependent manner. This increased vascular permeability continued up to six hours after heat treatment, after which time the tumor permeability recovered to normal levels (*126*). They explain this to be because of endothelial cell repair after this time. Heating of tumors above 43°C resulted in vascular hemorrhaging. When these effects were compared as a function of nanoparticle size, major differences between small (~7 nm) and large (100-400 nm) nanoparticles were observed (*124*). The smaller systems, albumin in this case, were relatively unaffected by treatment with hyperthermia. The larger nanoparticles, liposomes between 100 and 400 nm, on the other hand had low tumor accumulation without hyperthermia and significantly enhanced delivery with hyperthermia. This too was size dependent with the 100 nm liposomes having the greatest tumor delivery with hyperthermia, though still just as good as albumin without heat treatment. The explanation provided in this paper for this size dependency relates again to the increased pore size with heat treatment. While the smaller particles can freely extravasate due to the relatively large size of the intercellular openings in the endothelial layer, larger particles may be more restricted due to their similar size. When the tissue is heated and these openings are enlarged, this resistance may play less of a dominant role allowing them to permeate to a larger extent. When tested in a feline tumor model, similar enhancement of delivery was observed (*125*). Unfortunately, these nanoparticle systems continue to suffer with heterogeneous tissue distribution and poor interstitial penetration after thermal therapy (*128*).

Downloaded by MICHIGAN STATE UNIV on July 17, 2013 | http://pubs.acs.org
Publication Date (Web): July 8, 2013 | doi: 10.1021/bk-2013-1135.ch010

### 2.5. Need for Continued Investigation of New Delivery Enhancement Methods

Each of the above listed techniques will not likely be sufficient as a standalone means of enhancing the delivery of polymer therapeutics. Passive delivery by EPR remains the most attractive means of enhancing delivery, and many groups tailor the physicochemical properties of these conjugates to maximize the EPR effect. Unfortunately, as seen with the large number of clinical trials which do not show significant benefits, this alone will not likely translate these technologies into viable therapeutics with real benefit for patients. Clearly more efforts to enhance site specific delivery are required. In this context, delivery enhancement mechanisms which are more tumor selective are preferred. Hyperthermia, for example, has a degree of selectivity towards cancerous tissue; however the means of delivering the appropriate thermal dose without harming the surrounding healthy tissue remains a challenge. Therefore, an alternative means of delivering heat with greater tumor selectivity is preferred to enhance the accumulation of polymer therapeutics in solid tumors.


In Tailored Polymer Architectures for Pharmaceutical and Biomedical Applications; Scholz, C., et al.;
ACS Symposium Series; American Chemical Society: Washington, DC, 2013.

# 3. Guided Delivery with Plasmonic Photothermal Therapy (PPTT)

A recent method of selectively delivering heat to tumor tissue takes advantage of the plasmonic properties of colloidal gold. Of special interest in this regard is the unique capacity of these colloids to scatter and absorb light. Under conditions of particle SPR, strong light absorption results in particle heating. When located within a tumor mass, direct tissue heating can occur with laser light excitation. Termed PPTT, this heating process can be used as a means to induce tumor hyperthermia with therapeutic intentions (*129–131*).

In the following sections, AuNPs will be introduced as well as a description of their properties. Their use as antennas for PPTT will be described as well as the potential of using this technology to enhance the delivery of heat shock targeted polymer therapeutics to prostate tumors.

Downloaded by MICHIGAN STATE UNIV on July 17, 2013 | http://pubs.acs.org
Publication Date (Web): July 8, 2013 | doi: 10.1021/bk-2013-1135.ch010

## 3.1. Plasmonic Photothermal Therapy (PPTT)

The concept of PPTT was originally described by West and colleagues using gold nanoshells (*132*). In this landmark paper, they developed NIR absorbing PEGylated gold nanoshells which were delivered to breast carcinoma xenografts and heated with a NIR laser. Laser radiation (4 W/cm$^2$) of the tumors resulted in significant tumor heating ($\Delta T = 37.4°C$) and substantial tissue damage. When mice were treated with the same therapy and the tumors were allowed to grow, photothermal treatment resulted in cure of all tumors (*133*). Since these initial reports, a large number of papers have described use of this technique to thermally ablate tumors both *in vitro* and *in vivo* (*40*, *131*, *134–138*). In these studies, NIR absorbing GNRs or gold nanoshells were used to generate high temperatures to damage vasculature and through direct cell killing.

The majority of studies applying PPTT for tumor therapy have been done with tissue ablative intentions. Tumor heating above 50°C, well above the temperature required to ablate its vasculature, is not difficult to achieve using low-powered laser diodes and therefore cure of subcutaneous tumor models is widely reported (*132*, *133*, *136*, *138*). Of interest, however, is the possibility of using the precise control over heating to modulate the tumor microenvironment to facilitate the potency of other therapeutics. As mentioned earlier, several labs have used hyperthermia to improve the delivery of liposomes (*119*, *124–126*, *139*). The methods used however offer limited tissue control of heating in a well-defined and selective manner. Heating with a water bath provides a source of heat exterior to the skin at a predefined temperature, though direct control of temperature within the tumor core cannot be easily manipulated. Also, this method is not a clinically viable approach to heat most tumors. Treatment with high-energy radiofrequency probes can injure the tissue upon insertion of the probe and produces regions of high heat or hot spots immediately adjacent to the probe's surface and is not selective towards the cancerous tissue (*140*). For these reasons, PPTT may offer an advantage due to its selectivity towards cancerous tissue, depth of heat generation in tumors less than a few centimeter and precise control of heat delivery by modulating laser power output. Additionally, because


In Tailored Polymer Architectures for Pharmaceutical and Biomedical Applications; Scholz, C., et al.;
ACS Symposium Series; American Chemical Society: Washington, DC, 2013.

the AuNPs do not permeate far from the tumor's leaky vasculature, providing the sources of heat directly near blood vessels may offer better control of blood flow and vascular permeability.

There are several major disadvantages of PPTT that are worth discussing. First, intravenously administered AuNPs over 10 nm ultimately distribute mainly to the liver and spleen. This highlights a significant concern over their safety as they are non-degradable and not readily excreted. Second, the limited penetration depth of NIR light (< 2 cm) limits PPTT to tumors which are small in size and easily accessible with a fiber optic. Similarly, though the AuNPs are typically injected intravenously, PPTT is a localized therapy and may not be valuable to treat distant metastases. Finally, heterogeneous nanoparticle distribution in the tumor and limited access of tumor margins with the laser light increases the possibility of nonablative rims existing after therapy which may ultimately recur. Each of these disadvantages represents significant barriers to success which will likely limit this technology from existing as a standalone form of therapy.

Downloaded by MICHIGAN STATE UNIV on July 17, 2013 | http://pubs.acs.org
Publication Date (Web): July 8, 2013 | doi: 10.1021/bk-2013-1135.ch010

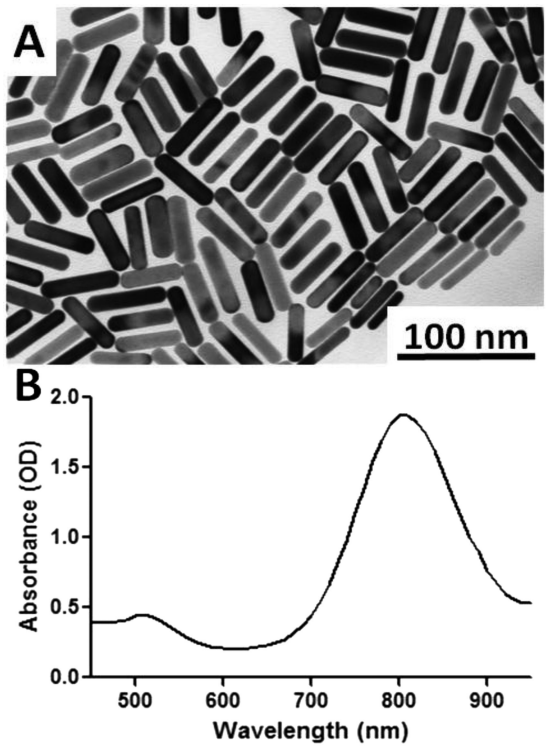


*Figure 1.* ***Characterization of GNRs****. (A) Transmission electron micrograph of GNRs; and (B) light absorption profile of GNRs with SPR peak at 800 nm. (Reproduced with permission from ref. (10). Copyright 2011 Elsevier.)*

### 3.2. Enhancement of Macromolecular Delivery by PPTT

While most studies have used PPTT to directly induce tissue damage by treating with high heat, a few have maintained lower temperatures and shown that this can result in greater blood perfusion and nanoparticle delivery (*141–144*). However, it is unclear if such enhanced delivery can occur for polymer therapeutics which are considerably smaller in size and are thus less susceptible to changes in vascular permeability due to heating (*123*, *124*). Therefore, to begin testing if such treatment could enhance the delivery of these therapeutics, a standard tumor permeability model, used extensively to characterize the EPR effect for polymer therapeutics, was adopted (*19*).

Downloaded by MICHIGAN STATE UNIV on July 17, 2013 | http://pubs.acs.org
Publication Date (Web): July 8, 2013 | doi: 10.1021/bk-2013-1135.ch010

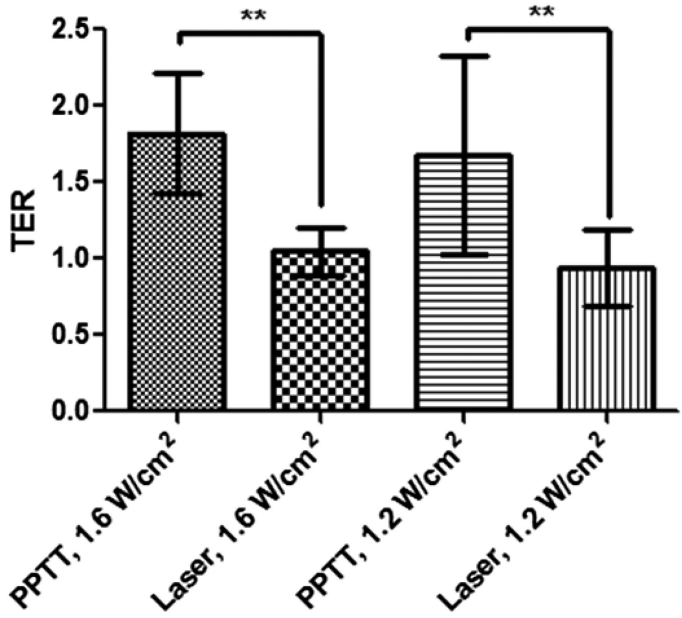


*Figure 2.* ***Evans blue dye (EBD) delivery thermal enhancement ratio (TER).*** ***Indicates a statistically significant difference ($p<0.01$) by one-way analysis of variance (ANOVA). Error bars represented as ± standard deviation. (Reproduced with permission from ref. (10). Copyright 2011 Elsevier.)*

Mice bearing sarcoma tumors (S180 tumor cells) were administered PEGylated GNRs with SPR peak at 800 nm (Figure 1) and allowed to rest for 24 hours to enable the nanoparticles to passively accumulate via EPR (*10*). In another study, this was found to result in 1.22% of the injected dose to be delivered to tumors (*51*). Evans blue dye (EBD) was then administered followed immediately by laser radiation of the animal's tumor to induce both moderate

(43°C) and severe (46°C) hyperthermia for 10 minutes. EBD was used in this case because it complexes with albumin and thus serves as a colorimetric tracer for this protein. After the animals were allowed to rest for 5 hours upon laser treatment, they were sacrificed and the tumor's EBD content was quantified.

Results from this initial study provided evidence that PPTT was capable of enhancing the delivery of macromolecules similar in size to most polymer therapeutics. Treatment of tumors with PPTT enhanced the delivery of albumin to these tumors by roughly 1.7-fold (Figure 2) (*10*). This enhancement was statistically independent of laser power and thus temperature, though the higher laser power (46°C temperature inside tumor) did result in some bruising and vascular damage. When the same laser power was tested in the absence of GNRs, no thermal enhancement of delivery was observed. This study confirmed that PPTT is a useful tool to improve the delivery of macromolecules such as proteins or polymer therapeutics (*10*).

Downloaded by MICHIGAN STATE UNIV on July 17, 2013 | http://pubs.acs.org
Publication Date (Web): July 8, 2013 | doi: 10.1021/bk-2013-1135.ch010

### 3.3. Heat Shock Targeting to Cancer Cells Treated with Hyperthermia

Once it was confirmed that PPTT could be used to facilitate the delivery of macromolecules, we sought to design a polymer therapeutic that would best complement this delivery mechanism. It was discussed in Section 2.2 that incorporation of targeting moieties that bind to receptors which have higher than normal expression in tumors can further improve delivery. However, receptor expression heterogeneity within the same tumor or across patient populations may reduce the viability of these approaches. In an effort to avoid this fundamental limitation and to take full advantage of tissue's response to heat induced stress, a unique targeting approach to extracellular heat shock proteins (HSP) was developed (*12*). It was hypothesized that specific targeting to HSPs in cells sensitized for targeting due to hyperthermic conditions would facilitate binding and uptake and therefore anticancer activity in this tissue.

The targeting ligand-receptor combination used for this particular application was the WIFPWIQL peptide which has known affinity for the glucose-regulated protein-78 (GRP78) receptor, a member of the HSP70 family of proteins (*145*). This combination is unique because while most HSPs are found only within the cytosol, this particular HSP has extracellular expression. To confirm that this peptide could target polymers to prostate cancer cells, it was conjugated to HPMA copolymers containing the anticancer drug aminohexylgeldanamycin (AHGDM) (*146*). For these conjugates, binding and anticancer activity confirmed targeting to prostate cancer cells due to their native expression of this receptor without sensitization with hyperthermia. This study showed that this targeting approach was viable even without hyperthermic treatment (*146*).

Next, the notion that hyperthermia could sensitize cells for heat shock targeting with this polymer-drug conjugate was tested (*12*). First, GRP78 receptor expression was measured as a function of time following treatment with heat shock (43°C, 30 min). Indeed, treatment in this way induced this receptor's expression 4-fold with peak expression occurring 8-12 hours post-heat shock (Figure 3A). Fluorescently labeled HPMA copolymers with and without the targeting peptide were then introduced to cells with and without prior treatment


In Tailored Polymer Architectures for Pharmaceutical and Biomedical Applications; Scholz, C., et al.;
ACS Symposium Series; American Chemical Society: Washington, DC, 2013.

with heat shock to evaluate binding and uptake. Confocal microscopy (Figure 3B) and flow cytometry (data not shown) showed that prior treatment of cells with hyperthermia allowed more of the targeted HPMA copolymers to be uptaken due to receptor induction (*12*). As expected based on results from the previous study (*146*), targeting alone without hyperthermic sensitization also resulted in some increased uptake, though not to the same extent.

### 3.4. PPTT Guided Delivery of Heat-Shock Targeted HPMA Copolymers

Following validation of the heat shock targeting approach *in vitro*, next we sought to use PPTT to guide the delivery of heat shock targeted HPMA copolymers to prostate tumors. In this study, PPTT is used to facilitate their delivery into the tumor interstitium from the vasculature, and heat shock targeting is used to retain these polymers within the tumor by binding to GRP78 and triggering intracellular delivery.

To test this, it was first necessary to confirm GRP78 tumor expression following treatment with PPTT. Mice bearing two prostate tumors which were previously administered PEGylated GNRs were laser radiated for 10 minutes such that the tumor temperature was raised to 43°C (Figure 4A) (*12*). In this experiment, only the right tumor was laser radiated while the left served as an untreated, internal control. Subsequent expression of GRP78, eight hours after treatment was then evaluated by immunohistochemistry (IHC). Indeed, heat shock treatment of the right tumors by laser radiation resulted in increased HSP expression compared to the untreated tumors (Figure 4B). These findings confirmed targeting sensitization using PPTT (*12*).

Next, the prostate tumor delivery of radiolabeled HPMA copolymers with and without heat shock targeting was evaluated following PPTT (*12*). Mice bearing two prostate tumors with GNRs were administered the radiolabeled conjugates immediately before 10 minutes of PPTT treatment of the right tumor at 43°C. Each animal was then sacrificed at specified time points and the radioactivity in each tumor was evaluated to quantify copolymer delivery. These studies show that PPTT resulted in a burst accumulation of all conjugates for up to four hours (Figure 4C). However, while the untargeted conjugates diffused back out of the tumor after four hours, the heat shock targeted copolymers were retained for an extended period of time. This increased retention is likely due to heat shock targeting while the receptor becomes increasingly available after PPTT. This prolonged retention begins to diminish after 12 hours, however, which is likely due to decreased receptor expression as the cells return to homeostasis. When the area under the tumor concentration vs. time curve was calculated for each experimental group, tumors which were treated with both PPTT and heat shock targeted conjugates had a four-fold increase in copolymer exposure (Figure 4D) (*12*).

The above results highlight the potential to use PPTT as a tool to guide delivery and use heat shock targeting to facilitate tumor retention and intracellular delivery. This method of delivery takes advantage of both passive and active targeting such that site specific delivery is optimized.


In Tailored Polymer Architectures for Pharmaceutical and Biomedical Applications; Scholz, C., et al.;
ACS Symposium Series; American Chemical Society: Washington, DC, 2013.

Downloaded by MICHIGAN STATE UNIV on July 17, 2013 | http://pubs.acs.org
Publication Date (Web): July 8, 2013 | doi: 10.1021/bk-2013-1135.ch010

Downloaded by MICHIGAN STATE UNIV on July 17, 2013 | http://pubs.acs.org
Publication Date (Web): July 8, 2013 | doi: 10.1021/bk-2013-1135.ch010



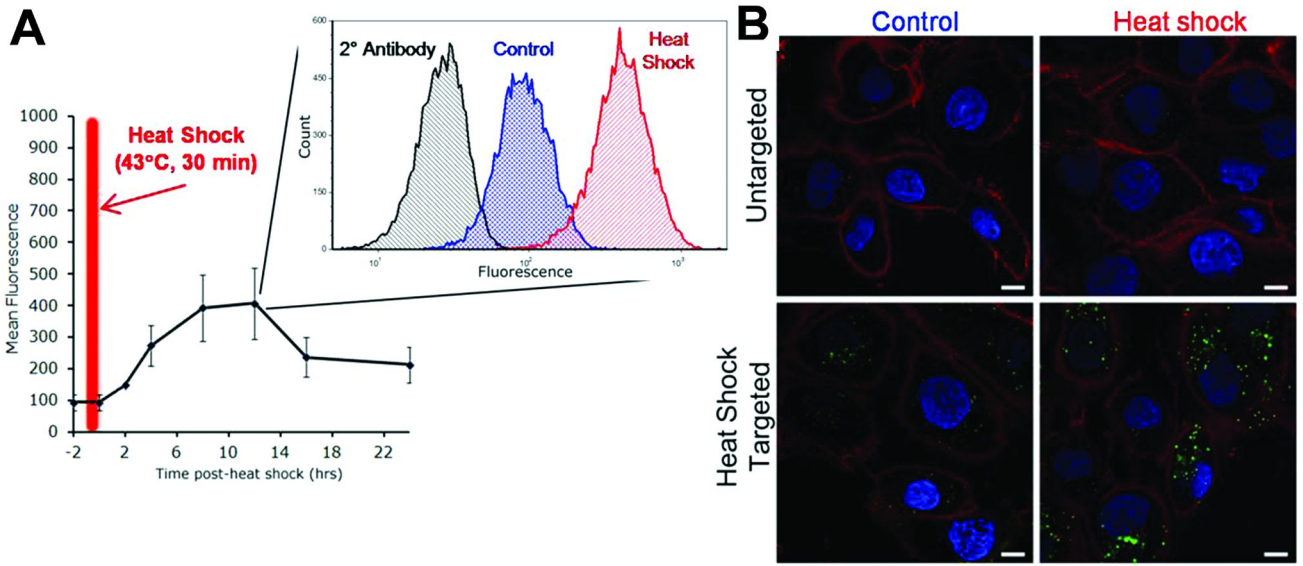


*Figure 3.* ***In vitro investigation of heat shock targeting.*** *(A) After induction of heat shock, the cell surface expression of the heat shock protein GRP78 in prostate cancer cells is quantified with peak expression occurring at 12 h. (B) Cellular binding and uptake of fluorescently labeled (green) HPMA copolymers in cells. Scale bar, 10 μm. Prior treatment with heat shock results in significantly increased uptake of heat shock targeted conjugates. (Reproduced with permission from ref. (12). Copyright 2012 American Chemical Society.)*

Downloaded by MICHIGAN STATE UNIV on July 17, 2013 | http://pubs.acs.org
Publication Date (Web): July 8, 2013 | doi: 10.1021/bk-2013-1135.ch010



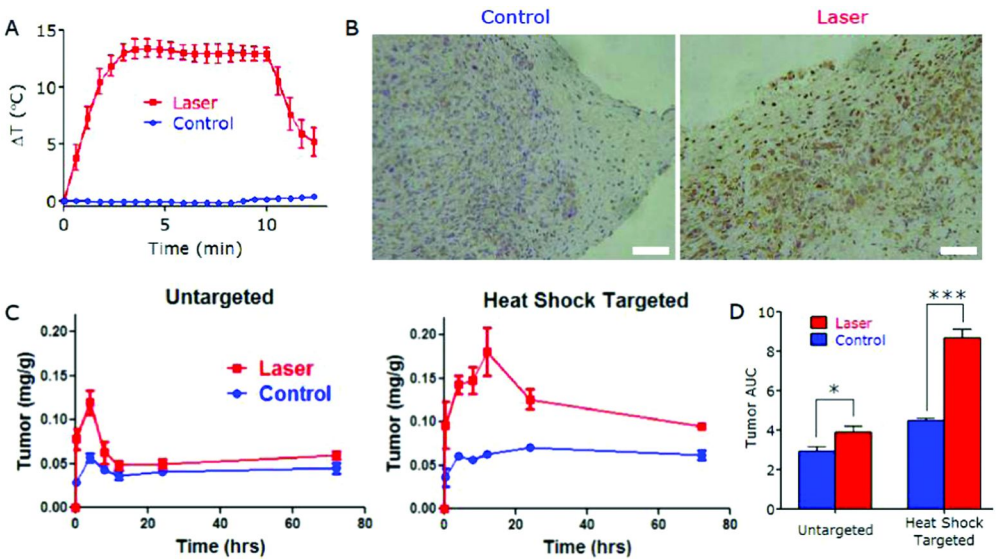


*Figure 4.* ***PPTT guided delivery of polymeric conjugates in mice.*** *(A) Changes in intratumoral temperatures during laser radiation (10 min) of left (control) and right (laser) tumors. (B) Cell expression of heat shock protein GRP78 (red color) in prostate tumors with or without laser treatment. Scale bar, 50 μm. Tumors which have been laser radiated have higher expression of GRP78. (C) Tumor accumulation of radiolabeled polymers (untargeted and heat shock targeted) with or without laser treatment. Laser radiation results in a burst accumulation (0-4 hours), which is only maintained (>24 hours) for the heat shock targeted polymers due to increased GRP78 expression. (D) Total area under the tumor concentration vs. time curve (AUC) indicates a four-fold increase in exposure to polymers. * and ***Indicates a statistically significant difference ($p<0.05$ and $p<0.001$ respectively) by one-way ANOVA. Error bars represented as ± standard deviation (A,D) and standard error of mean (C). (Reproduced with permission from ref. (12). Copyright 2012 American Chemical Society.)*

### 3.5. Intratumoral Distribution after Delivery with PPTT

While it has been shown that PPTT is capable of enhancing the accumulation of polymer therapeutics to tumors, this alone may not be sufficient to improve overall treatment outcome. As discussed earlier, this is because the dense interstitial matrix acts as a major barrier to transport and therefore delivery to areas which are distant from the viable vasculature. For this reason, delivery strategies which also increase tumor mass penetration are equally important (*26*).

It was hypothesized that treatment with PPTT would also increase the interstitial transport of polymer therapeutics due to favorable transport phenomena associated with tissue heating. To test this hypothesis, untargeted HPMA copolymers were labeled with gadolinium and their intratumoral distribution was visualized by magnetic resonance imaging (MRI) after treatment with PPTT (*11*). Mice were administered HPMA copolymer-Gd conjugates immediately before PPTT treatment of the right tumor. Subsequent $T_1$ flash and inversion recovery imaging of copolymer delivery by MRI was then acquired and analyzed. Results indicate that while the left (internal control) tumors did receive some copolymer delivery after two hours, the right (PPTT treated) tumors had significantly enhanced delivery (Figure 5) (*11*). This delivery profile appeared to have more pervasive distribution than the untreated tumors, though regions of limited delivery were still apparent. When tumors were treated with laser alone, i.e. no GNRs present, greater delivery was not observed.

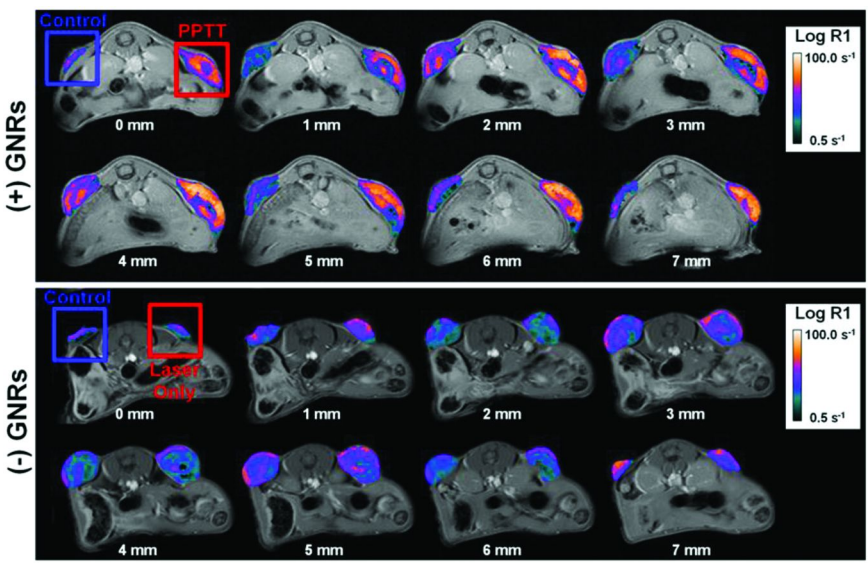


*Figure 5.* ***HPMA copolymer delivery two hours after treatment.*** *Laser treatment of the right tumor in animals previously administered GNRs (PPTT) facilitated significant enhancement of HPMA copolymer delivery in terms of both accumulation and overall tumor distribution (top row). Laser alone did not cause any increased delivery (bottom row). (Reproduced with permission from ref. (11). Copyright 2013 Elsevier.)*


In Tailored Polymer Architectures for Pharmaceutical and Biomedical Applications; Scholz, C., et al.; ACS Symposium Series; American Chemical Society: Washington, DC, 2013.

Downloaded by MICHIGAN STATE UNIV on July 17, 2013 | http://pubs.acs.org
Publication Date (Web): July 8, 2013 | doi: 10.1021/bk-2013-1135.ch010

Analysis of these images provided some additional insight. When regions of the tumor center, periphery and surrounding skin were calculated for thermal enhancement of delivery, each of these regions exhibited improved delivery with PPTT (Figure 6A) (*11*). This difference was however not statistically significant for the skin relative to laser alone. Similarly, a histogram of relaxation rate (R1) values indicates that a larger percentage of the tumor's cross-sectional area had more HPMA copolymers present (Figure 6B). Finally, fluorescence microscopy of tumor sections with fluorescently labeled HPMA copolymers corroborates these results. Together, this data suggests that treatment with PPTT facilitates greater interstitial transport and therefore tumor mass penetration of polymer therapeutics.

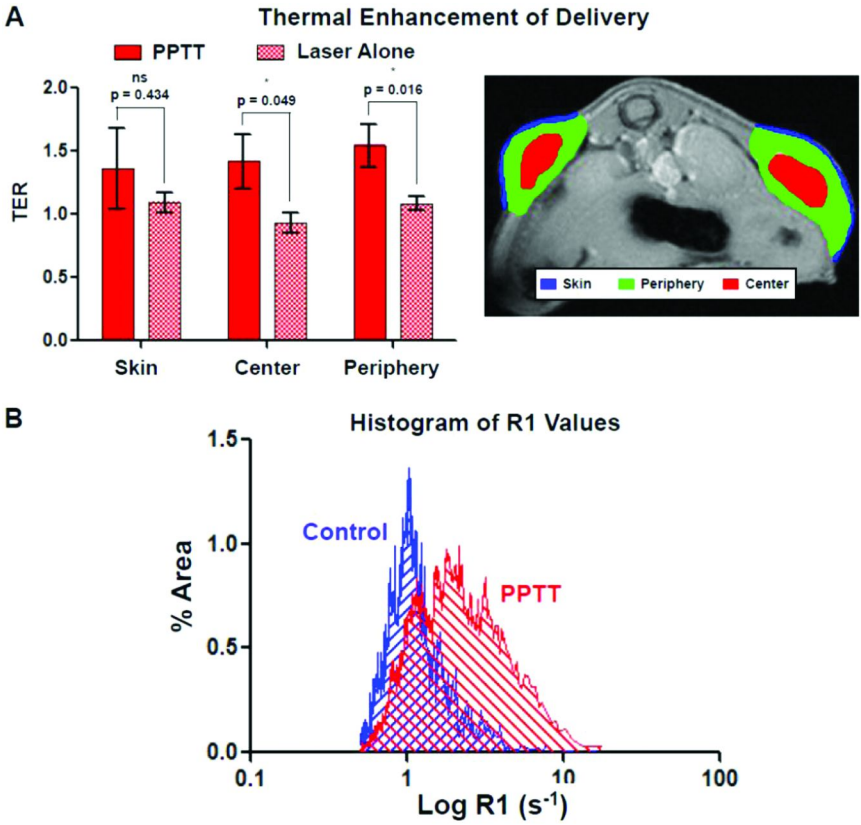


*Figure 6.* ***Image analysis of HPMA copolymer delivery.*** *Treatment of tumors with PPTT was capable of significantly enhancing the delivery of HPMA copolymers to the tumor's center and periphery (A, left). Treatment with laser alone, absence of GNRs, did not increase delivery. Representative ROIs for this analysis is also shown (A, right). A histogram of R1 values of both control and PPTT treated tumors is shown (B). This data shows the capability of PPTT to increase tumor mass distribution. *Indicates a statistically significant difference ($p < 0.05$) by t-test. Error bars represent ± standard error of the mean. (Reproduced with permission from ref. (11). Copyright 2013 Elsevier.)*


In Tailored Polymer Architectures for Pharmaceutical and Biomedical Applications; Scholz, C., et al.; ACS Symposium Series; American Chemical Society: Washington, DC, 2013.

Downloaded by MICHIGAN STATE UNIV on July 17, 2013 | http://pubs.acs.org
Publication Date (Web): July 8, 2013 | doi: 10.1021/bk-2013-1135.ch010

Downloaded by MICHIGAN STATE UNIV on July 17, 2013 | http://pubs.acs.org
Publication Date (Web): July 8, 2013 | doi: 10.1021/bk-2013-1135.ch010



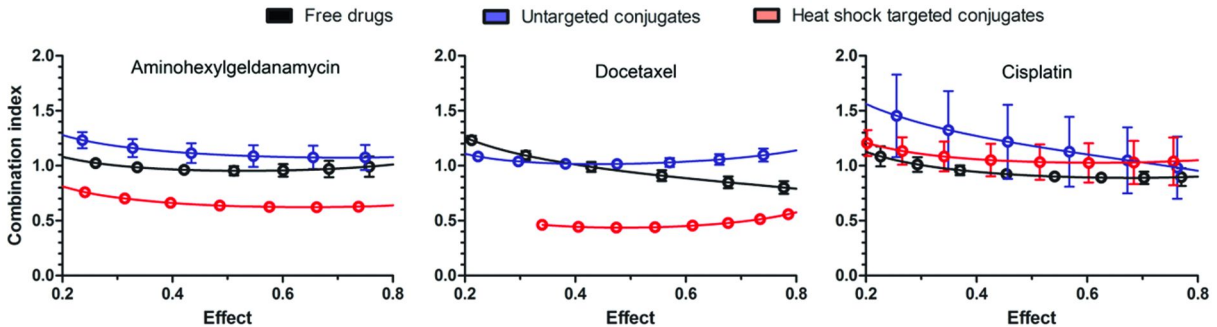


*Figure 7.* ***Combined in vitro effects of hyperthermia (43°C, 30 min.) incubation followed by treatment with heat shock targeted HPMA-copolymer drug conjugates, untargeted conjugates, or free drug controls.*** *Both aminohexylgeldanamycin and docetaxel bearing heat shock targeted conjugates showed marked synergism, with combination index values less than 1.0. Untargeted conjugates, free drug controls, and all cisplatin conjugates were additive to antagonistic in their combined effects. (Reproduced with permission from ref. (13). Copyright 2013 Elsevier.)*

Downloaded by MICHIGAN STATE UNIV on July 17, 2013 | http://pubs.acs.org
Publication Date (Web): July 8, 2013 | doi: 10.1021/bk-2013-1135.ch010

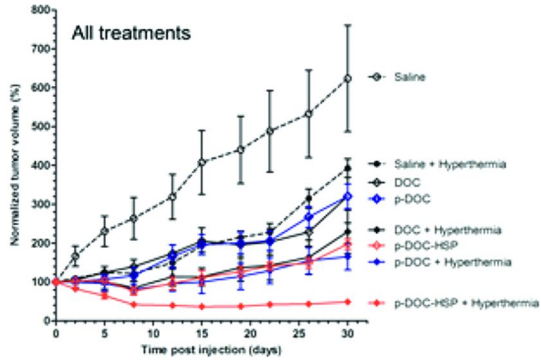


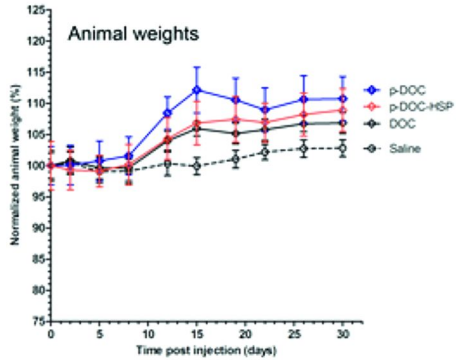


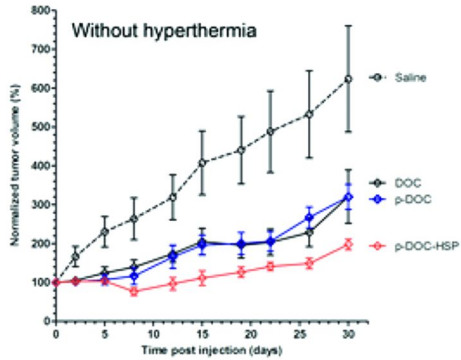


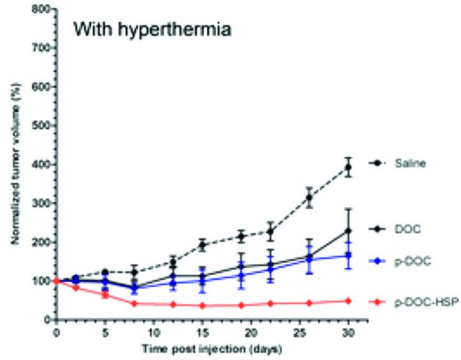



In Tailored Polymer Architectures for Pharmaceutical and Biomedical Applications; Scholz, C., et al.;
ACS Symposium Series; American Chemical Society: Washington, DC, 2013.

*Figure 8.* ***In vivo efficacy of hyperthermia (via PPTT) in combination with docetaxel therapy in athymic (nu/nu) mice bearing DU145 human prostate cancer tumor subcutaneous xenografts.*** *Animals were treated with a single dose of free DOC (DOC), untargeted HPMA copolymer-DOC (p-DOC), or heat shock targeted HPMA copolymer-DOC (p-DOC-HSP) at 10 mg/kg DOC equivalence. Treatment was assessed with and without hyperthermia (PPTT). Superior efficacy, with regression of approximately 50% over 30 days was observed for the combination of PPTT and heat shock targeted docetaxel therapy. No differences in animal weights between treatment groups were observed. (Reproduced with permission from ref. (13). Copyright 2013 Elsevier.)*

Downloaded by MICHIGAN STATE UNIV on July 17, 2013 | http://pubs.acs.org
Publication Date (Web): July 8, 2013 | doi: 10.1021/bk-2013-1135.ch010

### 3.6. *In vitro* Synergism of Heat Shock Targeted HPMA Copolymer-Drug Conjugates Following Hyperthermia

Building upon these results, a series of heat shock targeted HPMA copolymer-drug conjugates were synthesized bearing the anticancer drugs aminohexylgeldanamycin (AHGDM), docetaxel (DOC), or cisplatin. These drugs were selected based on previous work (*50*, *147*) and reports of synergism in combination with hyperthermia (*148–150*). The cytotoxic effects of a combination of hyperthermia (43°C, 30 min. incubation) and treatment with heat shock targeted drug conjugates, untargeted conjugates, or free drug controls was assessed *in vitro* using a cell viability assay (*13*). Combination index analysis (*151*) was used to determine if the combined effects of the combination (hyperthermia plus treatment) were antagonistic, additive, or synergistic. Marked synergism (combination index values less than 1.0) was observed for heat shock targeted conjugates bearing either AHGDM or DOC. Additive to slightly antagonistic effects were observed for all cisplatin conjugates, and AHGDM and DOC untargeted conjugates and free drug controls (Figure 7). These results demonstrate that prior treatment with hyperthermia can sensitize prostate cancer cells *in vitro* to heat shock targeted HPMA copolymer-drug conjugates. The heat shock targeted HPMA-copolymer DOC conjugate, due to its synergism and potency was then chosen for *in vivo* evaluation.

### 3.7. *In vivo* Efficacy of Heat Shock Targeted HPMA-Copolymer Docetaxel Conjugates and Hyperthermia Induced via GNR Mediated PPTT

Efficacy of the combination treatment of hyperthermia and heat shock targeted HPMA copolymer-DOC conjugates was evaluated in eight-week-old athymic (nu/nu) mice bearing DU145 subcutaneous tumor xenografts (*13*). Mice were intravenously administered a single dose of either heat shock targeted HPMA-copolymer-DOC, untargeted HPMA-copolymer-DOC, or free DOC via tail vein injection at a dose of 10 mg/kg docetaxel equivalence. Saline injection served as control. Hyperthermia was then induced immediately via GNR mediated PPTT as described in Section 3.4. Tumors on the right flank received hyperthermia (PPTT), and those on the left flank served as control. Tumor growth/regression was then monitored biweekly over a period of 30 days


In Tailored Polymer Architectures for Pharmaceutical and Biomedical Applications; Scholz, C., et al.;
ACS Symposium Series; American Chemical Society: Washington, DC, 2013.

(Figure 8). Various levels of efficacy were achieved for treatments without PPTT, with treatment with the targeted HPMA-copolymer DOC conjugate resulting in an increase of approximately 2X over 30 days. Increased levels of efficacy were observed for treatments in combination with PPTT, with the targeted HPMA-copolymer DOC conjugate resulting in tumor regression of approximately 50% over 30 days. These results demonstrate that this combination approach can indeed increase the delivery of chemotherapeutics to solid tumors, resulting in increased efficacy.

## 4. Conclusions

The delivery of polymer therapeutics and other nanomedicines is significantly restricted by not only the immune detection, but also the abnormal structure of solid tumors. Vascular heterogeneity, significant IFP, sluggish blood flow and poor perfusion limit therapeutic transport to most cancerous cells. However, these microenvironment abnormalities can also be exploited to selectively deliver nanocarriers to this tissue. Passive delivery by EPR and active targeting through receptor-ligand interactions have enabled use of several therapeutics in the clinic. Other methods to enhance delivery such as pharmacologic or physical modifications to the tumor's vasculature may be useful, though these strategies are not currently applied. Additionally, a new tool has been introduced to selectively induce tumor hyperthermia and therefore facilitate polymer therapeutic delivery. PPTT in combination with heat shock targeting has been shown to improve tumor accumulation, penetration and retention of polymeric conjugates. In the future, additional methods to alter the tumor microenvironment to allow greater delivery of macromolecules will likely be introduced. These methods will further unlock the tremendous potential of these drug delivery systems and help produce better treatments for cancer and other diseases.

## 5. Abbreviations

| | |
|---|---|
| AHGDM | Aminohexylgeldanamycin |
| ANOVA | Analysis of variance |
| AuNP | Gold nanoparticle |
| BBB | Blood-brain barrier |
| DOC | Docetaxel |
| DMXAA | 5,6-dimethylxanthenone-4-acetic acid |
| EBD | Evans blue dye |
| ECM | Extracellular matrix |
| EGFR | Epidermal growth factor receptor |
| EPR | Enhanced permeability and retention |
| GNR | Gold nanorod |
| GRP78 | Glucose regulated protein 78 kDa |
| HER2 | Human epidermal growth factor receptor 2 |
| HIFU | High-intensity focused ultrasound |


In Tailored Polymer Architectures for Pharmaceutical and Biomedical Applications; Scholz, C., et al.; ACS Symposium Series; American Chemical Society: Washington, DC, 2013.

Downloaded by MICHIGAN STATE UNIV on July 17, 2013 | http://pubs.acs.org
Publication Date (Web): July 8, 2013 | doi: 10.1021/bk-2013-1135.ch010

| | |
|---|---|
| HPMA | *N*-(2-hydroxypropyl)methacrylamide |
| HSP | Heat shock protein |
| HSP70 | Heat shock protein 70 kDa |
| ID | Injected dose |
| IFP | Interstitial fluid pressure |
| MTD | Maximum tolerated dose |
| MRI | Magnetic resonance imaging |
| NIR | Near infrared |
| NO | Nitric oxide |
| PDE | Partial differential equation |
| PEG | Poly(ethylene glycol) |
| PK1 | *N*-(2-hydroxypropyl)methacrylamide copolymer-doxorubicin |
| PPTT | Plasmonic photothermal therapy |
| RES | Reticuloendothelial system |
| RGD | Arg-Gly-Asp |
| SMANCS | Poly(styrene-*co*-maleyl-half-*n*-butylate)-neocarzinostatin |
| SPR | Surface plasmon resonance |
| TER | Thermal enhancement ratio |
| TNF-α | Tumor necrosis factor-α |
| VDA | Vascular disrupting agent |
| VEGF | Vascular endothelial growth factor |
| WIFPWIQL | Trp-Ile-Phe-Pro-Trp-Ile-Gln-Leu |

Downloaded by MICHIGAN STATE UNIV on July 17, 2013 | http://pubs.acs.org
Publication Date (Web): July 8, 2013 | doi: 10.1021/bk-2013-1135.ch010

## Acknowledgments

This research was supported by the National Institutes of Health (EB-R01EB7171), Utah Science, Technology, and Research (USTAR) Initiative, and a Department of Defense Prostate Cancer Predoctoral Training Award (PC094496) to AG.

## References

1. Strebhardt, K.; Ullrich, A. Paul Ehrlich's magic bullet concept: 100 years of progress. *Nat. Rev. Cancer* **2008**, *8*, 473–80.
2. Ringsdorf, H. Structure and properties of pharmacologically active polymers. *J. Polym. Sci., Part C: Polym. Symp.* **1975**, *51*, 135–153.
3. Duncan, R. The dawning era of polymer therapeutics. *Nat. Rev. Drug Discovery* **2003**, *2*, 347–360.
4. Malone, D. C.; Tran, T. T.; Poordad, F. F. Cost-efficacy analysis of peginterferon alfa-2b plus ribavirin compared with peginterferon alfa-2a plus ribavirin for the treatment of chronic hepatitis C. *J. Manag. Care Pharm.* **2005**, *11*, 687–694.
5. Tewey, M. Sigma-Tau Pharmaceuticals announces new ONCASPAR pricing. Sigma-tau Pharmaceuticals, Inc., 2011.

6. Nie, S. Understanding and overcoming major barriers in cancer nanomedicine. *Nanomedicine (London)* **2010**, *5*, 523–528.
7. Cedervall, T.; Lynch, I.; Lindman, S.; Berggård, T.; Thulin, E.; Nilsson, H.; Dawson, K. A.; Linse, S. Understanding the nanoparticle–protein corona using methods to quantify exchange rates and affinities of proteins for nanoparticles. *Proc. Natl. Acad. Sci. U.S.A.* **2007**, *104*, 2050–2055.
8. Jain, R. K. Vascular and interstitial barriers to delivery of therapeutic agents in tumors. *Cancer Metastasis Rev.* **1990**, *9*, 253–266.
9. Jain, R. K. Transport of molecules in the tumor interstitium: a review. *Cancer Res.* **1987**, *47*, 3039–3051.
10. Gormley, A. J.; Greish, K.; Ray, A.; Robinson, R.; Gustafson, J. A.; Ghandehari, H. Gold nanorod mediated plasmonic photothermal therapy: A tool to enhance macromolecular delivery. *Int. J. Pharm.* **2011**, *415*, 315–318.
11. Gormley, A. J.; Larson, N.; Banisadr, A.; Robinson, R.; Frazier, N.; Ray, A.; Ghandehari, H. Plasmonic photothermal therapy increases the tumor mass penetration of HPMA copolymers. *J. Controlled Release* **2013**, *166*, 130–138.
12. Gormley, A. J.; Larson, N.; Sadekar, S.; Robinson, R.; Ray, A.; Ghandehari, H. Guided delivery of polymer therapeutics using plasmonic photothermal therapy. *Nano Today* **2012**, *7*, 158–167.
13. Larson, N.; Gormley, A. J.; Frazier, N.; Ghandehari, H. Synergistic enhancement of cancer therapy using a combination of heat shock protein targeted HPMA copolymer-drug conjugates and gold nanorod induced hyperthermia. *J. Controlled Release* **2013** (in press).
14. Seymour, L.; Miyamoto, Y.; Maeda, H.; Brereton, M.; Strohalm, J.; Ulbrich, K.; Duncan, R. Influence of molecular weight on passive tumour accumulation of a soluble macromolecular drug carrier. *Eur. J. Cancer* **1995**, *31*, 766–770.
15. Peterson, H. I.; Appelgren, L. Tumour vessel permeability and transcapillary exchange of large molecules of different size. *Bibl. Anat.* **1977**, *15* (Pt 1), 262–265.
16. Peterson, H. I., Vascular and extravascular spaces in tumors: tumor vascular permeability. In *Tumor Blood Circulation: Angiogenesis, Vascular Morphology and Blood Flow of Experimental and Human Tumors*; Peterson, H. I., Ed.; CRS Press, Inc.: Boca Raton, FL, 1979; pp 77−85.
17. Larson, S. M. In *Mechanisms of Localization of Gallium-67 in Tumors*; Elsevier: New York, 1978; pp 193−203.
18. Pinsky, S. M.; Henkin, R. E. In *Gallium-67 Tumor Scanning*; Elsevier: New York, 1976; pp 397−409.
19. Matsumura, Y.; Maeda, H. A new concept for macromolecular therapeutics in cancer chemotherapy: mechanism of tumoritropic accumulation of proteins and the antitumor agent smancs. *Cancer Res.* **1986**, *46*, 6387–6392.
20. Maeda, H.; Wu, J.; Sawa, T.; Matsumura, Y.; Hori, K. Tumor vascular permeability and the EPR effect in macromolecular therapeutics: a review. *J. Controlled Release* **2000**, *65*, 271–284.

Downloaded by MICHIGAN STATE UNIV on July 17, 2013 | http://pubs.acs.org
Publication Date (Web): July 8, 2013 | doi: 10.1021/bk-2013-1135.ch010


In Tailored Polymer Architectures for Pharmaceutical and Biomedical Applications; Scholz, C., et al.;
ACS Symposium Series; American Chemical Society: Washington, DC, 2013.

21. Jain, R. K. Normalization of tumor vasculature: an emerging concept in antiangiogenic therapy. *Science* **2005**, *307*, 58–62.
22. Jain, R. K. Normalizing tumor vasculature with anti-angiogenic therapy: a new paradigm for combination therapy. *Nat. Med.* **2001**, *7*, 987–989.
23. Konerdingi, M.; Fait, E.; Gaumann, A.; Dimitropouloui, C.; Malkusch, W. Scanning electron microscopy of corrosion casts in the study of tumor. In *Angiogenesis: models, modulators, and clinical applications*; Maragoudakis, M. E., Ed.; Plenum Press: New York, 1998; Vol. 298, pp 429−447.
24. Baish, J. W.; Jain, R. K. Fractals and cancer. *Cancer Res.* **2000**, *60*, 3683–3688.
25. Hashizume, H.; Baluk, P.; Morikawa, S.; McLean, J. W.; Thurston, G.; Roberge, S.; Jain, R. K.; McDonald, D. M. Openings between defective endothelial cells explain tumor vessel leakiness. *Am. J. Pathol.* **2000**, *156*, 1363–1380.
26. Jain, R. K.; Stylianopoulos, T. Delivering nanomedicine to solid tumors. *Nat. Rev. Clin. Oncol.* **2010**, *7*, 653–664.
27. Sevick, E. M.; Jain, R. K. Viscous resistance to blood flow in solid tumors: effect of hematocrit on intratumor blood viscosity. *Cancer Res.* **1989**, *49*, 3513–3519.
28. Jain, R. K. Determinants of tumor blood flow: a review. *Cancer Res.* **1988**, *48*, 2641–2658.
29. Boucher, Y.; Jain, R. K. Microvascular pressure is the principal driving force for interstitial hypertension in solid tumors: implications for vascular collapse. *Cancer Res.* **1992**, *52*, 5110–5114.
30. Boucher, Y.; Baxter, L. T.; Jain, R. K. Interstitial pressure gradients in tissue-isolated and subcutaneous tumors: implications for therapy. *Cancer Res.* **1990**, *50*, 4478–4484.
31. Netti, P. A.; Berk, D. A.; Swartz, M. A.; Grodzinsky, A. J.; Jain, R. K. Role of extracellular matrix assembly in interstitial transport in solid tumors. *Cancer Res.* **2000**, *60*, 2497–2503.
32. Fukumura, D.; Jain, R. K. Tumor microenvironment abnormalities: causes, consequences, and strategies to normalize. *J. Cell. Biochem.* **2007**, *101*, 937–949.
33. Hobbs, S. K.; Monsky, W. L.; Yuan, F.; Roberts, W. G.; Griffith, L.; Torchilin, V. P.; Jain, R. K. Regulation of transport pathways in tumor vessels: role of tumor type and microenvironment. *Proc. Natl. Acad. Sci. U.S.A.* **1998**, *95*, 4607–4612.
34. Ramanujan, S.; Pluen, A.; McKee, T. D.; Brown, E. B.; Boucher, Y.; Jain, R. K. Diffusion and convection in collagen gels: implications for transport in the tumor interstitium. *Biophys. J.* **2002**, *83*, 1650–1660.
35. Yuan, F.; Dellian, M.; Fukumura, D.; Leunig, M.; Berk, D. A.; Torchilin, V. P.; Jain, R. K. Vascular permeability in a human tumor xenograft: molecular size dependence and cutoff size. *Cancer Res.* **1995**, *55*, 3752–3756.
36. Yuan, F.; Leunig, M.; Huang, S. K.; Berk, D. A.; Papahadjopoulos, D.; Jain, R. K. Mirovascular permeability and interstitial penetration of sterically

Downloaded by MICHIGAN STATE UNIV on July 17, 2013 | http://pubs.acs.org
Publication Date (Web): July 8, 2013 | doi: 10.1021/bk-2013-1135.ch010


In Tailored Polymer Architectures for Pharmaceutical and Biomedical Applications; Scholz, C., et al.;
ACS Symposium Series; American Chemical Society: Washington, DC, 2013.

stabilized (stealth) liposomes in a human tumor xenograft. *Cancer Res.* **1994**, *54*, 3352–3356.
37. Torchilin, V. Tumor delivery of macromolecular drugs based on the EPR effect. *Adv. Drug Delivery Rev.* **2011**, *63*, 131–135.
38. Adams, G. P.; Weiner, L. M. Monoclonal antibody therapy of cancer. *Nat. Biotechnol.* **2005**, *23*, 1147–1157.
39. Mehren, M.; Adams, G. P.; Weiner, L. M. Monoclonal antibody therapy for cancer. *Annu. Rev. Med.* **2003**, *54*, 343–369.
40. Loo, C.; Lowery, A.; Halas, N.; West, J.; Drezek, R. Immunotargeted nanoshells for integrated cancer imaging and therapy. *Nano Lett.* **2005**, *5*, 709–711.
41. Park, J.; Kirpotin, D.; Hong, K.; Shalaby, R.; Shao, Y.; Nielsen, U.; Marks, J.; Papahadjopoulos, D.; Benz, C. Tumor targeting using anti-her2 immunoliposomes. *J. Controlled Release* **2001**, *74*, 95–113.
42. Nurunnabi, M.; Cho, K. J.; Choi, J. S.; Huh, K. M.; Lee, Y. Targeted near-IR QDs-loaded micelles for cancer therapy and imaging. *Biomaterials* **2010**, *31*, 5436–5444.
43. Hattori, Y.; Maitani, Y. Enhanced in vitro DNA transfection efficiency by novel folate-linked nanoparticles in human prostate cancer and oral cancer. *J. Controlled Release* **2004**, *97*, 173–183.
44. Dixit, V.; Van den Bossche, J.; Sherman, D. M.; Thompson, D. H.; Andres, R. P. Synthesis and grafting of thioctic acid- PEG- folate conjugates onto Au nanoparticles for selective targeting of folate receptor-positive tumor cells. *Bioconjugate Chem.* **2006**, *17*, 603–609.
45. Stella, B.; Arpicco, S.; Peracchia, M. T.; Desmaële, D.; Hoebeke, J.; Renoir, M.; D'Angelo, J.; Cattel, L.; Couvreur, P. Design of folic acid-conjugated nanoparticles for drug targeting. *J. Pharm. Sci.* **2000**, *89*, 1452–1464.
46. Chithrani, B. D.; Chan, W. C. Elucidating the mechanism of cellular uptake and removal of protein-coated gold nanoparticles of different sizes and shapes. *Nano Lett.* **2007**, *7*, 1542–1550.
47. Yang, P. H.; Sun, X.; Chiu, J. F.; Sun, H.; He, Q. Y. Transferrin-mediated gold nanoparticle cellular uptake. *Bioconjugate Chem.* **2005**, *16*, 494–496.
48. Ishida, O.; Maruyama, K.; Tanahashi, H.; Iwatsuru, M.; Sasaki, K.; Eriguchi, M.; Yanagie, H. Liposomes bearing polyethyleneglycol-coupled transferrin with intracellular targeting property to the solid tumors in vivo. *Pharm. Res.* **2001**, *18*, 1042–1048.
49. Kursa, M.; Walker, G. F.; Roessler, V.; Ogris, M.; Roedl, W.; Kircheis, R.; Wagner, E. Novel shielded transferrin-polyethylene glycol-polyethylenimine/DNA complexes for systemic tumor-targeted gene transfer. *Bioconjugate Chem.* **2003**, *14*, 222–231.
50. Greish, K.; Ray, A.; Bauer, H.; Larson, N.; Malugin, A.; Pike, D. B.; Haider, M.; Ghandehari, H. Anticancer and antiangiogenic activity of HPMA copolymer-aminohexylgeldanamycin-RGDfK conjugates for prostate cancer therapy. *J. Controlled Release* **2011**, *151*, 263–270.

Downloaded by MICHIGAN STATE UNIV on July 17, 2013 | http://pubs.acs.org
Publication Date (Web): July 8, 2013 | doi: 10.1021/bk-2013-1135.ch010


In Tailored Polymer Architectures for Pharmaceutical and Biomedical Applications; Scholz, C., et al.;
ACS Symposium Series; American Chemical Society: Washington, DC, 2013.

51. Gormley, A. J.; Malugin, A.; Ray, A.; Robinson, R.; Ghandehari, H. Biological evaluation of RGDfK-gold nanorod conjugates for prostate cancer treatment. *J. Drug Targeting* **2011**, *19*, 915–924.
52. Arosio, D.; Manzoni, L.; Araldi, E. M. V.; Scolastico, C. Cyclic RGD functionalized gold nanoparticles for tumor targeting. *Bioconjugate Chem.* **2011**, *22*, 664–672.
53. Danhier, F.; Vroman, B.; Lecouturier, N.; Crokart, N.; Pourcelle, V.; Freichels, H.; Jérôme, C.; Marchand-Brynaert, J.; Feron, O.; Préat, V. Targeting of tumor endothelium by RGD-grafted PLGA-nanoparticles loaded with Paclitaxel. *J. Controlled Release* **2009**, *140*, 166–173.
54. Temming, K.; Schiffelers, R. M.; Molema, G.; Kok, R. J. RGD-based strategies for selective delivery of therapeutics and imaging agents to the tumour vasculature. *Drug Resist. Updates* **2005**, *8*, 381–402.
55. Sapra, P.; Allen, T. M. Internalizing antibodies are necessary for improved therapeutic efficacy of antibody-targeted liposomal drugs. *Cancer Res.* **2002**, *62*, 7190–7194.
56. Maruyama, K.; Ishida, O.; Takizawa, T.; Moribe, K. Possibility of active targeting to tumor tissues with liposomes. *Adv. Drug Delivery Rev.* **1999**, *40*, 89–102.
57. Allen, T. M.; Agrawal, A. K.; Ahmad, I.; Hansen, C. B.; Zalipsky, S. Antibody-mediated targeting of long-circulating (StealthR) liposomes. *J. Liposome Res.* **1994**, *4*, 1–25.
58. Kamps, J.; Koning, G.; Velinova, M.; Morselt, H.; Wilkens, M.; Gorter, A.; Donga, J.; Scherphof, G. Uptake of long-circulating immunoliposomes, directed against colon adenocarcinoma cells, by liver metastases of colon cancer. *J. Drug Targeting* **2000**, *8*, 235–245.
59. Goren, D.; Horowitz, A.; Zalipsky, S.; Woodle, M.; Yarden, Y.; Gabizon, A. Targeting of stealth liposomes to erbB-2 (Her/2) receptor: in vitro and in vivo studies. *Br. J. Cancer* **1996**, *74*, 1749–1756.
60. Bae, Y. H. Drug targeting and tumor heterogeneity. *J. Controlled Release* **2009**, *133*, 2–3.
61. Kirpotin, D. B.; Drummond, D. C.; Shao, Y.; Shalaby, M. R.; Hong, K.; Nielsen, U. B.; Marks, J. D.; Benz, C. C.; Park, J. W. Antibody targeting of long-circulating lipidic nanoparticles does not increase tumor localization but does increase internalization in animal models. *Cancer Res.* **2006**, *66*, 6732–6740.
62. Seymour, L. W.; Ferry, D. R.; Anderson, D.; Hesslewood, S.; Julyan, P. J.; Poyner, R.; Doran, J.; Young, A. M.; Burtles, S.; Kerr, D. J. Hepatic drug targeting: phase I evaluation of polymer-bound doxorubicin. *J. Clin. Oncol.* **2002**, *20*, 1668–1676.
63. Trere, D.; Fiume, L.; De Giorgi, L. B.; Di Stefano, G.; Migaldi, M.; Derenzini, M. The asialoglycoprotein receptor in human hepatocellular carcinomas: its expression on proliferating cells. *Br. J. Cancer* **1999**, *81*, 404–408.
64. Duncan, R.; Kopecek, J.; Rejmanova, P.; Lloyd, J. Targeting of *N*-(2-hydroxypropyl) methacrylamide copolymers to liver by incorporation of galactose residues. *Biochim. Biophys. Acta.* **1983**, *755*, 518–521.

Downloaded by MICHIGAN STATE UNIV on July 17, 2013 | http://pubs.acs.org
Publication Date (Web): July 8, 2013 | doi: 10.1021/bk-2013-1135.ch010


In Tailored Polymer Architectures for Pharmaceutical and Biomedical Applications; Scholz, C., et al.;
ACS Symposium Series; American Chemical Society: Washington, DC, 2013.

65. Duncan, R.; Seymour, L. C. W.; Scarlett, L.; Lloyd, J. B.; Rejmanova, P. Fate of *N*-(2-hydroxypropyl) methacrylamide copolymers with pendent galactosamine residues after intravenous administration to rats. *Biochim. Biophys. Acta.* **1986**, *880*, 62–71.
66. Seymour, L.; Ulbrich, K.; Wedge, S.; Hume, I.; Strohalm, J.; Duncan, R. *N*-(2-hydroxypropyl) methacrylamide copolymers targeted to the hepatocyte galactose-receptor: pharmacokinetics in DBA2 mice. *Br. J. Cancer* **1991**, *63*, 859–866.
67. Julyan, P. J.; Seymour, L. W.; Ferry, D. R.; Daryani, S.; Boivin, C. M.; Doran, J.; David, M.; Anderson, D.; Christodoulou, C.; Young, A. M. Preliminary clinical study of the distribution of HPMA copolymers bearing doxorubicin and galactosamine. *J. Controlled Release* **1999**, *57*, 281–290.
68. Chauhan, V. P.; Stylianopoulos, T.; Boucher, Y.; Jain, R. K. Delivery of molecular and nanoscale medicine to tumors: Transport barriers and strategies. *Annu. Rev. Chem. Biomol. Eng.* **2011**, *2*, 281–298.
69. Zlotecki, R. A.; Baxter, L. T.; Boucher, Y.; Jain, R. K. Pharmacologic modification of tumor blood flow and interstitial fluid pressure in a human tumor xenograft: network analysis and mechanistic interpretation. *Microvasc. Res.* **1995**, *50*, 429–443.
70. Li, C.; Miyamoto, Y.; Kojima, Y.; Maeda, H. Augmentation of tumour delivery of macromolecular drugs with reduced bone marrow delivery by elevating blood pressure. *Br. J. Cancer* **1993**, *67*, 975–980.
71. Nagamitsu, A.; Greish, K.; Maeda, H. Elevating blood pressure as a strategy to increase tumor-targeted delivery of macromolecular drug SMANCS: cases of advanced solid tumors. *Jpn. J. Clin. Oncol.* **2009**, *39*, 756–766.
72. Zlotecki, R. A.; Boucher, Y.; Lee, I.; Baxter, L. T.; Jain, R. K. Effect of angiotensin II induced hypertension on tumor blood flow and interstitial fluid pressure. *Cancer Res.* **1993**, *53*, 2466–2468.
73. Burton, M. A.; Gray, B. N.; Self, G. W.; Heggie, J. C.; Townsend, P. S. Manipulation of experimental rat and rabbit liver tumor blood flow with angiotensin II. *Cancer Res.* **1985**, *45*, 5390–5393.
74. Suzuki, M.; Hori, K.; Abe, I.; Saito, S.; Sato, H. A new approach to cancer chemotherapy: selective enhancement of tumor blood flow with angiotensin II. *J. Natl. Cancer Inst.* **1981**, *67*, 663–669.
75. Chaplin, D. J.; Hill, S. A.; Bell, K. M.; Tozer, G. M. Modification of tumor blood flow: Current status and future directions. *Semin. Radiat. Oncol.* **1998**, *8*, 151–163.
76. Seki, T.; Fang, J.; Maeda, H. Enhanced delivery of macromolecular antitumor drugs to tumors by nitroglycerin application. *Cancer Sci.* **2009**, *100*, 2426–2430.
77. Tozer, G. M.; Prise, V. E.; Chaplin, D. J. Inhibition of nitric oxide synthase induces a selective reduction in tumor blood flow that is reversible with L-arginine. *Cancer Res.* **1997**, *57*, 948–955.
78. Chan, R.; Babbs, C.; Vetter, R.; Lamar, C. Abnormal response of tumor vasculature to vasoactive drugs. *J. Natl. Cancer Inst.* **1984**, *72*, 145–150.
79. Brett, J.; Gerlach, H.; Nawroth, P.; Steinberg, S.; Godman, G.; Stern, D. Tumor necrosis factor/cachectin increases permeability of endothelial cell

Downloaded by MICHIGAN STATE UNIV on July 17, 2013 | http://pubs.acs.org
Publication Date (Web): July 8, 2013 | doi: 10.1021/bk-2013-1135.ch010

monolayers by a mechanism involving regulatory G proteins. *J. Exp. Med.* **1989**, *169*, 1977–1991.
80. Aicher, K. P.; Dupon, J. W.; White, D. L.; Aukerman, S. L.; Moseley, M. E.; Juster, R.; Rosenau, W.; Winkelhake, J. L.; Brasch, R. C. Contrast-enhanced magnetic resonance imaging of tumor-bearing mice treated with human recombinant tumor necrosis factor α. *Cancer Res.* **1990**, *50*, 7376–7381.
81. Paciotti, G. F.; Myer, L.; Weinreich, D.; Goia, D.; Pavel, N.; McLaughlin, R. E.; Tamarkin, L. Colloidal gold: a novel nanoparticle vector for tumor directed drug delivery. *Drug Delivery* **2004**, *11*, 169–183.
82. Farma, J. M.; Puhlmann, M.; Soriano, P. A.; Cox, D.; Paciotti, G. F.; Tamarkin, L.; Alexander, H. R. Direct evidence for rapid and selective induction of tumor neovascular permeability by tumor necrosis factor and a novel derivative, colloidal gold bound tumor necrosis factor. *Int. J. Cancer* **2007**, *120*, 2474–2480.
83. Zhao, L.; Ching, L. M.; Kestell, P.; Kelland, L. R.; Baguley, B. C. Mechanisms of tumor vascular shutdown induced by 5, 6-dimethylxanthenone-4-acetic acid (DMXAA): Increased tumor vascular permeability. *Int. J. Cancer* **2005**, *116*, 322–326.
84. Galbraith, S. M.; Rustin, G. J. S.; Lodge, M. A.; Taylor, N. J.; Stirling, J. J.; Jameson, M.; Thompson, P.; Hough, D.; Gumbrell, L.; Padhani, A. R. Effects of 5, 6-dimethylxanthenone-4-acetic acid on human tumor microcirculation assessed by dynamic contrast-enhanced magnetic resonance imaging. *J. Clin. Oncol.* **2002**, *20*, 3826–3840.
85. Sherwood, L. M.; Parris, E. E.; Folkman, J. Tumor angiogenesis: therapeutic implications. *N. Engl. J. Med.* **1971**, *285*, 1182–1186.
86. Carmeliet, P.; Jain, R. K. Principles and mechanisms of vessel normalization for cancer and other angiogenic diseases. *Nat. Rev. Cancer* **2011**, *10*, 417–427.
87. Winkler, F.; Kozin, S. V.; Tong, R. T.; Chae, S. S.; Booth, M. F.; Garkavtsev, I.; Xu, L.; Hicklin, D. J.; Fukumura, D.; di Tomaso, E. Kinetics of vascular normalization by VEGFR2 blockade governs brain tumor response to radiation:: Role of oxygenation, angiopoietin-1, and matrix metalloproteinases. *Cancer Cell* **2004**, *6*, 553–563.
88. Wildiers, H.; Guetens, G.; De Boeck, G.; Verbeken, E.; Landuyt, B.; Landuyt, W.; De Bruijn, E.; van Oosterom, A. T. Effect of antivascular endothelial growth factor treatment on the intratumoral uptake of CPT-11. *Br. J. Cancer* **2003**, *88*, 1979–1986.
89. Chauhan, V. P.; Stylianopoulos, T.; Martin, J. D.; Popović, Z.; Chen, O.; Kamoun, W. S.; Bawendi, M. G.; Fukumura, D.; Jain, R. K. Normalization of tumour blood vessels improves the delivery of nanomedicines in a size-dependent manner. *Nat. Nanotechnol.* **2012**, *7*, 383–388.
90. Griffon-Etienne, G.; Boucher, Y.; Brekken, C.; Suit, H. D.; Jain, R. K. Taxane-induced apoptosis decompresses blood vessels and lowers interstitial fluid pressure in solid tumors. *Cancer Res.* **1999**, *59*, 3776–3782.
91. Magzoub, M.; Jin, S.; Verkman, A. Enhanced macromolecule diffusion deep in tumors after enzymatic digestion of extracellular matrix collagen and its associated proteoglycan decorin. *FASEB J.* **2008**, *22*, 276–284.


In Tailored Polymer Architectures for Pharmaceutical and Biomedical Applications; Scholz, C., et al.; ACS Symposium Series; American Chemical Society: Washington, DC, 2013.

Downloaded by MICHIGAN STATE UNIV on July 17, 2013 | http://pubs.acs.org
Publication Date (Web): July 8, 2013 | doi: 10.1021/bk-2013-1135.ch010

92. Wong, C.; Stylianopoulos, T.; Cui, J.; Martin, J.; Chauhan, V. P.; Jiang, W.; Popović, Z.; Jain, R. K.; Bawendi, M. G.; Fukumura, D. Multistage nanoparticle delivery system for deep penetration into tumor tissue. *Proc. Natl. Acad. Sci. U.S.A.* **2011**, *108*, 2426–2431.
93. Serda, R. E.; Godin, B.; Blanco, E.; Chiappini, C.; Ferrari, M. Multi-stage delivery nano-particle systems for therapeutic applications. *Biochim. Biophys. Acta.* **2011**, *1810*, 317–329.
94. Yavuz, M. S.; Cheng, Y.; Chen, J.; Cobley, C. M.; Zhang, Q.; Rycenga, M.; Xie, J.; Kim, C.; Song, K. H.; Schwartz, A. G.; Wang, L. V.; Xia, Y. Gold nanocages covered by smart polymers for controlled release with near-infrared light. *Nat. Mater.* **2009**, *8*, 935–939.
95. ter Haar, G. Therapeutic ultrasound. *Eur. J. Ultrasound* **1999**, *9*, 3–9.
96. Aus, G. Current status of HIFU and cryotherapy in prostate cancer–a review. *Eur. Urol.* **2006**, *50*, 927–934.
97. Mitragotri, S. Healing sound: the use of ultrasound in drug delivery and other therapeutic applications. *Nat. Rev. Drug Discovery* **2005**, *4*, 255–260.
98. Hancock, H. A.; Smith, L. H.; Cuesta, J.; Durrani, A. K.; Angstadt, M.; Palmeri, M. L.; Kimmel, E.; Frenkel, V. Investigations into pulsed high-intensity focused ultrasound–enhanced delivery: Preliminary evidence for a novel mechanism. *Ultrasound Med. Biol.* **2009**, *35*, 1722–1736.
99. Mitragotri, S.; Blankschtein, D.; Langer, R. Ultrasound-mediated transdermal protein delivery. *Science* **1995**, *269*, 850–853.
100. Miller, D. L.; Pislaru, S. V.; Greenleaf, J. F. Sonoporation: mechanical DNA delivery by ultrasonic cavitation. *Somatic Cell Mol. Genet.* **2002**, *27*, 115–134.
101. Deng, C. X.; Sieling, F.; Pan, H.; Cui, J. Ultrasound-induced cell membrane porosity. *Ultrasound Med. Biol.* **2004**, *30*, 519–526.
102. Hynynen, K.; McDannold, N.; Sheikov, N. A.; Jolesz, F. A.; Vykhodtseva, N. Local and reversible blood-brain barrier disruption by noninvasive focused ultrasound at frequencies suitable for trans-skull sonications. *NeuroImage* **2005**, *24*, 12–20.
103. McDannold, N.; Vykhodtseva, N.; Hynynen, K. Targeted disruption of the blood–brain barrier with focused ultrasound: association with cavitation activity. *Phys. Med. Biol.* **2006**, *51*, 793–807.
104. Larina, I. V.; Evers, B. M.; Ashitkov, T. V.; Bartels, C.; Larin, K. V.; Esenaliev, R. O. Enhancement of drug delivery in tumors by using interaction of nanoparticles with ultrasound radiation. *Technol. Cancer Res. Treat.* **2005**, *4*, 217–226.
105. Yuh, E. L.; Shulman, S. G.; Mehta, S. A.; Xie, J.; Chen, L.; Frenkel, V.; Bednarski, M. D.; Li, K. C. P. Delivery of systemic chemotherapeutic agent to tumors by using focused ultrasound: Study in a murine model. *Radiology* **2005**, *234*, 431–437.
106. Frenkel, V.; Etherington, A.; Greene, M.; Quijano, J.; Xie, J.; Hunter, F.; Dromi, S.; Li, K. C. P. Delivery of liposomal doxorubicin (Doxil) in a breast cancer tumor model: investigation of potential enhancement by pulsed-high intensity focused ultrasound exposure. *Acad. Radiol.* **2006**, *13*, 469–479.

Downloaded by MICHIGAN STATE UNIV on July 17, 2013 | http://pubs.acs.org
Publication Date (Web): July 8, 2013 | doi: 10.1021/bk-2013-1135.ch010


In Tailored Polymer Architectures for Pharmaceutical and Biomedical Applications; Scholz, C., et al.;
ACS Symposium Series; American Chemical Society: Washington, DC, 2013.

107. Issels, R. Hyperthermia combined with chemotherapy–biological rationale, clinical application, and treatment results. *Onkologie* **2000**, *22*, 374–381.
108. Vega, V. L.; Charles, W.; De Maio, A. A new feature of the stress response: increase in endocytosis mediated by Hsp70. *Cell Stress Chaperones* **2009**, *15*, 517–527.
109. Vega, V. L.; De Maio, A. Increase in phagocytosis after geldanamycin treatment or heat shock: role of heat shock proteins. *J. Immunol.* **2005**, *175*, 5280–5287.
110. Song, C. W. Effect of local hyperthermia on blood flow and microenvironment: a review. *Cancer Res.* **1984**, *44*, 4721s–4730s.
111. Horsman, M. R. Tissue physiology and the response to heat. *Int. J. Hyperthermia* **2006**, *22*, 197–203.
112. Dudar, T. E.; Jain, R. K. Differential response of normal and tumor microcirculation to hyperthermia. *Cancer Res.* **1984**, *44*, 605–612.
113. Fujiwara, K.; Watanabe, T. Effects of hyperthermia, radiotherapy and thermoradiotherapy on tumor microvascular permeability. *Pathol. Int.* **2008**, *40*, 79–84.
114. Lefor, A. T.; Makohon, S.; Ackerman, N. B. The effects of hyperthermia on vascular permeability in experimental liver metastasis. *J. Surg. Oncol.* **1985**, *28*, 297–300.
115. Fajardo, L.; Schreiber, A.; Kelly, N.; Hahn, G. Thermal sensitivity of endothelial cells. *Radiat. Res.* **1985**, *103*, 276–285.
116. Hildebrandt, B.; Wust, P.; Ahlers, O.; Dieing, A.; Sreenivasa, G.; Kerner, T.; Felix, R.; Riess, H. The cellular and molecular basis of hyperthermia. *Crit. Rev. Oncol. Hematol.* **2002**, *43*, 33–56.
117. Kitchens, K. M.; El-Sayed, M. E.; Ghandehari, H. Transepithelial and endothelial transport of poly (amidoamine) dendrimers. *Adv. Drug Delivery Rev.* **2005**, *57*, 2163–2176.
118. Xu, L.; Chen, B.; Zhou, M. Change of individual vascular endothelial calcium during hyperthermia. *J. Therm. Biol.* **2006**, *31*, 302–306.
119. Kong, G.; Dewhirst, M. W. Hyperthermia and liposomes. *Int. J. Hyperthermia* **1999**, *15*, 345–370.
120. Huang, S. K.; Stauffer, P. R.; Hong, K.; Guo, J. W. H.; Phillips, T. L.; Huang, A.; Papahadjopoulos, D. Liposomes and hyperthermia in mice: increased tumor uptake and therapeutic efficacy of doxorubicin in sterically stabilized liposomes. *Cancer Res.* **1994**, *54*, 2186–2191.
121. Weinstein, J.; Magin, R.; Yatvin, M.; Zaharko, D. Liposomes and local hyperthermia: selective delivery of methotrexate to heated tumors. *Science* **1979**, *204*, 188–191.
122. Gaber, M. H.; Wu, N. Z.; Hong, K.; Huang, S. K.; Dewhirst, M. W.; Papahadjopoulos, D. Thermosensitive liposomes: extravasation and release of contents in tumor microvascular networks. *Int. J. Radiat. Oncol. Biol. Phys.* **1996**, *36*, 1177–1187.
123. Lammers, T.; Peschke, P.; Kühnlein, R.; Subr, V.; Ulbrich, K.; Debus, J.; Huber, P.; Hennink, W.; Storm, G. Effect of radiotherapy and hyperthermia on the tumor accumulation of HPMA copolymer-based drug delivery systems. *J. Controlled Release* **2007**, *117*, 333–341.

Downloaded by MICHIGAN STATE UNIV on July 17, 2013 | http://pubs.acs.org
Publication Date (Web): July 8, 2013 | doi: 10.1021/bk-2013-1135.ch010

124. Kong, G.; Braun, R. D.; Dewhirst, M. W. Hyperthermia enables tumor-specific nanoparticle delivery: effect of particle size. *Cancer Res.* **2000**, *60*, 4440–4445.
125. Matteucci, M. L.; Anyarambhatla, G.; Rosner, G.; Azuma, C.; Fisher, P. E.; Dewhirst, M. W.; Needham, D.; Thrall, D. E. Hyperthermia increases accumulation of technetium-99m-labeled liposomes in feline sarcomas. *Clin. Cancer Res.* **2000**, *6*, 3748–3755.
126. Kong, G.; Braun, R. D.; Dewhirst, M. W. Characterization of the effect of hyperthermia on nanoparticle extravasation from tumor vasculature. *Cancer Res.* **2001**, *61*, 3027–3032.
127. Chen, Q.; Krol, A.; Wright, A.; Needham, D.; Dewhirst, M.; Yuan, F. Tumor microvascular permeability is a key determinant for antivascular effects of doxorubicin encapsulated in a temperature sensitive liposome. *Int. J. Hyperthermia* **2008**, *24*, 475–482.
128. Liu, P.; Zhang, A.; Xu, Y.; Xu, L. X. Study of non-uniform nanoparticle liposome extravasation in tumour. *Int. J. Hyperthermia* **2005**, *21*, 259–270.
129. Huang, X.; Jain, P. K.; El-Sayed, I. H.; El-Sayed, M. A. Gold nanoparticles: interesting optical properties and recent applications in cancer diagnostics and therapy. *Nanomedicine* **2007**, *2*, 681–693.
130. Jain, P. K.; El-Sayed, I. H.; El-Sayed, M. A. Au nanoparticles target cancer. *Nano Today* **2007**, *2*, 18–29.
131. Huang, X.; Jain, P. K.; El-Sayed, I. H.; El-Sayed, M. A. Plasmonic photothermal therapy (PPTT) using gold nanoparticles. *Lasers Med. Sci.* **2008**, *23*, 217–228.
132. Hirsch, L. R.; Stafford, R. J.; Bankson, J. A.; Sershen, S. R.; Rivera, B.; Price, R. E.; Hazle, J. D.; Halas, N. J.; West, J. L. Nanoshell-mediated near-infrared thermal therapy of tumors under magnetic resonance guidance. *Proc. Natl. Acad. Sci. U.S.A.* **2003**, *100*, 13549–13554.
133. O'Neal, D. P.; Hirsch, L. R.; Halas, N. J.; Payne, J. D.; West, J. L. Photothermal tumor ablation in mice using near infrared-absorbing nanoparticles. *Cancer Lett.* **2004**, *209*, 171–176.
134. Stern, J. M.; Stanfield, J.; Lotan, Y.; Park, S.; Hsieh, J. T.; Cadeddu, J. A. Efficacy of laser-activated gold nanoshells in ablating prostate cancer cells in vitro. *J. Endourol.* **2007**, *21*, 939–943.
135. Stern, J. M.; Stanfield, J.; Kabbani, W.; Hsieh, J. T.; Cadeddu, J. A. Selective prostate cancer thermal ablation with laser activated gold nanoshells. *J. Urol.* **2008**, *179*, 748–753.
136. von Maltzahn, G.; Park, J. H.; Agrawal, A.; Bandaru, N. K.; Das, S. K.; Sailor, M. J.; Bhatia, S. N. Computationally guided photothermal tumor therapy using long-circulating gold nanorod antennas. *Cancer Res.* **2009**, *69*, 3892–3900.
137. Huang, X.; El-Sayed, I. H.; Qian, W.; El-Sayed, M. A. Cancer cell imaging and photothermal therapy in the near-infrared region by using gold nanorods. *J. Am. Chem. Soc.* **2006**, *128*, 2115–2120.
138. Dickerson, E. B.; Dreaden, E. C.; Huang, X.; El-Sayed, I. H.; Chu, H.; Pushpanketh, S.; McDonald, J. F.; El-Sayed, M. A. Gold nanorod assisted

Downloaded by MICHIGAN STATE UNIV on July 17, 2013 | http://pubs.acs.org
Publication Date (Web): July 8, 2013 | doi: 10.1021/bk-2013-1135.ch010

near-infrared plasmonic photothermal therapy (PPTT) of squamous cell carcinoma in mice. *Cancer Lett.* **2008**, *269*, 57–66.
139. Ponce, A. M.; Vujaskovic, Z.; Yuan, F.; Needham, D.; Dewhirst, M. W. Hyperthermia mediated liposomal drug delivery. *Int. J. Hyperthermia* **2006**, *22*, 205–213.
140. Tungjitkusolmun, S.; Staelin, S. T.; Haemmerich, D.; Tsai, J. Z.; Cao, H.; Webster, J. G.; Lee, F. T., Jr; Mahvi, D. M.; Vorperian, V. R. Three-dimensional finite-element analyses for radio-frequency hepatic tumor ablation. *IEEE Trans. Biomed. Eng.* **2002**, *49*, 3–9.
141. Diagaradjane, P.; Shetty, A.; Wang, J. C.; Elliott, A. M.; Schwartz, J.; Shentu, S.; Park, H. C.; Deorukhkar, A.; Stafford, R. J.; Cho, S. H. Modulation of in vivo tumor radiation response via gold nanoshell-mediated vascular-focused hyperthermia: characterizing an integrated antihypoxic and localized vascular disrupting targeting strategy. *Nano Lett.* **2008**, *8*, 1492–1500.
142. Park, J. H.; von Maltzahn, G.; Xu, M. J.; Fogal, V.; Kotamraju, V. R.; Ruoslahti, E.; Bhatia, S. N.; Sailor, M. J. Cooperative nanomaterial system to sensitize, target, and treat tumors. *Proc. Natl. Acad. Sci. U.S.A.* **2010**, *107*, 981–986.
143. Park, J. H.; Maltzahn, G. v.; Ong, L. L.; Centrone, A.; Hatton, T. A.; Ruoslahti, E.; Bhatia, S. N.; Sailor, M. J. Cooperative nanoparticles for tumor detection and photothermally triggered drug delivery. *Adv. Mater.* **2010**, *22*, 880–885.
144. Von Maltzahn, G.; Park, J. H.; Lin, K. Y.; Singh, N.; Schwöppe, C.; Mesters, R.; Berdel, W. E.; Ruoslahti, E.; Sailor, M. J.; Bhatia, S. N. Nanoparticles that communicate in vivo to amplify tumour targeting. *Nat. Mater.* **2011**, *10*, 545–552.
145. Arap, M. A.; Lahdenranta, J.; Mintz, P. J.; Hajitou, A.; Sarkis, Á.; Arap, W.; Pasqualini, R. Cell surface expression of the stress response chaperone GRP78 enables tumor targeting by circulating ligands. *Cancer Cell* **2004**, *6*, 275–284.
146. Larson, N.; Ray, A.; Malugin, A.; Pike, D. B.; Ghandehari, H. HPMA copolymer-aminohexylgeldanamycin conjugates targeting cell surface expressed GRP78 in prostate cancer. *Pharm. Res.* **2010**, *27*, 2683–2693.
147. Ray, A.; Larson, N.; Pike, D. B.; Gruner, M.; Naik, S.; Bauer, H.; Malugin, A.; Greish, K.; Ghandehari, H. Comparison of active and passive targeting of docetaxel for prostate cancer therapy by HPMA copolymer-RGDfK conjugates. *Mo.l Pharm.* **2011**, *8*, 1090–9.
148. Ito, A.; Saito, H.; Mitobe, K.; Minamiya, Y.; Takahashi, N.; Maruyama, K.; Motoyama, S.; Katayose, Y.; Ogawa, J. Inhibition of heat shock protein 90 sensitizes melanoma cells to thermosensitive ferromagnetic particle-mediated hyperthermia with low Curie temperature. *Cancer Sci.* **2009**, *100*, 558–64.
149. Takahashi, I.; Emi, Y.; Hasuda, S.; Kakeji, Y.; Maehara, Y.; Sugimachi, K. Clinical application of hyperthermia combined with anticancer drugs for the treatment of solid tumors. *Surgery* **2002**, *131*, S78–84.

Downloaded by MICHIGAN STATE UNIV on July 17, 2013 | http://pubs.acs.org
Publication Date (Web): July 8, 2013 | doi: 10.1021/bk-2013-1135.ch010

150. Istomin, Y. P.; Zhavrid, E. A.; Alexandrova, E. N.; Sergeyeva, O. P.; Petrovich, S. V. Dose enhancement effect of anticaner drugs associated with increased temperature in vitro. *Exp. Oncol.* **2008**, *30*, 56–9.
151. Chou, T. C.; Talalay, P. Quantitative analysis of dose-effect relationships: the combined effects of multiple drugs or enzyme inhibitors. *Adv. Enzyme Regul.* **1984**, *22*, 27–55.

Downloaded by MICHIGAN STATE UNIV on July 17, 2013 | http://pubs.acs.org
Publication Date (Web): July 8, 2013 | doi: 10.1021/bk-2013-1135.ch010


In Tailored Polymer Architectures for Pharmaceutical and Biomedical Applications; Scholz, C., et al.;
ACS Symposium Series; American Chemical Society: Washington, DC, 2013.

Downloaded by UNIV OF NORTH CAROLINA on July 20, 2013 | http://pubs.acs.org
Publication Date (Web): July 8, 2013 | doi: 10.1021/bk-2013-1135.ch011

## Chapter 11

# Fine-Tuning of Repeating Aminoethyelene Units in Poly(aspartamide) Side Chains for Enhanced siRNA Delivery

**Kanjiro Miyata,[1] R. James Christie,[1] Tomoya Suma,[2] Hiroyasu Takemoto,[3] Hirokuni Uchida,[3] Nobuhiro Nishiyama,[1,4] and Kazunori Kataoka[*,1,2,3]**

**[1]Center for Disease Biology and Integrative Medicine, Graduate School of Medicine; Graduate School of Engineering, The University of Tokyo, 7-3-1 Hongo, Bunokyo-ku, Tokyo 113-8656, Japan**
**[2]Department of Bioengineering and Graduate School of Engineering, The University of Tokyo, 7-3-1 Hongo, Bunokyo-ku, Tokyo 113-8656, Japan**
**[3]Department of Materials Engineering, Graduate School of Engineering, The University of Tokyo, 7-3-1 Hongo, Bunokyo-ku, Tokyo 113-8656, Japan**
**[4]Polymer Chemistry Division, Chemical Resources Laboratory, Tokyo Institute of Technology, R1-11, 4259 Nagatsuta, Midori-ku, Yokohama 226-8503, Japan**
**[*]E-mail: kataoka@bmw.t.u-tokyo.ac.jp.**

This chapter reviews our strategy for optimization of polycationic structures to improve siRNA delivery and reduce carrier toxicitiy. Improvement in carrier design is realized by modulating the number of repeating aminoethylene (RA) units in the side chain of a poly(aspartamide) derivative (PAsp(R)). Results reveal that the number of RA units in the PAsp(R) side chains affects their protonation behavior between extracellular and endosomal pHs in a distinctive "odd-even" manner. PAsp(R)s with even-numbered RA units induce acidic pH-responsive membrane disruption based on substantially increased protonation at the endosomal pH of 5.5. Ultimately, PAsp(R) with 4 RA units in each side chain demonstrated excellent transfection of siRNA due to accelerated endosomal escape as well as stable siRNA complexation.

© 2013 American Chemical Society
In Tailored Polymer Architectures for Pharmaceutical and Biomedical Applications; Scholz, C., et al.; ACS Symposium Series; American Chemical Society: Washington, DC, 2013.

# Introduction

Over the past two decades, a variety of polycationic materials have been developed to form polyion complexes (PICs) with oppositely charged nucleic acids, such as plasmid DNA (pDNA) and small interfering RNA (siRNA), for delivery into cells. Those efforts have revealed that PIC transfection efficiency is dramatically improved by specific polycationic structures (*1–4*). Indeed, PICs with poly(ethyleneimine) (PEI) or its derivatives demonstrate high transfection efficiency because of their ability to translocate from the endosome to the cytoplasm, triggered by protonation of their low pKa amines at the reduced endosomal pH (pH ~5.5) (*5*, *6*). In this regard, two possible mechanisms have been proposed to explain the endosomal escape behavior of such polycations. One is the "proton sponge effect", where endosome disruption occurs by increased osmotic pressure due to an influx of protons and chrolide ions into the endosomal compartment along with amine protonation (*5*, *6*). The other is disruption of endosomal membrane integrity by the binding of polycations to the negatively charged cellular membrane. Thus, polycations with increased cationic charges at the acidic endosomal pH can exert a stronger membrane disruptive effect (*4*, *6*). Despite efficient transfection in cultured cells, the considerable cytotoxicity of PEI has hampered its translation into a pharmaceutical agent, and thus, an optimized polycationic structure that allows more efficient transfection with lower cytotoxicity is needed.

In the present study, we demonstrate a systematic strategy for improved endosomal escape of siRNA with reduced carrier-associated toxicity. One of the major causes for the cytotoxicity of PEI is believed to be caused by cytoplasmic membrane disruption even at neutral pH, due to strong positive charges of PEI (*7*, *8*). Thus, it is assumed that less toxic endosomal escape should be realized by a polycation featuring a low degree of protonation (α) (or low density of cationic charges) at neutral pH but greatly increased α at acidic pH. Selective membrane disruption due to a larger change in the α between extracellular pH of 7.4 and endosomal pH of 5.5 (Δα) is targeted in the design of an endosome-escaping polycation. With regard to cationic structures with larger Δα values, we herein focus on the repeating aminoethylene (RA) unit (-$NHCH_2CH_2$-), which is the main repeating unit found in PEI.

When Δα values of a series of RA compounds are plotted against the number of repeating units in comparison with linear PEI (degree of polymerization (DP) of 520), a distinctive odd-even effect is found as shown in Figure 1, in which the Δα values converge with that of PEI in an up-and-down motion (*4*, *9*). Importantly, it is also found that "smaller" and "even"-numbered RA compounds possess a substantially larger Δα value.

To apply the above finding regarding larger Δα values to PIC-based siRNA delivery, we introduce the smaller and even numbered RA units, i.e. 2 and 4, into the side chains of a poly(aspartamide) derivative (PAsp(R)) by an aminolysis reaction of poly(β-benzyl L-aspartate) (PBLA) with diethylenetriamine (DET) and tetraethylenepentamine (TEP), respectively (*11*). Concurrently, control PAsp(R)s comprising an odd number of RA unit(s), i.e. 1 and 3, in the side chain are


In Tailored Polymer Architectures for Pharmaceutical and Biomedical Applications; Scholz, C., et al.;
ACS Symposium Series; American Chemical Society: Washington, DC, 2013.

Downloaded by UNIV OF NORTH CAROLINA on July 20, 2013 | http://pubs.acs.org
Publication Date (Web): July 8, 2013 | doi: 10.1021/bk-2013-1135.ch011

prepared using the same aminolysis reaction with ethylenediamine (EDA) and triethylenetetramine (TET), respectively (*11*). It is important to note that this aminolysis reaction provides a series of PAsp(R)s with the same DP and molecular weight distribution, as they are prepared from the same parent PBLA stock, which is necessary to accurately compare the effect of varying the RA units in polymer side chains. In the following sections, we describe the correlation between the Δα value of each PAsp(R) and its membrane disruptive effect, and then optimize the number of RA units for successful siRNA delivery with less toxic endosomal escape.

Downloaded by UNIV OF NORTH CAROLINA on July 20, 2013 | http://pubs.acs.org
Publication Date (Web): July 8, 2013 | doi: 10.1021/bk-2013-1135.ch011

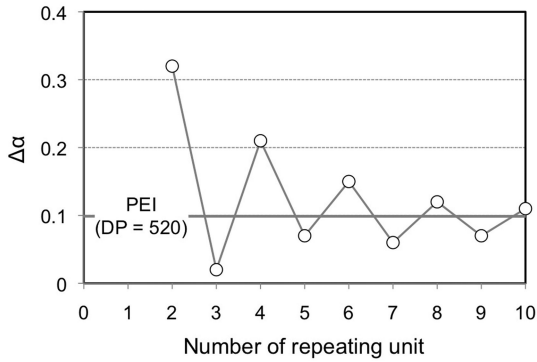


*Figure 1. Δα values of RA compounds plotted against the number of repeating aminoethylene units. The Δα values are calculated based on the Henderson-Hasselbalch equation with the pKa values of each RA compound as well as linear PEI with a DP of 520 (4, 9, 10).*

## Results and Discussion

PBLA with a DP of 92 and a Mw/Mn of 1.02 was used for the aminolysis reaction with EDA, DET, TET, or TEP to obtain the corresponding PAsp(R)s (termed PAsp(EDA), PAsp(DET), PAsp(TET), and PAsp(TEP), respectively) (Figure 2) (*11*, *12*). The prepared PAsp(R)s were subjected to a potentiometric titration at physiological ionic strength and temperature (150 mM NaCl and 37 °C) to determine their α values at pH 7.4 and 5.5 and their corresponding Δα values. As summarized in Table I, the obtained Δα values clearly exhibit an odd-even effect in the number of RA units in polymer side chains; PAsp(R)s bearing even-numbered RA units, i.e. PAsp(DET) and PAsp(TEP), showed a significantly larger Δα than those bearing odd-numbered RA units, i.e. PAsp(EDA) and PAsp(TET), as well as PEI. Thus, it is demonstrated that the unique protonation behavior of low molecular weight RA compounds (Figure 1) is maintained in the


In Tailored Polymer Architectures for Pharmaceutical and Biomedical Applications; Scholz, C., et al.;
ACS Symposium Series; American Chemical Society: Washington, DC, 2013.

side chain of PAsp(R) (Table I). Furthermore, the major protonated structures in each PAsp(R) side chain are estimated from the α values at pH 7.4 and 5.5. Corresponding to their large Δα values, PAsp(DET) and PAsp(TEP) distinctly alter their protonation state between pH 7.4 and 5.5 (Table I). It should be noted that the diprotonated diaminoethane structure ($-NH_2^+CH_2CH_2NH_3^+$) is adopted in PAsp(DET) and PAsp(TEP) at pH 5.5, providing a drastically increased cationic charge density.

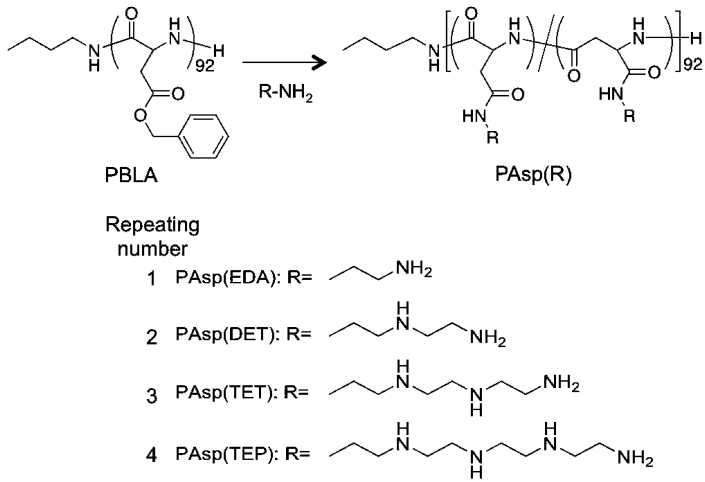


*Figure 2. Aminolysis reaction of PBLA with amine compounds and chemical structures of poly(aspartamide) derivatives bearing repeating aminoethylene units in the side chain.*

Next, the membrane disruptive effect of each PAsp(R) at pH 7.4 and 5.5 was quantitatively evaluated by a hemolysis assay with murine erythrocytes. In this assay, the amount of hemoglobin liberated from erythrocytes following incubation with PAsp(R) indicates the degree of membrane disruption activity (Figure 3) (*8*, *11*). At the extracellular pH of 7.4, all the PAsp(R)s show a low level of hemolysis activity (<5%), indicating appreciably decreased cytoplasmic membrane damage with the PAsp(R)s. This behavior is in sharp contrast with linear PEI (DP = ~500), which showed much higher hemolysis activity (~30%) (*11*). Interestingly, the odd-even effect is observed again for the hemolysis activity of PAsp(R)s at the endosomal pH of 5.5. PAsp(DET) and PAsp(TEP) with even-numbered RA units show significantly increased hemolysis activity at pH 5.5. This acidic pH-responsive membrane disruption behavior inherent to PAsp(DET) and PAsp(TEP) can be explained by their distinctively increased protonation state at pH 5.5, that is, acidic pH-selective generation of cationic structures with high charge density, such as the diprotonated diaminoethane (Table I), which can


In Tailored Polymer Architectures for Pharmaceutical and Biomedical Applications; Scholz, C., et al.;
ACS Symposium Series; American Chemical Society: Washington, DC, 2013.

Downloaded by UNIV OF NORTH CAROLINA on July 20, 2013 | http://pubs.acs.org
Publication Date (Web): July 8, 2013 | doi: 10.1021/bk-2013-1135.ch011

strongly bind to the cellular membrane (*8*). Note that the substantially lower pH-responsiveness of odd-numbered RA units is probably due to their alternating protonation state at pH 7.4, where further protonation is strongly suppressed by the neighboring protonated amines through electrostatic repulsion (*4*). The acidic pH-responsive membrane disruptive effect of PAsp(DET) and PAsp(TEP) observed in the hemolysis assay demonstrates their potential for endosomal membrane disruption with low cytoplasmic membrane damage.

Downloaded by UNIV OF NORTH CAROLINA on July 20, 2013 | http://pubs.acs.org
Publication Date (Web): July 8, 2013 | doi: 10.1021/bk-2013-1135.ch011

**Table I. α at pH 7.4 and 5.5, Δα, and representative protonation structure of each PAsp(R) side chain at pH 7.4 and 5.5 (*4*, *11*)**

| Polymer | RN* | α | | Δα | Representative protonation structure | |
|---|---|---|---|---|---|---|
| | | pH7.4 | pH5.5 | | pH7.4 | pH5.5 |
| PAsp(EDA) | 1 | 0.93 | 0.99 | 0.06 | 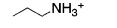 | 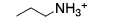 |
| PAsp(DET) | 2 | 0.51 | 0.82 | 0.31 | 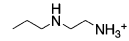 | 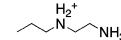 |
| PAsp(TET) | 3 | 0.56 | 0.66 | 0.10 | 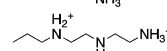 | 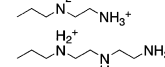 |
| PAsp(TEP) | 4 | 0.49 | 0.68 | 0.19 | 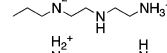 | 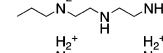 |

* RN: the repeating number of aminoethylene units in polymer side chain.

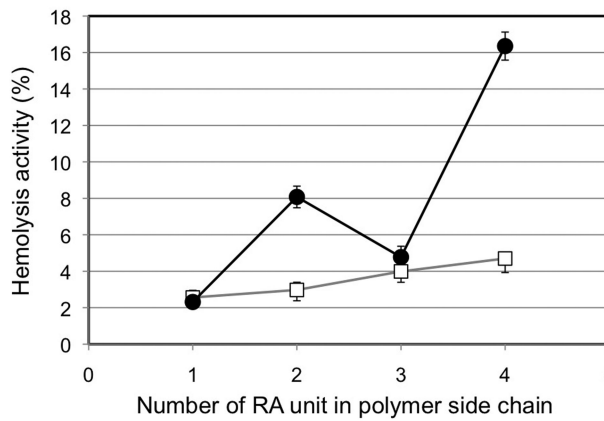


*Figure 3. Hemolysis activity of PAsp(R)s with varying numbers of RA units in polymer side chains at pH 7.4 (open square) and 5.5 (closed circle). The values for 100% and 0% are obtained from 0.2wt% Tween20 and a buffer solution without additives, respectively. Results are expressed as mean and SEM (N = 4) (11).*


In Tailored Polymer Architectures for Pharmaceutical and Biomedical Applications; Scholz, C., et al.;
ACS Symposium Series; American Chemical Society: Washington, DC, 2013.

Downloaded by UNIV OF NORTH CAROLINA on July 20, 2013 | http://pubs.acs.org
Publication Date (Web): July 8, 2013 | doi: 10.1021/bk-2013-1135.ch011

In order to determine siRNA delivery efficiency, each PAsp(R) was mixed with siRNA in a buffer solution to form PICs, and then applied to cultured murine melanoma cells stably expressing the luciferase gene (B16F10-Luc). In this assay, the luciferase gene is targeted for knockdown with anti-luciferase siRNA, and decreased luminescence indicates that gene silencing has occurred. Obviously, the gene silencing efficiency of siRNA PICs is affected by the number of RA units in the PAsp(R) side chains, where longer RA units allow more efficient gene silencing (Figure 4). Notably, PAsp(TEP) (or its PIC) achieves potent luciferase gene silencing with target siRNA, without affecting luciferase expression with non-target siRNA. This is in sharp constrast with linear PEI (DP = ~500), which considerably decreases the luciferase expression even with non-target siRNA, presumably due to severe cytotoxicity associated with the cytoplasmic membrane damage as indicated by the hemolysis assay. Excellent siRNA delivery with PAsp(TEP) is likely due to its acidic pH-responsive membrane disruption resulting in less toxic endosomal escape of siRNA PICs (Figure 3). Indeed, acceleated endosomal escape of PAsp(TEP) PICs is clearly oberved in cultured cells by a confocal laser scanning microscope using fluorescently-labeled siRNA and the late endosome/lysosome marker LysoTracker Green. Analyses of fluorescent signal overlap show that a major portion of labeled siRNAs observed in cells are not colocalized with the late endosomes/lysosomes (*12*).

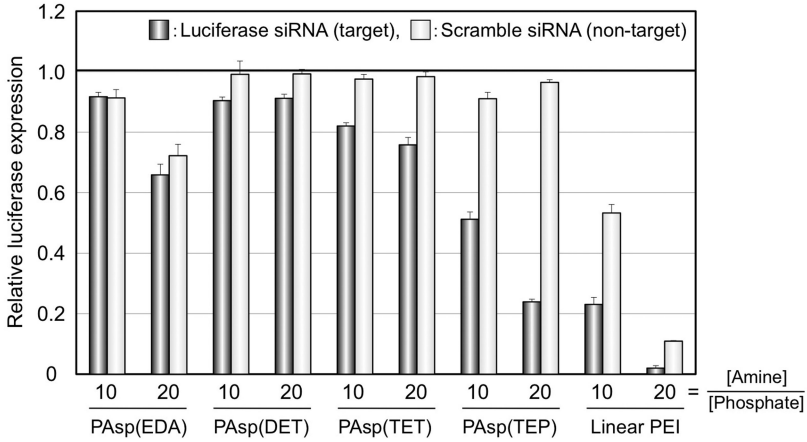


*Figure 4. Gene silencing efficinecy of PAsp(R)s containing varying numbers of RA units in polymer side chains in cultured B16F10-Luc cells. Each siRNA PIC was prepared at the ratio of [Amine in PAsp(R)]/[Phosphate in siRNA] = 10 or 20, and incubated with the cells at 100 nM siRNA for 48 h. Results are expressed as mean and SEM (N = 4). A part of this figure is used in the reference (12).*

With regard to the observed gene silencing results, the question arises as to why PAsp(DET) does not show a high level of gene silencing activity in spite of its acidic pH-responsitve membrane disruptive effect. Considering the fact that PAsp(DET) can significantly facilitate the endosomal escape of a much larger


In Tailored Polymer Architectures for Pharmaceutical and Biomedical Applications; Scholz, C., et al.;
ACS Symposium Series; American Chemical Society: Washington, DC, 2013.

nucleic acid, pDNA, inefficient siRNA delivery with PAsp(DET) could be due to events preceding endosomal entrapment, e.g., cellular uptake (*8*, *11*, *12*). A cellular uptake study using flow cytometric analysis reveals that the cellular uptake efficiency of siRNA PICs is enhanced with an increased number of RA units in PAsp(R) side chains (Figure 5). The cellular uptake profile corroborates well with gene silencing efficiency; higher cellular uptake of siRNA leads to more efficient gene silencing. It is worth mentioning that the cellular uptake efficiency of PAsp(EDA) and PAsp(DET) PICs is almost similar to that of naked siRNA, suggesting dissociation of their PICs in cell culture medium containing 10% fetal bovine serum, which could result in siRNA release prior to internalization. Thus, the stability of siRNA PICs with PAsp(DET) and PAsp(TEP) was further evaluated in culture medium by fluorescence correlation spectroscopy (FCS) with fluorescently-labeled siRNA (*12*). The hydrodynamic size of PAsp(DET) PICs decreases immediately (<10 min) to a size similar to that of naked siRNA (~6 nm), indicating dissociation of PICs and subsequent release of siRNA. In contrast, PAsp(TEP) PICs maintain their hydrodynamic size of over 100 nm for several hours, indicating that stable PIC formation allows efficent cellular uptake of the payload siRNA (*12*).

Downloaded by UNIV OF NORTH CAROLINA on July 20, 2013 | http://pubs.acs.org
Publication Date (Web): July 8, 2013 | doi: 10.1021/bk-2013-1135.ch011

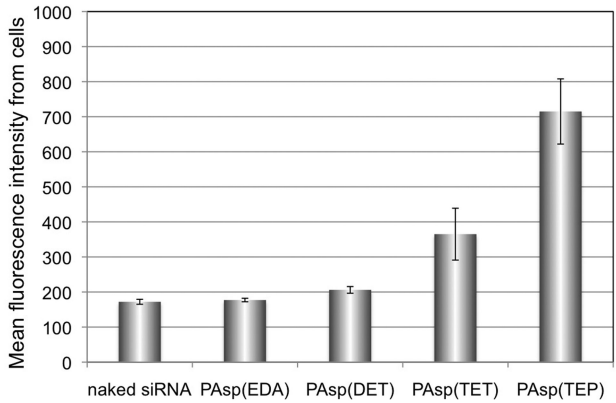


*Figure 5. Cellular uptake efficiency of fluorescently (Cy3)-labeled siRNA PICs prepared with PAsp(R) in cultured B16F10-Luc cells. The siRNA PICs were prepared at [Amine in PAsp(R)]/[Phosphate in siRNA] = 10 and incubated with cells at 100 nM siRNA for 12 h, followed by flow cytometric analysis. Results are expressed as the mean and SEM (N = 3). A part of this figure is used in the reference (12).*

The considerable difference in PIC stability between PAsp(DET) and PAsp(TEP) might be explained by the varying numbers (or densities) of cationic charges in PAsp(R) side chains. As shown in Table I, PAsp(TEP) side chains have twice as much cationic charges compared to PAsp(DET) at pH 7.4, which may contribute to stable complexation with siRNA through conformationally flexible and/or multipoint ion pair formation.


In Tailored Polymer Architectures for Pharmaceutical and Biomedical Applications; Scholz, C., et al.;
ACS Symposium Series; American Chemical Society: Washington, DC, 2013.

## Conclusions

In this chapter, the optimization of polycationic structures is demonstrated by varying the number of RA units in PAsp(R) side chains for successful siRNA delivery. Consequently, PAsp(TEP) with 4 RA units in the polymer side chains achieves strong sequence-specific gene silencing in cultured cells without considerable adverse side effects, presumably due to (i) accelerated endosomal escape associated with acidic pH-responsive membrane-disrupting functionality and (ii) efficient cellular uptake through stable complexation with siRNA. Thus, it is demonstrated that the fine-tuning of RA units in PAsp(R) side chain can dramatially improve the delivery ability of polycation-based PICs for enhanced siRNA delivery.

Downloaded by UNIV OF NORTH CAROLINA on July 20, 2013 | http://pubs.acs.org
Publication Date (Web): July 8, 2013 | doi: 10.1021/bk-2013-1135.ch011

## Acknowledgments

This work was finantially supported by the Funding Program for World-Leading Innovative R&D on Science and Technology (FIRST) from the Japan Society for the Promotion of Science (JSPS).

## References

1. Kabanov, A. V.; Kabanov, V. A. *Bioconjugate Chem.* **1995**, *6*, 7–20.
2. Kakizawa, Y.; Kataoka, K. *Adv. Drug Delivery Rev.* **2002**, *54*, 203–222.
3. Wagner, E. *Acc. Chem. Res.* **2012**, *45*, 1005–1013.
4. Miyata, K.; Nishiyama, N.; Kataoka, K. *Chem. Soc. Rev.* **2012**, *41*, 2562–2574.
5. Boussif, O.; Lezoualch, F.; Zanta, M. A.; Mergny, M. D.; Scherman, D.; Demeneix, B.; Behr, J. P. *Proc. Natl. Acad. Sci. U.S.A.* **1995**, *92*, 7297–7301.
6. Neu, M.; Fischer, D.; Kissel, T. *J. Gene Med.* **2005**, *7*, 992–1009.
7. Fischer, D.; Li, Y.; Ahlemeyer, B.; Krieglstein, J.; Kissel, T. *Biomaterials* **2003**, *24*, 1121–1131.
8. Miyata, K.; Oba, M.; Nakanishi, M.; Fukushima, S.; Yamasaki, Y.; Koyama, H.; Nishiyama, N.; Kataoka, K. *J. Am. Chem. Soc.* **2008**, *130*, 16287–16294.
9. Bencini, A.; Bianchi, A.; Garcia-Espana, E.; Micheloni, M.; Ramirez, J. A. *Coord. Chem. Rev.* **1999**, *188*, 97–156.
10. Smits, R. G.; Koper, G. J. M.; Mandel, M. *J. Phys. Chem.* **1993**, *97*, 5745–5751.
11. Uchida, H.; Miyata, K.; Oba, M.; Ishii, T.; Suma, T.; Itaka, K.; Nishiyama, N.; Kataoka, K. *J. Am. Chem. Soc.* **2011**, *133*, 15524–15532.
12. Suma, T.; Miyata, K.; Ishii, T.; Uchida, S.; Uchida, H.; Itaka, K.; Nishiyama, N.; Kataoka, K. *Biomaterials* **2012**, *33*, 2770–2779.

Downloaded by MICHIGAN STATE UNIV on July 17, 2013 | http://pubs.acs.org
Publication Date (Web): July 8, 2013 | doi: 10.1021/bk-2013-1135.ch012

## Chapter 12

# Dendrimer-Based RNA Interference Delivery for Cancer Therapy

**Leyuan Xu,[1] W. Andrew Yeudall,[2,3] and Hu Yang[*,1,3]**

**[1]Department of Biomedical Engineering, Virginia Commonwealth University, Richmond, Virginia 23284, United States**
**[2]Philips Institute of Oral and Craniofacial Molecular Biology, Virginia Commonwealth University, Richmond, VA 23298, United States**
**[3]Massey Cancer Center, Virginia Commonwealth University, Richmond, Virginia 23298, United States**
**[*]E-mail: hyang2@vcu.edu.**

RNA interference (RNAi) has emerged as a promising tool for cancer treatment. A strenuous ongoing effort for translation of RNAi into clinically acceptable therapy is the development of vectors for efficient and targeted RNAi delivery. In this chapter, we review RNAi-based cancer treatment and the utility of dendrimers in RNAi delivery.

To date, small-molecular-weight drugs remain dominant on the pharmaceutical market. In general, they interact with proteins such as enzymes within the cell or receptors on the cell surface to exert their desired therapeutic activities for treatment of various diseases. As for cancer chemotherapy, most of anticancer drugs are designed to be cytotoxic and induce apoptosis in cells. Nonetheless, lack of tumor specificity and acquisition of drug resistance are common problems associated with anticancer drugs and cause poor clinical outcomes. It is an important approach to modify existing drugs to improve their specificity and potency. Although discovery and development of new cytotoxic agents for cancer therapy remains a key focus, advances in fundamental understanding of cancer biology and identification of molecular targets have brought about new concepts in anticancer drug design and paved the way for development of molecularly targeted therapeutics. A paradigm shift in design of anticancer therapeutics has been brought about by a groundbreaking

© 2013 American Chemical Society
In Tailored Polymer Architectures for Pharmaceutical and Biomedical Applications; Scholz, C., et al.; ACS Symposium Series; American Chemical Society: Washington, DC, 2013.

discovery—RNA interference (RNAi) (*1*). In this chapter, we review RNAi for cancer treatment as well as the latest progress in RNAi delivery on the basis of dendrimers, which are an important class of macromolecules possessing highly branched nanoscale architectures with a high density of terminal groups on the surface.

## Brief Overview of RNAi

RNAi refers to the process of gene silencing (Figure 1) (*2*). In eukaryotic cells, the RNA endonucleases Drosha and Dicer recognize and cleave double-stranded RNA (dsRNA) into short double-stranded segment (~20-25 nt), which are known as small interfering RNA (siRNA) duplex, composed of a sense strand and an antisense strand. The siRNA duplex is phosphorylated at the 5′ end and hydroxylated at the 3′ end with two nucleotides overhung and, in turn, contributes to formation of the pre-RNA-induced silencing complex (pre-RISC), which includes (in mammals) one of four *Argonaute* proteins (AGO1-4) (*3*). Within the pre-RISC, the siRNA duplex is unwound, the sense strand is degraded, and the antisense or guide strand is integrated into the RISC. Once the bound siRNA within the RISC recognizes and hybridizes to its complementary messenger RNA (mRNA), the specific nucleases in the RISC then cleave the mRNA/siRNA hybrid. Subsequently, the cleaved mRNA is destroyed by the cells. Naturally, as mRNA encodes information for production of cellular proteins, its degradation induced by RNAi directly reduces expression of the corresponding protein (*4*).

For experimental (and therapeutic) purposes, two methods are commonly used to produce siRNAs. The first is to synthesize a dsRNA corresponding to the chosen sequence within the target gene. This dsRNA is then inserted into the cell, usually by transfection by any of the standard methods available. An alternative method is to generate a dsRNA corresponding to the target sequence in vivo from a precursor small hairpin RNA (shRNA). This involves synthesis of a double-stranded DNA of around 70bp, which is designed to contain tandem segments of both sense and antisense sequences corresponding to the target gene. This is ligated into a eukaryotic expression vector downstream of a suitable promoter (*e.g.*, U6), and is delivered to the cell. Once the vector is present in the cell and transcribed in the nucleus, it forms a dsRNA in a "hairpin" structure. This shRNA is transported into the cytoplasm and is processed, leading to the generation of a functional RISC.

## RNAi in Cancer Therapy

Cell surface receptors such as receptor tyrosine kinases, anti-apoptotic genes, survival factors or key participants in signaling pathways are essential for processes such as cell division, proliferation, survival and migration (*4*). Constant activation of these signaling pathways or overexpression of signaling molecules can lead to unchecked cell proliferation and migration, resulting in tumorigenesis.

Downloaded by MICHIGAN STATE UNIV on July 17, 2013 | http://pubs.acs.org
Publication Date (Web): July 8, 2013 | doi: 10.1021/bk-2013-1135.ch012


In Tailored Polymer Architectures for Pharmaceutical and Biomedical Applications; Scholz, C., et al.;
ACS Symposium Series; American Chemical Society: Washington, DC, 2013.

Downloaded by MICHIGAN STATE UNIV on July 17, 2013 | http://pubs.acs.org
Publication Date (Web): July 8, 2013 | doi: 10.1021/bk-2013-1135.ch012

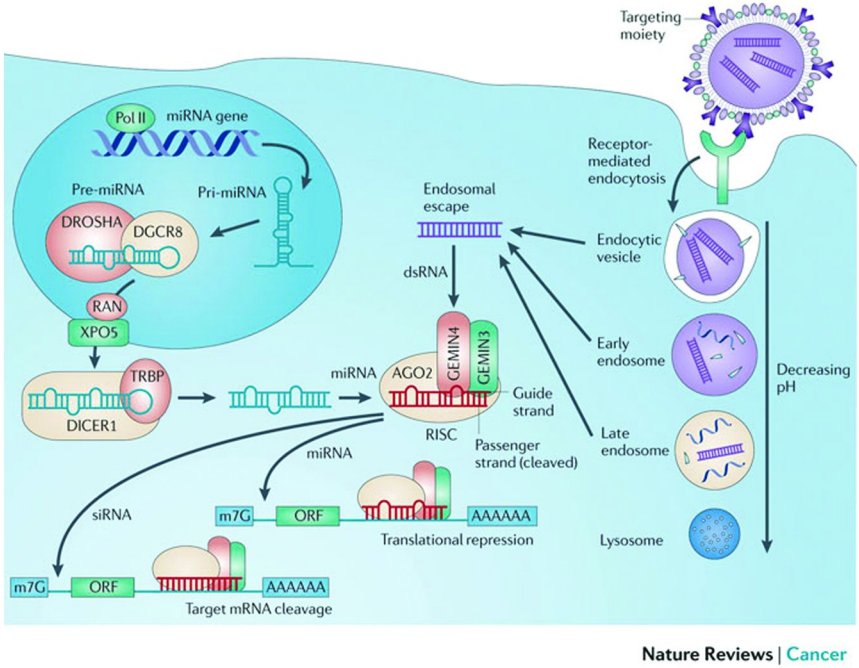


*Figure 1. Mechanism of RNAi following intracellular dsRNA delivery. (Reproduced from reference (2). Copyright 2013 Macmillan Publishers Ltd.)*

Ligands such as epidermal growth factor (EGF) stimulate EGFR dimerization and activate the intrinsic intracellular tyrosine kinase activity of the receptor (Figure 2) (*5*). This activation event enables recruitment of SH2-containing proteins to phosphotyrosine residues in the cytoplasmic portion of the receptor, including the adapter protein Grb2, phosphoinositide 3-OH kinase (PI3K) and phospholipase Cγ (*6*). These mediators trigger multiple signal transduction pathways such as MAPK, Akt and JNK pathways, leading to DNA synthesis and cell proliferation. EGFR overexpression on tumor cells, or mutation, can lead to hyperactivation and result in uncontrolled cell division that is characteristic of malignant disease. Based on the proposed role of EGFR as an oncoprotein, several anticancer therapeutics directly against EGFR have been developed, including the small molecule inhibitors Gefitinib and Erlotinib and the anti-EGFR antibody, Cetuximab, which have shown some utility in the treatment of several human cancers. In addition, EGFR-mediated drug delivery systems can be taken up more selectively by EGFR positive cells via EGFR-dependent endocytosis (*7*).


In Tailored Polymer Architectures for Pharmaceutical and Biomedical Applications; Scholz, C., et al.;
ACS Symposium Series; American Chemical Society: Washington, DC, 2013.

Downloaded by MICHIGAN STATE UNIV on July 17, 2013 | http://pubs.acs.org
Publication Date (Web): July 8, 2013 | doi: 10.1021/bk-2013-1135.ch012

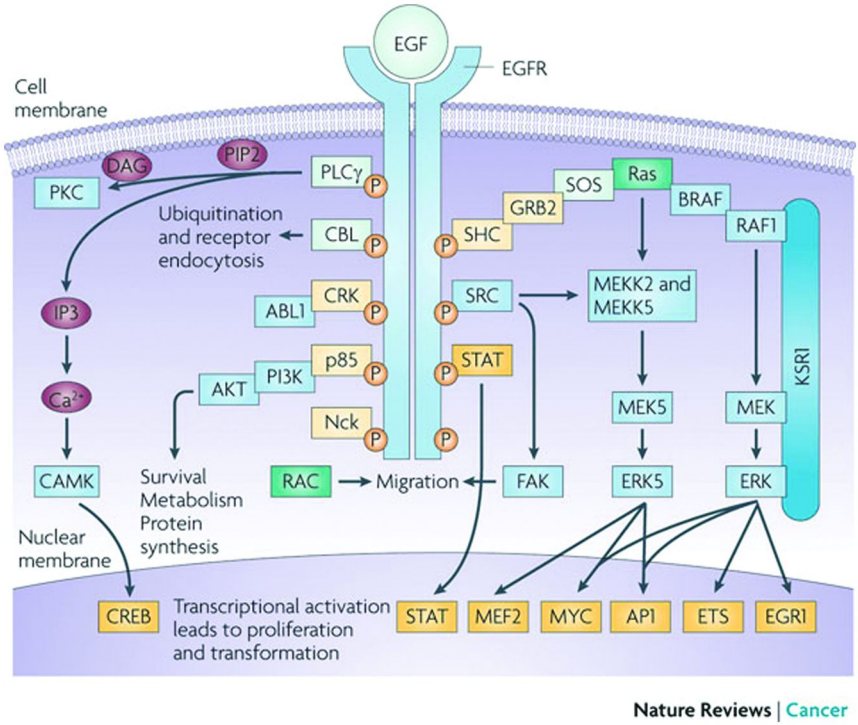


*Figure 2. The epidermal growth factor receptor signaling pathway. (Reproduced from reference (5). Copyright 2013 Macmillan Publishers Ltd.)*

Inhibiting EGFR signaling or blocking its pathway intermediates during carcinogenesis offers a new strategy to treat cancer. For instance, Wang et al. reported the role of a signaling intermediate, EPS8, in human head and neck squamous cell carcinoma (HNSCC) progression (*8*, *9*). Overexpression of EPS8 in tumor cells results in increased cell proliferation and migration along with elevated expression of matrix metalloprotease MMP-9, which is dependent on protein kinase B (Akt) activity. They found that EPS8 knockdown decreases tumorigenicity and MMP-9 expression. Furthermore, in clinical samples of squamous cell carcinoma, EPS8 expression was observed at elevated levels and correlated to MMP-9 expression (Figure 3) (*8*, *9*). Therefore, EPS8 may be a good candidate target for RNAi in the treatment of some cancers. In fact, a variety of molecular targets (Table I) have been identified and RNAi knockdown of those targets has been investigated for treating a broad spectrum of cancers including liver cancer, prostate cancer, *etc* (*10*). These delivery systems have been shown to improve siRNA stability and cancer-specificity, thus minimizing off-target and nonspecific immune stimulations.


In Tailored Polymer Architectures for Pharmaceutical and Biomedical Applications; Scholz, C., et al.;
ACS Symposium Series; American Chemical Society: Washington, DC, 2013.

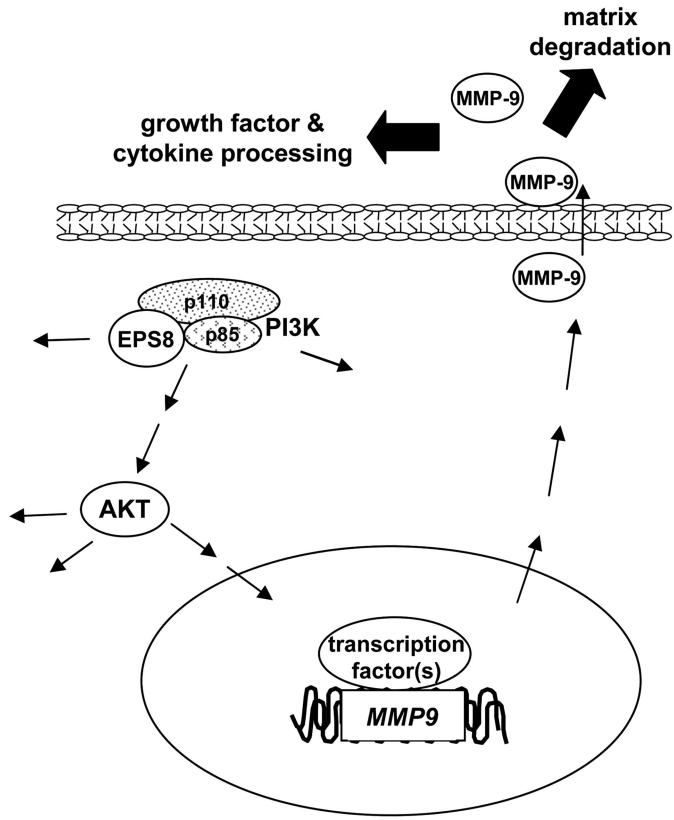


*Figure 3. Overexpression of EPS8 potentiates AKT activation in a PI3K-dependent manner, resulting in elevated transcription of MMP9 by a yet-to-be-determined mechanism. This results in enhanced MMP-9 activity, which is available to participate in degradation of extracellular matrix, thereby enhancing invasion. MMP-9 may also process growth factors, cytokines and chemokines, further stimulating cell growth and motility. (Reproduced from reference (9). Copyright 2013 Oxford University Press.)*

Downloaded by MICHIGAN STATE UNIV on July 17, 2013 | http://pubs.acs.org
Publication Date (Web): July 8, 2013 | doi: 10.1021/bk-2013-1135.ch012

Currently, clinical trials are ongoing to tackle cancer via RNAi-based gene therapies. Trial CALAA-01, acclaimed as the first targeted delivery of siRNA in humans (*11*), examined a targeted delivery system to deliver siRNA to reduce expression of the M2 subunit of ribonucleotide reductase (R2) (RRM2) to achieve inhibition of tumor growth. The R2 siRNA was complexed with cationic cyclodextrin and stabilized with adamantane polyethylene glycol (AD-PEG). A targeting ligand, human transferrin (Tf), was coupled to AD-PEG for selective delivery and enhanced uptake via transferrin receptor-mediated endocytosis (*12*). The evidence suggests that systematic administration of siRNA can result in specific gene (RRM2) inhibition at both mRNA and protein

levels at the site predicted for an RNAi mechanism of action. Analysis of tumor biopsies from melanoma patients following the treatment revealed that amounts of nanoparticles accumulated intracellularly correlated well with doses of nanoparticles administered.

**Table I. RNAi for Cancer Therapy. SOURCE: adapted from reference (*10*). Copyright 2013 Elsevier.**

| *Cancer type* | *Target gene* | *Administration Route* | *Ref (s).* |
|---|---|---|---|
| Liver | Bcl-2 | i.v. | (*14*) |
| Prostate | Integrin αv | i.t. | (*15*) |
| | CD31 | i.v. | (*16*) |
| | Bcl-2 | i.t. | (*14*) |
| | Raf-1 | i.v. | (*17*) |
| Breast | c-raf | i.v. | (*18*) |
| | RhoA | i.v. | (*19*) |
| | Her-2 | i.v. | (*20*) |
| Ovarian | EphA2 | i.v./i.p. | (*21*, *22*) |
| | FAK | i.p. | (*23*) |
| | ADRB2 | i.p. | (*24*) |
| | IL-8 | i.p. | (*25*) |
| | Her-2 | i.p. | (*26*) |
| Lung | EGFR | i.v. | (*27*) |
| | Akt1 | Inhalation | (*28*) |
| | TERT | i.t. | (*29*) |
| Gastric | VEGF | i.t. | (*30*) |
| Nasopharyngeal | Her-2 | i.t. | (*31*) |
| Glioblastoma | PTN | i.c. | (*32*) |
| Cervical | HPV18 type E6 and E7 | i.t. | (*33*) |
| Metastatic Ewing's sarcoma | EWS-FLI1 | i.v. | (*34*) |
| Melanoma | c-myc, MDM2, VEGF | i.t./i.v. | (*35*) |
| | EGFP | i.t. | (*36*) |

ABBREVIATIONS: i.v., intravenous; i.p., intraperitoneral; i.t., intratumoral; i.c., intracerebral.

Downloaded by MICHIGAN STATE UNIV on July 17, 2013 | http://pubs.acs.org
Publication Date (Web): July 8, 2013 | doi: 10.1021/bk-2013-1135.ch012


In Tailored Polymer Architectures for Pharmaceutical and Biomedical Applications; Scholz, C., et al.;
ACS Symposium Series; American Chemical Society: Washington, DC, 2013.

Another trial evaluated bi-shRNA-furin and granulocyte macrophage colony stimulating factor (GM-CSF) augmented autologous tumor cell vaccine for advanced cancer (FANG). The FANG vector was introduced to autologous tumor cells ex-vivo by electroporation, enabling transcription of the bi-shRNA furin and expression of the GM-CSF protein. Transfected tumor cells were irradiated, aliquoted, and cryopreserved until the time of injection (*13*). Autologous FANG vaccine produced both recombinant human GM-CSF(rhGMCSF) and bi-shRNAfurin. The GM-CSF protein helped recruit immune effectors to the site of intradermal injection and promote antigen presentation, while bi-shRNAfurin inhibited furin protein production at the post transcriptional and translational levels and consequently decreased both TGFβ1 and TGFβ2 expression. As a result of the phase I trial, local immunosuppression was reduced and tumor antigens and major histocompatibility complex (MHC) proteins promoted. Phase II trial in advanced melanoma has begun recently to examine immune responses to FANG.

Downloaded by MICHIGAN STATE UNIV on July 17, 2013 | http://pubs.acs.org
Publication Date (Web): July 8, 2013 | doi: 10.1021/bk-2013-1135.ch012

## Challenges to RNAi Therapy

In spite of high gene silencing potency, RNAi can cause specific and non-specific off-target effects. Specific off-target effects are usually caused by unintended suppression of an unrelated mRNA due to a certain degree of siRNA complementarity to unintended mRNAs. Nonspecific off-target effects include activating an immune response and toxicity (activation of Toll-like receptors) triggered directly by the siRNA/shRNA plasmid itself or the delivery system (*37*, *38*).

In addition to the off-target effects that impede therapeutic efficacy, barriers exist that reduce bioavailability of RNAi therapeutics. First, RNA encounters RNA-degrading ribonucleases present in the extracellular fluids during transport. Second, RNA may be absorbed nonspecifically by the liver, accessible mucosal surfaces, or body cavities (*4*). Third, RNA by itself has no specificity towards target cells and hardly enters the cell due to the presence of negative charges on the cell surface.

To address the barriers facing RNAi therapy, the use of vectors to deliver RNAi therapeutics has become an important approach. Vectors are expected to protect these molecules from degradation, reduce non-specific absorption, enhance cellular uptake and specificity, and facilitate transfection. As such, vectors need to be biocompatible and nonimmunogenic. In general, vectors are divided into two categories: viral vectors and synthetic vectors. Viral vectors have evolved functions to enter cells efficiently, but safety concerns have restricted their practical application. Synthetic vectors, particularly cationic polymers (*39–41*), have attracted considerable attention for gene transfer as they can potentially avoid toxicity and immunogenicity, provide high carrying capacity, achieve prolonged delivery, and allow low-cost manufacturing (*42*, *43*). Nonetheless, delivery efficiency of synthetic vectors for RNAi therapy is affected by factors such as assembly of nucleic acid/vector polyplexes, specificity,


In Tailored Polymer Architectures for Pharmaceutical and Biomedical Applications; Scholz, C., et al.;
ACS Symposium Series; American Chemical Society: Washington, DC, 2013.

uptake, endosomal escape, disassembly of polyplexes, and stability of siRNA in the cytoplasm (*43*). Endocytosis is a process involving multiple steps: binding, internalization, formation of endosomes, fusion with lysosomes, and lysis (*44*). Following endocytosis, endosomal escape is an important step that affects transfection efficiency.

In the past, a variety of synthetic vectors have been developed or studied to deliver DNA plasmids. Those vectors can be readily applied to deliver RNAi therapeutics in that both types of genetic material are packaged with vectors through electrostatic interactions. Because of the distinct tumor microenvironment and the unique surface characteristics of cancer cells, e.g., overexpression of EGFR, it seems practical to develop vectors to deliver RNAi molecules specifically to tumors through targeted delivery to avoid undesirable gene silencing effects on normal cells.

Downloaded by MICHIGAN STATE UNIV on July 17, 2013 | http://pubs.acs.org
Publication Date (Web): July 8, 2013 | doi: 10.1021/bk-2013-1135.ch012

## Dendrimers for RNAi Delivery

Numerous types of synthetic vectors and nanoparticulate delivery systems have been developed for delivery of nucleic acids including DNA and RNA. In this chapter, we review RNAi delivery on the basis of one important class of nanovectors, namely dendrimers.

### Structures and Properties of Dendrimers

Different from traditional polymers, dendrimers have a highly branched, three-dimensional architecture with very low polydispersity and high functionality, comprising an initiator core, several interior layers composed of repeating units, and multiple active terminal groups (Figure 4) (*45–48*). The number of branches and surface groups increase exponentially with increasing generation (G). The presence of numerous surface groups allows for high drug payload and multifunctionality. Dendrimer toxicity is generation- and dose-dependent (*49*). Higher generations tend to be more toxic and carboxylate-or hydroxyl-terminated PAMAM dendrimers are more cytocompatible than amine-terminated dendrimers. Dendrimers have been recognized as the most versatile compositionally and structurally controlled nanoscale building blocks throughout the fields of engineering, materials science, chemistry, and biology.

By virtue of their unique structures and properties, polycationic polyamidoamine (PAMAM) dendrimers have been extensively investigated for gene transfer (*45*, *50–52*). Polycationic dendrimers can form compacted polyplexes with nucleic acids in physiology pH. Furthermore, dendrimers can act as a "proton-sponge" to facilitate the escape of polyplexes from endosomes and lysosomes (*53*, *54*). In general, "proton-sponge" polymers contain a large number of secondary and tertiary amines with a $pK_a$ at or below physiological pH. They can adsorb protons released from ATPase and subsequently cause osmotic swelling and rupture of the endosome membrane to release the entrapped polyplexes.


In Tailored Polymer Architectures for Pharmaceutical and Biomedical Applications; Scholz, C., et al.;
ACS Symposium Series; American Chemical Society: Washington, DC, 2013.

Additionally, dendrimers facilitate transport of therapeutics across various cell membranes or biological barriers. For instance, PAMAM dendrimers rapidly cross adult rat intestine at high serosal transfer rates following endocytosis-mediated cellular internalization. Surface groups and molecular mass affect the dynamics of dendrimer cellular entry.

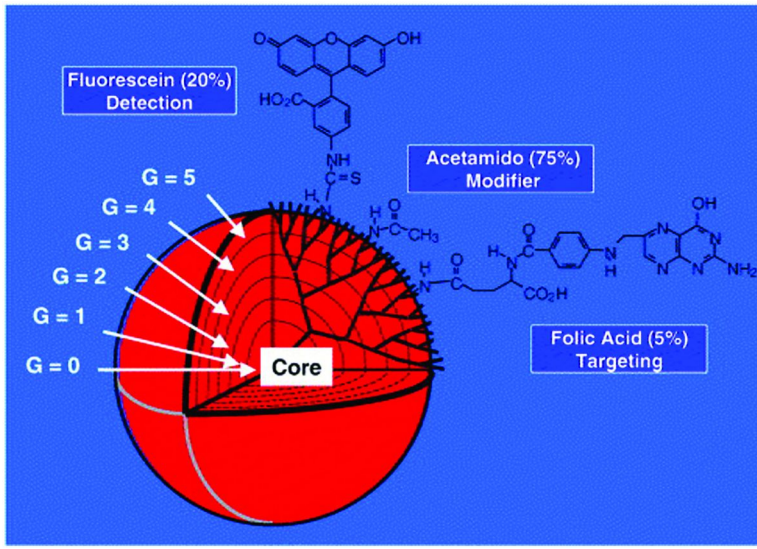


*Figure 4. Schematic presentation of dendrimers as nano-scaffold for the attachment of cell-specific ligands, modifiers, and fluorescence tags. Abbreviation: G: generation. (Reproduced from reference (48). Copyright 2013 Elsevier.)*

Downloaded by MICHIGAN STATE UNIV on July 17, 2013 | http://pubs.acs.org
Publication Date (Web): July 8, 2013 | doi: 10.1021/bk-2013-1135.ch012

## Examples of Dendrimer-Mediated RNAi Delivery

Dendrimers can be functionalized to carry a variety of functional moieties to enhance knockdown efficiency, achieve targeted delivery, and reduce off-target effects.

### *PEGylated Dendrimers*

Tang et al. reported the application of PEG-modified PAMAM dendrimers for siRNA delivery (*55*). They modified PAMAM dendrimer generations 5 and generation 6 with MPEG-5000. They found that PEG-modified dendrimers were capable of protecting complexed siRNA from RNase digestion. The in vitro studies revealed that PEG-modified dendrimers achieved similar knockdown effects in Cos7 cells compared to Lipofectamine 2000. They went on to study siRNA knockdown by the synthesized PEGylated PAMAM dendrimers in


In Tailored Polymer Architectures for Pharmaceutical and Biomedical Applications; Scholz, C., et al.;
ACS Symposium Series; American Chemical Society: Washington, DC, 2013.

animals. In this study, the authors intramuscularly injected PEG-modified dendrimer/siRNA against green fluorescence protein (GFP) polyplexes to C57BL/6 mice transiently infected with adenovirus or GFP transgenic mice and observed GFP suppression in both models. Interestingly, the authors noted that PEGylated PAMAM dendrimer G5.0 has higher transfection efficiency than PEGylated PAMAM dendrimer G6.0 and attributed it to a more flexible structure and a smaller size of G5.0 in contrast to G6.0. A structurally flexible vector tends to enhance compaction of siRNA and increase the fusion of the polyplexes with the cell membrane. A smaller size of polyplexes would bring about increased cellular uptake and enhanced release of the siRNA in the cell.

Downloaded by MICHIGAN STATE UNIV on July 17, 2013 | http://pubs.acs.org
Publication Date (Web): July 8, 2013 | doi: 10.1021/bk-2013-1135.ch012

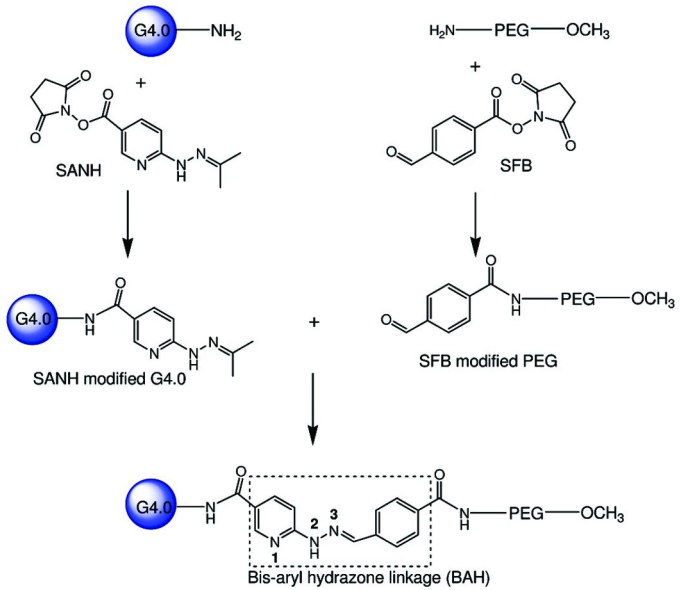


*Figure 5. Synthesis of PEGylated PAMAM dendrimers with BAH linkages. (Reproduced from reference (56). Copyright 2013 American Chemical Society.)*

*PEGylated Dendrimers with Bis-aryl Hydrazone (BAH) Linkages*

The "proton sponge" property conferred by amines in the dendrimer is crucial for successful gene delivery. However, surface modification of PAMAM dendrimers with PEG or other moieties has to utilize surface amine groups and inadvertently impairs dendrimer buffering capacity. To address this issue, Yuan et al. employed a new methodology to make PEGylated dendrimers by using a bis-aryl hydrazone (BAH) linker (Figure 5) (*56*). To use BAH to connect PEG to the dendrimer, PAMAM dendrimer G4.0 is activated with succinimidyl

4-hydrazinonicotinate acetone hydrazone (SANH), whereas monofunctional methoxypolyethylene glycol amine (PEG5000) is activated with succinimidyl 4-formylbenzoate (SFB). A subsequent coupling reaction between SFB-activated PEG and SANH-activated PAMAM forms a bis-aryl hydrazone linkage. It was found that use of BAH linkage simultaneously enables a high degree of PEGylation and an increase in buffering capacity of the dendrimer vector. Higher transfection efficiency was also observed for this vector compared to unmodified dendrimer (*56*). Although the utility of this new PEGylated dendrimer for RNAi delivery has yet to be reported, this new linker can be broadly used for dendrimer surface modification without compromising buffering capacity required for endosomal escape during RNAi intracellular transport.

Downloaded by MICHIGAN STATE UNIV on July 17, 2013 | http://pubs.acs.org
Publication Date (Web): July 8, 2013 | doi: 10.1021/bk-2013-1135.ch012

*Dendrimer-EGF Conjugates*

Epidermal growth factor receptor (EGFR) is preferentially overexpressed in multiple human solid tumors, including cancers of head and neck, lung, breast, colon, and brain. Tumor cells expressing a high level of EGFR can be more specifically targeted by a delivery system carrying EGFR ligand such as EGF. Following this rationale, Yuan et al. designed a dendrimer-EGF delivery system, in which EGF is covalently conjugated to PAMAM dendrimer G4.0 through a triglycine spacer (Figure 6) (*7*). They observed that dendrimer-EGF conjugates facilitated intracellular uptake in an EGFR-dependent manner without triggering EGFR signaling pathways in EGFR-overexpressing cells. Furthermore, they confirmed that dendrimer-EGF conjugates improved siRNA delivery and gene knockdown efficiency compared to commercial vectors and to unconjugated dendrimers. Particularly, they examined delivery of siRNA against yellow fluorescent protein (YFP siRNA) and shRNA against vimentin (shVIM). Approximately 70% suppression of YFP expression in YFP-expressing cells was achieved while approximately 40% suppression of vimentin expression was achieved. The enhanced knockdown efficiency of dendrimer-EGF conjugates compared to unmodified dendrimer or TransIT (a commercial keratinocyte transfection reagent) transfections indicates this delivery system is suitable for introduction of nucleic acids into cells via a receptor-targeted mechanism (*7*).

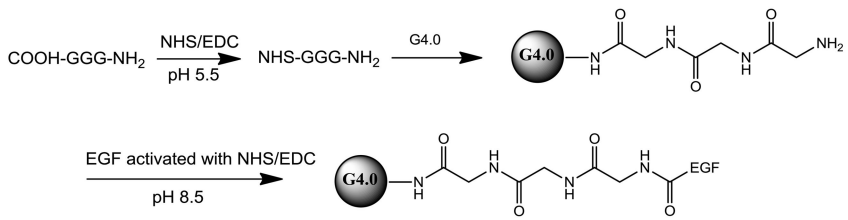


*Figure 6. Synthesis of dendrimer-EGF conjugates through triglycine spacer (GGG). (Reproduced from reference (7). Copyright 2013 Elsevier.)*


In Tailored Polymer Architectures for Pharmaceutical and Biomedical Applications; Scholz, C., et al.;
ACS Symposium Series; American Chemical Society: Washington, DC, 2013.

*Dendriworms*

Agrawal et al. developed a modular platform, namely dendriworm, for siRNA delivery (Figure 7) (*57*). To make dendriworms, cystamine core PAMAM dendrimers (generation 4) were reduced to dendrons and then coupled to near-infrared dye-labeled iron oxide nanoworms via a heterobifunctional linker, N-succinimidyl 3-(2-pyridyldithio)-propionate (SPDP). SPDP is a reducible linker, allowing rapid removal of dendrons from the conjugates in the reducing intracellular environment, which in turn helps improve siRNA delivery and diffusion inside the cell. The obtained dendriworms had 16-25 mV zeta potential and 80-110 nm hydrodynamic diameter. The authors used dendriworms to deliver EGFR siRNA for brain cancer treatment. In vitro studies show that EGFR expression in human glioblastoma cells was reduced by 70-80%, which was 2.5-fold more efficient than commercial cationic lipids. In particular, 0.5 mg/ml of dendriworm (11 μg of total siRNA) was infused into the EGFR-driven transgenic mice of glioblastoma in a period of 7 days. A significant amount of nanoparticles were delivered to the brain and lead to suppression of EGFR in the tumor.

Downloaded by MICHIGAN STATE UNIV on July 17, 2013 | http://pubs.acs.org
Publication Date (Web): July 8, 2013 | doi: 10.1021/bk-2013-1135.ch012

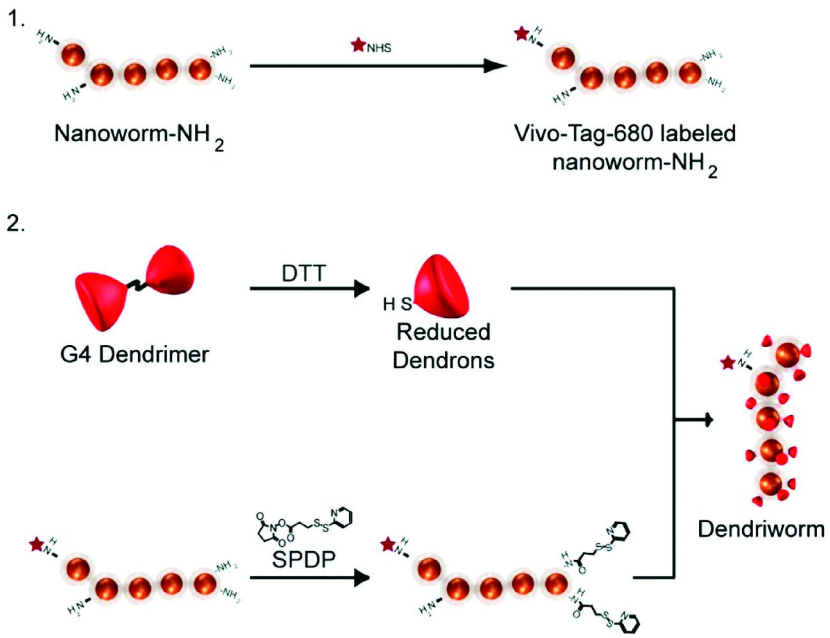


*Figure 7. Synthesis of dendriworms. (Reproduced from reference (57). Copyright 2013 American Chemical Society.)*

## Summary

Dendrimers display the evolving nature needed to incorporate a number of functionalities desirable for efficient delivery of RNAi. The biocompatibility, tumor specificity, and immunocompatibility of dendrimer-based nanovectors can be achieved through proper chemical modification at the periphery, and their composition, shape, and size can be precisely tuned to maximize transfection efficiency. Thus, dendrimer-based RNAi delivery is likely to meet the strict regulatory requirements of polymer-based therapeutics intended for use in humans.

Downloaded by MICHIGAN STATE UNIV on July 17, 2013 | http://pubs.acs.org
Publication Date (Web): July 8, 2013 | doi: 10.1021/bk-2013-1135.ch012

## Acknowledgments

This work was supported, in part, by the National Science Foundation (CAREER Award CBET0954957) and Jeffress Memorial Trust (J-1043).

## References

1. Fire, A.; Xu, S.; Montgomery, M. K.; Kostas, S. A.; Driver, S. E.; Mello, C. C. Potent and specific genetic interference by double-stranded RNA in Caenorhabditis elegans. *Nature* **1998**, *391*, 806–11.
2. Pecot, C. V.; Calin, G. A.; Coleman, R. L.; Lopez-Berestein, G.; Sood, A. K. RNA interference in the clinic: challenges and future directions. *Nat. Rev. Cancer* **2011**, *11*, 59–67.
3. Kawamata, T.; Tomari, Y. Making RISC. *Trends Biochem. Sci.* **2010**, *35*, 368–76.
4. Petrocca, F.; Lieberman, J. Promise and challenge of RNA interference-based therapy for cancer. *J. Clin. Oncol.* **2011**, *29*, 747–754.
5. Kolch, W.; Pitt, A. Functional proteomics to dissect tyrosine kinase signalling pathways in cancer. *Nat. Rev. Cancer* **2010**, *10*, 618–29.
6. Prenzel, N.; Fischer, O. M.; Streit, S.; Hart, S.; Ullrich, A. The epidermal growth factor receptor family as a central element for cellular signal transduction and diversification. *Endocr.-Relat. Cancer* **2001**, *8*, 11–31.
7. Yuan, Q.; Lee, E.; Yeudall, W. A.; Yang, H. Dendrimer-triglycine-EGF nanoparticles for tumor imaging and targeted nucleic acid and drug delivery. *Oral Oncol.* **2010**, *46*, 698–704.
8. Wang, H.; Teh, M. T.; Ji, Y.; Patel, V.; Firouzabadian, S.; Patel, A. A.; Gutkind, J. S.; Yeudall, W. A. EPS8 upregulates FOXM1 expression, enhancing cell growth and motility. *Carcinogenesis* **2010**, *31*, 1132–1141.
9. Wang, H.; Patel, V.; Miyazaki, H.; Gutkind, J. S.; Yeudall, W. A. Role for EPS8 in squamous carcinogenesis. *Carcinogenesis* **2009**, *30*, 165–74.
10. Oh, Y. K.; Park, T. G. siRNA delivery systems for cancer treatment. *Adv. Drug Delivery Rev.* **2009**, *61*, 850–862.
11. Davis, M. E. The first targeted delivery of siRNA in humans via a self-assembling, cyclodextrin polymer-based nanoparticle: from concept to clinic. *Mol. Pharm.* **2009**, *6*, 659–68.


In Tailored Polymer Architectures for Pharmaceutical and Biomedical Applications; Scholz, C., et al.; ACS Symposium Series; American Chemical Society: Washington, DC, 2013.

Downloaded by MICHIGAN STATE UNIV on July 17, 2013 | http://pubs.acs.org
Publication Date (Web): July 8, 2013 | doi: 10.1021/bk-2013-1135.ch012

12. Davis, M. E.; Zuckerman, J. E.; Choi, C. H.; Seligson, D.; Tolcher, A.; Alabi, C. A.; Yen, Y.; Heidel, J. D.; Ribas, A. Evidence of RNAi in humans from systemically administered siRNA via targeted nanoparticles. *Nature* **2010**, *464*, 1067–1070.
13. Senzer, N.; Barve, M.; Kuhn, J.; Melnyk, A.; Beitsch, P.; Lazar, M.; Lifshitz, S.; Magee, M.; Oh, J.; Mill, S. W.; Bedell, C.; Higgs, C.; Kumar, P.; Yu, Y.; Norvell, F.; Phalon, C.; Taquet, N.; Rao, D. D.; Wang, Z.; Jay, C. M.; Pappen, B. O.; Wallraven, G.; Brunicardi, F. C.; Shanahan, D. M.; Maples, P. B.; Nemunaitis, J. Phase I trial of "bi-shRNAi(furin)/GMCSF DNA/autologous tumor cell" vaccine (FANG) in advanced cancer. *Mol. Ther.* **2012**, *20*, 679–686.
14. Yano, J.; Hirabayashi, K.; Nakagawa, S.; Yamaguchi, T.; Nogawa, M.; Kashimori, I.; Naito, H.; Kitagawa, H.; Ishiyama, K.; Ohgi, T.; Irimura, T. Antitumor activity of small interfering RNA/cationic liposome complex in mouse models of cancer. *Clin. Cancer Res.* **2004**, *10*, 7721–7726.
15. Bisanz, K.; Yu, J.; Edlund, M.; Spohn, B.; Hung, M. C.; Chung, L. W.; Hsieh, C. L. Targeting ECM-integrin interaction with liposome-encapsulated small interfering RNAs inhibits the growth of human prostate cancer in a bone xenograft imaging model. *Mol. Ther.* **2005**, *12*, 634–643.
16. Santel, A.; Aleku, M.; Keil, O.; Endruschat, J.; Esche, V.; Durieux, B.; Loffler, K.; Fechtner, M.; Rohl, T.; Fisch, G.; Dames, S.; Arnold, W.; Giese, K.; Klippel, A.; Kaufmann, J. RNA interference in the mouse vascular endothelium by systemic administration of siRNA-lipoplexes for cancer therapy. *Gene Ther.* **2006**, *13*, 1360–70.
17. Pal, A.; Ahmad, A.; Khan, S.; Sakabe, I.; Zhang, C.; Kasid, U. N.; Ahmad, I. Systemic delivery of RafsiRNA using cationic cardiolipin liposomes silences Raf-1 expression and inhibits tumor growth in xenograft model of human prostate cancer. *Int. J. Oncol.* **2005**, *26*, 1087–1091.
18. Chien, P. Y.; Wang, J.; Carbonaro, D.; Lei, S.; Miller, B.; Sheikh, S.; Ali, S. M.; Ahmad, M. U.; Ahmad, I. Novel cationic cardiolipin analogue-based liposome for efficient DNA and small interfering RNA delivery in vitro and in vivo. *Cancer Gene Ther.* **2005**, *12*, 321–328.
19. Yamato, K.; Yamada, T.; Kizaki, M.; Ui-Tei, K.; Natori, Y.; Fujino, M.; Nishihara, T.; Ikeda, Y.; Nasu, Y.; Saigo, K.; Yoshinouchi, M. New highly potent and specific E6 and E7 siRNAs for treatment of HPV16 positive cervical cancer. *Cancer Gene Ther.* **2008**, *15*, 140–153.
20. Hogrefe, R. I.; Lebedev, A. V.; Zon, G.; Pirollo, K. F.; Rait, A.; Zhou, Q.; Yu, W.; Chang, E. H. Chemically modified short interfering hybrids (siHYBRIDS): nanoimmunoliposome delivery in vitro and in vivo for RNAi of HER-2. *Nucleosides, Nucleotides Nucleic Acids* **2006**, *25*, 889–907.
21. Landen, C. N., Jr.; Chavez-Reyes, A.; Bucana, C.; Schmandt, R.; Deavers, M. T.; Lopez-Berestein, G.; Sood, A. K. Therapeutic EphA2 gene targeting in vivo using neutral liposomal small interfering RNA delivery. *Cancer Res.* **2005**, *65*, 6910–8.
22. Landen, C. N.; Merritt, W. M.; Mangala, L. S.; Sanguino, A. M.; Bucana, C.; Lu, C.; Lin, Y. G.; Han, L. Y.; Kamat, A. A.; Schmandt, R.; Coleman, R. L.; Gershenson, D. M.; Lopez-Berestein, G.; Sood, A. K. Intraperitoneal

delivery of liposomal siRNA for therapy of advanced ovarian cancer. *Cancer Biol. Ther.* **2006**, *5*, 1708–1713.
23. Halder, J.; Kamat, A. A.; Landen, C. N., Jr.; Han, L. Y.; Lutgendorf, S. K.; Lin, Y. G.; Merritt, W. M.; Jennings, N. B.; Chavez-Reyes, A.; Coleman, R. L.; Gershenson, D. M.; Schmandt, R.; Cole, S. W.; Lopez-Berestein, G.; Sood, A. K. Focal adhesion kinase targeting using in vivo short interfering RNA delivery in neutral liposomes for ovarian carcinoma therapy. *Clin. Cancer Res.* **2006**, *12*, 4916–4924.
24. Thaker, P. H.; Han, L. Y.; Kamat, A. A.; Arevalo, J. M.; Takahashi, R.; Lu, C.; Jennings, N. B.; Armaiz-Pena, G.; Bankson, J. A.; Ravoori, M.; Merritt, W. M.; Lin, Y. G.; Mangala, L. S.; Kim, T. J.; Coleman, R. L.; Landen, C. N.; Li, Y.; Felix, E.; Sanguino, A. M.; Newman, R. A.; Lloyd, M.; Gershenson, D. M.; Kundra, V.; Lopez-Berestein, G.; Lutgendorf, S. K.; Cole, S. W.; Sood, A. K. Chronic stress promotes tumor growth and angiogenesis in a mouse model of ovarian carcinoma. *Nat. Med.* **2006**, *12*, 939–944.
25. Merritt, W. M.; Lin, Y. G.; Spannuth, W. A.; Fletcher, M. S.; Kamat, A. A.; Han, L. Y.; Landen, C. N.; Jennings, N.; De, G. K.; Langley, R. R.; Villares, G.; Sanguino, A.; Lutgendorf, S. K.; Lopez-Berestein, G.; Bar-Eli, M. M.; Sood, A. K. Effect of interleukin-8 gene silencing with liposome-encapsulated small interfering RNA on ovarian cancer cell growth. *J. Natl. Cancer Inst.* **2008**, *100*, 359–372.
26. Urban-Klein, B.; Werth, S.; Abuharbeid, S.; Czubayko, F.; Aigner, A. RNAi-mediated gene-targeting through systemic application of polyethylenimine (PEI)-complexed siRNA in vivo. *Gene Ther.* **2005**, *12*, 461–6.
27. Ma, Z.; Li, J.; He, F.; Wilson, A.; Pitt, B.; Li, S. Cationic lipids enhance siRNA-mediated interferon response in mice. *Biochem. Biophys. Res. Commun.* **2005**, *330*, 755–759.
28. Xu, C. X.; Jere, D.; Jin, H.; Chang, S. H.; Chung, Y. S.; Shin, J. Y.; Kim, J. E.; Park, S. J.; Lee, Y. H.; Chae, C. H.; Lee, K. H.; Beck, G. R., Jr.; Cho, C. S.; Cho, M. H. Poly(ester amine)-mediated, aerosol-delivered Akt1 small interfering RNA suppresses lung tumorigenesis. *Am. J. Respir. Crit. Care Med.* **2008**, *178*, 60–73.
29. Zhang, Z.; Yang, X.; Zhang, Y.; Zeng, B.; Wang, S.; Zhu, T.; Roden, R. B.; Chen, Y.; Yang, R. Delivery of telomerase reverse transcriptase small interfering RNA in complex with positively charged single-walled carbon nanotubes suppresses tumor growth. *Clin. Cancer Res.* **2006**, *12*, 4933–4939.
30. He, X. W.; Liu, T.; Chen, Y. X.; Cheng, D. J.; Li, X. R.; Xiao, Y.; Feng, Y. L. Calcium carbonate nanoparticle delivering vascular endothelial growth factor-C siRNA effectively inhibits lymphangiogenesis and growth of gastric cancer in vivo. *Cancer Gene Ther.* **2008**, *15*, 193–202.
31. Yoshizawa, T.; Hattori, Y.; Hakoshima, M.; Koga, K.; Maitani, Y. Folate-linked lipid-based nanoparticles for synthetic siRNA delivery in KB tumor xenografts. *Eur. J. Pharm. Biopharm.* **2008**, *70*, 718–725.
32. Grzelinski, M.; Urban-Klein, B.; Martens, T.; Lamszus, K.; Bakowsky, U.; Hobel, S.; Czubayko, F.; Aigner, A. RNA interference-mediated gene


In Tailored Polymer Architectures for Pharmaceutical and Biomedical Applications; Scholz, C., et al.; ACS Symposium Series; American Chemical Society: Washington, DC, 2013.

Downloaded by MICHIGAN STATE UNIV on July 17, 2013 | http://pubs.acs.org
Publication Date (Web): July 8, 2013 | doi: 10.1021/bk-2013-1135.ch012

silencing of pleiotrophin through polyethylenimine-complexed small interfering RNAs in vivo exerts antitumoral effects in glioblastoma xenografts. *Hum. Gene Ther.* **2006**, *17*, 751–766.
33. Fujii, T.; Saito, M.; Iwasaki, E.; Ochiya, T.; Takei, Y.; Hayashi, S.; Ono, A.; Hirao, N.; Nakamura, M.; Kubushiro, K.; Tsukazaki, K.; Aoki, D. Intratumor injection of small interfering RNA-targeting human papillomavirus 18 E6 and E7 successfully inhibits the growth of cervical cancer. *Int. J. Oncol.* **2006**, *29*, 541–548.
34. Hu-Lieskovan, S.; Heidel, J. D.; Bartlett, D. W.; Davis, M. E.; Triche, T. J. Sequence-specific knockdown of EWS-FLI1 by targeted, nonviral delivery of small interfering RNA inhibits tumor growth in a murine model of metastatic Ewing's sarcoma. *Cancer Res.* **2005**, *65*, 8984–8992.
35. Song, E.; Zhu, P.; Lee, S. K.; Chowdhury, D.; Kussman, S.; Dykxhoorn, D. M.; Feng, Y.; Palliser, D.; Weiner, D. B.; Shankar, P.; Marasco, W. A.; Lieberman, J. Antibody mediated in vivo delivery of small interfering RNAs via cell-surface receptors. *Nat. Biotechnol.* **2005**, *23*, 709–17.
36. Golzio, M.; Mazzolini, L.; Ledoux, A.; Paganin, A.; Izard, M.; Hellaudais, L.; Bieth, A.; Pillaire, M. J.; Cazaux, C.; Hoffmann, J. S.; Couderc, B.; Teissie, J. In vivo gene silencing in solid tumors by targeted electrically mediated siRNA delivery. *Gene Ther.* **2007**, *14*, 752–759.
37. Jackson, A. L.; Linsley, P. S. Recognizing and avoiding siRNA off-target effects for target identification and therapeutic application. *Nat. Rev. Drug Discovery* **2010**, *9*, 57–67.
38. Rao, D. D.; Vorhies, J. S.; Senzer, N.; Nemunaitis, J. siRNA vs. shRNA: similarities and differences. *Adv. Drug Delivery Rev.* **2009**, *61*, 746–759.
39. Lim, Y. B.; Kim, S. M.; Suh, H.; Park, J. S. Biodegradable, endosome disruptive, and cationic network-type polymer as a highly efficient and nontoxic gene delivery carrier. *Bioconjugate Chem.* **2002**, *13*, 952–7.
40. Mahato, R. I.; Henry, J.; Narang, A. S.; Sabek, O.; Fraga, D.; Kotb, M.; Gaber, A. O. Cationic lipid and polymer-based gene delivery to human pancreatic islets. *Mol. Ther.* **2003**, *7*, 89–100.
41. De Smedt, S. C.; Demeester, J.; Hennink, W. E. Cationic polymer based gene delivery systems. *Pharm. Res.* **2000**, *17*, 113–26.
42. Pack, D. W.; Hoffman, A. S.; Pun, S.; Stayton, P. S. Design and development of polymers for gene delivery. *Nat. Rev. Drug Discovery* **2005**, *4*, 581–93.
43. Luo, D.; Saltzman, W. M. Synthetic DNA delivery systems. *Nat. Biotechnol.* **2000**, *18*, 33–37.
44. Remy-Kristensen, A.; Clamme, J. P.; Vuilleumier, C.; Kuhry, J. G.; Mely, Y. Role of endocytosis in the transfection of L929 fibroblasts by polyethylenimine/DNA complexes. *Biochim. Biophys. Acta* **2001**, *1514*, 21–32.
45. Liu, M.; Frechet, J. M. J. Designing dendrimers for drug delivery. *Pharm. Sci. Technol. Today* **1999**, *2*, 393–401.
46. Esfand, R.; Tomalia, D. A. Poly(amidoamine) (PAMAM) dendrimers: from biomimicry to drug delivery and biomedical applications. *Drug Discovery Today* **2001**, *6*, 427–436.

Downloaded by MICHIGAN STATE UNIV on July 17, 2013 | http://pubs.acs.org
Publication Date (Web): July 8, 2013 | doi: 10.1021/bk-2013-1135.ch012

47. Newkome, G. R.; Yao, Z.; Baker, G. R.; Gupta, V. K. Micelles. Part 1. Cascade molecules: a new approach to micelles. A [27]-arborol. *J. Org. Chem.* **1985**, *50*, 2003–4.
48. Svenson, S.; Tomalia, D. A. Dendrimers in biomedical applications--reflections on the field. *Adv. Drug Delivery Rev.* **2005**, *57*, 2106–29.
49. Yang, H.; Kao, W. J. Dendrimers for pharmaceutical and biomedical applications. *J. Biomater. Sci., Polym. Ed.* **2006**, *17*, 3–19.
50. Eichman, J. D.; Bielinska, A. U.; Kukowska-Latallo, J. F.; Baker, J. R., Jr. The use of PAMAM dendrimers in the efficient transfer of genetic material into cells. *Pharm. Sci. Technol. Today* **2000**, *3*, 232–245.
51. Bielinska, A. U.; Yen, A.; Wu, H. L.; Zahos, K. M.; Sun, R.; Weiner, N. D.; Baker, J. R., Jr.; Roessler, B. J. Application of membrane-based dendrimer/DNA complexes for solid phase transfection in vitro and in vivo. *Biomaterials* **2000**, *21*, 877–887.
52. Schatzlein, A. G.; Zinselmeyer, B. H.; Elouzi, A.; Dufes, C.; Chim, Y. T. A.; Roberts, C. J.; Davies, M. C.; Munro, A.; Gray, A. I.; Uchegbu, I. F. Preferential liver gene expression with polypropylenimine dendrimers. *J. Controlled Release* **2005**, *101*, 247–258.
53. Takahashi, T.; Harada, A.; Emi, N.; Kono, K. Preparation of efficient gene carriers using a polyamidoamine dendron-bearing lipid: improvement of serum resistance. *Bioconjugate Chem.* **2005**, *16*, 1160–1165.
54. Sonawane, N. D.; Szoka, F. C., Jr.; Verkman, A. S. Chloride Accumulation and Swelling in Endosomes Enhances DNA Transfer by Polyamine-DNA Polyplexes. *J. Biol. Chem.* **2003**, *278*, 44826–44831.
55. Tang, Y.; Li, Y. B.; Wang, B.; Lin, R. Y.; van, D. M.; Zurcher, D. M.; Gu, X. Y.; Banaszak Holl, M. M.; Liu, G.; Qi, R. Efficient in vitro siRNA delivery and intramuscular gene silencing using PEG-modified PAMAM dendrimers. *Mol. Pharm.* **2012**, *9*, 1812–1821.
56. Yuan, Q.; Yeudall, W. A.; Yang, H. PEGylated polyamidoamine dendrimers with bis-aryl hydrazone linkages for enhanced gene delivery. *Biomacromolecules* **2010**, *11*, 1940–7.
57. Agrawal, A.; Min, D. H.; Singh, N.; Zhu, H.; Birjiniuk, A.; von Maltzahn, G.; Harris, T. J.; Xing, D.; Woolfenden, S. D.; Sharp, P. A.; Charest, A.; Bhatia, S. Functional delivery of siRNA in mice using dendriworms. *ACS Nano* **2009**, *3*, 2495–504.

Downloaded by MICHIGAN STATE UNIV on July 17, 2013 | http://pubs.acs.org
Publication Date (Web): July 8, 2013 | doi: 10.1021/bk-2013-1135.ch012

Downloaded by UNIV OF NORTH CAROLINA on July 20, 2013 | http://pubs.acs.org
Publication Date (Web): July 8, 2013 | doi: 10.1021/bk-2013-1135.ch013

## Chapter 13

# Challenges for PEGylated Proteins and Alternative Half-Life Extension Technologies Based on Biodegradable Polymers

**Ahmed Besheer,[*,1] Robert Liebner,[1] Martin Meyer,[2] and Gerhard Winter[1]**

**[1]Pharmaceutical Technology and Biopharmaceutics, Department of Pharmacy, Ludwig-Maximilians-Universität, Butenandtstrasse 5-13, D-81377 Munich, Germany**
**[2]Fresenius Kabi Deutschland GmbH, Pfingstweide 53, D-61169 Friedberg, Germany**
**[*]E-mail: ahmed.besheer@cup.uni-muenchen.de. Phone: +49 89 2180 77025. Fax: +49 89 2180 77020. Web: http://www.cup.uni-muenchen.de.**

PEGylation, the chemical conjugation of polyethylene glycol (PEG) to proteins, peptides and small molecules, is currently widely used to extend the half-life of therapeutic molecules, with 10 products already in the market. Despite its proven success, PEGylation may not be suitable for some of the newer protein binders, such as antibody fragments and protein scaffolds, which need to be administered in large doses for chronic therapy as concentrated solutions for subcutaneous injection. This short review highlights the deficiencies of PEGylation, as well as the industrially pursued alternatives based on biodegradable polymers. Eventually, the competitiveness of the newer techologies will be proven in comparative preclinical and clinical studies covering aspects like pharmacokinetics, pharmacodynamics, toxicity and stability.

© 2013 American Chemical Society
In Tailored Polymer Architectures for Pharmaceutical and Biomedical Applications; Scholz, C., et al.; ACS Symposium Series; American Chemical Society: Washington, DC, 2013.

# Introduction

Since the recombinant DNA revolution in the 80s, there has been a constant increase in the development of new protein therapies. To date, there are more than 200 approved biologicals on the market (*1*), with total sales amounting to 107.6 billion US$ in 2010 (*2*), and hundreds of candidates in the pipelines. Except for monoclonal antibodies (MAbs), the majority of the marketed and investigational biopharmaceuticals, such as cytokines, growth factors, and protein scaffolds, have a molecular size below the renal clearance threshold (i.e. < 60 kDa), and are thus rapidly eliminated through the kidneys. The introduction of PEGylation in the 70's by Davies and Abuchowsky (*3*, *4*) proved to be a valuable strategy to protect biopharmaceuticals and extend their circulation time, and led to the approval of the first PEGylated product, PEG-Adenosine deaminase (Adagen®) in 1990, and up to 10 PEGylated products currently on the market, with total sales exceeding 6 billion US$ (see Table 1). The technology, based on the chemical conjugation of poly(ethylene glycol) (PEG) to proteins, peptides or small molecules, is by far the established gold standard in half-life extension (HLE) (*5*), and it is not a mere life-cycle management option, but an enabling technology, without which some biotech products would have never reached the market.

Over the decades, the PEGylation technology has matured and gone through different generations to overcome problems with synthesis or purification (*6*). However, the technology faces new challenges that have emerged from the rapid developments in pharma's strategies and needs. These include the industry's increasing focus on therapies for chronic diseases (*7*), the evolution of new therapeutic drug classes, and the increasing need to administer high protein doses parenterally. For instance, the large market of MAbs (which represents more than one third of the biopharma market (*8*)) is witnessing a shift to smaller protein binders, such as MAb fragments or protein scaffolds (*9–11*). These promising "designer proteins" offer a number of advantages, such as: better tissue diffusion, lack of unwanted Fc-mediated effector functions, higher stability, easier and cheaper production as well as the circumvention of the complex IP situation associated with MAbs (*11*). However, their rapid elimination compared to the naturally long circulating antibodies (which have half-lives between 1-3 weeks) represents their Achilles' heel and reduces their competitiveness with MAbs (*12*). For such biologicals smaller than the renal filtration threshold, the application of a half-life extension technology is beneficial for the patient (to ensure their activity over long time periods, reduce administration frequency and increase patient compliance) and essential for the pharmaceutical industry (to enable market entry and increase competitiveness).

The challenge for these new therapeutic classes lies in the fact that they are usually required in large doses and must be administered parenterally, preferably by subcutaneous injection to allow self-administration. If PEGylation would be applied as a HLE technology, then questions such as the toxicity of high doses of the non-biodegradable PEG and the viscosity of its highly concentrated solutions would be raised, raising doubts about the safety and feasibility of PEGylation of

Downloaded by UNIV OF NORTH CAROLINA on July 20, 2013 | http://pubs.acs.org
Publication Date (Web): July 8, 2013 | doi: 10.1021/bk-2013-1135.ch013


In Tailored Polymer Architectures for Pharmaceutical and Biomedical Applications; Scholz, C., et al.;
ACS Symposium Series; American Chemical Society: Washington, DC, 2013.

such protein binders. This review tries to draw attention to these new challenges PEGylation is facing, and points to the emerging battery of alternative HLE technologies which might be able to overcome those limitations.

## Properties and Applications of PEG

PEG has a number of unique and interesting physicochemical properties, which were the subject of many studies and review articles (*13*, *14*). It is a polyether composed of a simple repeating unit, namely HO-($CH_2$-$CH_2$-O)$_n$-H. The oxygen molecules provide a polar component, while the ethylene units are responsible for a hydrophobic nature, rendering PEG amphiphilic and surface active (*15*). Accordingly, it is soluble in a number of organic solvents, as well as water over a wide range of molar masses (*16*). This high water solubility is peculiar, considering that its 2 neighbors; poly(propylene glycol) and poly(methylene glycol); are not soluble in water (*15*). This high hydrophilicity is attributed to the presence of PEG monomers in a gauche rather than a trans conformation, which facilitates the hydrogen bonding with water (*17*). Accordingly, each ethylene oxide unit is bound to 2-3 water molecules (the exact number depends on the method of determination and the molar mass (*18*, *19*)), with up to 8 layers (*20*) or 16 molecules (*21*) of structured water, and no free water exists in a 45 % v/v PEG solution. This strong hydration is responsible for the unusually high osmotic pressure of PEG solutions, and the much larger hydrodynamic radius of the PEG random coils in comparison to other polymers or proteins with similar molar mass (*22*).

Due to these favourable properties of PEG and its non-toxicity, non-immunogenicity and non-antigenicity (*5*), it finds many applications in the biomedical field, such as its use as a stabilizer in protein formulation, as an additive in protein purification by precipitation or aqueous two phase extraction, for reducing adsorption on surfaces and for coupling to proteins to increase their half-lives (*23*). In the latter case, PEGylation offers additional advantage, including the increase of protein solubility, better physical and thermal stability, reduced protease susceptibility, and reduced immunogenicity (*24*). In some rare cases, extra advantages could be conferred by PEGylation, such as the so-called "self-regulating pharmacokinetics" (*25*), as in the case of Pegfilgrastim (PEG-GCSF), the PEGylated protein's clearance is accelerated by neutrophil recovery, as it is cleared by internalization via G-CSF receptors present on the neutrophils (*25*). This unique example of a cytokine being removed from the body by its own biological effect eliminates the need for dose adjustment and allows the administration of a fixed dose (*26*).

## Limitations of PEGylation Technology

Despite the considerable advantages offered by PEGylation and the substantial progress in the technology, it still suffers from some limitations and drawbacks. These can be classified into:


In Tailored Polymer Architectures for Pharmaceutical and Biomedical Applications; Scholz, C., et al.;
ACS Symposium Series; American Chemical Society: Washington, DC, 2013.

Downloaded by UNIV OF NORTH CAROLINA on July 20, 2013 | http://pubs.acs.org
Publication Date (Web): July 8, 2013 | doi: 10.1021/bk-2013-1135.ch013

Downloaded by UNIV OF NORTH CAROLINA on July 20, 2013 | http://pubs.acs.org
Publication Date (Web): July 8, 2013 | doi: 10.1021/bk-2013-1135.ch013



**Table 1. List of marketed PEGylated proteins, their first approval, sales in 2010, indications and the companies which first commercialized them**

| | *PEGylated protein* | *Market entry* | *Sales 2010 (M US$)*[1] | *Indication* | *Company* |
|---|---|---|---|---|---|
| PEG–adenosine deaminase (Adagen®) | Adenosine deaminase | 1990 | 60 | Severe combined immunodeficiency disease (SCID) | Enzon |
| PEG–asparaginase (Oncaspar®) | Asparaginase | 1994 | 47 | Acute lymphoblastic leukemia | Enzon |
| PEG–interferon α2b (PEG–Intron®) | Interferon α2b | 2000 | 737 | Hepatitis C | Schering-Plough |
| PEG-interferon α2a (Pegasys®) | Interferon α2a | 2002 | 1,582 | Hepatitis C | Roche |
| Pegvisomant, (Somavert®) | Growth hormone receptor antagonist | 2002 | 157 | Acromegaly | Pfizer |
| PEG-filgrastim (Neulasta®) | Granulocyte colony stimulating factor | 2002 | 3,558 | Neutropenia | Amgen |
| PEG-epoetin-β (Mircera®)* | Erythropoetin | 2007 | 245 | Renal anaemia | Roche |
| Certolizumab Pegol (Cimzia®) | Fab fragment against TNF-α | 2008 | 264 | Rheumatoid arthritis and Crohn's disease | UCB |
| Pegloticase (Krystexxa®) | Urate oxidase | 2010 | n.a. | Chronic gout | Savient pharmaceuticals |
| Peginesatide (Omontys®) | Erythropoiesis stimulating agent | 2012 | n.a. | Anemia due to chronic kidney disease | Affymax and Takeda |

[1] From www.evaluatepharma.com.

In Tailored Polymer Architectures for Pharmaceutical and Biomedical Applications; Scholz, C., et al.;
ACS Symposium Series; American Chemical Society: Washington, DC, 2013.

## Raw Material and Conjugation Chemistry

The raw materials used for PEGylation can have profound effects on the PEGylation chemistry or the physicochemical properties and the stability of the product. One problem is that PEG is a synthetic polymer which shows a certain polydispersity. Although PEG polydispersity is relatively low (1.01 for low molar mass PEGs, increasing to a minimum of 1.2 for PEGs ≥ 20 kDa) (*27*), it leads to a polydispersity in the molar mass of the PEGylated protein. Changes in the polydispersity index (PDI) from batch to batch will influence the pharmacokinetics of the PEGylated product, and complicates its analysis and characterization (*6*).

Activated PEGs sometimes contain impurities which can affect the conjugation process or protein stability (*28*). For instance, PEGs are known to contain residual peroxides which accumulate upon storage due to light- or metal-induced auto-oxidation (*29*). The resulting protein oxidation can compromise protein stability and activity (*29*), and in some cases lead to degradation and chain scission of the PEG chain itself (*30*). This oxidation problem might be mitigated by purifying PEG from peroxides, use of antioxidants, as well as storage under nitrogen, away from light and at low temperatures (*28–30*). Another example for impurities in activated PEGs was recently published, describing the presence of an acetal-containing by-product in the raw material used for protein PEGylation. The slow hydrolysis of the acetal bond led to the release of the unPEGylated protein upon storage (*31*). Another important issue is the activity of the functionalized PEG, since the molar ratio of (active) PEG to protein is essential to control the degree of protein modification. However, the activity of functionalized PEG often varies from batch to batch, and it is recommended to check PEG's activity before use (*30*).

Proteins are usually PEGylated at nucleophilic sites, such as amino and thiol groups, and although there are many available coupling chemistries, each has its limitations. For instance, the maleimide-thiol conjugate is not stable under basic conditions, while the iodine released during the coupling of cysteine to iodo PEG can interact with the protein's tyrosine residues. The succinimidyl ester chemistry used for amine coupling can also form by-products by reaction with cysteine and tyrosine residues, leading to slow hydrolysis upon storage (*32*). Finally, the yield of mono-PEGylated protein can be low, due to the formation of multi-PEGylated products (*33*), or the formation of positional isomers (*30*), adding to the heterogeneity of the drug product. All the aforementioned problems point to the need for stringent control of the raw material, validation of the production methods and prudent characterization of the product (*31*) to ensure quality and reproducibility essential for regulatory approval and patient safety (*34*).

## Stability and Formulation

There is little information published about the formulation of PEGylated proteins (*28*), and practically nothing is published on their highly concentrated solutions. However, the following points are usually discussed as potential


In Tailored Polymer Architectures for Pharmaceutical and Biomedical Applications; Scholz, C., et al.;
ACS Symposium Series; American Chemical Society: Washington, DC, 2013.

Downloaded by UNIV OF NORTH CAROLINA on July 20, 2013 | http://pubs.acs.org
Publication Date (Web): July 8, 2013 | doi: 10.1021/bk-2013-1135.ch013

concerns for liquid formulations; namely 1) effect of PEGylation on protein stability, 2) effect on viscosity 3) effect on lyophilization (*25*)

*Protein Stability*

A protein's physical stability is usually due to the sum of conformational and colloidal stabilities (*35*). While many reports state that PEGylation increases the conformational (or thermodynamic) stability of proteins, such as increasing the melting point ($T_m$) of α-chymotrypsin by 6 °C (*36*), or that of recombinant human endostatin by 15 °C (*37*), there are few reports stating that PEGylation reduced $T_m$ for some proteins, such as the work of Gonnelli et al. on the PEGylation of azurin (*38*). Similarly, the generally held opinion that PEGylation increases colloidal stability and reduces aggregation tendency due to steric repulsion (*39*, *40*) is challenged by some reports, such as the work of Veronese et al., who reported an increased tendency for aggregation of G-CSF upon site specific PEGylation to a buried thiol group (*41*). These studies point to the fact that our understanding of the stabilization mechanisms and the interaction between PEG and the protein are far from being complete (*42*)

Downloaded by UNIV OF NORTH CAROLINA on July 20, 2013 | http://pubs.acs.org
Publication Date (Web): July 8, 2013 | doi: 10.1021/bk-2013-1135.ch013

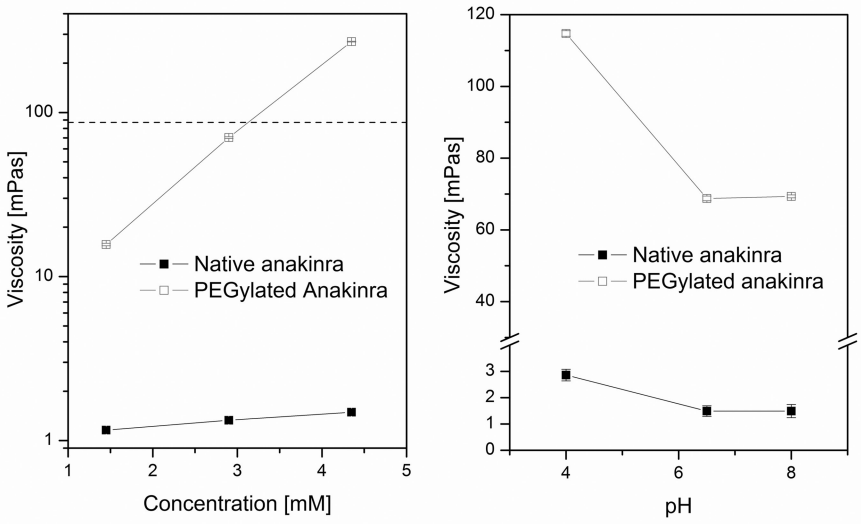


*Figure 1. (Left) Effect of high concentration on the viscosity of solutions of recombinant human interleukin 1 receptor antagonist (rhIL1ra, anakinra) and 40-kDa-monoPEGylated anakinra. Dashed line represents the viscosity of the marketed Cimzia® solution (200 mg/mL = 2.2 mM) as a reference. (Right) Effect of pH on the viscosity on anakinra and monoPEGylated anakinra. All measurements were performed using mVROC (Rheosese Inc, USA) at a shear rate of 314 $s^{-1}$.*


In Tailored Polymer Architectures for Pharmaceutical and Biomedical Applications; Scholz, C., et al.;
ACS Symposium Series; American Chemical Society: Washington, DC, 2013.

*Viscosity*

The viscosity of solutions of PEG or PEGylated proteins increases nonlinearly with the increase in concentration (*18*, *43*). For example, the viscosity of canine haemoglobin modified with 2, 4 and 6 molecules of 5 kDa PEG increased "in a slightly exponential fashion" with concentration, while the viscosity of unmodified haemoglobin remained nearly constant over the same concentration range (*43*). Similarly, the viscosity of PEGylated anakinra was 1-2 orders of magnitude higher than the native protein at the same molar concentration (see Figure 1). Several factors can further increase the viscosity, such as changes in pH (Figure 1), or the presence of PEG-protein interaction, as has been shown for the case of the interaction of PEG and type I soluble tumor necrosis factor receptor (*23*). With the current need for high concentration solutions for subcutaneous injections and the use of high molar mass PEGs, the viscosity can increase dramatically to a level that can compromise the injectability and reduce patient compliance.

Downloaded by UNIV OF NORTH CAROLINA on July 20, 2013 | http://pubs.acs.org
Publication Date (Web): July 8, 2013 | doi: 10.1021/bk-2013-1135.ch013

*Lyophilization*

Regarding lyophilization, it is known that free PEG chains tend to crystallize during freezing (*44*). This can be prevented by using sucrose to PEG weight ratios ≥ 5 (*44*). However, coupling PEG to proteins seemed to enhance PEG crystallization, leaving approximately 10 % of the PEG chains crystalline even with a sucrose : PEG ratio > 10 (*44*). Storage at 4 or 25 °C led to a dramatic increase in crystallinity, particularly in the high sucrose samples which had a low initial crystallinity (increasing from 3 % up to 90% by 4°C/0% RH and 100% by 25°C/60% RH) (*44*). Bhatnagar et al. finally note that the crystallized PEG fragments can function as a bulking agent in the freeze-drying process to reduce the time for primary drying and improve process economics (*44*). However, they (*44*) and other researchers (*45*) reported that PEGylation can adversely affect the stability of the lyophilized proteins. Additionally, PEG is highly hydrophilic and holds many water molecules, which are not easy to remove by lyophilization. This has implications to the lyophilization cycle, and the high residual moisture might affect protein stability (*28*).

**Activity**

PEGylation is known to reduce the in vitro and in vivo protein activity (*28*), even if the PEGylation site was distal to the binding site (*46*), due to steric hindrance of the receptor binding. For instance, PEGylation reduced the activity of interferon alpha-2a to only 7 % of the original molecules activity (*47*). This problem is usually overcome by increasing the dose and by the gained pharmacokinetic advantage, which outweighs the reduction in activity, making the overall balance in favour of PEGylation (*47*). However, this may not be the case for proteins which require high doses, since it will not be easy to increase the dose in order to compensate for the decreased activity.


In Tailored Polymer Architectures for Pharmaceutical and Biomedical Applications; Scholz, C., et al.;
ACS Symposium Series; American Chemical Society: Washington, DC, 2013.

Downloaded by UNIV OF NORTH CAROLINA on July 20, 2013 | http://pubs.acs.org
Publication Date (Web): July 8, 2013 | doi: 10.1021/bk-2013-1135.ch013

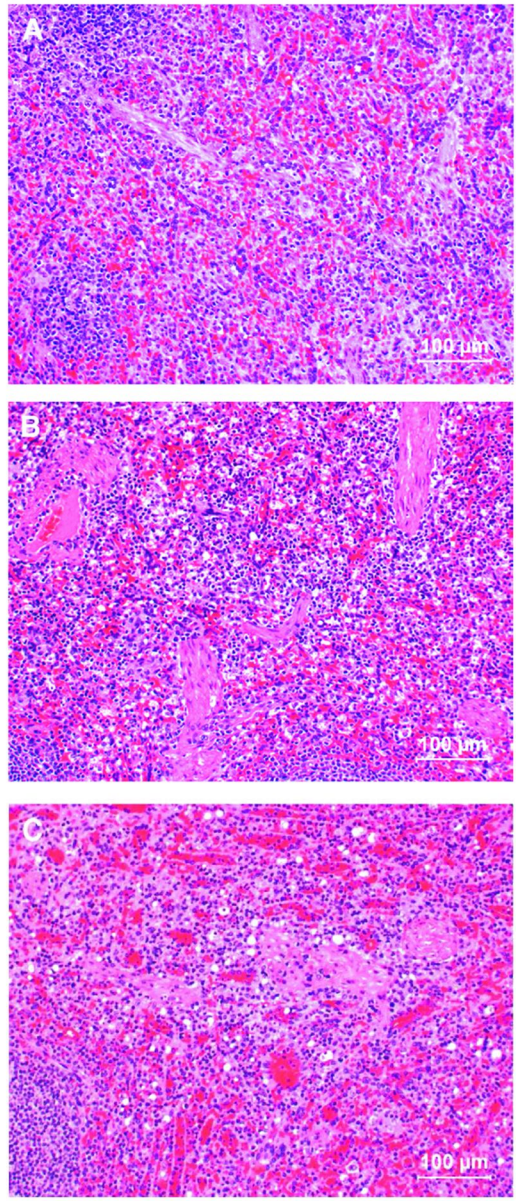


*Figure 2. Photomicrographs of spleen tissue in a control monkey collected on day 3 (A); maleimide-PEG-hemoglobin-treated monkey collected on day 3 (B); and day 13 (C). Monkeys were administered 21 mL/Kg of a 4.3 % w/v PEG-hemoglobin solution. Vacuoles were absent in control, but were moderate on day 3, and still observed, but less sever on day 13. Reproduced with permission from reference (48), Copyright 2007 Elsevier.*

## Toxicity

The most obvious toxicity problem with PEG is that it is not biodegradable. This problem is usually circumvented by using PEG with molar masses not more than 30-40 kDa, so that PEG can be renally eliminated. However, the fate of PEG in a polymer-protein conjugate can be different from the fate of PEG alone, probably due to receptor mediated cellular uptake of the protein part. This can cause vacuolation in several organs, such as the kidney, liver, spleen and bone marrow (*48*, *49*) (see for example Figure 2), a phenomenon which was not observed for PEG alone (*49*). After some time, the protein part degrades and the vacuoles are believed to be composed of PEG alone (*50*). Studies showed that larger vacuoles did not resolve even after 2 months, while the smaller ones did (*50*). Generally, vacuolation is an adaptive physiological response, with which cells can limit or contain damage, until the cell can retain its original status. This does happen in many cases, where vacuolation is considered to be fully reversible, however nothing is known about the homeostatic mechanisms by which the cell restores the status quo (*51*). In some cases, and for still unknown reasons, the cells can fail to limit the damage, leading to cell death (*51*). The routine regulatory toxicology studies are considered to be sufficient to evaluate the related risks, however especially when high dosis are applied or chronic administration is necessary, this aspect should be monitored.

Downloaded by UNIV OF NORTH CAROLINA on July 20, 2013 | http://pubs.acs.org
Publication Date (Web): July 8, 2013 | doi: 10.1021/bk-2013-1135.ch013

## Immunogenicity

Free PEG is known to be non-antigenic and does not induce antibody production (*5*, *14*, *25*). However, anti-PEG antibodies are produced when PEG is linked to particulates (such as PEGylated liposomes (*52*) and RBCs (*53*)) or by linking to proteins (*54*), particularly when coupled through aromatic linkers or when linked (close) to heterocyclic groups in the protein (*25*). In the case of particulate carriers, many publications reported that the PEG-coated particles induced anti-PEG antibodies in naïve animals quite readily and efficiently without the need for adjuvants, which leads to rapid elimination of a second injection of the PEGylated particles (a phenomenon known as accelerated blood clearance, ABC) (*55*). Anti-PEG antibodies against PEGylated proteins were also detected in the case of patients treated with PEG-asparaginase, PEG-uricase and certolizumab pegol (*56–58*). Additionally, new clinical studies found out that anti-PEG antibodies are abundant in the normal population (*53*). For instance, in 1984 Richter and Åkerblom found that 0.2 % of 453 healthy blood donors have anti-PEG antibodies in their sera, while 20 year later; Armstrong et al. have shown that ca. 25 % of 350 healthy donors had anti-PEG antibodies in their sera (*59*). This discrepancy may not be surprising, since the latter investigators used more sensitive methods, and more importantly, the incidence of anti-PEG antibodies increased due to the increased continuous exposure of the normal population to PEG in food additives, cosmetics and pharmaceuticals (*59*). Despite the successful use of many marketed PEGylated proteins, the clinical significance of anti-PEG antibodies has lately been drawn to focus as perhaps the underlying cause for the observed treatment failure in 10-50 % of the patients.


In Tailored Polymer Architectures for Pharmaceutical and Biomedical Applications; Scholz, C., et al.;
ACS Symposium Series; American Chemical Society: Washington, DC, 2013.

For instance, Armstrong et al. showed the existence of a strong correlation between the presence of anti-PEG antibodies in serum and the rapid clearance of PEG-asparaginase, rendering it a likely cause for the treatment failure in up to one third of the acute lymphoblastic leukemia patients receiving this therapy (*60*). Accordingly, the use of PEG-alternatives can lead to a possible amelioration of this problem (*61*).

## Alternative Half-Life Extension Technologies Based on Biodegradable Polymers

Downloaded by UNIV OF NORTH CAROLINA on July 20, 2013 | http://pubs.acs.org
Publication Date (Web): July 8, 2013 | doi: 10.1021/bk-2013-1135.ch013

Many alternative technologies have been developed to overcome PEG's disadvantages and to circumvent the complex IP landscape associated with PEGylation. These methods can be divided into:

1. Methods which reduce glomerular filtration through increasing the molecular size over the filtration cut-off-size. This is achieved either by chemical conjugation of the drug molecule to a polymer or a protein, or by recombinant fusion to a polypeptide.
2. Methods which increase the molecular size AND make use of the Fc neonatal receptor (FcRn) natural recycling mechanism. The latter is a well-known mechanism responsible for the exceptionally long half-lives of IgGs and albumin (*12*), where they bind to the FcRn in the slightly acidic environment of the endososme after pinocytic uptake by endocyte. Such binding prevents their degradation by lysosomal proteases and allows their recycling back to the circulation (*12*). Technologies which use this mechanism employ chemical conjugation or fusion of the molecule of interest to albumin or the Fc part of immunoglobulin.

This short review concentrates on industrially pursued biodegradable alternatives to PEGylation, which are based on polymers or polypeptides for increasing the protein size, while the interested reader is referred to excellent reviews regarding the methods utilizing the FcRn recycling mechanism (*12*, *62*, *63*).

### HESylation®

HESylation® involves the conjugation of the molecule of interest to hydroxyethyl starch (HES) (Scheme 1). HES is a biodegradable semi-synthetic polymer prepared by the hydroxyethylation of waxy maize starch fragments (*64*). The latter is a predominantly branched starch with poor water solublility, and a very short serum half-life due to rapid degradation by the serum amylase. Accordingly, hydroxyethylation is carried out to increase water solubility and reduce the biodegradation rate and extent by steric hindrance of amylase, thus increasing the circulation time (*65*). The molar mass of HES and the


In Tailored Polymer Architectures for Pharmaceutical and Biomedical Applications; Scholz, C., et al.;
ACS Symposium Series; American Chemical Society: Washington, DC, 2013.

average number of hydroxyethyl groups per glucose moiety (also known as the molar substitution, MS) can be adjusted to control the biodegradation rate, and accordingly the half-life of HESylated compounds (*65*, *66*).

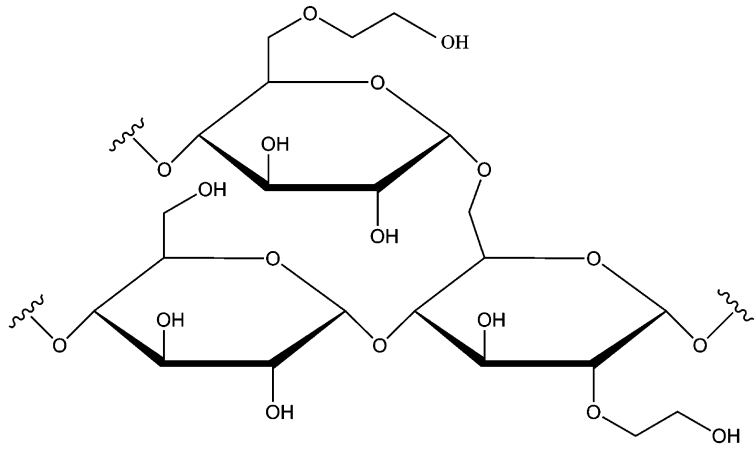


*Scheme 1. Structure of hydroxyethyl starch (HES)*

HES has been used for a long time as a plasma volume expander, where the first HES product was launched in the US in the 70s (*67*). Due to its high biocompatibility, biodegradability and proven safety record, it can be administered in doses up to 200 g/day (*67*). Additionally, the adverse effects to HES are generally regarded as mild and clinically insignificant, while its immunogenicity is considerably lower than albumin and dextran (*66*). This reduced immunogenicity is believed to be because of its structural similarity to glycogen (*65*).

Coupling to the target molecule can take place through activation of the abundant hydroxyl groups of HES, although this strategy can lead to multivalent coupling and product polymerization. A better approach, which is usually used for HESylation of molecules, involves the use of the naturally occurring single reducing end group of HES, allowing a specific 1:1 coupling to the molecule of interest using a wide variety of coupling chemistries (*68*). Enzymatically catalyzed conjugation is also feasible, for instance using aminated-HES or glutamine-containing HES for coupling to proteins using microbial transglutaminase (*69*).

Fresenius Kabi has performed a number of preclinical pharmacokinetic (PK) and pharmacodynamic (PD) studies with HESylated proteins. For instance, a PK study in dogs showed that it is possible to control the half-life of HESylated erythopoietin (EPO) by controlling the molar mass and molar substitution (MS) of HES, with high molar mass/high MS HES leading to three time longer half-life


In Tailored Polymer Architectures for Pharmaceutical and Biomedical Applications; Scholz, C., et al.;
ACS Symposium Series; American Chemical Society: Washington, DC, 2013.

Downloaded by UNIV OF NORTH CAROLINA on July 20, 2013 | http://pubs.acs.org
Publication Date (Web): July 8, 2013 | doi: 10.1021/bk-2013-1135.ch013

compared to Aranesp®, a marketed glycosylated form of EPO (*70*). Additionally, a PD study in mice showed a fourfold increase in hematocrit after treatment of mice with HES-EPO in comparison to unmodified EPO, as well as more than 1.5 fold increase in comparison to Aranesp® (*70*). The HES-EPO conjugate showed an *in vitro* and in *vivo* bioactivity profile well comparable to Mircera® (marketed PEG-EPO-conjugate). Similarly, the pharmacokinetics of HESylated IFNα was compared to PEGasys® (marketed PEG-IFNα-conjugate) in a study conducted in rabbits. The HES-IFNα-conjugate was more rapidly mobilized after s.c. injection. The AUC and $c_{max}$ values were roughly comparable for both substances (*70*).

Downloaded by UNIV OF NORTH CAROLINA on July 20, 2013 | http://pubs.acs.org
Publication Date (Web): July 8, 2013 | doi: 10.1021/bk-2013-1135.ch013

**Polysialylation**

Xenetic Biosciences couples polysialic acid (PSA), also known as columinic acid (CA) (Scheme 2), to biopharmaceuticals to increase their half-life. CA is a homopolymer of a-2,8-linked 5-N-acetylneuraminic acid (Neu5Ac). It is found on the capsule of neuroinvasive bacteria, and is believed to contribute to their virulence by camouflaging them, since it is found on host cells and cell surface proteins. This polysaccharide is biodegradable, as it is degraded intracellularly by neuraminidase.

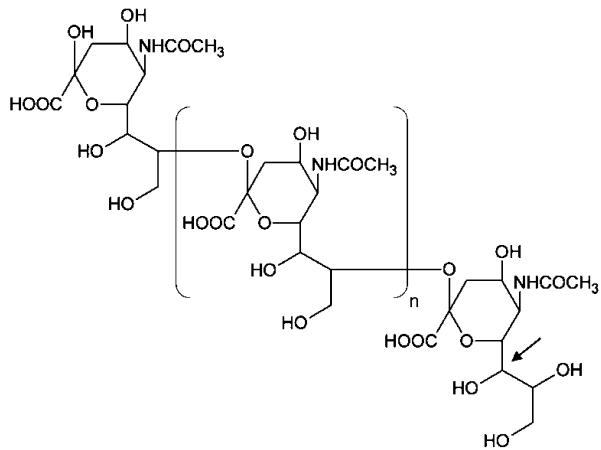


*Scheme 2. Structure of polysialic acid (PSA), also known as colominic acid (CA). The arrow shows the position of the non-reducing end, where periodate oxidation introduces an aldehyde group*

Coupling of CA to therapeutic molecules can be achieved through using the numerous carboxylate and hydroxyl groups, or better by periodate oxidation of the non-reducing end to form an aldehyde groupe, which can be directly used for a 1:1 coupling by reductive amination or through an activated linker (*71*). Recently, Lindhout et al. reported a genuine 2-step enzymatic coupling method, where in the

first step a Neu5Ac primer is added to the existing glycans on the target protein by a sialyltransferase. This is followed by polysialylation using the *Neisseria meningitidis* α2,8-polysialyltransferase (*72*).

There are several publications showing the feasibility of polysialilation for HLE. For instance, coupling 22 or 39 kDa PSA to insulin extended its hypoglycaemic effect over 6-9 h, compared to less than 3 h for the unmodified protein (*73*). Similarly, coupling CA to Fab fragments or single chain Fv regions (scFv) increases their half-life up to 5 fold (*74*, *75*). Additional benefits of polysialilation include reducing immunogenicity of the parent protein as well as increasing the the tumor uptake (*74*).

Downloaded by UNIV OF NORTH CAROLINA on July 20, 2013 | http://pubs.acs.org
Publication Date (Web): July 8, 2013 | doi: 10.1021/bk-2013-1135.ch013

## Recombinant PEG mimetics

Recombinant PEG mimetics are produced by genetic means through fusion of a long and flexible polypeptide chain to the N- or C-terminus of the therapeutic protein, and thus do not require additional conjugation and separation steps. Additionally, they can produce more homogeneous products, and the length of the fused chain can be precisely tailored to any desired length to control the plasma half-life.

### *PASylation*

XL-Protein GmbH uses the so called PASylation® technology, where the therapeutic protein is fused to a flexible polypeptide chain of 200 to 600 residues based on proline, alanine and serine (hence the name PASylation®). The 3 amino acids are neutral, thus avoiding changes in the protein's isoelectric point. Contrary to homopolymers based on proline, alanine or serine, which tend to form poly(proline) helix II, α-helix and ß-sheets, respectively, the polymer formed of defined sequences of the 3 amino acids forms a random coil in solution. Additionally, the fusion proteins showed a drastic increase in hydrodynamic radius, where an increase of 50 kDa (for PAS 600), appears as 0.5 MDa in analytical SEC (*76*). This leads to a 10-100 fold increase in the circulation time, depending on the length of the polypeptide tag (*76*). Possible advantages include production of the modified protein in one step, thus avoiding further processing and purification, and the possibility of production in *E. coli*. Additionally, PAS chains were resistant to serum proteases, but degradable by a kidney enzyme extract (*76*), indicating that they might be degraded intracellularly.

### *XTEN*

Amunix Inc. uses a similar technique, where they fuse the protein to an unstructured polypeptide based on alanine, glutamic acid, glycine, proline, serine and threonine. The presence of negatively charged amino acids helps in expanding the size of the unstructured chain by electrostatic repulsion, while the lack of hydrophobic amino acids ensures that the chain does not collapse or aggregate,


In Tailored Polymer Architectures for Pharmaceutical and Biomedical Applications; Scholz, C., et al.;
ACS Symposium Series; American Chemical Society: Washington, DC, 2013.

and reduces the likelihood of binding to MHC receptors and inducing an immune response (*77*). The effect of the XTEN technology on the half-life of proteins was demonstrated by coupling an 864 amino acid polypeptide based on ala (72 aa), glu (144 aa), gly (144 aa), pro (144 aa), ser (216 aa) and thr (144 aa) (*77*) to exenatide (a glucagon like peptide 1 (GLP1) agonist), which led to significant increase in the half-life (up to 125 fold), and a depot-like effect after subcutaneous administration (*77*). They could also show that "XTEN is not strongly immunogenic in mice and rabbits", where the repeated weekly injection of the modified exenatide in mice for 6 weeks, together with an adjuvant, lead to the production of a low titer of antibodies in only 5 out of 20 mice (*77*). Additionally, they used the ability to tune the half-life by changing the length of the XTEN chain, in order to develop a glucagon-XTEN fusion protein (with only 144 residues in the XTEN chain) for the protection against nocturnal hypoglycemia (*78*). It is worth noting that the "Xtended" proteins showed a reduced bioactivity (only 15% residual bioactivity for the Xtended glucagon) and receptor affinity (17 fold reduction in the EC50 of Xtended human growth hormone) (*76*), and it is not yet clear if this is only due to steric hindrance, or if the effect is aggravated by the electrostatic repulsion due to the high density of negative charges.

Downloaded by UNIV OF NORTH CAROLINA on July 20, 2013 | http://pubs.acs.org
Publication Date (Web): July 8, 2013 | doi: 10.1021/bk-2013-1135.ch013

## Benchmarking against PEG

Due to the plethora of available alternatives (including the technologies based on FcRn binding), there is a need for comparative studies to identify the strengths and weaknesses of each technique. For this purpose, PEGylation can serve as a benchmark for comparing the alternative HLE methods providing useful information to the pharmaceutical companies willing to licence these technologies, or for the regulatory bodies to identify benefits for patients and potential risks, or for the biotech companies developing and commercializing these technologies to prove their technologies' edge over PEGylation. Such benchmarking can be considered in the following areas:

### Pharmacokinetics

It is desirable to have a half-life equal to or superior to that obtained from PEGylation in order to allow less frequent dosing, e.g. (at least) weekly. A modest inferiority to PEG cannot be considered as a killer criterion for the HLE alternative, if other advantages still exist. It would be an added advantage if the technology does not interfere with the standard PK quantification methods which are established for PEGylated molecules.

### Pharmacodynamics

Ideally, the protein modification should not negatively affect binding affinity. However, the importance of in vitro binding should not be overestimated, since there is a lack of in vitro in vivo correlation (*25*).


In Tailored Polymer Architectures for Pharmaceutical and Biomedical Applications; Scholz, C., et al.;
ACS Symposium Series; American Chemical Society: Washington, DC, 2013.

## Toxicity

A biodegradable technology can certainly provide an edge over PEG, due to the safety concerns explained earlier. Accordingly, it should show an equal or superior safety profile in animals, and the biodistribution and fate (preferably of the conjugate and the constituting parts) should be elucidated. If the conjugate tends to accumulate in certain organs, like the liver or kidney, then the consequences of chronically administered high doses should be kept in mind. Additionally, information about immunogenicity is important. If the technology uses endogenously found components, there is a chance for development of antibodies against these components, which can lead to breaking of tolerance and serious side effects (*79*, *80*).

Downloaded by UNIV OF NORTH CAROLINA on July 20, 2013 | http://pubs.acs.org
Publication Date (Web): July 8, 2013 | doi: 10.1021/bk-2013-1135.ch013

## Formulation and Stability

Comparative studies regarding stress stability and shelf-life should show that the alternative methods are at least not inferior, if not better than PEGylation. For instance, a stability study for highly concentrated anakinra, PEG-anakinra and HES-anakinra showed that the latter had a much better stability upon storage at 40 °C for 8 weeks (see Figure 3). A reduction in viscosity supporting high dose s.c. administration and preventing problems in purification or analysis, compared to PEGylation, would certainly be an added advantage. The alternative methods should show ability to reduce or control product heterogenity and reproducibility (size variants, charge variants, coupling variants – including coupling stoichiometry). Additionally, the raw materials used should have high purity, should be free from toxic contaminants, and most importantly, have a low price.

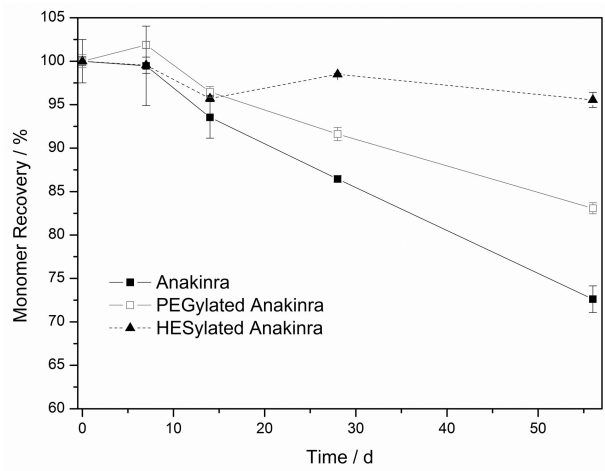


*Figure 3. Monomer recovery of 50 mg/mL anakinra, PEGylated anakinra and HESylated anakinra (protein-based concentration) as a function time upon stotage at 40 °C for 8 weeks.*


In Tailored Polymer Architectures for Pharmaceutical and Biomedical Applications; Scholz, C., et al.;
ACS Symposium Series; American Chemical Society: Washington, DC, 2013.

## Summary and Outlook

Although the PEGylation of biopharmaceuticals is an established half-life extension technology with a number of products reaching the market and others in the pipelines, it is facing a number of challenges, mainly the need to deliver high doses of therapeutic peptides and proteins to chronically ill patients through subcutaneous injection of highly concentrated solutions. Consequently, challenges arise particularly regarding toxicity (due to its non-biodegradability), lowered activity, formulation and high viscosity as well as immunogenicity. To overcome these challenges, many companies have developed a number of alternative technologies either based on increasing the molecular size or based on making use of the FcRn-based recycling mechanism. The former case involves many technologies based on biodegradable polymers, such as HESylation, Polysialylation, PASylation and Xten technologies. While HESylation and PASylation deliverd promising preclinical results and are about to enter clinical studies soon, both Polysialylation and the Xten technologies are already in clinical trials. Results of the clinical studies as well as benchmarking investigations against PEGylated proteins will eventually highlight the strengths of the newer technologies, and improve the therapy with biopharmaceuticals.

Downloaded by UNIV OF NORTH CAROLINA on July 20, 2013 | http://pubs.acs.org
Publication Date (Web): July 8, 2013 | doi: 10.1021/bk-2013-1135.ch013

## References

1. Walsh, G. *Nat. Biotechnol.* **2010**, *28* (9), 917–924.
2. R&D Pipeline News, Top 30 Biologics 2010; www. pipelinereview. com 2011 (accessed 06.11.2012).
3. Abuchowski, A.; van Es, T.; Palczuk, N. C.; Davis, F. F. *J. Biol. Chem.* **1977**, *252* (11), 3578–3581.
4. Abuchowski, A.; McCoy, J. R.; Palczuk, N. C.; van Es, T.; Davis, F. F. *J. Biol. Chem.* **1977**, *252* (11), 3582–3586.
5. Veronese, F. M.; Pasut, G. *Drug Discovery Today* **2005**, *10* (21), 1451–1458.
6. Veronese, F. M.; Mero, A.; Pasut, G. In *PEGylated protein drugs: Basic science and clinical applications*; Veronese, F. M., Ed.; Birkhäuser Verlag: Basel, Switzerland, 2009; p 113.
7. Pammolli, F.; Magazzini, L.; Riccaboni, M. *Nat. Rev. Drug Discovery* **2011**, *10*, 428–438.
8. Aggarwal, S. *Nat. Biotechnol.* **2011**, *29* (12), 1083–1089.
9. Sheridan, C. *Nat. Biotechnol.* **2007**, *25* (4), 365–366.
10. Moran, N. *Nat. Biotechnol.* **2011**, *29* (1), 5–6.
11. Skerra, A. *Curr. Opin. Biotechnol.* **2007**, *18*, 295–304.
12. Kontermann, R. E. *BioDrugs* **2009**, *23* (2), 93–109.
13. Chen, J.; Spear, S. K.; Huddleston, J. G.; Rogers, R. D. *Green Chem.* **2005**, *7* (2), 64–82.
14. Knop, K.; Hoogenboom, R.; Fischer, D.; Schubert, U. S. *Angew. Chem., Int. Ed.* **2010**, *49* (36), 6288–6308.
15. Israelachvili, J. *Proc. Natl. Acad. Sci. U.S.A.* **1997**, *94*, 8378.
16. Wattendorf, U.; Merkle, H. P. *J. Pharm. Sci.* **2008**, *97* (11), 4655–4669.


In Tailored Polymer Architectures for Pharmaceutical and Biomedical Applications; Scholz, C., et al.; ACS Symposium Series; American Chemical Society: Washington, DC, 2013.

17. Begum, R.; Matsuura, H. *J. Chem. Soc., Faraday Trans.* **1997**, *93* (21), 3839–3848.
18. Kirincic, S.; Klofutar, C. *Fluid Phase Equilib.* **1999**, *155*, 311–325.
19. Ninni, L.; Burd, H.; Fung, W. H.; Meirelles, A. J. A. *J. Chem. Eng. Data* **2003**, *48*, 324–329.
20. Eugene, M. *Cell Mol. Biol.* **2004**, *50* (3), 209–215.
21. Zalavsky, B. Y. *Aqueous two-phase partitioning: Physical chemistry and bioanalytical applications*; Marcel Dekker, Inc.: New York, 1995.
22. Asgeirsson, D.; Venturoli, D.; Fries, E.; Rippe, B.; Rippe, C. *Acta Physiol.* **2007**, *191* (3), 237–246.
23. Kerwin, B. A.; Chang, B. S.; Gegg, C. V.; Gonnelli, M.; Li, T. S.; Strambini, G. B. *Protein Sci.* **2002**, *11* (7), 1825–1833.
24. Bailon, P.; Berthold, W. *Pharm. Sci. Technol. Today* **1988**, *1* (8), 352–356.
25. Bailon, P.; Won, C. Y. *Expert Opin. Drug Delivery* **2009**, *6* (1), 1–16.
26. Yowell, S. L.; Blackwell, S. *Cancer Treat Rev.* **2002**, *28* (Suppl A), 3–6.
27. Veronese, F. M. *Biomaterials* **2001**, *22*, 405–417.
28. Payne, R. W.; Murphy, B. M.; Manning, M. C. *Pharm. Dev. Technol.* **2010**, 1–18.
29. Kumar, V.; Kalonia, D. S. *AAPS PharmSciTech* **2006**, *7* (3), 62.
30. Seely, J.; Buckel, S. D.; Green, P. D.; Richey, C. *BioPharm Int.* **2005**.
31. Zhang, B.; Towers, E. W.; Poppe, L.; Cockrill, S. L. *J. Pharm. Sci.* **2011**.
32. Chin, H.-W.; Gikanga, B.; Yang, Y.; Zhang, B. *J. Pharm. Sci.* **2011**, *100* (7), 2518–2525.
33. Lee, B. L.; Kwon, J. S.; Kim, H. J.; Yamamoto, S.; Lee, E. K. *Solid-Phase Bioconjugate Chem.* **2007**, *18*, 1728–1734.
34. Viegas, T. X.; Veronese, F. M. In *PEGylated protein drugs: Basic science and clinical applications*; Veronese, F. M., Ed.; Birkhäuser Verlag: Basel, Switzerland, 2009; p 113.
35. Chi, E. Y.; Krishnan, S.; Kendrick, B. S.; Chang, B. S.; Carpenter, J. F.; Randolph, T. W. *Protein Sci.* **2003**, *12* (5), 903–913.
36. Rodriguez-Martinez, J. A.; Sola, R. J.; Castillo, B.; Cintron-Colon, H. R.; Rivera-Rivera, I.; Barletta, G.; Griebenow, K. *Biotechnol. Bioeng.* **2008**, *101* (6), 1142–1149.
37. Nie, Y.; Zhang, X.; Wang, X.; Chen, J. *Bioconjugate Chem.* **2006**, *17* (4), 995–999.
38. Gonnelli, M.; Strambini, G. B. *Biochim. Biophys. Acta* **2009**, *1794*, 569–576.
39. Basu, A.; Yang, K.; Wang, M.; Liu, S.; Chintala, R.; Palm, T.; Zhao, H.; Peng, P.; Wu, D.; Zhang, Z.; Hua, J.; Hsieh, M. C.; Zhou, J.; Petti, G.; Li, X.; Janjua, A.; Mendez, M.; Liu, J.; Longley, C.; Zhang, Z.; Mehlig, M.; Borowski, V.; Viswanathan, M.; Filpula, D. *Bioconjugate Chem.* **2006**, *17* (3), 618–630.
40. Yu, P. Z.; Qin, D.; Qin, G. H.; Fan, B.; Ma, G. H.; Su, Z. G. *Process Biochem.* **2009**, *44* (12), 1340–1345.
41. Veronese, F. M.; Mero, A.; Caboi, F.; Sergi, M.; Marongiu, C.; Pasut, G. *Bioconjugate Chem.* **2007**, *18* (6), 1824–1830.
42. Yang, C.; Lu, D.; Liu, Z. *Biochemistry* **2011**, *50* (13), 2585–2593.

Downloaded by UNIV OF NORTH CAROLINA on July 20, 2013 | http://pubs.acs.org
Publication Date (Web): July 8, 2013 | doi: 10.1021/bk-2013-1135.ch013

43. Acharya, S. A.; Acharya, V. N.; Kanika, N. D.; Tsai, A. G.; Intaglietta, M.; Manjula, B. N. *Biochem. J.* **2007**, *405*, 503–511.
44. Bhatnagar, B. S.; Martin, S. W.; Hodge, T. S.; Das, T. K.; Joseph, L.; Teagarden, D. L.; Shalaev, E. Y.; Suryanarayanan, R. *J. Pharm. Sci.* **2011**, *100*, 3062–3075.
45. Tattini, V.; Parra, D. F.; Polakiewicz, B.; Pitombo, R. N. M. *Int. J. Pharm.* **2005**, *304* (1-2), 124–134.
46. Kubetzo, S.; Sarkar, C. A.; Plückthun, A. *Mol. Pharmacol.* **2005**, *68* (5), 1439–1454.
47. Fishburn, C. S. *J. Pharm. Sci.* **2008**, *97* (10), 4167–4183.
48. Young, M. A.; Malavalli, A.; Winslow, N.; Vandegriff, K. D.; Winslow, R. M. *Transl. Res.* **2007**, *149* (6), 333–342.
49. Bendele, A.; Seely, J.; Richey, C.; Sennello, G.; Shopp, G. *Toxicol. Sci.* **1998**, *42* (2), 152–157.
50. Webster, R.; Elliott, V.; Park, B. K.; Walker, D.; Hankin, M.; Taupin, P. In *PEGylated protein drugs: Basic science and clinical applications*; Veronese, F. M., Ed.; Birkhäuser Verlag: Basel, Switzerland, 2009; pp 127−146.
51. Henics, T.; Wheatley, D. N. *Biol. Cell* **1999**, *91* (7), 485–498.
52. Ishida, T.; Kiwada, H. *Int. J. Pharm.* **2008**, *354* (1-2), 56–62.
53. Garratty, G. *Transfusion Med. Rev.* **2004**, *18* (4), 245–256.
54. Garay, R. P.; El-Gewely, R.; Armstrong, J. K.; Garratty, G.; Richette, P. *Expert Opin. Drug Delivery* **2012**, *9* (11), 1319–1323.
55. Xu, L.; Anchordoquy, T. *J. Pharm. Sci.* **2011**, *100* (1), 38–52.
56. Singh, S. K. *J. Pharm. Sci.* **2011**, *100* (2), 354–387.
57. Schlesinger, N.; Yasothan, U.; Kirkpatrick, P. Pegloticase. *Nat. Rev. Drug Discovery* **2011**, *10* (1), 17–18.
58. Cimzia® Prescribing Information.
59. Armstrong, J. K. In *PEGylated protein drugs: Basic science and clinical applications*; Veronese, F. M., Ed.; Birkhäuser Verlag: Basel, Switzerland, 2009; pp 147−168.
60. Armstrong, J. K.; Hempel, G.; Koling, S.; Chan, L. S.; Fisher, T.; Meiselman, H. J.; Garratty, G. *Cancer* **2007**, *110* (1), 103–111.
61. Knop, K.; Hoogenboom, R.; Fischer, D.; Schubert, U. S. *Angew. Chem., Int. Ed.* **2010**, *49* (36), 6288–6308.
62. Kontermann, R. E. *Curr. Opin. Biotechnol.* **2011**, *22* (6), 868–876.
63. Dennis, M. S.; Zhang, M.; Meng, Y. G.; Kadkhodayan, M.; Kirchhofer, D.; Combs, D.; Damico, L. A. *J. Biol. Chem.* **2002**, *277* (38), 35035–35043.
64. Sommermeyer, K.; Hildebrand, U.; Cech, F.; Pfitzer, E.; Henning, K.; Weidler, B. *Starch* **1992**, *44* (5), 173.
65. Treib, J.; Baron, J. F.; Grauer, M. T.; Strauss, R. G. *Intensive Care Med.* **1999**, *25*, 258–268.
66. Brecher, M. E.; Owen, H. G.; Bandarenko, N. *J. Clin. Apheresis* **1997**, *12*, 146–153.
67. Jungheinrich, C.; Neff, T. *Clin. Pharmacokinet.* **2005**, *44* (7), 681.
68. Orlando, Ph.D. Thesis, Justus Liebig Universität, Giessen, 2003.
69. Besheer, A.; Hertel, T. C.; Kressler, J.; Mäder, K.; Pietzsch, M. *J. Pharm. Sci.* **2009**, *98* (11), 4420–4428.




In Tailored Polymer Architectures for Pharmaceutical and Biomedical Applications; Scholz, C., et al.; ACS Symposium Series; American Chemical Society: Washington, DC, 2013.



Downloaded by UNIV OF NORTH CAROLINA on July 20, 2013 | http://pubs.acs.org
Publication Date (Web): July 8, 2013 | doi: 10.1021/bk-2013-1135.ch013

70. Hey, T.; Knoller, H.; Vorstheim, P. In *Therapeutic proteins: Strategies to modulate their plasma half-lives*; Kontermann, R. E., Ed.; Wiley-VCH Verlag GmbH & Co.: Weinheim, Germany, 2012.
71. Gregoriadis, G.; Jain, S.; Papaioannou, I.; Laing, P. *Int. J. Pharm.* **2005**, *300* (1-2), 125–130.
72. Lindhout, T.; Iqbal, U.; Willis, L. M.; Reid, A. N.; Li, J.; Liu, X.; Moreno, M.; Wakarchuk, W. W. *Proc. Natl. Acad. Sci. U.S.A.* **2011**, *108* (18), 7397–7402.
73. Jain, S.; Hreczuk-Hirst, D. H.; McCormack, B.; Mital, M.; Epenetos, A.; Laing, P.; Gregoriadis, G. *Biochim. Biophys. Acta* **2003**, *1622* (1), 42–49.
74. Constantinou, A.; Epenetos, A. A.; Hreczuk-Hirst, D.; Jain, S.; Wright, M.; Chester, K. A.; Deonarain, M. P. *Bioconjugate Chem.* **2009**, *20* (5), 924–931.
75. Constantinou, A.; Epenetos, A. A.; Hreczuk-Hirst, D.; Jain, S.; Deonarain, M. P. *Bioconjugate Chem.* **2008**, *19* (3), 643–650.
76. Binder, U.; Skerra, A. In *Therapeutic proteins: Strategies to modulate their plasma half-lives*; Kontermann, R. E., Ed.; Wiley-VCH Verlag GmbH & Co. KGaA: Weinheim, Germany, 2012.
77. Schellenberger, V.; Wang, C. W.; Geething, N. C.; Spink, B. J.; Campbell, A.; To, W.; Scholle, M. D.; Yin, Y.; Yao, Y.; Bogin, O.; Cleland, J. L.; Silverman, J.; Stemmer, W. P. *Nat. Biotechnol.* **2009**, *27* (12), 1186–1190.
78. Geething, N. C.; To, W.; Spink, B. J.; Scholle, M. D.; Wang, C. W.; Yin, Y.; Yao, Y.; Schellenberger, V.; Cleland, J. L.; Stemmer, W. P.; Silverman, J. *PLoS One* **2010**, *5* (4), e10175.
79. Hayrinen, J.; Jennings, H.; Raff, H. V.; Rougon, G.; Hanai, N.; Gerardyschahn, R.; Finne, J. *J. Infect. Dis.* **1995**, *171* (6), 1481–1490.
80. Astronomo, R. D.; Burton, D. R. *Nat. Rev. Drug Discovery* **2010**, *9* (4), 308–324.

Downloaded by UNIV OF NORTH CAROLINA on July 20, 2013 | http://pubs.acs.org
Publication Date (Web): July 8, 2013 | doi: 10.1021/bk-2013-1135.ch013

Downloaded by UNIV OF MINNESOTA on July 17, 2013 | http://pubs.acs.org
Publication Date (Web): July 8, 2013 | doi: 10.1021/bk-2013-1135.ch014

Chapter 14

# Thermoresponsive Polymers with Functional Groups Selected for Pharmaceutical and Biomedical Applications

**Naohiko Shimada and Atsushi Maruyama***

**Institute for Materials Chemistry and Engineering,
Kyushu University,
Motooka 744-CE11, Nishi-ku, Fukuoka, Japan, 819-0395
*E-mail: maruyama@ms.ifoc.kyushu-u.ac.jp.**

Thermoresponsive polymers can be employed in design of smart devices for pharmaceutical and biomedical applications. For these purposes, the thermoresponsive polymers are modified with functional groups that allow control of stimuli-responsiveness and manipulating interactions with biocomponents. This review focuses on design and characteristics of thermoresponsive polymers. Firstly, we highlight some examples of 'lower critical solution temperature' LCST polymers with functional groups selected for pharmaceutical and biomedical applications. Next, we introduce 'upper critical solution temperature' UCST polymers. Although there are only a few examples of polymers that exhibit UCST-type phase behavior in an aqueous media, recent efforts to engineer the phase behavior and interactions with biocomponents by chemical modifications are discussed.

## Introduction

Polymers that change physicochemical properties in response to external stimuli, such as temperature, pH, light and/or magnetic field, have received attention in broad research areas including those related to microfluidics (*1*), textiles (*2*), and sensors (*3*). Polymers with non-linear changes (i.e., phase transitions) in solubility have been extensively explored. Thermoresponsive

© 2013 American Chemical Society
In Tailored Polymer Architectures for Pharmaceutical and Biomedical Applications; Scholz, C., et al.;
ACS Symposium Series; American Chemical Society: Washington, DC, 2013.

polymers that undergo phase transitions in response to modest temperature changes are best characterized of the stimulus-responsive polymers. Various types of smart or intelligent devices using thermoresponsive polymers have been proposed.

Thermoresponsive polymers are classified into two categories: One includes polymers that become insoluble upon heating above a lower critical solution temperature (LCST). The other category includes those that are insoluble below an upper critical solution temperature (UCST). Polymers having UCSTs or LCSTs near physiological temperature under physiological buffer conditions enable us to design smart devices for pharmaceutical and biomedical applications. Modification of the polymers with appropriate functional groups allows modulation of the polymer interactions with biocomponents such as proteins, nucleic acids, lipids, and cells. This review focuses on thermoresponsive polymers with functional groups that have been designed for pharmaceutical and biomedical applications.

Downloaded by UNIV OF MINNESOTA on July 17, 2013 | http://pubs.acs.org
Publication Date (Web): July 8, 2013 | doi: 10.1021/bk-2013-1135.ch014

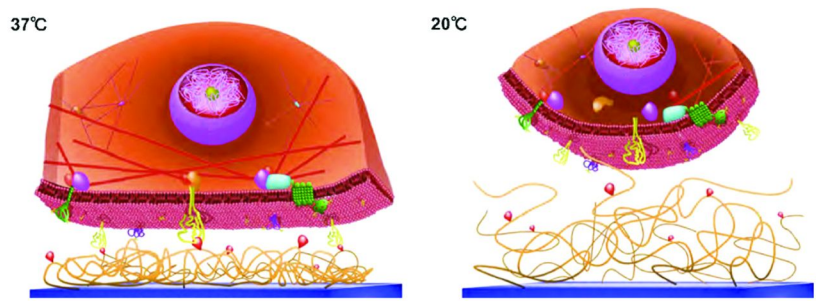


*Figure 1. Schematic illustration of temperature-responsive affinity control of the binding between integrin receptors on a cell and a dish coated with a thermoresponsive polymer modified with cell adhesion peptide. Reprinted with permission from (11), copyright (2007) Elsevier.*

## LCST-Type Polymers with Functional Groups

The LCST-type phase transition behavior is due to hydrophilic/hydrophobic property changes. Poly(N-isopropylacrylamide) (poly(NIPAm)) is one of the most useful LCST-type polymers for bio-related applications because its LCST is close to body temperature (32 °C) under physiological conditions. Okano and his colleagues have reported that cells cultured on a dish grafted with poly(NIPAm) can be detached as a cell sheet by cooling process (*4*), and the cell sheet has been clinically tested in repair of impaired heart function and of esophageal lesions (*5–7*). The same groups also synthesized 2-carboxyisopropylacrylamide (CIPAm), a derivative of NIPAm containing carboxylic groups. Cells were grown on dishes coated with poly(NIPAm-co-CIPAm) could be more rapidly detached


In Tailored Polymer Architectures for Pharmaceutical and Biomedical Applications; Scholz, C., et al.;
ACS Symposium Series; American Chemical Society: Washington, DC, 2013.

than those grown on poly(NIPAm) homopolymer, because the carboxylic groups of the polymer accelerate surface hydration of the dish (*8*). The carboxylic groups of the copolymers have also been utilized as site for modification of the polymer with peptides. Coating of the growth surface with copolymer modified with cell adhesion peptide (RGDS) facilitates the spreading of human umbilical vein endothelial cells without serum at temperatures above LCST; the cells detach at temperatures below LCST after cultivation (Figure 1) (*9*). The surface of chitosan, a polysaccharide with amino groups, copolymerizes with poly(NIPAm), and cells adhere to the copolymer and rapidly detach below LCST (*10*).

There are also many reports of use of LCST-type thermoresponsive polymers in drug delivery systems. Qin et al. reported that the anticancer drug, doxorubicin, entrapped by the thermosensitive block copolymer poly(ethylene oxide-*b*-NIPAm), is released upon cooling to below the LCST (*12*). Copolymers of 2-(dimethylamino)ethyl methacrylate (DMAEMA) and NIPAm form a complex with DNA and have a size of around 200 nm; these complexes have the potential to be taken up by cells (*13*).

The LCSTs of polymers can be tuned over wide range by copolymerization with hydrophobic or hydrophilic monomers. LCSTs of copolymers with ionic groups can be varied by alterations in the charged state of the groups. Based on this property, conversion of thermoresponsiveness to pH responsiveness by introduction of pH-sensitive ionic groups to LCST polymers was demonstrated. Poly(NIPAm-*co*-butylmethacrylate-*co*-acrylic acid) was used as delivery carrier for human calcitonin, which is a peptide hormone, in an oral drug delivery system (*14*). Calcitonin is not released from the complex with copolymer at low pH, but the calcitonin can be released at neutral pH at 37 °C because deprotonation of carboxylic acid induces an increase in LCST to above 37 °C at neutral pH. Soppimath et al. synthesized self-assembling, amphiphilic polymers, poly(NIPAm-co-*N,N*-dimethylacrylamide-co-10-undecenoic acid). Drugs encapsulated in nanoparticles assembled from this copolymer are released in acidic conditions at 37 °C, whereas the particles are stable at pH 7.4 (*15*).

As mentioned above, rational design concepts of smart polymers based on LCST-type polymers have been established. Sophisticated bio-devices tailored for pharmaceutical and biomedical applications were created by employing these polymers. LCST-type phase change was basically driven by considerable dehydration and hydrophilicity change. Thermoresponsive polymers that do not change hydrophilicity upon phase change would be interesting, because these polymer would not cause denaturation and damages of biocomponents owing to excess hydrophobic interactions.

## UCST-Type Polymers with Functional Groups

UCST polymers exhibit thermoresponsiveness on the basis of cohesive interactions, such as hydrogen bonding or electrostatic interactions, among polymer chains. The cohesive interactions are stabilized in low polarity solvents. There have been relatively few reports describing polymers with UCST-type behavior in an aqueous media, because both hydrogen bonds and


In Tailored Polymer Architectures for Pharmaceutical and Biomedical Applications; Scholz, C., et al.;
ACS Symposium Series; American Chemical Society: Washington, DC, 2013.

Downloaded by UNIV OF MINNESOTA on July 17, 2013 | http://pubs.acs.org
Publication Date (Web): July 8, 2013 | doi: 10.1021/bk-2013-1135.ch014

electrostatic interactions among polymer chains are destabilized by water and salts. Strong cohesive interactions between polymer chains is required to provide UCST behavior in an aqueous media. Poly(sulfobetaine)s (*16*, *17*), poly(*N*,*N*-dimethylaminoethyl methacrylate) in the presence of a multivalent anion such as $[Co(CN)_6]^{3-}$ (*18*), and poly(vinyl ether)s with pendant imidazolium salts (*19*) exhibit UCST-type phase transition behavior induced by electrostatic interactions among the polymer chains. Hydrogen bonding is also important in the UCST-type phase transition. One of the most familiar examples of a UCST-type polymer is poly(acrylic acid) (poly(AAc)) (*20*). Poly(AAc) and poly(acrylamide)(poly(AAm)) form a complex at low pH, because protonated carboxylic groups hydrogen bond with amide moieties of polyAAm (*21*). Katono et al. demonstrated release of drug incorporated in interpenetrating polymer network gels composed of poly(AAc) and poly(AAm-*co*-butylmethacrylate) in distilled water; release occurred as the temperature was increased above UCST (*22*).

Few polymers that exhibit UCST-type behavior under physiological buffer conditions are known. Recently, it was reported that polymers with multiple amide groups, including poly(*N*-acryloylglycineamide) and its derivatives, exhibit UCST-type behavior in a phosphate buffer at physiological pH (*23–25*). The utility of these polymers in pharmaceutical and biomedical applications will be restricted because the phase separation temperatures ($T_p$s) are less than 30 °C. As introduction of ionic and hydrophilic groups into the polymers usually results in a considerable decrease in $T_p$, these polymers are not good candidates for functionalization. Introduction of trace amounts of ionic groups into poly(*N*-acryloylglycineamide) actually reduces or prevents the UCST-type behavior (*26*).

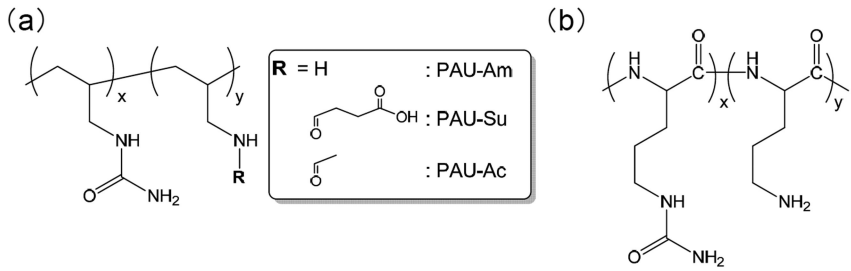


*Figure 2. Structural formula of poly(allylurea) derivatives (a) and poly(L-citrulline-co- L-ornithine).*

To exhibit UCST-type behavior in aqueous media, polymers must have groups with the ability to hydrogen bond and should have few ionizable groups. This hypothesis is supported by data on recently synthesized poly(acrylamide-*co*-acrylonitrile) and poly(methacrylamide) polymers. These non-ionic polymers have $T_p$s above 37 °C (*27*) and are thus candidates for


In Tailored Polymer Architectures for Pharmaceutical and Biomedical Applications; Scholz, C., et al.;
ACS Symposium Series; American Chemical Society: Washington, DC, 2013.

Downloaded by UNIV OF MINNESOTA on July 17, 2013 | http://pubs.acs.org
Publication Date (Web): July 8, 2013 | doi: 10.1021/bk-2013-1135.ch014

introduction of functional groups. Polymers with ureido groups, poly(allylurea) (PU) and poly(L-citrulline) (Figure 2), show UCST-type behavior under physiologically relevant pH and salt conditions (*28*). A UCST polymer with $T_p$ greater than 60 °C was obtained by controlling ureido content and molecular weight. Ionic amino groups (> 20 mol %) were introduced without reducing $T_p$ below the physiological range. The $T_p$ of poly(allylurea-*co*-allylamine) (PU-Am) can be regulated over the temperature range from 8 °C to 65 °C by changing amino group content (Figure 3). PUs having succinyl (PU-Su) or acetyl groups (PU-Ac) have also been obtained (*29*) and exhibit UCST behavior under physiological relevant conditions. The $T_p$s of the polymers with ionic groups change when the pH of the solution is changed. Furthermore, selective protein capture and separation is possible using PUs with different ionic groups (*29*). Poly(L-citrulline) derivatives , poly(L-citrulline-*co*-L-ornithine), also show UCST-type behavior (*28*). Because these derivatives are composed of naturally occurring amino acids, these polymers are biocompatible and biodegradable and hold promise for pharmaceutical and biomedical applications.

Downloaded by UNIV OF MINNESOTA on July 17, 2013 | http://pubs.acs.org
Publication Date (Web): July 8, 2013 | doi: 10.1021/bk-2013-1135.ch014

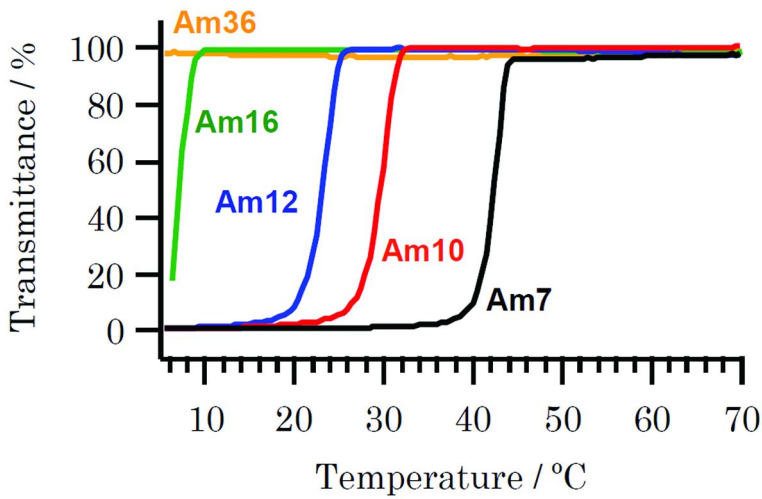


*Figure 3. UCST-type transmittance curves of PU-Ams at pH 7.5 in buffer containing 150 mM NaCl. The numbers indicate mol% of amino groups of PU-Am. Reprint with permission from (28), Copyright (2011) American Chemical Society.*

## Conclusion

Pharmaceutical and biomedical utilities of thermoresponsive polymers have been expanded by introduction of functional groups to the polymers. Bioconjugation, conversion of stimuli-responsiveness and manipulation of biocomponents were achieved by functionalizing thermoresponsive polymers.

Moreover, recent advances in UCST-type thermoresponsive polymers are particularly notable because these polymers would give us new strategies for material design that could not be achieved with LCST-type polymers.

## References


1. Argentiere, S.; Gigli, G.; Mortato, M.; Gerges, I., Blasi, L. Smart Microfluidics: The Role of Stimuli- Responsive Polymers in Microfluidic Devices. In *Advances in Microfluidics*; Kelly, R. T., Ed.; InTech: New York, 2012, pp 127−154.
2. Hu, J.; Meng, H.; Li, G.; Ibekwe, S. I. *Smart Mater. Struct.* **2012**, *21*, 053001.
3. Richter, A.; Paschew, G.; Klatt, S.; Lienig, J.; Arndt, K.-F.; Adler, H.-J. *Sensors* **2008**, *8*, 561–581.
4. Yamada, N.; Okano, T.; Sakai, H.; Karikusa, F.; Sawasaki, Y.; Sakurai, Y. *Makromol. Chem. Rapid Commun.* **1990**, *11*, 571–576.
5. Ohki, T.; Yamato, M.; Murakami, D.; Takagi, R.; Yang, J.; Namiki, H.; Okano, T.; Takasaki, K. *Gut* **2006**, *55*, 1704–1710.
6. Hata, H.; Matsumiya, G.; Miyagawa, S.; Kondoh, H.; Kawaguchi, N.; Matsuura, N.; Shimizu, T.; Okano, T.; Matsuda, H.; Sawa, Y. *J. Thorac. Cardiovasc. Surg.* **2006**, *132*, 918–924.
7. Nishida, K.; Yamato, M.; Hayashida, Y.; Watanabe, K.; Yamamoto, K.; Adachi, E.; Nagai, S.; Kikuchi, A.; Maeda, N.; Watanabe, H.; Okano, T.; Tano, Y. *N. Engl. J. Med.* **2004**, *351*, 1187–1196.
8. Ebara, M.; Yamato, M.; Hirose, M.; Aoyagi, T.; Kikuchi, A.; Sakai, K.; Okano, T. *Biomacromolecules* **2003**, *4*, 344–349.
9. Ebara, M.; Yamato, M.; Aoyagi, T.; Kikuchi, A.; Sakai, K.; Okano, T. *Biomacromolecules* **2004**, *5*, 505–510.
10. Wang, J.; Chen, L.; Zhao, Y.; Guo, G.; Zhang, R. *J. Mater. Sci.: Mater. Med.* **2009**, *20*, 583–590.
11. Yamato, M.; Akiyama, Y.; Kobayashi, J.; Yang, J.; Kikuchi, A.; Okano, T. *Prog. Polym. Sci.* **2007**, *32*, 1123–1133.
12. Qin, S.; Geng, Y.; Discher, D. E.; Yang, S. *Adv. Mater.* **2006**, *18*, 2905–2909.
13. Hinrichs, W.; Schuurmans-Nieuwenbroek, N.; Van De Wetering, P.; Hennink, W. *J. Controlled Release* **1999**, *60*, 249–259.
14. Serres, A.; Baudyš, M.; Kim, S. *Pharm. Res.* **1996**, *13*, 196–201.
15. Soppimath, K. S.; Tan, D. C. W.; Yang, Y. Y. *Adv. Mater.* **2005**, *17*, 318–323.
16. Schulz, D. N.; Peiffer, D. G.; Agarwal, P. K.; Larabee, J.; Kaladas, J. J.; Soni, L.; Handwerker, B.; Garner, R. T. *Polymer* **1986**, *27*, 1734–1742.
17. Chen, L.; Honma, Y.; Mizutani, T.; Liaw, D. J.; Gong, J. P.; Osada, Y. *Polymer* **2000**, *41*, 141–147.
18. Plamper, F. A.; Schmalz, A.; Muller, A. H. E. *J. Am. Chem. Soc.* **2007**, *129*, 14538–14539.
19. Yoshimitsu, H.; Kanazawa, A.; Kanaoka, S.; Aoshima, S. *Macromolecules* **2012**.
20. Buscall, R.; Corner, T. *Eur. Polym. J.* **1982**, *18*, 967–974.


Downloaded by UNIV OF MINNESOTA on July 17, 2013 | http://pubs.acs.org
Publication Date (Web): July 8, 2013 | doi: 10.1021/bk-2013-1135.ch014


In Tailored Polymer Architectures for Pharmaceutical and Biomedical Applications; Scholz, C., et al.;
ACS Symposium Series; American Chemical Society: Washington, DC, 2013.

21. Eustace, D. J.; Siano, D. B.; Drake, E. N. *J. Appl. Polym. Sci.* **1988**, *35*, 707–716.
22. Katono, H.; Maruyama, A.; Sanui, K.; Ogata, N.; Okano, T.; Sakurai, Y. *J. Controlled Release* **1991**, *16*, 215–227.
23. Nagaoka, H.; Ohnishi, N.; Eguchi, M. Thermoresponsive Polymer and Production Method Thereof. U.S. Patent 7,847,047, 2007.
24. Seuring, J.; Agarwal, S. *Macromol. Chem. Phys.* **2010**, *211*, 2109–2117.
25. Glatzel, S.; Laschewsky, A.; Lutz, J.-F. *Macromolecules* **2011**, *44*, 413–415.
26. Seuring, J.; Bayer, F. M.; Huber, K.; Agarwal, S. *Macromolecules* **2011**, *45*, 374–384.
27. Seuring, J.; Agarwal, S. *Macromolecules* **2012**, *45*, 3910–3918.
28. Shimada, N.; Ino, H.; Maie, K.; Nakayama, M.; Kano, A.; Maruyama, A. *Biomacromolecules* **2011**, *12*, 3418–3422.
29. Shimada, N.; Nakayama, M.; Kano, A.; Maruyama, A. *Biomacromolecules* **2013**, *14*, 1452–1457.

Downloaded by UNIV OF MINNESOTA on July 17, 2013 | http://pubs.acs.org
Publication Date (Web): July 8, 2013 | doi: 10.1021/bk-2013-1135.ch014

Downloaded by VIRGINIA TECH on July 20, 2013 | http://pubs.acs.org
Publication Date (Web): July 8, 2013 | doi: 10.1021/bk-2013-1135.ch015

Chapter 15

# Biomaterial-Induced Angiogenesis To Address Peripheral Vascular Disease: The Application of Sphere Templated Hydrogels

**Dale Terasaki,[2] Michael Sobel,[3] Colleen Irvin,[2] Errol Wijelath,[3] and Buddy D. Ratner*,[1,2]**

**[1]University of Washington Engineered Biomaterials (UWEB), University of Washington Seattle, Washington 98195**
**[2]Department of Bioengineering, University of Washington, Seattle, Washington 98195**
**[3]Department of Surgery, University of Washington, Seattle, Washington 98195**
***E-mail: ratner@uweb.engr.washington.edu.**

Peripheral arterial disease (PAD) is the atherosclerotic arterial occlusive disease of the legs that leads to muscle ischemia, disability, and limb loss. Therapeutic approaches that can restore circulation to ischemic limbs are needed. Here we explore the potential of a sphere-templated hydrogel scaffold with 30 micron diameter interconnected pores to induce an angiogenic response. A variant of this scaffold with 60 micron diameter parallel channels in addition to the 30 micron spherical pores was studied to determine if larger vessels might form in the larger channels. As a control, expanded polytetrafluoroethylene (PTFE) was studied. The three types of porous materials were implanted in mouse muscle for two weeks. The scaffold with 30 micron spherical pores showed the highest level of angiogenesis. However, only capillary-dimension blood vessels were seen in all materials.

© 2013 American Chemical Society
In Tailored Polymer Architectures for Pharmaceutical and Biomedical Applications; Scholz, C., et al.; ACS Symposium Series; American Chemical Society: Washington, DC, 2013.

Downloaded by VIRGINIA TECH on July 20, 2013 | http://pubs.acs.org
Publication Date (Web): July 8, 2013 | doi: 10.1021/bk-2013-1135.ch015

# Introduction

Peripheral arterial disease (PAD) is the atherosclerotic arterial occlusive disease of the legs that leads to muscle ischemia, disability, and limb loss. According to a 1999-2004 study, 12.2% of adults over the age of 60 suffered from PAD (*1*). Significant risk factors associated with PAD include smoking, hypertension and diabetes mellitus (*1*). Non-Hispanic black patients exhibited a higher prevalence of 19.2%. The overall prevalence rose to 23.2% for those over 80 years old. The need for effective treatment of PAD will escalate over the next few decades, as the number of patients over the age of 65 is predicted to increase from 35.3 million to 70.2 million by the year 2030 (*2*). Furthermore, a study that followed a large group of elderly men and women for ten years and assessed the mortality rates of those with PAD reported a 3-fold increase in mortality associated with PAD, even when controlling for age, sex, and other risk factor for cardiovascular disease (*3*).

Although mild to moderate PAD can be managed conservatively, more severe atherosclerotic obstructions of the leg arteries require surgical vascular grafting for relief of ischemia. And while natural graft conduits of autogenous veins work best for replacing these small diameter vessels, autogenous conduits are frequently not available, so prosthetic grafts are required (commonly ePTFE – expanded polytetrafluoroethylene). The critical problem with these small diameter prosthetic grafts is that host tissue ingrowth is severely limited by their structure and form. Without transmural tissue ingrowth and a native endothelium, they are persistently thrombogenic, and stimulate neointimal hyperplasia (*4*), leading to frequent graft failure. The ideal prosthetic graft material would permit and encourage the transmural ingrowth of host tissue, and the elaboration of a stable, durable endothelium.

Angiogenesis is the growth of capillaries from pre-existing blood vessels in the body. It occurs naturally in response to tissue growth and repair, yet it is also involved in various inflammatory diseases such as rheumatoid arthritis, psoriasis, and cancers (*5*). A related physiological process is arteriogenesis, which is the development of larger, collateral vessels sprouting from pre-existing arteries.

It has been observed in patients with vascular diseases that collateral vessels can develop to bypass an obstruction and restore flow. Clinically, there is an association between collateral vessels and higher survival rates after myocardial infarction (*6*). Researchers have been investigating arteriogenic therapy – the stimulation of arterial growth from preexisting arteries – as an approach to treat peripheral vascular disease. A number of review articles (*5*, *7*–*9*) have been published that document the progress of this research thrust.

The discovery and characterization of vascular endothelial growth factor (VEGF) and basic fibroblast growth factor (bFGF) in the late 1970's and in the 1980's led to many early efforts to explore angiogenesis and arteriogenesis for therapeutic applications. For example, one study assessed the effects of bFGF on blood flow to an ischemic canine myocardium (*10*). Dogs that were given bolus injections of bFGF showed a statistically significantly higher degree of collateral flow than those with no injection. This was demonstrated in the rabbit ischemic hind-limb model as well (*11*).


In Tailored Polymer Architectures for Pharmaceutical and Biomedical Applications; Scholz, C., et al.;
ACS Symposium Series; American Chemical Society: Washington, DC, 2013.

Therapeutic arteriogenesis is being explored by using other growth factors and novel modes of delivery. A marked increase in vascular density and vascular branching was observed when an osmotic pump was used to supply an ischemic rabbit hind limbs with VEGF (*12*). The rabbits treated with VEGF in this study also exhibited new hair growth and restored functionality in their limbs. Monocyte chemoattractant protein-1 (MCP-1) was also explored and evidence was observed of the angiogenic and arteriogenic functionality (*13*). In another study that utilized a rabbit hind limb ischemia model, plasmid gene therapy was employed to increase platelet derived endothelial growth factor (PD-ECGF) production (*14*) . Within 30 days of transfection, there was a significant increase in capillary density, arteriolar density, and calf blood pressure. Grundmann et al. (*15*) used an implantable infusion pump that released granulocyte-macrophage colony stimulating factor (GM-CSF) in a pig vascular occlusion model. Collateral conductance was shown to increase with the added stimulating factor.

Biomaterial scaffolds have been of great interest in the field of tissue engineering. The goal is to construct implantable materials of either biologic or synthetic origin to guide the in-growth/formation of native tissue and a native endothelium. Here we explore the use of precision engineered scaffolds that might encourage new blood vessel formation and could be used to construct optimized porous grafts that promote ingrowth and endothelialization. We have applied the process of sphere-templating for creating pro-angiogenic, anti-fibrotic scaffolds. We refer to the manufacture of these scaffolds as the "6S" process: sifting microspheres to a uniform size, sonicating the microspheres to close-pack them, sintering them together, surrounding them with the desired scaffold polymer, and solubilizing away the beads to yield interconnected pores. Marshall et al. discovered that pore size is strongly associated with vascular growth into sphere-templated materials (*16*). In the Marshall et al. experiments, scaffolds with pores of approximately 35μm diameter yielded the greatest density of blood vessels in a mouse subcutaneous model. The 6S scaffolds have been further enhanced by incorporating 60 μm diameter parallel channels running through the sphere-templated structure (*17*). These channels might allow larger blood vessels to form and to provide directionality for those vessels.

Downloaded by VIRGINIA TECH on July 20, 2013 | http://pubs.acs.org
Publication Date (Web): July 8, 2013 | doi: 10.1021/bk-2013-1135.ch015

## Experimental

### Scaffolds

*Scaffolds*

Three different groups of rod-shaped implants were used for the mouse implant study. The first group of scaffolds was comprised of poly(2-hydroxyethyl methacrylate)(PHEMA) fashioned to have longitudinal channels interconnected by spherical pores. These samples will be referred to as "channeled" scaffolds. The second group consisted of PHEMA implants with an interconnected porous geometry similar to the first group, but lacking the channels. These samples will be referred to as "porous" scaffolds. The third group was expanded


In Tailored Polymer Architectures for Pharmaceutical and Biomedical Applications; Scholz, C., et al.;
ACS Symposium Series; American Chemical Society: Washington, DC, 2013.

polytetrafluoroethylene (PTFE) with channel-like spaces in between the fibrils of the material. These samples were segments obtained from a commonly used clinical type of PTFE graft. This material was included as a control in order to contrast with the effects of the channeled architecture materials.

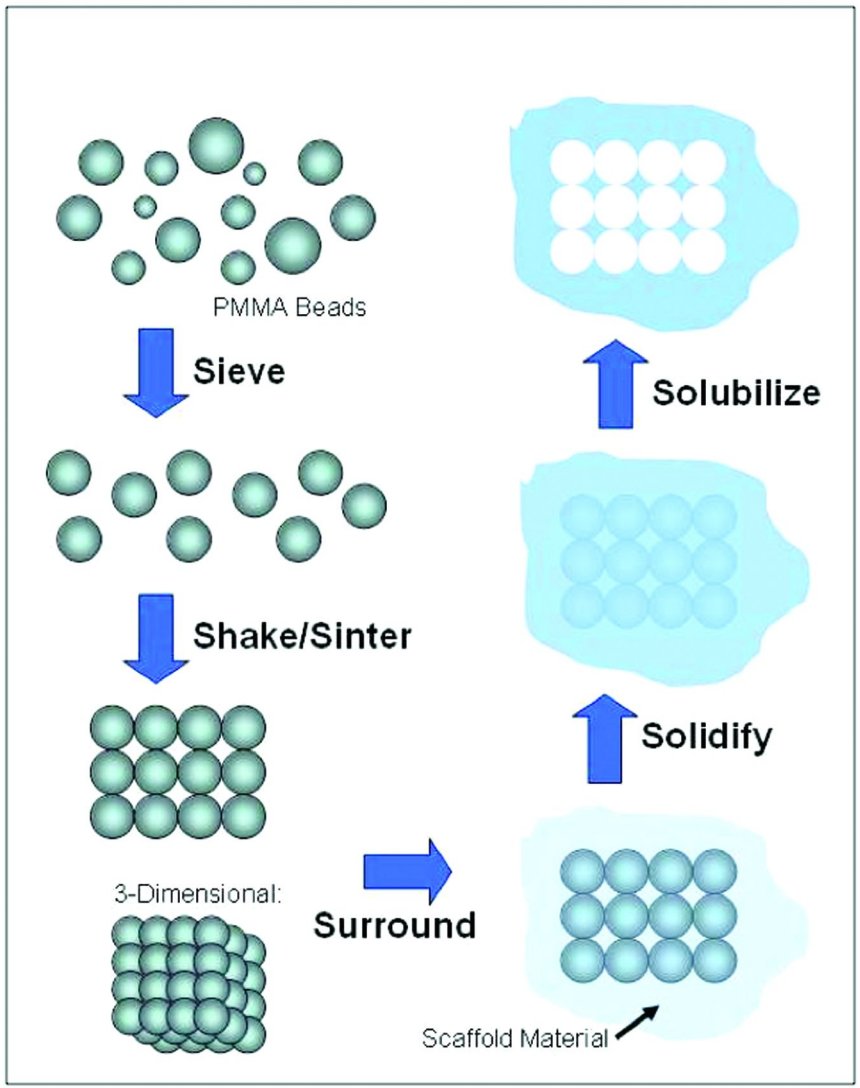


*Figure 1. A schematic representation of the "6S" process for fabricating scaffolds with uniform, interconnected pores.*

Downloaded by VIRGINIA TECH on July 20, 2013 | http://pubs.acs.org
Publication Date (Web): July 8, 2013 | doi: 10.1021/bk-2013-1135.ch015


In Tailored Polymer Architectures for Pharmaceutical and Biomedical Applications; Scholz, C., et al.;
ACS Symposium Series; American Chemical Society: Washington, DC, 2013.

*Fabrication of Scaffolds*

Porous scaffolds and channeled scaffolds were both fabricated using variants of the 6S sphere-templating process, and were composed of crosslinked pHEMA (*17*, *18*). As illustrated in Figure 1, PMMA beads are sieved to attain a uniformly sized fraction, shaken by sonication to ensure close packing, sintered together at >140°C, and surrounded by monomer solution under low vacuum pressure. The monomer mixture (purified HEMA monomer, tetraethylene glycol dimethacrylate crosslinking agent, ethylene glycol-water solvent and Irgacure 651) is then allowed to fully infiltrate the "bead cake" under atmospheric pressure. Upon UV initiation, the bead/polymer complex is immersed in solvents to remove the beads. Interconnected pores of approximately 30 microns in diameter were produced.

The channeled scaffolds were fabricated by a process developed at the University of Washington (*17*), a variant of the 6S process, as illustrated in Figure 2.

Downloaded by VIRGINIA TECH on July 20, 2013 | http://pubs.acs.org
Publication Date (Web): July 8, 2013 | doi: 10.1021/bk-2013-1135.ch015

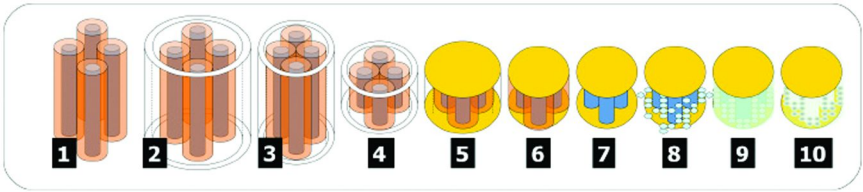


*Figure 2. Channeled scaffold fabrication: 1) Polycarbonate fibers with PMMA cladding are spun onto a reel. 2) Fiber bundles are inserted into shrink tubing. 3) Tubing is heated and compresses the fibers together. 4) Tubing is sectioned into smaller cylinders for ease of handling. 5) The ends of cylinders are glued to hold rods in place. 6) Shrink tubing is then cut away. 7) The PMMA cladding is dissolved away with xylenes. 8) Void spaces are filled with PMMA microbeads, which are then fused together by heating (see Figure 1). 9) Cylinders are infiltrated with HEMA monomer and allowed to polymerize. 10) PMMA and polycarbonate are dissolved away using as series of dichloromethane, acetone, ethanol, and water washes.*

The ePTFE materials were 0.6 mm wall thickness,with a porosity of 60 micron internodal distance (obtained from Atrium Medical, Hudson, NH). They were steam sterilized for 4 min before use. All samples were cut into approximately 5mm long rods with 1mm x 1mm square cross sections. These sizes were estimates in that the hydrogel samples exhibited varying swelling properties depending on the media.

**Implantation/Study Details**

An MTT cytotoxicity test and a gel-clot endotoxin assay were performed on all samples to ensure freedom from endotoxin and cytotoxic leachables.

Five male C57BL/6 mice were purchased from Charles River Laboratories (http://www.criver.com/). Mouse implantations were performed under aseptic conditions under the guidelines of the University of Washington IACUC. Ten scaffolds were implanted in 5 mice. Bilateral bicep femoris muscle implants of a single sample per muscle were performed on each mouse using Ketamine-Xylazine anesthesia cocktail. Each muscle incision was closed with a suture. Skin incisions were closed using wound clips. One dose of Buprenorphine was given per mouse for post surgical analgesia. Implants were explanted at two weeks and fixed in a zinc fixative. Non-specific stains included Trichrome, Picrosirius Red, and 4′,6-diamidino-2-phenylindole (DAPI). Immunohistochemical analysis consisted of MECA-32 staining. Not all implants could be found after excision and slide processing. Hence, there are fewer ePTFE samples than other scaffolds. Each explanted sample led to 12 or 30 sequential slides for the various stains desired.

Downloaded by VIRGINIA TECH on July 20, 2013 | http://pubs.acs.org
Publication Date (Web): July 8, 2013 | doi: 10.1021/bk-2013-1135.ch015

**Histological Analysis**

All paraffin-embedded tissue samples were sectioned into 5μm thick slices and placed in duplicate on slides. All histological images were acquired using a Nikon E800 Upright Microscope and Metamorph Version 6.3r7 software unless otherwise specified.

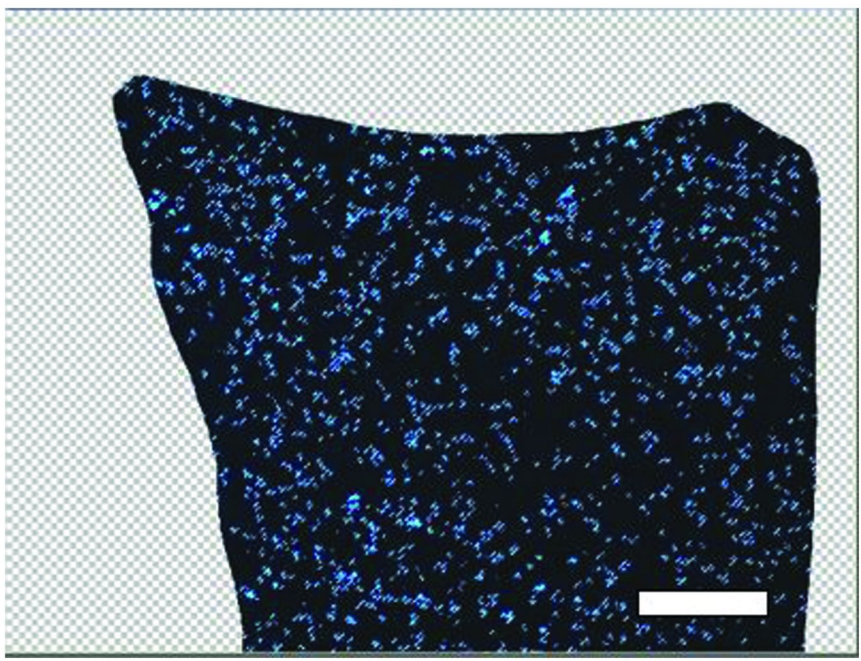

*Figure 3. A DAPI-stained image of a section of the porous scaffold. Scale Bar = 200 micron.*


In Tailored Polymer Architectures for Pharmaceutical and Biomedical Applications; Scholz, C., et al.;
ACS Symposium Series; American Chemical Society: Washington, DC, 2013.

Slides of each region of each scaffold group were stained with DAPI, and 10x micrographs were acquired. Using Adobe Photoshop CS4, an area of the image within the bounds of the scaffold was isolated as shown in Figure 3. Next, the blue nuclei were selected and the pixel area was recorded. The inverse, black pixel area was also recorded such that the ratio of blue nuclei pixel area to total pixel area could be calculated.

MECA-32 is a mouse panendothelial cell antigen. For counting MECA-32 positively stained cells, images at 20x magnification were selected in a staggered fashion from sections at each region of each implant. Next, a grid of 300 μm x 200 μm was overlaid in the Metamorph software (Figure 4). Positively stained cells were counted using a software-specific tool and these counts were exported to an Excel spreadsheet for further analysis. A positive cell was deemed to be noticeably stained (unstained cells exist in the image) and have a well-defined nuclei.

Downloaded by VIRGINIA TECH on July 20, 2013 | http://pubs.acs.org
Publication Date (Web): July 8, 2013 | doi: 10.1021/bk-2013-1135.ch015

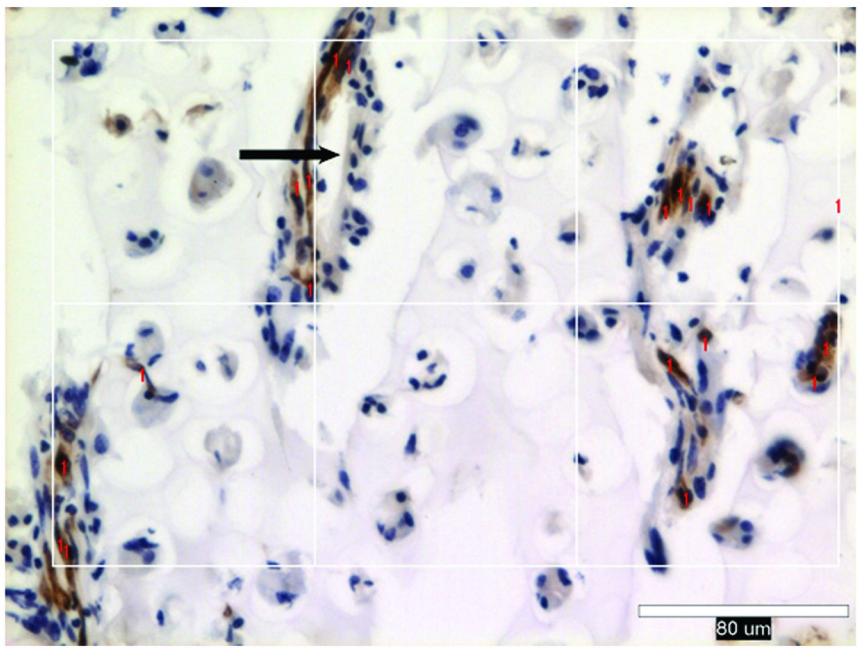


*Figure 4. An example of a MECA-32 stained slide: 20x magnified channeled scaffold with 300 μm x 200 μm grid. The "1's" indicate positive cell counts. The arrow points to a vessel lumen.*

MECA-32 lumen widths were calculated using calipers in the Metamorph software. Again, images from each region – if available – of each section were included in the analysis. A lumen was defined by the inner space between two long, parallel endothelial cells, or by the space within a circular endothelial "donut" shape. A well defined lumen is seen at the top of the image in Figure 4.

## Results

### In Vivo Study

Prior to implantation, a MTT cytotoxicity assay was performed. The implant samples showed equal or greater levels of cellular proliferation relative to the positive control. None of the samples tested positive for endotoxins using the gel-clot endotoxin assay. After explantation, DAPI staining and MECA-32 staining was performed. Figure 5 compares DAPI staining and MECA-32 staining for the PTFE and the porous scaffolds. Cells are dispersed more uniformly in the porous scaffold and in tissue adjacent to the porous scaffold. In contrast, the PTFE shows a heavy accumulation of inflammatory cells in the adjacent tissue compared to in the channels.

Downloaded by VIRGINIA TECH on July 20, 2013 | http://pubs.acs.org
Publication Date (Web): July 8, 2013 | doi: 10.1021/bk-2013-1135.ch015

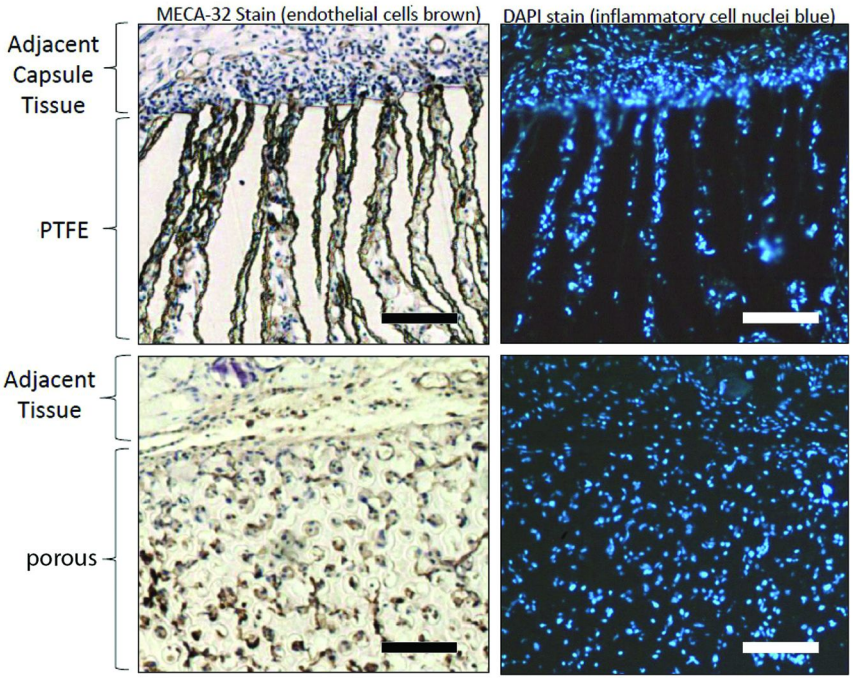


*Figure 5. DAPI and MECA-32 staining of the porous scaffold and the ePTFE material after 2 week implantation in mice. Scale bars are 100 microns.*

DAPI staining allows us to obtain information about general cellular infiltration within the scaffolds. The ratios of positively stained pixel area to total area for each scaffold type was determined using Adobe Photoshop CS3. These data are presented in Figure 6. There were statistically significant differences between the channeled and porous scaffolds, the channeled and PTFE scaffolds, and the porous and PTFE scaffolds (p-value $<0.005$, $<0.05$, $<0.005$, respectively).


In Tailored Polymer Architectures for Pharmaceutical and Biomedical Applications; Scholz, C., et al.;
ACS Symposium Series; American Chemical Society: Washington, DC, 2013.

Downloaded by VIRGINIA TECH on July 20, 2013 | http://pubs.acs.org
Publication Date (Web): July 8, 2013 | doi: 10.1021/bk-2013-1135.ch015

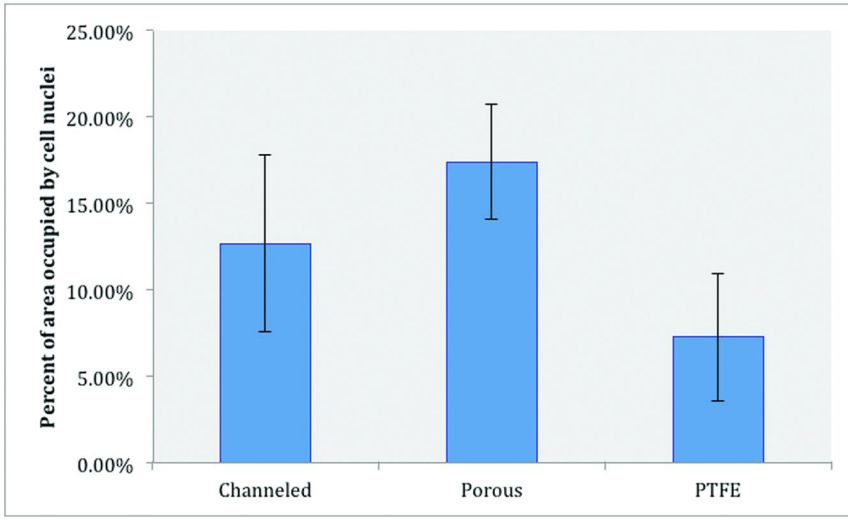


*Figure 6. Cellular infiltration data from DAPI images: N=17,15,5 for channeled, porous, and PTFE scaffolds, respectively. Error bars represent mean ±1 standard deviation.*

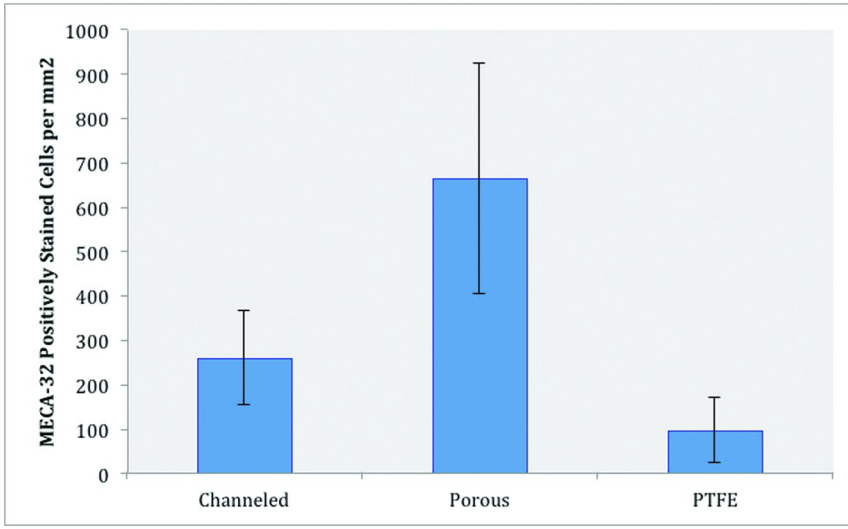


*Figure 7. MECA-32 Positive Cells: N=41, 31, 18 for channeled, porous, and PTFE scaffolds, respectively. Error bars represent mean ±1 standard deviation.*

Figure 7 shows the density of cells stained positive for MECA-32. The channeled scaffolds contained approximately 260 positively stained cells per cells/mm$^2$ while the porous scaffold had almost 700 cells/mm$^2$. PTFE showed the lowest endothelial cell content of the three scaffolds examined. There were statistically significant differences between the channeled and porous scaffolds, the channeled and PTFE scaffolds, and the porous and PTFE scaffolds (p-value <0.001, <0.001, <0.001, respectively).

Figure 8 depicts the average lumen widths of micro-vessels found in the three scaffold types. The micro-vessels observed within the channeled scaffolds exhibited an average width of 2.4 µm. There was a statistically significant difference between the channeled and porous scaffolds (p-value <0.001).

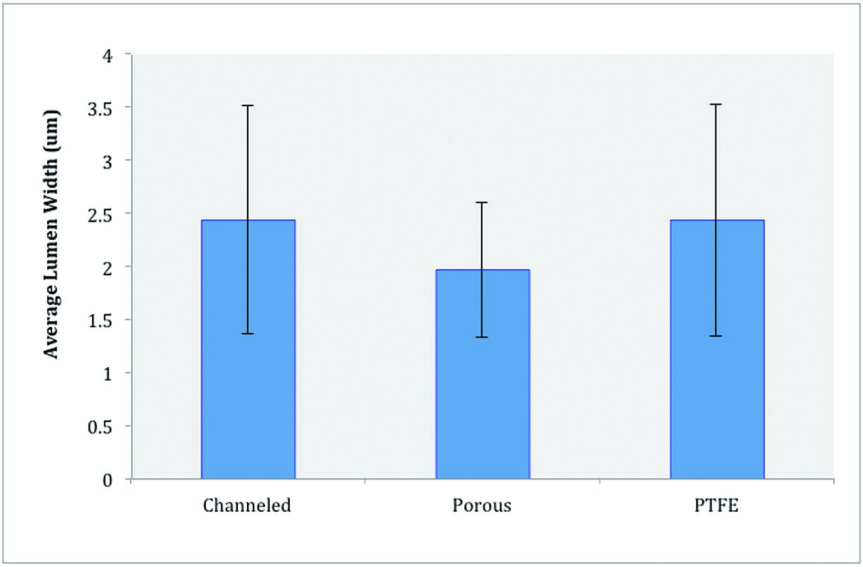


*Figure 8. Lumen Widths: N=83, 74, 16 for channeled, porous, and PTFE scaffolds, respectively. Error bars represent mean ±1 standard deviation.*

Downloaded by VIRGINIA TECH on July 20, 2013 | http://pubs.acs.org
Publication Date (Web): July 8, 2013 | doi: 10.1021/bk-2013-1135.ch015

## Discussion

This *in-vivo* study demonstrates that specifically engineered porous or channeled scaffolds have promise as an improved graft conduit material for peripheral arterial disease.

From the DAPI staining, it was determined that the porous scaffolds supported a greater degree of cellular infiltration than the PTFE samples. This is not surprising because the sphere-templated geometry allows for more void space, with a tightly controlled consistent architecture, Marshall et al. observed that sphere-templated materials consisted of approximately 67% void space by cross-sectional area (*19*). The ePTFE, in contrast, was noted in the current study to contain approximately twice as much solid material as void space and the


In Tailored Polymer Architectures for Pharmaceutical and Biomedical Applications; Scholz, C., et al.;
ACS Symposium Series; American Chemical Society: Washington, DC, 2013.

random, nodal structure of PTFE yielded significant heterogeneity in the size and distribution of void spaces. The channeled scaffolds contained more cells than the PTFE scaffolds but fewer than the porous controls.

From MECA-32 staining, it was found that vascular ingrowth did indeed occur within the channels and interconnected pores in the channeled scaffolds. However, the average lumen widths were small. They were statistically significantly larger than vessels in the porous scaffolds, but the potential for larger vessels with diameters approaching 60μm was not realized. Such larger vessels were observed in implants of this type into rat heart muscle (unreported data). Additionally, while the channeled scaffolds exhibited a greater concentration of endothelial cells than the PTFE samples, the porous scaffolds had the greatest number of endothelial cells by a large margin. Many papers have been published on the generation of new blood vessels in ischemic limbs and some of these have generated quantitative data on blood vessel density (*20–22*). However, due to different animal species and counting protocols, comparison between our study and other published studies is not feasible. Still it seems that the porous scaffold (the 6S scaffold) is highly angiogenic, and this property of the scaffold may encourage new blood vessel growth in the tissue external to the implant. Such enrichment of blood vessels in the region external to the scaffold has been noted (*23*). Also, the 6S implants are seen to heavily invaded by macrophages (*18*). Macrophages can be stimulated by porous materials to produce enhanced levels of cytokines (*24*). Since macrophages can secrete many of the cytokines associated with vascularized healing (VEGF, bFGF, etc), the presence of this enriched population of cells that are in a pro-healing phenotype (*17*) is potentially useful as a non-pharmacologic stimulator of angiogenesis.

Downloaded by VIRGINIA TECH on July 20, 2013 | http://pubs.acs.org
Publication Date (Web): July 8, 2013 | doi: 10.1021/bk-2013-1135.ch015

## Acknowledgments

Funding for these studies was provided by University of Washington Engineered Biomaterials (UWEB, National Science Foundation). Special thanks to Dr. Marc Takeno for assistance with images and microscopy.

## References

1. Ostchega, Y.; Paulose-Ram, R.; Dillon, C. F.; Gu, Q.; Hughes, J. P. Prevalence of Peripheral Arterial Disease and Risk Factors in Persons Aged 60 and Older: Data from the National Health and Nutrition Examination Survey 1999–2004. *J. Am. Geriatr. Soc.* **2007**, *55* (4), 583–589.
2. Purcell, P. Older Workers: Employment and Retirement Trends. *Monthly Labor Review*; Bureau of Labor Statistics: Washington DC, October 2000; pp 19−30.
3. Criqui, M. H.; Langer, R. D.; Fronek, A.; Feigelson, H. S.; Klauber, M. R.; McCann, T. J.; Browner, D. Mortality over a period of 10 years in patients with peripheral arterial disease. *N. Engl. J. Med.* **1992**, *326* (6), 381–386.

4. Zilla, P.; Bezuidenhout, D.; Human, P. Prosthetic vascular grafts: wrong models, wrong questions and no healing. *Biomaterials* **2007**Dec, *28* (34), 5009–27.
5. Helisch, A.; Schaper, W. Arteriogenesis: the development and growth of collateral arteries. *Microcirculation* **2003**Jan, *10* (1), 83–97.
6. Maseri, A.; Araujo, L.; Finocchiaro, M. Collateral devlopment and function in man. In *Collateral Circulation: Heart, Brain, Kidney, Limbs*; Schaper, W., Ed.; Kluwer Academic Publishers: New York, 1993; pp 381−402.
7. Germani, A.; Di Campli, C.; Pompilio, G.; Biglioli, P.; Capogrossi, M. C. Regenerative Therapy in Peripheral Artery Disease. *Cardiovasc. Ther.* **2009**, *27* (4), 289–304.
8. Lawall, H.; Bramlage, P.; Amann, B. Treatment of peripheral arterial disease using stem and progenitor cell therapy. *J. Vasc. Surg.* **2011**, *53* (2), 445–453.
9. Blum, A.; Balkan, W.; Hare, J. M. Advances in cell-based therapy for peripheral vascular disease. *Atherosclerosis* **2012**, *223* (2), 269–277.
10. Unger, E.F.; Banai, S.; Shou, M.; Lazarous, D.F.; Jaklitsch, M.T.; Scheinowitz, M.; Correa, R.; Klingbeil, C.; Epstein, S.E. Basic fibroblast growth factor enhances myocardial collateral flow in a canine model. *Am J Physiol* **1994**, *266* (4) (Pt 2), H1588–95.
11. Baffour, R.; Berman, J.; Garb, J.L.; Rhee, S.W.; Kaufman, J.; Friedmann, P. Enhanced angiogenesis and growth of collaterals by in vivo administration of recombinant basic fibroblast growth factor in a rabbit model of acute lower limb ischemia: dose-response effect of basic fibroblast growth factor. *J. Vasc. Surg.* **1992**Aug, *16* (2), 181–91.
12. Hopkins, S.P.; Bulgrin, J.P.; Sims, R.L.; Bowman, B.; Donovan, D.L.; Schmidt, S.P. Controlled delivery of vascular endothelial growth factor promotes neovascularization and maintains limb function in a rabbit model of ischemia. *J. Vasc. Sur.* **1998**, *27* (5), 886–895.
13. Hoefer, I.E.; van Royen, N.; Buschmann, I.R.; Piek, J.J.; Schaper, W. Time course of arteriogenesis following femoral artery occlusion in the rabbit. *Cardiovasc. Res.* **2001**, *49*, 609–617.
14. Yamada, N.; Li, W.; Ihaya, A.; Kimura, T.; Morioka, K.; Uesaka, T.; Takamori, A.; Handa, M.; Tanabe, S.; Tanaka, K. Platelet-derived endothelial cell growth factor gene therapy for limb ischemia. *J. Vasc. Surg.* **2006**, *44* (6), 1322–1328.
15. Grundmann, S.; Hoefer, I.; Ulusans, S.; Bode, C.; Oesterle, S.; Tijssen, J.G.; Piek, J.J.; Ivo Buschmann, I.; van Royen, N. Granulocyte-macrophage colony-stimulating factor stimulates arteriogenesis in a pig model of peripheral artery disease using clinically applicable infusion pumps. *J. Vasc. Surg.* **2006**, *43* (6), 1263–1269.
16. Marshall, A. J., Barker, T., Sage, E. H., Hauch, K. D.; Ratner, B. D. *Pore Size Controls Angiogenesis in Subcutaneously Implanted Porous Matrices*, Transactions of the 7th World Biomaterials Congress, Sydney, Austrailia, May 17−21, 2004; Curran Associates, Inc.: Red Hook, New York; p 710.
17. Madden, L. R.; Mortisen, D. J.; Sussman, E. M.; Dupras, S. K.; Fugate, J. A.; Cuy, J. L.; et al. Proangiogenic scaffolds as functional templates for

Downloaded by VIRGINIA TECH on July 20, 2013 | http://pubs.acs.org
Publication Date (Web): July 8, 2013 | doi: 10.1021/bk-2013-1135.ch015

cardiac tissue engineering. *Proc. Natl. Acad. Sci. U.S.A.* **2010**, *107* (34), 15211–15216.
18. Marshall, A. J.; Irvin, C. A.; Barker, T.; Sage, E. H.; Hauch, K. D.; Ratner, B. D. Biomaterials with Tightly Controlled Pore Size That Promote Vascular In-growth. *ACS Polym. Prepr.* **2004**, *45* (2), 100–101.
19. Marshall, AJ; Ratner, BD Quantitative Characterization of Sphere-Templated Porous Biomaterials. *AIChE J.* **2005**, *51*, 1221–1232.
20. Bush, R. L.; Pevec, W. C.; Ndoye, A.; Cheung, A. T. W.; Sasse, J.; Pearson, D. N. Regulation of new blood vessel growth into ischemic skeletal muscle. *J. Vasc. Surg.* **1998**, *28* (5), 919–928.
21. Lee, S. L.; Pevec, W. C.; Carlsen, R. C. Functional outcome of new blood vessel growth into ischemic skeletal muscle. *J. Vasc. Surg.* **2001**, *34* (6), 1096–1102.
22. Koffler, J.; Kaufman-Francis, K.; Shandalov, Y.; Egozi, D.; Pavlov, D. A.; Landesberg, A.; Levenberg, S. Improved vascular organization enhances functional integration of engineered skeletal muscle grafts. *Proc. Natl. Acad. Sci. U.S.A.* **2011**, *108* (36), 14789–14794.
23. Sussman, E. *Macrophage Polarity and Wnt Signaling in the Foreign Body Reaction*, Ph.D. Thesis, University of Washington, Seattle, Washington, 2011.
24. Bota, P.; Collie, A.; Puolakkainen, P.; Vernon, R. B.; Sage, E. H.; Ratner, B. D.; Stayton, P. S. Biomaterial topography alters healing in vivo and monocyte/macrophage activation in vitro. *J. Biomed. Mater. Res., Part B* **2010**, *95A*, 649–657.

Downloaded by VIRGINIA TECH on July 20, 2013 | http://pubs.acs.org
Publication Date (Web): July 8, 2013 | doi: 10.1021/bk-2013-1135.ch015

Downloaded by UNIV OF MINNESOTA on July 17, 2013 | http://pubs.acs.org
Publication Date (Web): July 8, 2013 | doi: 10.1021/bk-2013-1135.ch016

## Chapter 16

# Novel Cellulose Derivatives with Mitogenic and Osteogenic Activity

**Kai Zhang,[1] Dieter Peschel,[2] Steffen Fischer,[3] and Thomas Groth*,[2]**

**[1]Institute of Macromolecular Chemistry and Paper Chemistry, Darmstadt University of Technology, Petersenstr. 22, D-64287 Darmstadt, Germany**
**[2]Biomedical Materials Group, Institute of Pharmacy, Martin Luther University Halle-Wittenberg, Heinrich-Damerow-Straße 4, D-06120 Halle (Saale), Germany**
**[3]Institute of Plant and Wood Chemistry, Dresden University of Technology, Pienner Str. 19, D-01737 Tharandt, Germany**
***E-mail thomas.groth@pharmazie.uni-halle.de. Phone: (+49)-345-5528460. Fax: (+49)-345-5527379.**

Cellulose was sulfated by different routes to obtain cellulose sulfates (CS) with diverse degrees of sulfation ($DS_S$). Lower sulfated celluloses were either carboxylated at 6-O-position through a TEMPO-mediated oxidation or carboxymethylated at all hydroxyl groups (*2-O*, *3-O* and *6-O*-position) by chloroacetic acid. The chemical structure of products was characterized via elemental analysis, $^{13}C$ NMR and FT Raman spectroscopy, while the average degree of polymerization (DP) was studied using size exclusion chromatography. The bioactivity of these derivatives was studied towards their interactions with growth factors FGF-2 and BMP-2 having either a mitogenic/angiogenic or osteogenic activity, respectively. Competitive binding experiments showed an increase of binding of FGF-2 to CS with rising $DS_S$, but lower than heparin. No such dependency was observed for the carboxylated or carboxymethylated derivatives. Binding experiments with BMP-2 showed that CS with intermediate $DS_S$ had superior binding, although some binding was observed with carboxymethylated CS, too. Cell culture experiments exhibited a mitogenic effect for higher sulfated celluloses, but not for carboxy(methylated)

© 2013 American Chemical Society
In Tailored Polymer Architectures for Pharmaceutical and Biomedical Applications; Scholz, C., et al.; ACS Symposium Series; American Chemical Society: Washington, DC, 2013.

CS. Osteogenic activity measured by expression of alkaline phosphatase showed high effect for CS with intermediate $DS_S$ and moderate for carboxylated and carboxymethylated CS. Overall, these cellulose derivatives possess a cooperative activity with heparin-binding growth factors, which is highly dependent on the degree of derivatisation and type of functional groups.

## Introduction

Glycosaminoglycans (GAGs) are components of the extracellular matrix and cell surfaces and play important roles for the regulation of cell activities such as adhesion, migration, proliferation and differentiation (*1–3*). In many cases GAGs interact with proteins of regulatory activity in the surrounding of cells storing, activating and presenting these factors to the corresponding cellular receptors. Among the plethora of proteins interacting with GAG are many growth factors that regulate mitosis and differentiation of cells. For example, GAG as component of cell surface proteoglycans syndecans participate in the formation of growth factor-receptor-ligand complex and enhance signal transduction processes (*1*, *2*). Hence, GAGs are involved in many physiological and pathophysiological processes like development, wound healing, tumor development and metastasis (*4*, *5*).

A common scheme of GAG structure is a disaccharide unit consisting of an uronic acid and a N-acetyl or N-sulfoglucosamine (see Figure 2a). The glucosamine unit may carry additional sulfate groups mostly at 6-O-position, while the 2-O-position of uronic acid may be sulfated, too. Beside the different functionalization pattern of the hydroxyl groups also several glycoside linkages are known. Overall, both substitution patterns as well as positioning (e.g. $\alpha$ or $\beta$-configuration, 1,4 or 1,3-glycosidic bonds) of glycoside linkage make GAGs of specific tissue distribution and activity. One of the most well studied system is the interaction between fibroblast growth factor-2 (FGF-2) and heparan sulfate that shows a formation of distinct hydrogen bonds and ionic interaction of amino groups of FGF-2 and FGF-2-receptor with the carboxyl and sulfate groups of heparan sulfate (*6*). While these studies indicated an important role of hydrogen bonding (*7*), other groups claimed that particular ionic interactions are most important for interaction of GAGs with their ligands (*8*, *9*). For example, it has been reported that heparin oligosaccharides increased the FGF-2-induced proliferation, which was related to the degree of sulfation especially at *6-O*-position (*10*).

Despite the versatile functions of natural GAGs, they may differ strongly in the molecular composition depending on their sources, e.g. species dependency, batch-to-batch variability of heparin and heparan sulfate (*3*, *11*). Also the potential contamination by structural similar compounds represents significant risks for their pharmaceutical application (*12*, *13*). Thus, synthetic or semisynthetic compounds with GAG analogous structure or function have been searched for years. Different kinds of starting materials have been tried for the synthesis of these analogues, such as dextran, pullulan and colominic acid (*14–16*).



In Tailored Polymer Architectures for Pharmaceutical and Biomedical Applications; Scholz, C., et al.; ACS Symposium Series; American Chemical Society: Washington, DC, 2013.

Downloaded by UNIV OF MINNESOTA on July 17, 2013 | http://pubs.acs.org
Publication Date (Web): July 8, 2013 | doi: 10.1021/bk-2013-1135.ch016

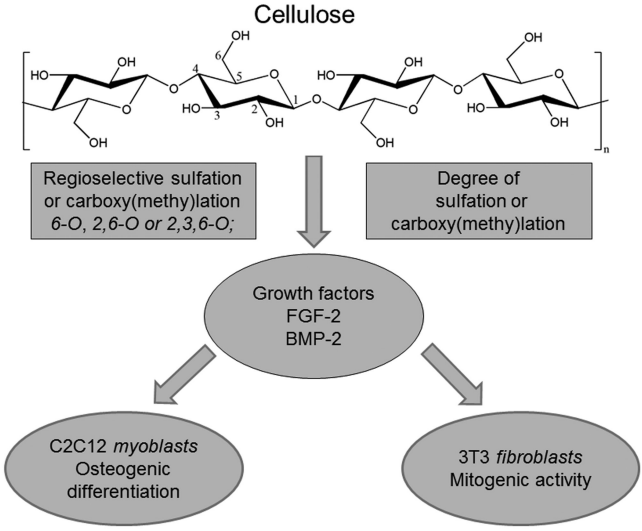


*Figure 1. Conceptual description of design of study with regioselelective derivatisation of chitosan and cellulose to achieve mitogenic activity in cooperation with growth factor FGF-2 and fibroblasts or osteogenic activity in cooperation with BMP-2 and C2C12 cells as model system.*

Downloaded by UNIV OF MINNESOTA on July 17, 2013 | http://pubs.acs.org
Publication Date (Web): July 8, 2013 | doi: 10.1021/bk-2013-1135.ch016

Cellulose is polysaccharides occurring in large quantity in nature and has a backbone consisting of *β*-(1,4)-linked glucose units. Due to its good biocompatibility and non-toxicity, cellulose is a suitable starting material for many compounds used in different fields including tissue engineering (*17*). In recent years, biomaterials based on cellulose have been investigated intensively. On the one hand, specific bioactive substituents have been attempted to be introduced into cellulose backbone such as in synthesis of novel cellulose-based biomaterials based on amino-functionalized cellulose (*18*, *19*). On the other hand, the distribution of the substituents has been proven important for their biological activities which refer to the regiochemistry of cellulose (*20*, *21*). Recently, cellulose was used as starting material for the synthesis of heparin-like compounds (*22*, *23*).

Thus, in this report, as shown schematically in Figure 1 derivatives from cellulose containing sulfate as well as carboxyl/carboxymethyl groups with predictable chemical structures were prepared, considering the structure of naturally occurring heparin and heparan sulfate. The biological activities of these derivatives were examined regarding their interactions with two heparin-binding growth factors, namely FGF-2 and bone morphogenic protein-2 (BMP-2). The mitogenic and osteogenic activity of these factors was studied with cultures of 3T3 fibroblasts or C2C12 myoblasts. Results are reported herein.

# Materials and Methods

## Materials

Microcrystalline cellulose (MCC) with an average DP of 276 was received from J. Rettenmaier & Söhne GmbH (Rosenberg, Germany). Pulp V-81 (AC, with 97.0% alpha cellulose) with an average DP of 1180 was purchased from Buckeye Technologies Inc. (Memphis, U.S.A.). Irradiated cellulose (IC) with an average DP of 113 was obtained after treating cellulose (DP ~ 500) with electron-beam. Heparin from porcine intestinal mucosa was obtained from Calbiochem (Gibbstown, U.S.A.). N,N-dimethyl formamide (DMF) was freshly distilled and water was demineralized before use. Other chemicals were all of analysis grade and used as received. Dialysis membrane from Spectrum Laboratories Inc. (Rancho Dominquez, U.S.A.) has an approximate molecular weight cut off of maximal 1000 Daltons.

Downloaded by UNIV OF MINNESOTA on July 17, 2013 | http://pubs.acs.org
Publication Date (Web): July 8, 2013 | doi: 10.1021/bk-2013-1135.ch016

## Synthesis of Cellulose Derivatives

The synthesis of cellulose derivatives was carried out as reported previously (*24*). The sulfation of cellulose was performed either as acetosulfation or as non-homogeneous direct sulfation. Briefly, 1 g cellulose was suspended in 50 ml anhydrous DMF at room temperature (RT) for over 14 h. Then, the reaction agent consisting of chlorosulfonic acid or chlorosulfonic acid/acetic anhydride in DMF was dropped into the suspension. After being kept at 50°C for 5 h, the solution was cooled down to RT and poured into saturated ethanolic solution of anhydrous sodium acetate. During the acetosulfation, the product was deacetylated in 1 M ethanolic solution of NaOH for over 15 h. After washing and dialysis against demineralized water, the products were lyophilized.

Cellulose sulfates (CS) containing carboxyl or carboxymethyl groups were synthesized based on earlier reports (*22*, *25*). Briefly, CS dissolved in water was oxidized through a 2,2,6,6-tetramethylpiperidine-1-oxyl (TEMPO)-mediated oxidation in order to prepare CS containing carboxyl groups. CS suspended in isopropyl alcohol was carboxymethylated using chloroacetic acid in the presence of NaOH.

## Characterization of Products

The contents of carbon, hydrogen and nitrogen were determined with Elemental Analyzer vario EL from Elementar (Hanau, Germany). The content of sulfur was measured with Elemental Analyzer Eltra CS 500 (Neuss, Germany). Total $DS_S$ of CS and CHS were calculated according to the equation: total $DS_S$ of CS = (S%/32)/(C%/72).

FT Raman spectra of the samples in small metallic discs were recorded on a Bruker MultiRam spectrometer (Bruker BioSpin GmbH, Ettlingen, Germany). A cw-Nd:YAG-laser with an exciting line of 1064 nm was applied as light source. The spectra were recorded over a range of 3500-150 $cm^{-1}$ using an operating spectral resolution of 3 $cm^{-1}$ and a laser power output of 100 mW.


In Tailored Polymer Architectures for Pharmaceutical and Biomedical Applications; Scholz, C., et al.;
ACS Symposium Series; American Chemical Society: Washington, DC, 2013.

The $^{13}C$ NMR spectra in $D_2O$ were recorded at RT on Bruker DPX 400 spectrometer with a frequency of 100.13 MHz, 30° pulse length, 0.35 acq. time and a relaxation delay of 3 s.

Size exclusion chromatography (SEC) was performed on a system containing a Waters 410 reflective index (RI) detector (Waters Corporation, Milford, MA) and PSS Suprema 3000 and 100 columns (Polymer Standards Service GmbH, Mainz, Germany). The columns have been calibrated with pullulan standards (Sigma–Aldrich, Buchs, Switzerland). The elution of the sample solution (0.05-0.07%) was carried out with 0.1 mol/l NaCl aqueous buffer as mobile phase. Empower Pro software (Waters Corporation) was used for analysis of data.

Downloaded by UNIV OF MINNESOTA on July 17, 2013 | http://pubs.acs.org
Publication Date (Web): July 8, 2013 | doi: 10.1021/bk-2013-1135.ch016

**Measurement of Affinity of Cellulose Derivatives to Growth Factors**

25 ng of growth factors fibroblast growth factor-2 (FGF-2) or bone morphogenic protein-2 (BMP-2) (Invitrogen, Karlsruhe, Germany) were mixed with 50 µl heparin agarose microparticel (Fluka, Saint Louis, U.S.A.) and 70 µl phosphate buffered saline (PBS, pH 7,4) for 30 min at RT. Then, samples were centrifuged at 6000 x g for 1 min. The supernatant was discarded and the sedimented microparticles were washed twice and resuspended in PBS. After that, 50 µl heparin agarose particles were mixed with 50 µl of cellulose derivatives dissolved in PBS at a concentration of 10 mg/ml. Thereafter the particle suspension was incubated further 30 min to allow the desorption of growth factors from the heparin agarose beads by competitive mechanism through cellulose derivatives. After centrifugation at 6000 x g, supernatants were transferred to a dot-blot apparatus (Roth, Karlsruhe, Germany) on a cellulose nitrate membrane (GE Healthcare, Buckinghamshire, UK). The quantity of transferred growth factors was detected by primary monoclonal mouse antibodies vs. FGF-2 (Sigma, Saint Louis, U.S.A.) and BMP-2 (R&D Systems, Wiesbaden-Nordenstadt, Germany) and a chemoluminescence kit ECL Plus (GE Healthcare, Buckinghamshire, UK) inkubiert. Blots were analyzed by densitometry using a CCD Camera (Diana 2, Raytest, Straubenhardt, Deutschland) and image analyzing software Image J (http://rsb.info.nih.gov/ij/download.html).

**Cell Culture**

The mouse 3T3-L1 fibroblast cells were obtained from ATCC (Manassas, U.S.A.). The myoblast cell line C2C12 that expresses osteogenic activity in the presence of BMP-2 was purchased from German Collection of Microorganisms and Cell Cultures (DSMZ, Braunschweig, Germany). The cells were cultured in 75 $cm^3$ culture flasks in Dulbecco's modified Eagle's medium (DMEM, Biochrom, Berlin, Germany, Berlin) containing 10% fetal bovine serum (Biochrom), antibiotics (100 U/ml penicillin, 100 µg/ml streptomycin, Biochrom) and 2 mM L-glutamine (Biochrom) named here as "normal growth medium" at 37°C in humidified atmosphere of 5% $CO_2$/95% air until nearly confluence. The cells were detached with 0.25% trypsin/0,02% ethylenediamine tetraacetic acid (EDTA, Biochrom). Trypsinization was stopped after 5 min by addition of DMEM with 10% FBS.


In Tailored Polymer Architectures for Pharmaceutical and Biomedical Applications; Scholz, C., et al.;
ACS Symposium Series; American Chemical Society: Washington, DC, 2013.

## Investigation of Mitogenic Effects of Cellulose Derivatives with 3T3 Fibroblasts

3T3-L1 fibroblast cells were seeded at a density of 10.000 cells/well in black 96 well plates (Greiner bio-one) in DMEM supplemented with 10% FBS and 1% penicillin-streptomycin-fungizone and cultured for 24 h. After washing the plates with DMEM only, the cellulose derivatives or heparin were applied to the cells in DMEM without FBS at a concentration range of 1 µg to 1000 µg/ml for 48 h in the presence of 10 ng/ml FGF-2. The proliferation was measured on the basis of the DNA content using the Quant -iT™ PicoGreen dsDNA quantification assay (Invitrogen, Karlsruhe, Germany). The fluorescent intensity was measured with an excitation wavelength of 485 nm and an emission wavelength of 520 nm by the plate reader Fluostar Optima. The proliferation was expressed as a ratio to the control (wells with 10 ng/ml FGF-2, only). All experiments were carried out with six wells per sample and dilution from which means and standard deviation were calculated.

Downloaded by UNIV OF MINNESOTA on July 17, 2013 | http://pubs.acs.org
Publication Date (Web): July 8, 2013 | doi: 10.1021/bk-2013-1135.ch016

## Measurement of Osteogenic Activity of Cellulose Derivatives with C2C12 Cells

The C2C12 cells were seeded at a density of 2 x $10^4$ cells per well in 96-well plates (Greiner) in DMEM with 10% FBS. After 18 h, the cells were washed quickly with PBS to remove serum. Then DMEM containing 2% FBS and 200 ng/ml BMP-2 (Invitrogen, Karlsruhe, Germany) with or without polysaccharides was added. The measurement of ALP activity was performed after 72 h. At the end of the incubation period, cells were lysed by addition of 50 µl of 0.5 % Triton 100 in distilled water for 30 min at RT at 300 rpm on an orbital shaker (IKA, Staufen, Germany). Then 20 µl of the lysate were transferred to a new 96-well plate and 40 µl of 1 mg/ml *p*-nitrophenylphosphate (Roth, Karlsruhe, Germany) in 0.5 M 2-amino-2-methyl-1-propanol buffer (AMP, Roth) pH 10.3 was added for the determination of ALP activity. The absorbance was measured at a wavelength of 405 nm in a microplate reader Optima FluoroStar (BMG Labtech, Offenburg, Germany) after 15 min incubation of the mixture at 37°C. All experiments were carried out with six wells per sample and dilution from which means and standard deviation were calculated.

The histochemical staining of alkaline phosphatase was done by fixing the cells with 5% glutaraldehyde for 15 min, washing with PBS and subsequent incubation with a mixture of 0,17 mg/ml 5-bromo-4-chloro-3-indolylphosphate (BCIP, Applichem, Darmstadt, Germany) and 0,33 mg/ml nitro blue tetrazolium (NBT, Applichem) in 0,375 M 2-amino-2-methyl-3-propanol buffer (pH=10,3) for 1 h at RT. The staining reaction was stopped by addition of 20 mM EDTA solution. Micrographs were taken with an inverted light microscope (Axiovert 100, (Carl Zeiss, Oberkochen, Germany) equipped with a CCD camera.


In Tailored Polymer Architectures for Pharmaceutical and Biomedical Applications; Scholz, C., et al.;
ACS Symposium Series; American Chemical Society: Washington, DC, 2013.

## Results and Discussion

### Synthesis and Characterization of Cellulose Derivatives

The cellulose derivatives were sulfated as well as further oxidized or carboxymethylated as described in the method section. The chemical structure of these compounds was elucidated using distinct analytical methods. Following this, various products were obtained with diverse total degrees of sulfation ($DS_S$), sulfation patterns and the presence of carboxyl groups (Figure 2B, Table 1 and 2). The total $DS_S$ were determined via elemental analysis, while the partial $DS_S$ was measured with $^{13}C$ NMR spectroscopy. Generally, an increasing total $DS_S$ was obtained using higher amounts of sulfating agents independent on the sulfation method either as acetosulfation or direct sulfation. However, the direct sulfation using chlorosulfonic acid could only be carried out using a high amount of chlorosulfonic acid of at least 3 mol per mol AGU, in order to obtain a water-soluble CS. By using high quantities of chlorosulfonic acid, CS with high total $DS_S$ were prepared even at room temperature (*24*).

Downloaded by UNIV OF MINNESOTA on July 17, 2013 | http://pubs.acs.org
Publication Date (Web): July 8, 2013 | doi: 10.1021/bk-2013-1135.ch016

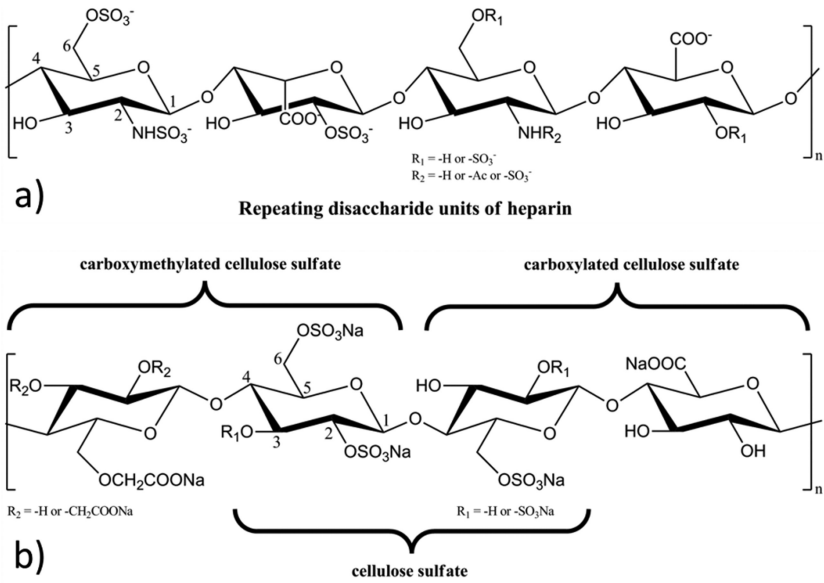


*Figure 2. Schematic representation of the chemical structure of (a) heparin and (b) cellulose derivatives.*


In Tailored Polymer Architectures for Pharmaceutical and Biomedical Applications; Scholz, C., et al.;
ACS Symposium Series; American Chemical Society: Washington, DC, 2013.

**Table 1. Synthesis of cellulose sulfates**

| *CS*[a] | *Starting materials* | *Molar ratio*[b] | *T (°C) / t (h)* | $DS_{S6}$[c] | $DS_{S2}$[c] | *total* $DS_S$[c] | $DS_{S3}$[c] |
|---|---|---|---|---|---|---|---|
| CS-0.31 | C2.5A | 2.35 | RT / 5 | 0.24 | 0.07 | 0.31 | 0 |
| CS-0.37 | AC | 0.85 | 60 / 5 | 0.33 | 0.04 | 0.37 | 0 |
| CS-0.58 | IC | 0.85 | 50 / 5 | 0.52 | 0.06 | 0.58 | 0 |
| CS-0.92 | AC | 3 | 50 / 5 | 0.77 | 0.15 | 0.92 | 0 |
| CS-0.97 | MCC | 3 | 50 / 5 | 0.73 | 0.24 | 0.97 | 0 |
| CS-1.57 | MCC | 3 | 50 / 6 | 0.91 | 0.55 | 1.57 | 0.11 |
| CS-1.69 | MCC | 3 | 50 / 5 | 1 | 0.69 | 1.84 | 0.15 |
| CS-1.80 | MCC | 4.5 | RT / 6 | 1 | 0.80 | 2.15 | 0.35 |
| CS-1.94 | MCC | 13 | RT / 3 | 1 | 0.94 | 2.28 | 0.34 |

[a] The sample were named as CS-x with x representing the sum of $DS_{S6}$ and $DS_{S2}$. [b] Molar ratio in mol sulphuric acid per mol AGU for CS-1.57 and CS-1.69; in mol chlorosulfonic acid per mol AGU and GlcN units for the other CS. 8 mol per mol AGU of acetic anhydride was used for the synthesis of CS-0.37, CS-0.58, CS-0.92, CS-0.97, CS-1.57 and CS-1.69. CS-1.57 was prepared in N,N-dimethylacetamide. [c] Total $DS_S$ was determined via elemental analysis and partial $DS_{S6}$ as well as $DS_{S2}$ of cellulose derivatives were analysed with liquid-state $^{13}C$ NMR spectroscopy. If no sulfation at *3-O*-position was detected via liquid-state $^{13}C$ NMR, the partial $DS_{S3}$ was taken as 0 and the total DS was the sum of $DS_{S6}$ and $DS_{S2}$. Otherwise, the $DS_{S3}$ is equal the difference between the total and partial $DS_S$.

Downloaded by UNIV OF MINNESOTA on July 17, 2013 | http://pubs.acs.org
Publication Date (Web): July 8, 2013 | doi: 10.1021/bk-2013-1135.ch016

By contrast, the acetosulfation led to water-soluble CS even when only a low amount of chlorosulfonic acid of 0.85 mol per mol AGU was used. The total $DS_S$ increased with higher amount of chlorosulfonic acid. However, a similar total $DS_S$ around 0.95 was measured using 3 mol chlorosulfonic acid per mol AGU, independent on the type of cellulose; either microcrystalline cellulose or alpha-cellulose, which possess different average DP. Sulfuric acid could also be used as sulfating agent. In comparison to chlorosulfonic acid, a significantly higher total $DS_S$ was achieved using an equal amount of 3 mol sulfating agent per mol AGU. Moreover, the *2-O*-position could be sulfated completely using sulfuric acid, whereas only 75% was sulfated using chlorosulfonic acid. This fact indicates that sulfuric acid is a more effective sulfating agent for the acetosulfation of cellulose compared to chlorosulfonic acid.

Figure 3 shows FT Raman spectra of CS or cellulose derivatives containing carboxyl/carboxymethyl groups with characteristic bands ascribed to vibrations of sulfate groups as well as carboxyl/ carboxymethyl groups. The signal around 1076 $cm^{-1}$ is attributed to symmetric stretching vibrations of O=S=O groups, while the bands between 824 and 843 $cm^{-1}$ are ascribed to symmetric stretching vibrations of C-O-S groups (*26*).


In Tailored Polymer Architectures for Pharmaceutical and Biomedical Applications; Scholz, C., et al.;
ACS Symposium Series; American Chemical Society: Washington, DC, 2013.

**Table 2. Synthesis of cellulose derivatives containing carboxyl/carboxymethyl groups**

| *Samples* | *Starting materials* | *Total* $DS_S$[c] | $DS_{COO}$[c] | $DS_{CM2}$[c] | $DS_{CM3}$[c] | $DS_{CM6}$[c] |
|---|---|---|---|---|---|---|
| Heparin[a] | | 1.26 | 0.54 | | | |
| CO-0.11[b] | CS-0.97 | 1 | 0.11 | | | |
| CO-0.67[b] | CS-0.37 | 0.37 | 0.67 | | | |
| CM-1.01[b] | CS-0.37 | 0.37 | | 0.3 | 0.25 | 0.46 |
| CM-1.47[b] | CS-0.31 | 0.31 | | 0.54 | 0.26 | 0.67 |

[a] Heparin has a partial $DS_{S2}$ of 0.83 and $DS_{S6}$ of 0.43 (*23*). [b] For preparation of CM-1.01 and 1.47, the carboxymethylation using 2 mol chloroacetic acid/4 mol NaOH per mol AGU were carried out in 75 or 150ml isopropyl alcohol, respectively. For the synthesis of CO-0.11 and 0.67, the combinations of oxidizing reagents - 2,2,6,6-tetramethylpiperidine-1-oxyl/NaBr/NaClO – of 0.05/1.5/8 and 0.1/3/16 mol per mol AGU were used, respectively. [c] Total $DS_S$ and $DS_{COO}$ were measured using liquid-state $^{13}C$ NMR spectroscopy. Partial $DS_{CM}$ were determined using $^{1}H$ NMR spectroscopy after the hydrolysis in 25% $D_2SO_4/D_2O$.

Within the FT Raman spectra of CO-0.67 and CM-1.47, also a weak signal around 1620 $cm^{-1}$ is visible, which is derived from the vibrations of COO-groups (*25*). It has been recently reported that the weak signal is due to the presence of the carboxylate groups (*27*). Moreover, the signals due to vibrations of cellulose backbone have decreased peak intensity or disappear after the derivatisation, e.g. the band at 1096 $cm^{-1}$ has a strongly reduced intensity.

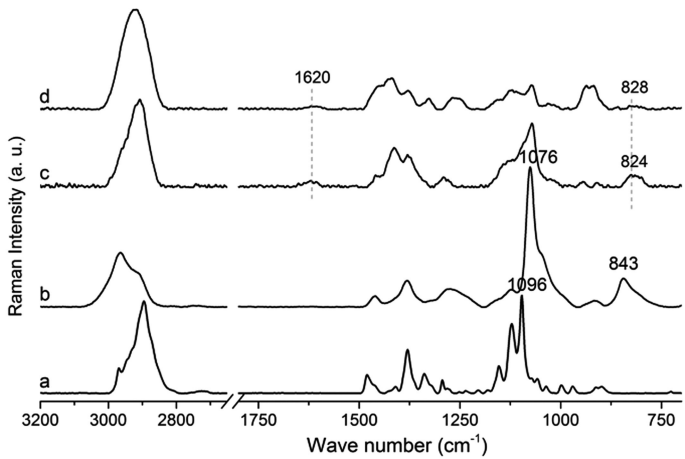


*Figure 3. FT Raman spectra (3200-700 $cm^{-1}$) of (a) microcrystalline cellulose; (b) CS-1.94; (c) CO-0.67 and (d) CM-1.47.*



In Tailored Polymer Architectures for Pharmaceutical and Biomedical Applications; Scholz, C., et al.; ACS Symposium Series; American Chemical Society: Washington, DC, 2013.

Downloaded by UNIV OF MINNESOTA on July 17, 2013 | http://pubs.acs.org
Publication Date (Web): July 8, 2013 | doi: 10.1021/bk-2013-1135.ch016

$^{13}C$ NMR spectroscopy provided more information about the derivatisation pattern. After the sulfation of cellulose, the C6 has a signal at 67 ppm, while the unmodified C6 at 60.5 ppm (Figure 4). With the sulfation at *2-O*-position, the signal of C1 shifts from 102.3 to 100.2 ppm. The partial $DS_S$, $DS_6$ and $DS_2$, of CS were measured according to the chemical shifts of C6-signals as well as C1-signals, respectively (*24*, *28*). The carbons of carboxyl groups show a chemical shift of 175.5 ppm representing the carbons at C6-position, as the TEMPO-mediated oxidation of cellulose has a regiospecifical character and only the primary groups can be oxidized (*29*, *30*). The degree of oxidation (DO) can be indirectly determined according to the changes of peak integrals after the oxidation of CS (*25*).

Downloaded by UNIV OF MINNESOTA on July 17, 2013 | http://pubs.acs.org
Publication Date (Web): July 8, 2013 | doi: 10.1021/bk-2013-1135.ch016

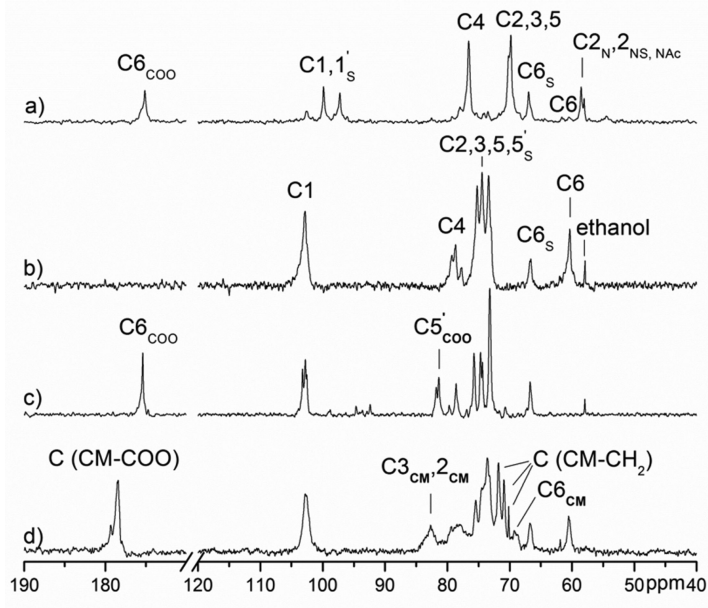


*Figure 4. $^{13}C$ NMR spectra (190-40 ppm) of (a) heparin, (b) CS-0.37, (c) CO-0.67 and (d) CM-1.47 in $D_2O$ at RT.*

Furthermore, the chemical shift of carbons in COO-groups of carboxymethyl groups is loctated at 178 ppm, while the carbons in $CH_2$-groups of carboxymethyl groups are between 70 and 73 ppm. For comparison, $^{13}C$ NMR spectrum of heparin is also shown in Figure 4a. The presence of two signals for C6 and $C6_S$ at 60.5 and 67 ppm is visible, indicating the sulfation at *6-O*-position. The chemical shifts at 58.5 ppm are ascribed to C2 of glucosamine units (*22*, *31*). Moreover, three signals are visible for C1, which is attributed to the presence of various building blocks in heparin: *α*-L-iduronic acid, *β*-D-glucuronic acid and *α*-D-glucosamine (*3*, *11*). All these building blocks can be sulfated at *2-O* or *2-N*-position, so that the signal of C1 at 102.5 ppm shifted to 99.8 and 97.2 ppm. Furthermore, the signal at 175 ppm is attributed carboxyl groups within the repeating units of heparin.


In Tailored Polymer Architectures for Pharmaceutical and Biomedical Applications; Scholz, C., et al.;
ACS Symposium Series; American Chemical Society: Washington, DC, 2013.

Another important property of these derivatives is the molecular weight. The molecular weights of obtained CS as well as CO/CM were determined via SEC. Based on the molecular weight, the degree of polymerization (DP) as number- and weight-averaged DP (referred to $DP_W$ and $DP_n$) were calculated (Table 3). Compared to the average $DP_n$ of starting cellulose, the cellulose derivatives showed significant lower $DP_n$, indicating a strong hydrolysis of cellulose chains during the sulfation as well as further oxidation or carboxymethylation (*22*, *25*, *29*).

**Table 3. Average DP of cellulose derivatives**

| *Samples* | $DP_W$ | $DP_n$ | $DP_W/DP_n$ |
|---|---|---|---|
| CS-0.37 | 741 | 288 | 2.57 |
| CS-0.92 | 372 | 121 | 3.07 |
| CS-0.97 | 365 | 180 | 2.03 |
| CS-1.57 | 247 | 119 | 2.08 |
| CS-1.69 | 655 | 166 | 3.95 |
| CS-1.80 | 188 | 94 | 2.01 |
| CS-1.94 | 82 | 52 | 1.58 |
| CO-0.67 | 159 | 112 | 1.19 |
| CM-1.47 | 817 | 248 | 3.29 |

Generally, the $DP_W$ and $DP_n$ decreased with increasing amount of sulfating agent chlorosulfonic acid. Using a low amount of 0.85 mol chlorosulfonic acid per mol AGU of AC, a low $DS_S$ of 0.37 was obtained, while the $DP_W$ and $DP_n$ were the highest among obtained CS. As shown in the SEC elution pattern (Figure 5), a slight fronting within the SEC chromatogram of CS-0.37 is visible, indicating the possible presence of another fraction with significantly higher DP. With other words, the polydispersity was high. Using a higher amount of 3 mol chlorosulfonic acid per mol AGU of AC, the total $DS_S$ increased to 0.92 and the $DP_W/DP_n$ were much lower than those of CS-0.37. A fronting is still visible within the SEC chromatogram of CS-0.92 (Figure 5). In comparison, for CS-0.97 starting from MCC using 3 mol chlorosulfonic acid per mol AGU, a relative symmetric SEC chromatogram was obtained and a low polydispersity was measured. This fact indicates that the starting cellulose has strong effects on the distribution of molecular weights, although no significant effect on the total $DS_S$ was observed. Moreover, the acetosulfation using 3 mol sulfuric acid per mol AGU led to CS with relative symmetric SEC chromatograms. After the direct sulfation using 13 mol chlorosulfonic acid per mol AGU, a total $DS_S$ of 2.28 was reached, while very low $DP_W$ and $DP_n$ of only 82 and 52 were obtained, too. Furthermore, the ratio of $DP_W/DP_n$ representing the polydispersity was the lowest


In Tailored Polymer Architectures for Pharmaceutical and Biomedical Applications; Scholz, C., et al.;
ACS Symposium Series; American Chemical Society: Washington, DC, 2013.

Downloaded by UNIV OF MINNESOTA on July 17, 2013 | http://pubs.acs.org
Publication Date (Web): July 8, 2013 | doi: 10.1021/bk-2013-1135.ch016

among prepared CS. Thus, the total $DS_S$ and the DP of CS are probably two opponents during the sulfation of cellulose, but both factors depend on the amount of used sulfating agent. The total DS increases with higher amount of sulfating agent, while the average DP ($DP_W$ and $DP_n$) decreases due to the hydrolysis during the sulfation. Another effect of hydrolysis is that the polydispersity decreases in correlation with higher amount of sulfating agent.

After the TEMPO-mediated oxidation of CS, a symmetric chromatogram was obtained for CO-0.67 (Figure 5). However, the molecular weight was much lower than the starting CS, indicating that a strong depolymerization of cellulose chains took place during the oxidation. As reported previously, cellulose undergoes a strong depolymerization during TEMPO-mediated oxidation (*29*, *30*).

Downloaded by UNIV OF MINNESOTA on July 17, 2013 | http://pubs.acs.org
Publication Date (Web): July 8, 2013 | doi: 10.1021/bk-2013-1135.ch016

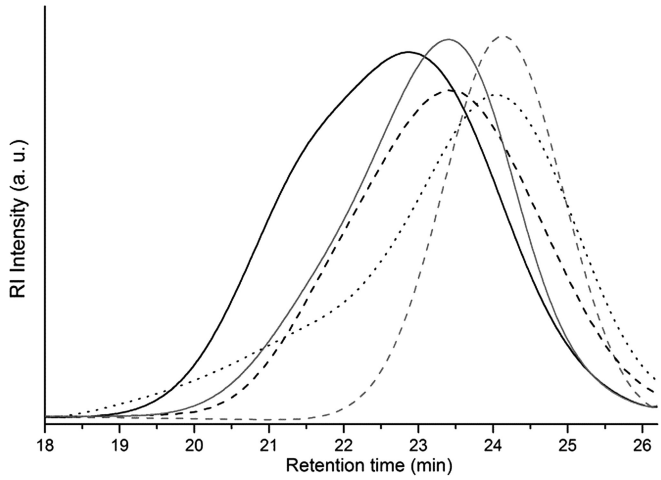


*Figure 5. SEC elution patterns (18-26.2 min) of CS-0.37 (dark solid line), CS-0.92 (dark dot line), CS-0.97 (grey solid line), CS-1.80 (dark dash line) and CO-0.67 (grey dash line).*

**Binding of Growth Factors FGF-2 and BMP-2 to Cellulose Derivatives**

Since a cooperative activity between semisynthetic heparinoid cellulose derivatives and growth factors requires the formation of a polysaccharide-growth factor complex, studies on binding affinity were carried out. The binding assay acts in a competitive manner to heparin that was used as control here. Figure 6A and B show the binding of growth factors FGF-2 and BMP-2 to cellulose sulfates (A), and carboxylated and carboxymethylated cellulose sulfates (B) as ratio of binding to heparin. It is visible in Figure 6A that the binding of CS to FGF-2 (white bars) was positively correlated to their total $DS_S$ with highest binding to most sulfated CS. However, the affinity of CS to FGF-2 was generally lower than


In Tailored Polymer Architectures for Pharmaceutical and Biomedical Applications; Scholz, C., et al.;
ACS Symposium Series; American Chemical Society: Washington, DC, 2013.

that of heparin expressed by the binding ration smaller than 1.0. Obviously, the sulfation only at *6-O*-position was not suffcient to allow binding of FGF-2 to cellulose derivatives. Only when the $DS_{S2}$ at *2-O*-position became larger than 0.5 (CS-1.57, see Table 1), there was a measurable quantity of bound FGF-2 detected. This is in line with studies using octasaccharides from heparan sulfate where a *6-O*-desulfation was not critical, while the sulfate at *2-O*-position was required for binding of FGF-2 (*32*).

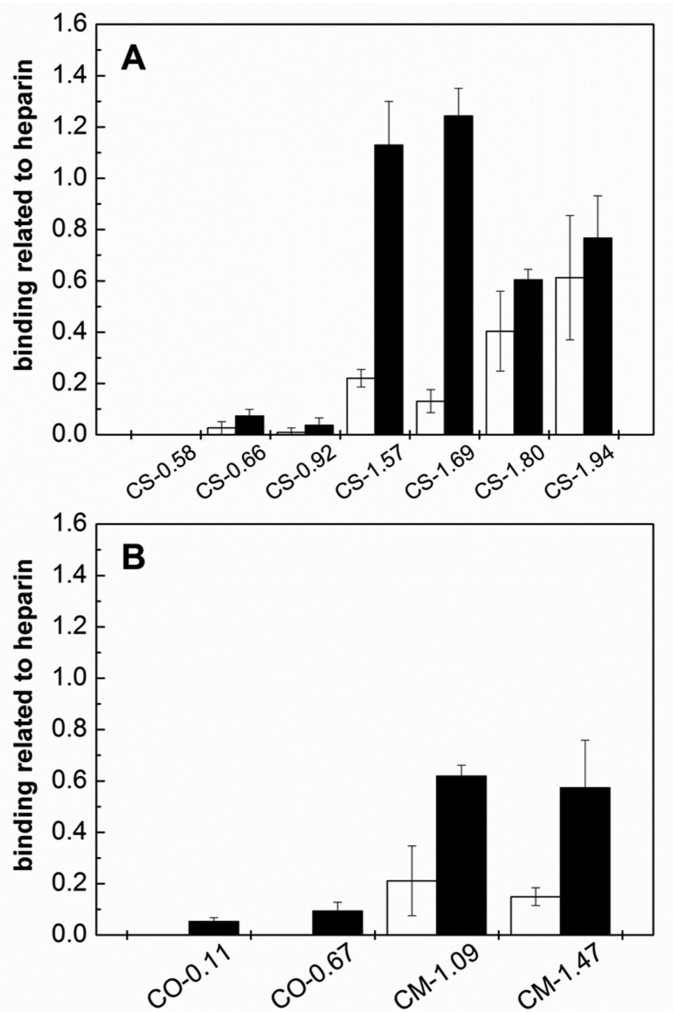


*Figure 6. Competitive binding assay of cellulose derivatives vs. heparin for FGF-2 (white bars) and BMP-2 (black bars). Results present ratio of binding related to heparin for (A) Cellulose sulfates, (B) Carboxylated and carboxymethylated cellulose.*


In Tailored Polymer Architectures for Pharmaceutical and Biomedical Applications; Scholz, C., et al.;
ACS Symposium Series; American Chemical Society: Washington, DC, 2013.

Downloaded by UNIV OF MINNESOTA on July 17, 2013 | http://pubs.acs.org
Publication Date (Web): July 8, 2013 | doi: 10.1021/bk-2013-1135.ch016

Carboxylated but lower sulfated CO-0.11 and CO-0.67 (see also Table 2), as shown in Figure 6B (white bars), did not express any detectable ability to interact with FGF-2, which is interesting because of their structural similarity to heparin with a carboxyl group at C6 and sulfate groups at *2-O* and *6-O*-position. Obviously, the lower degree of sulfation with a $DS_S$<1.0 hampered the binding of FGF-2 to the carboxylated CS. Interestingly, carboxymethylated CS showed some ability to bind FGF-2 in a competitive manner to heparin (Figure 6B). CM-1.09 and CM-1.47 shown in Figure 6B expressed about 20% binding of FGF-2 in comparison to the control. A reason for this ability might be the high degree of subsitution ascribed to carboxymethyl groups with $DS_{CM}$>1.0 despite the low $DS_S$<0.4. This fact indicates that not only sulfate but also carboxymethylated groups are involved in the binding of FGF-2 to cellulose derivatives. This assumption is backed by studies from Schlessinger et al. who claimed that the formation of hydrogen bonds and ionic interactions is crucial for the binding of FGF-2 to heparin (*6*).

Figure 6A and 5B also show the binding of BMP-2 to cellulose derivatives (black bars). In Figure 6A, it is visible that lower sulfated cellulose with a $DS_S$<1.0 did not express any ability to bind BMP-2. Interestingly the middle sulfated cellulose derivatives CS-1.57 and CS-1.69 expressed an affinity to BMP-2 higher than heparin, which declined significantly with further increase in total $DS_S$ because CS-1.80 and CS-1.94 had lower affinity than heparin. This contrasts the results of binding to FGF-2, where a continous rise of binding with increase in total $DS_S$ was observed. As well, no binding of BMP-2 to carboxylated CO-0.11 and CO-0.67 was detected here (see Figure 6B, white bars). However, both carboxymethylated derivatives, CM-1.09 and CM-1.47, expressed about 60% binding affinity of heparin probably due to the higher overall derivatisation degrees. In contrast to studies on binding of FGF-2, no studies on binding affinity have been done so far with BMP-2, although a recent study with chitosan sulfates on osteogenic differentiation of cells indicated important role of sulfation sites for the biological activity of BMP-2 (*33*)).

Downloaded by UNIV OF MINNESOTA on July 17, 2013 | http://pubs.acs.org
Publication Date (Web): July 8, 2013 | doi: 10.1021/bk-2013-1135.ch016

## Effects of Cellulose Derivatives and FGF-2 on 3T3 Fibroblast Growth

The mitogenic activity of cellulose derivatives was investigated in a range from 1 µg to 1 mg in the presence of 10 ng FGF-2/ml. Here the cell growth was characterized by DNA content and compared to the effect of 10 ng FGF-2/ml as control, only. All cellulose sulfates shown in Figure 7A yielded results comparable to heparin at a concentration of 1 mg/ml and increased the growth of 3T3 cells almost twofold compared to the control (FGF-2 with no addition of polysaccharides). However, cellulose derivatives with a $DS_S$<0.9 were not effective to achieve increased cell growth compared to FGF-2 alone and are not shown here. With increasing $DS_S$, the concentration of CS necessary to elevate the proliferation decreased down to 1 µg/ml for CS-1.94. In general, a stepwise, concentration related increase in proliferation from the lower to the higher sulfated derivatives was observed, It is remarkable that the derivative CS-1.94 showed a mitogenic activity higher than that of heparin at concentrations below 50 µg/ml.


In Tailored Polymer Architectures for Pharmaceutical and Biomedical Applications; Scholz, C., et al.;
ACS Symposium Series; American Chemical Society: Washington, DC, 2013.

Downloaded by UNIV OF MINNESOTA on July 17, 2013 | http://pubs.acs.org
Publication Date (Web): July 8, 2013 | doi: 10.1021/bk-2013-1135.ch016

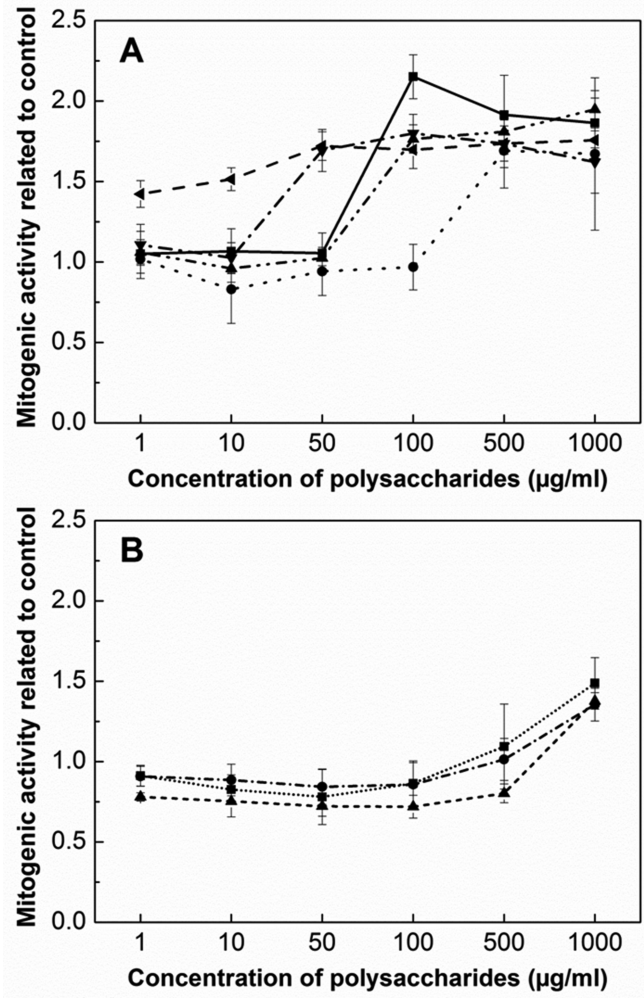


*Figure 7. Mitogenic activity of cellulose derivatives measured by proliferation of 3T3 fibroblasts in the presence of 10 ng/ml FGF-2 (control) and increasing quantities of cellulose derivatives and heparin. Results are expressed as ratio compared to control. (A) Cellulose sulfates CS-0.92 (circles and dotted line), CS-1.57 (triangles, dash-dot-dot line), CS-1.8 (rhombus and dash-dot line), CS-1.94 (triangles, dashed line) and heparin (squares and solid line); (B) Carboxylated cellulose CO-0.11 (squares and dotted line), carboxymethylated celluloses CM-1.09 (rhombus and dash-dot-line) and CM-1.47 (squares, dashed line). (Reproduced with permission from reference (22), Copyright 2012 Elsevier).*

The results for cell growth experiments with cellulose derivatives containing carboxyl/carboxymethyl groups are shown in Figure 7B. The results demonstrate that both carboxylated and carboxymethylated CS were only effective at high


In Tailored Polymer Architectures for Pharmaceutical and Biomedical Applications; Scholz, C., et al.;
ACS Symposium Series; American Chemical Society: Washington, DC, 2013.

concentrations of 500 µg/ml and 1 mg/ml with a maximum of about 1.5-fold mitogenic activity compared to FGF-2 control for CO-0.11. Compared to CS-0.92, which possessed similar partial $DS_S$ at *2-O* and *6-O*-positions (compare values in Table 1 and 2), CO-0.11 had a lower mitogenic activity especially at 500 µg/ml. This indicates a minor role of carboxyl groups in promotion of mitogenic activity of FGF-2. The carboxymethylated derivatives showed an increase up to 1.4-fold at the rather high concentration of 1 mg/ml. At concentrations lower than 500 µg/ml, a slight decrease in the proliferation compared to the control with FGF-2 was evident for all carboxylated and carboxymethylated derivatives, although previous studies have demonstrated that these derivatives are not toxic to cells (*22*).

Since it is desirable to obtain mitogenic effects already at minimal concentrations, CS seems to have clear advantages over carboxylated and carboxymethylated derivatives. The remarkable mitogenic activity of highly sulfated cellulose derivatives in comparison to heparin is certainly related to the difference in derivatisation degrees and sites. Heparin from porcine intestinal mucosa used in this study possesses a *6-O*-sulfation of only 0.43 (besides a *6-O*-carboxylation of 0.54) and a *2-O*-sulfation of 0.83 in comparison to 1.0 and 0.94 for CS-1.94, respectively (see Table 1 and 2 for comparison). Obviously, the higher $DS_S$ at these positions is related to the higher mitogenic activity of cellulose derivatives. Recent work indicated a dominant effect of ionic interaction between GAGs and their ligands (*34*). Hence, the increase in charge density of cellulose derivatives may contribute to an increased affinity to the ligand FGF-2. In fact, recent studies conducted by our group have shown that higher sulfated cellulose have a more protective effect on FGF-2 from proteolytic digestion by proteinases and cells that points to the formation of CS-FGF-2 complexes (*35*). Also other studies have shown a protection against proteolytic degradation of FGF-2 prolonging its biological activity not only for heparin, but also a (1,3)-β-galactan sulfate with a high $DS_S$ of 2.0, and other polysulfated compounds (*36*, *37*). Thus, a prolonged life time of FGF-2 can be expected as a major reason for the mitogenic activity particularly of highly sulfated cellulose derivatives. By contrast, the low mitogenic activity of carboxylated and carboxymethylated CS, despite the partly high degree of derivatisation, was unexpected because of the structural similarity to heparin. This indicates an essential role of sulfate groups for the binding of growth factor FGF-2. Other studies have shown no mitogenic activity of carboxymethyl cellulose with high $DS_{COO}$ of 1.5-2.4 per AGU and concentrations up to 60 µg/ml in the presence of FGF-2 with the same cell type (*38*), which was also seen in the current study with carboxylated and carboxymethylated CS.

Downloaded by UNIV OF MINNESOTA on July 17, 2013 | http://pubs.acs.org
Publication Date (Web): July 8, 2013 | doi: 10.1021/bk-2013-1135.ch016

## Effects of Cellulose Derivatives and BMP-2 on Osteogenic Differentiation of C2C12 Cells

In these experiments a selection of cellulose derivatives was used to study the effect on osteogenic differentiation of C2C12 myoblasts. This cell line has the ability of osteogenic differentiation that is characterized by expression of alkaline phosphatase and up regulation of several osteogenic genes. Here, C2C12 cells were exposed to 200 ng/ml growth factor BMP-2 (control) and cellulose

derivatives that expressed also a measurable ability to bind the growth factors (see Figure 6 A and B). Optimal concentrations of BMP-2 were found in previous experimental work (*23*). To show the effects of derivatives independently on the number of cells, ALP activity was normalized against the protein content and expressed as ratio to the control.

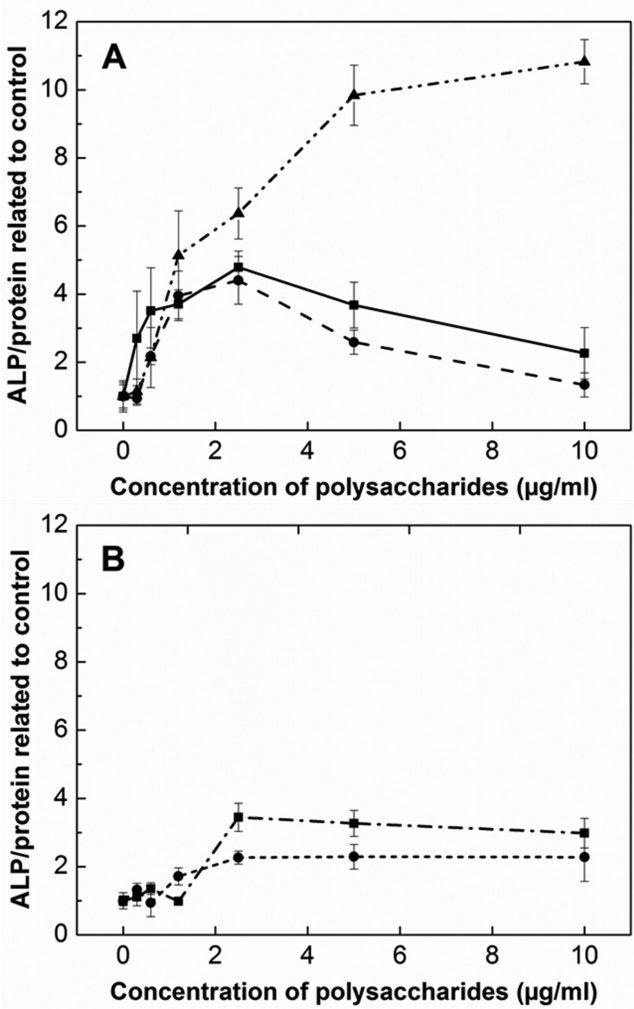


*Figure 8. Osteogenic activity of selected cellulose derivatives measured by expression of alkaline phosphatase (ALP) normalized to protein content of cells in the presence of 200 ng/ml BMP-2 (control) and increasing quantities of cellulose derivatives and heparin. Results are expressed as ratio compared to control. (A) Cellulose sulfates CS-1.57 (triangles, dash-dot-dot), CS-1.94 (rhombus, dashed line) and heparin (squares and solid line); (B) Carboxylated cellulose CO-0.67 (squares, dash-dot), and CM-1.47 (rhombus, dashed). (Reproduced with permission from reference (23), Copyright 2012 Elsevier).*



In Tailored Polymer Architectures for Pharmaceutical and Biomedical Applications; Scholz, C., et al.;
ACS Symposium Series; American Chemical Society: Washington, DC, 2013.

Downloaded by UNIV OF MINNESOTA on July 17, 2013 | http://pubs.acs.org
Publication Date (Web): July 8, 2013 | doi: 10.1021/bk-2013-1135.ch016

After the addition of polysaccharides, ALP activity was changing in a concentration dependent manner for all derivatives. Figure 8A shows that among the sulfated celluloses, CS-1.57 expressed the highest osteogenic activity with a monotone rise of ALP activity with increasing concentrations up to 10 μg/ml. It is interesting to note in Figure 8A that CS-1.57 expressed a higher osteogenic activity than heparin as indicated by the significantly higher expression of alkaline phosphatase (ALP). By contrast, the highest sulfated cellulose CS-1.94 showed only a weak enhancement of ALP activity at lower concentrations with values similar to heparin, while at concentrations higher than about 3 μg/ml the ALP expression decreased for both CS-1.94 and heparin. Out of the carboxylated/carboxymethylated cellulose derivatives, CO-0.67 caused a significantly stronger enhancement of ALP activity than CM-1.47 at 2.5 μg/ml (see Figure 8B). By contrast, CM-1.47 showed the lowest osteogenic activity of all compounds. In general, the osteogenic activity of these derivatives was lower in comparison to heparin. It should be noted that none of the derivatives was able to induce any significant ALP expression in C2C12 cells without the addition of BMP-2. This indicates strongly that the derivatives must act in a cooperative manner with BMP-2 to induce an osteogenic activity in C2C12 cells.

To visualize the effect of derivatives on the BMP-2 induced ALP secretion 5-bromo-4-chloro-3-indolylphosphate and nitro blue tetrazolium were used for histochemical staining of C2C12 cells (Figure 9). Here, only two derivatives were included that showed an expression of ALP in the quantitative assay. C2C12 cells showed a faint blue staining indicating the expression of ALP, when BMP-2 alone (200 ng/ml) was used (control). In comparison to that, a stronger staining was observed with CS-1.57 at the concentration of 2.5 μg/ml. However, there was no decrease of staining when the concentration of CS-1.57 was increased to 10 μg/ml. Similar findings were made for CO-0.67 at 2.5 μg/ml with no change at higher concentrations of the polysaccharide (not shown here) Overall, the histochemical staining confirmed the results of quantitative measurements of ALP activity in a qualitative manner.

Obviously, only middle sulfated cellulose with a $DS_S$ of around 1.6 was able to exert high binding affinity to BMP-2 as shown in the binding assay and to induce a strong osteogenic differentiation in C2C12 cells that increased with the rise of concentration from 1 to 10 μg/ml. In contrast, highly sulfated derivatives and also heparin expressed an inhibitory effect at concentrations higher than about 2 μg/ml. Other studies have shown that heparin concentrations as low as 1 μg/ml exerted an inhibitory action on BMP-2 activity and subsequent osteogenic differentiation of cells. It was observed that surface heparan sulfate proteoglycans and also heparin led to rapid endocytosis of BMP-2, which decreased the signal transduction processes via BMP-I-receptor and reduced expression of osteogenic markers like alkaline phosphatase in C2C12 cells (*39*). A recent work with chitosan sulfates showed that *6-O*-sulfation was critical for an osteogenic activity on C2C12 cells in the presence of BMP-2, while 2-*N*-sulfation was found to be inhibitory (*33*). A comparison of derivatisation pattern of CS shown in Table 1 and Table 2 (heparin) also indicates that a higher sulfation in *2-O*-position has an inhibitory effect, since both CS-1.94 and heparin have a $DS_S$ at *2-O*-position of 0.92 and 0.82, respectively. Contrary to previous study


In Tailored Polymer Architectures for Pharmaceutical and Biomedical Applications; Scholz, C., et al.;
ACS Symposium Series; American Chemical Society: Washington, DC, 2013.

Downloaded by UNIV OF MINNESOTA on July 17, 2013 | http://pubs.acs.org
Publication Date (Web): July 8, 2013 | doi: 10.1021/bk-2013-1135.ch016

of Zhou et al. (*33*), however, CS-1.57 did not express any inhibitory activity over the whole concentration range studied here, which was the case for chitosan sulfates (*33*). Such inhibitory activity was not observed for the carboxylated and carboxymethylated cellulose derivatives, although their osteogenic activity was low.

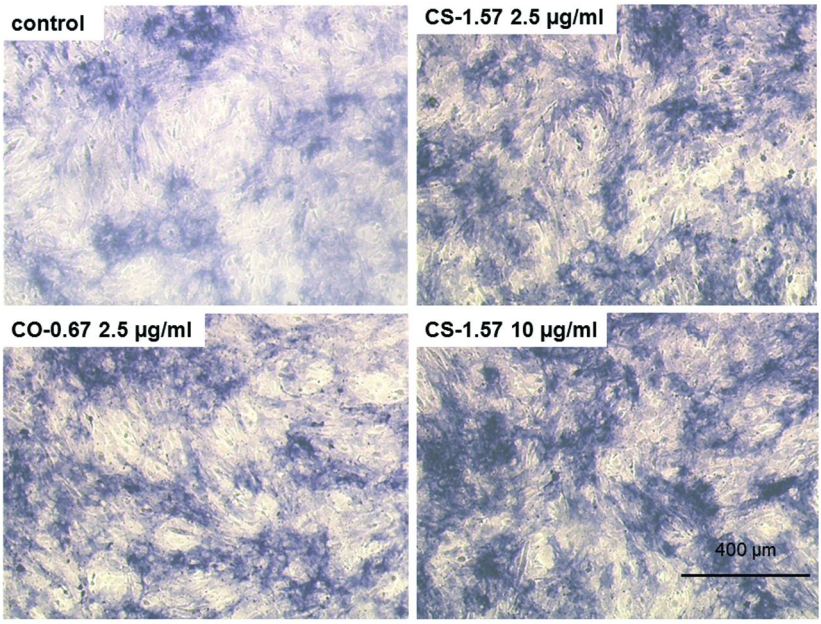


*Figure 9. Staining of alkaline phosphatase in C2C12 cells exposed to 200 ng BMP-2/ml (control) or addition of cellulose derivatives. Note that the increase in concentration of CS-1.57 causes also a stronger staining. (Reproduced with permission from reference (23), Copyright 2012 Elsevier).*

Downloaded by UNIV OF MINNESOTA on July 17, 2013 | http://pubs.acs.org
Publication Date (Web): July 8, 2013 | doi: 10.1021/bk-2013-1135.ch016

## Conclusions

Cellulose sulfates (CS) with various total and partial $DS_S$ were synthesized through two different sulfation processes as direct sulfation or acetosulfation. CS with total $DS_S$ up to 2.28 were obtained and distinct sulfation patterns were determined via $^{13}C$ NMR spectroscopy. Low sulfated celluloses could be further regiospecifically oxidized through TEMPO-mediated oxidation or carboxymethylated with chloroacetic acid. The molecular weights in the form of average DP of cellulose derivatives were determined via SEC and a general decrease of average DP with rising amount of sulfating agent was detected. The average DP of cellulose derivatives were reduced strongly after the TEMPO-mediated oxidation. CS with high partial $DS_S$ at *6-O-* and *2-O*-position showed higher mitogenic activity than heparin. While a high sulfation at *2-O*-position seemed to be mandatory for a mitogenic effect in cooperation with


In Tailored Polymer Architectures for Pharmaceutical and Biomedical Applications; Scholz, C., et al.;
ACS Symposium Series; American Chemical Society: Washington, DC, 2013.

the growth factor FGF-2, such high derivatisation was inhibitory for osteogenic activity in cooperation with the growth factor BMP-2. Both carboxylated and carboxymethylated exhibited some ability to bind both growth factors in the competitive binding assay with heparin. However there bioactivity on cells was low both regarding mitogenic and osteogenic activity. This was not expected due to some structural similarity to heparin, but the lower degree of derivatisation could be a reason for this fact. Some effect of the higher molecular weight could also be responsible, which was not discussed here in more detail because the differences in degree of polymerization between CS were not that large. The cellulose sulfates CS-1.94 and CS-1.57 seem to be interesting candidates for the application in tissue engineering as component of scaffolds or controlled drug release systems where angiogenic effects of FGF-2 and osteogenic differentiation of cells in the presence of BMP-2 are desired.

Downloaded by UNIV OF MINNESOTA on July 17, 2013 | http://pubs.acs.org
Publication Date (Web): July 8, 2013 | doi: 10.1021/bk-2013-1135.ch016

## Acknowledgments

The support by Dr. Erica Brendler is greatly appreciated. The financial support by German Research Foundation (Deutsche Forschungsgemeinschaft, grants: GR1290/7-1 and GR1290/7-2, FI755/4-1 and FI755/4-2 is gratefully acknowledged. We thank LOEWE – Soft Control (Landes-Offensive zur Entwicklung Wissenschaftlich-oekonomischer Exzellenz) for the financial support.

## References

1. Capila, I.; Linhardt, R. J. *Angew. Chem., Int. Ed.* **2002**, *41* (3), 391–412.
2. Liu, D.; Shriver, Z. *Semin. Thromb. Hemostasis* **2002**, *28*, 67–78.
3. Sasisekharan, R.; Raman, R.; Prabhakar, V. *Annu. Rev. Biomed. Eng.* **2006**, *8*, 181–231.
4. Casu, B. *Curr. Pharmaceutical Des.* **2004**, *10*, 939–949.
5. Laremore, T. N.; Zhang, F.; Dordick, J. S.; Liu, J.; Linhardt, R. J. *Curr. Opin. Chem. Biol.* **2009**, *13* (5-6), 633–40.
6. Schlessinger, J.; Plotnikov, A. N.; Ibrahimi, O. A.; Eliseenkova, A. V.; Yeh, B. K.; Yayon, A.; Linhardt, R. J.; Mohammadi, M. *Mol Cell* **2000**, *6* (3), 743–50.
7. Thompson, L. D.; Pantoliano, M. W.; Springer, B. A. *Biochemistry* **1994**, *33* (13), 3831–40.
8. Fromm, J. R.; Hileman, R. E.; Caldwell, E. E.; Weiler, J. M.; Linhardt, R. J. *Arch. Biochem. Biophys.* **1997**, *343* (1), 92–100.
9. Rusnati, M.; Coltrini, D.; Caccia, P.; Dell'Era, P.; Zoppetti, G.; Oreste, P.; Valsasina, B.; Presta, M. *Biochem. Biophys. Res. Commun.* **1994**, *203* (1), 450–8.
10. Pye, D. A.; Vives, R. R.; Turnbull, J. E.; Hyde, P.; Gallagher, J. T. *J. Biol. Chem.* **1998**, *273* (36), 22936–42.
11. Rabenstein, D. L. *Nat. Prod. Rep.* **2002**, *19* (3), 312–331.
12. Beni, S.; Limtiaco, J. F.; Larive, C. K. *Anal. Bioanal. Chem.* **2011**, *399* (2), 527–39.

13. Pan, J.; Qian, Y.; Zhou, X.; Pazandak, A.; Frazier, S. B.; Weiser, P.; Lu, H.; Zhang, L. *Nat. Biotechnol.* **2010**, *28* (3), 203–7.
14. Alban, S.; Schauerte, A.; Franz, G. *Carbohydr. Polym.* **2002**, *47*, 267–276.
15. Chaidedgumjorn, A.; Toyoda, H.; Woo, E. R.; Lee, K. B.; Kim, Y. S.; Toida, T.; Imanari, T. *Carbohydr. Res.* **2002**, *337*, 925–933.
16. Kunou, M.; Koizumi, M.; Shimizu, K.; Kawase, M.; Hatanaka, K. *Biomacromolecules* **2000**, *1* (3), 451–458.
17. Klemm, D.; Heublein, B.; Fink, H. P.; Bohn, A. *Angew. Chem., Int. Ed.* **2005**, *44* (22), 3358–93.
18. Genco, T.; Zemljič, L. F.; Bračič, M.; Stana-Kleinschek, K.; Heinze, T. *Macromol. Chem. Phys.* **2012**, *213* (5), 539–548.
19. Nikolajski, M.; Wotschadlo, J.; Clement, J. H.; Heinze, T. *Macromol. Biosci.* **2012**, *12* (7), 920–5.
20. Baumann, H.; Liu, C.; Faust, V. *Cellulose* **2003**, *10*, 65–74.
21. Groth, T.; Wagenknecht, W. *Biomaterials* **2001**, *22* (20), 2719–29.
22. Peschel, D.; Zhang, K.; Aggarwal, N.; Brendler, E.; Fischer, S.; Groth, T. *Acta Biomater.* **2010**, *6* (6), 2116–25.
23. Peschel, D.; Zhang, K.; Fischer, S.; Groth, T. *Acta Biomater.* **2012**, *8* (1), 183–93.
24. Zhang, K.; Brendler, E.; Geissler, A.; Fischer, S. *Polymer* **2011**, *52* (1), 26–32.
25. Zhang, K.; Peschel, D.; Klinger, T.; Gebauer, K.; Groth, T.; Fischer, S. *Carbohydr. Polym.* **2010**, *82* (1), 92–99.
26. Zhang, K.; Brendler, E.; Fischer, S. *Cellulose* **2009**, *17* (2), 427–435.
27. Zhang, K.; Fischer, S.; Geissler, A.; Brendler, E. *Carbohydr. Polym.* **2012**, *87* (1), 894–900.
28. Nehls, I.; Wagenknecht, W.; Philipp, B.; Stscherbina, D. *Prog. Polym. Sci.* **1994**, *19*, 29–78.
29. Saito, T.; Isogai, A. *Biomacromolecules* **2004**, *5* (5), 1983–9.
30. Hirota, M.; Furihata, K.; Saito, T.; Kawada, T.; Isogai, A. *Angew. Chem., Int. Ed.* **2010**, *49* (42), 7670–2.
31. Zhang, K.; Helm, J.; Peschel, D.; Gruner, M.; Groth, T.; Fischer, S. *Polymer* **2010**, *51* (21), 4698–4705.
32. Rider, C. C. *Biochem. Soc. Trans.* **2006**, *34* (Pt 3), 458–60.
33. Zhou, H.; Qian, J.; Wang, J.; Yao, W.; Liu, C.; Chen, J.; Cao, X. *Biomaterials* **2009**, *30* (9), 1715–24.
34. Seyrek, E.; Dubin, P. *Adv. Colloid Interface Sci.* **2010**, *158* (1-2), 119–29.
35. Weltrowski, A.; da Silva Almeida, M. L.; Peschel, D.; Zhang, K.; Fischer, S.; Groth, T. *Macromol. Biosci.* **2012**, *12* (6), 740–50.
36. Burgermeister, J.; Paper, D. H.; Vogl, H.; Linhardt, R. J.; Franz, G. *Carbohydr. Res.* **2002**, *337* (16), 1459–66.
37. Liekens, S.; Leali, D.; Neyts, J.; Esnouf, R.; Rusnati, M.; Dell'Era, P.; Maudgal, P. C.; De Clercq, E.; Presta, M. *Mol. Pharmacol.* **1999**, *56* (1), 204–13.
38. Hatanaka, K.; Ohtsuki, T.; Kunou, M. *Chem. Lett.* **1994**, *23*, 1407–1410.
39. Jiao, X.; Billings, P. C.; O'Connell, M. P.; Kaplan, F. S.; Shore, E. M.; Glaser, D. L. *J. Biol. Chem.* **2007**, *282* (2), 1080–6.

Downloaded by UNIV OF MINNESOTA on July 17, 2013 | http://pubs.acs.org
Publication Date (Web): July 8, 2013 | doi: 10.1021/bk-2013-1135.ch016


In Tailored Polymer Architectures for Pharmaceutical and Biomedical Applications; Scholz, C., et al.;
ACS Symposium Series; American Chemical Society: Washington, DC, 2013.

Downloaded by VIRGINIA TECH on July 20, 2013 | http://pubs.acs.org
Publication Date (Web): July 8, 2013 | doi: 10.1021/bk-2013-1135.ch017

## Chapter 17

# Tailoring Silk-Based Matrices for Tissue Regeneration

**A. Motta,[*,1,2] C. Foss,[1,2] and C. Migliaresi[1,2]**

**[1]Department of Industrial Engineering and BIOtech Research Center, University of Trento, via delle Regole 101, 38123 Mattarello (Trento), Italy**
**[2]European Institute of Excellence on Tissue Engineering and Regenerative Medicine. Trento, Italy**
**[*]E-mail: antonella.motta@ing.unitn.it.**

Silk fibroin has gained in the last years increasing interest as material for the fabrication of scaffolds for tissue engineering. Recently, the ability of silk fibroin to establish a direct cross-talk with the biological environment has been reported, showing the potential to promote cells adhesion, proliferation and metabolic activity forward the production both in vitro and in vivo of complex multifunctional tissues. After reviewing the main characteristics and applications of silk fibroin, the chapter focuses on the effect of processing on fibroin physical and biological properties, and addresses two particularly demanding tissue regeneration applications, i.e., cartilage and bone tissue engineering. Specifically, methods of production of silk fibroin non-woven nets, sponges and hydrogels are described and the possibility to induce in vitro vascularization of the scaffold prior the implantation is reported. Moreover, results on the ability of the material to support also the ostegenic differentiation of stem cells from other sources are discussed as preliminary to regenerative medicine therapy.

© 2013 American Chemical Society
In Tailored Polymer Architectures for Pharmaceutical and Biomedical Applications; Scholz, C., et al.;
ACS Symposium Series; American Chemical Society: Washington, DC, 2013.

# Tissue Engineering and a New Concept of Biocompatibility

The notion of tissue engineering has evolved since its first definition by the National Science Foundation in 1988 (*1*). With the passing of time, the aspiration to construct more and more complex tissues has become dominant, increasing the number of strategies explored in the field (*2*). In particular, the approach of tissue engineering implies the transfer of the medical treatment to a cellular level: the resources needed for tissue regeneration are introduced in the pathologic environment in a suitable configuration to optimize their activity and help the natural processes of self-repair. The main challenge of this strategy has lately become the control of the tridimensional development of the new tissue in a functional way (*3*).

Since functionality has become a fundamental requisite of the final regenerated tissue, the best combination of scaffold properties, cell source and *in vitro* signals must be defined for each application and, eventually, for each pathologic conditions which have to be treated. On this basis, new efforts have been made towards the definition and the control of the microenvironmental niche experienced by cells in the tissue-engineered system, such as oxygen concentration, pH, electric potential, cytokine gradients and mechanical forces (*2*). The main consequence of these issues is the extreme need of a detailed comprehension of cell behavior, both during normal tissue morphogenesis and during the repair and regeneration phases. Only in this case, cells could be guided with appropriate signals towards a functional restoration of damaged tissues.

The concept of biocompatibility has evolved in the same direction and its essence has become application-dependent (*4*). Today, biomaterials and scaffolds are designed to be biologically interactive and to establish a reciprocal dialogue with cells to contribute to the repair process. However, it has become evident that biological reactions induced by a material can be adverse or beneficial according to its application (*4*). Thus, the concept of biocompatibility has been enriched with a more complex meaning, resulting in a strong relationship between a biomaterial and its purpose (*5*).

Downloaded by VIRGINIA TECH on July 20, 2013 | http://pubs.acs.org
Publication Date (Web): July 8, 2013 | doi: 10.1021/bk-2013-1135.ch017

## The Active Role of the Scaffold

The scaffold has a central role among the components of the tissue-engineered system focused on the achievement of a complete tissue functionality. Indeed, it must provide spatio-temporally controlled signals to guide cell adhesion, migration, proliferation and activity (*6*). To that purpose, scaffold design should be based on the natural extracellular matrix (ECM), that is the best available model as it is a scaffold optimized by Nature itself. In fact, ECM provides adequate cell housing and instructs cell behavior through appropriate biochemical and biophysical signals. Thus, material, porosity, nano- and micro-topographic features and surface modification, such as the incorporation of bioactive molecules, should be developed according to this biomimetic principle (*6–8*), to offer the most suitable microenvironment to help cells build a functional tissue.


In Tailored Polymer Architectures for Pharmaceutical and Biomedical Applications; Scholz, C., et al.;
ACS Symposium Series; American Chemical Society: Washington, DC, 2013.

However, the complexity of the tissue-engineered system lies beyond the definition of the best scaffold properties. In fact, each component (scaffold, cells, bioactive molecules, *in vitro* mechanical stimuli) is strongly interdependent to the others, leading to a tangled system which has to be optimized in a synergistic way for each specific application (*9*). Recently, this optimization has been investigated using the new insights in developmental biology: latest hypotheses have stated that some mechanisms which take place during embryonic development can be exploited to induce tissue regeneration. Examples include endochondral ossification to obtain bone regeneration (*10*) or the use of progenitor cells common to endothelial cells and smooth muscle cells during embryogenesis for blood vessel tissue engineering (*11*); in this case, the biomaterial itself can be designed to guide an appropriate differentiation into the two kinds of cells and a functional organization of the vessel wall.

Under this point of view, a deep understanding of cell dictionary and signal transduction pathways during embryonic development becomes mandatory. Growth factors can be conjugated with scaffold biomaterials to have a control of their location and bioactivity (BMP-2 and BMP-7 for bone and cartilage regeneration, VEGF for blood vessel regeneration are a few examples) (*12*). The release of these stimulating molecules can be mainly controlled by the method of conjugation to the scaffold, such as chemical immobilization or physical encapsulation. Also in this case, scaffold properties become fundamental: shape, porosity and mechanical properties can influence not only the release, but also the subsequent signaling and cell responses (*12*). Again, a careful optimization is required.

In light of these considerations, a biomaterial for scaffold production is clearly an active part in tissue regeneration and has to possess not only an application-dependent biocompatibility but also a high versatility to allow the optimization of the final system. Silk fibroin is an example of such biomaterials and its properties will be described in the following paragraph.

Downloaded by VIRGINIA TECH on July 20, 2013 | http://pubs.acs.org
Publication Date (Web): July 8, 2013 | doi: 10.1021/bk-2013-1135.ch017

## Silk as an Adaptable Biomaterial

Silk fibroin is a biopolymer that displays complex molecular and supra-molecular structure, hierarchical organization, bioactivity due to molecular ligands, ability to self-assemble, resistance and adaptability. Silks (from cocoons and spiders nets) have attracted attention as bioactive proteins for various biomedical applications, but also as model fibers to understand other structural polymers (*13*, *14*).

Fibroin is one of the two proteins composing the silkworm silk filament, the outer core, about 25% by weight, being made by a family of proteins named sericins. Among the family of silks, silk from *Bombyx mori* silkworm is the most widely studied. The peculiar aspect of *Bombyx mori* silk fibroin molecule is the presence of two different amino acid sequences, VITTDSDGNE and NINDFDED, recognized by integrin promoting fibroblast growth, that were


In Tailored Polymer Architectures for Pharmaceutical and Biomedical Applications; Scholz, C., et al.;
ACS Symposium Series; American Chemical Society: Washington, DC, 2013.

identified in the N-terminal region of the heavy chain (*15*) lending the silk protein with multifunctional with bio-recognition capabilities. However different races of *Bombyx mori* exist and most studies refer to *Bombyx mori* polyhybrids, though different races of *Bombyx mori* and also different polyhybrids make silks with different amino acid compositions and molecular weight that in turn induce different biological responses (*16*).

Great interest has also risen in the use of fibroin isolated from A. pernyi as starting material for advanced biomedical applications (*17*). In comparison with *Bombyx mori*, the amino acid composition of *Antheraea pernyi* silk is characterized by an abundance of Alanine-Glycine-Serine-Tyrosine amino acid residues, and a significant amount of aspartic acid and arginine. The abundance of alanine favors the formation of alpha-helix conformation instead of beta-sheet. It also contains a significant amount of RGD (arginine-glycine-aspartic acid), a sequence that is known to be effective in cell attachment and is integrin-mediated (*18*). Non-mulberry silks are however more resistant to solvents than *Bombyx mori*. An issue in the use of A. pernyi in biomedical materials is to identify proper solvents and processing methods. While domestic silkworm, *Bombyx mori,* silk has been extensively exploited in the biomedical field during the last few decades, the transformation of wild (non-mulberry) silk from being a textile fiber to biomaterials is relatively new. Moreover, selected races of the domestic *Bombyx mori* produce constant composition and properties silks that eliminates any risks of batch-to-batch variations (*18*).

*Bombyx mori* silk threads have been used for many years in medicine as surgical sutures, which initially caused allergenic reactions in patients undergoing repeated surgical procedures. This problem, though, was full solved by removing the sericin and nowadays, silk sutures contain fibroin only and they cause no allergenic reaction whatsoever. Fibroin from *Bombyx mori* silk is currently considered to be highly biocompatible and immunological reactions or disease transmissions have never been reported (*19*).

Devices made from silk fibroin protein produced by the *Bombyx mori* silkworm are FDA approved and have been used in medicine for a wide variety of applications including surgical, drug delivery, and tissue engineering. Silk fibroin can be processed by various techniques to obtain different structures, i.e., gels, micro- and nanonets, sponges, films, with tailored mechanical and biological properties. By adjusting biopolymer architecture and chemical composition, it is possible to influence the formation of the extra cellular matrix (ECM) and ultimately guide cells to generate functional tissues (*20*). The potential of applying silk-based materials (mainly silk derived from *Bombyx mori* cocoons) to induce regeneration of various mammalian tissues such as bone, cartilage, tendon, myocardium and skin, is also increasingly reported (*21–28*). Multicomponent systems were also proposed, produced by combining silk fibroin with other proteins such as collagen or polysaccharides such as hyaluronic acid or chitosan (*29*, *30*) or synthetic polymers (*31*, *32*). *In vitro* and *in vivo* studies have already reported the promising use of silk fibroin as biomaterial for a variety of possible applications.

Downloaded by VIRGINIA TECH on July 20, 2013 | http://pubs.acs.org
Publication Date (Web): July 8, 2013 | doi: 10.1021/bk-2013-1135.ch017

Downloaded by VIRGINIA TECH on July 20, 2013 | http://pubs.acs.org
Publication Date (Web): July 8, 2013 | doi: 10.1021/bk-2013-1135.ch017

The peculiarity of silk is derived from its multi-functional nature such as adaptable mechanical performance, tailored degradability and bioactivity. Furthermore, the ability to process silk into various tunable materials and structures lends silk great potential for a number of therapeutic applications (Figure 1). Silk materials can differ widely in composition, structure and properties depending on the specific source as well as after processing (*33*). In particular, protein conformation is critical to biological functions, driving a different protein adsorption and/or cell-material cross talk. For instance, tailoring of the crystallinity degree and morphologies can be exploited to induce different blood responses in terms of platelet adhesion and activation (*34–38*). Changes in conformation as a consequence of processing result in variation in water content, crystalline domain extension, mechanical properties as well as bioactivity and biological behavior of the resulting material (*18*, *39–43*).

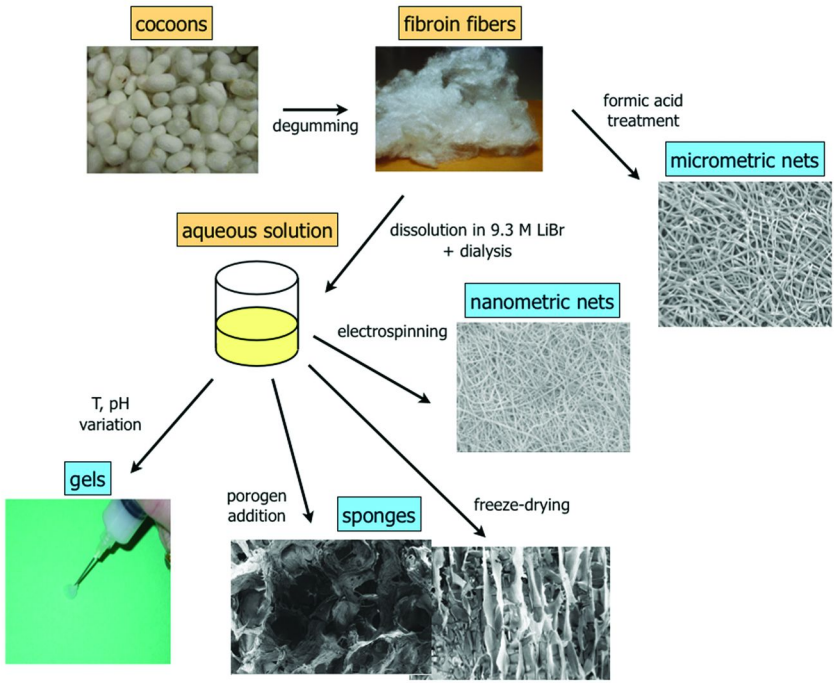


*Figure 1. Silk fibroin is purified by the degumming process. The resulting fibers can be partially solubilized with formic acid to obtain micrometric nets or completely dissolved in lithium bromide. After dialysis, the fibroin aqueous solution can be further processed to produce gels, sponges or nanometric nets.*

Degradability is also affected by silk fibroin inter- and supermolecular structure. Indeed, fibroin materials are stable or degradable, depending on the specific conformation (amount of beta sheet structure). In general, native fibroin fibers can be considered non-degradable, while degradation of regenerated fibers is very slow (years). Degradation of fibroin is proteolytic and usually mediated by a foreign body response. During degradation, less crystalline regions of the protein are broken in peptides which can be phagocytized by cells more easily (*19*).

Protein structure, scaffold morphology, biological and mechanical conditions at the implantation site can affect fibroin degradation rate. Several studies showed that films degraded faster than fibers if exposed to the same enzymes with a modification of fibroin molecular weight, an increase of protein crystallinity and a dramatic change in tensile strength (*19*). Also the degradation rate of fibroin porous sponges depends strongly on the production method, which determines differences in surface roughness and β-sheet content of the scaffolds (*44*).

Given the strong dependence of scaffold properties on fibroin processing conditions, in the following section a detailed description will be given regarding the production method and the resulting characteristics of silk-based scaffolds with different morphologies.

Downloaded by VIRGINIA TECH on July 20, 2013 | http://pubs.acs.org
Publication Date (Web): July 8, 2013 | doi: 10.1021/bk-2013-1135.ch017

*Non-Woven Nets*

Non-woven mats are an interesting option as a scaffold for tissue engineering thanks to their high surface area and rough topography for cell adhesion. Several techniques can be used to produce fibroin nets with fibers both in the nano- and in the micrometer range (*45–47*). The latter have been prepared with a partial solubilization of regenerated fibers in formic acid and small amounts of calcium chloride. Other techniques include homogenization, which can lead to fibers of 10-30 μm and pores with a diameter of about 300 μm (*46*). Scaffolds obtained have shown a quite relevant difference if compared with natural degummed fibers, mainly in terms of amino acid composition and crystallizable/polar/non -polar amino acid distribution. More relevant appeared to be however after scaffold processing the presence of a thin layer of fibroin hydrogel surrounding the fibroin fibers and richer in non-polar and polar amino acids than the parent fibroin, likely belonging to the fibroin L-chain. Such hydrogel layer possessed more light L-chain and P-25 constituents than the starting fibroin or fibroin of the net. TGA analysis results demonstrated that the native fibroin samples presented the greatest mass loss due to water content and thus the highest values of all the three factors listed above. On the contrary, the net samples lost the least amount of water, because of the less amorphous configuration portion and polar amino-acid content, which decrease the possibility to bind water even if the specific surface is higher than the coating layer. These scaffolds have shown to sustain adhesion and proliferation of several kinds of cells, including cheratinocytes, fibroblasts, osteoblasts and endothelial cells (*47–49*).


In Tailored Polymer Architectures for Pharmaceutical and Biomedical Applications; Scholz, C., et al.;
ACS Symposium Series; American Chemical Society: Washington, DC, 2013.

*Porous Sponges*

Fibroin-based sponges are characterized by tunable interconnected porosity and tailorable mechanical properties. Several techniques can be employed, such as particulate leaching (with salt or glucose as porogen) and freeze-drying, which may be eventually combined with gas foaming (*50*, *51*). In particular, salt leaching allows the formation of a more interconnected porosity and pore dimension can be modulated by the diameter of porogen grains. Two procedures have been developed for sponge production, the first implies the dissolution of fibroin in hexafluoro-2-propanol (HFIP). NaCl with a controlled granulometry is added to this solution and after solvent evaporation scaffolds are treated in methanol to induce the formation of β-sheet structures and make fibroin insoluble in water. Finally, several washing steps in distilled water can remove salt grains and porosity will reflect the arrangement of the voids left by the porogen. Thanks to this flexible technique, it is also possible to obtain porosity gradients if a suitable NaCl granulometry is used (*44*).

The use of toxic solvents such as HFIP and methanol is however a strong limitation for the production of a scaffold, and the above process can be completely conducted in an aqueous envi- ronment without losing the control on pore dimension and distribution. In addition, the final matrices have a faster degradation rate and surface proper- ties more suitable for cell adhesion (*52*). In this case, NaCl is directly added to a fibroin solution at 4-10% w/V in order to obtain an oversaturated solution, so that the surface of NaCl particles dissolves only partially. This leads to the gelation of fibroin in 3-5 days and hence to the formation of porous structures stable in water. As in the previous case, salt can be removed washing the sponges in distilled water (*44*).

The simplicity and versatility of this technique have allowed the production of blend scaffolds, combining silk fibroin with other polymers (examples included chitosan (*30*, *53*) and hyaluronic acid (*29*)) or inducing pre-mineralization with hydroxyapatite crystals (*54*). In addition, silk porous matrices have been conjugated to growth factors, such as BMP-2 (*55*) also loaded in synthetic microparticles (*56*).

Downloaded by VIRGINIA TECH on July 20, 2013 | http://pubs.acs.org
Publication Date (Web): July 8, 2013 | doi: 10.1021/bk-2013-1135.ch017

*Hydrogels*

Hydrogels are hydrated structures of hydrophilic polymeric chains, where water structure plays an important role in the physical behaviour of the gel. The nature of the adsorbed water can also determine the overall permeation of nutrients and cellular product through the gel.

Regenerated silk fibroin water solution gelation occurs primarily through the encouragement of macromolecular interactions among the hydrophobic side chains, initiating hydrogen bonding and resulting in physical cross-linking of the silk proteins. Fibroin-based hydrogels can be stabilized either by chemical or physical crosslinking and represent a bioactive substrate for a variety of attractive and practical applications (*44*, *57*). Several protocols were designed to obtain physical hydrogels, by changing different physical-chemical parameters of the


In Tailored Polymer Architectures for Pharmaceutical and Biomedical Applications; Scholz, C., et al.;
ACS Symposium Series; American Chemical Society: Washington, DC, 2013.

solution environment including protein concentration, temperature, and pH (*58*). Indeed, lowering the solution pH near to the isoelectric point of silk fibroin (pH = 3.8) reduces the repulsion forces between adjacent silk fibroin molecules, inducing physical cross-linking.

Other methods have been recently investigated to induce fibroin gelation. Wang et al. developed a method to induce gelation of silk fibroin through ultrasonication (*59*). By adjusting different sonication parameters, such as power and time, the authors were able to control the rate of silk fibroin gelation from minutes to hours. Motta et al. investigated the use of glycerol to induce gelation from silk fibroin solutions and compared the results with gels obtained at low temperature treatment (*60*).

Gas foaming of polymers using high pressure or supercritical $CO_2$ has emerged in recent years as a promising technique that avoids the use of organic solvents (*61*). While generally considered to be a weak solvent, at high pressures the solvating power of $CO_2$ in many polymers is comparable to that of a typical organic solvent making it a strong candidate for processing a breadth of materials (*62*, *63*).With this novel technique silk protein gelation can be considerably expedited under high pressure $CO_2$ with the formation of extensive β-sheet structures and stable hydrogels at processing times less than 2 h. In addition, high pressure $CO_2$ has shown a significant influence on hydrogel physical properties, such as porosity, sample homogeneity, swelling behavior and compressive properties, confirming the high feasibility of silk fibroin (*64*).

Chemical crosslinking can also be performed to prepare silk fibroin hydrogels. Genipin, a natural crosslinking agent extracted from the plant Gardenia jasminoides, has been successfully employed to cross-link silk fibroin solutions (*65*). In particular, genipin was used as stabilizing agent in multicomponent systems, such as fibroin-sericin, fibroin-chitosan, fibroin-hyaluronic acid (*29*, *66*).

## The Use of Silk Fibroin in Skeletal Tissue Engineering

In the following paragraphs, a brief overview will be given about the use of silk fibroin for bone and cartilage regeneration, focusing on how the versatility and feasibility of the scaffold production method have successfully led to promising results in these fields.

### Silk Fibroin in Bone Tissue Engineering

Bone defects can arise from traumas, tumors and infections, which require surgical intervention. Therapies for the subsequent bone augmentation include the use of autologous non-vascularized bone grafts from the iliac crest, distal femur or proximal tibia; autologous vascularized grafts, instead, are removed from the fibula and can participate to bone remodeling during tissue reconstruction but are more demanding and have a high probability of failure during the first year of implantation (*67*, *68*). Other treatments employ allografts, demineralized bone matrix or implants of synthetic materials (usually metals, ceramics or composites) to induce bone tissue restoration, but this challenging goal has not been fullfilled


In Tailored Polymer Architectures for Pharmaceutical and Biomedical Applications; Scholz, C., et al.;
ACS Symposium Series; American Chemical Society: Washington, DC, 2013.

Downloaded by VIRGINIA TECH on July 20, 2013 | http://pubs.acs.org
Publication Date (Web): July 8, 2013 | doi: 10.1021/bk-2013-1135.ch017

yet (*69*). In this perspective, the advanced tissue engineering principles have been applied to obtain the regeneration of a functional bone tissue.

Bone regeneration requires a scaffold with osteoconductive and osteoinductive properties, i.e. able to be populated by cells after implantation and substituted by new tissue starting from the surrounding; osteoinductive, if it is also to induce and guide differentiation of mesenchymal stem cells (MSC) in loco; or a combination of these two (*70*). Moreover, scaffold degradation rate should be compatible with the natural bone remodeling process (*71*).

The most important parameters to take into account to design a scaffold for bone tissue engineering are porosity and pore diameter distribution. In fact, scaffold morphology has to allow cell migration and help neo-angiogenesis after implantation. *In vivo* vascularization is a fundamental requirement to develop a functional tissue and insufficient blood vessels in bone can lead to a decrease of tissue formation and mass (*72*), due to limited nutrient supply and remotion of byproducts of metabolism and material degradation (*73*, *74*). In addition, studies demonstrated that vascularity supports MSCs and osteoblasts during tissue repair and osteogenesis follows angiogenesis in a bone fracture model (*75*, *76*). To induce neo-angiogenesis after implantation, current strategies include a scaffold design with nano/micro topography to facilitate vessel formation, angiogenetic growth factor delivery, co-culture of osteoblasts and endothelial cells or *in vivo* pre-vascularization (*77*). It has been reported that scaffold porosity should be over 60%, while the minimum pore diameter should be 100 μm to obtain osteogenesis and mineralization. Moreover, microporosity of pore walls (< 10 μm) can help cell attachment and differentiation, adsorbance of osteogenic proteins and mechanical stability at the fixation to the natural bone (*70*).

Several ceramic materials have been proposed for bone tissue engineering, especially hydroxyapatite (HA) as it is a physiological component of bone ECM and increases osteointegration. However, scaffolds resulted too brittle with a low degradation rate (*78*, *79*). On the other hand, the use of synthetic and natural polymers allows the control of scaffold morphology, to mimic in some extent the structural organization of the bone (*80*, *81*). In particular, silk fibroin sponges produced by salt leaching have shown to support the deposition and organization of bone mineralized extracellular matrix by human mesenchymal stem cells hMSC, both pure (*82*) and with the deposition of hydroxyapatite crystals, *in vitro* and *in vivo* (*83*, *84*).

In recent papers (*85*, *86*), fibroin sponges have shown to support also the ostegenic differentiation of stem cells from other sources, i.e. amniotic fluid stem cells (AFSCs). In fact, AFSCs displayed the ability to differentiate into osteoblasts when cultured in standard tissue culture plates for 28 days in osteogenic medium. In particular, the sequential expression of Runx2, osterix, osteopontin and osteocalcin during the culture period resembled the pathway of osteoblast differentiation, leading to the formation of typical mineral deposits and nodules. Subsequently, AFSCs were seeded on silk fibroin sponges for one week and then implanted subcutaneously in nude mice. On silk matrices, the osteogenic differentiation and the production of mineralized ECM were substantially enhanced after 4 weeks of implantation, when compared to collagen and poly-D,L-lactid acid (PDLLA) sponges used as a control (Figure 2).



In Tailored Polymer Architectures for Pharmaceutical and Biomedical Applications; Scholz, C., et al.;
ACS Symposium Series; American Chemical Society: Washington, DC, 2013.

Downloaded by VIRGINIA TECH on July 20, 2013 | http://pubs.acs.org
Publication Date (Web): July 8, 2013 | doi: 10.1021/bk-2013-1135.ch017

Downloaded by VIRGINIA TECH on July 20, 2013 | http://pubs.acs.org
Publication Date (Web): July 8, 2013 | doi: 10.1021/bk-2013-1135.ch017

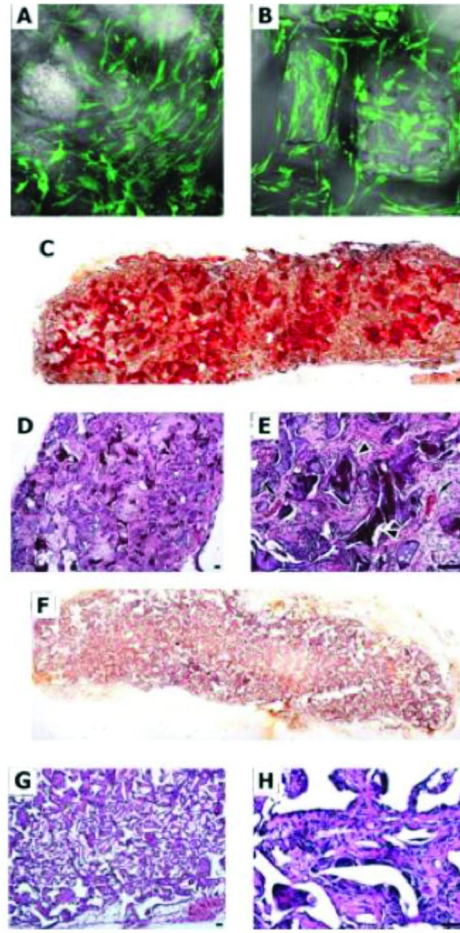


*Figure 2. Microscopical analysis of hAFSCs cultured on 3D silk fibroin (A, C-E) and PDLLA (B, F-H) scaffolds. In A and B, confocal images of cell-scaffold constructs after 7 days of culture (green live cells are superimposed to contrast images of scaffolds in gray). In C, F and D, E, G, H, histological images for Alizarin red and hematoxylin-eosin staining respectively after 28 days of ectopic implantation, showing more mineralized ECM and bone-like tissue structures with vascularization on silk fibroin scaffolds. (Reproduced with permission from ref. (85). Copyright 2011 Mary Ann Liebert, Inc.)*

Other silk-based matrices have successfully promoted bone regeneration, showing both osteoconductive and osteoinductive properties. Fini et al. (*22*) compared injectable silk fibroin hydrogels versus synthetic gels of poly-lactic-glycolic acid (PLGA). Authors demonstrated the biocompatibility of SF gels, which supported the proliferation, differentiation and synthetic activity of osteoblasts, increasing their expression of TGFβ-1 with respect to PLGA materials. Then, cell-free fibroin gels were implanted in a critical size rabbit

femur defect for 12 weeks. The treatment with SF hydrogels induced a significant higher amount of new bone formation with thicker and denser trabeculae, when compared to the synthetic control gel. On the other hand, empty defects did not heal spontaneously, demonstrating the osteoconductive ability of silk-based materials.

Besides the potential to support the regeneration of mineralized and functional bone tissue, silk fibroin has shown to sustain also the critical neo-angiogenesis of the new forming tissue both *in vitro* and *in vivo*. In fact, silk fibroin micrometric nets were co-cultured with human outgrowth endothelial cells (OEC) and primary human osteoblasts (OB) and after 4 weeks authors observed the formation of capillary tubes with increased length and area with respect to nets cultured with OEC alone. In addition, osteoblasts produced more extracellular matrix, especially collagen type I which is proven to be a pro-angiogenic substrate (*87*). Thus, the beneficial effect of co-culture on both cell types was demonstrated *in vitro*.

Downloaded by VIRGINIA TECH on July 20, 2013 | http://pubs.acs.org
Publication Date (Web): July 8, 2013 | doi: 10.1021/bk-2013-1135.ch017

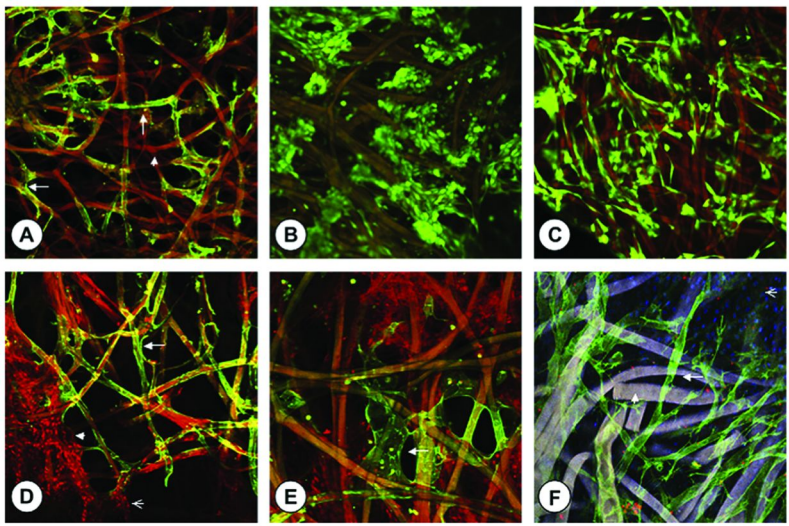


*Figure 3. Confocal images of HDMEC and OB cultured on silk fibroin scaffolds at different time points. In A, HDMEC grew on the fibers after 7 days of culture (live cells are stained in green with calcein-AM, dead cells in red with propidium iodide (PI); SF nets appear also in red – see arrowheads). In B, OB formed clumps between and on the fibers. C is an image of the co-culture of HDMEC and OB stained with calcein-AM and PI. D, E and F are images of the same co-culture at 3, 7 and 28 days respectively, where HDMEC are specifically stained with PECAM-1 (green) and PI (red) or DAPI (blue) are used for cell nuclei. Increasing the culture time, an extensive network of microcapillary-like structures (green, arrow) intertwined among silk fibroin fibers; OB are located in correspondence to stained nuclei in PECAM-1 negative regions. (Reproduced with permission from ref. (46). Copyright 2010 Elsevier.)*

Subsequently, the same scaffolds were co-cultured with human dermal microvascular endothelial cells (HDMEC) and OB (see figure 3), implanted subcutaneously in nude mice and after 2 weeks, pre-formed capillaries were still present, having a perfused lumen with red blood cells, evident from histomorphometry and immunohistochemistry analyses. Instead, no pre-formed capillaries, chimeric vessels or ingrowth of host capillaries were observed in the fibroin micrometric net alone or pre-cultured only with endothelial cells (*46*). In a following study (*88*), the significance of scaffold pre-seeding with osteoblasts for *in vivo* vascularization was further evaluated. In this case, silk fibroin nets were cultured only with human primary osteoblasts for 14 days before subcutaneous implantation and a rapid formation of host capillaries was observed after 2 weeks even without the contribution of an *in vitro* pre-formed network. Indeed, authors hypothesized that new bone ECM and soluble signals by osteoblasts in the scaffolds can serve as instructions for host endothelial cells and be physiologically provided at the right time and at the right place. Therefore, silk fibroin nets demonstrated to support the communication among cells and the efficient diffusion of pro-angiogenic factors, such as vascular endothelial growth factor VEGF. In addition, SF matrices tuned the migration of macrophages and multinucleated giant cells throughout the scaffolds, providing also the pro-angiogenic stimuli of inflammatory cells which is fundamental for vascularization and tissue repair.

Downloaded by VIRGINIA TECH on July 20, 2013 | http://pubs.acs.org
Publication Date (Web): July 8, 2013 | doi: 10.1021/bk-2013-1135.ch017

## Silk Fibroin in Cartilage Tissue Engineering

Degenerative joint diseases have a strong social and economical impact: for instance, in 2008 they represented the leading cause of chronic disability in the United States, affecting 20% of the adult population and forcing one third of patients to limit their daily activity and undergo surgical intervention; the total cost of osteoarthritis is estimated in 28.6 bilion dollars a year and it will rise because aged population is increasing (*89*). The situation is particularly problematic because all current treatments are unable to achieve a long-term repair of the joint. In the field of reparative surgery, therapies include arthroscopic debridement, abrasion arthroplasty and micro-fracture: these techniques stimulate the repair process inducing the release of mesenchymal stem cells from bone marrow into the damage site. However, fibrocartilage is formed with low resilience, reduced stiffness and weak wear resistance, thus it cannot withstand physiological loads in long term (*90*). Other options comprise mosaicplasty, which implies the remotion of osteochondral plugs (autografts) from not-bearing sites of the patient and the transplantation of these plugs in the site of injury, and Autologous Chondrocyte Transplantation (ACT), where lesions are filled with pre-cultured chondrocytes extracted from the patient, expanded *in vitro* and confined under a periosteal flap to the damaged site. Both these techniques are affected by lacking availability and morbidity of donor sites, low integration with the surrounding tissues, and difficulty in matching the topology of the graft to the shape of the injured site and the formation of fibrocartilage, as reported above (*89*, *91*). To overcome these limitations, the application of tissue engineering principles has shown a


In Tailored Polymer Architectures for Pharmaceutical and Biomedical Applications; Scholz, C., et al.;
ACS Symposium Series; American Chemical Society: Washington, DC, 2013.

great potential, because the morphological, biological, chemical and mechanical properties of the graft necessary to obtain a complete and durable repair of the joint can be tailored ad hoc (*90*, *92*).

A scaffold for cartilage regeneration should be characterized by a high and interconnected porosity to simulate what happens in the physiological environment, where chondrocytes are suspended and isolated in a dense ECM. The material has to be chosen according to several criteria, such as the type of damage (its extension, for instance), joint conditions after implantation (it may be conjugated with anti-inflammatory drugs), *in vitro* culture method (if mechanical stimulation is provided, scaffold material has to be able to sustain the applied load) (*93*, *94*).

Both natural and synthetic polymers have been proposed for cartilage tissue engineering (*93*). Natural materials have many advantages, including a known biocompatibility also because of ligands which can be recognized by cells. However, they may be difficult to find and process, have weak mechanical properties and a too high degradation rate (*70*, *95*). As previously described, silk fibroin has the potential to overcome these limitations because it is characterized by tailorable mechanical properties and degradation rate, besides the possibility to obtain matrices with a suitable morphology.

For these reasons, the use of silk-based matrices in cartilage tissue engineering have been widely explored. The feasibility of silk fibroin has been exploited to prepare hydrogels with encapsulated cells (*97*), porous sponges produced by freeze-drying (*96*, *97*) and salt leaching (*98–100*). Systematic studies have been reported, where *in vitro* cell responses of either articular chondrocytes or mesenchymal stem cells were evaluated in function of scaffold properties, such as fibroin concentration (*101*) and production method (*102*).

In a recent paper by Wang et al. (*103*), the properties of salt leaching fibroin sponges with two different pore diameter ranges (300-500 μm, SL300, and 500-1180 μm, SL500) were compared to freeze-dried silk scaffolds (FD) and combined with dynamic culture conditions. Rat chondrocytes from the resting zone of costochondral cartilage growth plate were cultured in a static environment or on a rocking platform for 15 days and cell proliferation, cell distribution, chondrogenic gene expression and new ECM deposition were evaluated. It was observed that the fibroin sponge with the highest porosity and pore size significantly improved chondrocyte proliferation, distribution and differentiation in terms of their round morphology and gene expression. Moreover, a hydrodynamic environment was beneficial in a way directly dependent on pore diameter with a higher production of cartilage matrix and limited hypertrophic differentiation (figure 4). Interestingly, the combination of high pore sizes and mechanical stimulation also increased the expression of integrin subunits α5, β1 and β3, corresponding to an upregulation of a fibronectin receptor with a predominant role in chondrocyte adhesion and mechanotransduction (*103*).

Starting from the promising pure fibroin materials, the optimization of scaffold properties for cartilage regeneration has been investigated by means of specific growth factors loading (*97*), genetically interfusion of RGD (arginine-glycine-aspartic acid) sequences (*104*) or the combination with other natural polymers (*105*).



In Tailored Polymer Architectures for Pharmaceutical and Biomedical Applications; Scholz, C., et al.;
ACS Symposium Series; American Chemical Society: Washington, DC, 2013.

Downloaded by VIRGINIA TECH on July 20, 2013 | http://pubs.acs.org
Publication Date (Web): July 8, 2013 | doi: 10.1021/bk-2013-1135.ch017

Downloaded by VIRGINIA TECH on July 20, 2013 | http://pubs.acs.org
Publication Date (Web): July 8, 2013 | doi: 10.1021/bk-2013-1135.ch017

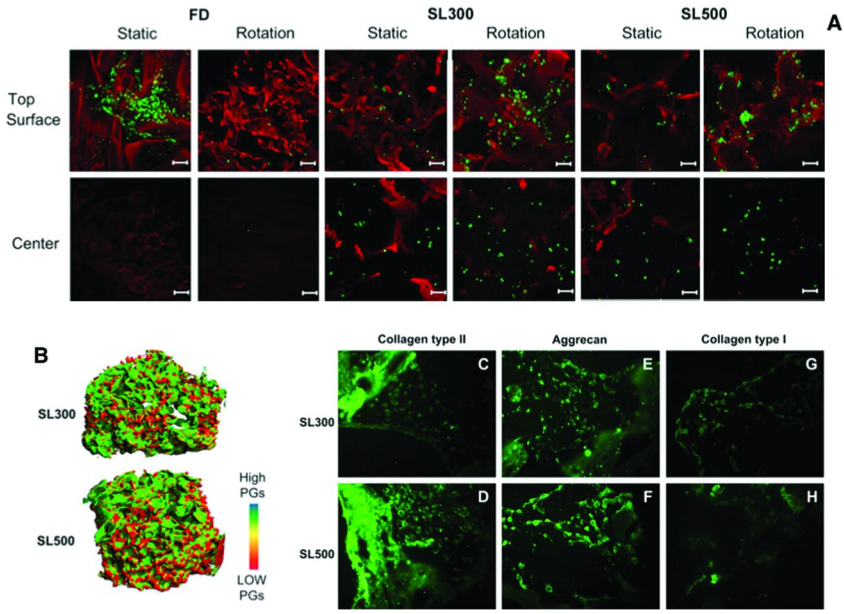


*Figure 4. In A, confocal images of cell viability and distribution in different silk fibroin scaffolds after 15 days of culture (green corresponds to live cells, while red stains dead cells and silk sponges, scale bar: 100 μm). In B, the production of proteoglycans PGs of SL300 and SL500 scaffolds after 30 days of rotation culture evaluated by microCT after staining with Hexabrix contrast agent. On the same constructs, the presence of collagen type II (C, D), aggrecan (E, F) and collagen type I (G, H) was detected by immunofluorescence (40x). (Reproduced with permission from ref. (103). Copyright 2010 Elsevier.)*

In particular, the aim of the combination of silk fibroin with polysaccharides such as chitosan and hyaluronic acid is to reproduce the characteristics of cartilage ECM, where glycosaminoglycans (GAG) are dispersed in a protein matrix of collagen type II. In a study by Silva et al. (*30*), blends of chitosan and silk fibroin at different concentrations were used to prepare freeze-dried sponges. Genipin, a natural and biocompatible cross-linker extracted from Gardenia fruits with weak anti-inflammatory properties, was employed to cross-link the scaffolds and induce the conformational change of fibroin into β-sheet crystalline structures. The resulting matrices showed a dependence of pore diameter, compressive modulus and water uptake on the silk fibroin-chitosan ratio. After no cytotoxicity was demonstrated, ATDC5 chondrocyte-like cells were cultured on the fibroin/chitosan sponges for 28 days. Scaffolds were able to sustain the maintenance of cell chondrocyte-like morphology and the migration and distribution throughout the whole structure. In particular, the scaffold with 50% wt of chitosan with respect to fibroin led to the highest cell proliferation and an increase of GAG deposition after the *in vitro* culture (*30*).

Lately, Foss et al. combined silk fibroin and hyaluronic acid (HA) to produce salt leaching sponges for cartilage regeneration (*29*). Besides the ability to retain a significant amount of water and to help the maintenance of chondrocyte phenotype, HA was used because of its known ability to decrease MMP and nitrogen oxide (NO) levels *in vitro* and inhibit cell apoptosis (*96*). For this reason, it may have a fundamental role in regulating the inflammatory process associated with osteoarthritis. In this study, matrices with a high and interconnected porosity were obtained by means of the salt leaching technique, using several hyaluronic acid concentration and the cross-linking with genipin to modulate scaffold properties. HA was incorporated into the scaffolds with different distributions according to the presence of cross-linking; in fact, HA acted as sericin during the spinning process, resulting in fibroin separation during the scaffold production. Protein separation was instead prevented by the cross-linking process, which caused a more interconnected arrangement of the two material components. In addition, the presence of hyaluronic acid influnced silk fibroin crystallinity and when combined to NaCl, had a synergistic effect to decrease the cross-linking degree of the scaffolds when compared to the pure fibroin cross-linked sponge (*29*).

These studies have clearly shown how silk fibroin offers the possibility to modulate scaffold properties to potentially achieve the functionality of the restored cartilage tissue. In addition, it provides the option to study the mechanisms underlying the regeneration process by the systematic variation of material variables.

Downloaded by VIRGINIA TECH on July 20, 2013 | http://pubs.acs.org
Publication Date (Web): July 8, 2013 | doi: 10.1021/bk-2013-1135.ch017

## References

1. Lanza, R.; Langer, R.; Vacanti, J. *Principles of Tissue Engineering*; Elsevier Academic Press: Waltham, MA, 2007.
2. Badylak, S. F.; Nerem, R. M. *Proc. Natl. Acad. Sci. U.S.A.* **2010**, *107*, 3285–3286.
3. Mikos, A. G.; Herring, S. W.; Ochareon, P.; Elisseeff, J.; Lu, H. H.; Kandel, R.; Schoen, F. J.; Toner, M.; Mooney, D.; Atala, A.; Van Dyke, M. E.; Kaplan, D.; Vunjak-Novakovjc, G. *Tissue Eng.* **2006**, *12*, 3307–3339.
4. Onuki, Y.; Bhardwaj, U.; Papadimitrakopoulos, F.; Burgess, D. J. *J. Diabetes Sci. Technol.* **2008**, *2*, 1003–1015.
5. Williams, D. F. *Biomaterials* **2008**, *29*, 2941–2953.
6. Kim, T. G.; Shin, H.; Lim, D. W. *Adv. Funct. Mater.* **2012**, *22*, 2446–2468.
7. Stoppato, M.; Carletti, E.; Maniglio, D.; Migliaresi, C.; Motta, A. *J. Tissue Eng. Regen. M.* **2011**, DOI:10.1002/term.516.
8. Stoppato, M.; Carletti, E.; Sidarovich, V.; Quattrone, A.; Unger, R. E.; Kirkpatrick, C. J.; Migliaresi, C.; Motta, A. *J. Bioact. Compat. Pol.* **2013**, in press.
9. Lenas, P.; Luyten, F. P.; Doblare, M.; Nicodemu-Lena, E.; Lanzara, A. E. *Artif. Organs* **2011**, *35*, 656–671.
10. Jukes, J. M.; Both, S. K.; Leusink, A.; Sterk, L. M. Th.; van Blitterswijk, C. A.; de Boer, J. *Proc. Natl. Acad. Sci. U.S.A.* **2008**, *105*, 6840–6845.

11. Krenning, G.; Moonen, J. A. J.; van Luyn, M. J. A.; Harmsen, M. C. *J. Tradit. Chin. Med.* **2008**, *18*, 312–323.
12. Lee, K.; Silva, E. A.; Mooney, D. J. *J. R. Soc., Interface* **2011**, *8*, 153–170.
13. Porter, D.; Vollrath, F. *Adv. Mater.* **2009**, *21*, 487–492.
14. Motta, A.; Floren, M.; Migliaresi, C. Silk fibroin in medicine. In *Silk: Properties, Production and Uses*; Nova Science Publishers, Inc.: Hauppage, NY, 2011; ISBN 978-1-62100-692-3, pp 189−222.
15. Yamada, H.; Igarashi, Y.; Takasu, Y.; Saito, H.; Tsubouchi, K. *Biomaterials* **2004**, *25*, 467–472.
16. Motta, A.; Maniglio, D.; Migliaresi, C.; Kim, H-J; Wang, X.; Hu, X.; Kaplan, D. L. *J. Biomater. Sci., Polym. Ed.* **2009**, *20*, 1875–1897.
17. Li, M.; Tao, W.; Lu, S.; Kuga, S. *Int. J. Biol. Macromol.* **2003**, *32*, 159–163.
18. Hardy, J. G.; Roemer, L. M.; Scheibel, T. R. *Polymer* **2008**, *49*, 4309–4327.
19. Altman, G. H.; Diaz, F.; Jakuba, C.; Calabro, T.; Horan, R. L.; Chen, J.; Lu, H.; Richmond, J.; Kaplan, D. L. *Biomaterials* **2003**, *24*, 401–416.
20. Kundu, B.; Kundu, S. C. *Progr. Polym. Sci.* **2010**, *35*, 116–127.
21. Wang, Y.; Kim, H.; Vunjak-Novakovic, G.; Kaplan, D. L. *Biomaterials* **2006**, *27*, 6064–6082.
22. Fini, M.; Motta, A.; Torricelli, P.; Niccoli Aldin, N.; Tschon, M.; Giardino, R.; Migliaresi, C. *Biomaterials* **2005**, *26*, 3527–3536.
23. Mandal, B. B.; Kundu, S. C. *Biotechnol. Bioeng.* **2008**, *100*, 1237–1250.
24. Kirkpatrick, C. J.; Fuchs, S.; Unger, R. E.; Motta, A; Reis, R.; Migliaresi, C. *Inflammation. Res.* **2007**, *62*, 540–540.
25. Jones, G.; Marshall, M.; El Haj, A. J.; Motta, A.; Cartmell, S. *Tissue Eng.* **2007**, *17*, 1765–1766.
26. Jones, G. L.; Motta, A.; Marshall, M.; El Haj, A. J.; Cartmell, S. H. *Biomaterials* **2009**, *30*, 5376–5384.
27. Di Felice, V.; De Luca, A.; Serrafico, C.; Di Marco, P.; Verin, L.; Motta, A.; Guercio, A.; Zummo, G. *ItaL. J. Anat. Embryol.* **2010**, *115*, 65–69.
28. Di Felice, V.; Serradifalco, C.; Rizzuto, L.; De Luca, A.; Rappa, F.; Barone, R.; Di Marco, P.; Cassata, G.; Puleio, R.; Verin, L.; Motta, A.; Migliaresi, C.; Guercio, A.; Zummo, G. *J. Tissue Eng. Regener. Med.* **2013**, in press.
29. Foss, C.; Merzari, E.; Migliaresi, C.; Motta, A. *Biomacromolecules* **2013**, in press.
30. Silva, S. S.; Motta, A.; Rodrigues, M. T.; Pinheiro, A. F. M.; Gomez, M. E.; Mano, J. F.; Reis, R. L.; Migliaresi, C. *Biomacromolecules* **2008**, *9*, 2764–2774.
31. Kemal, K.; Motta, A.; Fambri, L.; Migliaresi, C. *J. Biomater. Sci., Polym. Ed.* **2001**, *12*, 337–351.
32. Cassinelli, C.; Cascardo, G.; Morra, M.; Draghi, L.; Motta, A.; Catapano, G. *Int. J. Artif. Organs* **2006**, *29*, 881–892.
33. Motta, A.; Fambri, L.; Migliaresi, C. *Macromol. Chem. Phys.* **2002**, *203*, 1658–1665.
34. Santin, M.; Motta, A.; Freddi, G.; Cannas, M. *J. Biomed. Mater. Res.* **1999**, *46*, 382–389.

Downloaded by VIRGINIA TECH on July 20, 2013 | http://pubs.acs.org
Publication Date (Web): July 8, 2013 | doi: 10.1021/bk-2013-1135.ch017


In Tailored Polymer Architectures for Pharmaceutical and Biomedical Applications; Scholz, C., et al.;
ACS Symposium Series; American Chemical Society: Washington, DC, 2013.

Downloaded by VIRGINIA TECH on July 20, 2013 | http://pubs.acs.org
Publication Date (Web): July 8, 2013 | doi: 10.1021/bk-2013-1135.ch017

35. Santin, M.; Denyer, S. P.; Lloyd, A. W.; Motta, A. *J. Bioact. Compat. Polym.* **2002**, *17*, 195–208.
36. Fedel, M.; Engdogan, T.; Hasirci, N.; Morelli, A.; Chiellini, F.; Motta, A. *J. Bioact. Compat. Polym.* **2012**, *27*, 295–312.
37. Kaplan, D. L. In *Biomaterials. Novel Materials from Biological Sources*; Byrom, D., Ed.; Stockton Press: New York, 1991; pp 1–53.
38. Bini, E.; Knight, D. P.; Kaplan, D. L. *J. Mol. Biol.* **2004**, *335*, 27–40.
39. Servoli, E.; Maniglio, D.; Motta, A.; Predazzer, R.; Migliaresi, C. *Macromol. Biosci.* **2005**, *5*, 1175–1183.
40. Servoli, E.; Maniglio, D.; Motta, A.; Migliaresi, C. *Macromol. Biosci.* **2008**, *8*, 827–835.
41. Silva, S.; Maniglio, D.; Motta, A.; Mano, J. F.; Reis, R. L.; Migliaresi, C. *Macromol. Biosci.* **2008**, *8*, 766–774.
42. Maniglio, D.; Bonani, W.; Servoli, E.; Motta, A.; Migliaresi, C. *J. Bioact. Compat. Polym.* **2010**, *25*, 441–454.
43. MacIntosh, A. C.; Kearns, V. R.; Crawford, A.; Hatton, P. V. *J. Tissue Eng. Regener. Med.* **2008**, *2*, 71–80.
44. Vepari, C.; Kaplan, D. L. *Prog. Polym. Sci.* **2007**, *32*, 991–1007.
45. Bondar, B.; Fuchs, S.; Motta, A.; Migliaresi, C.; Kirkpatrick, C. J. *Biomaterials* **2008**, *29*, 561–572.
46. Unger, R. E.; Ghaanati, S.; Orth, C.; Sartoris, A.; Barbeck, M.; Halstenberg, S.; Motta, A.; Migliaresi, C.; Kirkpatrick, C. J. *Biomaterials* **2010**, *31*, 6959–6967.
47. Unger, R. E.; Peters, K.; Wolf, M.; Motta, A.; Migliaresi, C.; Kirkpatrick, C. J. *Biomaterials* **2004**, *25*, 5137–5146.
48. Fuchs, S.; Motta, A.; Migliaresi, C.; Kirkpatrick, C. J. *Biomaterials* **2006**, *27*, 5399–5408.
49. Unger, R. E.; Sartoris, A.; Peters, K.; Motta, A.; Migliaresi, C.; Kunkel, M.; Bulnheim, U.; Rychly, J.; Kirkpatrick, C. J. *Biomaterials* **2007**, *28*, 3965–3976.
50. Nakaoka, R.; Hsjong, S. X.; Mooney, D. J. *Tissue Eng.* **2006**, *12*, 2425–2433.
51. Karageorgiou, V.; Meinel, L.; Hofmann, S.; Volloch, V.; Kaplan, D. L. *J. Biomed. Mater. Res., Part A* **2004**, *71*, 528–537.
52. Kim, U. J.; Park, J.; Kim, H. J.; Wada, M.; Kaplan, D. L. *Biomaterials* **2005**, *26*, 2775–2785.
53. Silva, S. S.; Rodrigues, M. T.; Motta, A.; Gomes, M. E.; Mano, J. F.; Migliaresi, C.; Reis, R. L. *Tissue Eng., Part A* **2008**, *14*, 763–763.
54. Kim, H. J.; Kim, U. J.; Chunmei, L.; Wada, M.; Leisk, G. G.; Kaplan, D. L. *Bone* **2008**, *42*, 1226–1234.
55. Karageorgiou, V.; Tomkins, M.; Fajardo, R.; Meinel, L.; Snyder, B.; Wade, K.; Chen, J.; Vunjak-Novakovic, G.; Kaplan, D. L. *J. Biomed. Mater. Res., Part A* **2006**, *78*, 324–334.
56. Wang, X.; Wenk, E.; Zhang, X.; Meinel, L.; Vunjak-Novakovic, G.; Kaplan, D. L. *J. Controlled Release* **2009**, *134*, 81–90.
57. Migliaresi, C.; Motta, A.; Di Benedetto, A. Injectable scaffolds for bone and cartilage regeneration. In*Engineering of functional skeletal tissues*; Springer: Berlin, 2007; p 95−109.

58. Ayub, Z.; Arai, M.; Hirabayashi, K. *Biosci. Biotechnol. Biochem.* **1993**, *57*, 1910–1912.
59. Wang, X.; Kluge, J. A.; Leisk, G. G.; Kaplan, D. L. *Biomaterials* **2008**, *29*, 1054–1064.
60. Motta, A.; Migliaresi, C.; Faccioni, F.; Torricelli, P.; Fini, M.; Giardino, R. *J. Biomat. Sci., Polym. Ed.* **2004**, *15*, 851–864.
61. Mooney, D. J.; Baldwin, D. F.; Suht, N. P.; Vacanti, J. P.; Langer, R. *Biomaterials* **1996**, *17*, 1417–1422.
62. Shieh, Y.; Su, J.; Manivannan, G.; Lee, P. H. C.; Sawan, S. P.; Spall, D. W. *J. Appl. Polym. Sci.* **1996**, *59*, 707–717.
63. Floren, M.; Spilimbergo, S.; Motta, A.; Migliaresi, C. *J. Biomed. Mat. Res., Part B* **2011**, *99B*, 338–349.
64. Floren, M.; Spilimbergo, S.; Motta, A.; Migliaresi, C. *Biomacromolecules* **2012**, *13*, 2060–2072.
65. Kang, G. D.; Nahm, J. H.; Park, J. S.; Moon, J. Y.; Cho, C. S.; Yeo, J. H. *Macromol. Rapid. Commun.* **2000**, *21*, 788–791.
66. Motta, A.; Barbato, B.; Foss, C.; Torricelli, P.; Migliaresi, C. *J. Bioact. Compat. Polym.* **2011**, *26*, 130–143.
67. Muschler, G. F.; Nakamoto, C.; Griffith, L. G. *J. Bone Joint Surg. Am.* **2004**, *86*, 1541–1548.
68. Patterson, T. E.; Kumagai, K.; Griffith, L.; Muschler, G. F. *J. Bone Jt. Surg.* **2008**, *90*, 111–119.
69. Khan, S. N.; Cammisa, F. P., Jr; Sandhu, H. S.; Diwan, A. D.; Girardi, F. P.; Lane, J. M. *J. Am. Acad. Orthop. Surg.* **2005**, *13*, 77–86.
70. Karageorgiou, V.; Kaplan, D. L. *Biomaterials* **2005**, *26*, 5474–5491.
71. Rodrigues, M. T.; Gomes, M. E.; Reis, R. L. *Curr. Opin. Biotechnol.* **2011**, *22*, 726–733.
72. Patel, Z. S.; Young, S.; Tabata, Y.; Jansen, J. A.; Wong, M. E.; Mikos, A. G. *Bone* **2008**, *43*, 931–940.
73. Santos, M. I.; Reis, R. L. *Macromol. Biosci.* **2010**, *10*, 12–27.
74. Novosel, E. C.; Kleinhans, C.; Kluger, P. J. *Adv. Drug Delivery Rev.* **2011**, *63*, 300–311.
75. Glowacki, J. *Clin. Orthop.* **1998**, S82–89.
76. Gerber, H. P.; Ferrara, N. *Trends Cardiovasc. Med.* **2000**, *10*, 223–228.
77. Lin, A. S.; Barrows, T. H.; Cartmell, S. H.; Guldberg, R. E. *Biomaterials* **2003**, *24*, 481–489.
78. Ogose, A.; Hotta, T.; Kawashima, H.; Kondo, N.; Gu, W.; Kamura, T.; Endo, N. *J. Biomed. Mater. Res., Part B* **2005**, *72*, 94–101.
79. Muehrcke, D. D.; Shimp, W. M.; Aponte-Lopez, R. *Ann. Thorac. Surg.* **2009**, *88*, 1658–1661.
80. Rodrigues, M. T.; Gomes, M. E.; Viegas, C. A.; Azevedo, J. T.; Dias, I. R.; Guzòn, F. M.; Reis, R. L. *J. Tissue Eng. Regener. Med.* **2011**, *5*, 41–49.
81. Kim, H. J.; Kim, U. J.; Kim, H. S.; Li, C.; Wada, M.; Leisk, G. G.; Kaplan, D. L. *Bone* **2008**, *42*, 1226–1234.
82. Thimm, B. W.; Wuest, S.; Hofmann, S.; Hagenmueller, H.; Mueller, R. *Acta Biomater.* **2011**, *7*, 2218–2228.

Downloaded by VIRGINIA TECH on July 20, 2013 | http://pubs.acs.org
Publication Date (Web): July 8, 2013 | doi: 10.1021/bk-2013-1135.ch017


In Tailored Polymer Architectures for Pharmaceutical and Biomedical Applications; Scholz, C., et al.;
ACS Symposium Series; American Chemical Society: Washington, DC, 2013.

83. Zhao, J.; Zhang, Z.; Wang, S.; Sun, X.; Zhang, X.; Chen, J.; Kaplan, D. L.; Jiang, X. *Bone* **2008**, *45*, 517–527.
84. Bhumiratana, S.; Grayson, W. L.; Castaneda, A.; Rockwood, D. N.; Gil, E. S.; Kaplan, D. L.; Vunjak-Novakovic, G. *Biomaterials* **2011**, *32*, 2812–2820.
85. Maraldi, T.; Riccio, M.; Resca, E.; Pisciotta, A.; La Sala, G. B.; Ferrari, A.; Bruzzesi, G.; Motta, A.; Migliaresi, C.; Marzona, L.; De Pol, A. *Tissue Eng., Part A* **2011**, *17*, 2833–43.
86. Riccio, M.; Maraldi, T.; Pisciotta, A.; La Sala, G. B.; Ferrari, A.; Bruzzesi, G.; Motta, A.; Migliaresi, C.; De Pol, A. *Tissue Eng., Part A* **2012**, *18*, 1006–1013.
87. Fuchs, S.; Jiang, X.; Schmidt, H.; Dohle, E.; Ghanaati, S.; Orth, C.; A. Hoffman, A.; Motta, A.; Migliaresi, C.; Kirkpatrick, C. J. *Biomaterials* **2009**, *30*, 1329–1338.
88. Ghanaati, S.; Unger, R. E.; Webber, M. J.; Barbeck, M.; Orth, C.; Kirkpatrick, J. A.; Booms, P.; Motta, A.; Migliaresi, C.; Sader, R. A.; Kirkpatrick, C. J. *Biomaterials* **2011**, *32*, 8150–8160.
89. Sharma, L.; Kapoor, D.; Issa, S. *Curr. Opin. Rheumatol.* **2006**, *28*, 147–156.
90. Grayson, W. L.; Chao, P. H.; Marolt, D.; Kaplan, D. L.; Vunjak-Novakovic, G. *Trends Biotechnol.* **2008**, *26*, 181–189.
91. Beris, A. E.; Lykissas, M. G.; Papageorgiou, C. D.; Georgoulis, A. D. *Injury* **2005**, *36*, S14–S23.
92. Martin, I.; Miot, S.; Barbero, A.; Jakob, M.; Wendt, D. *J. Biomech.* **2007**, *40*, 750–765.
93. Nesic, D.; Whiteside, R.; Brittberg, M.; Wendt, D.; Martin, I.; Mainil-Varlet, P. *Adv. Drug Delivery Rev.* **2006**, *58*, 300–322.
94. Temenoff, S.; Mikos, A. G. *Biomaterials* **2000**, *21*, 431–440.
95. Chao, P. H. G.; Yodmuang, S.; Wang, X.; Sun, L.; Kaplan, D. L.; Vunjak-Novakovic, G. *J. Biomed. Mater. Res., Part B* **2010**, *95B*, 84–90.
96. Talukdar, S.; Nguyen, Q. T.; Chen, A. C.; Sah, R. L.; Kundu, S. C. *Biomaterials* **2011**, *32*, 8927–8937.
97. Uebersax, L.; Merkle, H. P.; Meinel, L. *J. Controlled Release* **2008**, *127*, 12–21.
98. Wang, Y.; Kim, U. J.; Blasioli, D. J.; Kim, H. J.; Kaplan, D. L. *Biomaterials* **2005**, *26*, 7082–7094.
99. Hofmann, S.; Knecht, S.; Langer, R.; Kaplan, D. L.; Vunjak-Novakovic, G.; Merkle, H. P.; Meinel, L. *Tissue Eng.* **2006**, *12*, 2729–2738.
100. Wang, Y.; Blasioli, D. J.; Kim, H. J.; Kim, H. S.; Kaplan, D. L. *Biomaterials* **2006**, *27*, 4434–4442.
101. Yan, L. P.; Oliveira, J. M.; Oliveira, A. L.; Caridade, S. G.; Mano, J. F.; Reis, R. L. *Acta Biomater.* **2012**, *8*, 289–301.
102. Makaya, K.; Terada, S.; Ohgo, K.; Asakura, T. *J. Biosci. Bioeng.* **2009**, *108*, 68–75.
103. Wang, Y.; Bella, E.; Lee, C. S. D.; Migliaresi, C.; Pelcaster, L.; Schwartz, Z.; Boyan, B. D.; Motta, A. *Biomaterials* **2010**, *31*, 4672–4681.
104. Kambe, Y.; Yamamoto, K.; Kojima, K.; Tamada, Y.; Tomita, N. *Biomaterials* **2010**, *31*, 7503–7511.
105. Bhardwaj, N.; Nguyen, Q. T.; Chen, A. C.; Kaplan, D. L.; Sah, R. L.; Kundu, S. C. *Biomaterials* **2011**, *32*, 5773–5781.

Downloaded by VIRGINIA TECH on July 20, 2013 | http://pubs.acs.org
Publication Date (Web): July 8, 2013 | doi: 10.1021/bk-2013-1135.ch017


In Tailored Polymer Architectures for Pharmaceutical and Biomedical Applications; Scholz, C., et al.;
ACS Symposium Series; American Chemical Society: Washington, DC, 2013.

Downloaded by VIRGINIA TECH on July 17, 2013 | http://pubs.acs.org
Publication Date (Web): July 8, 2013 | doi: 10.1021/bk-2013-1135.ch018

## Chapter 18

# Health and Safety via Surface Modification of Polyurethanes

**Kenneth J. Wynne,[*,1] Pinar Kurt,[1] Kennard Brunson,[1] Asima Chakravorty,[1] Murari Gupta,[1] Wei Zhang,[1] Lynn Wood,[2,3] and Dennis E. Ohman[2,3]**

**[1]Department of Chemical and Life Science Engineering, Virginia Commonwealth University, 601 West Main Street, Richmond, Virginia 23284**
**[2]Department of Microbiology and Immunology, VCU Medical Center, Virginia Commonwealth University Richmond, 5-040 Sanger Hall, 1101 E. Marshall Street, Richmond, Virginia 23298**
**[3]McGuire Veterans Affairs Medical Center, 1201 Broad Rock Blvd., Richmond, Virginia 23249**
**[*]E-mail: kjwynne@vcu.edu.**

Alkylammonium containing polymers are well known to effect contact kill of pathogenic bacteria. For coatings, alkylammonium function is needed only at the surface and not in the bulk. This paper describes a blend strategy that is "processing friendly" and aims at development of modifiers for conventional coating or molding operations. Specifically, the temporal instability of a polyurethane modifier with a copolyoxetane soft block having trifluoroethoxymethyl (3F) and C12 quaternary (dimethyldodecyl ammonium) side chains was overcome by utilizing a $–CF_2CF_2H$ (4F) fluorous side chain and increasing the C12 mole fraction (U-4F-C12(0.34)). Characterization of a 2 wt% base polyurethane modified with 2 wt% U-4F-C12(0.34) validated a soft block surface modification model. Biocidal effectiveness (100% kill of spray on challenges of Gram+/- bacteria) was retained after storage for at least a month under ambient conditions of temperature

© 2013 American Chemical Society
In Tailored Polymer Architectures for Pharmaceutical and Biomedical Applications; Scholz, C., et al.; ACS Symposium Series; American Chemical Society: Washington, DC, 2013.

and humidity. This stability was correlated with zeta potential measurements of accessible near surface charge. These results suggest zeta potential measurements hold promise as a physical method for assessing effectiveness of polycation contact kill and polycation stability in contact with aqueous systems.

## 1. Introduction

Infection is a serious medical complication associated with health care environments. The 5-10% incidence of infections for hospital patients is well documented (*1*, *2*) Sources of bacteria include health care equipment such as cell phones, pagers, computer keyboards, doorknobs, and electrocardiograph leads (*3*). Modes of transmission of antibiotic resistant pathogens occur in obvious ways such as touches, coughs, and sneezes.

A study of Pennsylvania hospitals found that catheter associated urinary tract infections, designated CAUTIs, constituted over 60% of nosocomial infections (*4*). Women are particularly susceptible to UTIs (*5*). The majority of UTIs are caused by resistant strains of *Escherichia coli* (*6*) but infections are also caused by other Gram +/- bacterial strains (*7*).

Biocidal polymers offer promise in helping curb the spread of infections by providing coatings for biomedical devices or molded articles. Such polymers may be classified as biocide release or non-release contact kill. Biocide release systems are the most advanced in that commercial products are available. A recent review covers recent advances in contact kill systems (*8*). A brief description of biocide release coatings is provided below followed by the development of surface modifiers that introduce contact kill into conventional polymers.

### A. Biocide Release

The most commonly encountered strategy is *biocide release*. This approach is implemented by mixing polymeric materials with an FDA approved antibiotic or biocide (*9–11*). The active agent leaches from the tubing, coating, or other article and effects bacterial kill. A test of efficacy is carried out by placing a disk or similar object in contact with bacteria seeded on agar. A characteristic "zone of inhibition" forms a halo of killed bacteria around the article due to leached biocide. Although few laboratories report results, this is an important test to distinguish between biocide leaching and contact kill.

Polymer materials employing release of silver ($Ag^+$) are increasingly common (*12*, *13*). However, some bacterial strains are inherently resistant to silver (*14*) and some develop resistance (*15*, *16*). More research is needed to understand whether this situation is as serious as the buildup of antibiotic resistance and to understand effects on eukaryotic cells (*17*). Bacterial strains develop resistance against antibiotics since the mechanism of action is based on disruption of metabolic pathways via genetic alteration in cells. Some bacteria strains such as methicillin-resistant *Staphylococcus aureus* (MRSA) are of current concern because of increasing resistance to antibiotics (*18*, *19*).

Downloaded by VIRGINIA TECH on July 17, 2013 | http://pubs.acs.org
Publication Date (Web): July 8, 2013 | doi: 10.1021/bk-2013-1135.ch018


In Tailored Polymer Architectures for Pharmaceutical and Biomedical Applications; Scholz, C., et al.;
ACS Symposium Series; American Chemical Society: Washington, DC, 2013.

## B. Contact Kill

As the designation indicates, *contact kill* occurs when bacteria impinge on a solid surface. The two main classes of materials that effect contact kill do so either by a covalently bound *surface oxidant* that is renewed periodically or by membrane disruption, typically brought about by *surface accessible positive charge*.

### *1. Oxidative Kill*

This area was pioneered by Worley and Sun, who showed that introduction of hydantoin generates oxidative biocidal surfaces after conversion of amide (-CON-H) to chloramide (-CON-Cl) (*20–24*). Oxidative kill is unparalleled for rapid kinetics, typically effecting 100% kill in a few minutes. Chloramine and related functionality must be renewed periodically by treatment with bleach, which is convenient for applications such as water disinfection and treatment of fabrics used in nosocomial environments (*23*, *25*). Worley has continued to develop various strategies to effect oxidative kill and applications of this technology (*21*, *26–30*). Inspired by this research, we developed hydantoin based surface modified polyurethanes (*31*). These findings on oxidative kill will not be reviewed in this article, which focuses on surface concentration of quaternary (quat) polycations.

### *2. Polycations at Surfaces*

Contact kill occurs when a bacterium impinges on a surface with tethered polycations. As noted above, we focus on solid surfaces with quaternary nitrogen functionality. The mechanism by which surface quat functionality interacts with pathogenic organisms for contact kill has been discussed but the details are not clear (*32–35*). For coatings and thin films, a mechanistic analogy is drawn below to cell wall disruption proposed for solution borne polycations that have been studied extensively by authors including Tew (*36–38*), Kuroda (*39*), and Tiller (*40*).

In a 1986 solution study, Ikeda showed that a 1 h exposure of *Bacilus subtilis* cells and protoplasts to polycations resulted in release of $K^+$ (*41*). This release likely plays an important role in cell death as $K^+$ concentration in cells is much higher than the surrounding medium. That is, thermodynamically driven $K^+$ diffusion is one factor thought responsible for rapid cell lysis from osmotic shock (Eq 1). Solution borne polycations with multiple sites for conjugation through the formation of polysalts account for rapid chemisorption, release of $K^+$, and the formation of insoluble bioconjugates (*41*). Along with release of $K^+$ (or other inorganic cations) is likely that disruption of cell proton motive force ($\Delta p$) occurs ($\Delta p$ results from the difference in pH between intracellular pH ($pH_i$) and extracellular pH ($pH_o$)) (*42*, *43*).



In Tailored Polymer Architectures for Pharmaceutical and Biomedical Applications; Scholz, C., et al.;
ACS Symposium Series; American Chemical Society: Washington, DC, 2013.

Downloaded by VIRGINIA TECH on July 17, 2013 | http://pubs.acs.org
Publication Date (Web): July 8, 2013 | doi: 10.1021/bk-2013-1135.ch018

$$P[A^+]_n\ nB^-\ +\ [Cell^{n-}]\ nK^+\ \rightarrow\ [Cell^{n-}]P[A^+]_n\ +\ nK^+B^-\qquad \text{Eq 1.}$$

Where: $P[A^+]_n$ represents a polycation

$B^-$ is an associated anion

$Cell^{n-}$ represents a bacterium

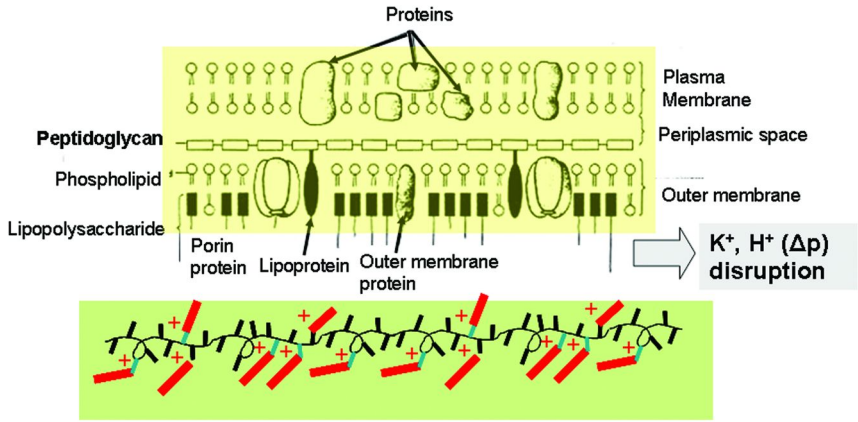


*Figure 1. A model for contact kill by disruption of bacterial membrane (negative, yellow) and $K^+$ / $H^+$ diffusion leading to cell death; coating (green, positive) has near surface accessible quaternary polycations, represented by red bars.*

A combination of (1) negatively charged phospholipid exchange (*8*) with negatively charged counter ions associated with quat cations (Eq 1) and (2) outflow of $K^+$ driven by osmotic pressure analogous to findings for water soluble polycations (*41*) and (3) disruption of cell proton motive force (Δp) seems likely for contact kill by surface concentrated polycations (Figure 1). A combination of these thermodynamically driven processes is consistent with 100% kill for high concentrations of sprayed on pathogen challenges in 30 min (*44*) as diffusion of species such as $K^+$ and $H^+$ would be rapid. While evidence for proposed mechanisms of kill is difficult to acquire (*8*), Santore has confirmed that bacterial chemisorption to solid surfaces bearing a positive charge is strongly favored (*45*).

## 2. Quats at Surfaces

Figure 2 provides a schematic that represents homogeneous, covalently bound polycations (Figure 2A) and surface modified coatings (Figure 2B). Either can give surface accessible quaternary function.


In Tailored Polymer Architectures for Pharmaceutical and Biomedical Applications; Scholz, C., et al.; ACS Symposium Series; American Chemical Society: Washington, DC, 2013.

Downloaded by VIRGINIA TECH on July 17, 2013 | http://pubs.acs.org
Publication Date (Web): July 8, 2013 | doi: 10.1021/bk-2013-1135.ch018

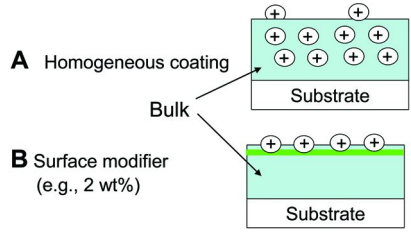


*Figure 2. Schematic for **A**, polymers containing quaternary function and **B**, surface modified coatings.*

Downloaded by VIRGINIA TECH on July 17, 2013 | http://pubs.acs.org
Publication Date (Web): July 8, 2013 | doi: 10.1021/bk-2013-1135.ch018

## A. Homo-Quats

A good deal of research has described the homogeneous incorporation of alkylammonium function in coatings (*46–49*), and thin films (*50*, *51*). An example of homogeneous incorporation of quaternary function is provided by Cooper's report of chain extender modification (*33*). Depending on the percent alkylpyridinium content, water uptake was 22 to 49 wt %, which negatively affected mechanical properties. For optimum compositions, contact kill was up to 95% against a sprayed challenge of *Staphylococcus aureus*. Hard block functionality trapped in the bulk may have resulted in an insufficient surface accessible quaternary charge for higher efficiency. With a similar functional group, quaternized polystyrene-*b*-poly(4-vinylpyridine) copolymers containing fluorous moieties showed good antimicrobial activity against *Staphylococcus aureus*. Bactericidal effectiveness was correlated with the molecular composition and organization in the top 2-3 nm (*52*).

Quaternized polyethylene imine has been extensively studied by Klibanov (*53*). Thin coatings have been found to generate highly effective C12-quaternary antimicrobial surfaces. Thus, in the absence of inter- or intramolecular associative forces that sequester charge, surface accessible C12-quat function is robust and strongly antimicrobial (*54*).

## B. Surface Modification

Coatings with quaternary function concentrated at the surface are depicted in Figure 2B. Surface modified coatings represented by Figure 2B have been obtained by several methods including plasma treatment and subsequent functionalization (*55*, *56*) and photografting (*57*) and grafting to or from surfaces (*32*, *51*, *57*).

Due to entropic considerations, chain ends tend to be excluded from the bulk (*58*). End group surface concentration was used by Tiller in the photopolymerization of acrylate monomers and crosslinkers along with polyoxazoline macromonomers having biocidal quarternary ammonium end groups (*59*).


In Tailored Polymer Architectures for Pharmaceutical and Biomedical Applications; Scholz, C., et al.;
ACS Symposium Series; American Chemical Society: Washington, DC, 2013.

In the research described below, we focus on a straightforward blend method for surface functionalization of polyurethanes. Because this approach involves an additive for conventional polyurethanes, this blend surface modification may be translated to a large scale process.

### *1. Generation 1 Surface Modifiers (SMs)*

The attractive features of "processing friendly" surface modifiers motivated our research in polyurethanes (*31*, *60*, *61*). Prior work showed that polyurethane soft blocks are surface-concentrated (*62–64*). Thus, we have explored functional P[AB]-copolyoxetane diols **1** in a new approach to surface modification. Here, A and B designate repeat units or side chains. A model for this concept applied to quaternary surface function is shown in Figure 3. The surface concentrated functional soft block of the SM is shown in red along with side chains A and B. Economy is thus ensured by using the P[AB]-soft block polyurethane as a minor constituent in the blend.

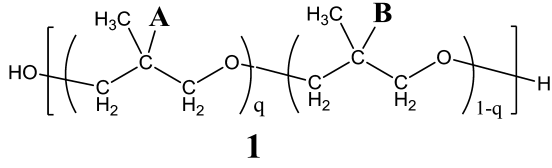


**1**

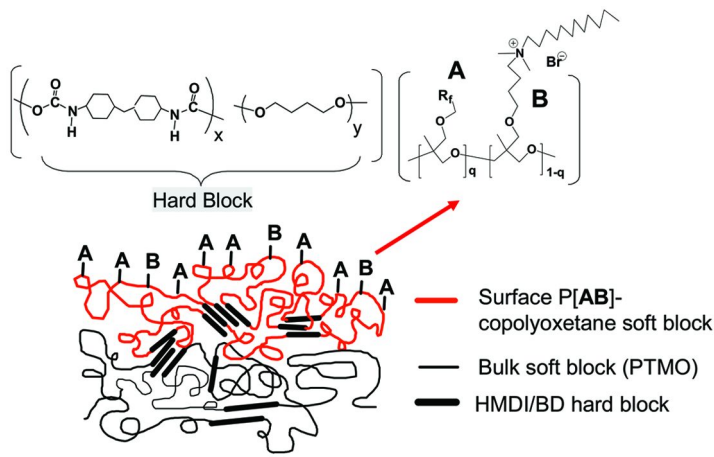


*Figure 3. Schematic of P[AB]-polyurethane surface modification. Here, A is a fluorous group and B is a C12 quat.*

The model shown in Figure 3 has been used to guide the development of quaternary alkylammonium antimicrobial SMs (*31*, *44*, *65*). Herein, we focus on SMs with fluorous side chains A having $R_f$ = -$CF_3$ (3F) and -$CF_2CF_2H$ (4F),


In Tailored Polymer Architectures for Pharmaceutical and Biomedical Applications; Scholz, C., et al.; ACS Symposium Series; American Chemical Society: Washington, DC, 2013.

Downloaded by VIRGINIA TECH on July 17, 2013 | http://pubs.acs.org
Publication Date (Web): July 8, 2013 | doi: 10.1021/bk-2013-1135.ch018

respectively and B = C12 quat. Both of these modifiers effect contact kill due to quat functionality (*44*, *65*) but the morphological and functional stability of the modified surfaces are dramatically different. The synthesis, initial surface characterization and biotesting for the 3F modifier have been published (*44*, *65*). Details for the 4F modifier, which was prepared in a similar fashion, will be published separately.

The bulk polyurethane is $H_{12}$MDI-BD(50)-PTMO-1000, where the hard block is 4,4′-(methylene bis(p-cyclohexyl isocyanate) ($H_{12}$MDI) and butanediol (BD) and poly(tetramethylene oxide) PTMO-1000 is the soft block. This base polyurethane with a Shore D hardness of 47 ±2 was selected for its similarity to commercially available aliphatic polyurethanes that are used in many applications such as biomedical materials and sports equipment. A notable difference for the base polyurethane described herein is a purification scheme that ensures no water contamination during a sensitive dynamic contact angle experiment (*66*).

The focus of initial discussion is a "first generation" SM $H_{12}$MDI-BD(50)-3F-C12(0.11), Figure 3, (1-q) = 0.11. This SM is designated U-3F-C12(0.11). $M_n$ for the soft block is 5.1 kDa. Coatings were generated by dipping or spreading tetrahydrofuran (THF) or THF-isopropanol (THF-IPA) solutions of 2 wt% U-3F-C12(0.11) and base polyurethane. The compositional rationale and other details may be found elsewhere (*44*).

2 wt% U-3F-C12(0.11) coatings were tested against aerosol challenges ($10^6$ CFU/mL) of Gram negative (*Pseudomonas aeruginosa, Escherichia coli*) *and* Gram positive (*Staphylococcus aureus*) bacteria. After 30 min residence, bacteria were stripped, serially diluted and plated for colony counts. 2 wt% U-3F-C12(0.11) coatings effected 100% kill, a 3.6-4.4 log reduction of Gram +/- bacteria. A zone of inhibition test showed no biocide release for SM modified compositions. This encouraging result was attributed to good block/soft block phase separation, a cation/co-repeat group ratio mimicking natural biocidal proteins (*67*), and a semifluorinated "chaperone" or low surface energy moiety that aids in alkylammonium surface-concentration.

Downloaded by VIRGINIA TECH on July 17, 2013 | http://pubs.acs.org
Publication Date (Web): July 8, 2013 | doi: 10.1021/bk-2013-1135.ch018

## *2. Generation 1 Not Stable!*

A denouement began with biocidal testing on the same coatings as a function of time to assess durability of contact kill. Figure 4 shows aerosol test results for 2 wt% U-3F-C12(0.11) coatings within a few days and after two weeks at ambient temperature. To our surprise, the modified coating had lost biocidal effectiveness. Several sets of tests showed that contact biocidal kill for 2 wt% PU-**8**-5100 ranged from 0-50%.

To gain insight into loss of contact biocidal effectiveness, TM-AFM imaging was performed as a function of time. Figure 5 shows the TM-AFM 3D height image for a 2 wt% U-3F-C12(0.11) coating after 2 d and 2 wk at ambient temperature. One to two days after the coating was generated, the image in Figure 5A was almost featureless, as reported earlier (*44*).

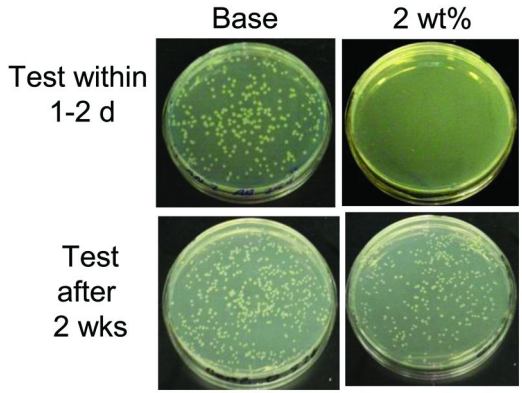


*Figure 4. Agar plates after a spray challenge of P. aeruginosa: Left, base polyurethane control; Right, 2 wt% U-3FC12(0.11).*

The 3D height image shown in Figure 5B shows a radical change after two weeks aging at ambient temperature. The vertical (z scale) is increased to 1000 nm compared to the image in Figure 5A to capture the formation of multiple features up to ~10 μm wide and 100 – 200 nm high. Longer aging in air results in further complexities that we assign to surface phase separation of the U-3F-C12(0.11) modifier.

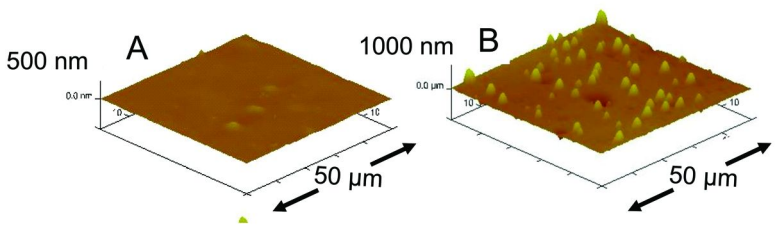


*Figure 5. TM-AFM 3D height image for a 2 wt% U-3F-C12(0.11) coating after 2 d (A) and 2 wk (B) at ambient temperature.*

Based on biotesting and AFM imaging, we now realize that the solution coating process results in a metastable state. Quaternary charge is accessible and contact antimicrobial effectiveness is high. With time, phase separation occurs, partly driven by the immiscibility of the 3F side chains. The phase separated domains must sequester quaternary charge leading to ineffective contact antimicrobial kill.


In Tailored Polymer Architectures for Pharmaceutical and Biomedical Applications; Scholz, C., et al.;
ACS Symposium Series; American Chemical Society: Washington, DC, 2013.

Downloaded by VIRGINIA TECH on July 17, 2013 | http://pubs.acs.org
Publication Date (Web): July 8, 2013 | doi: 10.1021/bk-2013-1135.ch018

Downloaded by VIRGINIA TECH on July 17, 2013 | http://pubs.acs.org
Publication Date (Web): July 8, 2013 | doi: 10.1021/bk-2013-1135.ch018

*3. Streaming Potential Measurements for Quantifying near Surface Quaternary Charge*

Solution test methods provide quantitative estimates of antimicrobial effectiveness including minimum inhibitory concentrations (MICs), minimum biocidal concentrations (MBCs) and kill kinetics (*68*). However, methods for estimating biocidal effectiveness for surface bound polycation coatings are widely varying and do not often permit unambiguous comparisons. Regardless of the procedure, testing coatings for antimicrobial effectiveness is tedious and carries an element of personal risk, as Gram negative (*Pseudomonas aeruginosa, Escherichia coli*) and Gram positive (*Staphylococcus aureus*) are opportunistic pathogenic bacteria. A rapid, quantitative measurement of surface accessible quaternary ammonium charge was therefore sought. Measurement of quaternary charge density has often employed fluorescein dye binding and release of bound dye by an ion exchange surfactant such as dodecyl trimethyl ammonium chloride (*34*, *69*–*72*). This method failed for polyurethanes modified with quaternary SMs because of nonspecific dye adsorption and slow desorption (*73*).

Streaming potential measurements have long been known for quantifying surface charge, particularly on colloidal particles (*74*). Assessing surface accessible charge for thin films formed by alternating polyelectrolyte deposition was elegantly demonstrated by Adamczyk (*75*). Alternating positive and negative potentials attested to the charge of the last polyelectrolyte deposited. Streaming potentials have also been employed for studying antimicrobial function of polyelectrolyte multilayers comprising poly(allyl amine) hydrochloride and poly(sodium 4-styrene sulfonate (*76*).

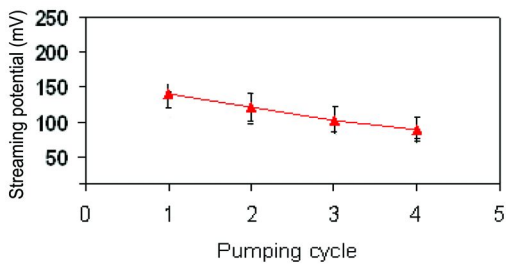


*Figure 6. Streaming potentials for a 2 wt% U-3F-C12(0.11) coating as a function of capillary pumping cycle (~20 s per cycle).*

In an initial examination of streaming potential measurements on modified polyurethanes the microfluidic method developed by Alvarez (*77*) was adapted (*73*). The inside of a 100 μm capillary was coated with the desired polyurethane and streaming potentials were obtained using a 1 mM KBr solution (Figure 6) (*73*). The good news was an initial streaming potential above 100 mV for a 2 wt% U-3F-C12(0.11) coating. The high near surface accessible charge agrees with excellent


In Tailored Polymer Architectures for Pharmaceutical and Biomedical Applications; Scholz, C., et al.;
ACS Symposium Series; American Chemical Society: Washington, DC, 2013.

near term contact antimicrobial effectiveness (Figure 4, 1-2 d). The bad news was a rapid decrease in streaming potentials over the course of only four pumping cycles (*73*). Streaming potentials scale to charge density so that the results for the 2 wt% U-3F-C12(0.11) coating indicate a precipitous decrease (~50%) in accessible near surface quaternary charge in < 2 min.

Compared to the relatively slow (2 wk) deactivation of quaternary charge density in air (biotesting, AFM), streaming potential measurements show loss of surface accessible positive charge for 2 wt% U-3F-C12(0.11) takes only a few minutes. Apparently, water plasticization of the near surface SM domain results in an acceleration of phase separation that sequesters quat function.

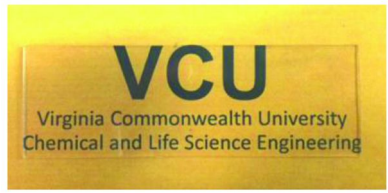


*Figure 7. Image of a 2 wt% U-4F-C12(0.34) coated glass slide.*

Downloaded by VIRGINIA TECH on July 17, 2013 | http://pubs.acs.org
Publication Date (Web): July 8, 2013 | doi: 10.1021/bk-2013-1135.ch018

## *4. Generation 2 Modifier*

The unexpected temporal instability of 2 wt% U-3F-C12(0.11) has led to the development of alternative SMs that will achieve long term contact antimicrobial effectiveness. One of these is based on the replacement of $–CF_3$ by $–CF_2CF_2H$ (Figure 3). H-bonding was proposed by Ellison to explain decreased surface tension upon replacement of terminal $-CF_3$ by $–CF_2H$ (*78*). Thus replacement of 3F with amphiphilic 4F seemed attractive based on the notion that $CF_2$**H** hydrogen bonding would provide an enthalpic contribution enhancing the free energy of mixing.

The polyurethane modifier U-4F-C12(0.34) was prepared by a method paralleling that described previously for the 3F analog (Figure 3, $R_f = -CF_2CF_2H$, q = 0.34) (*44*). The weight fraction of C12 was increased to 0.34 compared to 0.11 for generation 1 modifier based on preliminary experiments that showed enhanced modified surface stability. By $^1$H-NMR end group analysis, $M_n$ for 4F-C12(0.34) diol was 6.0 kDa. Copolyoxetane diol and polyurethane solution characterization ($^1$H-NMR, GPC) will be provided in a separate publication.

Unlike the 3F polyurethane SM, U-4F-C12(0.34) was insoluble in THF. DMAC (dimethyl acetamide) was used as an alternative solvent for deposition of 2 wt% U-4F-C12(0.34). An overnight thermal treatment in vacuum (120 °C) removed solvent. Optically transparent coatings resulted (Figure 7); coating thickness was typically 160 μm.


In Tailored Polymer Architectures for Pharmaceutical and Biomedical Applications; Scholz, C., et al.;
ACS Symposium Series; American Chemical Society: Washington, DC, 2013.

Based on the hypothesis that stable, accessible near surface charge would be a predictor of long term antimicrobial effectiveness, zeta potential measurements were a priority. As noted above, we developed a capillary method for this purpose (*73*). However, coating the inside of a 100 μm capillary is tedious and subsequent characterization of the coating surface problematical.

In a new approach, zeta potential measurements were carried out on drip coated microscope slides using a SurPASS electrokinetic analyzer and clamping cell (Anton PAAR). For these initial measurements, pH was constant at ~7. For the SurPASS, each run consists of a forward and backward pumping cycle taking ~15 min. Three runs (~ 45 min) provided a more demanding test of stability in dilute polyelectrolyte ($10^{-3}$ M KBr) compared to the capillary method (~ 2 min) used previously (*73*).

Downloaded by VIRGINIA TECH on July 17, 2013 | http://pubs.acs.org
Publication Date (Web): July 8, 2013 | doi: 10.1021/bk-2013-1135.ch018

**Table 1. Zeta potentials for 2 wt% U-4F-C12(0.34) relative to base polyurethane**

| | *Zeta potential (mV)* | |
|---|---|---|
| *Run* | *1 wk* | *4 wks* |
| 1 | 42.1 | 39.8 |
| 2 | 41.0 | 37.6 |
| 3 | 38.8 | 35.8 |

Reported here are initial zeta potential measurements for 2 wt% U-4F-C12(0.34) relative to base polyurethane HMDI-BD(50)-PTMO(1000). Zeta potentials for polymer coatings are known to be affected by pH (*79*). Initial measurements reported here were carried out at pH 7.

Compared to base polyurethane (-37± 4 mV), zeta potentials for 2 wt% U-4F-C12(0.34) were positive. Table 1 lists zeta potentials relative to base polyurethane at < 1 wk and > 4 wk. Zeta potentials for 2 wt% U-4F-C12(0.34) were diminished 5-10% after one month storage in air at ambient temperature. Each set of zeta potential tests amounted to ~2 h immersion in 1 mM NaBr. Interestingly, the diminution observed over the course of the three runs for the first test at < 1 wk (42.1 → 38.8 mV) was restored to some degree for the first run after 4 wk in air (39.8 mV). However, the final value after four weeks "aging" in air (35.8 mV). was10% less than the corresponding value after 1 wk.

The stability of zeta potentials for 2 wt% U-4F-C12(0.34) supports the hypothesis that -$CF_2$**H** hydrogen bonding provides enthalpic stabilization of the modified surface. However, a detailed study is warranted to confirm these initial results.

Spray challenges of *Pseudomonas aeruginosa*, *Escherichia coli*, and *Staphylococcus aureus* were carried out as described previously (*44*). The residence time for each bacterial challenge ($10^6$ cfu/ml) was 1 h. Table 2 shows


In Tailored Polymer Architectures for Pharmaceutical and Biomedical Applications; Scholz, C., et al.;
ACS Symposium Series; American Chemical Society: Washington, DC, 2013.

percent kill for the pathogen challenges after one hour residence time. Within experimental error, complete kill was observed within 1 wk and after 4 wks at ambient temperature. These results are important in validating the model shown in Figure 3 for surface concentration of the U-4F-C12(0.34) modifier. Importantly, the biocidal effectiveness after storage of at least a month under ambient conditions of temperature and humidity also provide support for the use of zeta potentials as a predictor for polycation contact kill.

**Table 2. Percent kill of spray challenges for U-4F-C12-34. Residence time for each challenge ($10^6$ cfu/ml) was 1 h**

| *Challenge* | *< 1 wk* | *> 4 wk* |
|---|---|---|
| *Pseudomonas aeruginosa* | 100 | 95 |
| *Escherichia coli* | 100 | 100 |
| *Staphylococcus aureus* | 99 | 90 |

Downloaded by VIRGINIA TECH on July 17, 2013 | http://pubs.acs.org
Publication Date (Web): July 8, 2013 | doi: 10.1021/bk-2013-1135.ch018

## 3. Conclusion

Fluorous side chain A in polyurethanes with P[AB] copolyoxetane soft blocks act as chaperones for surface concentration of functional side chain B. However, unanticipated new surface morphologies and new surface phenomena can arise from A-side chain / B-side chain interactions invalidating the simple model shown in Figure 3. In the present work, the temporal instability of the U-3F-C12(0.11) modifier was avoided by utilizing a $–CF_2CF_2H$ (4F) fluorous side chain and increasing the C12 mole fraction. The results for U-4F-C12(0.34) are important in validating the model shown in Figure 3. Biocidal effectiveness was demonstrated after storage for at least a month under ambient conditions of temperature and humidity. This stability was correlated with zeta potential measurements of accessible near surface charge. These results suggest zeta potential measurements hold promise as a physical method for assessing effectiveness of polycation contact kill and polycation stability in contact with aqueous systems.

In summary, polyurethanes with P[AB] copolyoxetane soft blocks are effective and potentially processing-compatible surface modifiers for conventional polyurethanes. This surface modification approach is “green” in the sense that only a minimal amount of surface modifier (2 wt% or less) is leveraged so as to effect a radical change in surface function. In addition, the 4F chaperone is “green” in avoiding the use of perfluorinated eight carbon moieties that are likely PFOA precursors.


In Tailored Polymer Architectures for Pharmaceutical and Biomedical Applications; Scholz, C., et al.;
ACS Symposium Series; American Chemical Society: Washington, DC, 2013.

Downloaded by VIRGINIA TECH on July 17, 2013 | http://pubs.acs.org
Publication Date (Web): July 8, 2013 | doi: 10.1021/bk-2013-1135.ch018

## Acknowledgments

K.J.W. thanks the National Science Foundation (DMR- grants DMR-0207560, DMR-0802452, and DMR-1206259) and the VCU School of Engineering Foundation for support of this research. This work was also supported by Public Health Service Grant AI-19146 from the National Institute of Allergy and Infectious Disease (D.E.O.), and in part by Veterans Administration Medical Research Grant I01BX000477 (D.E.O.). K.J.W. also thanks Ray Ottenbrite for being a great colleague and friend for over 30 years.

## References

1. Friedman, N. D.; Korman, T. M.; Fairley, C. K.; Franklin, J. C.; Spelman, D. W. *J. Infect.* **2002**, *45*, 47.
2. Hacek, D. M.; Suriano, T.; Noskin, G. A.; Krusynski, J.; Reisberg, B.; Peterson, L. R. *Am. J. Clin. Pathol.* **1999**, *111*, 647.
3. Borer, A.; Gilad, J.; Smolyakov, R.; Eskira, S.; Peled, N.; Porat, N.; Hyam, E.; Trefler, R.; Riesenberg, K.; Schlaeffer, F. *Emerging Infect. Dis.* **2005**, *11*, 1160.
4. Maki, D. G.; Tambyah, P. A. *Emerging Infect. Dis.* **2001**, *7*, 342.
5. Nicolle, L. E. *Women's Health* **2005**, *1*, 39.
6. Shigemura, K.; Tanaka, K.; Adachi, M.; Yamashita, M.; Arakawa, S.; Fujisawa, M. *J. Infect. Chemother.* **2011**, *17*, 646.
7. Shigemura, K.; Arakawa, S.; Tanaka, K.; Fujisawa, M. *J. Infect. Chemother.* **2009**, *15*, 18.
8. Bieser, A. M.; Tiller, J. C. *Macromol. Biosci.* **2011**, *11*, 526.
9. Medlin, J. *Environ. Health Perspect.* **1997**, *105*, 290.
10. Hazzizalaskar, J.; Helary, G.; Sauvet, G. *J. Appl. Polym. Sci.* **1995**, *58*, 77.
11. Nurdin, N.; Helary, G.; Sauvet, G. *J. Appl. Polym. Sci.* **1993**, *50*, 663.
12. Muller, G.; Winkler, Y.; Kramer, A. *J. Hosp. Infect.* **2003**, *53*, 211.
13. Holder, I. A.; Durkee, P.; Supp, A. P.; Boyce, S. T. *Burns* **2003**, *29*, 445.
14. Johnson, J. R.; Delavari, P.; Azar, M. *Antimicrob. Agents Chemother.* **1999**, *43*, 2990.
15. Silver, S. *FEMS Microbiol. Rev.* **2003**, *27*, 341.
16. Silver, S.; Phung, L. T.; Silver, G. *J. Ind. Microbiol. Biotechnol.* **2006**, *33*, 627.
17. Marambio-Jones, C.; Hoek, E. M. V. *J. Nanopart. Res.* **2010**, *12*, 1531.
18. Diekema, D. J.; Pfaller, M. A.; Schmitz, F. J.; Smayevsky, J.; Bell, J.; Jones, R. N.; Beach, M. *Clin. Infect. Dis.* **2001**, *32*, S114.
19. Borer, A.; Gilad, J.; Yagupsky, P.; Peled, N.; Porat, N.; Trefler, R.; Shprecher-Levy, H.; Riesenberg, K.; Shipman, M.; Schlaeffer, F. *Emerging Infect. Dis.* **2002**, *8*, 966.
20. Worley, S. D.; Sun, G. *Trends Polym. Sci.* **1996**, *4*, 364.
21. Eknoian, M. W.; Worley, S. D. *J. Bioact. Compat. Polym.* **1998**, *13*, 303.
22. Eknoian, M. W.; Worley, S. D.; Bickert, J.; Williams, J. F. *Polymer* **1999**, *40*, 1367.

23. Sun, G.; Worley, S. D. In *Modified Fibers with Medical and Specialty Applications*; Edwards, J. V., Buschle-Diller, G., Eds.; Springer: Dordrecht, The Netherlands, 2006; p 81.
24. Kenawy, E. R.; Worley, S. D.; Broughton, R. *Biomacromolecules* **2007**, *8*, 1359.
25. Sun, G.; Worley, S. D. *J. Chem. Educ.* **2005**, *82*, 60.
26. Sun, G.; Allen, L. C.; Luckie, E. P.; Wheatley, W. B.; Worley, S. D. *Ind. Eng. Chem. Res.* **1995**, *34*, 4106.
27. Kocer, H. B.; Worley, S. D.; Broughton, R. M.; Huang, T. S. *React. Funct. Polym.* **2011**, *71*, 561.
28. Cerkez, I.; Kocer, H. B.; Worley, S. D.; Broughton, R. M.; Huang, T. S. *React. Funct. Polym.*, *72*, 673.
29. Cerkez, I.; Kocer, H. B.; Worley, S. D.; Broughton, R. M.; Huang, T. S. *J. Appl. Polym. Sci.*, *124*, 4230.
30. Cerkez, I.; Kocer, H. B.; Worley, S. D.; Broughton, R. M.; Huang, T. S. *Cellulose*, *19*, 959.
31. Makal, U.; Wood, L.; Ohman, D. E.; Wynne, K. J. *Biomaterials* **2006**, *27*, 1316.
32. Lee, S. B.; Koepsel, R. R.; Morley, S. W.; Matyjaszewski, K.; Sun, Y. J.; Russell, A. J. *Biomacromolecules* **2004**, *5*, 877.
33. Grapski, J. A.; Cooper, S. L. *Biomaterials* **2001**, *22*, 2239.
34. Tiller, J. C.; Liao, C. J.; Lewis, K.; Klibanov, A. M. *Proc. Natl. Acad. Sci. U.S.A.* **2001**, *98*, 5981.
35. Lin, J.; Qiu, S. Y.; Lewis, K.; Klibanov, A. M. *Biotechnol. Prog.* **2002**, *18*, 1082.
36. Tew, G. N.; Scott, R. W.; Klein, M. L.; De Grado, W. F. *Acc. Chem. Res.* **2009**, *43*, 30.
37. Som, A.; Navasa, N.; Percher, A.; Scott, R. W.; Tew, G. N.; Anguita, J. *Clin. Vaccine Immunol.* **2012**, *19*, 1784.
38. Tew, G. N.; Scott, R. W.; Klein, M. L.; Degrado, W. F. *Acc. Chem. Res.* **2010**, *43*, 30.
39. Sovadinova, I.; Palermo, E. F.; Urban, M.; Mpiga, P.; Caputo, G. A.; Kuroda, K. *Polymers* **2011**, *3*, 1512.
40. Waschinski, C. J.; Barnert, S.; Theobald, A.; Schubert, R.; Kleinschmidt, F.; Hoffmann, A.; Saalwachter, K.; Tiller, J. C. *Biomacromolecules* **2008**, *9*, 1764.
41. Ikeda, T.; Hirayama, H.; Yamaguchi, H.; Tazuke, S.; Watanabe, M. *Antimicrob. Agents Chemother.* **1986**, *30*, 132.
42. Kashket, E. R. *Annu. Rev. Microbiol.* **1985**, *39*, 219.
43. Kakinuma, Y. *Microbiol. Mol. Biol. Rev.* **1998**, *62*, 1021.
44. Kurt, P.; Wood, L.; Ohman, D. E.; Wynne, K. J. *Langmuir* **2007**, *23*, 4719.
45. Gon, S.; Kumar, K. N.; Nusslein, K.; Santore, M. M. *Macromolecules* **2012**, *45*, 8373.
46. Majumdar, P.; Lee, E.; Patel, N.; Ward, K.; Stafslien, S. J.; Daniels, J.; Chisholm, B. J.; Boudjouk, P.; Callow, M. E.; Callow, J. A.; Thompson, S. E. M. *Biofouling* **2008**, *24*, 185.

Downloaded by VIRGINIA TECH on July 17, 2013 | http://pubs.acs.org
Publication Date (Web): July 8, 2013 | doi: 10.1021/bk-2013-1135.ch018

47. Pant, R. R.; Buckley, J. L.; Fulmer, P. A.; Wynne, J. H.; McCluskey, D. M.; Phillips, J. P. *J. Appl. Polym. Sci.* **2008**, *110*, 3080.
48. Majumdar, P.; He, J.; Lee, E.; Kallam, A.; Gubbins, N.; Stafslien, S. J.; Daniels, J.; Chisholm, B. J. *J. Coat. Technol. Res.* **2010**, *7*, 455.
49. Ye, S. J.; Majumdar, P.; Chisholm, B.; Stafslien, S.; Chen, Z. *Langmuir* **2010**, *26*, 16455.
50. Milovic, N. M.; Wang, J.; Lewis, K.; Klibanov, A. M. *Biotechnol. Bioeng.* **2005**, *90*, 715.
51. Huang, J. Y.; Koepsel, R. R.; Murata, H.; Wu, W.; Lee, S. B.; Kowalewski, T.; Russell, A. J.; Matyjaszewski, K. *Langmuir* **2008**, *24*, 6785.
52. Krishnan, S.; Ward, R. J.; Hexemer, A.; Sohn, K. E.; Lee, K. L.; Angert, E. R.; Fischer, D. A.; Kramer, E. J.; Ober, C. K. *Langmuir* **2006**, *22*, 11255.
53. Schaer, T. P.; Stewart, S.; Hsu, B. B.; Klibanov, A. M. *Biomaterials* **2012**, *33*, 1245.
54. Park, D.; Wang, J.; Klibanov, A. M. *Biotechnol. Prog.* **2006**, *22*, 584.
55. Gottenbos, B.; van der Mei, H. C.; Klatter, F.; Nieuwenhuis, P.; Busscher, H. J. *Biomaterials* **2002**, *23*, 1417.
56. Vasilev, K.; Griesser, S. S.; Griesser, H. J. *Plasma Processes Polym.* **2011**, *8*, 1010.
57. Huang, J.; Murata, H.; Koepsel, R. R.; Russell, A. J.; Matyjaszewski, K. *Biomacromolecules* **2007**, *8*, 1396.
58. Jalbert, C.; Koberstein, J. T.; Hariharan, A.; Kumar, S. K. *Macromolecules* **1997**, *30*, 4481.
59. Waschinski, C. J.; Tiller, J. C. *Biomacromolecules* **2005**, *6*, 235.
60. Makal, U.; Wynne, K. J. *Langmuir* **2005**, *21*, 3742.
61. Wynne, K. J.; Makal, U.; Kurt, P.; Gamble, L. *Langmuir* **2007**, *23*, 10573.
62. Andrade, J. D.; Tingey, K. G. *Langmuir* **1991**, *7*, 2471.
63. Garrett, J. T.; Lin, J. S.; Runt, J. *Macromolecules* **2002**, *35*, 161.
64. Ratner, B. D.; Yoon, S. C.; Kaul, A.; Rahman, R. In *Polyurethanes in biomedical engineering II*; Planck, H., Syre, I., Dauner, M., Egbers, G., Eds.; Elsevier: New York, 1986; Vol. 3, p 213.
65. Kurt, P.; Gamble, L. J.; Wynne, K. J. *Langmuir* **2008**, *24*, 5816.
66. Uilk, J. M.; Mera, A. E.; Fox, R. B.; Wynne, K. J. *Macromolecules* **2003**, *36*, 3689.
67. Tew, G. N.; Liu, D. H.; Chen, B.; Doerksen, R. J.; Kaplan, J.; Carroll, P. J.; Klein, M. L.; DeGrado, W. F. *Proc. Natl. Acad. Sci. U.S.A.* **2002**, *99*, 5110.
68. Chakrabarty, S.; King, A.; Kurt, P.; Zhang, W.; Ohman, D. E.; Wood, L. F.; Lovelace, C.; Rao, R.; Wynne, K. J. *Biomacromolecules* **2011**, *12*, 757.
69. Goddard, J. M.; Hotchkiss, J. H. *Prog. Polym. Sci.* **2007**, *32*, 698.
70. Kugler, R.; Bouloussa, O.; Rondelez, F. *Microbiology* **2005**, *151*, 1341.
71. Ledbetter, J. W., Jr.; Bowen, J. R. *Anal. Chem.* **1969**, *41*, 1345.
72. Murata, H.; Koepsel, R. R.; Matyjaszewski, K.; Russell, A. J. *Biomaterials* **2007**, *28*, 4870.
73. Gupta, M. L.; Brunson, K.; Chakravorty, A.; Kurt, P.; Alvarez, J. C.; Luna-Vera, F.; Wynne, K. J. *Langmuir* **2010**, *26*, 9032.
74. Stanley, J. S. *J. Phys. Chem.* **1954**, *58*, 533.

Downloaded by VIRGINIA TECH on July 17, 2013 | http://pubs.acs.org
Publication Date (Web): July 8, 2013 | doi: 10.1021/bk-2013-1135.ch018


In Tailored Polymer Architectures for Pharmaceutical and Biomedical Applications; Scholz, C., et al.;
ACS Symposium Series; American Chemical Society: Washington, DC, 2013.

75. Adamczyk, Z.; Zembala, M.; Warszynski, P.; Jachimska, B. *Langmuir* **2004**, *20*, 10517.
76. Lichter, J. A.; Rubner, M. F. *Langmuir* **2009**, *25*, 7686.
77. Pu, Q. S.; Elazazy, M. S.; Alvarez, J. C. *Anal. Chem.* **2008**, *80*, 6532.
78. Ellison, A. H.; Fox, H. W.; Zisman, W. A. *J. Phys. Chem.* **1953**, *57*, 622.
79. Kirby, B. J.; Ernest, F.; Hasselbrink, J. *Electrophoresis* **2004**, *25*, 203.

Downloaded by VIRGINIA TECH on July 17, 2013 | http://pubs.acs.org
Publication Date (Web): July 8, 2013 | doi: 10.1021/bk-2013-1135.ch018

Downloaded by PURDUE UNIVERSITY on July 20, 2013 | http://pubs.acs.org
Publication Date (Web): July 8, 2013 | doi: 10.1021/bk-2013-1135.ch019

## Chapter 19

# Antimicrobial Polymers: Molecular Design as Synthetic Mimics of Host-Defense Peptides

**Edmund F. Palermo,[1] Satyavani Vemparala,[2] and Kenichi Kuroda*[,1,3]**

**[1]Macromolecular Science and Engineering Center, University of Michigan, Ann Arbor, Michigan 48109, United States**
**[2]The Institute of Mathematical Sciences, CIT Campus, Taramani, Chennai 600113, India**
**[3]Department of Biologic and Materials Sciences, School of Dentistry, University of Michigan, Ann Arbor, Michigan 48109, United States**
***E-mail: kkuroda@umich.edu.**

The development of new antimicrobials effective against drug-resistant bacterial infections is a significant scientific challenge, requiring new molecular targets and antimicrobial strategies. Amphiphilic synthetic polymers have been utilized as a new molecular platform to mimic the structural features and antimicrobial functions of naturally occurring host-defense antimicrobial peptides. We have developed cationic amphiphilic random methacrylate copolymers which displayed a broad spectrum of inhibitory activity while maintaining low toxicity and low susceptibility to resistance in bacteria. The polymer-based antimicrobial design will provide a new versatile strategy for creation of a diversity of antimicrobial agents to fight against resistant bacteria.

## Introduction

### Emerging Issue of Antibiotic Resistance

The emergence of drug-resistance in pathogenic bacteria is significant threat to public health (*1*–*6*). These resistances can arise from antibiotic misuse, giving pressure for selection of resistant subpopulation in bacteria. These resistant strains spread to communities and public places including schools, causing invasive infections. In recent years, the number of new antibiotics in

© 2013 American Chemical Society
In Tailored Polymer Architectures for Pharmaceutical and Biomedical Applications; Scholz, C., et al.; ACS Symposium Series; American Chemical Society: Washington, DC, 2013.

the development pipeline dramatically declined, reducing available treatment options (*7*). Therefore, there is an urgent need to create new antibiotics which can overcome the existing resistance mechanisms of bacteria without contributing to the development of multi-drug resistance. However, the development of new antimicrobials effective against drug-resistant bacteria is a scientific challenge because the new antibiotic design requires new molecular targets and antimicrobial strategies rather than modifying existing drugs or their formulations.

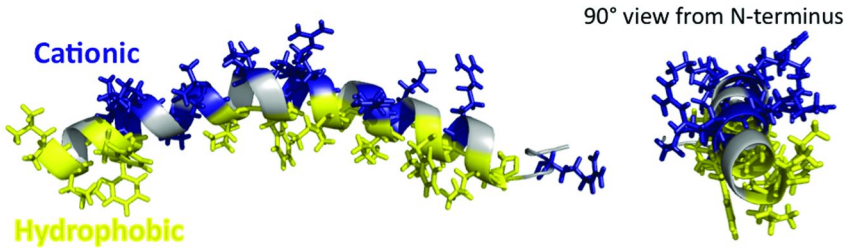


*Figure 1. α-helical cationic antimicrobial peptide LL-37. Cationic residues (blue) and hydrophobic reduces (yellow) are segregated into the opposite sides of helix. The backbone structure was colored gray. These images were created using the structure of human LL-37 from coordinates in PDB ID 2K6O (Wang, G. Structures of human host defense cathelicidin LL-37 and its smallest antimicrobial peptide KR-12 in lipid micelles, J. Biol. Chem.* ***2008****, 283, 32637−32643) with Pymol Open-Source 0.99rc6.*

Downloaded by PURDUE UNIVERSITY on July 20, 2013 | http://pubs.acs.org
Publication Date (Web): July 8, 2013 | doi: 10.1021/bk-2013-1135.ch019

**Antimicrobial Peptides as New Antibiotics**

One approach has been centered in implementation of host-defense antimicrobial peptides, which are components of the innate immune system. Host-defense antimicrobial peptides act as "Nature's antibiotics" which protect the host from bacterial infections by controlling growth of bacteria or killing them without harming the host (mammalian) cells (*8–14*). These peptides target bacterial cell membranes and disrupt membrane structures, causing leakage of cellular components, breakdown of membrane potential, and cell death. These peptides are relatively small (20-50 amino acids) and have generally cationic and hydrophobic residues, which provide cationic, amphiphilic properties. One of the classes is α -helical peptides including magainins and cathelicidin LL-37 (Figure 1). These peptides are in the form of random coil in solution, but they adopt helical conformation when bound to bacterial cell membranes. The unique feature of these peptides is the amphiphilic structure of helix, in which cationic and hydrophobic residues are segregated into the different sides of helix. The peptides selectively attack bacteria over human cells because of preferential electrostatic binding of cationic peptides to bacterial cell surfaces with high net negative charges as compared to human cells. The amphiphilic helical peptides accumulate on bacterial membrane surfaces and insert into the membrane, resulting in disintegration of membrane structures or formation of

membrane pores. Several molecular mechanisms have been proposed to describe the membrane disruption (Figure 2). These modes of actions contrast to those of traditional antibiotics such as penicillin, which are generally enzyme inhibitors or DNA replication inhibitors with specific molecular targets.

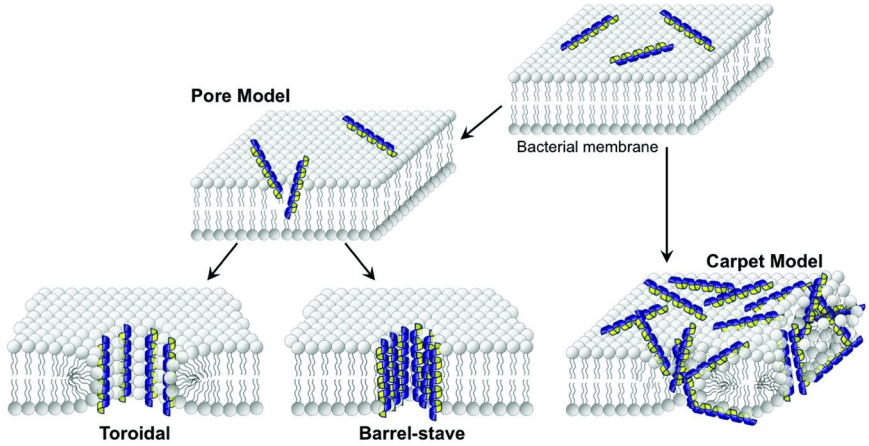


*Figure 2. Proposed models for membrane disruption by α-helical antimicrobial peptides. Cationic residues of peptides are colored blue while hydrophobic residues are yellow.*

Downloaded by PURDUE UNIVERSITY on July 20, 2013 | http://pubs.acs.org
Publication Date (Web): July 8, 2013 | doi: 10.1021/bk-2013-1135.ch019

## Synthetic Mimics of Antimicrobial Peptides

Since the discovery of host-defense peptides, many efforts have been made to develop natural antimicrobial peptides as new antibiotic drugs because of their reduced susceptibility to bacterial resistance. However, implementation of antimicrobial peptides and derivatives meets significant obstacles associated with poor pharmacokinetics *in vivo*, low stability due to susceptibility to proteolysis, and high manufacturing cost, preventing large-scale production (*15*). One approach to address these issues is to create synthetic mimics of antimicrobial peptides. The unique feature of antimicrobial peptides is that the molecular mechanism of antimicrobial action does not rely on the specific interactions with receptors or enzymes in bacteria. This was initially evidenced by the fact that D-enantiomer magainin showed the same level of activity compared to natural magainin (*16*). On the other hand, a class of antimicrobial peptides has cationic and hydrophobic side chains in common and adopt secondary conformations such as helix upon binding to lipid membranes, displaying segregated amphiphilic structures (Figure 1). It is, however, interesting that no common consensus sequences have been found yet (*10*). These findings suggest that the amphiphilic conformations with segregated cationic and hydrophobic residues, rather than the exact amino acid sequences or chemical structures, are likely key determinants for the antimicrobial activity. This inspired researchers to create synthetic molecules which can display segregated amphiphilic structures based on synthetic backbones


In Tailored Polymer Architectures for Pharmaceutical and Biomedical Applications; Scholz, C., et al.;
ACS Symposium Series; American Chemical Society: Washington, DC, 2013.

as new antimicrobial agents. The examples include antimicrobial β-peptides (*17*) and peptoids, which can adopt helical conformations with segregated amphiphilic structures (Figure 3) (*18*, *19*). In general, these peptidomimetics are resistant to proteolysis and expected to have prolonged lifetime and activity in physiological conditions. This design principle was also applied to arylamide derivatives (Figure 3) (*20–22*). Although these arylamides are not designed to form helical structures, the rigid backbone presents the segregated amphiphilic conformation. These studies suggest that the amphiphilic structures are key determinants for antimicrobial activity, not requiring natural peptide sequences and backbones.

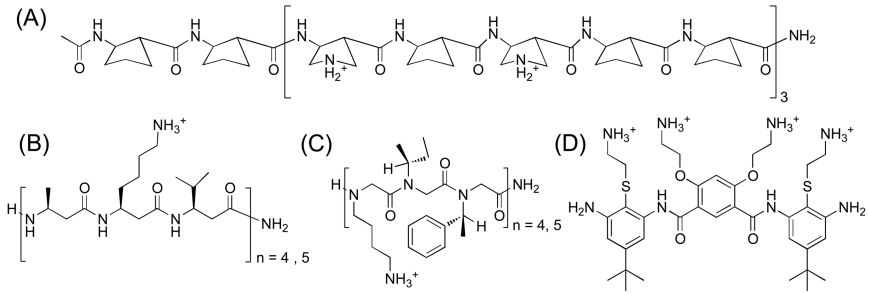


*Figure 3. Synthetic mimics of antimicrobial peptides. (A) β-peptide β-17 (23), (B) β-peptide (24), (C) peptoid (19), and (D) arylamide (20).*

Downloaded by PURDUE UNIVERSITY on July 20, 2013 | http://pubs.acs.org
Publication Date (Web): July 8, 2013 | doi: 10.1021/bk-2013-1135.ch019

**Antimicrobial Polymers**

Although these approaches using peptide-like oligomers showed promising results, it has been of great interest to utilize molecular frameworks which can facilitate the development and use of antimicrobials for potential applications. To that end, the molecular design was further extended to include synthetic polymer backbones such as polymethacrylate (Figure 4) (*25–30*). These polymers are designed to have low molecular weights (MWs) (a few kDa) and primary ammonium and hydrophobic groups in side chains to mimic antimicrobial peptides. This contrasts to traditional antimicrobial or disinfecting polycations with quaternary ammonium groups modified with hydrophobic moieties such as long alkyls and relatively high MWs (*30–32*). The antimicrobial peptide-mimetic polymers showed potent activity against a panel of bacteria and minimal hemolytic activity against human erythrocytes. These polymers are not designed to form defined secondary conformations such as the α-helix, and the polymer conformation is rather random coils. The polymers have also random sequences of cationic and hydrophobic groups along the polymer backbone as well as distribution in the molecular size. Despite these heterogeneities in terms of conformation and chemical structures, these polymers are potent antimicrobial, suggesting that random amphiphilic structures can also mimic the antimicrobial activity of natural peptides.

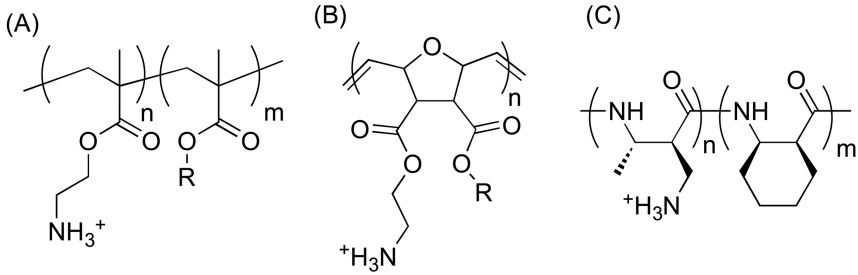


*Figure 4. Examples of antimicrobial polymers based antimicrobial peptide-mimetic design: (A) polymethacrylate (33), (B) polynorbornene (34), and (C) nylon (35, 36).*

Downloaded by PURDUE UNIVERSITY on July 20, 2013 | http://pubs.acs.org
Publication Date (Web): July 8, 2013 | doi: 10.1021/bk-2013-1135.ch019

### Amphiphilic Random Copolymers with Antimicrobial Activity

Our research has focused on evaluating the potential for amphiphilic polymers to serve as antimicrobial agents (*26*, *28*). We sought to develop a rational design of synthetic polymers based on a methacrylate platform. Previously, we demonstrated that the methacrylate random copolymers displayed antimicrobial activity against a broad spectrum of bacteria including methicillin-resistant *Staphylococcus aureus* (MRSA) without adverse toxicity to human cells (*37*, *38*). Bacteria cultured with the copolymers did not develop resistance after 21 passages while the inhibitory concentration of conventional antibiotics increased up to 500 times (*37*). The broad spectrum of inhibitory activity while maintaining low toxicity and low susceptibility to resistance in bacteria are the hallmarks of naturally occurring host defense peptides (*8*, *10*, *14*).

## Results and Discussion

### Snorkeling Effect

Our previous research indicated that the primary ammonium groups of antimicrobial methacrylate copolymers bind effectively to lipids because of their complexation with phosphate lipid headgroups (*39*). In addition, sum frequency generation (SFG) vibrational spectra of polymers in a lipid bilayer showed that the hydrophobic groups of polymers are oriented parallel to the surface normal of lipid bilayer, suggesting that the hydrophobic groups of polymers are inserted into the hydrophobic core of lipid bilayers (*40*). Accordingly, we hypothesized that the amphiphilic structure of random copolymers ought to be capable of a "snorkeling effect" exerted by elongated spacer arms in the cationic side chains. In transmembrane helical peptides, the snorkel effect refers to stabilization of transmembrane conformation of peptides upon elongation of the cationic linker groups, which reach to the lipid water interface while the hydrophobic peptide is located in the hydrophobic membrane core (*41*, *42*). As an analogy to this concept, we supposed that elongating the cationic side chain spacer groups of copolymers

might enhance insertion of the polymer backbone into the hydrophobic membrane core, facilitating membrane disruption ultimately. To test this hypothesis, we synthesized a library of cationic, amphiphilic copolymers with different length of cationic spacer groups (Figure 5) (*38*).

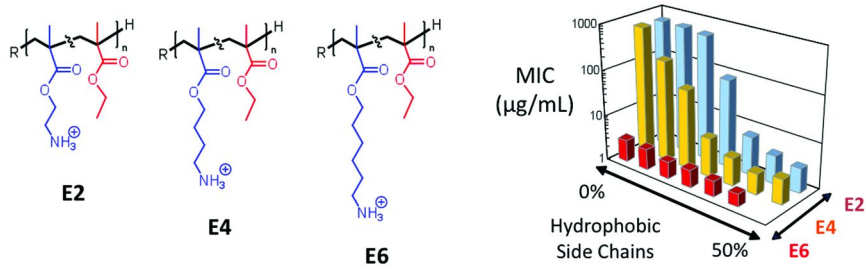


*Figure 5. Tuning antimicrobial activity of amphiphilic methacrylate copolymers by snorkeling effect. (A) Chemical structures of polymers with different lengths of cationic spacer arms. The copolymers have ethyl groups as hydrophobic side chains (0 to 50 mole %). (B) Minimum inhibitory concentration (MIC) of polymers for E. coli. Data are from Ref. (38).*

For each spacer group (E2: ethylene, E4: butylene, E6: hexylene), we first prepared a series of copolymers with varying percentages of ethyl side chains as hydrophobic co-monomer ethyl methacrylate (EMA) to examine the snorkeling effect on their antimicrobial activity (*38*). The elongated spacer groups endowed the copolymers with much more potent inhibitory ability against *Escherichia coli* and *S. aureus*. The copolymers with ethylene spacers (E2 polymers) and butylene (E4 polymers) showed potent antimicrobial activity against *E. coli* (MIC < 20 μg/mL) when the percentage of ethyl methacrylate (EMA) comonomer is grater than 45 mol. % or 30 mol.% respectively. On the other hand, the copolymers with hexylene spacer groups (E6 polymers) exhibited high antimicrobial activity (MIC ~ 10 μg/mL) even with 0% EMA, and the activity is not sensitive to the EMA contents. In addition to the antimicrobial activity, we also evaluated the lytic activity of polymers to human red blood cells (hemolysis). In general, the hemolytic activity was increased as the spacer length was increased. The E6 polymers were highly hemolytic with HC50 (polymer concentration for 50% hemolysis) ~ 3 μg/mL. Among the polymer series in this study, the E4 copolymers showed the highest selectivity index ($HC_{50}$/MIC) which implies that the butylene spacer groups are the most effective against bacteria without causing harm to human cells.

## Computational Modeling

Inspired by the antimicrobial activity controlled by the new designed based on the cationic spacer groups, we further examined the details of membrane binding of polymers via molecular dynamic simulations (*38*).


In Tailored Polymer Architectures for Pharmaceutical and Biomedical Applications; Scholz, C., et al.;
ACS Symposium Series; American Chemical Society: Washington, DC, 2013.

Downloaded by PURDUE UNIVERSITY on July 20, 2013 | http://pubs.acs.org
Publication Date (Web): July 8, 2013 | doi: 10.1021/bk-2013-1135.ch019

For this study, we used a pre-equilibrated bilayer patch of zwitterionic POPE (1-palmitoyl-2-oleoyl phosphatidylethanolamine) and anionic POPG (1-palmitoyl-2-oleoyl phosphatidylglycerol) in a 7:3 mixture, which is a common formulation used to mimic bacterial cell membranes (*43*). Three model polymers with spacer arm lengths ($E2_{model}$, $E4_{model}$, and $E6_{model}$) were constructed (Figure 6). These polymers have the degree of polymerization (DP) of 10 and fraction of EMA comonomer, $f_{HB}$ of 0.3. The mole fraction $f_{HB}$ = 0.3 was selected because we are interested in the polymers with potent antimicrobial activity and low hemolytic activity (*38*).

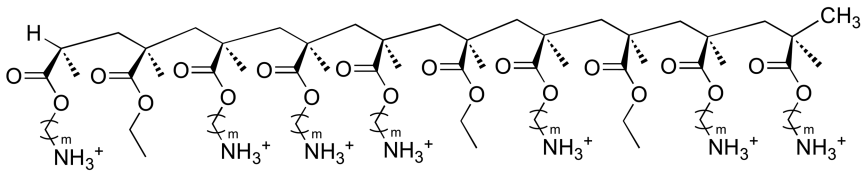


*Figure 6. Monomer sequence and structures of model copolymers. The copolymers have different length of cationic spacer arms: ethylene (m = 2) for E2 $_{model}$, butylene (m = 4) for E4$_{model}$, and hexane (m = 6) for E6$_{model}$. The copolymer structures have an isotactic sequence, and the ratio of cationic monomers and EMA co-monomers is 7:3. These groups are unevenly distributed, modeling the random sequence of polymers (38).*

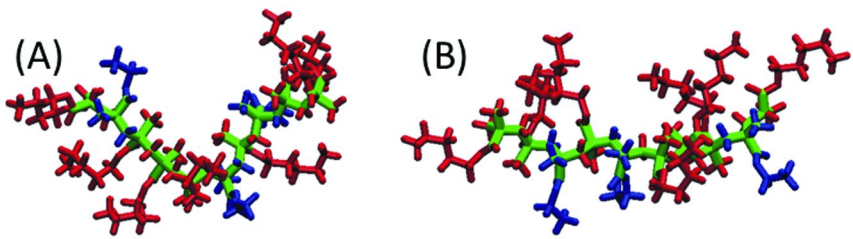


*Figure 7. The average conformation of the copolymer E4$_{model}$ in water (A) and at the water-lipid interface (B). The cationic and EMA ethyl side chains are colored red and blue, respectively. The polymer backbones are colored green. All three systems were simulated under isothermal-isobaric ensemble conditions (305 K temperature and 1 atm pressure). See Reference (38) for experimental details. Adapted with permission from Ref. (38). Copyright 2012 American Chemical Society.*



In Tailored Polymer Architectures for Pharmaceutical and Biomedical Applications; Scholz, C., et al.; ACS Symposium Series; American Chemical Society: Washington, DC, 2013.

Downloaded by PURDUE UNIVERSITY on July 20, 2013 | http://pubs.acs.org
Publication Date (Web): July 8, 2013 | doi: 10.1021/bk-2013-1135.ch019

Each polymer was first placed in aqueous phase above POPE-POPG (7:3) bilayers, and the three systems were simulated for 100 ns each. Counter-ions were added to each system for overall charge neutrality. In general, the three polymers in water adopted compact structures, and the side groups are randomly oriented with respect to the polymer backbone. This is likely because the exposure of hydrophobic polymer backbone and ethyl side chains of EMA to water needs to be minimized, resulting in the compact conformation in water. The results also indicated that no predominant conformations were observed for polymers in water. On the other hand, simulations of polymers interacting with lipid-water interface revealed that the polymer backbones are predominantly oriented parallel to the membrane surface, with the hydrophobic groups projected into the membrane core, and the ammonium groups projected to the water-membrane interface. These results were represented by the two snapshots of conformations of polymer $E4_{model}$ in water and at the lipid-water interface as shown in Figure 7. $E4_{model}$ polymer adopts an extended conformation with well-separated hydrophobic and charged side groups near the lipid interface, whereas the conformation in water is crescent-shaped and no predominant amphiphilic structure can be observed. Yethiraj and coworkers also previously demonstrated that random copolymer models of β-peptides form the segregated amphiphilic structure upon binding to lipid membrane (*44*).

Simulations of the three polymers with bacteria-type POPE-POPG bilayers suggest that the depth of insertion of the polymers into the lipid bilayer depends on the cationic length of the spacer arm groups (Figure 8); the center of mass of the copolymer chains along the membrane normal moves towards the hydrophobic membrane core as the spacer arms are elongated. The polymer backbone of $E4_{model}$ and $E6_{model}$ polymers are stretched in the membranes. The pendant ammonium groups are located near the water-lipid interface while the ethyl groups of EMA co-monomers are rather oriented to the hydrophobic core of membranes. Apparently, the cationic and hydrophobic ethyl side chains of the copolymer are segregated in the opposite side of the polymer backbones.

Downloaded by PURDUE UNIVERSITY on July 20, 2013 | http://pubs.acs.org
Publication Date (Web): July 8, 2013 | doi: 10.1021/bk-2013-1135.ch019

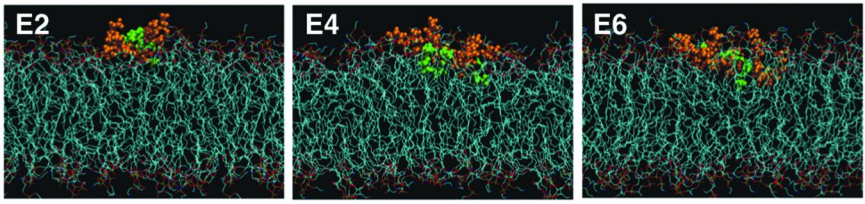


*Figure 8. Amphiphilic copolymers with different spacer arm lengths ($E2_{model}$, $E4_{model}$, and $E6_{model}$), interacting with bacteria-type lipid bilayer at the end of 100 ns simulations. Water is not shown for clarity. The ammonium spacer arm groups and hydrophobic ethyl groups of EMA comonomers are colored orange and green, respectively. Reproduced with permission from Ref. (38). Copyright 2012 American Chemical Society.*


In Tailored Polymer Architectures for Pharmaceutical and Biomedical Applications; Scholz, C., et al.;
ACS Symposium Series; American Chemical Society: Washington, DC, 2013.

Downloaded by PURDUE UNIVERSITY on July 20, 2013 | http://pubs.acs.org
Publication Date (Web): July 8, 2013 | doi: 10.1021/bk-2013-1135.ch019

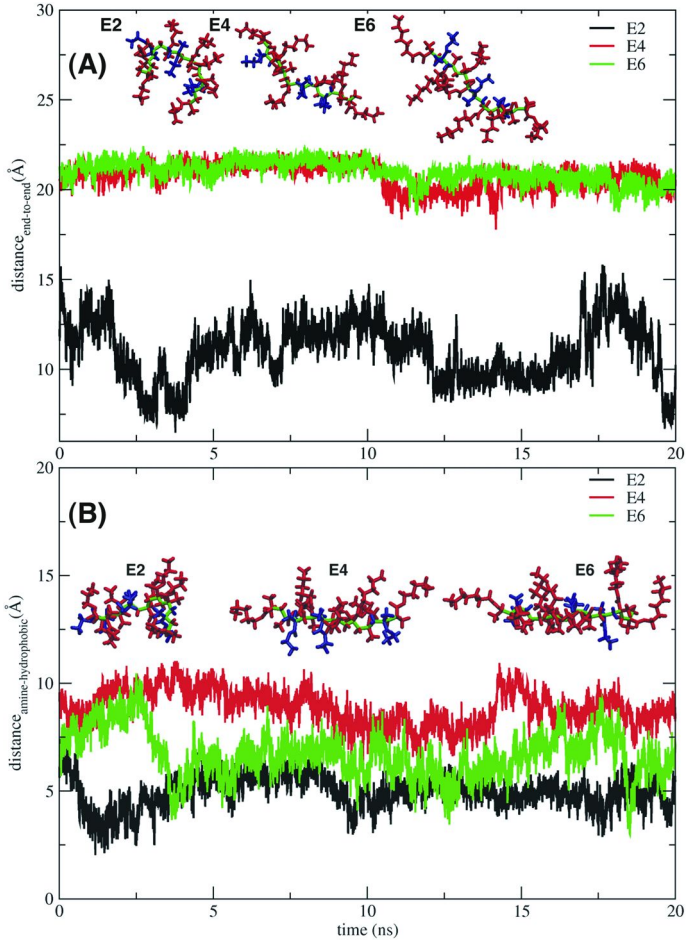


*Figure 9. (A) End-to-end distances of the polymers in the last 20ns of simulation (B) distance between the centers of mass of the ethyl and amine groups in the polymers Insets: average conformation of the copolymers at the end of 100 ns of simulation in the (A)XY plane (perpendicular to membrane normal) (B) parallel to the membrane normal. The cationic and EMA ethyl side chains are colored red and blue, respectively. The polymer backbones are colored green. Adapted with permission from Ref. (38). Copyright 2012 American Chemical Society.*

The development of global amphiphilic structure by methacrylate copolymers was also quantified by examining the parameters of polymer conformations. The end-to-end distance of polymer chains is a measure to describe how much polymers chains are stretched (Figure 9). The end-to-end distance of $E4_{model}$ and $E6_{model}$ polymers in the last 20ns of simulation appears to be constant to


In Tailored Polymer Architectures for Pharmaceutical and Biomedical Applications; Scholz, C., et al.;
ACS Symposium Series; American Chemical Society: Washington, DC, 2013.

be ~20 Å (Figure 9A). The theoretical length for a fully extended conformation of polymer chains with DP = 10 is 23-24 Å based on the chemical structure. This result indicates that $E4_{model}$ and $E6_{model}$ polymers are in highly stretched conformations. Once these polymer chains are inserted in the hydrophobic core of membranes, the polymer chains extend to maximize the interaction between the hydrophobic polymer backbone and acyl chains of lipids for stabilization. The average distances between the center of mass of the ethyl and amine groups in the polymers are ~7 and ~9 Å for $E4_{model}$ and $E6_{model}$. The theoretical maximum distances for complete segregation of these side chains would be ~16 and ~18 Å, respectively (see Figure 9B). This results support the distinctive segregation of cationic spacer arms and hydrophobic ethyl groups of EMA comonomer to opposite faces (Figure 9). In analogy to the snorkeling effect observed with transmembrane peptide helices, the increased spatial separation between the cationic ammonium and hydrophobic ester groups would facilitate deeper membrane insertion.

These random copolymers are not designed to adopt defined secondary structures such as α-helix. These results may indicate that the formation of such amphiphilic structures in lipid membranes may determine their antimicrobial activity rather than the random sequence and molecular weight distribution, and random coil conformation although the exact molecular details of antimicrobial mechanism is not clear at this point. Gellman and coworkers previously demonstrated that cationic amphiphilic random nylon copolymers showed potent activity by tuning the balance of cationic and hydrophobic groups (*35*, *36*). Their studies also reached the similar conclusion that such amphiphilic conformation of polymers and peptides in lipid membranes is a general phenomenon for antimicrobial activity.

Downloaded by PURDUE UNIVERSITY on July 20, 2013 | http://pubs.acs.org
Publication Date (Web): July 8, 2013 | doi: 10.1021/bk-2013-1135.ch019

## Summary and Outlook

Cationic amphiphilic random copolymers showed potent antimicrobial activity and minimal toxicity to human cells, demonstrating their potential as new antimicrobials. The copolymers are also effective against drug resistant bacteria and do not contribute to the development of new resistance mechanisms in bacteria. These polymers likely act on bacterial cell membranes and disrupt the membrane integrity, which mimic the function of natural antimicrobial peptides. The antimicrobial activity can be tuned by altering the cationic spacer arm length, which control the depth of polymer insertion into the lipid membrane, representing the snorkeling effect. The random copolymers have flexible backbones and distribution in the molecular length or molecular weight, which are distinctively different from the defined structures and sequences of antimicrobial peptides. However, many types of polymers have already been utilized as platforms of antimicrobial polymers, and they showed potent activity against a panel of bacteria. The polymer-based strategy to create new antimicrobials will be versatile and can provide a diversity of antimicrobial agents to fight against resistant bacteria.


In Tailored Polymer Architectures for Pharmaceutical and Biomedical Applications; Scholz, C., et al.;
ACS Symposium Series; American Chemical Society: Washington, DC, 2013.

## Acknowledgments

We would like to thank Dr. Gregory Caputo at Rowan University and Dr. Haruko Takahashi at University of Michigan for help to prepare figures.

## Conflict of interest

K. Kuroda is a co-inventor on a patent application filed by the University of Pennsylvania covering "Antimicrobial Copolymers and Uses Thereof". The patent application has been licensed to PolyMedix Inc. (Radnor, PA). PolyMedix did not play a role in the design and conduct of this study, in the collection, analysis, or interpretation of the data, or in the preparation, review, or approval of the article.

Downloaded by PURDUE UNIVERSITY on July 20, 2013 | http://pubs.acs.org
Publication Date (Web): July 8, 2013 | doi: 10.1021/bk-2013-1135.ch019

## References

1. Fernandes, P. *Nat. Biotechnol.* **2006**, *24*, 1497–1503.
2. Fischbach, M. A.; Walsh, C. T. *Science* **2009**, *325*, 1089–1093.
3. Levy, S. B. *The Antibiotic Paradox. How Miracle Drugs Are Destroying the Miracle*; Plenum Press: New York, 1992.
4. Levy, S. B. Antibiotic resistance: An Ecological Imbalance. In *Antibiotic Resistance: Origins, Evolution, Selection and Spread*, 207 ed.; Chadwick, D. J., Goode, J., Eds. Wiley: Chichester, 1997; pp 1−14.
5. Levy, S. B.; Marshall, B. *Nat. Med.* **2004**, *10*, S122–S129.
6. Nathan, C. *Nature* **2004**, *431*, 899–902.
7. Rodriguez de Castro, F.; Naranjo, O. R.; Marco, J. A.; Violan, J. S. *Semin. Respir. Crit. Care Med.* **2009**, *30*, 161–71.
8. Brogden, K. A. *Nat. Rev. Microbiol.* **2005**, *3*, 238–250.
9. Fjell, C. D.; Hiss, J. A.; Hancock, R. E. W.; Schneider, G. *Nat. Rev. Drug Discovery* **2012**, *11*, 37–51.
10. Hancock, R. E. W.; Sahl, H. G. *Nat. Biotechnol.* **2006**, *24*, 1551–1557.
11. Matsuzaki, K. *Biochim. Biophys. Acta, Biomembr.* **1999**, *1462*, 1–10.
12. Nguyen, L. T.; Haney, E. F.; Vogel, H. J. *Trends Biotechnol.* **2011**, *29*, 464–472.
13. Shai, Y. *Biopolymers* **2002**, *66*, 236–248.
14. Zasloff, M. *Nature* **2002**, *415*, 389–395.
15. Marr, A. K.; Gooderham, W. J.; Hancock, R. E. W. *Curr. Opin. Pharm.* **2006**, *6*, 468–472.
16. Wade, D.; Boman, A.; Wahlin, B.; Drain, C. M.; Andreu, D.; Boman, H. G.; Merrifield, R. B. *Proc. Natl. Acad. Sci. U.S.A.* **1990**, *87*, 4761–4765.
17. Cheng, R. P.; Gellman, S. H.; DeGrado, W. F. *Chem. Rev.* **2001**, *101*, 3219–3232.
18. Chongsiriwatana, N. P.; Patch, J. A.; Czyzewski, A. M.; Dohm, M. T.; Ivankin, A.; Gidalevitz, D.; Zuckermann, R. N.; Barron, A. E. *Proc. Natl. Acad. Sci. U.S.A.* **2008**, *105*, 2794–2799.
19. Patch, J. A.; Barron, A. E. *J. Am. Chem. Soc.* **2003**, *125*, 12092–12093.


In Tailored Polymer Architectures for Pharmaceutical and Biomedical Applications; Scholz, C., et al.; ACS Symposium Series; American Chemical Society: Washington, DC, 2013.

20. Choi, S.; Isaacs, A.; Clements, D.; Liu, D. H.; Kim, H.; Scott, R. W.; Winkler, J. D.; DeGrado, W. F. *Proc. Natl. Acad. Sci. U.S.A.* **2009**, *106*, 6968–6973.
21. Goodman, C. M.; Choi, S.; Shandler, S.; DeGrado, W. F. *Nat. Chem. Biol.* **2007**, *3*, 252–262.
22. Liu, D. H.; Choi, S.; Chen, B.; Doerksen, R. J.; Clements, D. J.; Winkler, J. D.; Klein, M. L.; DeGrado, W. F. *Angew. Chem., Int. Ed.* **2004**, *43*, 1158–1162.
23. Porter, E. A.; Wang, X.; Lee, H.-S.; Weisblum, B.; Gellman, S. H. *Nature* **2000**, *404*, 565–565.
24. Liu, D.; DeGrado, W. F. *J. Am. Chem. Soc.* **2001**, *123*, 7553–7559.
25. Gabriel, G. J.; Som, A.; Madkour, A. E.; Eren, T.; Tew, G. N. *Mater. Sci. Eng., R* **2007**, *57*, 28–64.
26. Kuroda, K.; Caputo, G. A. *WIREs Nanomed. Nanobiotechnol.* **2012**.
27. Li, P.; Li, X.; Saravanan, R.; Li, C. M.; Leong, S. S. J. *RSC Adv.* **2012**, *2*, 4031–4044.
28. Palermo, E. F.; Kuroda, K. *Appl. Microbiol. Biotechnol.* **2010**, *87*, 1605–1615.
29. Timofeeva, L.; Kleshcheva, N. *Appl. Microbiol. Biotechnol.* **2011**, *89*, 475–492.
30. Munoz-Bonilla, A.; Fernandez-Garcia, M. *Prog. Polym. Sci.* **2012**, *37*, 281–339.
31. Kenawy, E. R.; Worley, S. D.; Broughton, R. *Biomacromolecules* **2007**, *8*, 1359–1384.
32. Tashiro, T. *Macromol. Mater. Eng.* **2001**, *286*, 63–87.
33. Kuroda, K.; DeGrado, W. F. *J. Am. Chem. Soc.* **2005**, *127*, 4128–4129.
34. Lienkamp, K.; Madkour, A. E.; Musante, A.; Nelson, C. F.; Nusslein, K.; Tew, G. N. *J. Am. Chem. Soc.* **2008**, *130*, 9836–9843.
35. Mowery, B. P.; Lee, S. E.; Kissounko, D. A.; Epand, R. F.; Epand, R. M.; Weisblum, B.; Stahl, S. S.; Gellman, S. H. *J. Am. Chem. Soc.* **2007**, *129*, 15474–15476.
36. Mowery, B. P.; Lindner, A. H.; Weisblum, B.; Stahl, S. S.; Gellman, S. H. *J. Am. Chem. Soc.* **2009**, *131*, 9735–9745.
37. Sovadinova, I.; Palermo, E. F.; Urban, M.; Mpiga, P.; Caputo, G. A.; Kuroda, K. *Polymers* **2011**, *3*, 1512–1532.
38. Palermo, E. F.; Vemparala, S.; Kuroda, K. *Biomacromolecules* **2012**, *13*, 1632–1641.
39. Palermo, E. F.; Lee, D. K.; Ramamoorthy, A.; Kuroda, K. *J. Phys. Chem. B* **2011**, *115*, 366–375.
40. Avery, C. W.; Palermo, E. F.; McLaughin, A.; Kuroda, K.; Chen, Z. *Anal. Chem.* **2011**, *83*, 1342–1349.
41. Mishra, V. K.; Palgunachari, M. N.; Segrest, J. P.; Anantharamaiah, G. M. *J. Biol. Chem.* **1994**, *269*, 7185–7191.
42. Monne, M.; Nilsson, I.; Johansson, M.; Elmhed, N.; von Heijne, G. *J. Mol. Biol.* **1998**, *284*, 1177–1183.
43. Wilkinson, S. G. *Microbial Lipids*; Academic Press: London, 1988; Vol. 1.
44. Mondal, J.; Zhu, X.; Cui, Q. A.; Yethiraj, A. *J. Phys. Chem. B* **2010**, *114*, 13585–13592.

Downloaded by PURDUE UNIVERSITY on July 20, 2013 | http://pubs.acs.org
Publication Date (Web): July 8, 2013 | doi: 10.1021/bk-2013-1135.ch019


In Tailored Polymer Architectures for Pharmaceutical and Biomedical Applications; Scholz, C., et al.;
ACS Symposium Series; American Chemical Society: Washington, DC, 2013.

Downloaded by VIRGINIA TECH on July 17, 2013 | http://pubs.acs.org
Publication Date (Web): July 8, 2013 | doi: 10.1021/bk-2013-1135.ch020

Chapter 20

# Discrimination of Influenza Virus Strains and Super High Sensitive Detection of Viruses Using Sugar Chip and Sugar-Chain Immobilized Gold Nanoparticles

**Yasuo Suda,*[,1,2,3] Xu Zhang,[1,2] Yuko Takahashi,[1] Risa Yokoyama,[2] Mami Nagatomo,[2] Kazue Aoyama,[2] Toshiomi Okuno,[3] Shigeru Saito,[4] Saeko Morikawa,[5] Satoshi Hiroi,[5] Tetsuo Kase,[5] Naoki Murakami,[6] Junichiro Nishi,[7] and Masahiro Wakao[1]**

**[1]Department of Chemistry, Biotechnology and Chemical Engineering, Graduate School of Science and Engineering, Kagoshima University, 1-21-40, Kohrimoto, Kagoshima 890-0065, Japan**
**[2]SUDx-Biotec Corporation, 1-42-1, Shiroyama, Kagoshima 890-0013, Japan**
**[3]Department of Microbiology, Hyogo College of Medicine, 1-1, Mukogawa, Hyogo 663-8501, Japan**
**[4]INFOCOM CORPORATION, 2-34-17, Jingu-mae, Shibuya-ku, Tokyo 150-0001, Japan**
**[5]Osaka Pref. Inst. of Public Health, 1-3-69, Nakamichi, Higashinari-ku, Osaka 537-0025, Japan**
**[6]Murakami Clinic for Children, 9-1, Ohtaki, Kagoshima 892-0805, Japan**
**[7]Graduate School of Medical and Dental Sciences, Kagoshima University, 8-35-1, Sakuragaoka, Kagoshima 890-0075, Japan**
**E-mail: ysuda@eng.kagoshima-u.ac.jp.**

A sugar-chain-immobilized chip (named Sugar Chip, SC) and gold nano-particles (SGNP) were developed. Using these tools, nano-biotechnology methods were developed to discriminate the viral strains and to detect viruses high sensitively. Influenza viruses bind to neuraminic acid containing sugar-chains on the cell surface at the first stage of infection. The binding potency of type A influenza viruses was evaluated using surface plasmon resonance (SPR) imaging and SC immobilized with 6 kinds of sugar-chains containing N-acetylneuraminic acid and 2 kinds of sugar-chains with no N-acetylneuraminic

© 2013 American Chemical Society
In Tailored Polymer Architectures for Pharmaceutical and Biomedical Applications; Scholz, C., et al.; ACS Symposium Series; American Chemical Society: Washington, DC, 2013.

acid. The relative binding potency of viruses to 8 kinds of sugar-chains immobilized on the SC varied even though the viruses were classified in the same serotype. Using 242 strains of influenza virus, we obtained 1976 data sets, created a database, and developed an algorithm based on the nearest neighbor with Euclidean distance to estimate the most similar strains according to the relative sugar-chain binding potency. Based on the database and the algorithm, we estimated the influenza virus strains most similar to the 2009 pandemic viruses (H1N1pdm2009) that were obtained from clinical isolates. In addition, based on the binding data, we found that the sugar-chain, heparin, binds to every virus, which allowed us to prepare heparin-immobilized gold nano-particles. Then, using these nano-particles, we established a novel technique for a super sensitive detection method of influenza viruses in combination with a real time quantitative polymerase chain reaction (real time qPCR). Using this method, we were able to detect influenza viruses that existed in the saliva of asymptomatic patients. Supportive clinical evaluations, during the 2011-2012 season, for influenza diagnosis were also obtained.

Downloaded by VIRGINIA TECH on July 17, 2013 | http://pubs.acs.org
Publication Date (Web): July 8, 2013 | doi: 10.1021/bk-2013-1135.ch020

## Introduction

Sugar-chains are increasingly being recognized as important partners in receptor-ligand binding and cellular signaling (*1*), and also known as receptor molecules for the viral infection (*2–4*). We have developed sugar-chain immobilized chip, named Sugar Chip (SC), and sugar-chain immobilized gold nano-particle (SGNP) (*5–8*). In brief, sugar-chains obtained from natural source or by the chemical synthesis were conjugated with our original linker molecule to prepare ligand-conjugates, and then immobilized on the gold chip to prepare SC, or to gold nano-particle to prepare SGNP. SC can be used for the sensor chip of surface plasmon resonance (SPR) apparatus for high-throughput analysis of proteins, since the binding interaction with SPR can be evaluated without any labeling of proteins. SGNP was used for the visual detection, as SGNPs lost the plasmon absorption when the interaction occurred between sugar-chains on SGNP and analyte, such as protein, in solution. We found that SGNP was also useful for the capturing and concentration of viruses at a very low concentration (*9*).

It was found that the hemagglutinin (HA) of type A influenza virus binds to N-acetylneuraminic acid containing sugar-chain (*2*). In addition, we know that the HA of influenza virus isolated from avian preferentially binds to α2-3 N-acetylneuraminic acid, whereas the virus from human is recognized by α2-6 N-acetylneuraminic acid (*10*, *11*). Ryan-Poirier *et al.* reported that the type A influenza viruses from human has distinct binding potency to trisaccharide containing gangliosides, where the neuraminic acid moiety is located at the


In Tailored Polymer Architectures for Pharmaceutical and Biomedical Applications; Scholz, C., et al.;
ACS Symposium Series; American Chemical Society: Washington, DC, 2013.

non-reducing end of the trisaccharide (*12*). It was shown that the binding potency to the trisaccharide varied for each strains classified even in the same subtype serologically determined by experimental animal sera, indicating a new method for the discrimination of influenza virus strains based on the binding interaction to the structures of receptor oligosaccharides. In our knowledge, this is the first attempt for the discrimination of influenza virus strains based on the sugar-chain binding potency of viruses.

In this paper, we report two subjects; the discrimination of influenza virus strains based on the sugar-chain binding property using SC, and the super high sensitive detection of influenza viruses using SGNP. The latter has been already applied to the clinical research.

Downloaded by VIRGINIA TECH on July 17, 2013 | http://pubs.acs.org
Publication Date (Web): July 8, 2013 | doi: 10.1021/bk-2013-1135.ch020

## Discrimination of Influenza Virus Strains

### Influenza Virus Strains

Over 240 strains of influenza viruses from human and avian sources are listed in Table I including old vaccine strains. These viruses were cultivated in Madin-Darby canine kidney (MDCK) cells or in chicken eggs according to the manual of National Institute of Infectious Diseases (NIID), Japan (http://www.nih.go.jp/niid/ja/labo-manual.html). After cultivation, the viruses were purified by the ultra-centrifugation (24,000 rpm, 90 min. 15 °C) using sucrose gradient (*13*). The concentration of the virus was determined using hemagglutinin unit (HAU) with hemagglutination test with chicken erythrocytes (Nippon Biotest Lab, Japan) (*14*). All experiments with living viruses were done in a biosafety level-2 laboratory.

### Preparation of Sugar Chip (SC)

Sugar-chains (Figure 1) used for the discrimination of influenza virus strains with SC experiments were purchased or synthesized as follows: Galβ1-4Glc and Neu5Acα2-6Galβ1-4Glc were from Nacalai Tesuque (Kyoto, Japan), and Neu5Acα2-3Galβ1-4Glc was from Dextra Laboratories Ltd.. (Berkshire, UK). Galβ1-4GlcNAcβ1-6Glc, Neu5Acα2-3Galβ1-4GlcNAcβ1-6Glc and Neu5Acα2-6Galβ1-4GlcNAcβ1-6Glc were synthesized chemo-enzymatically in our lab. Neu5Acα2-3Galβ1-3GlcNAcβ1-6Glc and Neu5Acα2-6Galβ1-3GlcNAcβ1-6Glc were also prepared by us chemically. These sugar-chains were then conjugated with the mono-valent linker molecule to prepare ligand-conjugates for the immobilization of sugar-chains on the gold-coated chip (*5*, *6*), in which the sugar unit at the reducing end lost the sugar structure and worked as a hydrophilic linker between the mono-valent linker molecule and sugar-chains. The overview for the preparation of array-type SC, spotter and SPR-imaging apparatus are shown in Figure 2. The surface of gold-coated chip (Toyobo Co. Ltd., Osaka, Japan) was oxydatively washed with UV ozone cleaner (Structure Probe Inc. West Chester, PA, USA) for 20 minutes. Then, 1 μl of the 5% glycerol containing aqueous solution of the 12 kinds of ligand-conjugates with the fixed concentration of 500 μM were spotted on the chip with automatic spotter (Toyobo) according to the manual of the manufacture. The spotted chip was kept in stand for 1


In Tailored Polymer Architectures for Pharmaceutical and Biomedical Applications; Scholz, C., et al.;
ACS Symposium Series; American Chemical Society: Washington, DC, 2013.

hour at room temperature and washed sequentially with water, PBS containing 0.05% Tween-20 (PBS-T) and water, and dried at room temperature. In addition, for the control sugar-chains, heparin, GlcNAcα1-6Glc, GlcNAcβ1-6Glc and GalNAcα1-6Glc were immobilized similarly.

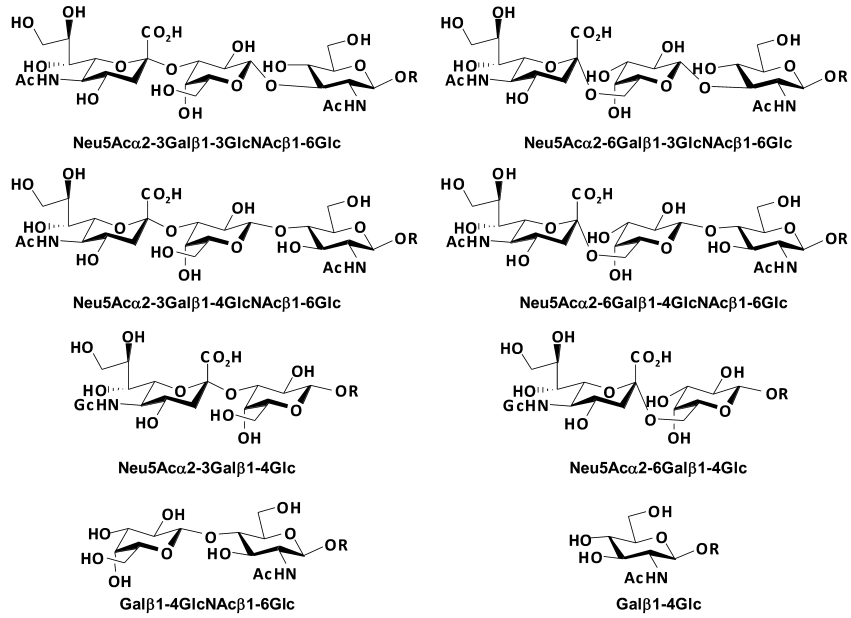


*Figure 1. Sugar-Chains immobilized on array type Sugar Chip for the discrimination of virus strains; Note: R = 6Glucose.*

Downloaded by VIRGINIA TECH on July 17, 2013 | http://pubs.acs.org
Publication Date (Web): July 8, 2013 | doi: 10.1021/bk-2013-1135.ch020

## SPR Imaging and Bio-informatics

The SC immobilized with 12 kinds of sugar-chains as described above was set on prism with a refraction oil ($n_D$ =1.700, Cargill Laboratories Inc., Cedar Grove, NJ, USA) in an SPR Imaging apparatus (MultiSPRinter™, Toyobo). The SPR measurements were carried out according to the manual of the manufacture using PBS-T as a running buffer at the flow rate 150 μl/min at room temperature. To check the specificity of sugar-chains immobilized on the chip, the binding potency against lectins, *Sambucus nigra* agglutinin (SNA) and *Ricinus communis* agglutinin (RCA120) from Vector Laboratories (Burlingame, CA, USA), *Sambucus sieboldiana* agglutinin (SSA) from J-OIL MILLS, Inc (Tokyo, Japan) and *Wheat germ* agglutinin (WGA) from SEIKAGAKU Corp. (Tokyo, Japan), was evaluated prior to the influenza viruses. The concentration of lectins was fixed at 2 μM in PBS-T. Three doses (100, 50, 25 HAU) of virus solution in PBS-T were applied to examine the binding potency.


In Tailored Polymer Architectures for Pharmaceutical and Biomedical Applications; Scholz, C., et al.;
ACS Symposium Series; American Chemical Society: Washington, DC, 2013.

Downloaded by VIRGINIA TECH on July 17, 2013 | http://pubs.acs.org
Publication Date (Web): July 8, 2013 | doi: 10.1021/bk-2013-1135.ch020



**Table I. 242 Influenza virus strains**

| | | | | | | | | | |
|---|---|---|---|---|---|---|---|---|---|
| 1 | A/OSAKA/1529/2007-2 | 51 | A/OSAKA/899/2007-3 | 101 | A/OSAKA/09/2007 | 151 | A/Kobe/1/2003 | 201 | A/CHIBA/75/2005-1 |
| 2 | A/duck/HK/313/4/78-1 | 52 | A/OSAKA/64/2008-1 | 102 | A/OSAKA/730/2007 | 152 | A/OSAKA/734/2007 | 202 | A/OSAKA/894/2007-3 |
| 3 | A/Aichi/2/68-1 | 53 | B/GIFU/31/2005-2 | 103 | A/NewCaledonia/20/99 | 153 | B/3107/18/2005 | 203 | B/Shangdong/7/97 |
| 4 | A/Turkey/Wisconsin/6118/68-2 | 54 | A/Sichuan/2/87-1 | 104 | B/GIFU/55/2005 | 154 | B/Victoria/2/87-1 | 204 | A/Okuda/57-3 |
| 5 | A/duck/HK/24/5/76-1 | 55 | A/duck/HK/313/4/78-5 | 105 | A/CHIBA/92/2005-1 | 155 | B/GIFU/16/2005 | 205 | A/OSAKA/14/2007-1 |
| 6 | A/duck/HK/24/5/76-2 | 56 | A/CHIBA/130/2005-2 | 106 | B/OSAKA/297/2007-2 | 156 | A/OSAKA/37/2007 | 206 | A/OSAKA/739/2007-1 |
| 7 | A/Osaka/17/2006 | 57 | A/OSAKA/1072/2007-1 | 107 | A/OSAKA/31/2008-1 | 157 | B/GIFU/4/2005 | 207 | A/OSAKA/1529/2007-1 |
| 8 | A/Fukuoka/1/70-1 | 58 | A/OSAKA/56/2007-2 | 108 | A/OSAKA/337/2007-1 | 158 | A/OSAKA/708/2007-1 | 208 | A/OSAKA/824/2007 |
| 9 | A/Mallard/Astrakhan/263/82-1 | 59 | A/OSAKA/30/2007-1 | 109 | A/OKINAWA/5/2007 | 159 | B/Kobe/3/2003 | 209 | A/OSAKA/38/2008-2 |
| 10 | A/OSAKA/708/2007-2 | 60 | A/Memphis/1/71-1 | 110 | A/OSAKA/1480/2007 | 160 | A/OSAKA/121 | 210 | B/GIFU/2/2005 |
| 11 | A/OKINAWA/17/2007-2 | 61 | A/Kobe/54/2002 | 111 | B/GIFU/66/2005 | 161 | A/OSAKA/39/2007 | 211 | A/KYUSHU/29/2005-2 |

*Continued on next page.*

Downloaded by VIRGINIA TECH on July 17, 2013 | http://pubs.acs.org
Publication Date (Web): July 8, 2013 | doi: 10.1021/bk-2013-1135.ch020



**Table I. (Continued). 242 Influenza virus strains**

| | | | | | | | | | |
|---|---|---|---|---|---|---|---|---|---|
| 12 | A/OSAKA/335/2007-1 | 62 | A/OSAKA/48/2007 | 112 | B/3107/46/2005 | 162 | A/OSAKA/899/2007-1 | 212 | B/OSAKA/464/ 2007-2 |
| 13 | A/Panama/2007/99-1 | 63 | A/Tokyo/6/73-1 | 113 | A/OSAKA/60/ 2007-1 | 163 | A/OSAKA/1527/2007-3 | 213 | B/OSAKA/308/ 2007 |
| 14 | A/OSAKA/121/2007-2 | 64 | A/Aichi/2/68-4 | 114 | A/OSAKA/45/2007 | 164 | B/Kobe/21/2007 | 214 | B/GIFU/36/2005-2 |
| 15 | A/Panama/2007/99-2 | 65 | A/OSAKA/735/ 2007-2 | 115 | B/OSAKA/339/ 2007-2 | 165 | A/OSAKA/586/2007 | 215 | A/OSAKA/573/ 2007 |
| 16 | A/OSAKA/316/2007-1 | 66 | A/OSAKA/13/2007 | 116 | A/OSAKA/345/2007 | 166 | A/GIFU/25/2005-2 | 216 | A/OSAKA/547/ 2007 |
| 17 | A/3107/27/2005-2 | 67 | A/OSAKA/41/2007-1 | 117 | A/OSAKA/19/2007 | 167 | B/GIFU/48/2005 | 217 | A/OSAKA/873/ 2007-2 |
| 18 | A/FM/1/47-1 | 68 | B/Yamanashi/166/ 98-2 | 118 | A/OSAKA/15/2007 | 168 | B/OSAKA/451/2007 | 218 | A/OSAKA/875/ 2007 |
| 19 | A/OSAKA/700/2007-2 | 69 | A/3107/31/2005 | 119 | A/OSAKA/07/ 2007-2 | 169 | A/OSAKA/16/2007 | 219 | A/OSAKA/2/2008 |
| 20 | A/OSAKA/38/2007-2 | 70 | A/KYUSHU/29/ 2005-1 | 120 | A/OSAKA/479/ 2007-2 | 170 | A/Memphis/1/71-3 | 220 | A/Kobe/7/2002 |
| 21 | A/OSAKA/71/2007-2 | 71 | B/GIFU/59/2005 | 121 | A/OSAKA/42/2007 | 171 | A/OSAKA/772/2007 | 221 | A/Tokyo/6/73-4 |
| 22 | A/Fukuoka/1/70-3 | 72 | B/GIFU/8/2005-2 | 122 | B/3107/14/2005 | 172 | A/Czechoslovakia/ DUCK/1/1956 | 222 | B/OSAKA/348/ 2007 |
| 23 | A/Sydney/5/97-2 | 73 | B/OSAKA/355/2007 | 123 | B/Kobe/5/2006 | 173 | A/OSAKA/10/2007 | 223 | A/OSAKA/877/ 2007 |

Downloaded by VIRGINIA TECH on July 17, 2013 | http://pubs.acs.org
Publication Date (Web): July 8, 2013 | doi: 10.1021/bk-2013-1135.ch020



| | | | | | | | | | |
|---|---|---|---|---|---|---|---|---|---|
| 24 | A/OSAKA/1348/2007 | 74 | A/GIFU/43/2005-1 | 124 | A/okuda/57-2 | 174 | A/OSAKA/58/2007-2 | 224 | A/CHIBA/92/2005-2 |
| 25 | A/Guizhou/54/89-1 | 75 | A/OSAKA/59/2007 | 125 | A/GIFU/58/2005-2 | 175 | A/OSAKA/20/2007-2 | 225 | A/OSAKA/854/2007-2 |
| 26 | A/Duck/Australia/341/83 | 76 | A/CHIBA/89/2005 | 126 | A/OSAKA/422/2007-2 | 176 | B/Nagasaki/1/87-4 | 226 | A/OSAKA/1007/2007-1 |
| 27 | A/Duck/Alberta/60/76-1 | 77 | A/OSAKA/587/2007 | 127 | B/GIFU/32/2005 | 177 | A/OSAKA/422/2007-1 | 227 | A/OSAKA/1009/2007 |
| 28 | A/OSAKA/1348/2007 | 78 | A/Sydney/5/97-3 | 128 | A/OSAKA/64/2008-2 | 178 | B/Victoria/2/87-2 | 228 | A/OSAKA/1000/2007 |
| 29 | A/OSAKA/57/2007-1 | 79 | A/Wyoming/3/2003-2 | 129 | B/GIFU/19/2005 | 179 | A/OSAKA/921/2007-1 | 229 | A/GIFU/58/2005-1 |
| 30 | B/GIFU/57/2005 | 80 | A/OKINAWA/18/2007 | 130 | A/OSAKA/684/2007 | 180 | A/OSAKA/121/2007-1 | 230 | A/OSAKA/36/2007 |
| 31 | A/OSAKA/08/2007-1 | 81 | A/OSAKA/1312/2007 | 131 | A/CHIBA/130/2005-3 | 181 | A/CHIBA/65/2005-2 | 231 | A/OSAKA/1013/2007 |
| 32 | A/Turkey/Outario/6118/68-2 | 82 | A/OSAKA/4/2008 | 132 | A/Kitakyushu/159/93-1 | 182 | A/OKINAWA/15/2007 | 232 | A/NewCaledonia/20/1999 |
| 33 | A/Chicken/Germany/N/49 | 83 | A/OKINAWA/17/2007-1 | 133 | A/OSAKA/600/2007 | 183 | B/3107/40/2005-1 | 233 | B/OSAKA/304/2007 |
| 34 | B/GIFU/22/2005-2 | 84 | A/KYUSHU/27/2005 | 134 | A/YAMAGATA/32/1989 | 184 | A/Kobe/3/2003 | 234 | A/okuda/57-6 |
| 35 | B/GIFU/60/2005-2 | 85 | A/duck/HK/24/5/76-4 | 135 | A/OSAKA/1352/2007 | 185 | A/OSAKA/38/2008-3 | 235 | A/OSAKA/1349/2007 |

*Continued on next page.*

Downloaded by VIRGINIA TECH on July 17, 2013 | http://pubs.acs.org
Publication Date (Web): July 8, 2013 | doi: 10.1021/bk-2013-1135.ch020



**Table I. (Continued). 242 Influenza virus strains**

| | | | | | | | | | |
|---|---|---|---|---|---|---|---|---|---|
| 36 | B/GIFU/65/2005 | 86 | A/Kitakyushu/159/93-5 | 136 | B/GIFU/64/2005 | 186 | A/Sichuan/2/87-2 | 236 | B/GIFU/34/2005 |
| 37 | B/GIFU/50/2005-2 | 87 | A/OKINAWA/16/2007-2 | 137 | A/OSAKA/739/2007-2 | 187 | A/OSAKA/708/2007-1 | 237 | A/CHIBA/65/2005-1 |
| 38 | A/OSAKA/205/2007 | 88 | A/Niigata/102/81-1 | 138 | A/Wyoming/3/2003-1 | 188 | A/Tokyo/6/73-3 | 238 | A/Tokyo/6/73-2 |
| 39 | A/OSAKA/205/2007 | 89 | A/OSAKA/27/2008-2 | 139 | A/Yamanashi/2/77-1 | 189 | B/Kobe/1/2002 | 239 | A/Kobe/2/05-1 |
| 40 | B/GIFU/56/2005 | 90 | A/NewYork/55/2004 | 140 | A/OSAKA/282/2007 | 190 | A/OSAKA/1527/2007-2 | 240 | A/Tokyo/6/73-6 |
| 41 | B/3107/38/2005-2 | 91 | A/Fukuoka/c29/85-1 | 141 | A/GIFU/43/2005-3 | 191 | A/OSAKA/894/2007-2 | 241 | A/OSAKA/35/2007 |
| 42 | A/OSAKA/40/2007-1 | 92 | A/Adachi/1/0532 | 142 | A/OSAKA/340/2007 | 192 | A/3107/13/2005 | 242 | A/Beijing/262/95-1 |
| 43 | A/Shimane/DUCK/124R/80 | 93 | B/Kobe/1/2003 | 143 | B/Kobe/62/2005 | 193 | A/OSAKA/31/2008-2 | | |
| 44 | B/Nagasaki/1/87-1 | 94 | A/OSAKA/64/2007 | 144 | A/OSAKA/717/2007 | 194 | A/OKINAWA/7/2007 | | |
| 45 | A/OSAKA/921/2007-2 | 95 | A/OSAKA/479/2007-1 | 145 | A/GIFU/25/2005-1 | 195 | A/CHIBA/75/2005-2 | | |
| 46 | A/OSAKA/07/2007-1 | 96 | A/OSAKA/1170/2007 | 146 | A/OSAKA/27/2008-1 | 196 | A/Kobe/6/05 | | |
| 47 | A/Guizhou/54/89-3 | 97 | A/GIFU/43/2005-4 | 147 | A/KYUSHU/29/2005-3 | 197 | A/OSAKA/1351/2007 | | |
| 48 | A/WUHAN/359/1995 | 98 | A/ENGLAND/DUCK/1956 | 148 | A/Memphis/1/71-2 | 198 | A/Yamanashi/2/77-2 | | |

| | | | | | | | | | |
|---|---|---|---|---|---|---|---|---|---|
| 49 | A/3107/44/2005-1 | 99 | A/OSAKA/854/ 2007-1 | 149 | A/beijing/262/95-2 | 199 | B/GIFU/52/2005-2 | | |
| 50 | B/Yamanashi/166/98-1 | 100 | A/3107/22/2005 | 150 | B/GIFU/26/2005 | 200 | A/OSAKA/1234/2007 | | |

Downloaded by VIRGINIA TECH on July 17, 2013 | http://pubs.acs.org
Publication Date (Web): July 8, 2013 | doi: 10.1021/bk-2013-1135.ch020

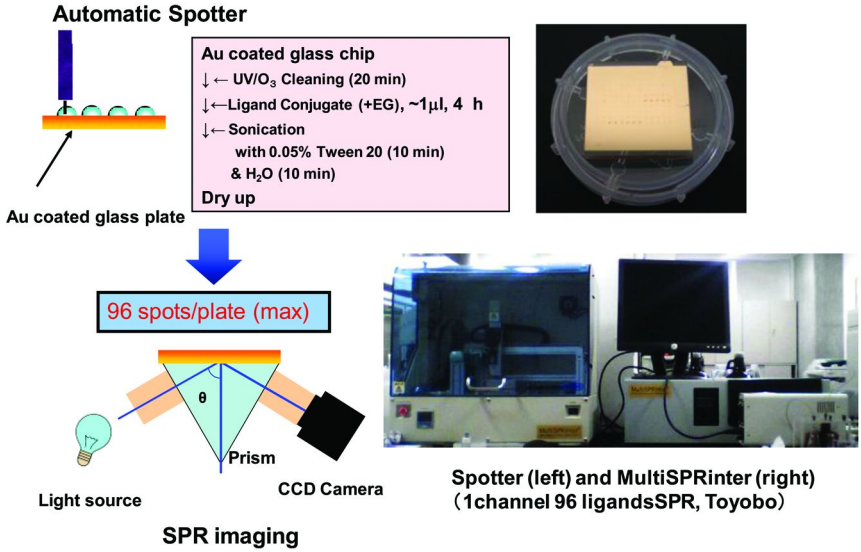


*Figure 2. Overview of the preparation of array-type sugar chip, spotter and apparatus for SPR-imaging.*

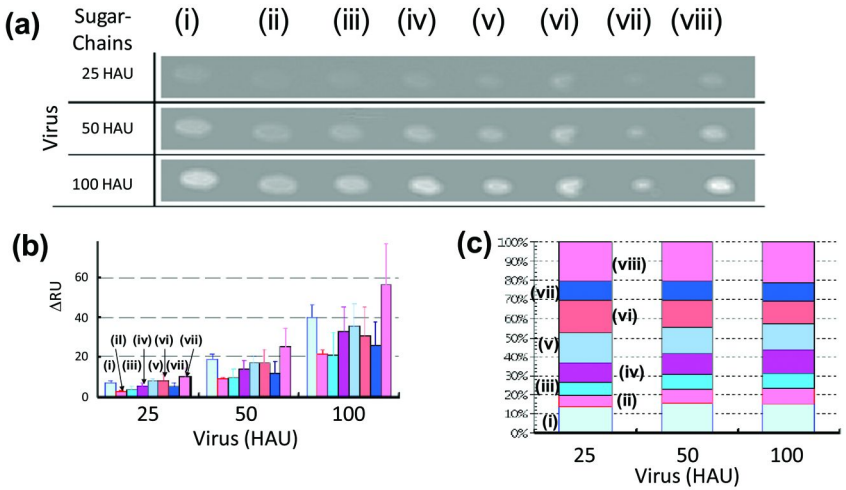


*Figure 3. Binding Patterns of Influenza Virus Type A Sydney Strain (H3N2). (a) Row data of the binding in SPR-imaging; (b) Quantification from the brightness of each spots; (c) Relative binding potency. Sugar-chains immobilized on the chip are (i) Galβ1-4Glc, (ii) Galβ1-4GlcNAcβ1-6Glc, (iii) Neu5Acα2-3Galβ1-4Glc, (iv) Neu5Acα2-6Galβ1-4Glc, (v) Neu5Acα2-3Galβ1-3GlcNAcβ1-6Glc , (vi) Neu5Acα2-6Galβ1-3GlcNAcβ1-6Glc, (vii) Neu5Acα2-3Galβ1-4GlcNAcβ1-6Glc, (viii) Neu5Acα2-6Galβ1-4GlcNAcβ1-6Glc.*

Downloaded by VIRGINIA TECH on July 17, 2013 | http://pubs.acs.org
Publication Date (Web): July 8, 2013 | doi: 10.1021/bk-2013-1135.ch020


In Tailored Polymer Architectures for Pharmaceutical and Biomedical Applications; Scholz, C., et al.;
ACS Symposium Series; American Chemical Society: Washington, DC, 2013.

The binding phenomena of a type A influenza virus [A/Sydney/5/97(H3N2)] is apparent in Figure 3. The SPR intensity of spots on the chip, which indicates the binding potency of the virus to each sugar-chain, increased with increasing the HAU of the virus (Figure 3a). The intensities were then quantified (Figure 3b) by calculating an average of the brightness at 8 independent points in one spot, and used as a relative binding value to the total (the summation of the averaged value for the eight spots) as shown in Figure 3c. The averaged relative binding values were reproducible in the separate experiment at each HAU of the virus solution, respectively. Similarly, the binding potencies of other influenza virus strains were evaluated.

Downloaded by VIRGINIA TECH on July 17, 2013 | http://pubs.acs.org
Publication Date (Web): July 8, 2013 | doi: 10.1021/bk-2013-1135.ch020

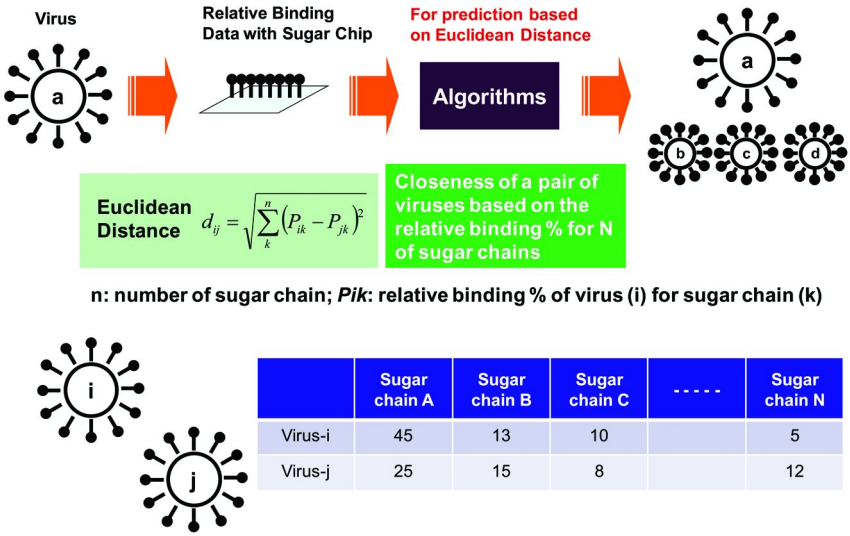


| | Sugar chain A | Sugar chain B | Sugar chain C | - - - - - | Sugar chain N |
|---|---|---|---|---|---|
| Virus-i | 45 | 13 | 10 | | 5 |
| Virus-j | 25 | 15 | 8 | | 12 |

*Figure 4. Outline of creating database and algorithms for the Prediction of Influenza Virus Strains.*

To discriminate virus strains, we developed an algorithm based on the nearest neighbor method; this was used to evaluate the similarity of the relative binding potencies (Figure 4). First, the profiles of the relative binding values of all influenza virus strains were stored in a database. Secondly, closeness between a query profile for unknown virus strain and all profiles in the database was calculated using Euclidean distance. Finally, the influenza virus strain showing the smallest distance was outputted as the estimated strain.


In Tailored Polymer Architectures for Pharmaceutical and Biomedical Applications; Scholz, C., et al.;
ACS Symposium Series; American Chemical Society: Washington, DC, 2013.

Downloaded by VIRGINIA TECH on July 17, 2013 | http://pubs.acs.org
Publication Date (Web): July 8, 2013 | doi: 10.1021/bk-2013-1135.ch020



**Table II. Prediction of influenza virus strains which have similar sugar-chain binding property to H1N1pdm2009. Values are Euclid distance based on the 8 kinds of sugar-chain binding potency of each H1N1pdm2009 strain harvested at different city in Osaka to the strains in the database.**

| *Strain 2206 (Ikeda City)* | | *Strain 2374 (Hirakata City)* | | *Strain 2738 (Toyonaka City)* | |
|---|---|---|---|---|---|
| B/3107/46/2005 | 0.07926 | A/OSAKA/58/2007(H1N1) | 0.067551 | A/OSAKA/58/2007(H1N1) | 0.112306 |
| A/OSAKA/56/2007(H1N1) | 0.081174 | A/KYUSHU/27/2005(H3N2) | 0.07728 | A/CHIBA/89/2005(H3N2) | 0.114183 |
| A/OSAKA/42/2007(H3N2) | 0.091075 | B/Shangdong/7/97 | 0.078355 | A/OSAKA/1007/2007(H3N2) | 0.116495 |
| A/Panama/2007/99(H3N2) | 0.092016 | A/CHIBA/89/2005(H3N2) | 0.083351 | B/Shangdong/7/97 | 0.123825 |
| B/GIFU/50/2005 | 0.093645 | B/Victoria/2/87 | 0.084835 | A/GIFU/25/2005(H3N2) | 0.130453 |
| A/OSAKA/39/2007(H3N2) | 0.096249 | A/GIFU/43/2005(H3N2) | 0.085149 | B/Victoria/2/87 | 0.131778 |
| A/Memphis/1/71(H3N2) | 0.096252 | A/Turkey/Wisconsin/6118/68 (H9N2) | 0.085628 | A/OSAKA/13/2007(H3N2) | 0.132157 |
| A/Aichi/2/68(H3N2) | 0.09662 | A/Guizhou/54/89(H3N2) | 0.086749 | B/3107/46/2005 | 0.132264 |
| B/OSAKA/339/2007 | 0.09858 | A/Yamanashi/2/77(H3N2) | 0.087258 | A/CHIBA/65/2005(H3N2) | 0.133026 |
| A/Tokyo/6/73(H3N2) | 0.099208 | A/Turkey/Outario/6118/68 (H8N4) | 0.089927 | A/OSAKA/09/2007(H3N2) | 0.135879 |
| A/OSAKA/45/2007(H1N1) | 0.10019 | A/CHIBA/92/2005(H3N2) | 0.090089 | A/CHIBA/92/2005(H3N2) | 0.137999 |
| A/Fukuoka/1/70(H3N2) | 0.101103 | A/OSAKA/854/2007(H3N2) | 0.09134 | A/Aichi/2/68(H3N2) | 0.138005 |
| A/OSAKA/708/2007(H3N2) | 0.101309 | A/OSAKA/09/2007(H3N2) | 0.093565 | A/CHIBA/75/2005(H3N2) | 0.141959 |
| A/OSAKA/700/2007(H1N1) | 0.101683 | B/3107/46/2005 | 0.096054 | A/3107/31/2005(H1N1) | 0.1439 |
| A/OSAKA/739/2007(H3N2) | 0.101711 | A/OSAKA/13/2007(H3N2) | 0.096427 | A/Tokyo/6/73(H3N2) | 0.144144 |

| *Strain 2206 (Ikeda City)* | | *Strain 2374 (Hirakata City)* | | *Strain 2738 (Toyonaka City)* | |
|---|---|---|---|---|---|
| A/duck/HK/24/5/76(H3N2) | 0.102449 | A/CHIBA/65/2005(H3N2) | 0.096751 | B/Yamanashi/166/98 | 0.144172 |
| A/OSAKA/1348/2007(H3N2) | 0.104783 | A/CHIBA/75/2005(H3N2) | 0.097055 | B/3107/18/2005 | 0.146569 |
| A/OSAKA/71/2007(H3N2) | 0.105125 | A/GIFU/58/2005(H3N2) | 0.097128 | B/3107/14/2005 | 0.151262 |
| A/OSAKA/40/2007(H3N2) | 0.109358 | B/Yamanashi/166/98 | 0.097557 | A/OKINAWA/17/2007(H3N2) | 0.153379 |
| A/OSAKA/41/2007(H3N2) | 0.110227 | A/Tokyo/6/73(H3N2) | 0.097853 | A/GIFU/43/2005(H3N2) | 0.157006 |
| A/OSAKA/38/2007(H3N2) | 0.111358 | A/CHIBA/130/2005(H3N2) | 0.098322 | A/CHIBA/130/2005(H3N2) | 0.157694 |
| A/OSAKA/59/2007(H1N1) | 0.112235 | A/3107/31/2005(H1N1) | 0.100535 | A/GIFU/58/2005(H3N2) | 0.157802 |

Downloaded by VIRGINIA TECH on July 17, 2013 | http://pubs.acs.org
Publication Date (Web): July 8, 2013 | doi: 10.1021/bk-2013-1135.ch020



In Tailored Polymer Architectures for Pharmaceutical and Biomedical Applications; Scholz, C., et al.;
ACS Symposium Series; American Chemical Society: Washington, DC, 2013.

The developed algorithm and database were then applied to the 2009 pandemic viruses (H1N1pdm2009) harvested in Ikeda City, Toyonaka City, and Hirakata City in Osaka prefecture, Japan, respectively. Three H1N1pdm2009 viruses were cultured independently using MDCK cells, purified by sucrose gradient/ultracentrifugation, diluted to 50 HAU with PBS-T, and applied to SC immobilized as described above. From the evaluation, the three H1N1pdm2009 viruses have high score of similarity for similar type A (H1N1) strains of influenza virus which were harvested in Osaka prefecture in 2007 (Table II).

Vaccine strains to prevent influenza infections are predicted every year based on the epidemic information of the previous year. Therefore, the resultant vaccine may not be effective all the time against seasonal virus strains, especially type A. According to our data in this report, an easier and quicker profiling or discrimination of the epidemic strain of type A influenza virus is possible for the prediction and preparation of the more effective vaccine strains.

Downloaded by VIRGINIA TECH on July 17, 2013 | http://pubs.acs.org
Publication Date (Web): July 8, 2013 | doi: 10.1021/bk-2013-1135.ch020

## High Sensitive Detection of Influenza viruses: Concentration of Viruses with Heparin-GNP and Their Real-Time PCR Amplification

Although the binding potency of each strain to 8 kinds of sugar-chains varied, it was found that all the strains bind to heparin based on the SPR imaging analysis (Figure 5). Thus heparin proved to be a useful ligand to capture and concentrate viruses from a solution. Heparin-GNP was prepared using the ligand-conjugate of heparin (mean Mw = 17,500) and our mono-valent linker molecule (*9*). The diameter of Heparin-GNP was estimated to be 10-20 nm by the transmittance electron microscopy (TEM) analysis (Figure 6), which was purified by precipitation with a centrifugation at 12,000 x *g* for 40 min. To 500 μL of virus solution was added 10 μL of Heparin-GNP with a gentle agitation. After incubation for 30 min at room temperature, the mixture was centrifuged at 10,000 x *g* for 10 minutes, and the supernatant was removed. In this stage of mixing, it was predicted that specific binding should occur between the Heparin-GNPs and viruses, and the resulting binding complex could be collected. By centrifugation at 10,000 x *g* for 10 min, precipitates, which were expected to include viruses, were obtained. Resulting precipitates were re-suspended in 10 μL of RNase free water, and heated at 100 °C for 10 minutes to destroy virus particle and release RNA. For a control, 10 μL of the original virus solution before Heparin-GNP treatment was heated at 100 °C for 10 min. For the clinical samples, 250 μL of or saliva was collected from patients who agreed with our clinical research. 250 μL of MEM medium containing anti-microorganism was added to the saliva, and concentrated using the Heparin-GNP technique as described above. The RT reaction, followed by the qPCR amplification, was carried out using Thermal Cycler Dice Real Time System (Takara Bio Inc., Otsu, Japan) with a commercial reagent (One Step SYBR Prime Script RT-PCR Kit II (Perfect Real Time), Takara) according the standard protocol attached. Primers used for these reactions were designed for the gene encoded to M-protein of influenza virus type A and


In Tailored Polymer Architectures for Pharmaceutical and Biomedical Applications; Scholz, C., et al.;
ACS Symposium Series; American Chemical Society: Washington, DC, 2013.

B as follows; Type A: forward: 5′GGA CTG CAG CGT AGA CGC TT, riverse: 5′CAT YCT GTT GTA TAT GAG GCC CAT, Type B: forward: 5′AAA TAC GGT GGA TTA AAT AAA AGC AA, riverse: 5′CCA GCA ATA GCT CCG AAG AAA. The cycling reaction for the amplification was done using Thermal Cycler Dice Real Time System as follows; initial denaturation step (95 °C for 10 sec), 40 cycles of 95 °C for 5 sec followed by 60 °C for 30 seconds. The purity of the amplified fragment (cDNA) was checked by the melting curve analysis (denaturation at 95 °C for 15 sec followed by step-up elevation of the temperature from 60 to 95 °C by 0.5 °C in 30 sec increments). The data analysis, including determination of threshold cycle (Ct) value and dissociation temperature of the synthesized cDNA, was performed using the software that was loaded in the system. Concentration factors (*CFs*) relative to non-treated samples (control) were calculated according to the following equation; $CF = 2^{\Delta Ct}$, where ΔCt is the value of non-treated control sample (Ct) minus that of the objective sample.

Downloaded by VIRGINIA TECH on July 17, 2013 | http://pubs.acs.org
Publication Date (Web): July 8, 2013 | doi: 10.1021/bk-2013-1135.ch020

(a)

| | 1 | 2 | 3 | 4 | 5 | 6 | 7 | 8 | 9 | 10 | 11 | 12 |
|---|---|---|---|---|---|---|---|---|---|---|---|---|
| A | Gaβ4Gc [Lactose] | Gaβ4GcNAc β6Gc [typeII] | NeuAca23 Gaβ4Gc [S23Lac] | NeuAca26 Gaβ4Gc [S26Lac] | NeuAca23Ga β3 GcNAcβ6Gc [S23Type I] | NeuAca26Ga β3 GcNAcβ6Gc [S26Type I] | NeuAca23Ga β4 GcNAcβ6Gc [S23Type II] | NeuAca26Ga β4 GcNAcβ6Gc [S26Type II] | GcNAca6Gc | GcNAcβ6Gc | GaNAca6Gc [Tn] | Heparin |
| B | Heparin | Gaβ4Gc [Lactose] | Gaβ4GcNAc β6Gc [typeII] | NeuAca23 Gaβ4Gc [S23Lac] | NeuAca26 Gaβ4Gc [S26Lac] | NeuAca23Ga β3 GcNAcβ6Gc [S23Type I] | NeuAca26Ga β3 GcNAcβ6Gc [S26Type I] | NeuAca23Ga β4 GcNAcβ6Gc [S23Type II] | NeuAca26Ga β4 GcNAcβ6Gc [S26Type II] | GcNAca6Gc | GcNAcβ6Gc | GaNAca6Gc [Tn] |
| C | GaNAca6Gc [Tn] | Heparin | Gaβ4Gc [Lactose] | Gaβ4GcNAc β6Gc [typeII] | NeuAca23 Gaβ4Gc [S23Lac] | NeuAca26 Gaβ4Gc [S26Lac] | NeuAca23Ga β3 GcNAcβ6Gc [S23Type I] | NeuAca26Ga β3 GcNAcβ6Gc [S26Type I] | NeuAca23Ga β4 GcNAcβ6Gc [S23Type II] | NeuAca26Ga β4 GcNAcβ6Gc [S26Type II] | GcNAca6Gc | GcNAcβ6Gc |
| D | GcNAcβ6Gc | GaNAca6Gc [Tn] | Heparin | Gaβ4Gc [Lactose] | Gaβ4GcNAc β6Gc [typeII] | NeuAca23 Gaβ4Gc [S23Lac] | NeuAca26 Gaβ4Gc [S26Lac] | NeuAca23Ga β3 GcNAcβ6Gc [S23Type I] | NeuAca26Ga β3 GcNAcβ6Gc [S26Type I] | NeuAca23Ga β4 GcNAcβ6Gc [S23Type II] | NeuAca26Ga β4 GcNAcβ6Gc [S26Type II] | GcNAca6Gc |
| E | GcNAca6Gc | GcNAcβ6Gc | GaNAca6Gc [Tn] | Heparin | Gaβ4Gc [Lactose] | Gaβ4GcNAc β6Gc [typeII] | NeuAca23 Gaβ4Gc [S23Lac] | NeuAca26 Gaβ4Gc [S26Lac] | NeuAca23Ga β3 GcNAcβ6Gc [S23Type I] | NeuAca26Ga β3 GcNAcβ6Gc [S26Type I] | NeuAca23Ga β4 GcNAcβ6Gc [S23Type II] | NeuAca26Ga β4 GcNAcβ6Gc [S26Type II] |
| F | NeuAca26Ga β4 GcNAcβ6Gc [S26Type II] | GcNAca6Gc | GcNAcβ6Gc | GaNAca6Gc [Tn] | Heparin | Gaβ4Gc [Lactose] | Gaβ4GcNAc β6Gc [typeII] | NeuAca23 Gaβ4Gc [S23Lac] | NeuAca26 Gaβ4Gc [S26Lac] | NeuAca23Ga β3 GcNAcβ6Gc [S23Type I] | NeuAca26Ga β3 GcNAcβ6Gc [S26Type I] | NeuAca23Ga β4 GcNAcβ6Gc [S23Type II] |
| G | NeuAca23Ga β4 GcNAcβ6Gc [S23Type II] | NeuAca26Ga β4 GcNAcβ6Gc [S26Type II] | GcNAca6Gc | GcNAcβ6Gc | GaNAca6Gc [Tn] | Heparin | Gaβ4Gc [Lactose] | Gaβ4GcNAc β6Gc [typeII] | NeuAca23 Gaβ4Gc [S23Lac] | NeuAca26 Gaβ4Gc [S26Lac] | NeuAca23Ga β3 GcNAcβ6Gc [S23Type I] | NeuAca26Ga β3 GcNAcβ6Gc [S26Type I] |
| H | NeuAca26Ga β3 GcNAcβ6Gc [S26Type I] | NeuAca23Ga β4 GcNAcβ6Gc [S23Type II] | NeuAca26Ga β4 GcNAcβ6Gc [S26Type II] | GcNAca6Gc | GcNAcβ6Gc | GaNAca6Gc [Tn] | Heparin | Gaβ4Gc [Lactose] | Gaβ4GcNAc β6Gc [typeII] | NeuAca23 Gaβ4Gc [S23Lac] | NeuAca26 Gaβ4Gc [S26Lac] | NeuAca23Ga β3 GcNAcβ6Gc [S23Type I] |

(b)

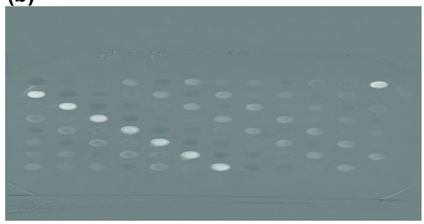

(c)

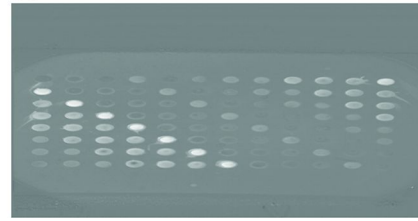

*Figure 5. Examples of the virus binding to sugar-chains on the array-type SC; (a) sugar-chains, (b) binding image of A/OSAKA/422/2007(H1N1); (c) binding image of A/OKINAWA/12/2007(H3N2).*


In Tailored Polymer Architectures for Pharmaceutical and Biomedical Applications; Scholz, C., et al.;
ACS Symposium Series; American Chemical Society: Washington, DC, 2013.

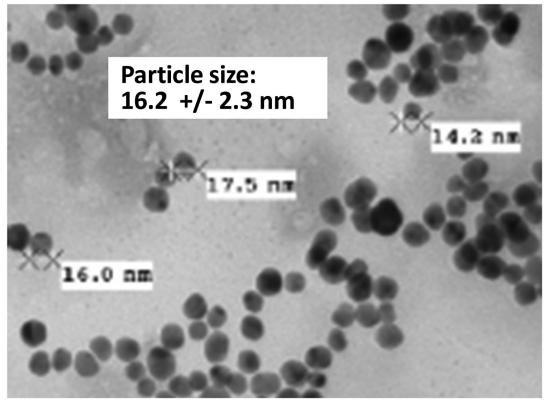


*Figure 6. Transmittance electro microscopy (TEM) image of Heparin-GNP.*

Downloaded by VIRGINIA TECH on July 17, 2013 | http://pubs.acs.org
Publication Date (Web): July 8, 2013 | doi: 10.1021/bk-2013-1135.ch020

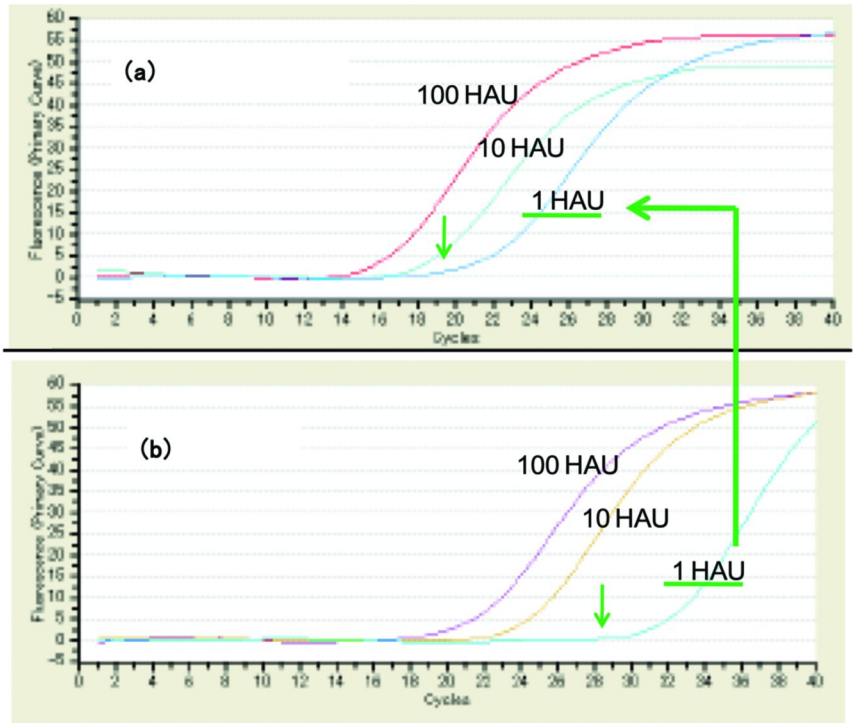


*Figure 7. RT-qPCR analysis of type A influenza virus [A/Wyoming/3/ 2003(H3N2)]; (a) With capturing and concentration using Heparin-GNP, (b) Without Capturing and concentration.*


In Tailored Polymer Architectures for Pharmaceutical and Biomedical Applications; Scholz, C., et al.;
ACS Symposium Series; American Chemical Society: Washington, DC, 2013.

As shown in Figure 7, it was found that the Ct value of 1 HAU of influenza Wyoming strain drastically decreased from ~30 to ~20 by the capturing and concentrating the virus with Heparin-GNP, thus indicating that the *CF* was around 1000. Using clinical samples (patient's nasal mucosal swabs), it was found that our technique, using Heparin-GNP, was at least 100 fold more sensitive than a regular RT-qPCR method (Table III). In the regular RT-qPCR method, without capturing and concentration, the viral RNA was not detected in the 1/100 diluted sample with PBS, however, the viral RNA was detected even in 1/1000 diluted sample when the technique that we developed with capturing and concentration using Heparin-GNP was used. Since, it is known that trace amounts of influenza viruses exist in the patient's saliva, the saliva represents an alternative, easy and non-painful way to collect samples compared with nasal swabs. Based on this premise, the influence of saliva on the capturing and concentration of virus using Heparin-GNP was evaluated (Table IV). The efficiency of Heparin-GNP procedure was not altered with or without adding saliva in 20 % to the 15 HAU virus solution, therefore, no inhibition of saliva activity was observed by the binding interaction between heparin on the gold nano-particle and viral receptor proteins.

Downloaded by VIRGINIA TECH on July 17, 2013 | http://pubs.acs.org
Publication Date (Web): July 8, 2013 | doi: 10.1021/bk-2013-1135.ch020

**Table III. Comparison of sensitivity using clinical samples (nasal swab from H1N1pdm09 patients)**

| Sample# | Dilution with PBS | With Capturing and Concentration using Heparin-GNP | | | Without Capturing and Concentration | | |
|---|---|---|---|---|---|---|---|
| | | Ct | Tm | Positive | Ct | Tm | Positive |
| 1 | ×1 | 30.27 | 83.63 | ● | 33.1 | 83.84 | ● |
| | ×1/10 | 29.64 | 83.64 | ● | 35.63 | 83.84 | ● |
| | ×1/100 | 34.24 | 83.77 | ● | 37.1 | 77.12 | |
| | ×1/1000 | 35.88 | 83.72 | ● | 39.7 | 77.08 | |
| 2 | ×1 | 29.09 | 84.01 | ● | 31.34 | 84.13 | ● |
| | ×1/10 | 34.46 | 84.14 | ● | 34.7 | 84.29 | ● |
| | ×1/100 | 32.91 | 84.19 | ● | 35.5 | 76.44 | |
| | ×1/1000 | 35.86 | 84.22 | ● | 39.12 | 77.84 | |
| 3 | ×1 | 28.48 | 83.79 | ● | 33.32 | 84.02 | ● |
| | ×1/10 | 33.16 | 83.93 | ● | 37.99 | 84.13 | ● |
| | ×1/100 | 35.05 | 83.65 | ● | 41.31 | 76.28 | |
| | ×1/1000 | 37.55 | 83.74 | ● | 38.38 | 76.67 | |
| 4 | ×1 | 28.67 | 83.71 | ● | 30.35 | 83.98 | ● |
| | ×1/10 | 33.64 | 83.96 | ● | 34.83 | 84.07 | ● |
| | ×1/100 | 32.59 | 83.92 | ● | -- | 62.87 | |
| | ×1/1000 | 35.12 | 83.94 | ● | 38.23 | 78.69 | |
| N.C. | | | | | 33.92 | 76.19 | |


In Tailored Polymer Architectures for Pharmaceutical and Biomedical Applications; Scholz, C., et al.;
ACS Symposium Series; American Chemical Society: Washington, DC, 2013.

**Table IV. Influence of saliva for capturing and concentration of influenza viruses**

| | *Saliva (μl)* | *PBS (μl)* | *run* | *Ct(CP)* | *Tm #1* |
|---|---|---|---|---|---|
| samples (15HAU) | 100 | 400 | Without Capturing and Concentration | 22.94 | 83.14 |
| | | | With Capturing and Concentration using Heparin-GNP | 18.82 | 83.2 |
| | 0 | 500 | Without Capturing and Concentration | 21.55 | 82.99 |
| | | | With Capturing and Concentration using Heparin-GNP | 18.86 | 83.09 |
| control | P.C. | | | 14.58 | 83.38 |
| | N.C. | | | 36.4 | 78.09 |

Downloaded by VIRGINIA TECH on July 17, 2013 | http://pubs.acs.org
Publication Date (Web): July 8, 2013 | doi: 10.1021/bk-2013-1135.ch020

Using our method with saliva samples, we found asymptomatic patients of influenza during the pandemic in the summer of 2009. The situation occurred as follows: a student was sickened with influenza during a summer training camp of a sports club. The camp was terminated immediately by the president of the university. Other members returned to university next day. Then, saliva samples of other members, who were all very healthy, were analyzed by our newly developed system. From 28 students' saliva samples, it was found that 8 samples contained type A influenza viruses (data not shown). Consequently, asymptomatic patients, who were not yet visibly sicken by influenza, were disclosed.

We then performed a systematic clinical research in the season of 2011-2012 by comparing diagnostic results between conventional immune-chromatography kit using nasal swab and our method using saliva (Table V). A total of 109 children and 74 adults, who visited Kagoshima University Hospital or Murakami Clinic for Children due to the influenza-like symptoms were investigated, according to their agreement for a comparative diagnosis. Using the conventional kit with nasal swabs, 46/109 children and 46/74 adults patients were concluded as not infected with influenza. However, using our method, it was detected that the saliva samples of 26 children from the 46 and 24 adults from the 46 patients contained type A or B influenza viruses. These results indicated that over 50% of patients were mis-diagnosed as false-negative by the conventional kit.

Based on the clinical data, our method was significantly more useful for the early diagnosis of influenza because of its high sensitivity and easy collection of sample (saliva). Therefore, our method, using Heparin-GNP and RT-qPCR, is very effective for the prevention of outbreaks inside a hospital environment by checking medical doctors/nurses and patients for underlying disease, such as diabetes, cancer and immune-deficiency.


In Tailored Polymer Architectures for Pharmaceutical and Biomedical Applications; Scholz, C., et al.;
ACS Symposium Series; American Chemical Society: Washington, DC, 2013.

**Table V. The Clinical Research of influenza infection in 2011-12 season: Comparison of diagnostic results between conventional kit using nasal swab and our method using saliva**

| Patients | Conventional kit | Our method using saliva | | |
|---|---|---|---|---|
| | | A | B | Negative |
| Adults (N = 74) | A+ | 25 | 0 | 0 |
| | B+ | 1 | 2 | 0 |
| | Negative | 24 | 0 | 22 |
| Children (N = 109) | A+ | 54 | 0 | 2 |
| | B+ | 1 | 5 | 1 |
| | Negative | 23 | 3 | 20 |

Downloaded by VIRGINIA TECH on July 17, 2013 | http://pubs.acs.org
Publication Date (Web): July 8, 2013 | doi: 10.1021/bk-2013-1135.ch020

## Acknowledgments

We appreciate Prof. Hiroko Tsutsui (Hyogo College of Medicine), Prof. Yasuo Suzuki (Chubu University) and Dr. Soichi Nukuzuma (Hyogo Prefectural Institute of Public Health and Environmental Sciences) for the discussion and providing influenza virus strains, and Dr. Satoshi Koizumi (Kyowa Hakko Kogyo Co., Ltd.) for providing β1-4 galactose transferase. We also thank to the kind suggestions/advices for this paper by Prof. Raphael M. Ottenbrite, who was a supervisor of YS at Virginia Commonwealth University for his heparin work in 1988. This work was supported in parts by grants from the Japan Science and Technology Agency (YS) and the Japan Ministry of Health, Labor and Welfare (YS).

## References

1. Varki, A. *Essentials of Glycobiology*; Varki, A., Cummings, R., Esko, J., Freeze, H.; Hart, G.; Marth, J., Eds; Cold Spring Harbor Laboratory Press: Cold Spring Harbor, NY, 1999, and references therein.
2. Skehel, J. J.; Wiley, D. C. *Annu. Rev. Biochem.* **2000**, *69*, 531–569.
3. Gagneux, P.; Cheriyan, M.; Hurtado-Ziola, N.; van der Linden, E. C.; Anderson, D.; McClure, H.; Varki, A.; Varki, N. M. *J. Biol. Chem.* **2003**, *278*, 48245–48250.
4. Lycke, E.; Johansson, M.; Svennerholm, B.; Lindahl, U. *J. Gen. Virol.* **1991**, *72*, 1131–1137.
5. Suda, Y.; Kishimoto, Y.; Nishimura, T.; Yamashita, S.; Hamamatsu, M.; Saito, A.; Sato, M.; Wakao, M. *Polym. Prepr.* **2006**, *47*, 156–157.

6. Suda, Y.; Arano, A.; Fukui, Y.; Koshida, S.; Wakao, M.; Nishimura, T.; Kusumoto, S.; Sobel, M. *Bioconjugate Chem.* **2006**, *17*, 1125–1135.
7. Wakao, M.; Saito, A.; Ohishi, K.; Kishimoto, Y.; Nishimura, T.; Sobel, M.; Suda, Y. *Bioorg. Med. Chem. Lett.* **2008**, *18*, 2499–2504.
8. Nakamura-Tsuruta, S.; Kishimoto, Y.; Nishimura, T.; Suda, Y. *J. Biochem.* **2008**, *143*, 833–839.
9. Zhang, X.; Nakamura-Tsuruta, S.; Haruyama, M.; Yokoyama, R.; Nagatomo, M.; Wakao, M.; Nakajima, K.; Aoyama, K.; Okuno, T.; Morikawa, S.; Hiroi, S.; Kase, T.; Nose, H.; Nishi, J.; Okamoto, M.; Baba, M.; Suda, Y. *Polym. Prepr.* **2012**, *53*, 671–672.
10. Ito, T.; Couceiro, J. N.; Kelm, S.; Baum, L. G.; Krauss, S.; Castrucci, M. R.; Donatelli, I.; Kida, H.; Paulson, J. C.; Webster, R. G.; Kawaoka, Y. *J. Virol.* **1998**, *72*, 7367–7373.
11. Gamblin, S. J.; Haire, L. F.; Russell, R. J.; Stevens, D. J.; Xiao, B.; Ha, Y.; Vasisht, N.; Steinhauer, D. A.; Daniels, R. S.; Elliot, A.; Wiley, D. C.; Skehel, J. J. *Science* **2004**, *303*, 1838–1842.
12. Ryan-Poirier, K.; Suzuki, Y.; Bean, W. J.; Kobasa, D.; Takada, A.; Ito, T.; Kawaoka, Y. *Virus Res.* **1998**, *56*, 169–176.
13. Ishihama, A.; Nagata, K. *CRC Crit. Rev. Biochem.* **1988**, *23*, 27–76.
14. Sever, J. L. *J. Immunol.* **1962**, *88*, 320–329.

Downloaded by VIRGINIA TECH on July 17, 2013 | http://pubs.acs.org
Publication Date (Web): July 8, 2013 | doi: 10.1021/bk-2013-1135.ch020

# Editors' Biographies

## Carmen Scholz

Dr. Carmen Scholz is a Professor of Chemistry at the University of Alabama in Huntsville. She received a Diploma (MS) in Polymer Chemistry and a Doctorate degree in Chemistry from the University of Technology in Dresden, Germany. Dr. Scholz worked at the University of Massachusetts in Amherst and in Lowell and at Tokyo Science University prior to taking a faculty position in Alabama in 1998. Dr. Scholz's research concentrates on biocompatible and biodegradable polymers. She worked for several years with the Boston Retinal Implant Project and designed and synthesized block copolymers for the modification of biomedically relevant surfaces. Her group's research into bacterial polyesters developed the first gene delivery system based on medium-chain length polyhydroxyalkanoates. She has published more than 50 scientific articles, edited three ACS Series Books and organized several symposia at ACS National Meetings. She is an executive officer in the North Alabama local section of ACS.

## Jörg Kressler

Prof. Jörg Kressler is a Professor of Physical Chemistry at the Martin Luther University Halle-Wittenberg, Germany. He received a Diploma (MS) in Technical Chemistry and a Doctorate degree in Chemistry from the University of Technology in Dresden, Germany. Dr. Kressler was postdoc at the University of Massachusetts in Amherst and at the Tokyo Institute of Technology, Japan. After a stay as an Assistant Professor at the Albert Ludwigs University in Freiburg, he became a full Professor in Halle in 1997. His work is related to the physical chemistry of polymers with applications in medicine and pharmacy. He focuses on polyphilic polymers and their interactions with phospholipid model membranes and cell membranes. He has published more than 200 scientific articles and holds several patents.

Downloaded by PURDUE UNIVERSITY on July 20, 2013 | http://pubs.acs.org
Publication Date (Web): July 8, 2013 | doi: 10.1021/bk-2013-1135.ot001

© 2013 American Chemical Society
In Tailored Polymer Architectures for Pharmaceutical and Biomedical Applications; Scholz, C., et al.;
ACS Symposium Series; American Chemical Society: Washington, DC, 2013.

# Subject Index


**A**

Alkaline phosphatase (ALP), 276
ALP. *See* Alkaline phosphatase (ALP)
Alternative half-life extension technologies
  HESylation®, 224
  hydroxyethyl starch (HES), structure, 225*s*
  polysialic acid (PSA), structure, 226*s*
  polysialylation, 226
  recombinant PEG mimetics
    PASylation, 227
    XTEN, 227
Anti-CSC nanomedicines, 133
Anti-CSC therapies, current strategies employed, 132
Antimicrobial polymers, 322
  amphiphilic copolymers, different spacer arm lengths, 326*f*
  amphiphilic methacrylate copolymers, tuning antimicrobial activity, 324*f*
  amphiphilic random copolymers with antimicrobial activity, 323
  antibiotic resistance, emerging issue, 319
  computational modeling, 324
  copolymer $E4_{model}$, average conformation, 325*f*
  end-to-end distances and distance between centers of mass, 327*f*
  examples, 323*f*
  α-helical antimicrobial peptides, membrane disruption, 321*f*
  α-helical cationic antimicrobial peptide LL-37, 320*f*
  model copolymers, monomer sequence, and structures, 325*f*
  as new antibiotics, 320
  snorkeling effect, 323
  summary and outlook, 328
  synthetic mimics, 321, 322*f*
Anti-prostate CSC nanomedicine, 134
  CD133 expression in spheres and prostasphere formation, 140*f*
  cell surface marker expressions, 138*f*
  growths of FACS sorted CD133+ and CD133- cells, 139*f*
  Hh signaling
    inhibition, 135
    pathway, 135
  HPMA copolymer-cyclopamine conjugate, design, and synthesis, 136
  RC-92a/hTERT cells
    changes of cell viabilities and CD133+ prostate CSC percentages, 144*f*
    characterization of CSCs, 129
    cytotoxicity of cyclopamine and apoptosis levels, 142*f*
    evaluations of cyclopamine and HPMA copolymer-cyclopamine conjugate, 141
    prostasphere formation, 143*f*
  Sonic hedgehog (SHh) pathway, 135
  thiazolidine-2-thione (TT) functional groups, 136*t*
ATR-FTIR. *See* Attenuated total reflectance-fourier transform infrared (ATR- FTIR)
Attenuated total reflectance-fourier transform infrared (ATR-FTIR), 80

**B**

Benchmarking against PEG
  formulation and stability, 229
  pharmacodynamics, 228
  pharmacokinetics, 228
  protein-based concentration, monomer recovery, 229*f*
  toxicity, 229
Bioactive-based poly(anhydride-esters) (PAEs)
  as delivery systems
    poly(anhydride-ester) electrospun fibers, 34
    poly(anhydride-ester) hydrogels, 31
    poly(anhydride-ester) microspheres, 30
    SAPAE microspheres, 31*f*
  electrospun fibers, SEM images, 34*f*
  hydrolytic degradation of polymer, 28*f*
  introduction, 27
  physically crosslinked hydrogels preparation, 33*f*
  polymerization methods, 29
  PVP and SAPAE, chemical structures, 32*f*
  summary, 35
  swelling ratio ($Q$) variation, PVP content, 33*t*
  synthesis of SAPAEs, melt-condensation polymerization, 29*f*
Biomaterial-induced angiogenesis




In Tailored Polymer Architectures for Pharmaceutical and Biomedical Applications; Scholz, C., et al.; ACS Symposium Series; American Chemical Society: Washington, DC, 2013.

Downloaded by 217.118.78.91 on July 17, 2013 | http://pubs.acs.org
Publication Date (Web): July 8, 2013 | doi: 10.1021/bk-2013-1135.ix002

channeled scaffold fabrication, 249*f*
discussion, 254
example of MECA-32 stained slide, 251*f*
histological analysis, 250
implantation/study details, 249
introduction, 246
peripheral arterial disease (PAD), 245
porous scaffold, DAPI-stained image, 250*f*
scaffolds, 247
fabrication, 249
6S process, 248*f*
summary, 255
in vivo study
cellular infiltration data from DAPI images, 253*f*
lumen widths, 254*f*
MECA-32 positive cells, 253*f*
porous scaffold, DAPI, and MECA-32 staining, 252*f*
Bone tissue engineering, parameters, 289

## C

Cancer stem cells (CSC), 127
versus clonal evolution, 128
future perspectives, 144
growth and maintenance, regulation, 130
key properties
resistance to anti-cancer therapies, 130
self-renewal and differentiation, 129
Cancer therapy, dendrimer-based RNA interference delivery, 197
dendrimers as nano-scaffold, schematic presentation, 205*f*
epidermal growth factor receptor signaling pathway, 200*f*
EPS8 potentiates AKT activation, overexpression, 201*f*
mechanism of RNAi following intracellular dsRNA delivery, 199*f*
PEGylated PAMAM dendrimers, synthesis, 206*f*
Cartilage tissue engineering, 293
silk fibroin, 292
Clonal evolution model and cancer stem cell model, 129*f*
Combating HIV-1 entry and fusion, 105
HIV-$1_{HXB2}$ viral infectivity inhibition, 115*f*
HR2 peptide–PEG conjugates, 119*t*
introduction, 106
peptide modified copolymers, properties, 114*t*
polyvalent side chain peptide–synthetic polymer conjugates, 110
CDR H3 peptide, feasibility, 111
chain length dependency, 112
degree of polymerization (DP), 112
inhibit infection of HOS CCR5 cells, 112
pentafluorophenyl methacrylate, polymerization, 113*s*
3-step ester-amide/thiol-ene post-polymerization modification strategy, 111
CSC model, challenges, 131

## D

DAPI. *See* 4′,6-Diamidino-2-phenylindole (DAPI)
Degree of polymerization (DP), 112, 190, 261
Dendrimer-EGF conjugates, 207
4′,6-Diamidino-2-phenylindole (DAPI), 250
DP. *See* Degree of polymerization (DP)

## E

Enhanced siRNA delivery
aminolysis reaction of PBLA with amine compounds, 192*f*
cellular uptake efficiency of fluorescently (Cy3)-labeled siRNA PICs, 195*f*
conclusions, 196
Δα values of RA compounds, 191*f*
introduction, 190
PAsp(R)
gene silencing efficiency, 194*f*
hemolysis activity, 193*f*
representative protonation structure, 193*t*
structures, 192*f*
poly(aspartamide) side chains, 189
results and discussion, 191

## F

FACS. *See* Fluorescent activated cell sorting (FACS)



In Tailored Polymer Architectures for Pharmaceutical and Biomedical Applications; Scholz, C., et al.; ACS Symposium Series; American Chemical Society: Washington, DC, 2013.

Downloaded by 217.118.78.91 on July 17, 2013 | http://pubs.acs.org
Publication Date (Web): July 8, 2013 | doi: 10.1021/bk-2013-1135.ix002

Fatty acid modified poly(glycerol adipate), 39
conclusion, 50
expanded $^{13}C$ NMR spectra of PGA, 47*f*
experimental section
acylation of PGA backbone with fatty acid chains, 41
differential scanning calorimetry (DSC), 42
materials, 41
polymer nanoparticle preparation, 42
synthesis of PGA, 41
transmission electron microscopy (TEM), 42
$^{1}H$-$^{13}C$ COSY NMR spectrum of PGA measured in $CDCl_3$, 46*f*
melting temperature, crystallization temperature, specific enthalpy of melting, degree of crystallinity, 48*t*
poly(glycerol adipate) backbone and esterification reaction, 43*f*
prepare poly(glycerol adipate), experimental setup, 44*f*
results and discussion
DSC measurements, 47
synthesis of PGA backbone, 43
temperature dependence of regioselectivity, 46
thermogravimetry, 48
transmission electron microscopy, 48
S20 nanoparticles, cryo-TEM image, and negative-stain TEM, 49*f*
SEC measurements of PGA, 45*t*
thermal gravimetric analysis (TGA) thermograms, 49*f*
Fluorescent activated cell sorting (FACS), 129

## G

GAGs. *See* Glycosaminoglycans (GAGs)
Glycosaminoglycans (GAGs), 260
GNR. *See* Gold nanorod (GNR)
Gold nanorod (GNR), 173

## H

HC. *See* Hydroxycinnamic acid (HC)
HC-based PAEs (HCPAEs), 33
HCPAEs. *See* HC-based PAEs (HCPAEs)
HES. *See* Hydroxyethyl starch (HES)
High sensitive detection of influenza viruses
capturing and concentration, influence of saliva, 348*t*
comparison of sensitivity, clinical samples, 347*t*
heparin-GNP, TEM image, 346*f*
influenza infection, clinical research, 349*t*
type A influenza virus, RT-qPCR analysis, 346*f*
virus binding, examples, 345*f*
HIV-1 entry and fusion inhibition, 109*f*
HIV-1 fusion inhibiting peptides, PEGylation, 116
addition of cysteine containing mutant HR2 peptides to PEG-acrylate, 118*s*
glycoprotein41 (gp41) polypeptide and HR2 derived C41 wild-type peptide, 117*f*
HR2 mutant peptide–PEG conjugates, efficacy, 120*f*
HR2 peptide–PEG conjugates, degradation half-lives, 121*f*
HIV-1 life cycle, 108*f*
HPMA copolymer-cyclopamine conjugate, 134, 137*f*
design and synthesis, 136
Hydroxycinnamic acid (HC), 28
Hydroxyethyl starch (HES), 54

## I

Influenza virus strains
binding patterns of influenza virus, 340*f*
discrimination, 333
high sensitive detection, 344
introduction, 332
prediction, 342*t*
creating database and algorithms, 341*f*
preparation of array-type sugar chip, spotter and apparatus, 340*f*
preparation of sugar chip (SC), 333
SPR imaging and bio-informatics, 334
sugar-chains immobilized, 334*f*
242 influenza virus strains, 335*t*

## L

LCST. *See* Lower critical solution temperature (LCST)
List of marketed PEGylated proteins, 218*t*
Lower critical solution temperature (LCST), 236
Low-molar mass glycerides, 40



In Tailored Polymer Architectures for Pharmaceutical and Biomedical Applications; Scholz, C., et al.; ACS Symposium Series; American Chemical Society: Washington, DC, 2013.

Downloaded by 217.118.78.91 on July 17, 2013 | http://pubs.acs.org
Publication Date (Web): July 8, 2013 | doi: 10.1021/bk-2013-1135.ix002

Downloaded by 217.118.78.91 on July 17, 2013 | http://pubs.acs.org
Publication Date (Web): July 8, 2013 | doi: 10.1021/bk-2013-1135.ix002

## M

Models of cancer heterogeneity, 128

## N

Nascent poly(amino acid) chains, secondary structures
amide I (carbonyl stretching) and amide II (NH bending) bands, 80*f*
CD data for PAA oligomers in acetonitrile, secondary structure prediction, 78*t*
investigation, amino acid oligomers, 75*t*
investigation by ATR- FTIR spectroscopy, 80
n-Hex-p(Cbz-L-Cys), 83*f*
n-Hex-p(TFA-L-Lys), n-Hex-p(Cbz-L-Cys), and n-Hex-p(bz-L-Glu), 82*f*
summary of amide I and amide II band positions, 81*t*
n-Hex-p(Cbz-*L*-Cys) oligomers, secondary structure, 79*t*
*N*-hexylamino-poly(bz-L-glutamate), 76*f*
poly(Cbz-L-cysteine), 76*f*
poly(Cbz-L-lysine), 77*f*
poly(TFA-L-cysteine), 75*f*
secondary structure of PAA oligomers, circular dichroism (CD), 74
secondary structures of PAA's by FTIR, 82*f*
urea interfering with β-sheet formation, 79*f*
Novel cellulose derivatives, 259
affinity to growth factors, 263
ALP activity, 276
average DP, 269*t*
binding of growth factors FGF-2 and BMP-2, 270
BMP-2, effects on osteogenic differentiation, 274
$^{13}$C NMR spectra of heparin, CS-0.37, CO-0.67, and CM-1.47, 268*f*
cell culture, 263
cellulose sulfates, synthesis, 266*t*
characterization of products, 262
competitive binding assay, 271*f*
containing carboxyl/carboxymethyl groups, 267*t*
effects of cellulose derivatives and FGF-2 on 3T3 fibroblast growth, 272
heparin and cellulose derivatives, chemical structure, 265*f*
introduction, 260
materials, 262
microcrystalline cellulose, 267*f*
mitogenic activity, 261*f*, 273*f*
mitogenic effects, 264
osteogenic activity, 264, 275*f*
SEC elution patterns, 270*f*
staining of alkaline phosphatase, 277*f*
synthesis and characterization, 265

## O

Oligomeric poly(amino acid)s, secondary structure, 69
amino acid N-carboxyanhydrides (NCAs), amine-initiated ring-opening polymerization, 73*f*
β-sheets and α-helices, 71
introduction, 70
PEGylated PAA block copolymers, 72
poly(amino acid) polymerization mechanisms, 71

## P

PAsp(R). *See* Poly(aspartamide) derivative (PAsp(R))
PEGylated dendrimers, 205
PEGylated proteins and alternative half-life extension technologies, 215
PEGylation technology challenges, 216
PEGylation technology limitations, 217
activity, 221
immunogenicity, 223
raw material and conjugation chemistry, 219
spleen tissue, photomicrographs, 222*f*
stability and formulation, 219
lyophilization, 221
protein stability, 220
viscosity, 221
viscosity of solutions, 220*f*
toxicity, 223
PGA. *See* Poly(glycerol adipate) (PGA)
Poly(aspartamide) derivative (PAsp(R)), 190
Polyesters based on glycerol, 40
Poly(glycerol adipate) (PGA), 39
Polymeric micelles as drug carriers, 87
Polymeric micelles stabilization by complex formation with metal ion, 91



In Tailored Polymer Architectures for Pharmaceutical and Biomedical Applications; Scholz, C., et al.;
ACS Symposium Series; American Chemical Society: Washington, DC, 2013.

polymers and ligands, molecular structures, 92*f*
electrostatic interactions, 87
EPR (enhanced permeability and retention) effect, 88
schematic illustration, 89*f*
fluorescence intensity ratio for $I_1$ to $I_3$ peaks of pyrene, 96*f*
HA-coated micelle, 96
Hep-coated micelles, HA-coated micelles, and CMDex-coated micelles, flow cytometric analysis, 98*f*
importance, 90
molecular structures of polymers, polyion complex formation, 93*f*
platinum complexes and PEG-b-polyglutamate, molecular structures, 91*f*
by polyion complex formation, 93
temperature-responsive micelle formation, 94*f*
Poly(*N*-vinyl-2-pyrrolidone) (PVP), 32
Poly(oxazoline) block copolymers
ABA self-assembling triblock copolymers, 55
cancer treatment, liposomal delivery, 53
cationic ring-opening polymerization, 55*f*, 56
drug delivery applications, 54
introduction and motivation, 53
polysiloxanes as hydrophobic cores, 56
Polyoxazoline containing triblock block copolymers
ABA triblock copolymer, synthesis, 62*f*
aqueous-based binary solvent system, 64
click-based triblock copolymer synthesis, 60*f*
copper-catalyzed alkyne-azide cycloaddition methodology, 61*t*
$^1$H NMR spectra of $N_3$-PDMS-$N_3$, PMOXA, and CuAAC product PMOXA-PDMS-PMOXA, 63*f*
proof of triblock, 64
triblock copolymer, self-assembly
large unilamellar vesicles, 65
nanoscale vesicles, 66
PMOXA-PDMS-PMOXA triblock copolymer vesicles, 66*f*
vesicles, range of 1-5μm, 65*f*
triblock formation via click chemistry, 59
triblock synthesis by macroinitation, 57
Generation I, Generation II, $^1$H NMR spectrum, 58*f*
Generation III and $^1$H NMR spectrum, 59*f*
Polytetrafluoroethylene (PTFE), 245
Polyvalent HIV-1 entry inhibitors, 107
Properties and applications of PEG, 217
Protein therapies, 216
PTFE. *See* Polytetrafluoroethylene (PTFE)
PVP. *See* Poly(*N*-vinyl-2-pyrrolidone) (PVP)

## R

RA. *See* Repeating aminoethylene (RA)
Repeating aminoethylene (RA), 189
RES. *See* Reticulo-endothelial system (RES)
Reticulo-endothelial system (RES), 54
RNAi delivery, dendrimers
examples
dendrimer-EGF conjugates, synthesis, 207*f*
dendriworms, 208
PEGylated dendrimers, bis-aryl hydrazone (BAH) linkages, 206
synthesis of dendriworms, 208*f*
structures and properties, 204
summary, 209
RNA interference (RNAi), 197
brief overview, 198
cancer therapy, 198, 202*t*
RNAi therapy, challenges, 203

## S

SA. *See* Salicylic acid (SA)
SA-containing PAEs (SAPAEs), 28
Salicylic acid (SA), 28
SAPAEs. *See* SA-containing PAEs (SAPAEs)
Secondary structures of nascent poly(amino acid) chains, 74
Solid tumors
abbreviations, 173, 174
introduction, 151
polymer therapeutics, enhanced delivery, 151
PPTT guided delivery
characterization of GNRs, 162*f*
combined in vitro effects of hyperthermia incubation, 170*f*
enhancement of macromolecular delivery, 163
evans blue dye (EBD) delivery thermal enhancement ratio (TER), 163*f*



In Tailored Polymer Architectures for Pharmaceutical and Biomedical Applications; Scholz, C., et al.; ACS Symposium Series; American Chemical Society: Washington, DC, 2013.

Downloaded by 217.118.78.91 on July 17, 2013 | http://pubs.acs.org
Publication Date (Web): July 8, 2013 | doi: 10.1021/bk-2013-1135.ix002

heat shock targeted HPMA copolymer-drug conjugates, in vitro synergism, 172
heat shock targeted HPMA-copolymer docetaxel conjugates, in vivo efficacy, 172
heat shock targeting, in vitro investigation, 166*f*
heat shock targeting to cancer cells, hyperthermia, 164
heat-shock targeted HPMA copolymers, 165
HPMA copolymer delivery, 168*f*, 169*f*
hyperthermia, in vivo efficacy, 171*f*
intratumoral distribution after delivery, 168
plasmonic photothermal therapy (PPTT), 161
polymeric conjugates in mice, 167*f*
tools for improved delivery
delivering nanomedicines, 154
hyperthermia, 159
need for continued investigation, 160
passive targeting and EPR Effect, 153
pharmacologic enhancement of delivery, 156
physical enhancement of delivery, 158
receptor-mediated active targeting, 155
translatability of EPR, 154
transvascular transport, 158
tumor necrosis factor-α (TNF-α), 157
vascular disrupting agents (VDAs), 157
Surface modification of polyurethanes
biocide release, 304
conclusion, 314
contact kill
model, 306*f*
oxidative kill, 305
polycations at surfaces, 305
health and safety, 303
introduction, 304
polymers containing quaternary function and surface modified coatings, 307*f*
quats at surfaces, 306
2 wt% U-3F-C12(0.11) coating, TM-AFM 3D height image, 310*f*
agar plates after spray challenge of P. aeruginosa, 310*f*
generation 2 modifier, 312
generation 1 not stable, 309
generation 1 surface modifiers (SMs), 308
homo-quats, 307
image of 2 wt% U-4F-C12(0.34) coated glass slide, 312*f*
P[AB]-polyurethane surface modification, 308*f*
quantifying near surface quaternary charge, 311
streaming potentials, capillary pumping cycle, 311*f*
surface modification, 307
U-4F-C12-34, percent kill of spray challenges, 314*t*
zeta potentials, base polyurethane, 313*t*

## T

Thermoresponsive polymers
introduction, 235
LCST-type polymers with functional groups, 236
poly(allylurea) derivatives and poly(L-citrulline-co- L-ornithine), 238*f*
temperature-responsive affinity control, 236*f*
UCST-type polymers with functional groups, 237
UCST-type transmittance curves of PU-Ams, 239*f*
Tissue engineering, active role of scaffold, 282
Tissue regeneration
confocal images of HDMEC and OB cultured, 291*f*
hAFSCs cultured, microscopical analysis, 290*f*
silk as adaptable biomaterial, 283
*Bombyx mori*, 284
hydrogels, 287
non-woven nets, 286
porous sponges, 287
process-dependent bioactivity of silk fibroin, 285
silk fibroin, purification by degumming process, 285*f*
silk fibroin scaffolds, confocal images of cell viability and distribution, 294*f*
tailoring silk-based matrices, 281
use of silk fibroin, bone tissue engineering, 288



In Tailored Polymer Architectures for Pharmaceutical and Biomedical Applications; Scholz, C., et al.; ACS Symposium Series; American Chemical Society: Washington, DC, 2013.

Downloaded by 217.118.78.91 on July 17, 2013 | http://pubs.acs.org
Publication Date (Web): July 8, 2013 | doi: 10.1021/bk-2013-1135.ix002

**U**

UCST. *See* Upper critical solution temperature (UCST)
Upper critical solution temperature (UCST), 236

**V**

Vascular angiogenic growth factor (VEGF), 157, 246
VEGF. *See* Vascular angiogenic growth factor (VEGF)
Viral strains, 331

Downloaded by 217.118.78.91 on July 17, 2013 | http://pubs.acs.org
Publication Date (Web): July 8, 2013 | doi: 10.1021/bk-2013-1135.ix002


In Tailored Polymer Architectures for Pharmaceutical and Biomedical Applications; Scholz, C., et al.;
ACS Symposium Series; American Chemical Society: Washington, DC, 2013.